Sediment Dispersion at the New Auckland Marine Disposal Ground, Northeast New Zealand

A thesis

submitted in fulfilment

of the requirements for the degree

of

Doctor of Philosophy

at

The University of Waikato

by

BRYNA KATHRYN FLAIM

THE UNIVERSITY OF
WAIKATO
Te Whare Wānanga o Waikato

2012

This book is dedicated to my mom, Kathryn Erskine Flaim,
who probably never imagined that I would end up writing a book about mud in the ocean,
but who I know would have been the first in line to read it.

ABSTRACT

A controversial history of near shore dredged material disposal east of Auckland, New Zealand, starting in the mid-1980s, resulted in the use of a temporary deep water site that did not satisfy the requirements of the London Dumping Convention. In New Zealand, since most maintenance dredged material contains a low level of contamination, it is a common requirement that open-sea disposal sites are retentive, so that impacts can be monitored. In 2007, preliminary investigations for a proposed site located on New Zealand's northeast shelf were initiated. Indications that the site was suitable prompted Maritime New Zealand (MNZ) to grant a permit for a trial disposal of 5,000 m^3 of muddy dredged material on the condition that disposal operations were monitored to assess the potential for dispersion of the material beyond the boundary of the site. The overall aim for this thesis research, based on the questions raised by MNZ, was to determine the potential for dispersion at the AMDG and classify the site based on its dispersive qualities. This aim was approached in three ways: (*i*) investigation of the hydrodynamic setting, (*ii*) measurement of the disposal process and the resultant plume, and (*iii*) development and implementation of a model designed to simulate the disposal characteristics under conditions not observed in the field.

The first two approaches involved measurement campaigns, which were undertaken in 2008 and 2010. The 2008 campaign primarily focused on investigation of the hydrodynamic setting through the deployment of a long-term upward facing ADP, which was complemented by hydrological measurements (CTD), and nearby wind records. The 2010 campaign corresponded to the trial disposals at the AMDG, where 4 disposals were monitored using a range of techniques. Stationary water sampling and OBS turbidity measuring stations were positioned in the vicinity of the disposal location with the intention of recording data that could be used to calibrate backscatter data recorded with a vessel-mounted ADCP. These data were supplemented by additional pre- and post-disposal measurements, such as sediment cores, MBES backscatter, dynamic penetrometer profiles, and under water video imagery, which provided information on the depositional fate of the disposed material. Therefore, measurements were collected during all stages of the disposal process, providing a unique dataset for a deep-water disposal site.

Due to the low number of published studies on disposal plume dispersal and the site specific nature of the process, it was not known in advance what the most efficient and practical techniques for monitoring the plume were. The identification of optimal measuring methods was a secondary outcome of this work. It was found that, due to the transient nature of the plume, stationary sampling techniques were not able to satisfactorily record the plume because its position was difficult to predict. Taking sequential measurements along transects proved to be the optimal approach for tracking the plume. Specifically, backscatter data from the vessel-mounted ADCP records provided the best perspective on the spatial and temporal characteristics of the disposal plume. MBES bathymetry data recorded after the completion of all disposals was ultimately inconclusive regarding depositional fate because the deposits were less than 20 cm thick and, therefore, unresolvable at the water depths of the AMDG and the frequency of the system employed. However, a backscatter map,

developed from the same MBES dataset, corroborated some of the findings from the plume monitoring surveys by showing the impact locations of the disposed loads, which appeared as lighter gray patches (higher density substrate) amongst the darker gray natural site sediment areas.

Analysis of ADCP backscatter data obtained during the trial disposals indicated that the extent of horizontal dispersion was greatest in the surface region (500 - 800 m) due to stronger current velocities that occur as a result of the decreased influence of friction from the seabed and the increased influence of wind-driven currents. However, in all cases, after the descent of the dredged material to the seabed during the first few minutes, the maximum concentrations were always located near the seabed where horizontal dispersion was low (~200 m). Based on these findings, it was concluded that the weak ambient forcing mechanisms have the potential for the greatest dispersion, rather than the dynamic forces associated with the disposal process. It was found that while generally producing low ambient current velocities, the dominant forcing mechanisms at the AMDG were temporally variable, which could lead to a range of different dispersion characteristics. Tides, wind, and the East Auckland Current (EAUC) were identified as the predominant drivers. Tidal currents were relatively slow (2-10 cm/s), but in general appeared to be more important than wind-driven currents in the surface zone. The influence of the EAUC varied during the field campaigns, where its influence appeared to be weak during the monitored trial disposals, but strong during the long-term deployment of 2008. This variability corresponds to the findings of other studies undertaken on the dynamics of the northeast coast region.

The short-term mechanisms of the disposal process, additionally captured in the ADCP backscatter records, showed similar characteristics to those previously described in the literature (i.e., 1-*Convective Descent*, 2-*Dynamic Collapse*, and 3-*Passive Dispersion*). However, through analysis of the rate of dilution throughout the 3 phases, an additional transitional phase was identified. This phase, observed both spatially (with distance from the disposal location) and temporally (with time after disposal), was characterised by a decreased rate of dilution. From the findings, an alternative conceptual model for the disposal process was developed in which the transitional phase was described as a turbulent zone, where water at the interface of the dynamic zone is set in circular motion, therefore, preventing dilution at a particular location or time. After momentum is reduced enough, the turbulent forces give way to the diffusive forces and passive dispersion becomes the dominant mode for dispersion.

The main finding of this research was that the potential for dispersion beyond the boundary of the AMDG is low indicating that the site behaves retentively. This finding is partly a result of the low velocities of the ambient currents, but also because of the operational limitations of the tug-towed disposal method employed for disposal. For minimising the dispersion potential of the AMDG for future operations at the site, it is recommended that the disposal method remain unchanged, that material types more susceptible to dispersion not be disposed there, and that disposal not be undertaken when tidal currents are aligned with the wind direction for winds greater than 20 knots.

ACKNOWLEDGEMENTS

The completion of this thesis and the pending proposal for long-term use of the Auckland Marine Disposal Ground (AMDG) represent the culmination of a project which was first conceived in 2006 by Professor Terry Healy, and Simon Male and Allan Drinkrow of Kaipara Ltd./Coastal Resources Ltd.

Terry's passing in July 2010 was a tragedy that touched many, many people, from his industry partners all over New Zealand, to his academic colleagues at University of Waikato and across the globe, vast numbers of Bachelor's, Master's, and PhD students, and of course his family. Terry was known for his passion, work-ethic, and his uncanny ability to just make things happen. I was lucky enough to bear witness to his ways and I will always be grateful to him.

When Terry passed, he was actively supervising a number of students. Drs. Willem de Lange and Karin Bryan accepted the burden of taking over supervision of, in addition to their own students, all of Terry's students. I applaud their efforts; the added work load must have been oppressive. In my case, Willem took over as my chief supervisor, and Karin, along with Dr. Conrad Pilditch, continued on in their supportive roles. From my perspective, the transition was as smooth as one could hope for and I am so grateful for Willem's tolerance for my incessant questions, impromptu drop-ins, and his editing efforts on what became a rather verbose thesis. As tragic as the circumstances were, I am lucky to have been able to work with Willem and take advantage of his vast knowledge.

The roles of my other two supervisors, while less labour intensive, were no less significant. Karin and Conrad both managed to provide me with supportive and encouraging words when I often didn't even know I needed them, which were especially helpful in the difficult time after Terry passed. I would also like to acknowledge their efforts to unite the coastal and marine students through their numerous backyard barbeques and through the Coastal Marine Seminar Series. These activities have created sense of camaraderie among the students despite the diverse range of research topics we were all involved in.

Thank you to Vicki Moon for the crash course on geo-mechanics, Dave Campbell for all your hard work and support, Sydney Wright for managing all the crazy scientists, and Jacinta Parenzee, Annette Rodgers, Chris McKinnon, Craig Hoskings, and Louise Fisk for continually and (mostly) happily helping me with one thing or another over the years.

A special thanks needs to be given to Dirk Immenga who was absolutely instrumental (pun intended!) throughout the entirety of my research project. I often tested his legendary skills in organisation and planning with my elaborate field plans and I'm sure he often just wanted to throw me overboard. Despite all that, we managed to develop a great working relationship and I am eternally grateful for all the hard work he put into my project. Speaking of field work, I couldn't have undertaken such rigorous field campaigns without the help of the following people: Mike Roycroft, Gary Larsen, Lyall Campbell, Sean Kelly,

Sebastien Boulay, Simon Weppe, Andrew Wood, Remy Zyngfogel, Nina Stark, Denise Bruesewitz, and Alex Schimel.

Over the years, I was able to get access to resources that were not immediately available to me in the Earth and Ocean Department. The accessibility of such things as software, field instruments, datasets, and most importantly knowledge, demonstrates the willingness of colleagues in the coastal science community of New Zealand to support the next generation of researchers. I would like to thank in particular, Ben Tuckey, Colin Roberts, Pierre Hovelt, and Rathika Jebamony of DHI New Zealand for free access to and guidance in using the MIKE by DHI model suites; Rob Bell, Andrew Swales, Carolyn Lundquist, Glen Reeve, and Nicole Hancock of NIWA Hamilton for model data, instrument and lab access, and valuable advice; LINZ and the Royal New Zealand Navy for MBES data; Jae Staite of North Port for water level data; Pete McComb, Dave Johnson, and Brett Beamsley of MetOcean Solutions Ltd. for access to the Sontek ADP, model data and for the many email advice sessions; Craig Stevens and Brett Grant of NIWA Wellington for access to the drogue/drifter set-up; Tara Ross-Watt of Martime New Zealand for discussions on the history of dredged material disposal in the Auckland area; Prof. David Hamilton and Chris McBride of the Department of Biological Sciences at University of Waikato for access to and advice in using the BIOFISH; Chris Hendy, Annie Barker, and Lisa Pearson of the Department of Chemistry at University of Waikato for access to and advice in using the gravity corer; Prof. Achim Kopf of University of Bremen for access to *Nimrod* and for his editing efforts; the German Research Association (via MARUM and GLOMAR, University of Bremen) and the German Academic Exchange Service (DAAD) for travel and expenses associated with bringing *Nimrod* to New Zealand; Tam Larkin, Mark Liew, and Jiae Erin Lee of the Department of Civil and Environmental Engineering at University of Auckland for access to and advice in using lab shear strength equipment; and finally, Peter Longdill and Jonathan Sharples for their expertise on the northeast shelf of New Zealand and guidance on how best to analyse and interpret data collected there.

I was lucky enough to receive a Waikato Doctoral Scholarship followed by an extension to that scholarship, which covered my living expenses for more than 3 years. I couldn't have done that without the help of Gwenda Pennington and the scholarships office, along with Professor Cam Nelson from the Department of Earth and Ocean Science. Kaipara Ltd./Coastal Resources Ltd. provided research funding and were always supportive of my research endeavours. Jenny Robertson of UniLink made accessing those funds a breeze.

Thank you to Gegar, Rafael, Nina, Deb, Denise, Rachel, Natalie, Clarisse, and Alex (giver of kittens) for your support and friendship over the years. A girl's gotta have some people to lean on sometimes. Thanks for being there to prop me up ☺.

And finally, thank you to my dad and my sister, for listening to me rant and rave over skype, sending me care-packages from California, and for clearing your schedules for me when I came home for visits. I am so lucky to have you two in my life.

PREFACE

The research presented in this thesis was initiated in 2007 as a collaboration between Kaipara Ltd./Coastal Resources Ltd. and the Coastal Marine Group of the University of Waikato to provide the necessary scientific information for a proposal to establish a new disposal area for dredged sediments originating in the east Auckland region of New Zealand. It follows on from preliminary work comprising my Master of Science project, completed in 2008.

The main body of this thesis comprises three Chapters (3-5) with Chapters 1, 2, and 6 serving to tie together the main findings and provide the monographic structure. I assume responsibility for all aspects presented herein including: field campaigns, laboratory assessments, data analysis, written expression of the work, and collation of the thesis.

Publications and reports produced in association with this research include:

Flaim, B.K., Healy, T.R., and Weir, P. (2010). Establishment of a dredged material disposal site in the Exclusive Economic Zone: New Zealand. *Coastal Management*, 38(5), 474-500.

- The content of this paper is sourced mainly from the findings of the MSc portion of this research project, but written and published during the PhD. Aspects pertaining to the management angle of the project that occurred after completion of the MSc were included in the paper. The paper can be viewed in Appendix II of this thesis.

Flaim, B.K., Healy, T.R., and de Lange, W.P. (2009). Tidal components of flow at a proposed dredged material disposal site on the continental shelf, northeast New Zealand. Paper presented at Coasts and Ports 2009, Wellington, New Zealand.

- The content of this paper is tied to Chapters 3 (tidal data observations) and Chapter 5 (a preliminary modelling study). The paper is included in Appendix II of this thesis.

Flaim, B.K., Stark, N., Moon, V., de Lange, W.P., Healy, T.R., and Kopf, A. (2011). Monitoring a dredged material disposal site on the continental shelf using

the dynamic penetrometer *Nimrod*. Paper presented at Coastal Sediments 2011, Miami, Florida.

- A side project aimed at determining the fate of disposed sediment at the AMDG through assessment of geotechnical properties of the seabed comprised the content of the above paper. The research is linked to the aims of Chapter 4 of this thesis but, was not included as it was not a main focus. The paper is included in Appendix II of this thesis.

Flaim, B.K. and Healy, T.R. (2008). Proposal for dredged sediment disposal on the continental shelf in the EEZ: Environmental Impact Assessment. Coastal Marine Group, University of Waikato, Hamilton, New Zealand. 96 p.

- A consulting report produced on behalf of Kaipara Ltd./Coastal Resources Ltd. for submission to Maritime New Zealand for consideration of the initial proposal. The EIA was developed during the MSc portion of this project, but is included in Appendix III of this thesis to provide perspective on the research direction taken throughout the project's various stages.

Flaim, B.K. and de Lange, W.P. (2011). Post-disposal monitoring of the Auckland Marine Disposal Ground. Coastal Marine Group, University of Waikato, Hamilton, New Zealand. 186 p.

- A consulting report produced on behalf of Kaipara Ltd./Coastal Resources Ltd. for submission to Maritime New Zealand after completion of the disposal operations and the post-disposal monitoring surveys in July 2010. The details of several datasets not covered in the thesis are included in this report and it is, therefore, cited periodically throughout the thesis. The report is included in Appendix III of this thesis.

Establishment of the AMDG as long-term site for disposal operations is still on-going. Currently, a monitoring plan for long-term use of the site is being developed which is required before a new permit can be approved. The content of the monitoring plan will draw heavily on the experiences and outcomes of the field campaigns described in this thesis.

TABLE OF CONTENTS

LIST OF FIGURES

LIST OF TABLES

TABLE OF ACRONYMS

ADCP	Acoustic Doppler Current Profiler (RD Instruments®)
ADP	Acoustic Doppler Profiler (Sontek®)
AMDG	Auckland Marine Disposal Ground
ATB	Above the bed
BSWD	Blended Sea Winds dataset from the National Oceanographic and Atmospheric Administration (NOAA) National Climatic Data Center (NCDC)
CMA	Coastal Marine Area
CTD	Conductivity Temperature Depth
DOAG	Disposal Options Advisory Group
EAUC	East Auckland Current
EDG	Explosives Dumping Ground
EEZ	Exclusive Economic Zone
ENU	East, North, Up coordinate system
LINZ	Land Information New Zealand
MAE	Mean Absolute Error
MBES	Multibeam Echo Sounder
MI	Mokohinau Islands wind data (CliFlo and Blended Sea Winds) and tide gauge/model output (NIWA) location
MNZ	Maritime New Zealand
NIMBY	Not In My Back Yard
NIWA	National Institute of Water and Atmospheric Research
NTU	Nephelometric turbidity units
NZTM	New Zealand Transverse Mercator Coordinate Projection
SBES	Single beam echo sounder
SEM	Scanning Electron Microscope
SI	Slipper Island wind data (CliFlo and Blended Sea Winds) station
SIO	Southern Oscillation Index
SSC	Suspended solids concentration (mg/L)
SSS	Side-scan sonar
TEU	Twenty foot equivalent unit, standard measure of container volumes
WD	Wind-driven (with respect to residual currents)

TABLE OF SYMBOLS

A	area of the hemispherical discharge (m^2)
A_D	surface area of the density current (m^2)
A_I	area of impact (m^2)
AL	all acoustic losses
A_o	effective area of the orifice (m^2)
C_v	volume concentration scatterers
c	the speed of sound (m/s)
D	sediment grain size diameter (m)
D_{Di}	difference in density of the density current (kg/m^3)
D_{Fs}	dispersion factor relative to space
D_{Ft}	dispersion factor relative to time
d_z	difference in depth (m)
E	entrainment
e	entrainment coefficient
F	negative buoyancy
Fr	densimetric Froude number
f	frequency (Hz) of the acoustic signal
g	gravitational acceleration (m/s^2)
H	water depth (m)
H_D	potential density current thickness (m)
H_{Di}	initial thickness of the density current (m)
h_{10}	height 10 m above the sea surface
h_w	height from which wind velocity (w_w) was measured
I	insertion speed (m/s)
k	wave number of acoustic energy
k_1	constant in the sonar equation
L_s	density current propagation distance (m)
M_D	volume of the density current (m^3)

R_{Di} initial radius of the density current (m)

R_I radius of the area of impact (m)

RT_{s1} mean relative turbidity at space 1

RT_{s5} mean relative turbidity at space 5

RT_{t1} mean relative turbidity at time 1

RT_{t4} mean relative turbidity at time 4

RV ensonified volume

r_g radius (m) of a particle

r_h radius of the hemispherical discharge cloud (m)

$\bar{r}$ effective radius of the orifice (m)

S proportion of sediments settling directly at the point of impact

S_F spread factor

SL source level from transducer

S_v volume backscattering strength

t_i time for material to pass through hopper doors

t_{PD} time post-disposal (s)

U_{crit} sediment entrainment threshold velocity (m/s)

u_{24} non-tidal cross-shore current from the surface-most ADP bin (24 m below the surface)

u_w cross-shore component of the wind-driven current

u_{w0} synthetic cross-shore surface current

V volume of the hemispherical discharge cloud (m^3)

V_0 discharged volume (m^3)

V_{Di} initial velocity of the density current (m/s)

V_s volume of solid particles disposed as a mass (m^3)

v_{24} non-tidal alongshore current from the surface-most ADP bin (24 m below the surface)

v_w alongshore component of the wind-driven current

v_{w0} synthetic alongshore surface current

$\bar{v}$ vector velocity of the discharged material (m/s)

$\bar{v}_a$ vector velocity of the ambient water (m/s)

W_{fE} early-phase down-fall velocity (m/s)

W_{fi} down-fall velocity of the mass of disposed sediments at the moment of impact

W_{fK} down-fall velocity (m/s)

W_{fL} late-phase down-fall velocity (m/s)

W_{fM} average down-fall velocity (m/s)

W_s natural settling velocity of sediment particles (m/s)

w_{10} wind velocity (m/s) 10 m above the sea surface

w_w wind velocity (m/s) at a known height above the sea surface

w_x measured cross-shore wind speed component

w_y measured alongshore wind speed component

x_1 weight (g) of the rinsed and dried filter paper

x_2 weight (g) of the re-dried filter paper following filtration

y volume (l) of sample filtered

Z height of the orifice above the bottom (m)

z water depth (m)

z_E maximum turbidity depth of the disposal cloud (m)

z_L leading edge depth of the high turbidity region corresponding to the 0.35 relative turbidity contour (m)

α Hellman coefficient taken as 0.11 for open-ocean conditions

β angle of spread of the plume of descending material (°)

β_k parameter defined by the submerged weight, sediment grain size, water viscosity, and an experimental parameter

γ_s submerged weight

γ_u derived depth-scaling value used to produce the inferred cross-shore wind-driven current

γ_v derived depth-scaling value used to produce the inferred alongshore wind-driven current

Δt time after disposal (min)

Δx maximum cross-shore dispersion distance

Δy	maximum alongshore dispersion distance
θ	direction of dispersion
λ	wavelength (m) of the acoustic signal
μ	viscosity of water
ρ	density of water (kg/m^3)
P	magnitude of dispersion (m)
ρ_d	bulk (wet) density of dredged material (kg/m^3)
ρ_e	excess density of the density current (kg/m^3)
ρ_{plume}	density of the suspended sediment component of the disposal plume after impact with the seafloor (kg/m^3)
ρ_s	density of solid particles (kg/m^3)
φ_β	dimensionless parameter determined experimentally for determination of W_{fK}

CHAPTER 1
INTRODUCTION

1.1 Open-Water Disposal of Dredged Material

There are several well-accepted methods for the handling of dredged material in modern times. The preference for each is situation dependent and is likely influenced by such aspects as the local implementation of the international convention on disposal at sea, available resources for dredging and disposal of the material, the level of contamination of the dredged material, and the availability and feasibility of the various disposal options.

For example, in The Netherlands and the north of Germany, a common practice is to dispose dredged material in sub-aquatic confined 'depots' where potential environmental effects are confined to a single location (Palumbo, 2007). Other present day options for the handling of dredged material are being used in Australia and Japan in the form of land reclamation (e.g., Gladstone Harbour; Sparkes (2012)) and beneficial reuse (e.g., construction and restoration of native habitats, Naito and Nakamura (2009)).

In the past and still today, open sea or 'marine' disposal of dredged material has been a viable option for the handling of dredged material. In the United States, marine disposal has been undertaken since the early 1900s in such places as San Francisco in association with the development boom after the California Gold Rush of 1849 (Chin & Ota, 2001). In those times, disposals were mostly un-documented, but today, a well-established program for disposal site establishment, operation, and monitoring is run by the US Army Corps of Engineers.

1.1.1 The Role of Sediment Dispersion

With the ratification of the London Dumping Convention and the 1996 Protocol, marine disposal has become less favourable where alternative options exist, such as those used in The Netherlands. However, there are still many examples where marine disposal is still the favoured option. In the US, there are many current sites for marine disposal along its coasts that accommodate a large percentage of material dredged from near shore areas (e.g., the San Francisco Deep Ocean

Disposal Site (SF-DODS), Los Angeles/Long Beach (LA-2), San Diego 100 Fathom (LA-5), and Miami Ocean Dredged Material Disposal Site (ODMDS) (EPA, 2012).

In those cases, marine disposal sites are chosen based on their retentive characteristics so that material there can be monitored for potential negative impacts. However, there are also examples where dispersive sites are preferred, for example, in the case where a near shore disposal site acts as an artificial sediment source for a severely eroded beach (Foster et al., 1996). Retentive sites effectively function as aquatic containment sites, similar to those commonly used in Europe, but without physical containment barriers. In that respect, it is necessary to undertake substantial site assessment investigations to determine the nature of the site and whether or not it will be suitable for disposal operations.

Whether a marine site is required to be retentive or dispersive is usually dependant on the levels of contaminants within the material intended for disposal (McAnally & Adamec, 1987). Dispersive sites may be appropriate if the material is uncontaminated and needs to be re-introduced to the local littoral system as in the aforementioned example. For the case of slightly contaminated sediments (within the acceptable range for marine disposal), it is necessary that the material remain within the boundary of this site so that negative impacts, both toxic and chronic, are limited to that area only.

In such a case, the stability of the site in terms of dispersion must be known before disposal operations at the site can begin (McAnally & Adamec, 1987). Field surveys, numerical modelling, and ‘back-of-the-envelope’ calculations can be used to determine the dispersive potential of a site (e.g., Aarninkhof and Luijendik (2010), Hands and Allison (1991), Langtry et al. (2009), and Wu et al. (2006)). Numerical modelling approaches are also capable of identifying optimal site operation conditions making it possible to determine where is the best place to release the material within the boundary of the site on any given set of conditions so that the sediment plume will not be transported outside the boundary of the site before concentrations have reduced to background levels (Aarninkhof & Luijendik, 2010; Langtry et al., 2009).

1.1.2 Dispersion Assessment

There are four main approaches for assessing dispersion or the potential for dispersion at a marine disposal site: (1) *in situ* plume monitoring, (2) numerical modelling of disposal fate and sediment dispersion, (3) inference from hydrodynamic observations, and (4) pre- and post-disposal benthic investigations

Early studies reviewed by Truitt (1988) relied heavily on the first approach through deployment of optical turbidity sensors and collection of water samples for determination of suspended sediment concentration (SSC) at the time of disposal. These studies provided the basis for the currently understood model for the disposal process based on the observation of remarkably similar patterns of dispersion after release of sediment into the water column, which will be described in detail in Chapter 2. It is understood today that point-based measurements are limited in resolution; however, in the past, disposal sites were typically located in water depths less than 50 m, where at least vertical resolution requirements are less demanding. However, considerable resources were still required to accurately observe the plume using point-based measurements.

To overcome gaps in knowledge, researchers began to develop numerical models designed to simulate the disposal process. This second approach aimed to gain insights into the disposal process while making it possible to bypass or, at least, decrease the dependency on the difficult and often fruitless task of monitoring disposal processes in the field. However, traditional *in situ* field research was not discontinued; rather, the aim of field studies shifted to data collection for the purposes of model development.

Some of the first commercial models of dredged material fate were created by the US Army Corps of Engineers (USACE). The USACE model, DIFID (Disposal From Instantaneous Dump), was a pre-cursor to the more well-known STFATE (Short Term Fate) and LTFATE (Long Term Fate) that simulate the short-term fate and long-term fate of material disposed at sea (McAnally & Adamec, 1987). DIFID was developed primarily on the basis of model developments by Koh and Chang (1973). The STFATE and LTFATE models have been described and applied in such reports as Johnson and Fong (1995), Scheffener (1992) and

Scheffner and Tallent (1992). Moritz and Randall (1995) attempted to improve modelling capabilities with the model ODAMS by including the prediction of fate after disposal of multiple dumps, which is the common case in reality, especially at large disposal sites. In response, to some extent, the USACE also created the model MDFATE, which had much the same capabilities as ODAMS.

Other modelling attempts have been reported, such as the work undertaken by Wolanski et al. (1992), which compared field observations to model results and found that models should account not just for wave induced velocities, but for wave turbulence as well to accurately simulate the maintenance of the high turbidity suspension at the bed after disposal, which is highly susceptible to advection from the disposal area. Models specifically focusing on the *Dynamic Collapse* phase (density current) have been undertaken by Doneker et al (2004) and Drapeau et al. (1999). Those efforts examined energy budgets in relation to the formation of density currents after impact of the disposed material with the seabed and predicted characteristics of associated dispersion.

Recent studies that describe efforts to make modelling and application of model results more user-friendly, demonstrate a maturity in the field of modelling of disposal mechanics (Aarninkhof & Luijendik, 2010; Howlett et al., 2000). They indicate that in general, the processes are well understood and simulated results can give users reliable estimates. Models of disposal mechanics are now at a stage where results can be applied in field cases, such as to answer the question of optimal disposal location in order to minimise adverse impacts through scenario simulations.

Today, through the understanding developed from early *in situ* assessments and models, the dispersion potential of a site can be inferred from numerical predictions based on hydrodynamic observations, which can be measured at a site at any time. This combination incorporates approaches two and three and makes it possible to determine if material disposed at a site would disperse beyond its boundaries without the need to physically dispose material there. Marine disposal sites currently used in the US are established and operated based on this combination of approaches and also complemented by approach four: pre- and post-disposal benthic measurements (EPA/USACE, 2008; Germano and

Associates Inc., 2010; Weston Solutions Inc., 2010). These comparative measurements allow for identification of the signature of deposited dredged material, which can, subsequently, be used to verify the predictions made using the hydrodynamic observations and numerical simulations.

Previous studies employing, primarily, approach 4 have evaluated findings related to the long-term fate of disposed dredged material by assessing mound migration and consolidation, re-entrainment, and redistribution using a variety of monitoring methods. Volumetric observations from Multibeam echosounder (MBES) bathymetric data is a relatively simple method that is commonly used (Li et al., 2009; Preston et al., 2003; Wienberg et al., 2004). Another form of data available from MBES systems is backscatter, which can give information on seabed characteristics and is being increasingly favoured over, or at least used in conjunction with, the more traditional technique of side-scan sonar (Preston et al., 2003; Wienberg & Bartholomä, 2005). This type of data is especially useful in monitoring disposal areas when the disposed material has characteristics distinct from the surrounding seabed, and can provide information at a very high resolution. Seabed classification techniques such as these, however, are usually accompanied by sediment grab sampling and photography as a means of ground-truthing the acoustically acquired datasets.

In the US, the combination of approaches 2, 3, and 4 is the accepted strategy for establishment and monitoring of marine disposal sites. Most likely, the conspicuous absence of approach 1, the physical measurement of the disposal plume, is due to the associated difficulties, such as the short duration and transient nature of the plume, timing of monitoring surveys with disposal events, and availability of instrumentation for sufficient resolution. Furthermore, it seems that in the US case, the preference to avoid introducing sediment at the site before knowing whether the site is dispersive or retentive is more important than directly measuring the plume for an accurate understanding of the dispersive characteristics of the site.

However, in the context of other areas of research, the need to understand and observe sediment plume dynamics has continued. To deal with the above mentioned difficulties of measuring sediment plumes, employment of acoustic

technology has become more and more widespread especially in research areas, such as bottom boundary layer measurements (Lynch et al., 1997), estuarine suspended sediment dynamics (Dinehart & Burau, 2005; Shi et al., 1997), turbidity currents (Traykovski et al., 2000), and dredging-related plumes (Hitchcock & Bell, 2004; Reine et al., 2002).

Use of acoustic technology can provide turbidity information based on the acoustic signature of the denser plume-affected water on a greater spatial and temporal scale than that obtained from point-based optical sensors and water samples. This technology has also been applied, to a limited extent, in the study of plumes arising from the disposal of dredged material. Early applications used acoustic sounders that provided imagery of the sediment plume and that allowed mainly for qualitative assessments (e.g., Bokuniewicz et al. (1978); Drapeau et al. (1992); Joyce (1979); and Wolanski et al. (1992)). Later, opportunistic use of the backscatter intensity information stored in Acoustic Doppler Current Profiler (ADCP) records allowed for quantitative measurement and examination of the spatial and temporal evolution of plumes associated with the disposal process (e.g., Siegel et al. (2009); Tsai et al. (1992); and Tsai et al. (1995)). Calibration of the backscatter intensity data to SSC values in mg/l, the traditional measure of SSC, is difficult, however, as it requires collection of SSC at high spatial and temporal resolution. The studies cited above, reported findings in the original units of decibels (dB), the logarithm of the acoustic intensity, and still managed to show meaningful results on the evolution of the plume.

The effort to align ADCP backscatter data showing relative turbidity patterns to the more meaningful measure of mg/l is great, however, as evidenced by numerous studies on the topic (e.g., Gartner (2004); Hill (2003); Hoitink and Hoekstra (2005); Holdaway et al. (1999); Schettini et al. (2010); and Tubman et al. (1994)). Though, few such studies are available that focus specifically on plumes arising from disposal of dredged material (Wu et al., 2003; Wu et al., 2006).

In circumstances where there is a need to employ approach 1 and physically monitor the plume arising from disposal of dredged material to assess dispersion, the use of acoustic technology offers the highest resolution of the plume dynamics

while requiring the least logistical effort. Furthermore, such high resolution data could provide new insights into the currently understood dynamics of the disposal process.

1.1.3 Moving Offshore

An emerging trend of increased offshore marine industry can be illustrated by examples of evaluations of wind energy (Dvorak et al., 2010), aquaculture (Troell et al., 2009), mining (Lambert, 2001), and oil industry (Freudenburg & Gramling, 1994) in this zone. Aside from other reasons, NIMBY[1] concerns are a likely motivator for this shift (e.g., Giddings (2011)). Similar motivations have led to the identification of offshore areas as potential suitable areas for disposal site establishment (Chin & Ota, 2001; Disposal Options Advisory Group, 1994).

Use of offshore areas for industrial activities, while seemingly advantageous in some respects, leads to a range of feasibility issues mainly related to the increased water depth and exposure to more extreme meteorological conditions. These issues arise not just in association with the activity itself, but more importantly in association with the methods that are typically used to assess the site suitability for the desired activity.

Traditional methods for site assessment in near shore areas are not always appropriate for offshore areas. In the case of determining site suitability for disposal of dredged material, it is sometimes necessary, for example, to make observations of suspended sediment concentration at the surface, as well as near the seabed, and along the length of the water column in between. When the water depth is 20 m, point observations (e.g., water samples or turbidity measurements) every 5 m water depth starting at the surface and ending at the bed would sufficiently represent the vertical profile. For such a profile then, 4 sampling locations would be required; however, if that sampling scheme were applied to an offshore site with water depths in excess of 100 m, 20 or more sampling locations

[1] NIMBY (Not In My Backyard) describes the situation where residents oppose development based on geographic proximity, rather than being fundamentally opposed to the effects that may arise (Delogu, 1990). Increased industrialisation of the ocean environment will be opposed by local residents with effects on visual amenities serving as the commonly cited effects. The very same residents, however, may believe that the project proposed is suitable, as long as it is located somewhere else.

would be needed to accurately describe the SSC profile. Deployment, operation, and retrieval of such a set-up is both cost and practically prohibitive. Furthermore, it will be shown that, due to the transient nature of disposal plumes, far more than one profile is necessary to accurately track its movements.

Tracking of a disposal plume may not always be required for determining site suitability (e.g., US site assessment strategy). However, in states that do not have an extensive history of disposal and no accepted strategy for assessment, such as some island nations, it can be useful to undertake observations of the plume. In this scenario, it is therefore clear that water depth is a limiting factor for the employed assessment methods. In deep water conditions, a safer and more effective strategy is through the use of remote sensing techniques (e.g., acoustic technology) that bypass the physical limitations of direct measurements over a substantial horizontal and vertical space.

1.2 Narrowing the Focus: The East Auckland Case

Auckland, one of New Zealand's major cities, is home to one of the oldest and busiest ports in the nation, the Ports of Auckland (Figure 1.1). Most of the port's development was undertaken in the late 1800s. At the time, the port was visited by relatively few vessels, but it was expanded in response to the increase in New Zealand's population and the proportional growth in the amount of imported and exported goods transiting the surrounding oceans.

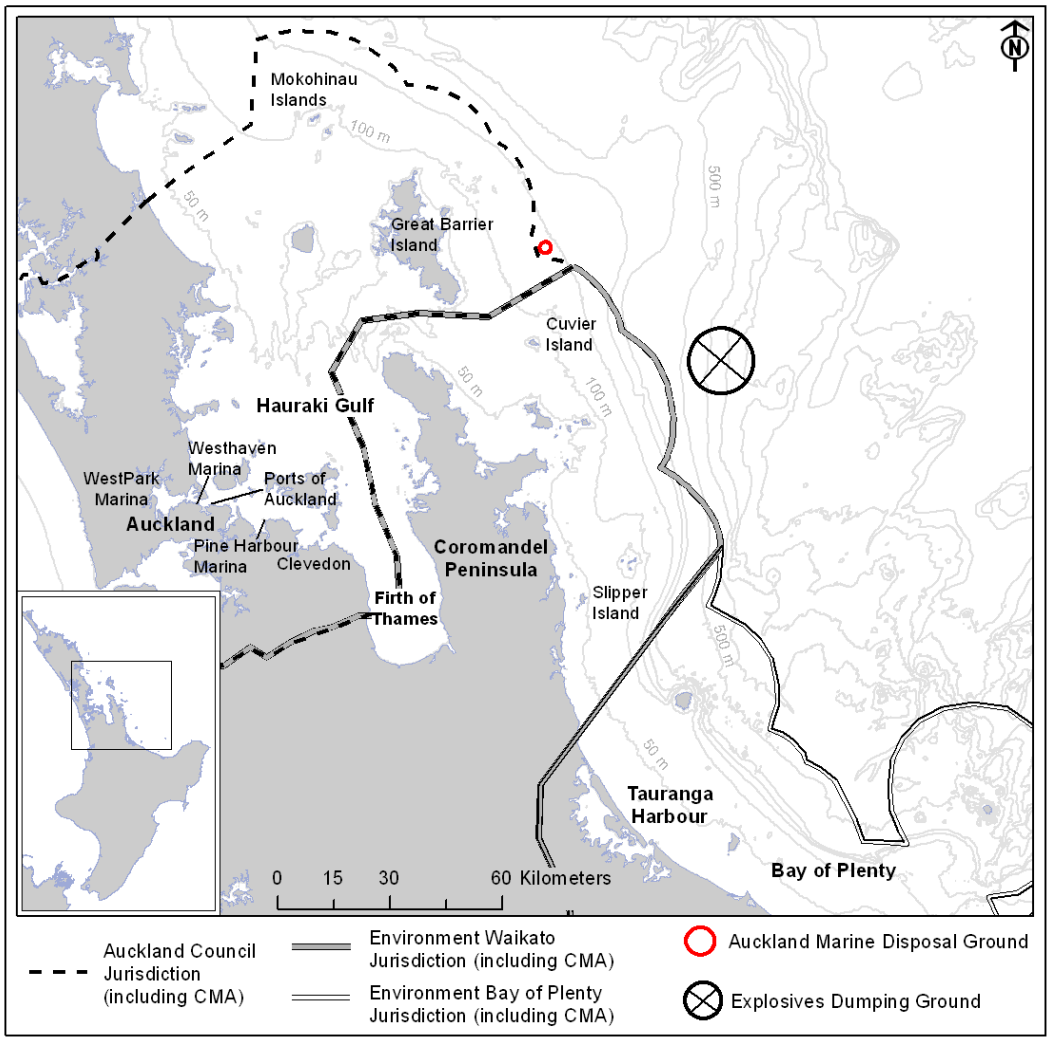

Figure 1.1 East Auckland region of the North Island of New Zealand including locations discussed in the text.

Today, the Ports of Auckland are a hub for international and domestic freight shipping services, as well as the cruise liner market, handling 37 % of New Zealand's annual trade by value, and each year accommodating 70 or so cruise liners, which result in an average economic benefit for each visit of $1.1 million.

New Zealanders are a sea-going people and Aucklanders are no exception to that, as nostalgically portrayed by Peart (2007). With more than 150,000 registered vessels in the Auckland area alone (Auckland Council, 2010), recreational boating is a much loved cultural past-time for many (Johnson, 1987; Ministry for Culture and Heritage, 2009). Several marinas, both private and government owned, in the Auckland area serve to accommodate a number of the area's recreational and commercial vessels.

1.2.1 Infilling of Auckland Coastal Areas

Common to both the ports and the marinas of Auckland is the problem of siltation of berths and channels. This type of bathymetry change is commonly characterised by a tendency for a natural adjustment back to an equilibrium state or depth following over-deepening by dredging especially in coastal areas where there is an excess of available sediment (Hume, 1983).

In the Auckland watersheds, relatively steep topography and high annual rainfall combined with erosion inducing land-use practices, such as farming and large earth works projects, lead to a significant amount run-off and thus siltation in near shore areas (Healy, 2002). This is particularly true on the eastern coast of Auckland where coastal areas lie within the sheltered area of the Hauraki Gulf (Figure 1.1), where open coast energy is dissipated by a bounding peninsula (the Coromandel Peninsula) and barrier islands (Great Barrier Island and others), which results in higher rates of deposition (Healy, 2002).

Maintaining a safe navigable depth is crucial and thus leads to the need for *maintenance dredging*; removal of in-filled material to restore the originally dredged depth (Yell & Riddell, 1995).

New Zealanders' attraction to the coast for its aesthetic, commercial, and cultural value will likely lead to more and more new coastal development, and thus also the need for *capital works dredging*; the dredging of previously undisturbed coastal areas for the purposes of expansion of already existing engineered coastal spaces or the development of new ones.

1.2.2 The Ongoing Need for Dredging

Although the frequency and intensity of dredging operations in Auckland has decreased since the 19th and 20th Centuries (Johnson, 1987), there are plenty of examples of ongoing maintenance and planned capital works dredging activities. For example, in 2009, consent was granted to Ports of Auckland for berth deepening at one of their container terminals to accommodate the next generation of container ships carrying 5,000 to 7,000 TEU (twenty foot equivalent unit, a standard industry measure of container volumes), which follows the channel deepening for similar purposes in 2007 (Ports of Auckland Ltd., 2009). Recently, several berths at Westhaven Marina (Figure 1.1) in downtown Auckland were enlarged to accommodate 90 m super-yachts in anticipation of the influx of visitors due to the Rugby World Cup 2011 (New Zealand Press Association, 2010). Other marinas in the Auckland area, such as Westpark and Pine Harbour (Figure 1.1), experience active infilling and require regular maintenance dredging to remain navigable. Another trend contributing to the need for maintenance and capital works dredging is the development of canal estates, which incorporate residential communities and berthing sites for the wealthy recreational boaters (Peart, 2006). One such development in Clevedon, part of rural south Auckland (Figure 1.1), has been under consideration on and off since the 1980s (Crossley, 2010).

1.2.3 Disposal of Dredged Material: A Contentious History

Despite the obvious need for dredging, since the late 1980s the topic has been accompanied by controversy over the disposal of the dredged material. The adoption of the Resource Management Act 1991 and the London Dumping Convention 1972 (International Maritime Organisation, 2003), and the establishment of a large marine park in the Auckland Territorial Seas (hereafter referred to as a Coastal Marine Area (CMA) (Figure 1.1)) in 2000 added to the complexity of identifying a long-term solution for the disposal of material dredged from east Auckland-area ports and marinas. Flaim et al. (2010) reviewed the difficulties that port and marina operators experienced in establishing and maintaining operating open sea disposal sites in the east Auckland area over the last 30 years. It was suggested that the combination of a general increase in

concern for the environment, 'NIMBY' perspectives, and a legislative body seemingly reluctant to defy a few passionate, public activists also contributed to the gridlock.

Following submission of a consent application to dispose dredged material by Ports of Auckland in the early 1990s, a Disposal Action Advisory Group (DOAG) was formed to examine the options available for disposal of dredged material from the Port of Auckland, including both maintenance activities, as well as capital works (Disposal Options Advisory Group, 1994). Their findings and recommendations were presented in a series of reports that addressed harbour edge, land, and marine disposal possibilities (Disposal Options Advisory Group, 1994). The disposal option recommendations resulting from the DOAG examinations are summarised below.

For highly contaminated dredged material:

- port reclamation, and
- approved sanitary landfill.

For maintenance dredging that meet regulatory guidelines (i.e., only slightly contaminated):

- port reclamation, and
- marine disposal in water deeper than 100 m.

For capital works dredging (assumed to be uncontaminated):

- port reclamation
- marine disposal in water deeper than 100 m.

In general, under New Zealand disposal guidelines, material disposed at sea should deposited within the site boundaries and not be subject to re-suspension and dispersion beyond the boundaries of the site. This guideline allows for future monitoring of disposed materials and for more accurate assessment of potential environmental impacts, and is in line with the London Dumping Convention

(1972) to which New Zealand is a party (International Maritime Organisation, 2003). The DOAG determined that, near Auckland, coastal areas at water depths deeper than 100 m were not likely to be influenced by a high energy hydrodynamic environment that would re-disperse the disposed material. Another potential benefit to preventing the establishment of sites in water depths less than 100 m is that the 100 m depth contour in the Auckland region occurs outside the boundaries of the Hauraki Gulf (Figure 1.1), which is well-known for its cultural, commercial, aesthetic, and recreational assets[2]. At the time, and no doubt still today, for many reasons (some proven and some seemingly emotional) there was a strong perception that disposal operations tainted the Gulf environment. Establishment of future disposal sites outside the Hauraki Gulf provided the best compromise for all interested parties.

Following the reporting of the DOAG conclusions, New Zealand's Maritime Safety Authority, now Maritime New Zealand (MNZ), intervened and began to award consents for disposal of dredged material originating from the east Auckland coastal areas at the Explosives Dumping Ground (EDG) located in the Exclusive Economic Zone (EEZ) (Figure 1.1). Being located in the EEZ, the EDG is under the jurisdiction of MNZ rather than the regional authority, Auckland Council, which regulates Auckland coastal areas to the 12 nm limit only. The EDG was established primarily for the Royal New Zealand Navy to permanently dispose of abandoned World War II munitions at water depths that are inaccessible to the public. These munitions have been found in shallow coastal zones, well within reach of recreational divers and, therefore, represent a public threat that requires mitigation. The site has never been surveyed or monitored exclusively for dredged material disposal because the extreme water depth and danger in sampling in the vicinity of the munitions make such activities virtually impossible. Therefore, the impacts from years of disposal operations at the EDG

[2] The general admiration for the Hauraki Gulf for all its values culminated in the establishment of the Hauraki Gulf Marine Park in 2000 and the enactment of the Hauraki Gulf Marine Park Act 2000 (New Zealand Government, 2000). The Act was not designed to add another layer of bureaucracy, but rather to integrate the management of the Gulf (including its islands and catchments), establish the Park, establish management objectives, recognise the relationship of *tangata whenua* (Maori term for the indigenous peoples of New Zealand) with the Gulf and its islands, and establish a forum. As such, the Act holds few teeth, in the legislative sense, but has possibly provided an added incentive and/or reason for not awarding new consents for disposal of dredged material within the east Auckland CMA [NB: the latter statement is a personal opinion of the author, however it is one also held by others (*pers. comm*., T. Ross-Watt)].

and effects on the surrounding areas are unknown. When the site was first used for dredged material disposal (mid-1990s), long-term consents were granted with little regulation as to the quantity of material being placed there. Under recent management regimes, however, dredged material disposal is capped at 50,000 m^3 per annum, a portion of which is allocated to each applicant to alleviate some of the need, but applications routinely exceed the total allocations (*pers. comm.*, T. Ross-Watt). The EDG is generally considered a temporary solution (*pers. comm.*, T. Ross-Watt). In order to acquiesce with the London Dumping Convention, it was always the intention to establish a new site that was more easily monitored, but still in line with the recommendations of the DOAG.

1.2.4 Establishment of the New Auckland Marine Disposal Ground

In 2007, a new marine disposal site was proposed on the continental shelf 25 km east of Great Barrier Island in the EEZ (Figure 1.1). Details on the site selection process are reviewed in Flaim et al. (2010). In December 2009, following an in depth desktop study, a preliminary field survey, and consultations with likely stakeholders, the findings of which are reported in Flaim et al. (2010), MNZ awarded short-term consent for disposal of 5,000 m^3 of material dredged from Pine Harbour Marina (Figure 1.1) at the proposed site. As part of the consent requirements, MNZ required that disposals be monitored to assess the dispersion potential at the site during a range of weather and sea state conditions (those which could be feasibly monitored). The aim in allowing the short-term consent to pass was to confirm whether the disposed material would remain within the boundaries of the site. To determine the long-term suitability of the site for on-going use by Auckland area ports and marinas, MNZ planned to base their decisions largely on the findings of the dispersion surveys.

To date, no studies, other than those associated with this project, have been undertaken at the new Auckland Marine Disposal Ground (AMDG) for the purpose of assessing its long-term suitability for disposal of dredged material, or for any other purposes. Long-term suitability is typically based on several factors, many of which can be addressed prior to disposal operations. Dispersion potential is more difficult to quantify both in theory and in practice. This thesis includes

and expands on the findings of the commissioned dispersion surveys with the intention of addressing the dispersion issue from several different angles. The outcome of this research will be of value to MNZ and possible future users of the new disposal ground.

1.3 Aims and Objectives

The overall aim of this research is to evaluate the dispersion potential at the AMDG and determine whether the site is retentive or dispersive. Knowledge of these characteristics is critical for determining the long-term suitability of the site for on-going use because potential adverse impacts from disposal operations may be either contained within the boundary of the site in the case of the former, or, in the case of the latter, they may occur at unknown locations where the effects cannot be monitored.

This aim is to be met by achieving the following objectives:

1. resolve the forcing mechanisms and influences driving the hydrodynamics on the continental shelf in the region of the new disposal ground;

2. determine the site-specific processes involved in the disposal of dredged material;

3. assess the potential for loss of disposed sediment from the disposal site; and

4. recommend operational restrictions on disposal methodology to minimise dispersal during disposal.

To meet the above objectives, a data collection and modelling program was undertaken to provide information focused on:

- the water column structure and currents at the disposal grounds;

- the benthic environment at the disposal ground;

- sediment pathways and plume behaviour in the vicinity of the disposal ground; and

- conditions leading to optimal site operation.

1.4 Benefits and Innovations of this Research

In answering the above practical questions, more general conclusions will come to light that can be translated to many other situations around the world. Namely, the need to move disposal offshore to satisfy concerned stakeholders is a universal trend with more and more development in near shore areas. The experience reported here can therefore be used to streamline similar processes in countries around the world.

Primarily, general conclusions about monitoring and investigating deep water sites to satisfy aims to move offshore can be put into a global context as, presumably, this is a trend that will persist in the future. Furthermore, this work draws general conclusions on the applicability of current knowledge of the disposal process and how it may vary in relation to the use of deeper and deeper sites.

From a scientific point of view, this research is relatively uncommon in that data has been collected at all stages of the disposal process. The applied nature of dredged material disposal related research often means that there is only the opportunity for predictive measures, such as numerical simulations and some 'post-disposal' ground-truthing. This research will bring a unique perspective to a topic that has deep roots in the history of coastal engineering.

At present, there are at least a dozen, if not more, commercial enterprises along the east Auckland coastal sector that may at present, or at some point in the future, be in need of a disposal option for dredged sediment. In a worst case scenario, sedimentation can threaten the commercial viability of these businesses; as if it is not removed it can prevent safe passage of vessels, which are the life blood of any establishment serving as a maritime link. MNZ has taken the lead in finding a suitable disposal option for the interested parties, first by allowing temporary use of the EDG and then by awarding short-term consent to dispose dredging at the AMDG to assess the suitability for ongoing use. The findings of this research will weigh heavily on the decision-making process for awarding long-term consent for

disposal at the site which would solve a decades-long problem in the east Auckland coastal area.

Finally, the northeast coast of New Zealand has been studied rather extensively, but as intimated previously, the focus has been on the coastal areas within the Hauraki Gulf. Shelf areas are relatively unknown especially at the scale that the present research has addressed.

This research, therefore, has two main implications: 1) on a national scale, knowledge gaps on the northeast coast shelf environment will be further filled, and 2) the possibility of establishing disposal grounds in shelf areas will be highlighted. On a global scale, such conclusions may provide an alternative for other countries under-going similar problems now or in the future.

1.5 Thesis Structure

1.5.1 Chapter 2 – General Background

Chapter 2 includes a summary of the generally accepted theories behind the processes of open-water disposal of dredged material. Specific aspects influencing this process will also be reviewed. Also included in this chapter is a description of the physical setting of the northeast coast shelf region, the location of the AMDG, based on previous studies undertaken in the area. Focus will be given to what is known about the hydrodynamic regime and the benthic environment, as these are aspects that affect or are affected by disposal operations at the AMDG.

1.5.2 Chapter 3 – Hydrodynamic Observations

The potential for dispersion at a dredged material disposal site is largely dependent on the hydrodynamic setting. Hydrodynamic drivers such as tides, geostrophic flows, and wind ultimately determine the type, direction, and magnitude of sediment transport. With no previous hydrodynamic or hydrologic observations recorded at the AMDG, and only a few related studies in nearby areas, this chapter will attempt to characterise the major water column drivers and the resultant flows to better understand the potential for dispersion at the site.

1.5.3 Chapter 4 – The Disposal Process and Dispersion Pathways

A pilot study, consented by MNZ, was undertaken to physically measure the dispersion due to disposal of dredged material at the study site. In this chapter, other factors influencing dispersion potential at the site, such as nature of the material to be disposed, dredging technique, and disposal procedure, will be reviewed with a focus on the specific scenario in which the pilot study was carried out. The results of surveys undertaken over a range of weather and sea conditions are presented to substantiate conclusions about dispersion pathways, dispersion magnitude, and the overall disposal efficiency of the AMDG. Complementary post-disposal monitoring data will also be presented to support the findings of the dispersion surveys.

1.5.4 Chapter 5 – Hydrodynamic and Mud Transport Models

Chapter 5 describes the process for developing *i*) a regional scale 2-dimensional hydrodynamic model and *ii*) a local scale 3-dimensional hydrodynamic and mud transport model for simulation of the disposal events monitored during the pilot study (Chapter 4). The capability of the model for simulation of the disposal process is discussed including recommendations for improvements. Following model development, idealised scenarios are simulated to gain a better understanding of dispersion processes under conditions that were not monitored previously in the field. From the results, recommendations are made optimal environmental conditions for minimising the dispersion of disposed material.

1.5.5 Chapter 6 – Summary and Conclusions

Chapter 6 summarises the findings of this thesis. The dispersion potential of the AMDG is described with reference to the conclusions made in the previous chapters and classification (retentive or dispersive) for the purposes of ongoing use is assigned. Implications and considerations for ongoing use of the AMDG for disposal of dredged material are detailed. The innovations and advancements of the work presented in each of the three main Chapters are summarised and suggestions are made on areas of further study that would benefit this research.

CHAPTER 2
THEORETICAL REVIEW AND SITE SETTING: A GENERAL BACKGROUND

2.1 Introduction

Assessment of the Auckland Marine Disposal Ground (AMDG), in terms of the potential for dispersion of the dredged material disposed there, first requires an understanding of the processes that may be of influence. The aim of this chapter, therefore, is to provide an overview from the international and national literature on the state of the art research and the current understanding of the processes involved in the open-water disposal of dredged material, as well as of the setting of the northeast coast of New Zealand, where the AMDG is situated. The reviews provided will focus mainly on research that is directly relevant to the specific case of disposal at the AMDG to provide the appropriate background for topics discussed in the following chapters. The specific aspects that are pertinent to this research are:

- **Section 2.2.1 - the processes understood to be involved in disposal at open-water disposal sites, with specific focus on deep water sites:**

  A review of the state-of-the-art understanding of the disposal process puts into context much of the theory applied in Chapter 4 of this thesis and provides the basis for findings that improve the current understanding;

- **Sections 2.2.2-2.2.3 - the potential environmental impacts involved in open water disposal of dredged material, with a focus on dispersion as a delivery mechanism for impacts and the influencing factors:**

  While not directly related to the research presented in this study, a review of the environmental impacts associated with marine disposal of dredged material highlights the importance of the research and, as such, also the motivation of the research. The topic of potential impacts is particularly important as they arise as a direct result of the main focus of the study: sediment dispersion; and

- **Section 2.3 - previous studies that provide insight into the physical setting of the AMDG:**

  A review of the current knowledge of the physical setting of the AMDG functions in several ways: 1) previous knowledge led to the choice of the AMDG as a potential site, 2) many aspects previously discovered were referred to explicitly within the main data chapters of this thesis and, thus, require explanations, and 3) the review highlights the lack of specific knowledge about the AMDG, and, therefore, makes more poignant the new contributions described herein.

With respect to the research undertaken and described in Chapters 3-5, the reviews provided in this chapter, in a general sense, serve to narrow the focus and to help identify those attributes that are significant and require further examination.

2.2 The Disposal Process

Disposal of dredged material at open-water disposal sites has been studied extensively over the last decades starting approximately in the 1970s. This field of study began in response to a growing public consciousness of environmental issues, and the need to understand the disposal processes better so that impacts could be minimised (Herbich, 1981; Tay et al., 2008). The bulk of the basic theoretical knowledge has been described in technical reports produced as part of the Dredged Material Research Program (DMRP) (e.g., Bokuniewicz et al. (1978); Holliday (1978); and Nichols et al. (1978)) and more recently, the Dredging Operations Environmental Research Program (DOER) (e.g., Puckett (1998) and Swanson et al. (2000)) associated with the U.S. Army Corps of Engineers (USACE). In recent years, dredging and disposal programs have tended to focus more on the management and monitoring of disposal sites (e.g., Canada's Disposal at Sea Program within Environment Canada and the European Dredging Association (EUDA)).

Relatively few studies have been published in international peer-reviewed journals, but due to its applied nature, the topic has been popular in the field of

coastal engineering, and has been covered more extensively in the form of conference proceedings.

2.2.1 A Conceptual Review

During the dredging process, material extracted from the seabed by any number of methods (refer to Yell and Riddell (1995) for descriptions) and destined for open-water disposal, is often placed onto a holding barge called a 'hopper'. After the hopper is filled, it is either driven or towed to the disposal site where the hull of the hopper can be split open (a split-hull hopper), or two large doors on the bottom of the hopper can be opened and the dredged material will insert into the water column to commence descent. Alternative methods for emptying the hopper do exist (e.g., pipeline disposal, McAnally and Adamec (1987) and Neal et al. (1978)), but those will not be discussed here because they were not used in the operations at the AMDG.

There have been no major advances in the understanding of the key processes involved in the disposal of dredged material since the early work published in the 1970s (e.g., Bokuniewicz et al.(1978); Koh (1971); Koh and Chang (1973)). Truitt (1988) reviewed the findings of field studies focusing on the disposal of dredged material through the mid-1980s, in which, like in most other descriptions, the disposal process is described as occurring in three main phases: *Convective Descent* (Phase 1), *Dynamic Collapse* (Phase 2), and *Passive Dispersion* (Phase 3) (Figure 2.1).

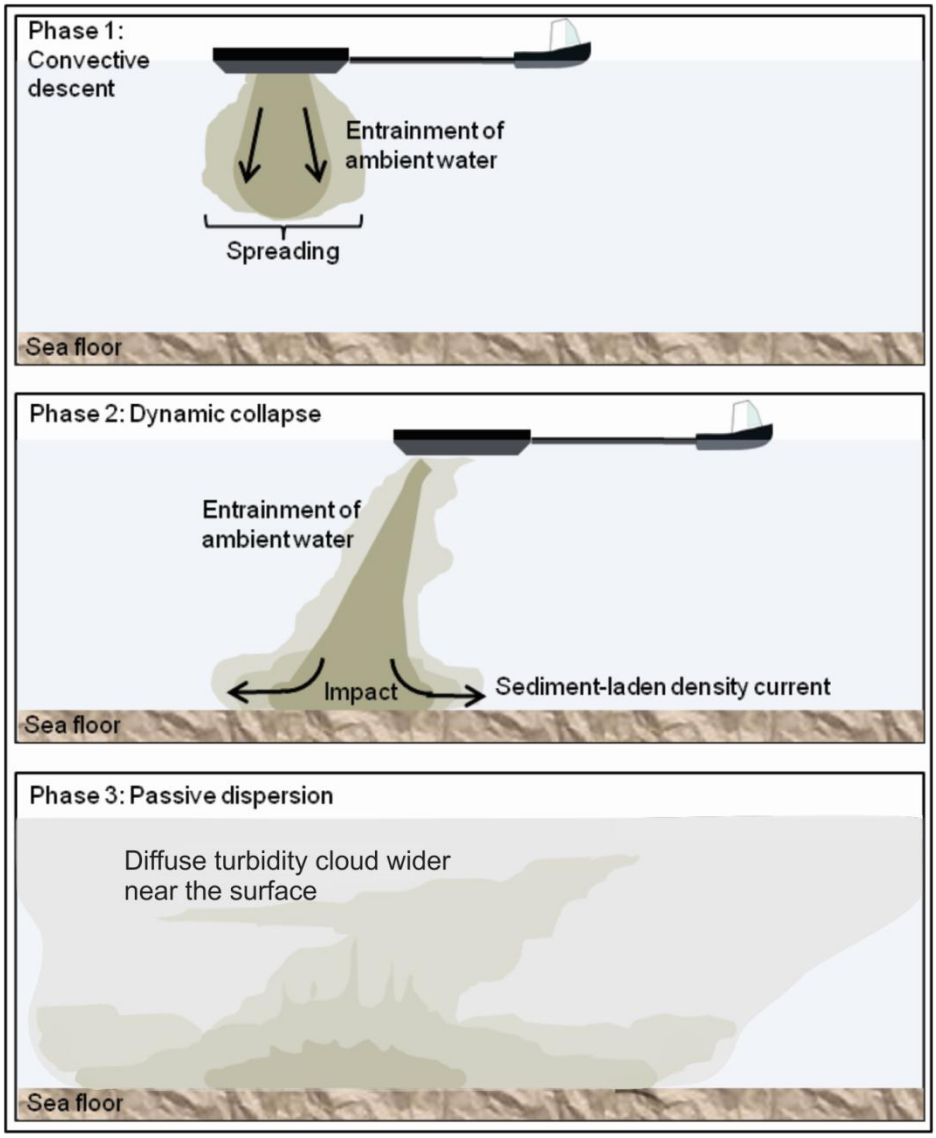

Figure 2.1 Schematic diagram of the 3 main phases that occur during the process disposal of dredged material (not drawn to scale).

During *Convective Descent*, the dredged material descends through the water column as a dense fluid-like jet. The speed of the descending jet is largely governed by its own negative buoyancy, which is a function of the grain densities, the water density, the volume disposed, and gravity (Krishnappan, 1975). Sometimes larger aggregates or 'clods' of material descend faster than the jet and may be present at the leading edge or even precede it, depending the characteristics of the dredged material. Around the perimeter of the jet, ambient water can become entrained, which can act to increase the volume significantly (up to 70 times, as reported by Truitt (1988) and based on the equations of Bokuniewicz et al. (1978)). This increase in volume, which essentially translates to horizontal sediment dispersion, has been described dimensionally by

Krishnappan (1975) to be a function of the water depth of the site, the submerged specific weight of the disposed material, the grain size diameter, and the viscosity of the water. The buoyancy of the material at the perimeter of the jet increases, usually leading to a loss of some of the disposed material in the upper water column through advection by the ambient current. The proportion lost is commonly cited as 1 – 5 % of the disposed load ((Bokuniewicz et al., 1978; Bokuniewicz & Gordon, 1980; Gordon, 1974; Truitt, 1988)).

Following *Convective Descent*, the descending material collapses, usually on impact with the seabed, but in some cases, can also collapse mid-column at a density layer having equal buoyancy to that of the descending material. This phase is called *Dynamic Collapse* and can be coupled with the generation of a density current produced by the excess energy available following collapse. Material that does not deposit immediately on impact is transported in the dense surge that propagates radially away from the point of impact. The speed of the density current is dependent on the height of the surge above the bed, which is, in turn, dependent on the radius and speed of the descending jet at the moment of impact, the densimetric Froude number, the ratio of the difference density of the surge to the ambient water density, and gravity (Drapeau et al., 1999). Surge height is usually approximated as 20 % of the water depth and the propagation distance is in the range of 100 m from the area of impact (Gordon, 1974), but there is evidence that these values are depth dependant. For example, Tsai et al. (1995) reported values of 25 % and 150 m for surge thickness proportion and distance, respectively, in 10 m of water, whereas those values in 100 m of water were 70 % and 100 m. However, the detection threshold may also be a factor in the measured thicknesses and propagation distances, which is dependent on the type of instrumentation used to measure the surge. After sufficient energy is lost, the density current slows down, at which point suspended material can either settle on the seabed or be advected with the ambient current.

The passive transport of material in suspension after surge propagation is said to be part of the third phase of the disposal process, *Passive* (or long-term) *Dispersion*. However, passive dispersion actually begins during the *Convective Descent* phase when diluted material around the perimeter of the jet is lost to the

ambient current. Passive dispersion is dominant when all the dynamic momentum of the disposed load (due to its negative buoyancy) is spent and the material is no longer moving as a result of its own force. At this point, transport is a function of the grain settling velocity and the speed of the ambient current. If the ambient current speed is greater than the critical velocity for deposition, then the grain will stay in suspension and be transported in the direction of the ambient current and, likewise, if the current speed is lower than the deposition velocity, the grain will deposit on the seabed (McCave, 1984). Passive dispersion continues until all the material settles to the seabed, which can occur over an area much greater then area covered during the first two phases depending on the local hydrodynamics.

In a broader sense, this 3-phase model for the disposal process is governed primarily by the sediment induced density difference between the mass of disposed material and that of the surrounding water. This density difference drives the initial negative buoyancy of the descending material and, thus, all the processes that occur thereafter. When the density difference is negligible (e.g., after the density surge has propagated away from the point of impact), transport of the sediments is dependent on the individual grain (or floc) density, which primarily determines the settling velocity. Therefore, the density of the two mediums (water and sediment), and the difference between them, form the basis for the current understanding of the disposal process.

2.2.2 Environmental Impacts

The general negative public perception of environmental impacts arising from disposal of dredged material at sea most likely stem from a few unfortunate incidents, where some poor choices were made, mostly owing to the fact that in the early days, impacts were still poorly understood and therefore difficult to mitigate (Fredette & French, 2004). In New Zealand, one incident occurred in the late 1980s when dredged material was disposed at what turned out to be a snapper[3] feeding and spawning ground (Grace, 1988). Not long after, controversy developed over a nearby site, where it was found that there was a significant loss of material away from the site due to dispersive processes (Parliamentary

[3] Snapper (*Pagrus auratus*) are a commercially and recreationally important fish species in New Zealand.

Commissioner for the Environment, 1995). Similar incidents may have been the impetus for the on-going resistance and difficulty related to establishment of disposal sites elsewhere in the world (e.g., the cases of disposal of dredgings from the Port of Oakland (Kagan, 1994) and the Port of Los Angeles (Anderson et al., 2002) in the United States).

With the exception of rare cases, such as those described above, the impacts perceived by the public are often exaggerations and not necessarily based the current science (Fredette & French, 2004). For example, the concentration of a sediment plume visible to the human eye at the sea surface is around 15 mg/l. While such a plume may appear alarming, in actual fact negative impacts on marine organisms are typically only sensed at much higher concentrations (e.g., in the range of 100 – 10,000 mg/l depending on the organism and the exposure time (Wilber & Clarke, 2001)).

Disposal of dredged material at open-water sites is not completely without potential for environmental impacts, however. There are two main types that can arise: i) toxic effects, due to high SSC levels, which include smothering and high concentrations of contaminants if present, and ii) chronic effects, due to the long-term persistence of SSC and contaminant levels elevated slightly above background levels.

Usually, toxic effects tend to be greatest during and immediately after disposal because SSC, and possibly also contaminant levels, tend to be high. However, as the period between disposals is longer than the time it takes for concentrations to reduce to background levels, the persistence of toxic effects tends be low. Chronic effects, on the other hand, are usually associated with resuspension of the deposited material (Eggleton & Thomas, 2004; Langtry et al., 2009; Scott & Redmond, 1989), which would be the case if the material is regularly entrained by currents and/or waves.

Within the disposal zone, it is generally accepted that impacts will be severe, mostly due to the smothering of benthic organisms (toxic effects). However, if the

'like-on-like' approach[4] is followed, recolonisation can occur rapidly, in the form of vertical, lateral, or recruitment migration, several months to a year after disposal, depending on the state of the community prior to burial (Bolam et al., 2011; Bolam et al., 2006; Fredette & French, 2004; Maurer et al., 1986). In the case of a deep-water disposal site, where the influence of waves is rarely felt and ambient near-bed currents are weak, resuspension of deposited material will be uncommon and, thus, also chronic effects. Therefore, focus tends to be given to ensuring that the impacts are minimised outside the disposal zone (Langtry et al., 2009) and to do that, it is necessary to determine and understand the dispersion characteristics of a disposal site.

2.2.3 The Role of Dredged Material

Transport of sediments associated with the disposal process depends not only on the characteristics of the water column (i.e., depth, ambient current, and density), but also the physical and bulk properties of the material being disposed. Physical properties refer to the mineralogy, texture, and sorting of the sediments, which, in part, influence the bulk properties of the sediment (e.g., porosity, shear strength, and bulk density).

The influence of physical properties on the transport of dredged material during the disposal process was demonstrated at an inner shelf disposal site (20 - 30 m water depth), near the Port of Tauranga on the northeast coast of New Zealand's North Island. Contrary to the generally accepted model for dispersion (described in Section 2.2.1), no density surge was formed after impact of the material with the bed, and very little passive dispersion was observed (Warren, 1992). These aspects were attributed primarily to the sandy, disaggregated texture of the dredged material.

[4] A disposal approach which aims to place dredged material at locations where the naturally occurring sediment is similar in texture and composition to the material being disposed, with the understanding that the disposed material will behave similarly to the site sediment. The benefit of this approach is that more accurate predictions on the fate of the disposed material can be made assuming there is a previous understanding of the sediment transport characteristics of the site. Additionally, using this approach ensures that changes to the benthic habitat due to disposal, will be minimised.

Bulk properties tend to influence dispersion during the disposal process especially in the case that some of the *in situ* structure is maintained during dredging, or re-established during consolidation within the hopper prior to disposal or at the bed following deposition. For example, sediment beds primarily composed of fine silts and clays will most likely have a higher shear strength than beds composed of sands, due to their propensity for cohesion (Mitchener & Torfs, 1996). In general, dredged material possessing high shear strength will be less susceptible to dispersion during the disposal process. Several other bulk properties can give an indication as to the susceptibility of a specific material to dispersion during the disposal process, such as water content and bulk density; however shear strength in particular may be the most effective measure as it not only indicates the degree that *in situ* structure will be maintained, but also as it is feasible to measure *in situ* with a hand-held field shear vane.

The likelihood that the *in situ* structure will be maintained is linked to method used for dredging. Bulk properties of removed sediments can be altered from the *in situ* state as a result of the mechanical or hydraulic reworking by the dredger and the subsequent increase in water content. For example, bucket dredging minimises reworking and water content increases because some of the *in situ* structure of the sediment is preserved, whereas cutterhead suction dredging typically results in a dredged slurry with 10 - 20 % solids by dry weight (McAnally & Adamec, 1987; USACE, 1983).

Dredged material that is highly reworked and possessing a high water-content will be more susceptible to entrainment and dispersion during the disposal process. As such, the disposed material will be less likely to descend dynamically as negatively buoyant aggregates and more as individual particles suspended in a slurry with a buoyancy closer to that of the ambient water. These principles were proven by Bokuniewicz and Gordon (1980) in a study of the deposition characteristics of dredged material. Once the dredged material is loaded into the hopper, it is possible that it can undergo re-consolidation if sufficient time passes under the right conditions before transport and disposal.

2.3 Setting of the Northeast Shelf of New Zealand and the AMDG

The physical environment and underlying hydrodynamics play an important role in the dispersive characteristics of an open-water disposal site. As was previously mentioned, sites proposed for disposal operations need to be classified as either retentive or dispersive (McAnally & Adamec, 1987). Such characteristics are determined primarily by the local oceanography (e.g., tides, currents, and waves), which is, in part, influenced by the physiography of the region. Aspects, such as the naturally occurring seabed sediments, can give an indication of the classification type. The following sections, therefore, review the current knowledge relating to the physiography, seabed characteristics, and oceanography of the northeast coast region, where the AMDG is located.

2.3.1 Physiography and Sediments

Physiography

The islands of New Zealand comprise an emergent portion of continental crust along the boundary of two major plates in the southern ocean (de Lange et al., 2003; Sharples, 1998). The southern half of the North Island and the South Island are mostly aligned with the plate boundary, whereas the northern half of the North Island deviates from it, such that the northeast coast of the North Island is situated at an angle of about 60° from the axis of the rest of the land mass. This positioning has particular implications for wind exposure and boundary current flows at the coastlines along the upper half of the North Island. These implications will be described in following sections.

New Zealand's continental shelf is large in surface area (300,000 km^2) and variable in width (Sharples, 1998). The shelf along the northeast coast is no exception, ranging from just 11 km to 100 km (Harris, 1985). Along the northernmost sector of the northeast coast, the shelf slopes at a mostly gentle angle that decreases from NW to SE along the coast and tends to increase in width in the same direction (Rogers, 2012). Proceeding southeast along the coastline, the shelf continues to increase in width and decrease in slope to a pivot point

approximately aligned with Great Barrier Island (see depth contours in Figure 1.1), after which shelf widths begin to decrease again. There, the shelf is at its widest point, appearing as a lobe protruding out from the shelf areas to the north and south. From the 50 m isobath to the shelf edge (~200 m), the average slope gradient is about 0.004. The AMDG, situated about 25 km east of Great Barrier, is located midway across this wide shelf platform.

In the area of the AMDG, the slope gradient is 0.01, with water depths that range from 130 m to 160 m, increasing from southwest to northeast (Flaim and de Lange (2011); Appendix III). MBES data and underwater video recorded at the AMDG indicate a generally flat seabed with little to no distinguishable morphologic features (Flaim & de Lange, 2011; Flaim & Healy, 2008).

Sediments

As a part of the OS 20/20 Bay of Islands Coastal Survey Project undertaken from 2008-2010, a large number of sediment samples were collected at water depths ranging from the nearshore to those at the shelf edge along the east Northland coastline of New Zealand (Bowden et al., 2010). Samples comprising the 'Southern Sector' of the survey, were located in the vicinity of transect H shown in Figure 2.2, located slightly north of Whangarei Harbour (for reference, Whangarei Harbour is located at the northwest corner of Figure 1.1). Results of sediment analyses of the samples collected near this transect, as reported by Rogers (2012), are summarised here because they are likely to be similar to nearby areas to the south, where the AMDG is located.

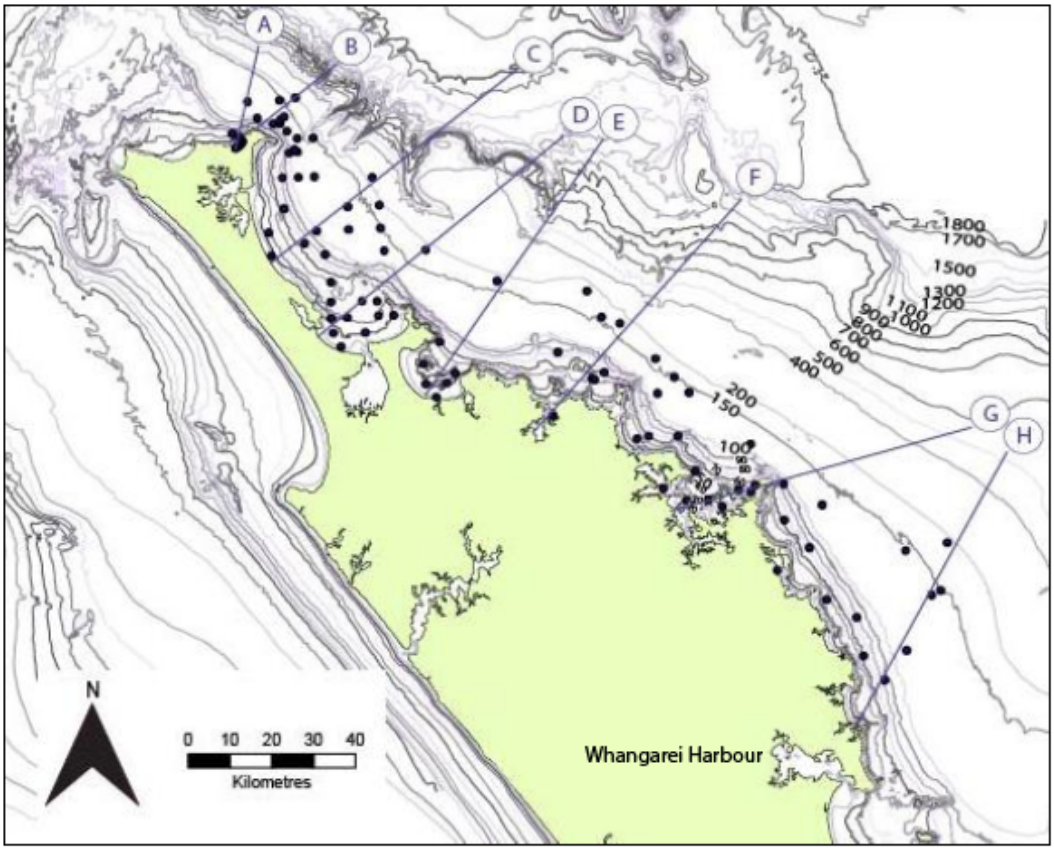

Figure 2.2 Survey transects and sample locations of the OS 20/20 Bay of Islands Coastal Survey Project conducted from 2008-2010 on the eastern coastline of Northland, New Zealand. Transect H corresponds to the 'Southern Sector', and is the nearest to the shelf region to the south that is the focus of this thesis (adapted from Rogers (2012)).

Grain size and textural analysis showed that in the southern sector of the survey area, sediment could be classified mainly as muddy sand (mS) and gravelly muddy sand (gmS), with a small component of sandy mud (sM), based on the Folk classification method. The mud component was determined to be dominated by medium to coarse silts, with very little contribution from clay sized material. The sandy component was dominated by very fine to fine grained material, with a small contribution of coarse sized fractions. Gravel was not a common textural class found in the southern sector of the survey area. Overall, sediments in the southern region were well- to very well-sorted.

Mineralogy analyses showed that southern sector shelf sediments tended to be low in quartz, feldspar, heavy minerals, and volcanic rock fragments, but high in sedimentary rock fragments and calciclastic (skeletal) grains. Calciclastic grains were dominated by bivalves as well as planktic benthic foraminifera skeletal types, which contributed predominantly to the gravel and sand fractions, respectively. High calcite content that tended to increase with depth, characterised

the sediments in this sector due to the predominance of skeletal grains. Skeletal grains were not well preserved, which, along with grain size sorting patterns, suggests that sediment in this region is relict and may have been exposed to high energy environments during the peak of the last glaciation.

Another survey undertaken in 2002, as a part of a proposal to establish a marine reserve on the east coast of Great Barrier Island, contributed to the basic knowledge of the northeastern shelf habitats (Sivaguru & Grace, 2002) (see Figure 2.3 for the location of the proposed reserve, the area where samples were collected). Samples were collected mainly at water depths greater than 80 m, up to 120 m, and thus are most likely also indicative of seabed characteristics slightly to the southeast at the location of the AMDG.

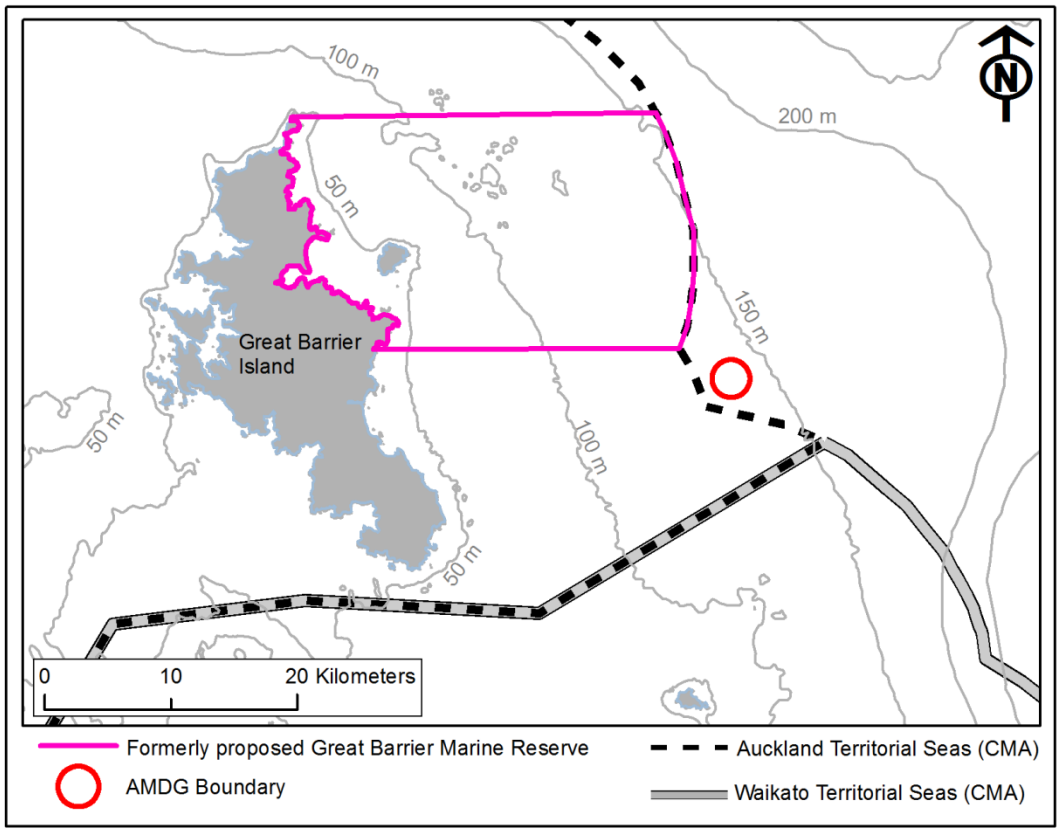

Figure 2.3 Location of the former proposed Great Barrier Marine Reserve.

Focus was given mainly to the benthic faunal species collected in the sediment samples, although descriptions of the general characterisitcs of each sample site were included based on under water video footage and observations of sediments prior to sieving for benthic species. The deepest site (120 m) was described as having scattered silt-covered boulders on a muddy sediment bottom (Sivaguru &

Grace, 2002). These observations correspond with the findings of Rogers (2012) that the shelf sediments east of Whangarei Harbour are predominately muddy sands, with silt comprising the main mud component. This indicates a low-energy environment, where currents and waves are not strong enough to suspend material from the surface of the boulders.

Naturally occurring sediment characteristics at the AMDG were reported by Flaim and de Lange (2011) in accordance with requirements by Maritime New Zealand (MNZ) to investigate the effects of disposal of dredged material there in April 2010. For details of sediment characteristics beyond that which is described below, please refer to Flaim and de Lange (2011), included in Appendix III.

It was found that sediments at the AMDG were composed of approximately 55 % fractions less than 63 µm (silts and clay), where silt sized grains were dominant. Very fine and fine sands comprised approximately 30 % of the overall distribution. The percentage of sand decreased with increasing grain size. A preliminary assessment of the mineralogical properties of the site sediment was undertaken using x-ray diffraction (XRD), which gave an indication of the mineral composition based on the position of the various peaks within the spectrum. Indications from rough estimates of the 5 samples analysed indicated that calcite was the dominant mineral in all samples[5]. Quartz was common in all samples, though not abundant. Plagioclase feldspar was present, but less common than quartz. Clay minerals were also present in all samples, but less common than quartz. The fast-scanning method used did not allow for reliable interpretation of the individual clay minerals, but there was an indication of one or more of the following clay minerals: smectite, chlorite, illite, and halloysite. Grain size and mineralogical characteristics of sediments from the AMDG are similar to those reported by Rogers (2012) for shelf areas to the north.

Sediment cores retrieved from the site showed consistent trends in color and length. In general, all cores had a characteristic thin (4-7 cm), soft layer, grayish yellow in color (Munsell colour code: 2.5Y 7/2), overlying a denser, thicker (5-10 cm) layer, light gray in colour (Munsell colour code: 2.5Y 7/1) (Figure 2.4).

[5] Interpretations of XRD analyses were provided by Professor Cam Nelson, Department of Earth and Ocean Science, University of Waikato.

It was not uncommon to observe sediment billowing up from the sediment surface into the overlying water within the core, as the core was shifted onto the vessel deck after retrieval (Figure 2.4). The softness of the upper layer, and its propensity to become suspended into the overlying water suggests a weakly consolidated, almost fluid-like layer that can be easily eroded. That such a low density sediment layer is present at the site, suggests that normal nearbed flow conditions are very low energy, but also that there is sufficient turbulence to impede consolidation. The lower layer was characterised by a slightly different gray colour shade and appeared to be denser based on visual observations.

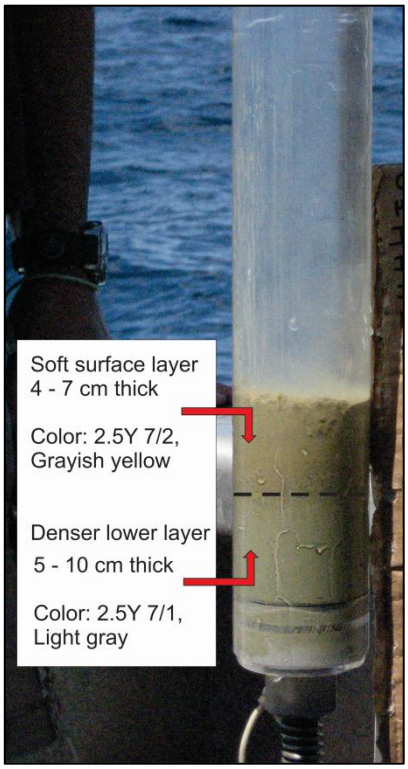

Figure 2.4 Photo of a representative sediment core collected near the centre of the AMDG prior to disposal operations. Colour codes are based on the Munsell colour descriptions.

A geo-mechanical assessment of the seabed across the AMDG, based on deceleration measurements recorded by a dynamic penetrometer, indicated that shear strength increased from approximately 0.5 kPa to 1.2 kPa at a depth of 13 cm below the seabed surface (Flaim et al., 2011). This pattern was consistent at all sampled locations. These results show that indeed, surface sediments were not strongly consolidated and that sediments increased in density with depth, as was indicated by visual observations of sediment cores, but overall the seabed at the AMDG is characterised by low strength seabed sediments.

2.3.2 Oceanography

New Zealand's geographic isolation from neighbouring continents makes it vulnerable to the influence of the surrounding ocean, but due to the relatively large land mass, the regional oceanography also shows some characteristics of continent-driven hydrodynamics (Sharples, 1998). These attributes contribute to a unique and sometimes complex hydrodynamic setting.

Water masses

The North Island of New Zealand receives a large portion of its oceanic waters from the South Pacific sub-tropical gyre. This water originates in the Coral Sea and travels southward along the Australian coastline as the East Australian Current (EAC), a weak western boundary current (de Lange et al., 2003). At the approximate latitude of 35°S, the EAC then turns east and flows across the Tasman Sea as the Tasman Front (TF), a transitional zone characterised by the changing water properties of the EAC as it travels eastward (Heath, 1985) (Figure 2.5). This flow is intercepted by the New Zealand land mass, at which point most of the subtropical water wraps around the northern tip of New Zealand and travels southeast along New Zealand's northeast coast, where it is then becomes known as the East Auckland Current (EAUC) (Sharples, 1998).

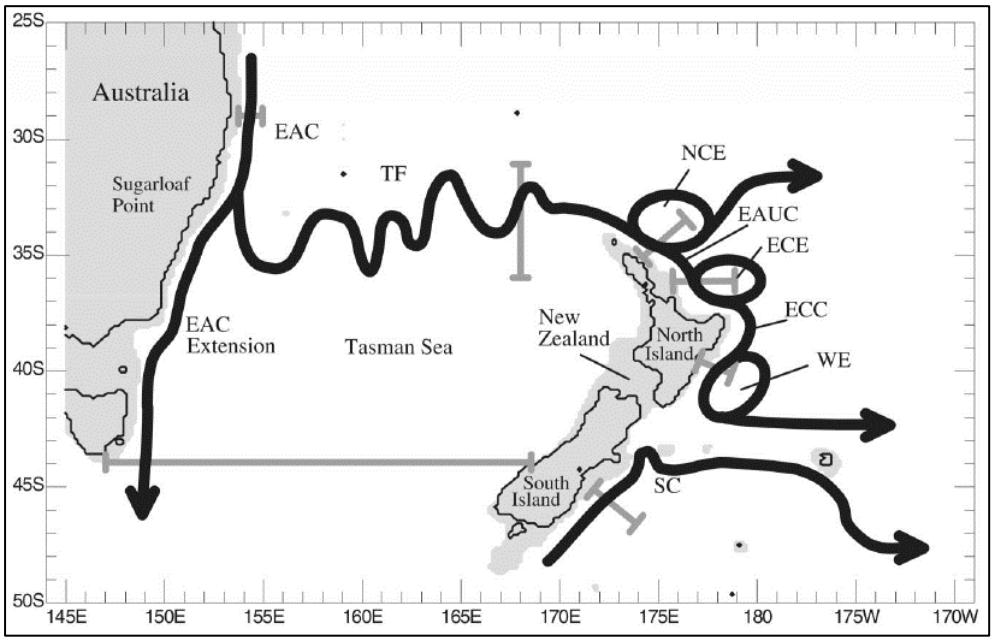

Figure 2.5 Boundary currents surrounding New Zealand including the East Australian Current (EAC), Tasman Front (TF), and the East Auckland Current (EAUC) (source: Tilburg et al. (2001)).

The EAUC is characterised by relatively warm temperatures (17-21°C) and high salinities (~35.7), having originated in sub-tropical areas (Harris, 1985). Periodically, surface intrusions of the EAUC onto the northeast shelf can occur mainly due to persistent summertime easterly winds (at least 10-12 m/s) that are relatively common in the northeast region (Sharples, 1997). Inner and outer shelf waters tend to increase in temperature and salinity with proximity to the EAUC (Sharples, 1997), which typically resides along the shelf margin (Sharples, 1998), except during summer periods as mentioned above. The front representing the boundary between neritic waters and those of the EAUC is characterised by a temperature gradient of more than 2°C (Sharples, 1997). Development of a seasonal thermocline, beginning in October, to a depth of approximately 40 m by late summer, occurs in the shelf regions of the northeast coast (de Lange et al., 2003)

Tides

Tidal currents on northeast coast of the North Island are typically in the range of 10-20 cm/s (Stanton et al., 2001); however somewhat lower values were observed in the Bay of Plenty region (Figure 1.1) (Longdill, 2007). Like all other New Zealand regions, tides are predominantly semi-diurnal, with the M_2 tide as the principal constituent.

This wave travels anti-clockwise as a trapped Kelvin wave around the bathymetric platform (Heath, 1985), which on the northeast coast, ranges in width from 11 km-100 km (Harris, 1985). It has a period of 12.42 h with typical current amplitudes of 5-10 cm/s (Sharples & Greig, 1998). Other semi-diurnal constituents, such as the N_2 and the S_2, are weak on the east coast (Heath, 1985).

Diurnal constituents in this region are generally complex, owing to the variable bathymetry between the east coast and the amphidrome located east of New Zealand (Stanton et al., 2001). The largest of these diurnal components are the K_1 and O_1 and while generally less important than the semi-diurnal components, (Walters et al., 2001), both Heath (1985) and Longdill (2007) reported larger-than-expected flows for the K_1 in the region.

Internal tides can occur under certain conditions in the northeast shelf region, namely stratified summer conditions, when the main barotropic tidal constituent (M_2) is induced to split into its baroclinic harmonics (M_4 and M_6) through interaction with a significant bathymetric feature, such as a deep oceanic ridge (Sharples & Greig, 1998). The internal waves may then break on the shelf edge adding significant energy to the local current regime (Sharples et al., 2001).

Residual Currents

Shelf-associated residual currents may arise due to local oceanic flows, as described above, wind stress, density gradients, or internal tides, and are usually larger than tidal currents (Sharples & Greig, 1998).

The EAUC is a weak and variable boundary current, dependent on seasonal and inter-annual variation (e.g., El Niño/Southern Oscillation (ENSO) fluctuations) (de Lange et al., 2003), with typical speeds of 15-30 cm/s (Brodie, 1960; Denham et al., 1984) and a mean transport ranging from 9-34 Sv in the outer Hauraki Gulf region (Figure 1.1) (Roemmich & Sutton, 1998; Stanton et al., 1997). The seasonal and inter-annual variations in the EAUC result in changes in both the strength and location of the current over time (de Lange et al., 2003).

At the mid-shelf Coromandel region (see Figure 1.1), two basic, shore-parallel, current regimes have been observed: a weak, calm-weather southerly directed current (10-20 m/s), and a stronger current (~40 m/s) associated with storms (Bradshaw et al., 1994). It was considered that the former current situation is associated with the nearby propagation of the EAUC, and the latter driven by wind stress. To the north, mean shore-parallel currents directed to the southeast (20-30 cm/s) were also observed and associated with the EAUC (Sharples & Greig, 1998).

Evidence of locally derived wind driven currents have been observed in the Bay of Plenty region (see Figure 1.1) as seen by an offshore directed flow in the top 10 m of the water column in response to northwesterly winds, followed approximately one inertial period later by a compensating shore-directed flow below 30 m water depth (Longdill et al., 2008). This response was characterised

as a transient upwelling event made possible by the stratified spring/summer conditions, which decoupled the upper layer from the rest of the water column.

Coastal trapped waves are an example of non-locally derived wind effects that have the capacity to constitute, at times, a significant forcing mechanism along the northeast coast of New Zealand and in the vicinity of the AMDG. Coastal trapped waves can develop as a result of the relationship between periodic, but stationary, wind forcing, a resultant change in the vorticity of the water column, and the slope of the shelf (Huyer, 1990). Their combined effect can result in the propagation of waves along the shelf significant distances from their origin (Huyer, 1990) that can comprise a large portion of the sea level and alongshore current variability (e.g., Battisti and Hickey (1984) and Chapman (1987)). On the northeast coast of New Zealand, the presence of coastal trapped waves has yet to be specifically verified, but the potential for them has been noted by Longdill (2007) and Bell and Goring (1996), and limited evidence has been reported by Stephens et al. (2001) and de Lange (2003).

The effects of internal tides have been observed at the shelf margin to the north of the location of the AMDG, where the associated cross-shelf energy flux was calculated to be ~400 W m^{-1}, which was significantly greater than that due to the barotropic tide or inertial shear (Sharples et al., 2001). The additional energy flux due to the generation of the internal wave was suggested as the dominant mechanism driving diapycnal nutrient supply in the summer in that region.

Waves

Unlike the exposed west coast of New Zealand, the east coast is sheltered from prevailing winds by the land mass, which results in a wave climate that is significantly lower energy than that of the west coast. Pickrill and Mitchell (1979) described the east coast wave climate as: wave heights (H) between 0.5 m and 2 m, periods (T) ranging from 6-9 s, and variable steepness, indicative a mixed swell and local sea environment with weak seasonal variability. Similar low energy conditions were produced by wave hindcast modelling of the New Zealand region, which gave a mean wave height of 1.9 m and a maximum of 8.9 m and periods ranging from 5-13 s (Gorman et al., 2003). The wave hindcast results also

showed a positive correlation with ENSO, indicating a moderate tendency towards enhanced wave heights during La Niña conditions.

The low energy wave climate in the northeast coast region suggests that it would not be an important sediment transport mechanism during the disposal process of dredged material at the AMDG. There are two main considerations for sediment transport due to waves: *i*) increased turbulence near the surface, which may increase the settling time for the fine component entrained in that area; and *ii*) resuspension of deposited material due to wave interaction with the bed.

Although increased settling time implies that a surface plume will persist longer, the turbulence will also act to dilute the plume faster. Thus the implications are that the net effect may be zero. An additional consideration, in this case, is that operational limitations mean that material cannot be brought to the site in rough conditions (swell not exceeding 2.5 m with winds from the north to southeast, or 3 m on a northwest to south wind (*pers. comm.*, Simon Male)). Therefore, surface turbulence will not usually be significant.

The other more important factor is the potential for resuspension at the bed following deposition. This long-term effect can be linked to chronic environmental impacts if, for example, extreme waves during storm conditions regularly resuspend the disposed material exposing the nearbed region to increased turbidity and possibly increased contaminant levels (Eggleton & Thomas, 2004; Langtry et al., 2009; Scott & Redmond, 1989). In such a case, the regularity of the resuspension events and the associated current strength should be considered.

If sufficient time passes before an extreme event, consolidation of the deposited material over time will result in an increased critical threshold for erosion (e.g., Endler (2009) and Halka et al. (1991)), such that the percentage of extreme events capable of overcoming the threshold condition will decrease. This will, therefore, result in a decrease in the occurrence of resuspension over time. Considering that the northeast coast is not characterised as a high energy environment, it is likely that consolidation processes will dominate over resusupension processes.

Furthermore, if resuspension is initiated, but sufficient current speeds are not maintained, then the material will form a relatively stationary nepheloid layer above the bed, which will eventually resettle in place (Wolanski et al., 1992). In this situation, it may be possible that the nepheloid layer would disperse in the downslope direction as a sediment-laden gravity current (Kneller & Buckee, 2000; Traykovski et al., 2000), provided the slope and the excess density of the layer is sufficient to initiate movement (Traykovski et al., 2000). At the AMDG, the shelf is only gently inclined (gradient=0.01), and it is not likely that a wave-induced nepheloid layer would develop at the required concentrations (~20 g/l, e.g., Traykovski et al. (2000)) so, significant momentum would not likely be obtained.

The speed required for resuspension is in the range of 20 – 30 cm/s assuming unconsolidated muddy dredged material (Clyde & Christian, 1993). Based on deep water wave theory, and a typical wave period in the northeast coast region (5-13 s; Gorman et al. (2003)), a minimum sustained wave height of 14 m would be required to produce the near-bed velocities needed to entrain deposited dredged material. Twenty year wave hindcast model results indicated a maximum wave height of 8.9 m (Gorman et al., 2003), so it is not probable that wave action will be able to resuspend deposited material at the AMDG.

2.4 Summary

Based on extensive previous work, there is a solid, basic understanding of the underlying processes involved in the disposal of dredged material at open-water disposal sites. The 3-phases (*Convective descent*, *Dynamic collapse*, and *Passive dispersion*) involved in the disposal process are well-understood in the context of the sites previously studied. The governing forces driving the disposal process are primarily dependent on the density difference between the disposed material and that of the ambient water. The 3 disposal phases occur in response to a successive reduction in the inherent density difference due to entrainment and dilution along the interface of the two mediums. However, to date, research in this area has been mainly limited to disposal sites at water depths approximately less than 50 m, so it is not as clear whether the developed model is valid for the deep water situation at the AMDG.

Current knowledge on the oceanography, and the physiography and sedimentology of the northeast coast region and at the AMDG suggests that the site would exhibit 'retentive' behaviours, where dispersion of dredged material disposed there would be minimal. However, there are still many gaps in the knowledge related to the dispersive characteristics of the site that cannot be deduced from previous studies in the region. Specific areas that require further research include:

- A detailed understanding of the hydrodynamic and hydrographic setting;
- Assessment of the relevance of the commonly accepted conceptual model of the disposal process to that which occurs at the AMDG especially considering the significant water depth there;
- Site classification as either dispersive or retentive for determining its suitability for the proposed long-term usage under requirements of regulating authority;
- A specific understanding of the potential for dispersion during the variable weather and sea conditions common to the northeast coast region.

CHAPTER 3

FORCING MECHANISMS OF THE SHELF ENVIRONMENT AT THE AUCKLAND MARINE DISPOSAL GROUND: DATA OBSERVATIONS

3.1 Introduction

The coastal seas around New Zealand are forced by a variety of both short-term and long-term variations in the local currents. On the continental shelf, these variations can be brought about by tides, meteorological events, and local oceanic flows, among others (Sharples & Greig, 1998). All of these mechanisms have the potential to mobilise and disperse sediments which can then be deposited elsewhere. Whether the effect is positive or negative, sediment movements cause a change to both the dispatching and receiving environments.

Dispersion of dredged material disposed at an open-sea site, therefore, is largely dependent on the local hydrodynamic processes. Generally, a site is classified prior to use as either dispersive or non-dispersive for the purpose of determining the type of dredged material that may be appropriate for disposal there (McAnally & Adamec, 1987). The site classification process, along with knowledge of the sediments intended for disposal, involves a detailed understanding of the regional and local hydrodynamics which are determinants the main sediment transport pathways and potential for dispersion.

3.2 Motivation and Relevance to the Thesis Objectives

The AMDG is the first dredged material disposal site in the deep waters beyond the territorial seas of New Zealand that has been established in compliance with the international laws on disposal at sea. The laws require careful characterisation and ongoing monitoring to establish how the site functions with respect to disposal operations aiming to identify potential for adverse environmental impacts. Understanding and characterising the hydrodynamic setting of the site is a key factor in classifying whether it is dispersive or non-dispersive.

There is no precedent for studying an area of New Zealand's continental shelf for the express purpose of establishing a dredged material disposal site. Forcing mechanisms in deeper waters differ greatly from those in the near shore areas so it

is not possible to make assumptions based on what is known of the historical disposal grounds within the nearby Hauraki Gulf and apply that knowledge to the AMDG. Furthermore, while there is a substantial body of work looking at the forcing mechanisms of the Hauraki Gulf, its northern shelf boundary, the Coromandel coast, and the Bay of Plenty (Black et al., 2000; Bradshaw et al., 1991; Longdill et al., 2008; Proctor & Greig, 1989; Sharples, 1997; Sharples & Greig, 1998; Sharples et al., 2001), very little research has been undertaken in the region directly east of Great Barrier Island (beyond the eastern boundary of the Gulf (Figure 1.1)) where the AMDG is located. It is, therefore, critical to establish the forcing mechanisms there and attempt to draw conclusions with dredged material disposal operations in particular as the frame of reference.

The findings of this chapter are additionally important for developing a numerical model that can reliably predict the dispersion pathways in conditions that have yet to be measured physically at the site.

3.3 Chapter Aims

The aim of this chapter is to characterise the hydrodynamic and hydrologic setting of the AMDG using measured data and determine the importance of the various forcing mechanisms with respect to dispersion of disposed dredged material. This will be achieved by detailing the shelf environment in terms of:

- water column structure;
- tidal currents;
- residual currents;
- local wind effects[6];

[6] The nature of the data available only allowed for conclusions related to local wind effects (e.g. upwelling and locally sourced wind-driven currents). Non-local wind effects, such as the development of coastally trapped waves and their influence on sediment dispersion at the AMDG, are a potentially important (Bell & Goring, 1996; Stephens et al., 2001), albeit periodic, forcing mechanism at the AMDG considering its proximity to shelf-break (Huyer, 1990). However, identification of such effects would require a dedicated and extensive deployment campaign focussing on a wide range of environmental variables along a length of the shelf on the order of 1000 km and covering most of the shelf width in that region (e.g., Freeland et al. (1986) and Schumann and Brink (1990)). Within the limitations of this research project (e.g. funding and time), such a field campaign was not possible.

- internal tides; and
- the main mechanisms that are likely to influence the dispersion of dredged material.

3.4 Data Sources and Sampling Methodology

For the purposes of this study, numerous dedicated research voyages were undertaken between 2008 and 2010 to collect several types of data related to shelf current patterns, water column structure and characteristics, and the seabed environment. Herewith, only datasets related to the aims of this chapter will be described. Non-related datasets will be detailed in following chapters and appendices.

Physical sampling of the shelf environment was, for the most part, limited to the boundaries of the AMDG and areas immediately adjacent to it at water depths ranging from approximately 130 m – 160 m (Figure 3.1). The long-term mooring deployment and all other sampling surveys were undertaken from the MV Star Keys and the MV Ten-Sixty. Each voyage included 2–4 representative Conductivity Temperature Density (CTD) profiles from various locations within or near the AMDG (Figure 3.1 and Table 3.1). Over the 2 year field campaign period of this research CTD profiles were recorded at times representing important seasonal changes in the water column structure.

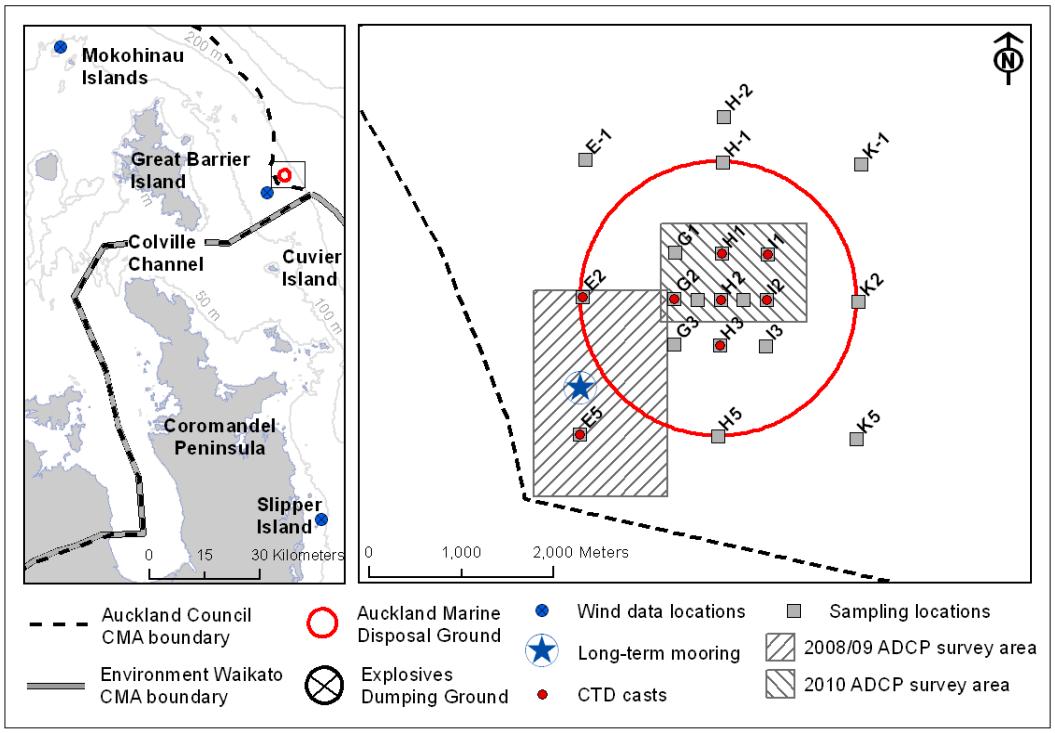

Figure 3.1 Locations of sampled data at the AMDG. The long-term ADP location appears outside the site boundary because the site was shifted northeast of its original location after the deployment due to an overlap with the Auckland CMA.

Table 3.1 Hydrographic data collection details including site ID, water depth, sample depth, site coordinates, and sampling times at the AMDG.

Site ID	Water Depth (m)	Sample Depths (m)	NZTM easting	NZTM northing	Data Collection Times (NZST)
ADP Deployment					
E5	140	19 to 131	1850212	5988128	26/09/08 to 27/11/08
Current meter Deployment					
E5	140	135	1850212	5988128	26/09/08 to 16/10/08
Temperature Sensor Deployment					
E5	140	133	1850212	5988128	26/09/08 to 27/11/08
CTD casts					
E2	142	0 to 142	1850239	5989629	26/09/08
E5	140	0 to 140	1850212	5988128	26/09/08; 04/06/09; 23/11/09
G2	144	0 to 144	1851239	5989610	26/09/08; 25/04/10
H1	145	0 to 145	1851748	5990101	26/09/08; 20/03/10; 10/04/10
H2	145	0 to 145	1851739	5989601	20/03/10; 10/04/10; 15/04/10; 21/04/10; 25/04/10
H2/I2	145	0 to 145	185 1990	5989601	21/04/10
H3	144	0 to 144	1851730	5989101	04/06/09
I1	147	0 to 147	1852249	5990092	15/04/10
I2	146	0 to 146	1852239	5989592	10/04/10; 21/04/10; 25/04/10
ADCP Surveys					

Site (new)	centre	145	4 to 128	As above	10/04/2010; 0830 – 1200
Site (new)	centre	145	4 to 128	As above	15/04/2010; 1000 – 1130
Site (new)	centre	145	4 to 128	As above	21/04/2010; 0915 – 1130
Site (new)	centre	145	4 to 128	As above	25/04/2010; 1030 – 1130
Temperature Sensor (short-term)					
Site (old)	centre	140	1	See Figure 3.1	08/11/2008; 0615 – 1400
Site (old)	centre	140	1	As above	23/11/2009; 1230 – 1430
Site (new)	centre	145	1	As above	10/04/2010; 0830 – 1200
Site (new)	centre	145	1	As above	15/04/2010; 1000 – 1130
Site (new)	centre	145	1	As above	21/04/2010; 0915 – 1130
Site (new)	centre	145	1	As above	25/04/2010; 1030 – 1130

Due to the significant water depth and distance from the coast, only one long-term deployment for recording the current patterns was possible. This occurred over the spring season of 2008 (Figure 3.1 and Table 3.1). Additional short-term ADCP surveys (down-ward facing/boat-mounted) were undertaken in April (autumn) 2010 (Figure 3.1 and Table 3.1).

3.4.1 CTD Profiles

Profiles of salinity, temperature, and density were obtained with a SEABIRD® SBE 19+ Seacat Profiler. All profiles were obtained using the same instrument in 'marine' mode. The device was serviced and calibrated by SeaBird Electronics at recommended intervals. Density values derived by the CTD profiler are not directly measured, but calculated from temperature, conductivity, and pressure and therefore do not reflect density variations due to the presence of suspended particles.

3.4.2 ADP and Current Meter Records

Moored Records

Current speed and direction data were recorded by a SONTEK® 250 kHz Acoustic Doppler Profiler (ADP) and an InterOcean® S4 A EM current meter.

The ADP also housed a temperature sensor which recorded data for the same period. The sensor was located near the transducer head. The ADP averaged currents over a 10-minute interval each hour and the temperature sensor sampled at an interval of 1 Hz over the 10-minute averaging interval each hour (Appendix Table I.1)

The ADP and temperature records were 63 days long starting on 26 September 2008 NZST (Table 3.1) The S4 current meter sampled at a rate of 2 Hz for 10 minute bursts every hour for 20 days also starting on 26 September 2008 NZST (Table 3.1). Due to a power failure after 20 days, the S4 data record is significantly shorter than the ADP record. For the purposes of this research, the S4 data was averaged over the 10 minute burst for the length of the record giving one sample for each hour. This allowed for incorporation with the ADP data record resulting in a more complete velocity profile during the period in which the two records coincided.

The ADP and S4 were deployed at the seabed as a weighted instrument string with the ADP suspended at 7 m above the bed (ATB) by a 160 kg buoyancy frame and the S4 below that at 5 m ATB (Figure 3.2). Attaching the instrument string to the seabed weight was an acoustic release used for instrument retrieval at the end of the monitoring period. The 250 kHz ADP returned acceptable signal to ratios over a distance of 112 m from the transducer head, not including the 1.5 m blanking distance. Data from the top 20 m of the water column was corrupted due to waves and air bubbles and is therefore not discussed in the following sections.

In the following analyses, current velocities are often presented as vector components. Current vectors were first rotated relative to true north and as the local bathymetric contours are oriented approximately north to south, east/west and north/south directed currents are considered ‘cross-shore’ and ‘alongshore’, respectively (Figure 1.1). In the case of the vector components, a standard Cartesian coordinate system was adopted where positive x-values are directed Cross-shore (east) and positive y-values are directed alongshore (north).

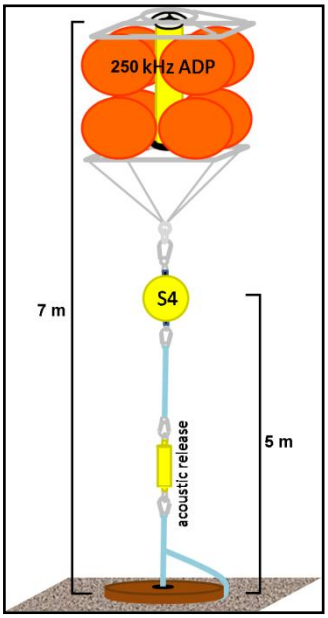

Figure 3.2 Diagram of mounting set up for the long-term moored instrument deployment.

Boat-Mounted ADCP Surveys

Difficulties with the deployment and retrieval of the moored instrument string meant that it was not possible to carry out multiple long-term deployments over different seasons which would allow for a more complete description of the hydrodynamic setting at the AMDG. To supplement the one long-term record, current speed and direction were recorded using a down-ward facing, boat-mounted RD Instruments® 300 kHz Workhorse Sentinel Acoustic Doppler Current Profiler (ADCP) during 5 separate short-term surveys (Figure 3.3 and Table 3.1). The ADCP also housed a temperature sensor which was located near the transducer head. Temperature data was recorded during each of the short-term surveys for the length of each survey (Table 3.1). The survey undertaken in November 2008 will be discussed in this chapter; however, those surveys undertaken in April 2010 will be covered in Chapter 4 of this thesis.

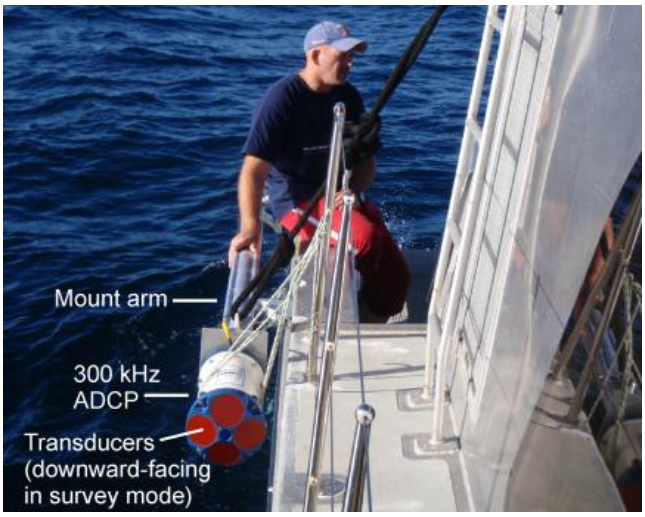

Figure 3.3 Photo of the RD Instruments® 300 kHz ADCP attached to the swinging mount arm. This set-up was used for each of the short-term downward facing ADCP surveys.

The ADCP was configured to ping 8 times per ensemble for the length of each recorded transect (Appendix Table I.2). Temperature data was recorded once per ensemble for the length of each survey transect. A recurring problem attributed to a combination of the power supply on the survey vessel, cable length, and a high ping rate resulted in a reasonably consistent blind spot with a loss of current data beyond a depth of approximately 75 – 100 m. These issues were not resolved until after the short-term surveys were completed.

As with the long-term current data records, vectors were rotated relative to true north and thus oriented with the local bathymetry. A moving average filter based on a local regression using weighted linear least squares and a 1st degree polynomial model was applied to smooth and remove outliers from the records of each ADCP depth bin. Given that the short-term surveys spanned less than the length of a tidal cycle, the data records are mainly regarded as 'snapshots' of the vertical current structure of the AMDG on the day of each survey.

3.4.3 Local Wind Data

Wind data (surface wind speed and surface wind direction) were retrieved as time series from the National Institute of Water and Atmospheric Research (NIWA) online climate database 'CliFlo' (National Institute of Water and Atmospheric Research (NIWA)). Data from meteorological stations at the Mokohinau Islands (MI), Slipper Island (SI) were accessed for the period of December 2005 – December 2010 (Appendix Table I.3 and Figure 3.1). Wind data were used for

direct analysis and comparison to the measured shelf currents and also for a general analysis on the local wind climate of the northeast coast.

Additionally, wind data were obtained from the National Oceanographic and Atmospheric Administration (NOAA) National Climatic Data Center (NCDC) Blended Sea Winds dataset (BSWD) (Zhang et al., 2006). This dataset contains globally gridded, high resolution ocean surface vector winds and wind stresses on a global 0.25° grid. Wind speeds are generated by blended observations from up to 6 satellites and wind directions come from NCEP Reanalysis 2 (NRA-2) (National Oceanographic and Atmospheric Administration (NOAA)). Six-hourly wind speed components were retrieved for the nodes nearest the long-term deployment location (Site E5), MI, and SI (Appendix Table I.4 and Figure 3.1) and interpolated to an hourly interval for comparison to the CliFlo data records.

In order to compare CliFlo wind data records to the BSWD records, CliFlo records were scaled to reflect a 10 m surface wind using the Hellmann relation (see Kaltschmitt et al (2007))

$$w_{10} = w_w \left(\frac{h_{10}}{h_w} \right)^{\alpha} \qquad \text{Equation 3-1}$$

where w_{10} is the velocity of the wind (m/s) at a height 10 m above a surface, w_w is the velocity of the wind (m/s) at a known height above the surface, h_{10} is the height 10 m, h_w is the height from which the velocity w_w was measured, and α is the Hellmann coefficient taken as 0.11 for open-ocean conditions after Hsu et al. (1994). All further descriptions and discussions of the CliFlo wind records are with reference to the 10 m scaled values.

3.5 Local Wind Climate

As a potentially important forcing mechanism on the hydrodynamic setting of the AMDG, the wind climate of the northeast shelf needs to be evaluated. Having a good understanding of the wind climate will make easier the identification of any possible correlations with shelf currents. Due to its great distance from land, there is a paucity of measured wind data from the AMDG. New Zealand's national climate database (CliFlo) (National Institute of Water and Atmospheric Research

(NIWA)), includes two measuring locations nearby at Cuvier Island (25 km distance) and along the Colville Channel (50 km distance) (Figure 3.1), however these stations were no longer operational at the onset of this study. The nearest measuring stations with data records coinciding with the period of this study were at MI and SI which are 65 km and 80 km away, respectively (Appendix Table I.3 and Figure 3.1).

General wind climate patterns were evaluated by assessing the 5-year hourly surface wind speed and direction data records from the CliFlo dataset at MI and SI (Appendix Table I.3 and Figure 3.1). For a more detailed assessment of the study period, the NOAA BSWD (Zhang et al., 2006) was utilised by extracting component wind speeds at nodes corresponding Site E5 at the AMDG, MI, and SI (Appendix Table I.4 and Figure 3.1).

3.5.1 Blended Sea Winds Accuracy

The accuracy of the BSWD was assessed to determine if it could be used to represent the wind climate at the AMDG. To do this, wind records at the nodes nearest the MI and SI were compared to those of the CliFlo dataset for the same locations.

The full BSWD extraction period (1 Sept 2008 – 1 May 2010) covers the two main field study periods (2008 deployment: 26 Sept – 28 Nov & 2010 survey period: 20 Mar – 26 Apr). The periods outside these date ranges were included in the extraction for application in numerical simulations and for general information. Comparisons based on linear regressions of the BSWD and the CliFlo data for the full period show an acceptable level of accuracy at MI location, with the cross-shelf wind speed component ($R^2 = 0.82$) better represented than the along-shelf wind speed component ($R^2 = 0.53$) (Figure 3.4). At SI, the cross-shelf component ($R^2 = 0.57$) is acceptable, though not highly accurate, and the along-shelf component ($R^2 = 0.48$) is represented poorly. During the 2008 deployment period alone, the BSWD appears to represent the measured CliFlo datasets significantly better (Figure 3.4). At MI, the R^2-values were 0.86 and 0.72 for the cross-shelf and along-shelf wind components, respectively. At SI, the accuracy was somewhat lower with R^2-values of 0.67 and 0.68 for cross- and along-shelf components, respectively. The BSWD poorly represents the CliFlo datasets

during the 2010 survey period with only the cross-shelf component of wind speed at MI showing an acceptable level of accuracy ($R^2 = 0.80$). The R^2-values were 0.24, 0.46, and 0.36 for the MI along-shelf, SI cross-shelf, and SI along-shelf components, respectively.

It appears that overall the BSWD is a fairly good representation of wind speeds along the northeast shelf considering it is from a low-resolution global dataset. In general, the data coming from MI is better than that coming from SI and the cross-shelf wind is better represented than the along-shelf wind at both locations. The low level of accuracy during the 2010 survey period, suggests that the data should not be used for analysis during that period. In which case, the best alternative is likely to be the CliFlo wind data from MI (as it is the closest station to the AMDG) for ongoing analysis during the 2010 survey period. During the 2008 deployment period, however, the BSWD accuracy appears to be of an acceptable level and the data record from the node nearest Site E5 is likely to be the best option for further analysis and comparison to other datasets collected the AMDG during that period.

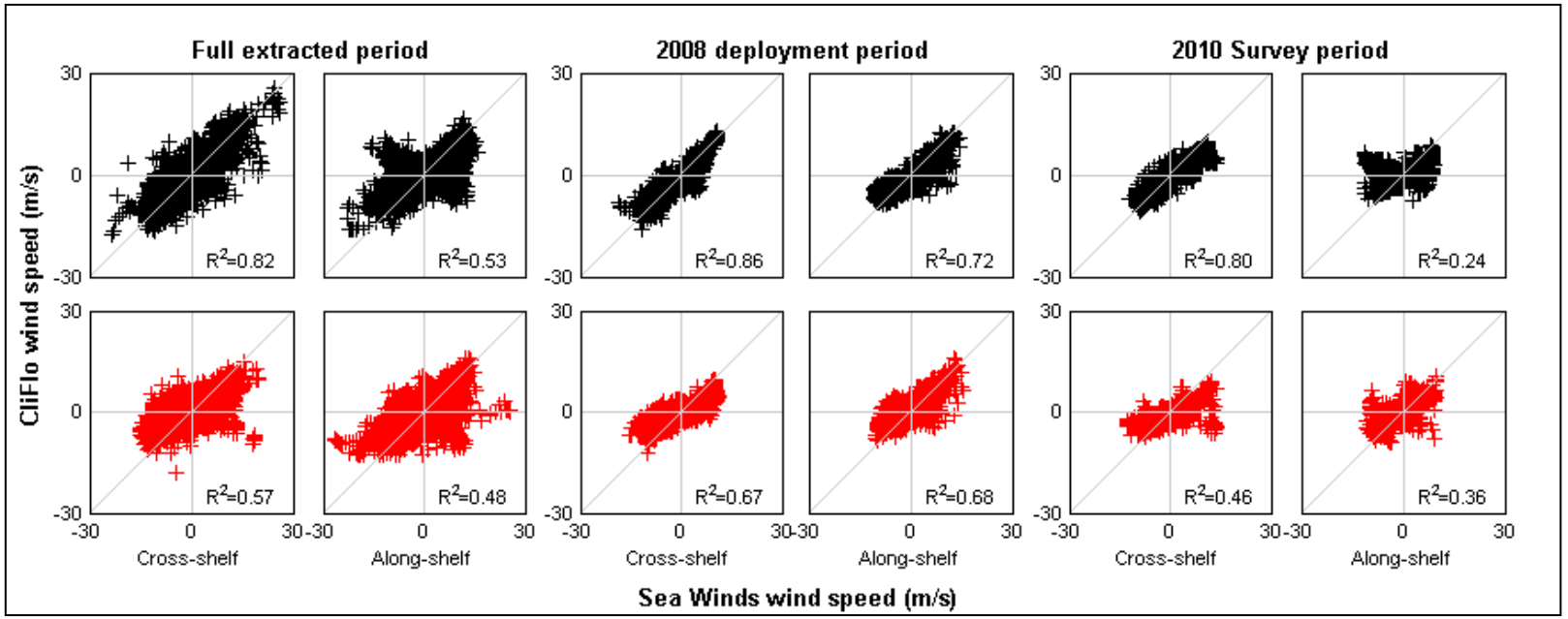

Figure 3.4 Scatter plots and R^2 values from linear regression of BSWD and CliFlo data component wind speeds (cross-shelf and along-shelf) at the Mokohinau Islands (black) and Slipper Island (red). Plots for the full extracted period (1 Sept 2008 - 1 May 2010), the 2008 deployment period (26 Sept -27 Nov 2008 NZST), and the 2010 survey period (20 Mar -26 April 2010) are shown.

3.5.2 Predominant Wind Patterns

The 5 year period (December 2005 – December 2010) wind records were grouped seasonally as: summer (December – February), autumn (March – May), winter (June – August), and spring (September – November). Data records from both the MI and SI CliFlo stations were plotted as wind roses to examine wind patterns for the two locations on the northeast shelf (Figure 3.5).

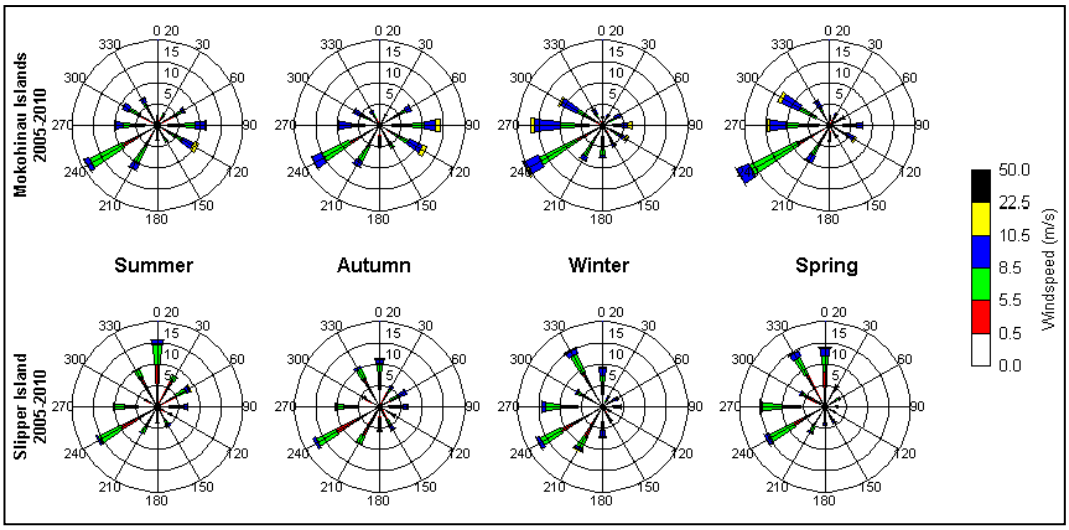

Figure 3.5 Seasonal wind rose plots for Mokohinau Island (MI) and Slipper Island (SI) during the period of December 2005 - December 2010.

The primary wind direction in all seasons at both locations was from the southwest, where samples comprised at least 15 % of the record in all cases (Figure 3.5 and Table 3.2). At MI, the records from the southwest ranged from ~18 – 24 % seasonally which was somewhat higher than those at SI between ~16 and 17 %. At MI, the secondary directions for all seasons except autumn were also from the southwest quadrant. In autumn, the secondary direction was from the east. At SI, secondary directions were from the north/northwest with the exception of spring which was from the southwest. It should also be noted that north-westerlies also occurred frequently, especially in winter and spring at both MI and SI.

At MI, maximum wind speeds ranged from 18 m/s in autumn to 28 m/s in winter. All maximum wind speeds were recorded as coming from the east/southeast quadrant. The average wind speed at MI ranged from 5.3 m/s in summer to 6.6 m/s in winter. The percent of calm records (<0.5 m/s) was highest in autumn at 1.4 % and lowest in winter and spring at 0.4 %. Maximum wind speeds at SI

ranged from 17 m/s in autumn, to 22 m/s in winter and averages ranged from 4.1 m/s in summer to 4.9 m/s in winter. The percent of calm records at SI did not vary significantly throughout the seasons.

Table 3.2 Wind climate details for the period of December 2005 - December 2010 at the Mokohinau Island (MI) and Slipper Island (SI) CliFlo stations.

Location	1° dir (°)	*f* (%)	2° dir (°)	*f* (%)	Max spd (m/s)	Dir (°)	Avg spd (m/s)	σ	% Calms *
MI									
Summer	240	18.9	210	11.6	20.7	110	5.3	2.9	0.7
Autumn	240	17.5	90	14.3	18.1	90,120	5.7	3.2	1.4
Winter	240	20.7	270	16.8	28.7	118	6.6	3.4	0.4
Spring	240	24.3	270	14.8	20.7	100	6.1	3.1	0.4
SI									
Summer	240	15.9	360	15.8	17.9	60	4.1	2.2	0.7
Autumn	240	17.4	360	11.2	16.7	140	4.3	2.4	0.9
Winter	240	17.4	330	15.3	21.9	90	4.9	2.9	0.7
Spring	240	15.7	270	15.4	17.5	360	4.7	2.5	0.8

*Calms: Wind speed < 0.5 m/s

Another seasonal pattern can be seen in the frequency of easterly wind, especially at MI. In summer and autumn at MI, the frequency of records from 60° - 120° was 29.3 % and 34.7 %, respectively. In winter and spring, the frequency of easterly winds was 18.9 % and 18.6 %, respectively. At SI, the frequency of easterlies was 19.4 %, 17.7 %, 10.7 %, and 9.8 % for summer, autumn, winter, and spring, respectively. The averaged differences between the summer/autumn and winter/spring seasons were 13.2 % and 8.3 % for MI and SI, respectively.

3.5.3 Wind Climate of the Study Periods

During the 2008 long-term deployment period, 26 September – 27 November, the predominant wind direction was ~240° which occurred during 18 % of the deployment period (Table 3.3 and Figure 3.6). The secondary direction was from ~270°, occurring during 14 % of the deployment. Overall, wind speeds measured from the western and eastern directions made up 52 % and 30 % of the records during the 2008 period, respectively. The maximum wind speed recorded was 17 m/s from 324°, the average was 8.4 m/s, and there were 0 % calm record

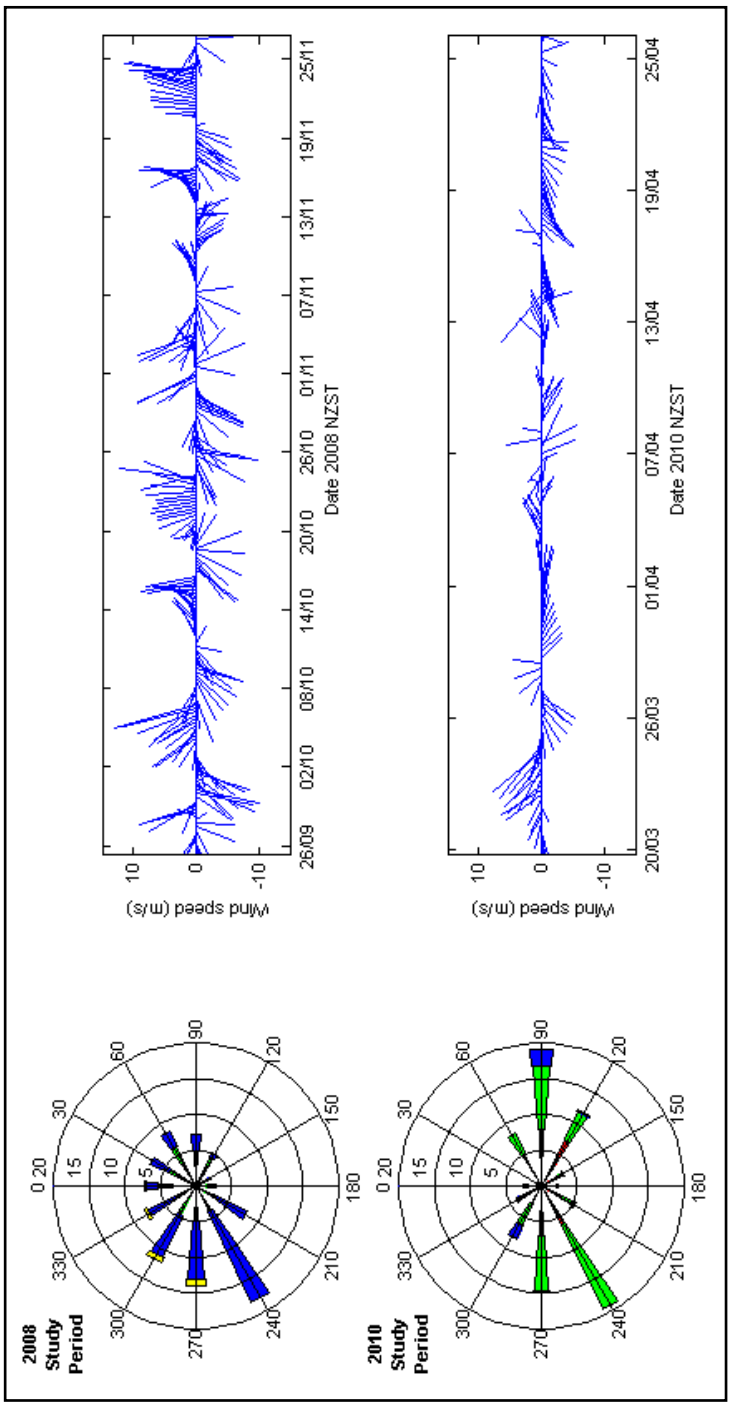

Figure 3.6 Wind record plots (rose and feather) for the 2008 study period (top) and the 2010 study period (bottom). Scale of the feather plots are indicated by either the positive or negative y-axes.

The 2010 study period, 20 March – 26 April, also showed a predominant wind direction of ~240° and a secondary direction of 270° with both directions measured approximately 19 % of the record (Table 3.3 and Figure 3.6). Overall, 52 % and 43 % of the records were measured as coming from the western and eastern directions, respectively. During this time, the maximum wind speed was 11.7 m/s coming from 310°, the average was 5.4 m/s and 0.7 % of the records were calm.

Table 3.3 Wind climate details for the 2008 and 2010 study periods.

Location	1° dir (°)	*f* (%)	2° dir (°)	*f* (%)	Max spd (m/s)	Dir (°)	Avg spd (m/s)	σ	% Calms *
2008									
Spring	240	18.1	270	14	16.7	324	8.4	2.4	0.0
2010									
Autumn	240	19.3	90	19.1	11.7	310	5.4	1.9	0.7

*% Calms: Wind speed < 0.5 m/s

3.5.4 Discussion

General wind climate patterns were examined for the period of December 2005 – December 2010 using wind speed and direction records from the NIWA National Climate Database (CliFlo) at the Mokohinau Islands and Slipper Island both located along the northeast coast of the North Island. According to the Southern Oscillation Index (SIO) as published by the Australian Government Bureau of Meteorology (2011), this five year period included two El Niño periods (2006 & 2009) and four La Niña periods (2005, 2007, 2009, and 2010). Thus, it is likely to be a good representation of a range of climate conditions for the purposes of a general assessment of the northeast coast wind climate. In the northeast of New Zealand, El Niño events typically bring about westerlies and southerlies in the summer and winter respectively, and in autumn and spring, south-westerlies are more common (Gordon, 1985). La Niña years tend to bring about less south-westerly winds (Jiang et al., 2004). The predominance of south-westerly winds during the period examined suggests that El Niño events dominated the period examined.

Generally speaking, winds in the northeast region are light and from the southwest mainly. These patterns are in line with climate conditions described by Bradshaw et al (1991), Brodie (1960), and Harris (1985) which associate the predominant

low speed west and south-westerlies with the passage of mid-latitude anticyclones to the east and northeast approximately once per week. Higher speed intermittent northerly and easterly winds can also occur in association with the less frequent passage of subtropical low pressure systems (Bradshaw et al., 1991; Harris, 1985). The present analysis supports this claim as the maximum wind speeds and lower frequency records were consistently recorded from either the east or the north (Table 3.2).

Seasonal wind patterns along the northeast coast are commonly described as predominant westerlies in the winter and spring and easterlies in the summer (Chang et al., 2003; Sharples, 1997; Sharples & Greig, 1998; Zeldis et al., 2004). For the period analysed here, this pattern was realised to the extent that the frequency of easterly winds was greater in summer and autumn than in winter and spring, but easterly winds were never found to be predominant.

Differences in patterns between MI and SI can be attributed, in large part, to the locality with respect to the coastline and in smaller part to the land aspect. The Mokohinau Islands are positioned at the northern boundary of the Hauraki Gulf approximately 60 km from the coast where it is exposed to a large wind fetch, whereas Slipper Island is only a couple kilometres from the coast and thus much more sheltered from the predominant winds. The land aspect at the latitude of MI is situated northwest-southeast and that at SI is closer to north-south. Differences in the immediate environment of the anemometers on each island may also contribute to the greater frequency of recorded northerly winds at SI.

Wind records during the two study periods generally reflect the 5 year patterns for the corresponding seasons. However, during the 2008 study period, average wind speeds were somewhat higher (2-3 m/s) and the maximum wind speed was lower (1-3 m/s) than the spring 5 year records for MI and SI indicating overall higher wind speeds at the AMDG, but somewhat less variability. This is possibly due to the offshore position site and nearby morphologic features such as the Colville Channel which may act to focus the wind (Figure 3.1). The spring-time westerly pattern was evident in the 2008 period with the predominant south-westerlies, but also with north-westerly wind as the third most frequent wind direction.

During the 2010 study period, the secondary wind direction was from the east which reflects well the autumn 5 year pattern at MI, but not at SI which was from the north. It is possible that the early autumn timing of the 2010 period shows some remnants of the 'summer easterly' pattern and maybe more so than in other years as the frequency during this period is approximately 5 % higher than in the combined years (Table 3.2 and Table 3.3). Alternatively, increased winds from the east could be a result of La Niña climate conditions which were predominant in 2010 based on the SIO as published by the Australian Bureau of Meteorology (2011). Average wind speeds during the 2010 study period matched those of the 5 year dataset for autumn at both MI and SI within ~1 m/s, but the maximum wind speed was significantly lower (5-7 m/s) suggesting a more settled period for average autumn conditions.

3.6 Thermal Characteristics and Water Column Structure of the AMDG

CTD profiles and temperature time series were recorded intermittently between 2008 and 2010. It was not possible to collect data at regular intervals throughout an annual cycle which would allow for a detailed assessment of seasonal changes in the water column properties at the AMDG, however the data that was collected, albeit covering more than 2 annual cycles, gives an indication of the seasonal variability which appears to be similar to what has been reported in previous studies of the northeast coast (Garner, 1961; Harris, 1985; Longdill, 2007; Sutton & Roemmich, 2001).

3.6.1 Seasonal Variation

For the present study, no temperature data were collected for the summer months of December through February, however a CTD cast from the end of March 2010 shows temperatures of 20.4°C and 14.4°C at the surface and bed, respectively and a thermocline depth of approximately 60 m (Figure 3.7a). The average temperature profile of four casts recorded in April 2010 showed a weakening isotherm structure with a thermocline depth at approximately 80 m and temperatures ranging from 19.7°C at the surface to 14.5°C at the bed (Figure 3.7b). Cooling and thermocline deepening was evident in casts recorded in June 2009 (winter) and September 2008 (early spring) where the latter showed

temperatures ranging 16.5°C – 15.5°C, surface to bed and a weak thermocline at approximately 120 m (Figure 3.7c). The September cast showed a surface temperature of 15.3°C and a bed temperature of 13.6°C with no distinct thermocline (Figure 3.7d). A late spring cast was recorded in November 2009 which showed warming in the near-surface waters to 17.5°C accompanied by early evidence of thermocline development, but bed temperatures remained cool at 13.9°C similar to the September cast recorded the previous year (Figure 3.7e).

To broaden the perspective of seasonal temperature and water column structure patterns, the five CTD casts described above were combined with a near-bed temperature time series recorded in September 2008 and near-surface temperature recorded in November 2008 (see Table 3.1) These data were interpolated to derive 'generic' seasonal isotherms that are indicative of the period between late March and late November at the AMDG (Figure 3.7f). Despite the lack of data in the summer months, the important seasonal processes are well-represented. Warm stratified conditions in late summer/early spring leads to cooling and deepening of the thermocline and the transition to nearly fully-mixed cold water of the late winter/early spring months. Finally, as water begins to warm again leading into early summer there is evidence of redevelopment of the thermocline which foreshadows the warm stratified conditions of the summer months.

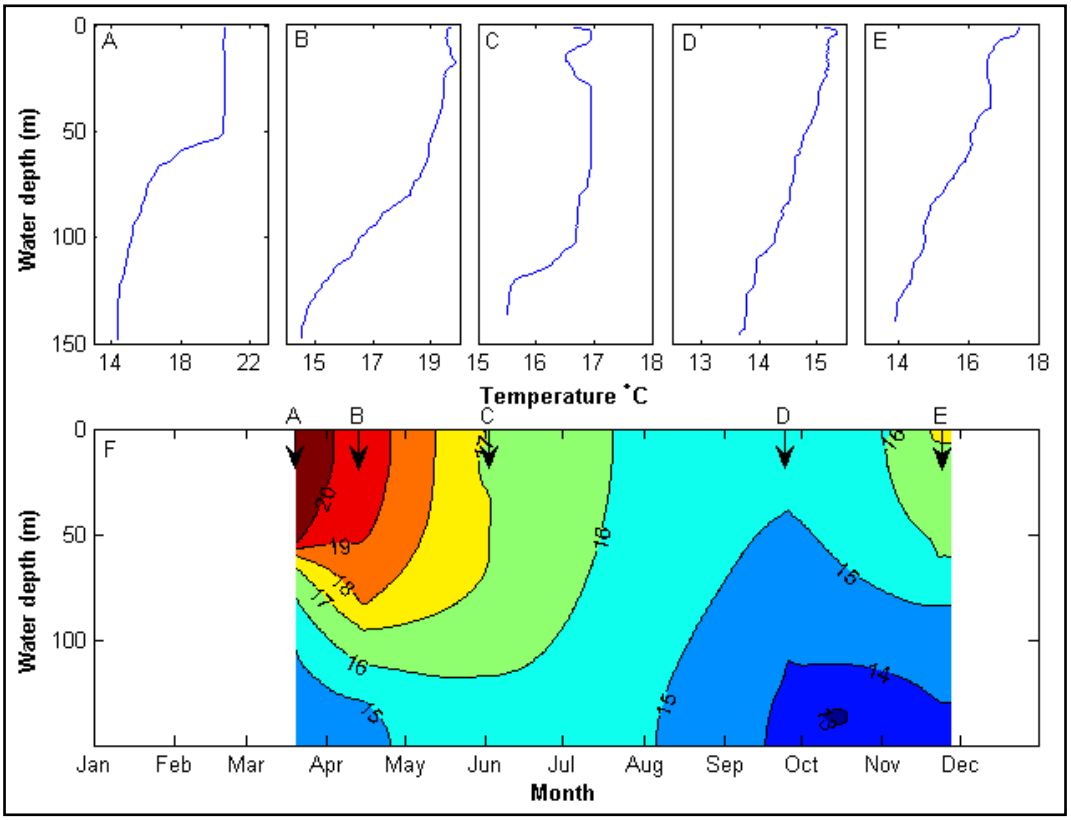

Figure 3.7 Temperature profiles from CTD casts recorded in A) Mar 2010, B) Apr 2010 (average of 4 casts recorded on 10, 15, 21, and 25 Apr), C) Jun 2009, D) Sept 2008, and E) Nov 2009 at the AMDG. F) Seasonal isotherms derived from combined and interpolated temperature data including casts (A – E; positions labelled at the top of plot), a near bed time series recorded from 26 Sept – 27 Nov 2008, and near-surface temperature data recorded in Nov 2008 (see Table 3.1).

3.6.2 Study Periods

Temperature data recorded during the 2008 and 2010 study periods are described in detail below to more clearly define the hydrologic setting and structural aspects of the water column during each period.

2008 Deployment Period

The long-term deployment, beginning on 26 September 2008, included a near-bed temperature record (Table 3.1). On the day of deployment a CTD cast was recorded which showed a nearly fully-mixed water column ranging from approximately 15°C at the surface to just under 14°C seabed with no distinct thermocline (Figure 3.7d). The near-bed temperature record, recorded approximately 10 m ATB, started at approximately 14°C and slowly declined by 0.5°C until 8 October when it then rapidly declined a further 1°C (Figure 3.8). Between 10 October and 18 October the temperature fluctuated between about 12.5°C and 13°C, after which point, the temperature remained at a relatively

stable 13°C with a slight increase to approximately 13.5°C by the end of the record in late November. No CTD casts beyond the one recorded on the day of deployment were recorded during the 2008 study period so potential changes in the structure of the water column coinciding with the rapid near-bed temperature decline and subsequent period of depressed temperatures are unknown.

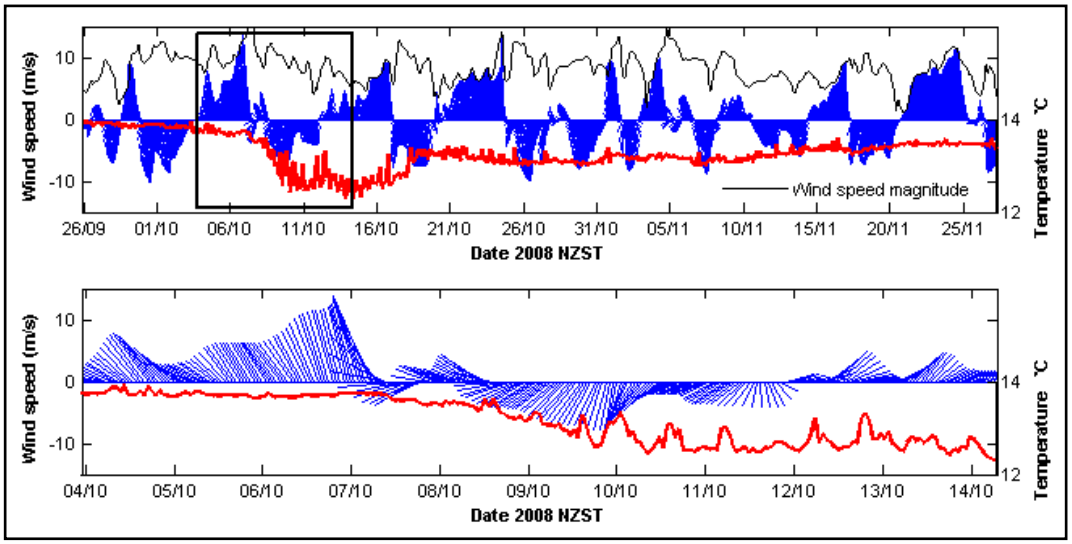

Figure 3.8 Top: near-bed temperature data recorded 26 Sept - Nov 27 2008 (red line and right-hand y-axis) and wind speed vectors and magnitude (black line and left-hand y-axis) for the corresponding period. Bottom: close-up of period outlined by black box in the top plot.

2010 Survey Period

In April 2010, a series of surveys were undertaken each of which included CTD casts to assess the hydrologic and structural properties of the water column on each day. To examine the late summer/early autumn period as a whole, the four casts recorded in April (on the 10th, 15th, 21st, and 25th) are presented below (Figure 3.9b-e) alongside a CTD cast recorded just before the April 2010 survey period on March 20 (Figure 3.9a). The April casts included in Figure 3.9 comprised the mean April temperature profile described in the previous section (Figure 3.7b).

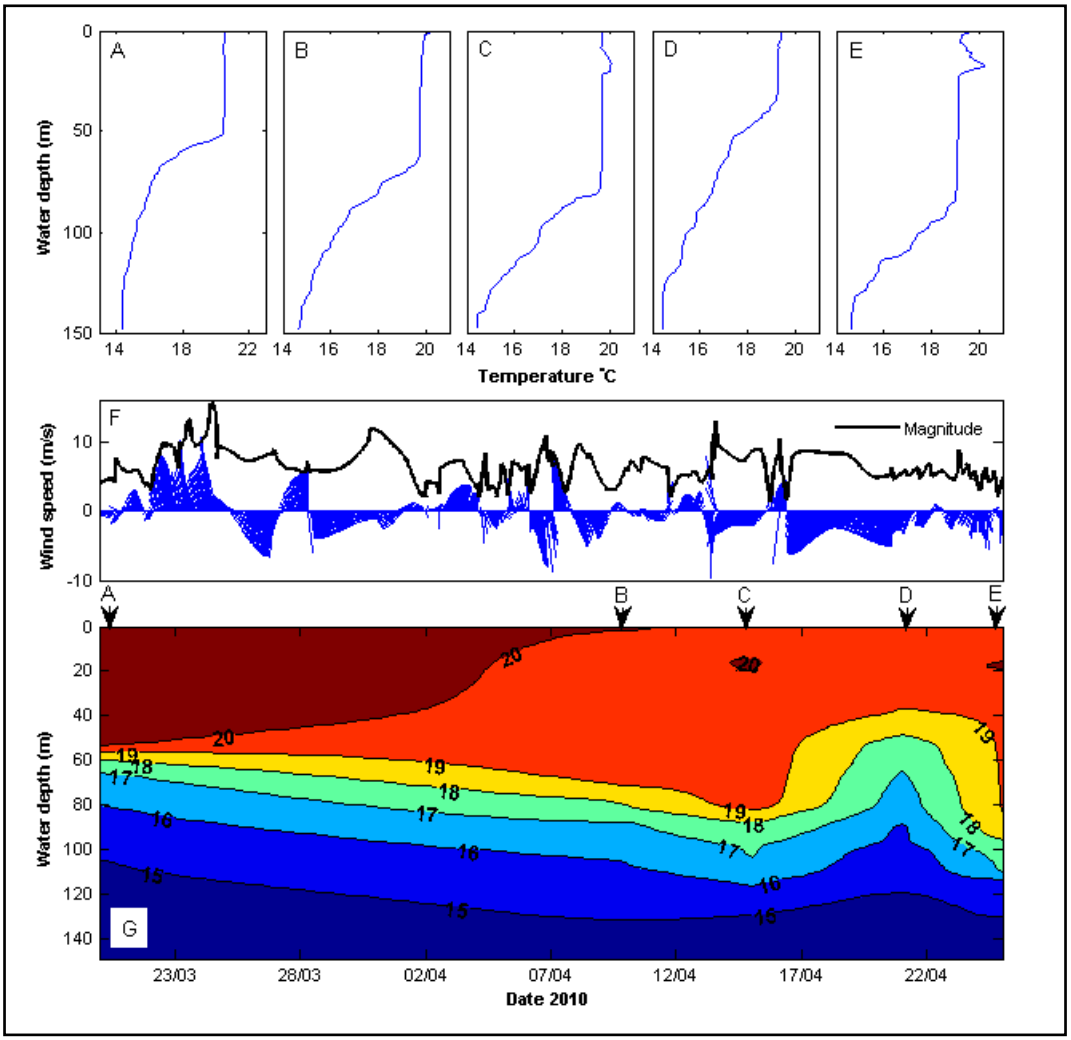

Figure 3.9 Temperature profiles from CTD casts recorded on A) 20 Mar, B) 10 Apr, C) 15 Apr, D) 21 Apr, and E) 25 Apr 2010 at the AMDG. F) Wind speed vectors and magnitude (black line) for the corresponding period. G) Seasonal isotherms derived from combined and interpolated temperature profiles (A-E; positions labelled at the top of plot).

A thermocline was present in the profiles of all five casts above which the temperature was constant to the surface. Small interruptions in the mixed surface layer where the temperature increased slightly at approximately 20 m below the surface are evident in the profiles recorded on April 15 and 25 (Figure 3.9c&e). The temperature change was most pronounced on April 25 with a maximum increase of approximately 1.5°C. Density and salinity profiles corresponding to the four April CTD casts shown in Figure 3.9 are plotted in Figure 3.10. Interruptions in both the density and salinity surface mixed layers corresponding to those in the temperature profiles can be seen (Figure 3.10b&f; d&h). The spikes in the profiles of April 25 occur over 5 m with the maximum/minimum end the ranges for temperature, density, and salinity occurring over just 0.6 m, the equivalent of 3 data points. Slightly surface-ward of the low density/low salinity data spikes in the profiles from April 15 and 25 are narrow regions where the

records deviate slightly in the opposite direction away from the mixed layer norm (i.e. higher density/higher salinity). These changes are much less pronounced than those immediately below them, but are still notable. In both cases, the corresponding temperature records are warmer than the mixed layer norm.

These observations indicate that on April 15 and April 25, the CTD cast profiled a narrow band of warmer, denser, and more saline water overlying a slightly thicker layer of warmer, less dense, and less saline water. Both layers were positioned between 15 and 20 m below the surface within the surface mixed layer which was present on all four survey days.

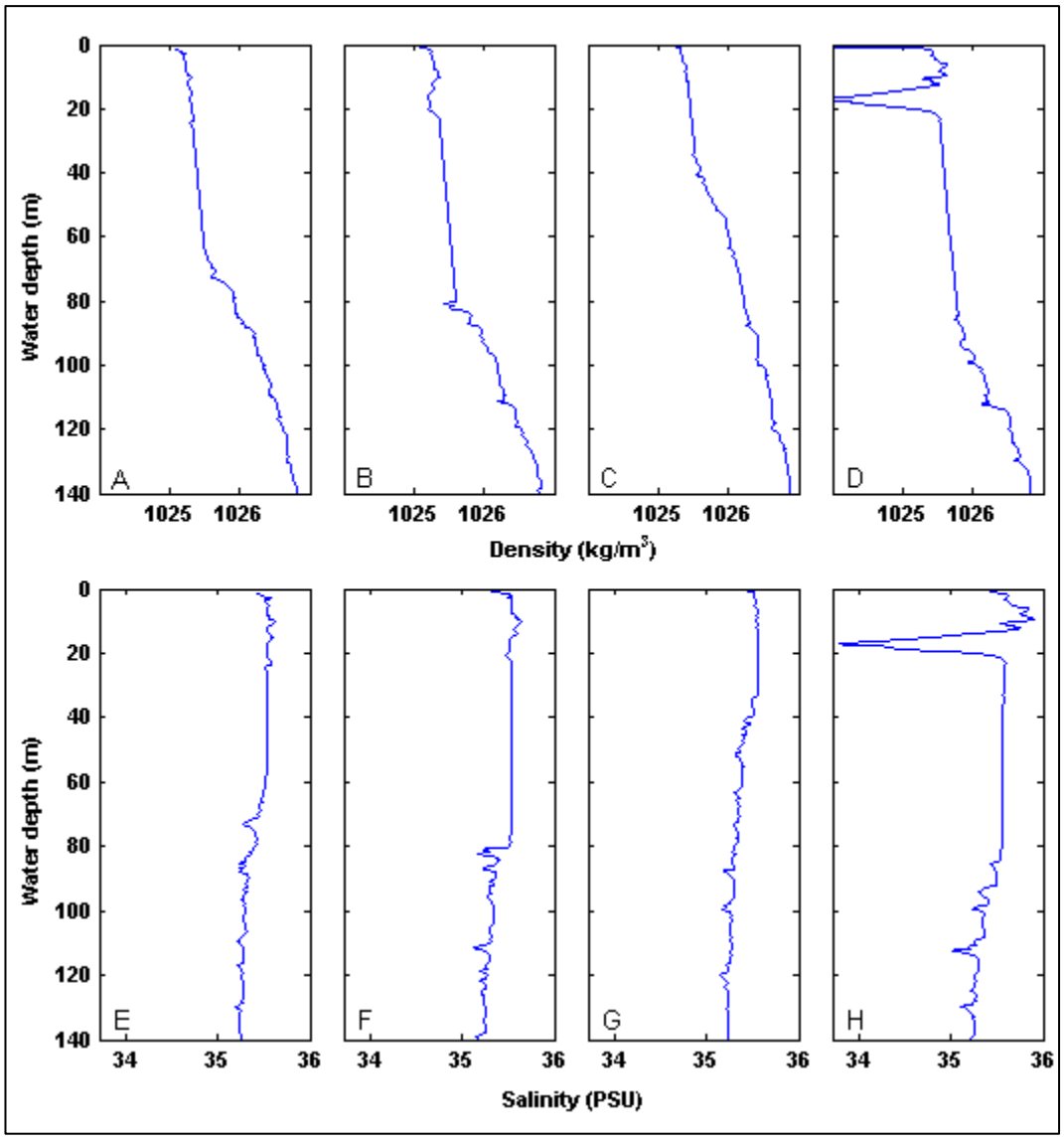

Figure 3.10 Density and salinity profiles from CTD casts recorded on A&E) 10 Apr, B&F) 15 Apr, C&G) 21 Apr, and D&H) 25 Apr 2010 at the AMDG.

Aside from the perturbations described above, temperatures were relatively constant in April following a slight decrease in the surface temperature from

20.4°C in March to just less than 20°C in April with bed temperatures remaining at approximately 14.5°C throughout the period (Figure 3.9a-e). However, the depth of the thermocline, and thus the structure of the water column, was variable in this period. Starting on 20 March, the thermocline was situated at approximately 60 m water depth. Three weeks later on 10 April, the thermocline had deepened by 10 m, reaching 70 m water depth. Just five days later, it had deepened by a further 10 m, reaching 80 m water depth on 15 April. However, six days after that on 21 April, the depth of the mixed layer had decreased by approximately 50 m so that the thermocline was situated only 30 m below the surface. At the end of the study period on 25 April, the typical seasonal structure had been re-established and the thermocline was again observed at 80 m water depth. Figure 3.9g illustrates the thermocline fluctuations during the 2010 study period through interpolation of the five temperatures profiles and derivation of the isotherm structure.

3.6.3 Discussion

Seasonal temperature and water column structure patterns at the AMDG were constructed from data collected over two years for the period between late March and late November. The derived seasonal thermal structure appears to correspond well with that reported by Garner (1961) for shelf waters east of Great Barrier Island in similar months. The data can therefore be regarded as representative of generic seasonal patterns at the AMDG.

The constructed period, though not inclusive of a summer period, implies that which has been reported in other studies along the northeast coast: stratification which becomes fully developed in February and March with surface and bed temperatures ranging from 20°C - 22°C and 14°C - 16°C, respectively (Garner, 1961; Harris, 1985; Longdill, 2007; Sutton & Roemmich, 2001). The onset of autumn conditions are characterised by cooling and a deepening of the thermocline until conditions become fully mixed in the winter months. Winter water column temperatures are correlated to latitude, so that temperatures at the AMDG appear to be somewhat warmer than that within the Bay of Plenty to the south (~14°C) (Longdill, 2007), but somewhat cooler than the northern Hauraki Gulf shelf waters (~16°C) (Harris, 1985). This correlation was also reported by Sutton and Roemmich (2001) for areas north of New Zealand. At the AMDG,

warming in the surface waters and re-development of the thermocline was observed in the end of November; however, it is possible that this process may actually begin somewhat earlier as evidenced by Longdill (2007) and Harris (1985) in shelf waters to the south and north, respectively.

The patterns described above are generally considered to be driven by regular seasonal climate variation related to incident solar radiation (Harris, 1985). These patterns may vary inter-annually by means of ENSO climate patterns, such that El Niño conditions bring on cooler temperatures and La Niña conditions tend to bring on warmer temperatures, but in general the seasonal patterns remain fairly steady year to year. Shorter term temperature and water column structure variability can, however, occur sporadically as a result of wind patterns. For instance, the warm sub-tropical waters of the EAUC which typically flow south/southeast along the continental slope of the northeast coast under prolonged easterly wind conditions can migrate westward into the surface waters of the shelf causing the water temperature there to increase for a time (Sharples, 1997). Similarly, offshore winds (west/northwest) have been shown to cause up-welling along the coast bringing cooler near-bed water to the surface in response the offshore movement of the warmer surface water (Longdill et al., 2008; Sharples & Greig, 1998; Zeldis, 2004). It should be noted though that even though these events can be regarded as short-term, ENSO climate patterns can influence their occurrence by increasing or decreasing the persistence of south-westerly (El Niño) or northern quadrant (La Niña) winds.

Neither up-welling nor EAUC surface intrusion appear to have occurred in full extent during the 2008 study period, but there is evidence of other short-term changes in the temperature profile at the AMDG that cannot be completely explained by seasonal climate variability. During the 2008 study period there was an abrupt decrease in temperature near the bed that lasted 10 days in the middle of October, a month when continued cooling would not normally be expected. One possible explanation can be suggested by considering the local wind climate. The four days prior to the decline in temperature near the bed were characterised by prolonged north-westerly winds followed by somewhat weaker westerlies, and then a settled period (Figure 3.8). It is possible that these ‘up-welling-favourable’ conditions may have initiated offshore flow of the surface waters sufficiently to

induce at least a weak near-bed counter flow of cool water from offshore that may or may not have resulted in a small up-welling event closer to the coast. At its position on the shelf, fully up-welled water would not often be expected at the AMDG, but counter-flow may explain the decrease in near-bed temperature for the period following the prolonged north-westerlies. The settled period following the north-westerly pulse are likely to have left inertial motions unobstructed, which may explain the duration of the depressed near-bed temperatures well after the up-welling-favourable conditions had ceased.

The 2010 study period occurred during autumn when a gradual deepening of the thermocline would normally be expected leading into fully-mixed winter conditions. Indeed, this effect appeared to have been taking place starting at least in the end of March and throughout the majority of April. The coinciding wind climate was characterised as weak in intensity and variable in origin, as is common for autumn conditions (Figure 3.9f). However, starting on 16 April a period of relatively strong winds from the south occurred which lasted until 21 April. On the same day, the thermocline was recorded at only 30 m water depth as opposed to 80 m only 6 days prior. Mixing in the upper water column resulting from the strong wind pulse was likely the cause of the thermocline rise. Following cessation of the wind pulse, no more than four days passed before the thermocline had re-established at 80 m as evidenced by the temperature profile recorded on 25 April (Figure 3.9e-g).

Superimposed on the normal thermocline fluctuations of the season, however, were several other notable features. Near surface temperature, density and salinity data spikes, both above and below the surface mixed layer norm recorded on two of the four April 2010 survey days suggest the possible influence of other processes (Figure 3.9 and Figure 3.10). Surface intrusion of the EAUC over the shelf, would be expressed in hydrologic terms as the presence of warmer, denser, and more saline water as the boundary current is sub-tropical (warmer) and oceanic (denser and more saline) (de Lange et al., 2003; Sharples, 1997). The narrow layer of water with the same hydrological properties comprising the surface-ward component of the data spikes on April 15 and 25 may be explained as such; however, the evidence is not strong as it is only 1-2 m in thickness (Figure 3.9c&e and Figure 3.10b&f; d&h). One would expect a more vertically

continuous increase in temperature, at least to the depth of the mixed layer, and persistent north-easterly or easterly winds which were not observed in this period (Figure 3.9f). Furthermore, the deeper slightly thicker layer of warmer, *less* dense, and *less* saline water certainly cannot be explained as EAUC intrusion.

More likely, the lower component of the data spikes represent a transient pulse of water which originated from the hopper, in which portions, especially in the case of the cast on April 25, may even be spurious (e.g. the 3 data points comprising the extreme end of the range of the records that deviated from the mixed layer norm). Hydrological properties of near-shore Auckland areas tend to be warmer due to water depth, as well as less dense and less saline due to coastal input of freshwater run-off (Loomb & Healy, 2000; Oldman et al., 2004). Water incorporated in the material dredged from Pine Harbour Marina would be expected to have properties characteristic of near-shore areas, which therefore could explain at least the lower portion of the data spikes observed with the surface mixed layer on April 15 and 25 (Figure 3.9c&e and Figure 3.10b&f; d&h).

It should be noted, however, that if the parcels of water comprising the spikes in the profiles on those two days were in fact originating from the hopper, the elevated turbidity that could be expected to be associated with them would normally cause an increase in density, whereas in these cases, the density in the lower portion of the data spikes were lower than the norm. This is most likely due to the fact that density derived from the CTD records is not a direct measurement, but calculated from the temperature, salinity, and pressure measurements, so suspended sediment would not be represented. For a back-of-the-envelope confirmation, the minimum density recorded on April 25 within the near surface data spikes was approximately 1024 kg/m^3. For neutrally buoyant or negatively buoyant conditions that would be expected from turbid water, the actual density would have to be at least equal to the ambient density (~1026 kg/m^3) which corresponds to an excess mass of sediment per cubic metre of 2 kg or 2 g/l. Although this seems reasonable for a turbid plume, in actual fact, the CTD casts were recorded after the surface plume was no longer visible, so a suspended sediment concentration (SSC) as high as 2 g/l would not be expected. The same rationale applied to the spike observed in the profile from April 15 does seem

more feasible however. The spike in that case could be associated with a suspended sediment concentration of approximately 0.5 g/l which is entirely possible as a transient plume remnant not visible from the surface. Possibly, some large floating debris associated with the load of disposed material contributed to the scale of data spike observed on April 25.

3.7 ADP and S4 Derived Tidal Current Observations

Tides can be regarded as an important underlying forcing mechanism present in the world's oceans. Their influence varies in time and space, but in a regular and highly predictable way. Described in the following sections, is a detailed assessment of tidal currents at the AMDG which was undertaken in order to better understand the tidal motions and determine their contribution to sediment dispersion at the site.

3.7.1 Data Processing

Hourly current data recorded by an ADP and a S4 deployed at the AMDG were analysed using the T_TIDE tidal harmonic analysis package (Pawlowicz et al., 2002) in the MATLAB® environment. Using these programs, the tidal signal was predicted as the sum of a finite set of sinusoids set at specific frequencies which are related to the astronomical motions that influence the tides. Derived parameters include the amplitude, phase, and confidence interval for each constituent which allows for robust interpretation of the results (Pawlowicz et al., 2002). Non-tidal (residual) currents were also derived in this process by removing the predicted tidal signal from the raw data.

3.7.2 Results

At the AMDG, the tidal current magnitude was at a maximum at 19 cm/s and an average of 6 cm/s for the deployment period. The maximum tidal current amplitude was 16 cm/s in the cross-shore direction, and 11 cm/s in the alongshore direction (Figure 3.11 and Figure 3.12). Cross-shore tidal currents diminished in amplitude with depth, with maximum near-surface and near-bed velocities of 16 and 8 cm/s, respectively. In the alongshore direction, tidal currents were generally more consistent with depth though slower compared to cross-shore tidal currents.

However, between the depths of 115 – 131 m, the average alongshore tidal current was on the order of 2 cm/s greater than near-surface alongshore tidal currents.

In the cross-shore direction, the tidal component of the data record ranged from 25 % – 65 %, with the maximum and minimum tidal contribution occurring at 60 and 20 m below the surface, respectively (Figure 3.13). In the alongshore direction, the tidal component was somewhat lower with minimum and maximum contributions of 4 % and 25 %, occurring at 20 and 80 m below the surface, respectively.

The tidal form factor ranged from 0.25 – 0.5 through the water column indicating the dominance of the semi-diurnal tides at the AMDG (Figure 3.13) though diurnal tidal constituents were also influential at a statistically significant (95 %) level (Table 3.4 and Figure 3.15). The important semi-diurnal constituents included the M_2, S_2, and N_2 (principle lunar, principle solar, and lunar ellipse), but only the M_2 was significant throughout the water column (Table 3.4). The important diurnal constituents included the K_1 and O_1 (principle lunar-solar and principle lunar), and likewise, only the K_1 was significant throughout the water column (Table 3.4). The M_m (monthly lunar) tidal constituent also appears to have had an important influence at mid-water column depths during the measurement period (Table 3.4).

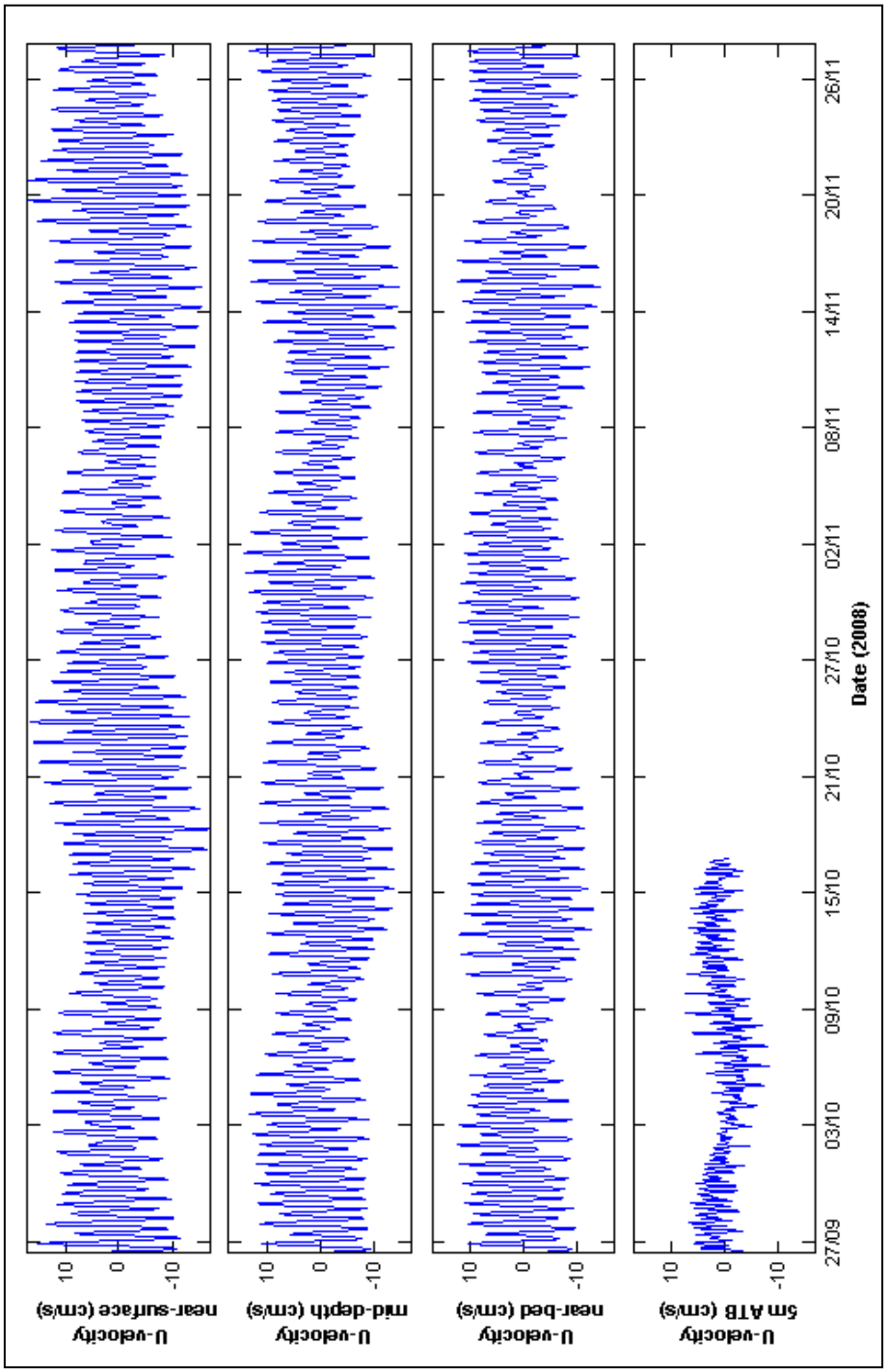

Figure 3.11 Tidally influenced cross-shore (u) velocities (cm/s) at the AMDG from a 63 day ADP record and a 20 S4 record. Velocities were rotated relative to true north to align approximately with the local bathymetry. ADP bins have been averaged over the near-surface (19-43 m depth), mid-depth (43-115 m depth), and near-bed (115-131 m depth) and the S4 data was recorded 5 m ATB.

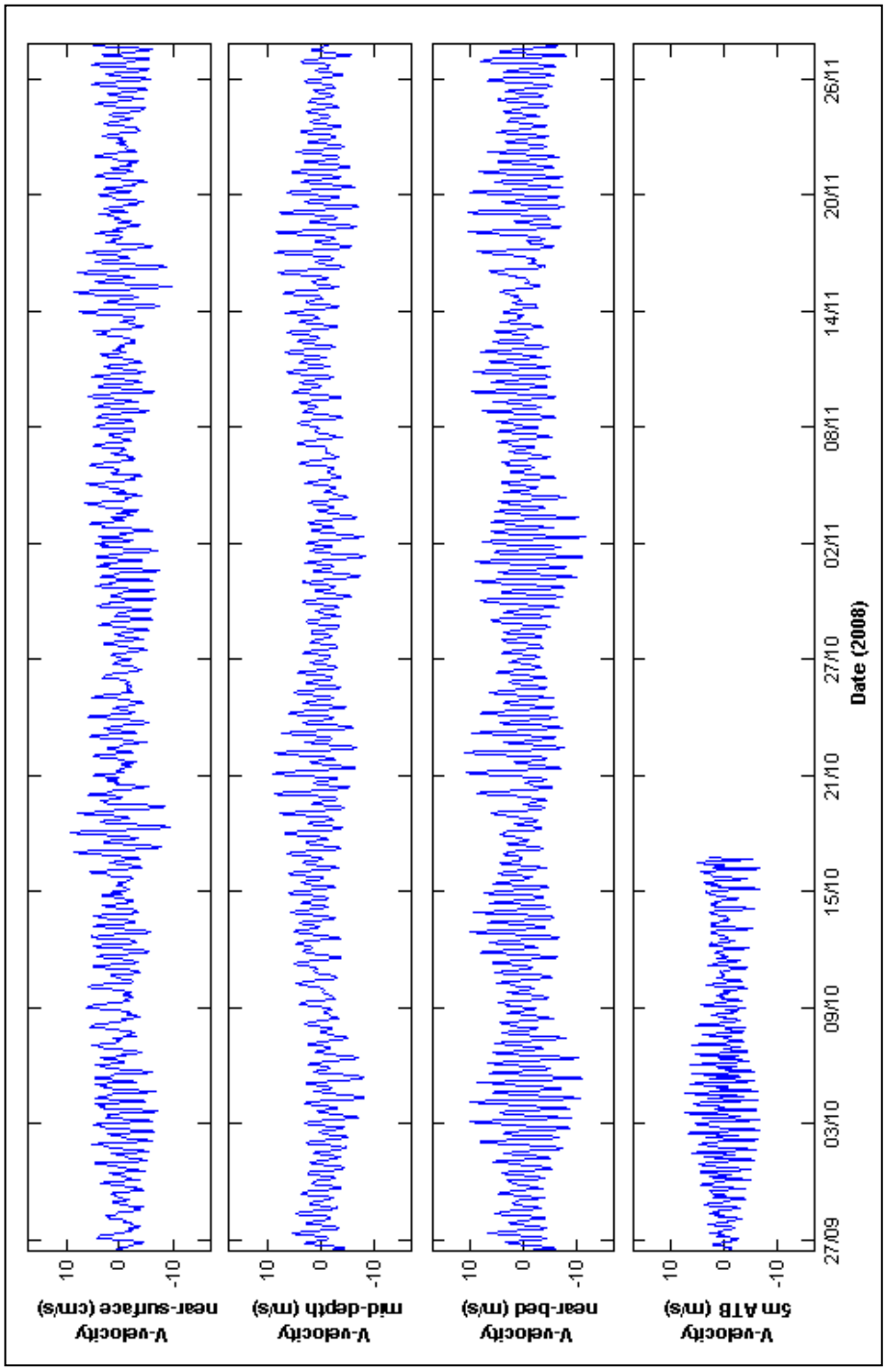

Figure 3.12 Tidally influenced along-shore (v) velocities (cm/s) at the AMDG from a 63 day ADP record and a 20 S4 record. Velocities were rotated relative to true north to align approximately with the local bathymetry. ADP bins have been averaged over the near-surface (19-43 m depth), mid-depth (43-115 m depth), and near-bed (115-131 m depth) and the S4 data was recorded 5 m ATB.

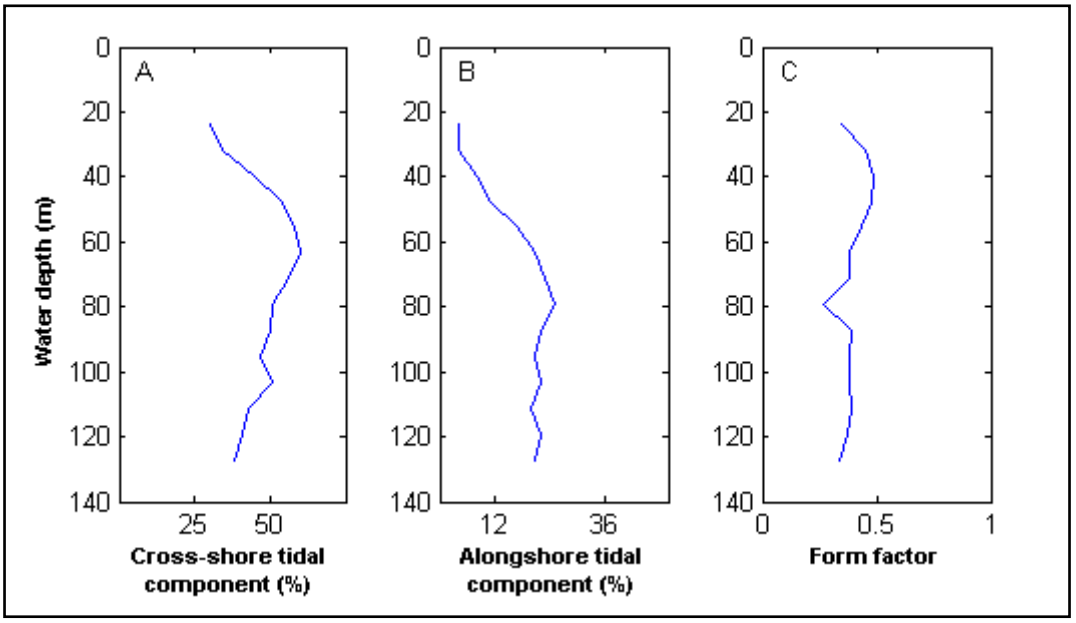

Figure 3.13 Profiles of (a) percent cross-shore tidal component, (b) percent alongshore tidal component, and (c) form factor at the AMDG from the 63 day ADP record. Profiles based each 8 m bin of non-corrupt ADP data.

The dominant constituent, with a major-axis amplitude of approximately 8 cm/s, was the M_2 (Table 3.4; Figure 3.14; Figure 3.15). The K_1 and M_m tidal constituents had major-axis amplitudes ranging from 2 – 3 cm/s and those of the O_1, N_2 and S_2 were between 1 and 2 cm/s. The M_m, N_2, and S_2 displayed some vertical variation in the major axis amplitude, with higher velocities at mid-depth, near-surface and near-bed, respectively. Others showed little or no variation in amplitude with depth. All ellipses were oriented approximately normal to the local bathymetry (E-W) and all but the M_2 rotated in the anti-clockwise direction. Notably, the orientation angle of the M_2 decreased while the phase angle increased with depth. The other constituents generally displayed either similar or retarded phases with depth.

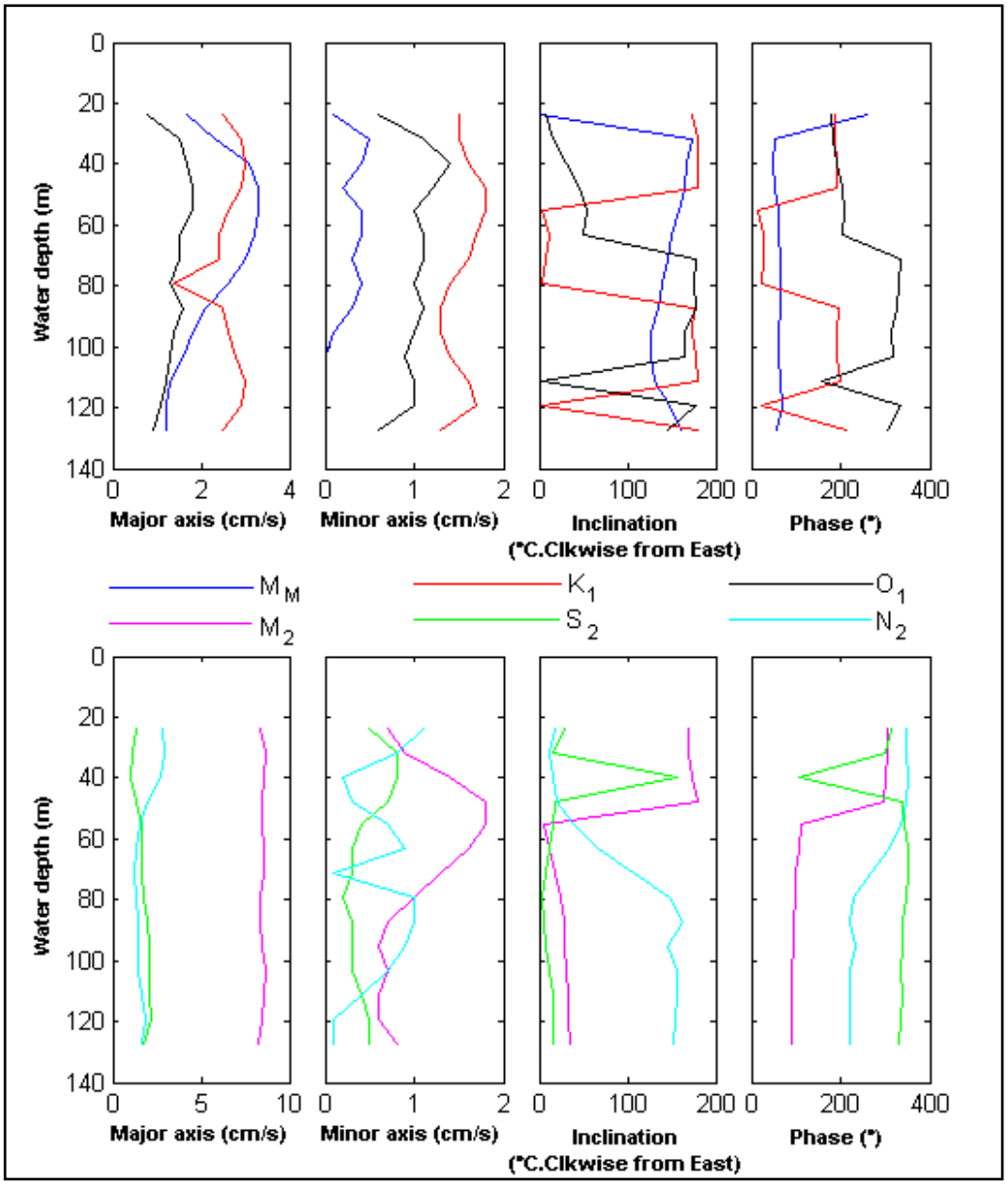

Figure 3.14 Profiles of tidal ellipse parameters for the M_m (blue), K_1 (red), O_1 (black), M_2 (magenta), S_2 (green), and N_2 (cyan) tidal constituents at the AMDG from the 63 day ADP record. Profiles based each 8 m bin of non-corrupt ADP data.

Table 3.4 Monthly (M_M), diurnal (K_1, O_1), and semi-diurnal (M_2, S_2, N_2) tidal ellipse parameters from the long-term ADP and S4 current meter deployments. Semi-major and semi-minor axis amplitudes are in cm/s. Inclination is in degrees counter-clockwise from east. Phase is in degrees relative to equilibrium tide at Greenwich. The 14 bins of usable ADP data correspond to water depths 24 – 128 m (mid-bin depth) and S4 data correspond to 135 m. (DA) is the ellipse parameters for the depth-averaged tidal currents. Significant constituents (95% level) are marked with a (*). Where the record was too short to separate the constituent a (-) is shown.

Water depth	M_m				K_1				O_1				M_2				S_2				N_2			
	Major	Minor	Inc	Phase	Major	Minor	Inc	Phase	Major	Minor	Inc	Phase	Major	Minor	Inc	Phase	Major	Minor	Inc	Phase	Major	Minor	Inc	Phase
24	1.7	0.1	1.23	261	*2.5	1.5	174	187	0.8	0.6	8	177	*8.3	0.7	169	307	1.3	0.5	29	312	2.8	1.1	19	348
32	2.3	0.5	173	51	*2.9	1.5	179	189	1.5	1.1	15	185	*8.7	0.9	170	307	1.1	0.8	16	303	2.9	0.8	12	347
40	*3.1	0.4	168	47	*3	1.6	180	192	*1.7	1.4	30	192	*8.6	1.4	174	303	1	0.8	157	107	2.7	0.2	16	352
48	*3.3	0.2	165	53	*2.9	1.8	179	192	*1.8	1.2	46	203	*8.5	1.8	179	297	1.3	0.7	18	338	*2	0.3	21	348
56	*3.3	0.4	158	61	*2.6	1.8	4	13	*1.8	1	54	208	*8.5	1.8	6	110	*1.6	0.4	16	344	*1.5	0.7	39	334
64	*3.2	0.4	151	62	*2.4	1.7	12	26	*1.5	1.1	50	205	*8.6	1.6	12	106	*1.7	0.3	12	350	*1.3	0.9	66	308
72	*3	0.3	145	64	*2.4	1.6	8	26	1.5	1.1	178	335	*8.6	1.3	18	101	*1.7	0.3	8	353	*1.2	0.1	107	266
80	*2.6	0.4	139	67	*1.4	1.4	3	22	1.3	1	176	330	*8.4	1	24	98	*1.8	0.2	3	346	1.3	1	147	230
88	*2.1	0.3	135	67	*2.5	1.3	176	194	1.6	1.1	177	326	*8.4	0.7	28	96	*2	0.3	5	338	1.4	1	162	219
96	*1.8	0.1	127	63	*2.6	1.3	174	190	1.4	1	165	313	*8.5	0.6	29	93	2.1	0.3	7	337	1.4	0.9	146	233
104	*1.6	0	126	59	*2.8	1.4	177	193	*1.3	0.9	165	316	*8.7	0.7	31	92	*2.1	0.3	12	336	1.4	0.7	156	221
112	1.3	0	130	65	*3	1.6	180	198	*1.2	1	4	159	*8.6	0.6	32	92	2.1	0.4	15	337	1.7	0.4	156	221
120	1.2	0	148	68	*2.9	1.7	3	24	*1.1	1	177	334	*8.5	0.6	34	91	2.2	0.5	16	335	1.9	0.1	155	221
128	1.2	0	161	57	*2.5	1.3	179	211	*0.9	0.6	146	304	*8.2	0.8	35	89	1.8	0.5	17	331	1.7	0.1	152	220
135	-	-	-	-	0.5	0.1	4	6	1	0.2	157	168	*2.8	1.3	91	265	1.5	0.4	141	0.55	-	-	-	-
DA	*2.1	0.1	153	33	*2.7	1.5	180	196	*1.3	1.1	13	169	*8	1.5	17	103	*1.7	0.4	14	336	*1.6	0.6	7	6

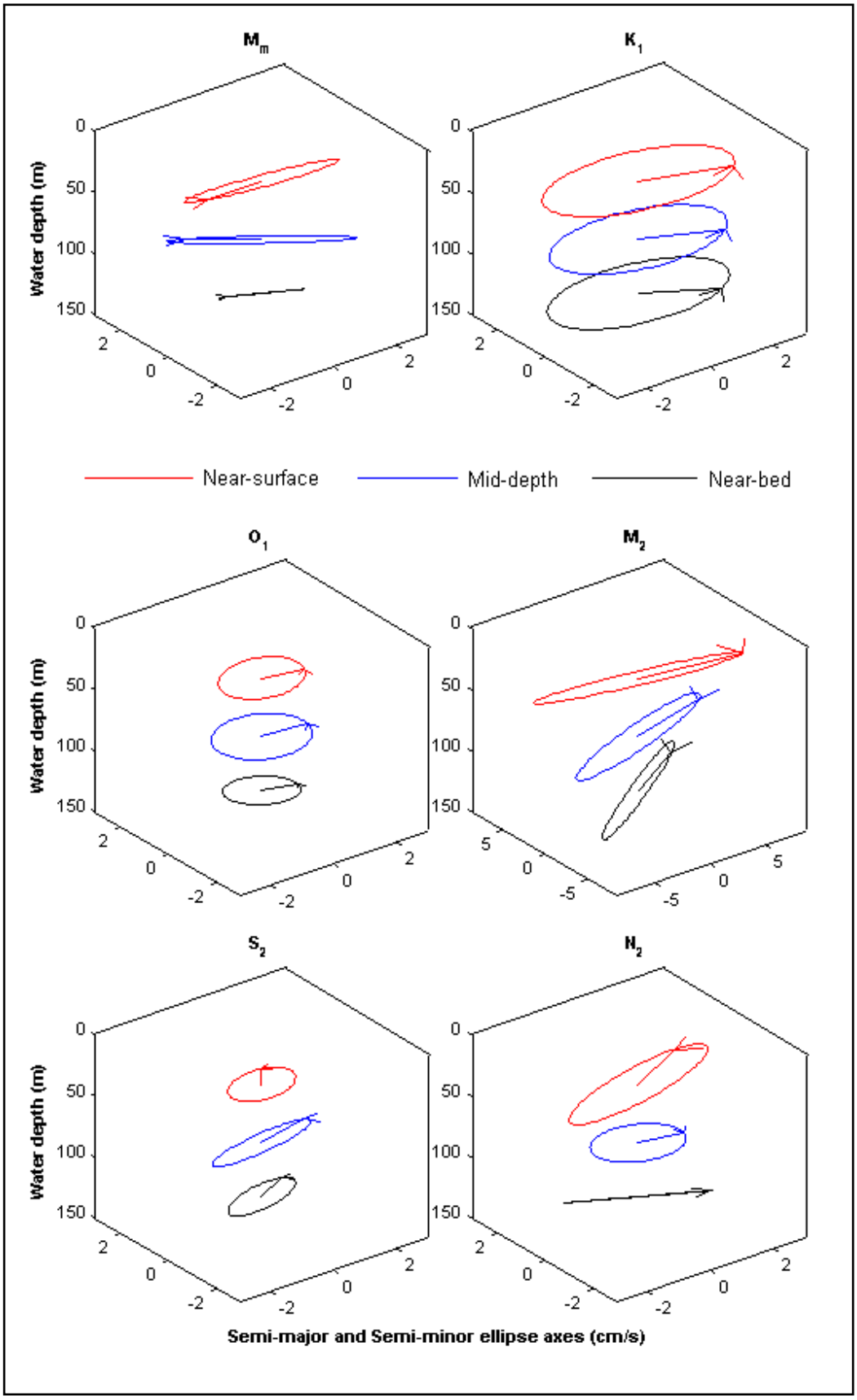

Figure 3.15 M_M, K_1, O_1, M_2, S_2, and N_2 tidal ellipses from the AMDG based on the predicted tidal signal of the 2008 ADP deployment. Red, blue, and black ellipses represent the tidal signal averaged from 19-43 m, 43-115 m, and 115-131 m water depth, respectively. Note the different x and y scales for the M_2 ellipses.

Internal tides

Interactions of the barotropic tide with the bathymetry in shelf break and slope regions can cause vertical perturbations in the structure of the water column which may initiate the on- or off-shelf flow of internal tidal period waves known as an internal or baroclinic tide (Sharples et al., 2001). Internal tides can influence the variance of the tidal current amplitude substantially depending on proximity to the location of generation (Heath, 1984). Previous studies have shown internal tides to play a role in mixing of nutrients across the pycnocline (Holligan et al., 1985; Sharples et al., 2001) and have been suggested as a possible source of enhanced sediment transport (Heath, 1984).

Evidence of internal tides has been documented from many locations around New Zealand's continental shelf including: west coast, South Island (Heath, 1984; Vennell & Moore, 1993); west coast, North Island (Stanton, 1977); Kermadec Ridge, northeast of the North Island (Chiswell & Moore, 1999); Chatham Rise, east of the South Island (Chiswell, 2000); and most notably on the northeast shelf c. 100 km north of the AMDG (Sharples & Greig, 1998; Sharples et al., 2001). The proximity of the AMDG to the location of the latter 2 studies suggests that internal tides may be present and at times influence sediment dispersion in much the same way that internal tides can enhance nutrient mixing.

A straightforward method for identifying internal tides is by examining time series of isotherm structure (Chiswell, 2000; Sharples et al., 2001; Stanton, 1977), but this requires instrument deployments beyond that which was possible in this study. One near-bed temperature time series the length of the long-term ADP deployment was recorded however. Spectral analysis of this record showed a strong semi-diurnal (M_2) signal and also significant variability of the shallow water harmonics M_4 and M_6 (Figure 3.16). This signature has been shown to be related to internal tide activity (Sharples & Greig, 1998).

Spectral analysis of cross-shore and along-shore currents (raw-surface, raw-near-bed, barotropic-only and baroclinic-only (derivation after Sharples et al, (2001))) support the dominance of the semi-diurnal M_2 signal and the presence of the shallow water harmonics observed in the temperature variability (Figure 3.16). It appears that there is also significant variance at the diurnal frequency (likely the

K_1 mainly) and also at the inertial frequency $2\pi/f$. These peaks were present in the raw records both near the surface and at near the bed (Figure 3.17). By splitting the raw currents into barotropic (depth-averaged) and baroclinic (raw with depth-averaged removed) components, it is apparent that the diurnal variability is limited to the barotropic component and the inertial and shallow water harmonic variances are only significant in the baroclinic component (Figure 3.17).

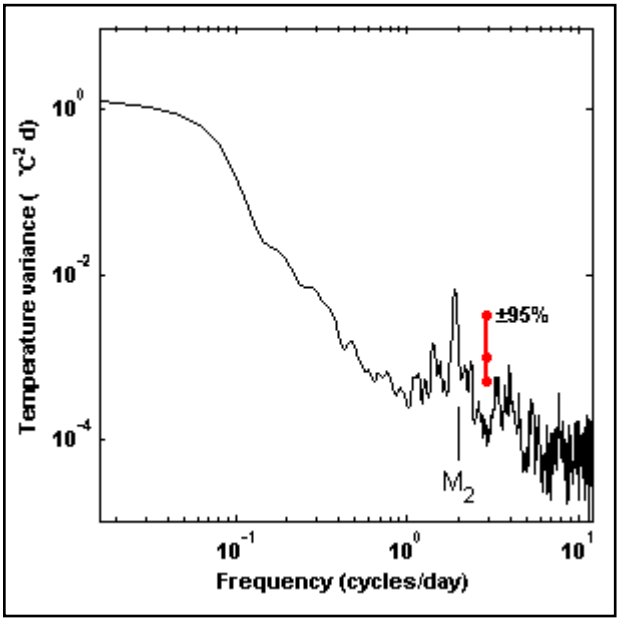

Figure 3.16 Variance in the temperature record at a depth of 135 m from the long-term ADP deployment location. The spectrum was averaged with a cosine bell filter, with 10 degrees of freedom.

Evidence of internal tides has also been identified through vertical variation of tidal ellipse parameters, specifically inclination and phase (e.g. Vennell and Moore, (1993) and Sharples et al, (2001)). Figure 3.14 shows vertical variation in inclination and phase in all the important constituents, however, only the M_2 and K_1 were significant at the 95% level throughout the water column. The mid-depth phase and inclination shift of the M_2 suggests a dominant first-mode internal wave, but that of the K_1 indicates the presence of higher-mode waves. Examination of the cross-shelf and along-shelf baroclinic-only currents show further evidence of 'typical' first-mode internal wave features in the M_2 ellipse at the AMDG, with current amplitudes at a maximum at the surface and near the bed and a phase change of approximately 180° at mid-depth in both the cross-shore and along-shore components (Figure 3.18).

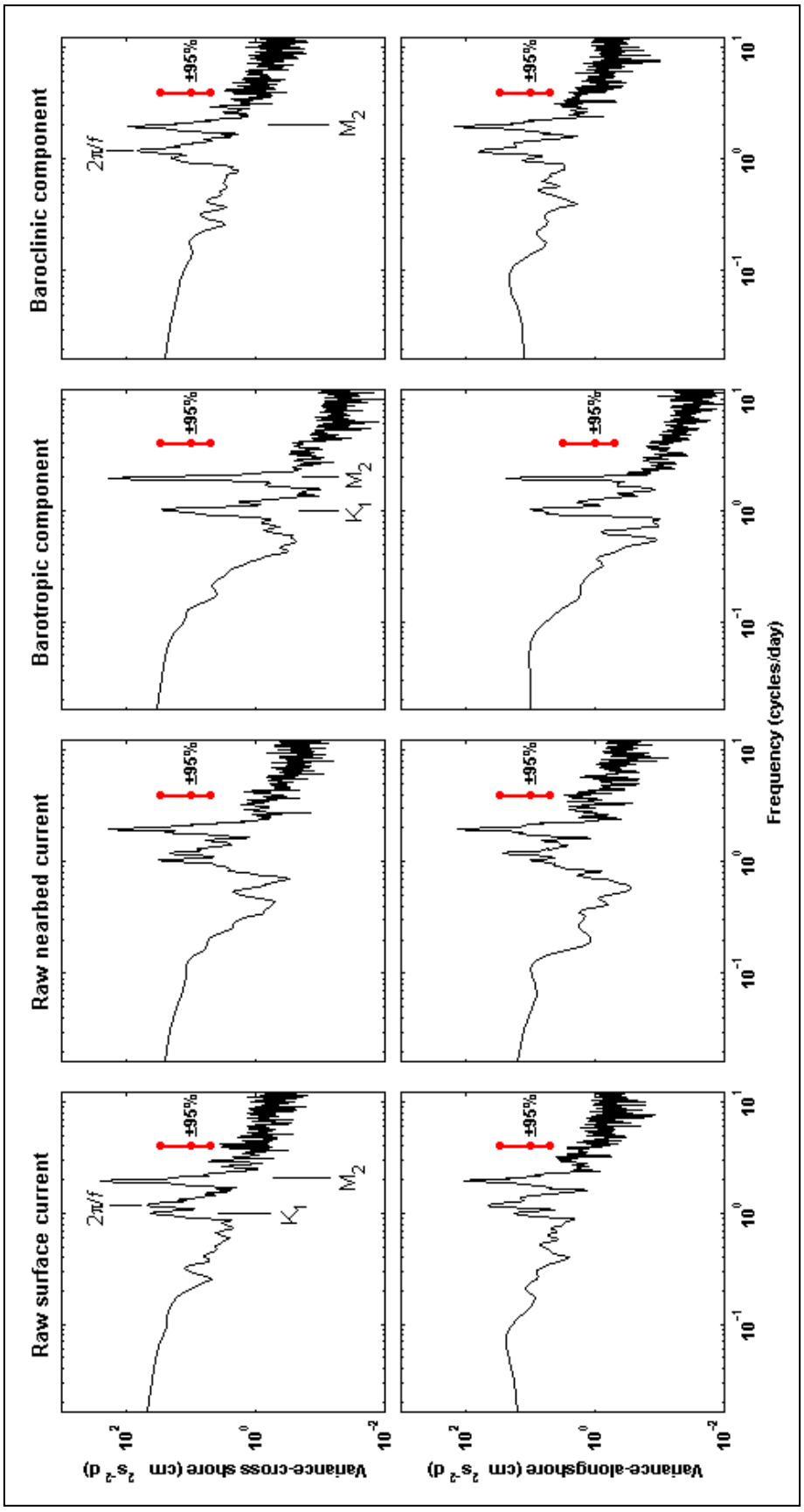

Figure 3.17 Variance of cross-shore and alongshore raw-surface, raw-near-bed, barotropic, and baroclinic currents at the ADP deployment location. The spectra were averaged with a cosine bell filter, with 10 degrees of freedom.

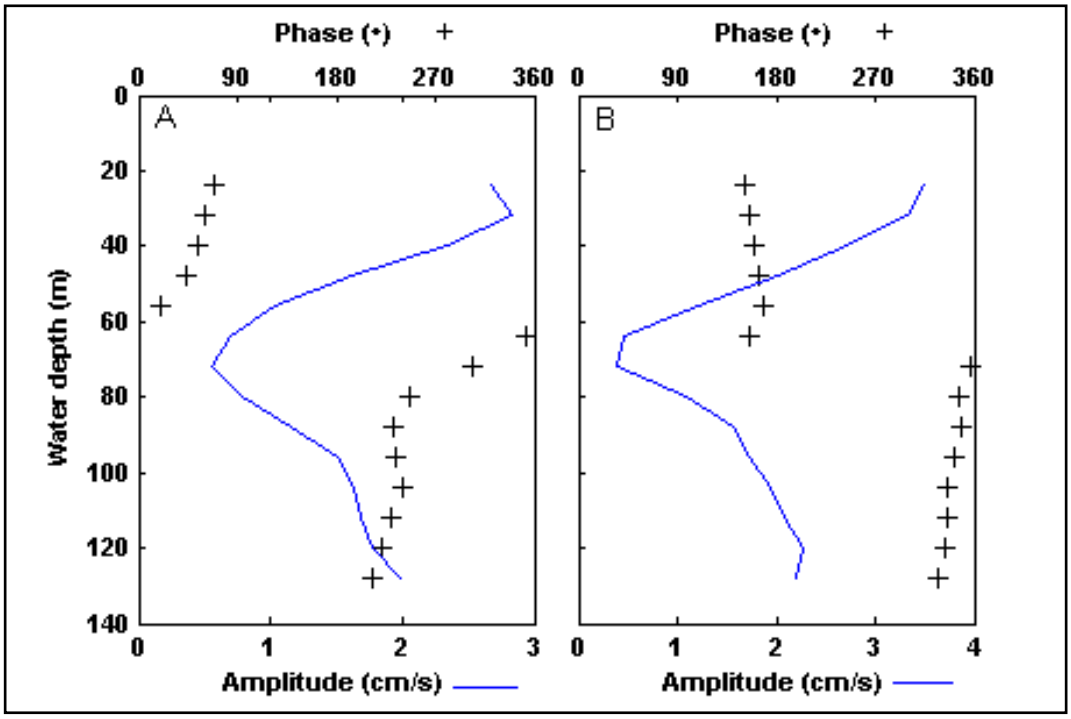

Figure 3.18 Baroclinic tide profiles of the M_2 tidal constituent for the period of the long-term ADP deployment. (a) Cross-shore baroclinic current amplitude and phase and (b) alongshore baroclinic amplitude and phase.

With a first-mode internal wave, higher current shear at mid-depths would be expected. To assess this, vertical current shear was calculated for the length of the long-term ADP deployment (calculation method following Sharples et al, (2001)). Figure 3.19b shows that higher current shear occurs at near-surface depths regularly throughout the deployment. Between 25/10 and 25/11, higher shear can be seen at the interior of the water column (approximately mid-depth) which appears to be only semi-attached to more regular near-surface shearing. There is also a hint of enhanced shear closer to the beginning of the deployment, but to a lesser extent than that later in the record. The wind record for this period does not indicate that exceptionally strong or prolonged winds were the source of the higher interior shear (Figure 3.19a). The near-bed temperature record showed rapid cooling accompanied by strong semi-diurnal periodicity for approximately 10 days prior to the period of high interior shear and was followed for the remainder of the deployment period by a more stable temperature approximately 1 degree cooler than that recorded at the start of the deployment (Figure 3.19c). It is important to note that the temperature record was recorded well below the height of the first ADP bin, so a direct comparison of the temperature record to the shear values was not possible.

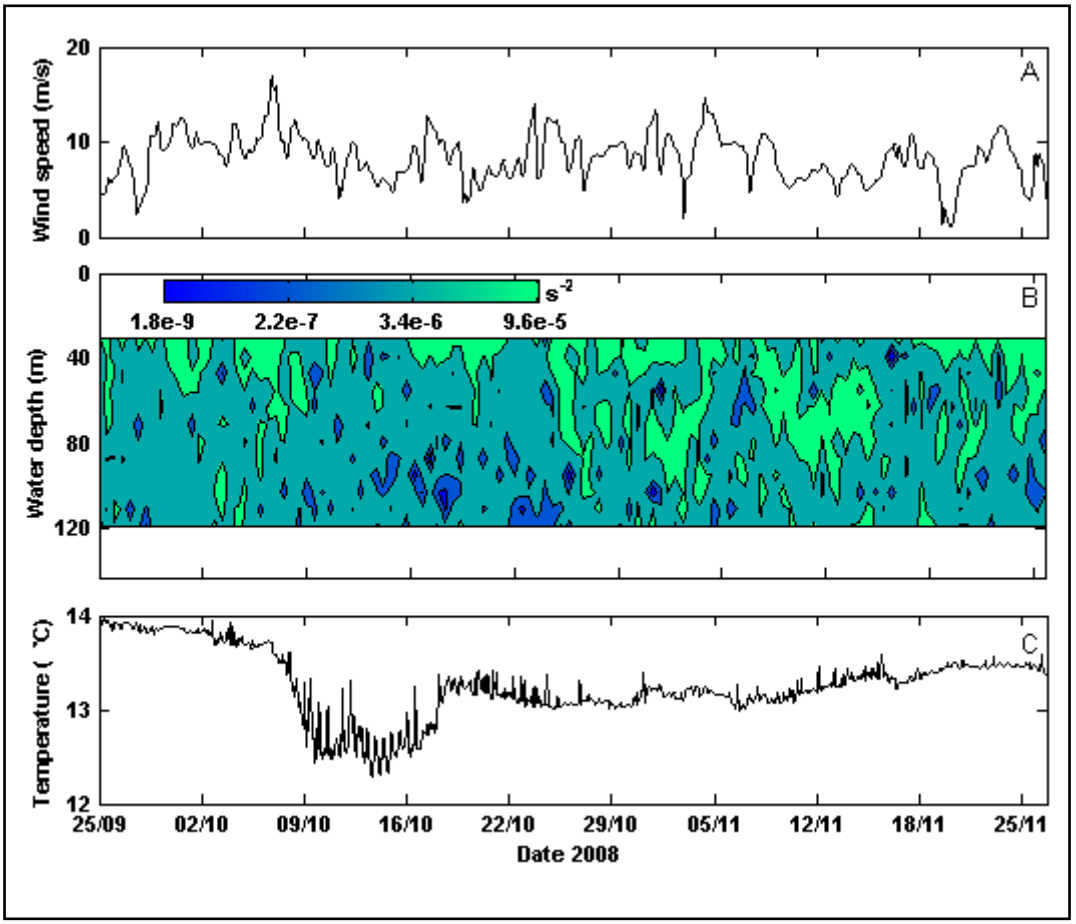

Figure 3.19 (a) Wind speed at the Blended SeaWinds node nearest the ADP deployment location. (b) Squared current shear (s^{-2}) for the long-term ADP deployment averaged over one tidal cycle window for the entire deployment. (c) Temperature record from a depth of 135 m over the same time period at the ADP deployment location.

3.7.3 Discussion: Tidal Forcing

Tidal currents at the AMDG were found to be similar to the range of 10 – 20 cm/s reported by Stanton et al (2001). Generally speaking, the cross-shore tidal signal was stronger than the alongshore signal (Figure 3.13). Constriction and shallowing through the Colville Channel southeast of the AMDG may contribute to the disparity (Figure 3.1). Predominant tidal constituents were similar to those reported by Stanton et al (2001) and Sharples and Greig (1998) for the New Zealand shelf and more specifically in the latter, the northeast shelf. The M_2 tide was observed to be the dominant constituent with a major-axis current amplitude very similar to that reported by Sharples and Greig (1998), however, at the AMDG the M_2 tidal ellipse was observed to be rotating clockwise which diverges from the generally accepted knowledge that it propagates anticlockwise as a coastally-trapped Kelvin wave (de Lange et al., 2003; Heath, 1985; Sharples, 1998; Stanton et al., 2001; Walters et al., 2001). It is possible that, at times,

propagation of the tidal wave in the area of the AMDG may follow a more localised propagation path around Great Barrier Island which varies from the principal anti-clockwise rotation around New Zealand's land mass. Strong phase differences at the entrances to the Hauraki Gulf (e.g. the Colville Channel (Figure 3.1)) which might result from a localised propagation path may also have contributed to the strong cross-shore tidal signals similar, though on a smaller scale, to the dynamics of the Cook Strait between the North and South Islands of New Zealand (Heath, 1985).

Other important semi-diurnal constituents were the S_2 and the N_2 which had very similar major-axis current amplitudes (1-2 cm/s) with significance limited mainly to mid-depths. This is somewhat surprising because typically the S_2 tidal energy is thought to be weak on the east coast due to a nearby amphidromic node leading to a greater tidal admittance discrepancy with other semi-diurnal constituents (Heath, 1985; Stanton et al., 2001; Walters et al., 2001). The diurnal K_1 tidal constituent imparted the second largest influence behind the M_2, with tidal current variability somewhat larger than that reported by Sharples and Greig (1998) for sites to the north and somewhat smaller than that reported by Longdill (2007) for sites to the south of the AMDG. The K_1 tidal admittance in the present case was stronger than that of the O_1 contrary to the findings of Longdill (2007) who reported similar amplitudes for the M_2, K_1, and O_1.

Another notable difference in tidal current features of the AMDG is the added influence of the M_m (monthly lunar) tidal constituent which has not been reported as significant by any other New Zealand studies. In the present case, 95% significance was mainly limited to mid-depth waters, but the current amplitude in general rivalled that of the K_1, with a depth-averaged major-axis current amplitude only 0.6 cm/s lower. It is possible that the influence of the M_m is more pronounced in deeper and more exposed shelf waters and indeed this theory is supported by review of long-period tides by Hendershott and Munk (1970) that suggests that long-period tidal signals tend to be insignificant in coastal areas possibly due to damping by continental shelf topography. As there have been no other studies including long-term ADP deployments at locations with similar characteristics to the AMDG on the northeast shelf, however, it is not possible to confirm this as a potential explanation.

Internal wave activity occurring during the ADP deployment at the AMDG was generally consistent with a weak first-mode semi-diurnal (M_2) tidal period wave. Additional variability at the shallow water harmonic periods and the inertial period suggest a steepening and breaking of the internal wave with additional input from vertical shearing and inertial oscillations. These findings are similar to that observed at a study site c. 100 km to the north (Sharples et al., 2001).

It should be noted that the shear values derived for this period and location were several orders of magnitude lower that reported by Sharples et al, (2001) for the area to the north of the AMDG, however, the range of values is comparable so it is still reasonable to suggest that the shearing patterns may have been influenced by internal tide activity. Internal tide energy is more pronounced closer to the generating area and may be quickly damped with movement away (Stanton, 1977). The shelf width in the region studied by Sharples et al, (2001) is significantly narrower than that at the AMDG and the study sites were considerably closer to shelf-break, so it is not unexpected that the magnitude of shearing related internal tide activity measured at the AMDG was significantly lower than that of the previous study to the north

3.8 Residual Current Observations

3.8.1 Data Processing: Current and Wind Records

Time series of residual currents recorded during the long-term ADP deployment were calculated by removing the tidal signal from the raw data through harmonic analysis (see Pawlowicz et al (2002)) followed by low-pass filtering (36 hour folding period e.g. Allen and Kundu (1978); Lentz and Winant (1986); and Dever (1997). These 'sub-inertial' currents were examined to identify flow features excluding the effects of tidal and inertial oscillations. However, lagged correlation analysis of the residual currents and local winds was undertaken using residual currents with only tidal oscillations removed because low-pass filtering can introduce a serial correlation which may result in erroneous correlations (Ebisuzaki, 1997).

Wind data retrieval and processing are described in Section 3.4.3. All wind and residual current data were oriented relative to true north and aligned

approximately with the local bathymetry. Positive cross-shore values (*x*,*u*) were directed east (offshore) and positive alongshore values (*y*,*v*) were directed north.

3.8.2 Features of the Residual Current Flow Field

During the long-term ADP deployment, currents were predominantly driven by non-tidal forcing as evident in Figure 3.13(a&b). Cross-shore flows possessed a slightly larger tidal component than those in the alongshore direction, but it is clear from Figure 3.20(b-d) that the trajectories of the raw currents versus currents with the tidal component removed are essentially the same. This indicates that the tidal currents did not have a significant impact on the net flow direction during the measurement period.

Maximum mean residual velocities of 4.3 cm/s and 5.2 cm/s were recorded at 48 m and 56 m below the surface in the cross-shore direction and alongshore directions, respectively (Table 3.5). Minimum mean residual velocities were measured from 136 m below the surface at 1.3 cm/s and 0.2 cm/s cross-shore and alongshore, respectively. Residual currents were predominantly directed towards the south and east (Figure 3.20a) which resulted in a net flow trajectory for the measurement period towards the southeast (Figure 3.20b-c). This pattern was evident throughout the water column, but at slightly larger magnitudes near the surface and at mid-depths, with a cumulative flow distance of 200, 190, and 111 m east; and 150, 177, and 45 m south near the surface, at mid-depths, and near the bed, respectively during the measurement period.

Instantaneous velocities showed the opposite pattern to the time-averaged velocities with a maximum in the cross-shore direction (17 cm/s) rather than in the alongshore direction (11 cm/s). Generally speaking, residual currents recorded during the measurement period were relatively consistent in speed and direction with respect to time, as well as in the velocity profile, with the cross-shore residual current directed east and the alongshore current was directed south (Table 3.5 and Figure 3.21a&b).

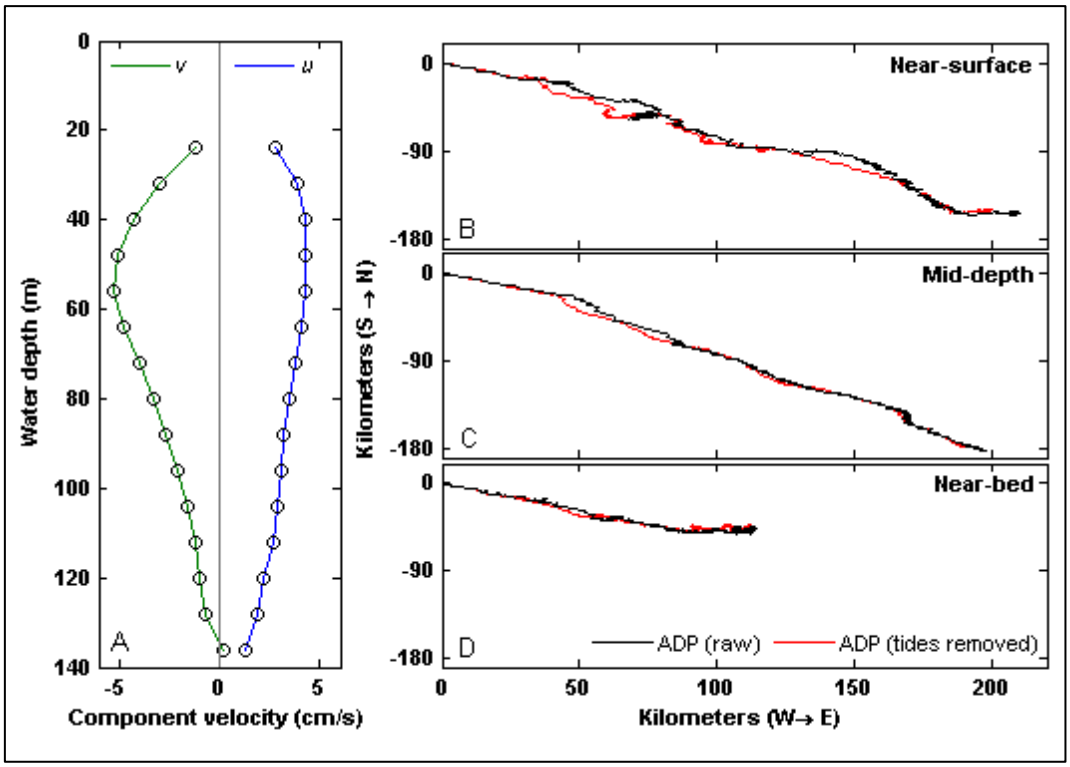

Figure 3.20 (a) Mean cross-shore (*u*, blue) and alongshore (*v*, green) sub-inertial currents (cm/s) for the period of 25 September - 27 November 2008; mid-depth of each ADP bin is indicated by open circles. (b - d) Progressive vector diagrams of depth-averaged (near-surface: 19 - 43 m; mid-depth: 43 - 115 m; near-bed: 115 - 131 m) raw (black) and tides-removed (red) currents for the same period as in (a).

Table 3.5 Statistics of sub-inertial cross-shore and alongshore velocities at the AMDG during the long term ADP deployment (25 September – 27 November 2008).

	Cross-shore (*u*, cm/s)		Alongshore (*v*, cm/s)	
Mid-depth bin (m)	**Mean**	**Std**	**Mean**	**Std**
24	2.78	4.39	-1.18	4.06
32	3.90	3.99	-2.96	3.63
40	4.30	3.53	-4.29	3.18
48	4.31	3.30	-5.10	2.86
56	4.23	3.23	-5.21	2.60
64	4.04	3.07	-4.71	2.45
72	3.81	2.99	-4.01	2.41
80	3.49	2.95	-3.29	2.47
88	3.19	2.84	-2.64	2.63
96	3.03	2.75	-2.04	2.79
104	2.88	2.79	-1.58	2.92
112	2.67	2.95	-1.22	3.02
120	2.23	2.91	-0.96	2.91
128	1.86	2.82	-0.73	2.72
136[+]	1.26	2.89	0.21	2.96
Depth avg.	3.27	2.04	-2.77	1.41

All record lengths 1498 h except [+](491 h)

A closer look at the temporally varying sub-inertial current flow fields reveals some degree of variability in the flow patterns (Figure 3.21a&b). Cross-shore sub-inertial currents were more vertically consistent with respect to direction than alongshore sub-inertial currents which often showed a weak flow reversal at depth. The predominantly eastwards flow of the cross-shore currents was interrupted by two periods of weak and short, but distinct westerly flow which was established throughout the water column (Figure 3.21a). The first period occurred between 3 and 5 October and notably the corresponding alongshore current maintained the predominant southwards flow (Figure 3.21b). The second period occurred not long after the first, between 11 and 15 October. Similar to the first period, the direction reversal was established throughout the water column and the corresponding alongshore currents did not exhibit a comparable reversal. Another notable feature occurred close to the end of the measurement period on 26 November. At that time, the cross-shore currents were directed towards the east as was common during the measurement period, but the corresponding alongshore currents were directed northwards rather than to the south. This event appears to have been initiated on approximately 24 November with the strongest pulse occurring on 26 November by which time the alongshore reversal was observed throughout the water column. After 26 November, it appears that the atypical flow pattern deteriorated and likely returned to the familiar east and south directed pairing.

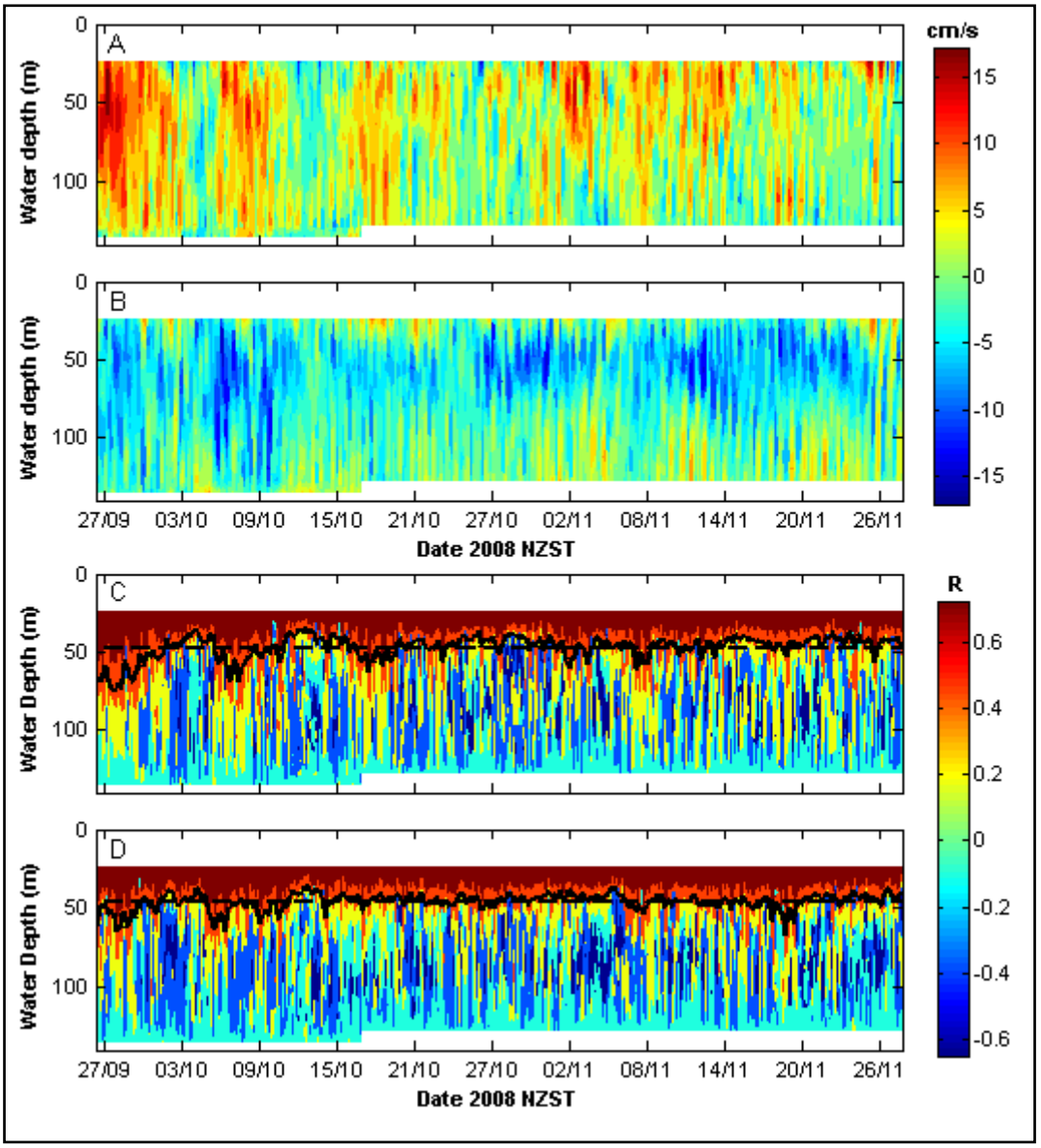

Figure 3.21 Contour plot of sub-inertial (a) cross-shore and (b) alongshore current velocities (cm/s) and autocorrelation (R) of the (c) cross-shore and (d) alongshore velocity profile with the velocity of the surface-most bin of the long-term ADP record at the AMDG. Black lines (c & d) represent the depth of the running mean (solid) and time-averaged mean (dashed) significant (95% level) correlation with the surface-most layer.

Vertical autocorrelation analysis of the residual currents (only tides removed) showed that positive correlation with the surface-most ADP bin (mid-bin depth 24 m) was significant (95 % level, R=0.53) to an average depth of 47 m and 46 m in the cross-shore and alongshore directions, respectively (Figure 3.21c&d). The surface correlation depth increased noticeably during two periods at the beginning of the measurement period. Between 25 September and 3 October, the surface correlation depth increased to a maximum of approximately 70 m in the cross-shore direction and 60 m in the alongshore direction. Between 6 October and 9

October, the surface correlation depth increased again to a maximum at 65 m and 60 m in the cross-shore and alongshore directions, respectively.

3.8.3 Residual Current and Wind Correlation

To isolate the wind-driven component from the residual velocity field, lagged cross-correlation analysis was undertaken on the detrended data records from the 6 surface-most ADP bins of the long-term deployment based on the autocorrelation results highlighted in Figure 3.21c&d. Detrended wind data from both the MI CliFlo station and the BSWD node nearest the ADP deployment location (see Section 3.5 for details on the wind records) were cross-correlated to the residual velocity measurements. Figure 3.22 shows the correlations between the cross-shore residual currents (u) and either the cross-shore (w_x) or alongshore (w_y) wind component within the maximum lag range of 40 hours (approximately twice the inertial period) to minimise spurious peaks. Figure 3.23 shows the lagged cross-correlations of the alongshore residual currents (v) with the cross-shore (w_x) and alongshore (w_y) wind components. Blue stem plots are the lagged correlations with respect to the MI CliFlo wind record and the black stem plots are that with the BSWD record. The dashed lines indicate the upper and lower 95 % confidence bounds.

The correlation patterns of the two different wind records were essentially the same, but often with a slight offset in the lag time which is not unexpected as the locations of the two records differed by approximately 65 km. Peak correlations in all instances occurred at the surface-most water depth (mid-bin depth 24 m) (Table 3.6). Correlations were, overall, weak with a maximum of 0.21 occurring between the cross-shore residual current (u) and alongshore wind (w_y). Correlations with the cross-shore wind (w_x) were weaker than that with the alongshore wind (w_y) and exhibited a correlation reversal between 40 and 50 m below the surface. With respect to cross-shore wind (w_x), cross-shore currents (u) shifted from positively-correlated to negatively-correlated with depth meaning that the component current was directed in the opposite direction of the corresponding wind component at depth. Alongshore currents (v) were negatively-correlated near the surface moving to positively-correlated with depth indicating that the current component opposed the corresponding wind component in this case near the surface and matched the wind component at depth. On the

other hand, correlations with alongshore wind (w_y) were in both instances positive with respect to all depth layers analysed, but diminished steadily with distance from the surface. In all cases, currents lagged winds in the range of 5-10 hours (Table 3.6).

Table 3.6 Cross-correlation details for the surface-most ADP bins for the measurement period (25 September – 27 November 2008). Insignificant correlations at the 95 % level are marked by *. Record length is 1498 h.

Mid-depth ADP bin (m)	Cross-shore (*u*)				Alongshore (*v*)			
	w_x		w_y		w_x		w_y	
	R	Lag (h)	R	Lag (h)	R	Lag (h)	R	Lag (h)
24	0.1	7	0.21	4	-0.11	3	0.19	8
32	*0.04	7	0.1	4	-0.06	4	0.15	8
40	*-0.05	5	0.06	5	*0.02	5	0.1	9
48	-0.1	4	*0.05	7	*0.01	5	0.08	9
56	-0.13	4	0.08	10	0.06	5	*0.04	10
64	-0.14	3	0.1	10	0.09	5	*0.01	11

R is the correlation level; lags are in hours

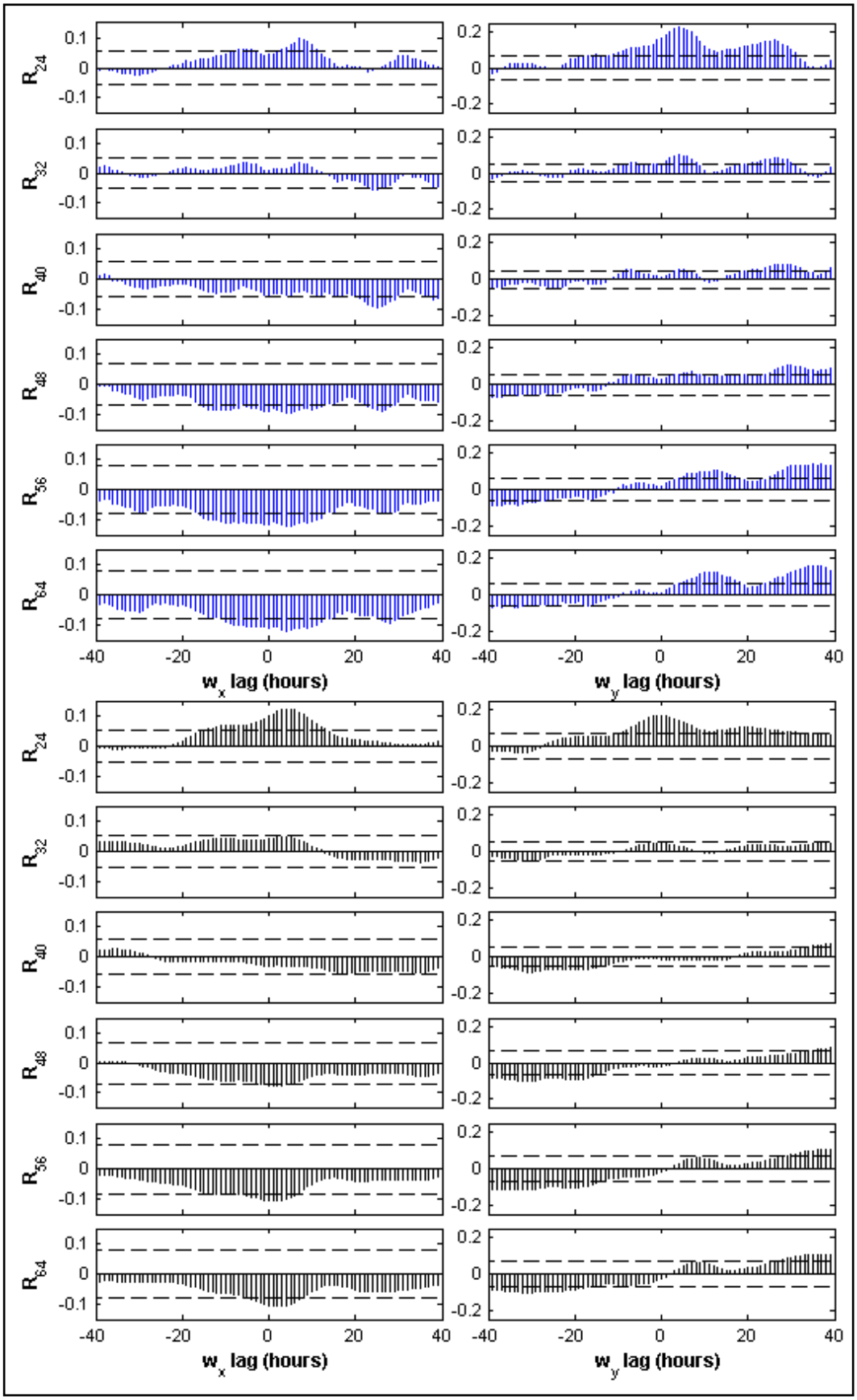

Figure 3.22 Lagged correlations of cross-shore residual currents to cross-shore (w_x) and alongshore (w_y) winds at Mokohinau Islands (blue) and the Blended SeaWinds node nearest the deployment site (black). R-subscript is the correlation at the mid-bin water depth (m) corresponding to the six surface-most ADP bins. Dashed lines are the 95% conf. bounds.

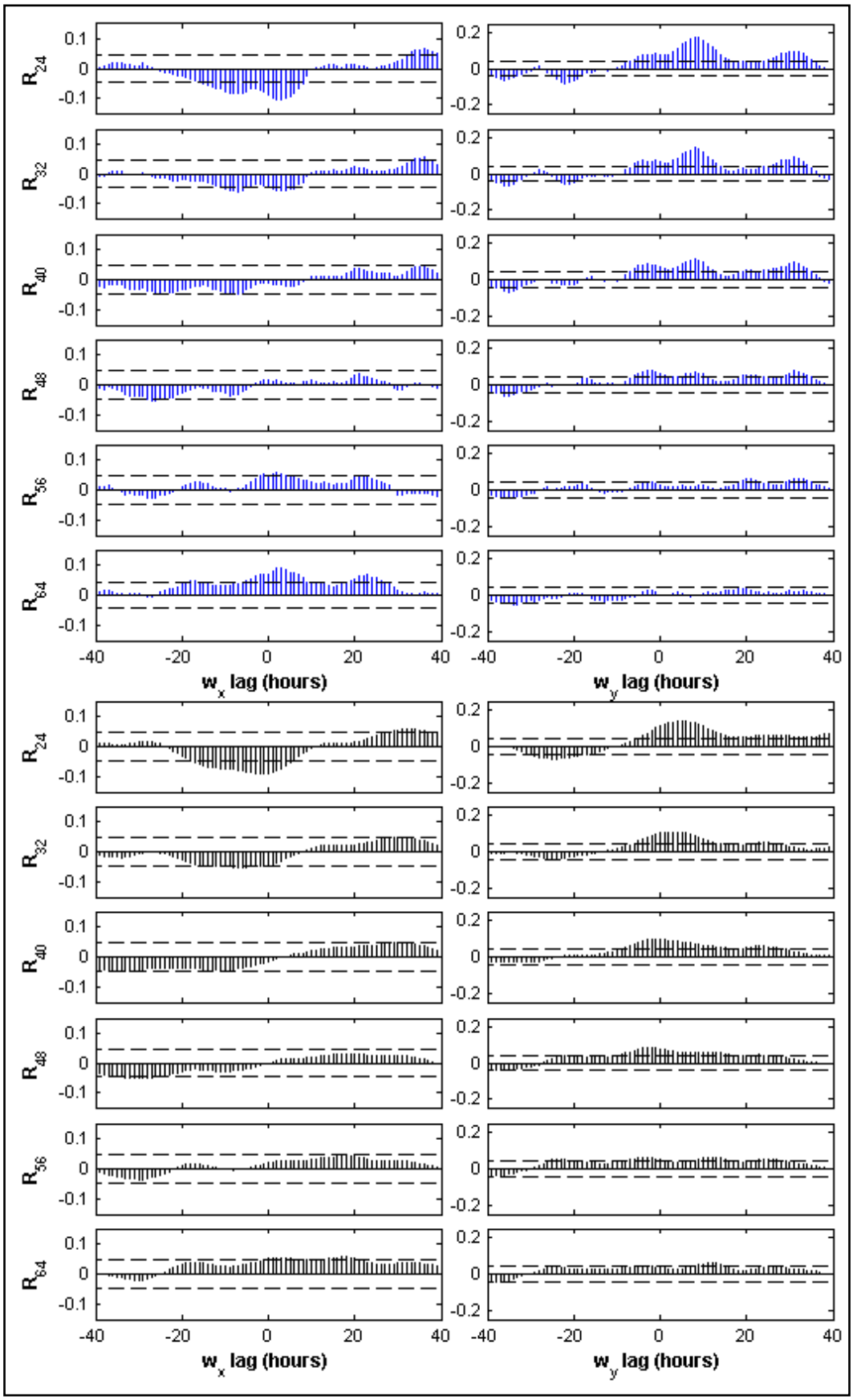

Figure 3.23 Lagged correlations of along-shore residual currents to cross-shore (w_x) and alongshore (w_y) winds at Mokohinau Islands (blue) and the Blended SeaWinds node nearest the deployment site (black). R-subscript is the correlation at the mid-bin water depth (m) corresponding to the six surface-most ADP bins. Dashed lines are the 95% conf. bounds.

3.8.4 Wind Driven Currents

To fully understand the influence of the wind on residual currents at the AMDG, multiple regression analysis was undertaken on the 4 surface-most ADP bin data records with respect to the lag-adjusted MI CliFlo wind record in order to infer the wind-driven (WD) current components. Lags were applied initially to the cross-shore and alongshore components of wind speed to adjust for the lag interval derived in the cross-correlation analysis (Table 3.6). Next, multiple linear regression was undertaken to compute the regression coefficients between each possible combination of wind speed and residual current components (Table 3.7).

Table 3.7 Multiple linear regression coefficients and statistics for the residual currents from the 4 surface-most ADP bins (*u* and *v*) and wind speeds from the Mokohinau Islands CliFlo wind record (w_x and w_y). Data duration is 62.4 days (25 September – 27 November 2008).

	Mid-depth bin (m)	Regression coeff. (w_x)		Regression coeff. (w_y)		F-statistic		Lag interval applied (hr)*	
		a	**P-value**	***b***	**P-value**	**Value**	**P-value**	***u*:w_x**	***v*:w_y**
Along shore (*v*)	24	-1.38E-03	3.39E-04	3.47E-03	1.12E-10	29.36	6.67E-03	3	8
	32	-6.45E-04	7.37E-02	2.77E-03	3.45E-08	17.63	2.70E-08	4	8
	40	-1.84E-04	0.569	1.83E-03	4.47E-05	8.71	1.74E-04	5	9
	48	8.59E-05	0.77	1.01E-03	0.012	3.14	0.044	5	9
		c	**P-value**	***d***	**P-value**	**Value**	**P-value**	***u*:w_x**	***v*:w_y**
Cross-Shore (*u*)	24	1.30E-03	7.35E-04	4.60E-03	0	44.55	0	7	4
	32	4.28E-04	0.254	1.95E-03	1.77E-04	7.97	3.62E-04	7	4
	40	-6.69E-04	0.043	7.95E-04	0.083	3.54	0.029	5	5
	48	-1.05E-03	3.19E-04	8.78E-04	0.030	9.03	1.27E-04	4	5

*in all cases residual current components followed wind components; lag intervals were applied accordingly.

Regression coefficients were then applied such that:

$$v_w = aw_x + bw_y \qquad \text{Equation 3-2}$$

and

$$u_w = cw_x + dw_y \qquad \text{Equation 3-3}$$

where v_w and u_w are the alongshore and cross-shore components of the WD current; *a*, *b*, *c*, and *d* are the derived regression coefficients (see Table 3.7); and w_x and w_y are the measured cross-shore and alongshore wind speed components. Time series of the inferred WD current components during the measurement period are plotted with the sub-inertial currents in Figure 3.24 and Figure 3.25. Progressive vector diagrams of the same time series are shown in Figure 3.26.

Inferred WD currents were strongest at the surface-most ADP bin (mid-depth bin, 24 m) and diminished approximately with depth in both the cross-shore and alongshore direction (Figure 3.24 and Figure 3.25). Alongshore and cross-shore WD currents were similar in magnitude throughout the depths analysed, with a mean surface-most (24 m) velocity of 1.23± cm/s and 1.71±1.11 cm/s, respectively and a mean bottom-most velocity (48 m) of 0.34±0.22 cm/s and 0.56±0.44 cm/s (Table 3.8).

Table 3.8 Statistics (mean, standard deviation, and depth scaling value (γ_u and γ_v) for the inferred wind-driven cross-shore (u_w) and alongshore (v_w) current for the 4 surface-most ADP bin data records.

Mid-bin depth (m)	u_w, cm/sec			v_w, cm/sec		
	Mean	STD	γ_u	Mean	STD	γ_v
24	1.71	1.11	-	1.23	1.04	-
32	0.7	0.46	0.41	0.92	0.73	0.74
40	0.38	0.32	0.54	0.59	0.44	0.64
48	0.56	0.44	1.47	0.34	0.22	0.57
			Avg =0.81			Avg =0.65

Notably, removing the inferred WD currents from the non-tidal residual current did not have a significant effect on the current trajectory during the measurement period (Figure 3.26). The greatest influence of the wind was at the surface-most ADP bin (24 m); however the residual current was still directed towards the southeast. The inferred WD current 24 m below the surface is plotted as an inset in Figure 3.26a and shows that WD current was actually directed toward the northwest, but had a cumulative trajectory of only ~30 km during the measurement period. Thirty-two meters below the surface, the WD current was also directed northwest, but with only a cumulative trajectory of ~12 km (Figure 3.26b). At the 2 bottom-most depths (40 and 48 m), the WD currents were more closely aligned with the residual current towards the southwest, but were further diminished in magnitude and so did not contribute to or alter the residual current trajectory greatly (Figure 3.26c&d).

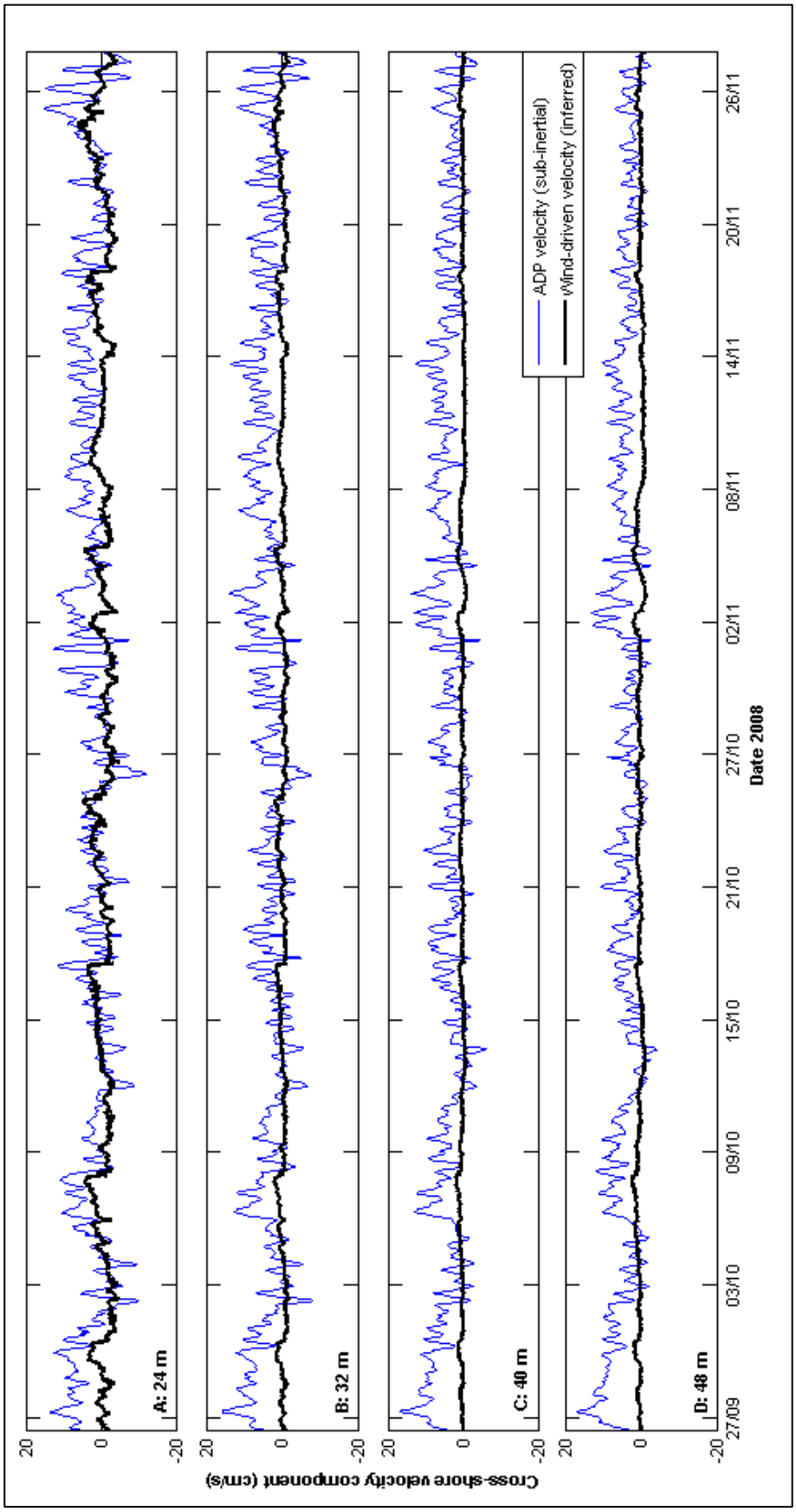

Figure 3.24 Cross-shore velocity (wind-driven and sub-inertial) for the 4 surface-most ADP bins during the deployment period (25 September – 27 November 2008).

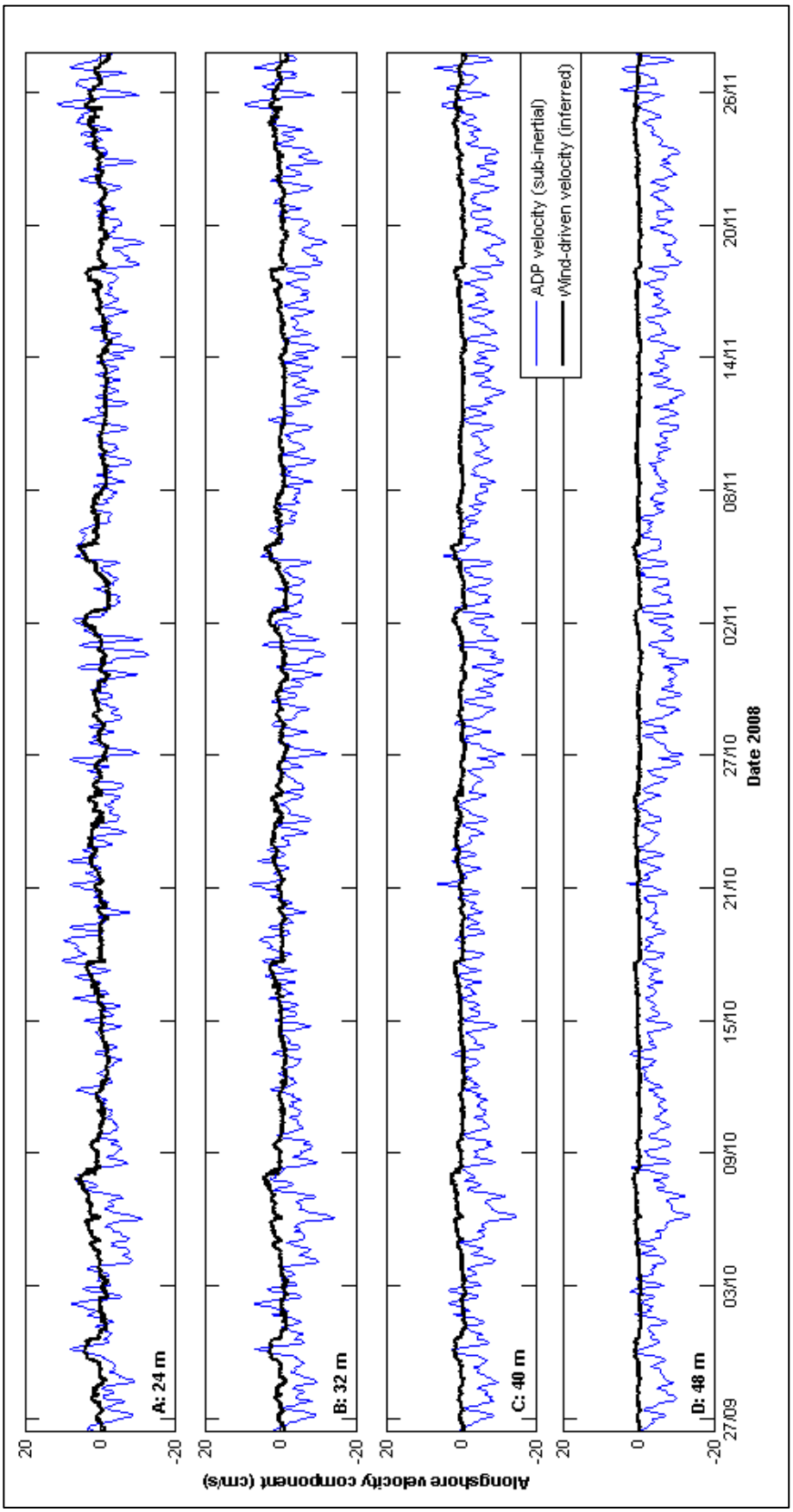

Figure 3.25 Alongshore velocity (wind-driven and sub-inertial) for the 4 surface-most ADP bins during the deployment period (25 September – 27 November 2008).

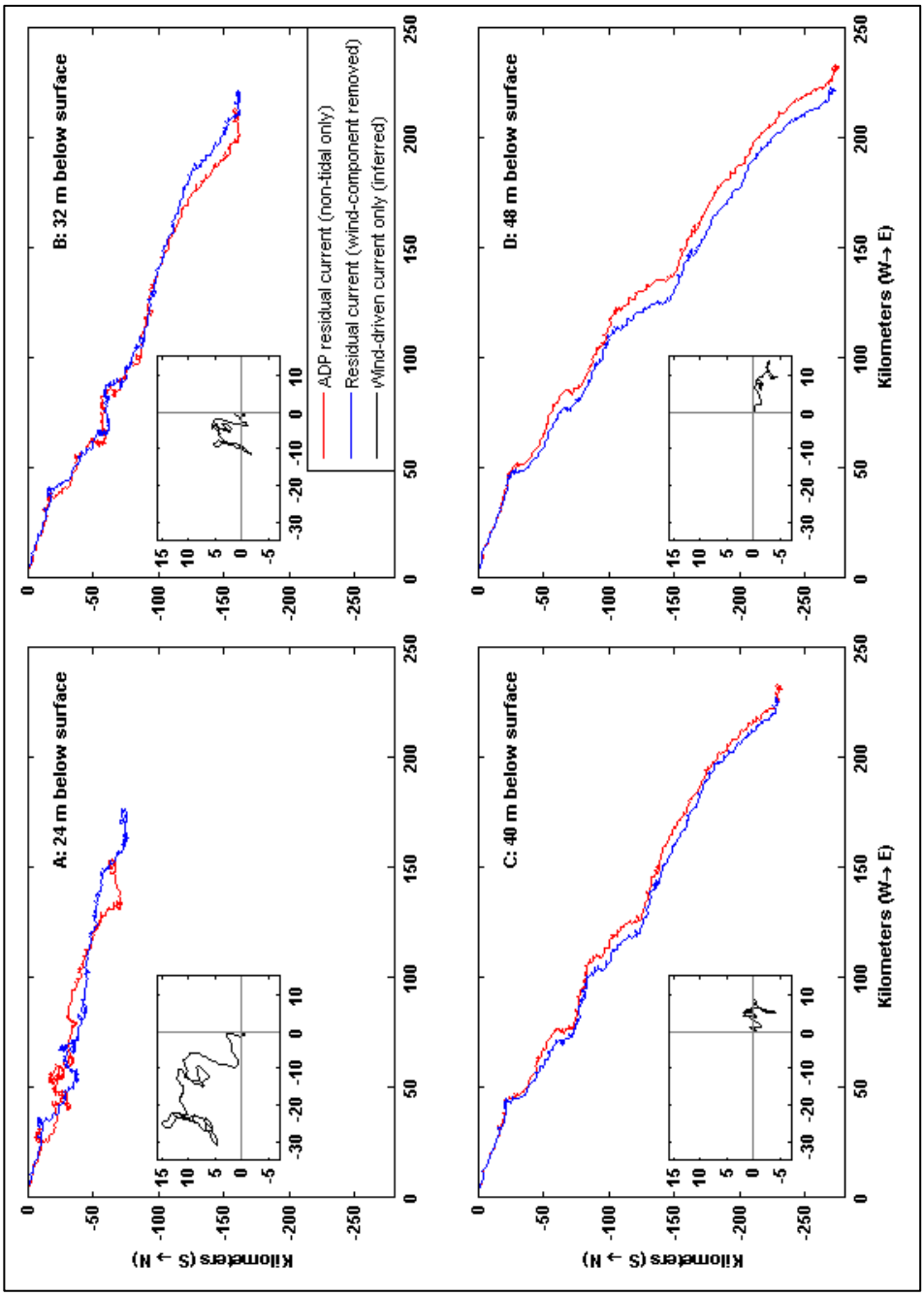

Figure 3.26 Progressive vector diagrams of the trajectories of the residual current (non-tidal only) (red), the residual current with the inferred wind-driven component removed (blue), and inset: the inferred wind-driven current (black) for the 4 surface-most ADP bins for the measurement period of 25 September – 27 November 2008 at the AMDG.

It is probable that the magnitude of the wind influence is underestimated in the above derivation because it is based solely on the inferred wind-driven currents at depths between 24 and 48 m. Intuitively, the magnitude of the wind effects should increase with proximity to the surface. A scale factor for the cross-shore (γ_u) and alongshore (γ_v) WD current was calculated from the mean velocity ratio between each of the 4 depth records (Table 3.8). The average scale factor was then applied stepwise starting with the 24 m WD current components through to 0 m, thereby synthetically obtaining the wind-driven current components at the surface for the measurement period at the AMDG. Assuming that the non-tidal, non-wind-driven residual current is relatively constant between 0 and 24 m below the surface, the total residual surface current was then estimated as the synthetic 0 m wind-driven current plus the non-tidal residual current derived from the surface-most bin (24 m) of the ADP record, hereafter referred to as the synthetic surface current.

Surface wind-driven currents are commonly estimated to be approximately 1-3 % of the measured wind speed (Davies, 1983; Tomczak, 1964). To substantiate the validity of the scaling procedure, a time series comprising 2 % of the measured wind speed during the ADP deployment period was plotted against the synthetic surface current (Figure 3.27). The scaled synthetic surface current magnitude was approximately 50 % of the surface current estimated as 2 % of the wind speed. The averaged scaling factors likely do not accurately reflect the mean vertical velocity ratios for the depths between 0 and 24 m so the synthetic surface current should be viewed as an underestimate of the total residual surface current.

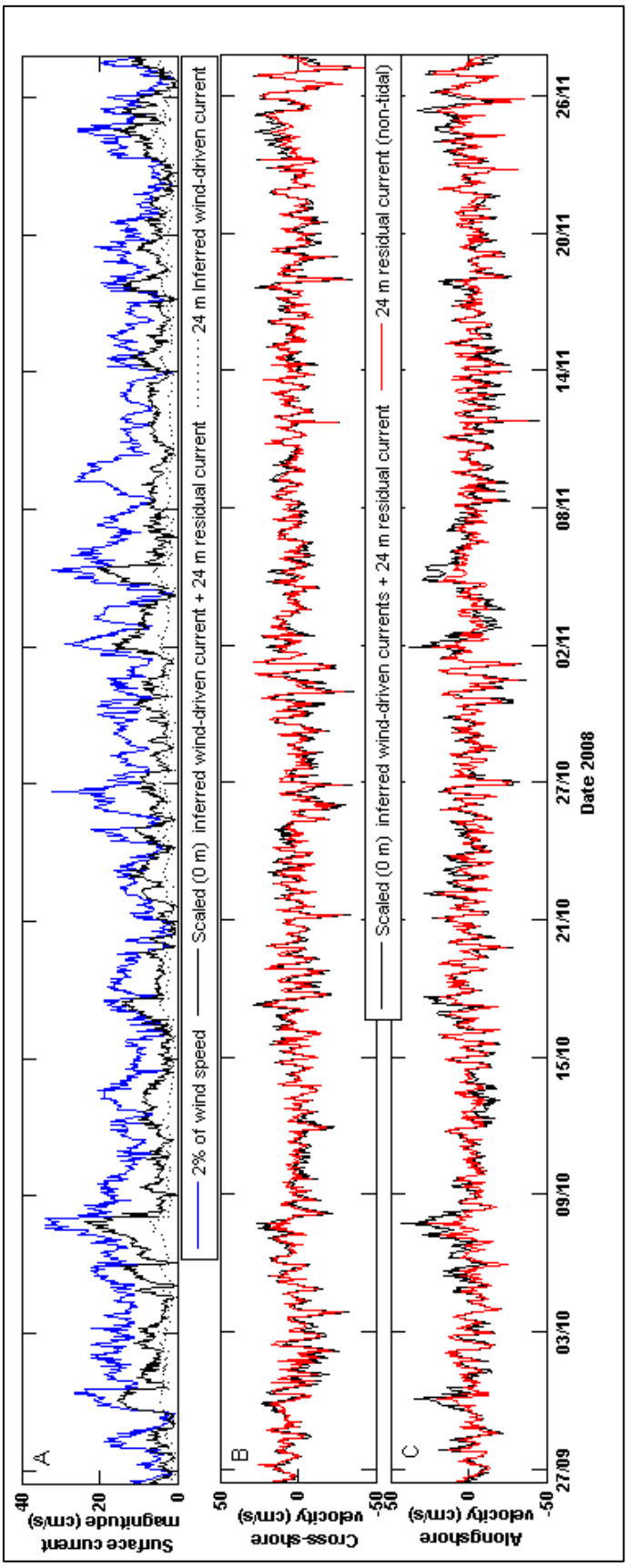

Figure 3.27 Time series of (a) surface current magnitude (cm/sec) at 0 m below the surface estimated as 2% of the wind speed (blue), at 0 m below the surface estimated from scaled inferred wind-driven current + the non-tidal 24 m residual current (black) (synthetic surface current), and inferred wind-driven current at 24 m below the surface (dashed black); (b and c) component current velocity (cm/s) at 0 m from scaled inferred wind-driven current + the non-tidal 24 m residual current (black) (synthetic surface current) and at 24 m from non-tidal residual currents (red) during the measurement period (25 September – 27 November 2008).

As components, the synthetic surface current increased the range of the 24 m non-tidal residual current by approximately 5 cm/s (Figure 3.27b&c and Table 3.9), with a maximum cross-shore velocity of 50 cm/s compared to 46 cm/s and a maximum alongshore velocity of 45 cm/s compared to 38 cm/s.

Table 3.9 Statistics of the synthetic surface current and the non-tidal residual current from the surface-most ADP bin (24 m below the surface. Data records are 1498 h. Synthetic surface current obtained by addition of the 0 m scaled inferred wind-driven current to the 24 m non-tidal residual current.

	Synthetic surface current		24 m non-tidal residual current	
	u_{w0}, (cm/s)	v_{w0}, (cm/s)	u_{24}, (cm/s)	v_{24}, (cm/s)
Maximum	50	45	46.3	37.6
Mean	8	8.7	6.9	6.6
STD	9.9	11.1	8.4	8.3

The synthetic surface current exhibited a more meandering character compared to the 24 m non-tidal residual current (Figure 3.28). The net distance accumulated was lower by approximately 30 km, but the trajectory path incorporated significant northerly and southerly additions not present in the deeper record.

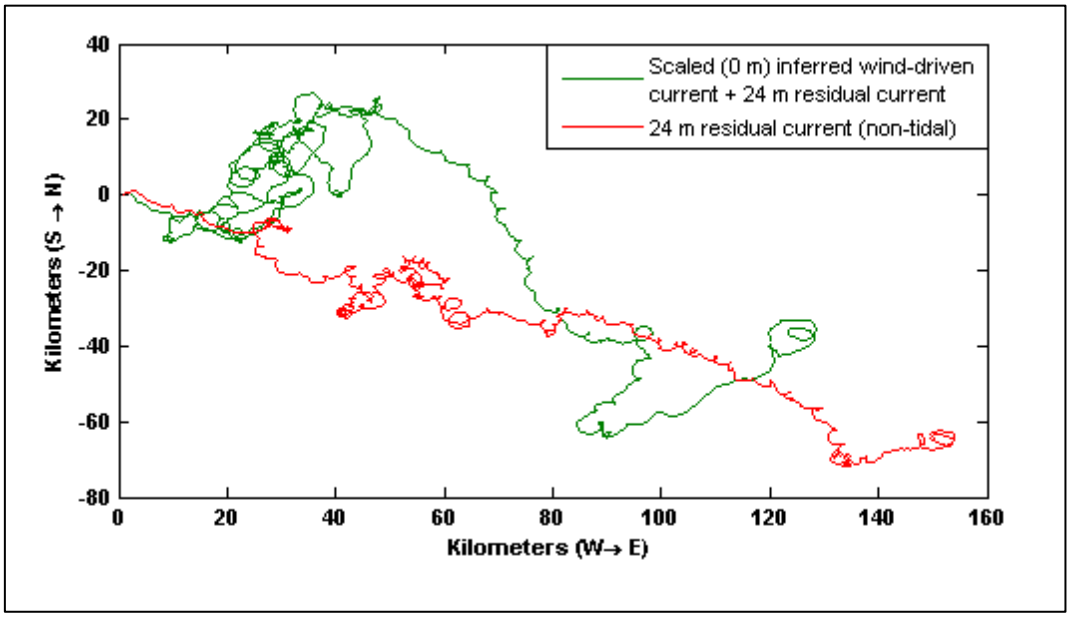

Figure 3.28 Progressive vector diagram of the trajectories of the ADP residual current (non-tidal only) 24 m below the surface (red), and the synthetic surface current (0 m below the surface) (green) estimated as the scaled inferred wind-driven current + the non-tidal 24 m residual current for the measurement period of 25 September – 27 November 2008 at the AMDG.

3.8.5 Discussion: Non-Tidal Forcing

Non-tidal flows recorded during the long-term ADP deployment period indicated a consistent south-easterly directed current with only short-lived and weak flow

reversals. Typical flow speeds were significantly lower than those observed by Sharples and Greig (1998) who reported speeds of 20 -30 cm/s. In this study maximums of only 17 cm/s and 11 cm/s were observed in the cross-shore and alongshore directions, respectively. The lower speeds may be related to the relatively wide shelf in the region compared to the narrow shelf in the region of the study by Sharples and Grieg (1998), but also the lack of data in the surface 20 m most likely contributed to the lower observed speeds.

Overall, correlation of the non-tidal currents to local winds during the measurement period was weak, but this is not surprising as the wind speeds were low compared to those reported in other studies undertaken in nearby areas (Longdill et al., 2008; Sharples & Greig, 1998; Zeldis et al., 2004) and additionally ADP data was corrupt in the surface 20 m where the strongest correlations would have been expected. However, some characteristics of a wind-driven residual current were observed. Namely, the strongest correlation to the wind was detected between the alongshore wind and the cross-shore current such that in a northerly wind (from the north) the cross-shore surface current was directed east which is consistent with Ekman-style dynamics. However, as the predominant wind direction during the measurement period was from the SW (Figure 3.6), up-welling and down-welling tendencies were not likely a significant factor.

Inferred wind-driven currents from 24 m below the surface and deeper made up only a small component of the residual flows suggesting that at those depths, the influence of the wind at least during the measurement period was small. The derived synthetic surface current indicates that wind-driven surface currents make up a larger component of the residual current and imply a typical flow speed more similar to that reported by Sharples and Grieg (1998). However, even with the wind-driven component included, the derived surface current still appears to be directed predominantly toward the southeast.

Variations in the sub-inertial residual currents and their corresponding correlation with surface flows highlighted some residual flow characteristics that were atypical compared to the majority of the data record. Starting on approximately 25 September the surface correlation depth increased by approximately 25 m (Figure 3.21c), which was immediately followed by a full vertical reversal of the cross-

shore current to the west between 3 October and 5 October (Figure 3.21a). Following a short interim period when flows were again directed to the east, a second deepening of the surface correlation depth occurred between 6 October and 9 October. Similar to the first, immediately following the second deepening event, a second full vertical reversal of cross-shore currents towards the west occurred between 11 October and 15 October.

These patterns suggest that strong mixing events which would have resulted in a deepened mixed layer may have initiated the two westward residual current pulses. Supporting this theory is the near-bed temperature record which showed a rapid decrease in temperature starting on 8 October likely the result of cooler slope waters propagating westward onto the shelf in response to the westerly flow reversals (Figure 3.8).

At first glance, it would not be unreasonable to assume that the initial decline in temperature was associated with the second deepening and flow reversal events because the dates are more closely aligned. However, a closer look at the temperature record shows a short-lived increase in temperature on 12 October lasting only 1 day after which point the temperature declined again. That increase is likely to be correlated to the short interim period before the second deepening event, which would indicate a lag of approximately 3 days for a near-bed conserving flow reversal.

It is difficult to determine if that is a reasonable lag time because complementary data on a potential associated up-welling event either at or inshore of the AMDG was not collected. However, 3 days is significantly longer than the lag of c. 1 day between up-welling favourable wind events and fully upwelled conditions reported by Longdill et al. (2008) and Zeldis et al. (2004) especially considering that it is unknown whether the estimated lag in this case was associated with fully upwelled conditions or simply just a near-bed flow reversal.

Furthermore, if the atypical residual current patterns were indeed associated with the observed decrease in temperature during the same period, then a corresponding correlation to the alongshore wind would have been expected. The strongest lagged correlation did occur between the cross-shore residual current and the alongshore wind speed; however, at a depth of 24 m below the surface,

the correlation was weak at 0.21 (Figure 3.22). It is not certain whether the corresponding surface correlation would be strong enough to initiate a near-bed flow reversal.

Another possible explanation is that the depressed near-bed temperature could have been result of a combination of wind gusts not normally favourable for up-welling and the effects of centrifugal up-welling. This phenomenon has been observed or suggested in other studies of New Zealand's shelf and can be described as the centrifugal effects of flow past convex coastal bends (Cresswell, 1994; Sharples & Greig, 1998; Shirtcliffe et al., 1990; Zeldis et al., 2004).

Sharples et al. (1998) suggested the possibility that the observed up-welling at a northeast coast shelf site c. 100 km north of the AMDG may very well include a significant contribution simply as a result of curvature of the flow of the East Auckland Current (EAUC) which would not require favourable wind stress.

Centrifugal up-welling from the EAUC was also proposed by Zeldis et al. (2004) as an explanation for a decrease in the near-bed temperature at outer shelf and slope moorings at study sites nearby those discussed by Sharples et al. (1998). The cooling at the bed was observed between September (spring) and December (summer) when the opposite would be expected and precisely during the same months that the decrease in the near-bed temperature was observed in this study.

Shirtcliffe et al. (1990) observed centrifugal up-welling at the northwest coast of New Zealand's South Island, which was related to a bending of the northerly flowing Westland Current past the Challenger Plateau. At the AMDG, the analogous scenario is the potential interaction of the south-easterly flowing EAUC with the large bathymetric lobe feature comprising the slope and shelf edge approximately normal to the AMDG (Figure 3.1). Indeed, the influence of this bathymetric feature has been suggested by Black et al. (2000) as having an impact on shelf baroclinic circulation in the region and no doubt warrants further investigations.

The predominant south-easterly flowing residual current and the possibility of nearby centrifugal up-welling suggest that the EAUC may be an important forcing mechanism at the AMDG. As the AMDG is located approximately midway across

the shelf, a strong presence of the EAUC there would contradict the traditionally held knowledge that the EAUC flow path is typically off the shelf or along the shelf edge (de Lange et al., 2003; Sharples, 1998).

Sharples (1997) observed that during prolonged north-easterlies the warm sub-tropical waters of the EAUC intruded onto the shelf, but the fundamental difference here is that it appears that the EAUC may have been situated at least as far onto the shelf as the location of the AMDG and its presence was nearly vertically uniform in direction. Sutton and Roemmich (2001) showed a strong correlation between EAUC and the SOI which suggests that there may be significant variation in its properties (i.e. magnitude, transport volume, and width) depending on the corresponding wind patterns associated with either El Niño or La Niña conditions. Ridgeway and Godfrey (1997) reported that during weak periods, the East Australian Current, the feeder current for the EAUC, decreased in speed and increased in width, whereas during strong periods, the flow path was characterised by increased speed and a narrow path. In principle, the same mechanisms should apply to the EAUC. During a low transport year, the flow would be expected to decrease and spread out to possibly include the mid to outer shelf areas in its path southeast along the coast. This would result in a somewhat slower residual current directed uniformly to the southeast (in the vertical), analogous to the one that was identified in this study.

3.9 Summary and Conclusions

The hydrodynamic forcing mechanisms at play in the region of the AMDG have some unique attributes not apparent in areas to the north and south. The likely factors contributing to the somewhat specialised hydrodynamics are the width of the shelf and its unusual shape, as well as the presence of Great Barrier Island to the east. The main findings of this chapter are highlighted conceptually in Figure 3.29.

The influence of the tides in this region is relatively small contributing approximately 25 % to the overall flow. In general, the tidal characteristics are similar to those of nearby regions such as the dominance of the semi-diurnal M_2 tidal constituent having an approximate amplitude of 8 cm/s. Contrary to the norm though, the M_2 tide propagates clockwise which, while not likely impacting the

principal flow patterns, intimates the influence of local pathways associated with the presence of Great Barrier Island and the Hauraki Gulf.

Seemingly unique to the study area is the significance of the monthly M_m tidal constituent which may be related to the distance of the AMDG from the coast (Hendershott & Munk, 1970). During the measurement period, this constituent exhibited an influence on par with the diurnal K_1 constituent, which has typically been found to be the second most important tidal wave along the northeast coast (Longdill, 2007; Sharples & Greig, 1998). The influence of a strong M_m may be more apparent during lunar perigee when the percent tidal component may increase in the area of the AMDG. Evidence of a first-mode internal tide was also observed and though its presence did not appear to enhance shelf flows greatly, during periods of stratification which are common in summer on the northeast shelf, an internal tide may have the effect of increasing the potential for dispersion of suspended sediment at the site.

Non-tidal currents showed a predominant south-easterly directed flow. This trend was consistent throughout the water column varying only by a decrease in magnitude with proximity to the bed. Compared to measurements in other areas, the typical observed speeds were somewhat lower than expected with peak flows occurring at the depth of the mixed layer. Wind effects on the non-tidal flows appeared small during the measurement period, but some evidence of Ekman-style dynamics was observed. If fully upwelled conditions developed at the AMDG, potential for resuspension or advection of deposited dredged material may occur (e.g. Gao and Jia (2002)), however the distance of the site from the coast suggests that up-welling would not occur directly at the AMDG and consolidation of deposited material over time would further decrease the likelihood of such processes (Halka et al., 1991). Conclusions on the influence of the wind could, however, benefit from additional ADP measurements during periods of stronger winds and which include the surface 20 m of the water column.

The evidence suggests that the dominant south-easterly flow that exists in absence of the tidal and wind components is likely to be the dominant forcing mechanism at the AMDG. It has been proposed that the EAUC is the source of this residual flow and if so, implies that its magnitude may vary seasonally and also inter-

annually (Sharples, 1997; Stanton et al., 1997; Sutton & Roemmich, 2001; Zeldis et al., 2004).

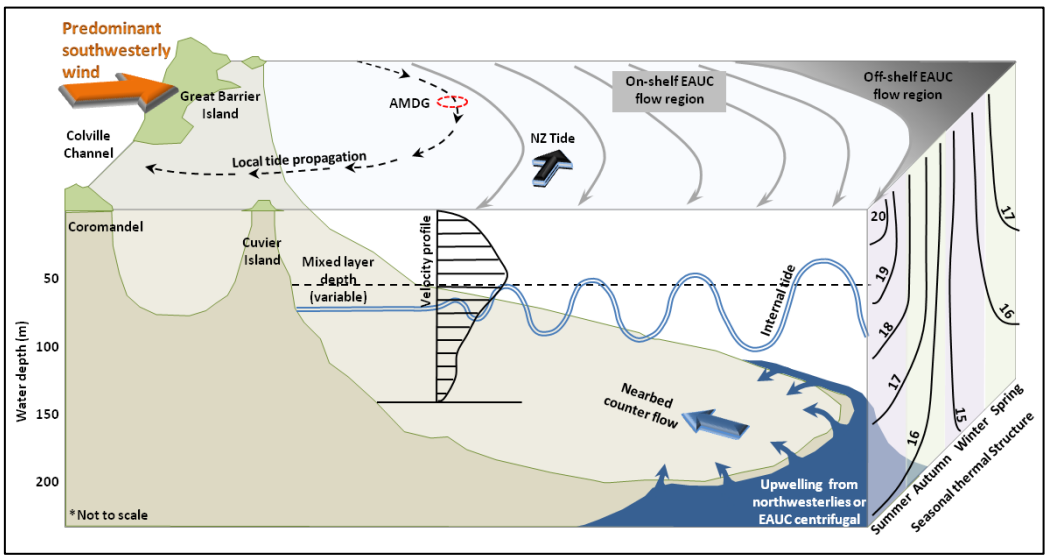

Figure 3.29 Diagram of the major hydrodynamic and hydrologic features influencing the AMDG. Diagram is not drawn to scale.

3.9.1 Implications for Site Dispersion

Based on the long-term ADP data record and the conditions under which the data was recorded, a passive particle suspended in the water column has the potential to disperse between 2 km and 6 km per day. At the limits of the mixed layer, the potential for dispersion is greatest (see Figure 3.20a and Figure 3.21c&d) and if there is a strong density gradient associated with this zone, fine particles in the silt to clay range could become trapped and undergo focused long-term dispersion along the pycnocline where speeds may be strongest (e.g. Wang and Jiang (2008); Trocine and Trefry (1983)).

However, passive (long-term) dispersion typically only applies to 1-5 % of the disposed material (Truitt, 1988). The majority of the disposed material would be expected to disperse dynamically (in the short-term) (i.e. under its own momentum) (Bokuniewicz & Gordon, 1980; Gordon, 1974). With the negative buoyancy of the descending jet and the exaggerated fall velocities of aggregated and/or flocculated sediments, very high ambient velocities would be required to overcome the momentum of the descending material. The typical residual velocities measured at the AMDG are relatively low for the region (<15 cm/s), owing most likely to the width and depth of the shelf in the region, thus, it is likely that the ambient velocity will be lower than the critical velocity for

deposition for the majority of the material disposed under most conditions that are conducive to disposal operations (see Section 3.8).

For the period of the long-term ADP record, the AMDG exhibited characteristics of a non-dispersive site in that the likelihood that disposed dredged material will be dispersed beyond the site boundaries is low. However, the measurement period was not characterised by particularly strong winds or storm conditions, which can enhance the ambient velocity through wind-driven currents and increased wave orbital velocities (see Section 3.5). Therefore, although the measurement period spanned a season, it was essentially a snap-shot of the hydrodynamics that may occur at the AMDG. There may also be potential for enhancement of the ambient current velocity through strong internal tides, up-welling related near-bed flows, which had only minimal influence during the measurement period, and via variability in the position and strength of the EAUC.

3.9.2 Relevance to Thesis Aims and Objectives

The majority of the findings in this Chapter focussed on the resolution of the important hydrodynamic forcing mechanisms at the AMDG and provided the basis for completion of Objective 1 of this thesis. Additional conclusions developed in the studies presented in Chapters 4 and 5 enhance the knowledge gained from the work presented here, and further contribute to the completion of Objective 1. Indirectly, the work presented in this Chapter also adds to the understanding of the site specific processes involved in the disposal of dredged material (Objective 2) by virtue of the dependence of sediment dispersion pathways on hydrodynamic processes. Conclusions made in Chapter 4 on important transport pathways will draw on the findings from this Chapter. Estimates of potential transport distances of suspended particles based on the long-term ADP record presented here represent quantifiable conclusions on the potential for loss of sediment from the disposal site and, therefore, contribute to the completion of Objective 3; however, additional findings related to this objective are presented in Chapters 4 and 5.

CHAPTER 4

A PILOT STUDY FOR UNDERSTANDING SITE SPECIFIC PROCESSES AND PATHWAYS OF SEDIMENT DISPERSION DUE TO DREDGED MATERIAL DISPOSAL

4.1 Introduction

Even though the Auckland Marine Disposal Ground (AMDG) is positioned beyond the territorial seas, supposedly outside the region of historical controversy when it comes to dredged material disposal, after preliminary studies and an environmental impact assessment in 2009, it seemed as though the AMDG was too much of an unknown entity and was not likely to be approved for long-term use. However, through some forward-thinking on the part of Maritime New Zealand (MNZ), a short-term consent was awarded instead, to serve as a pilot-study, the main purpose of which was to determine the potential for sediment dispersion at the site through direct *in situ* measurements immediately following disposal of dredged material at the site.

It was envisaged by MNZ that during disposal of the allocated 5000 m^3 of material, measurements on the dispersion and fate of the disposed material would be undertaken in a variety of weather and sea conditions so as to obtain a comprehensive perspective regarding sediment dispersion characteristics from the data collected at the site. That outlook would weigh heavily in the decision-making process for long-term consent.

4.2 Motivation and Relevance to the Thesis Objectives

The most reliable method for understanding the dispersion pathways and behaviour of sediment disposed at a dredged material disposal site is through physical in situ measurements[7]. Such measurements can lead to direct

[7] The use of tracers may serve to enhance physical *in situ* measurements. Although, examples of the use of tracers to track fine sediments are limited, it is possible to 'tag' dredged material with a fluorescent tracer powder such that the tracer is incorporated into the natural aggregates within the storage vessel (Louisse et al., 1986). In this case, quantification of the tracer requires carefully planned and intensive seafloor sampling as well as specialised tracer recovery technology which may only lead to recovery of a small percentage of the original volume (in the case deep offshore sites, often less than 10%) and has been typically limited to sediments with particle sizes less than 15 µm (Black et al., 2007). In the present case, with a particle size range easily exceeding 15 µm, the above method would not be suitable. Another method that can be employed is the sampling of 'tagged' sediments suspended in the water column, rather than those deposited on the sea floor,

observations of whether a disposal site is dispersive or non-dispersive and thus give answers as to the long-term suitability of the site for various disposal operations. However, this type of evaluation is not the historical norm in New Zealand, and the Auckland region in particular, as a result of laws that require that the character of a proposed disposal site be known prior to disposal of any material. This catch-22 scenario is understandable as it is preferable to avoid potential environmental impacts, but it creates a problem in that it is not possible to fully understand the character of a disposal site and the behaviour of sediment disposed within the site without witnessing it first-hand. This makes it difficult to classify a site as dispersive or non-dispersive prior to undertaking disposal operations. Extrapolation from hydrodynamic measurements and numerical modelling can be helpful in ascertaining a 'best-guess', but as has been the case in Auckland, such techniques have proven insufficient for awarding a consent. In recent years, this issue has likely been at the root of difficulties in establishing new disposal sites within the Auckland CMA (Flaim et al., 2010).

The work included in this chapter is relatively unique around the world and especially New Zealand. Much of the research done on dispersion of dredged material took place in the 1980s in the US (e.g. Bokuniewicz and Gordon (1980); Gordon (1974); McAnally and Adamec (1987)) prior to the modernisation and streamlining of various methods for measuring sediment dispersion. In New Zealand, most related research has been undertaken under private contracts without published results (*pers.comm.*, R. Liefting); one exception being research undertaken by Warren (1992) in connection to disposal of maintenance dredgings from Port of Tauranga, New Zealand.

The findings of this chapter have led to interpretations on sediment dispersion at the AMDG, in particular the site-specific processes involved in the disposal of

using a device that attaches a time stamp to the sample allowing for temporal quantification of tracer dispersion (Black et al., 2004). Paramagnetic properties of the tracer allow for separation from untagged sediments. This method would appear to be appropriate for the case of tracking dispersed dredged material, but it would still require the incorporation of the tagged sediments into the hopper load of dredged material so that the natural features of the disposal process are represented in the tracer study. Addition of a tracer would be beneficial in that the amounts recovered would, with no doubt, be representative of the material that originated in the hopper, but the study could not be undertaken effectively in absence of the release of a large amount of muddy material. This raises the question whether addition of a tracer to a hopper load of material to be disposed would be any more effective than simply tracking the sediment itself as was the case in the present study.

dredged material and the potential for loss of disposed material beyond the site boundaries. Additional conclusions on the viability of the different measuring techniques were drawn, which is significant because, as previously indicated, the topic of dredged material disposal is not heavily published in contemporary international literature meaning that advances in field methodologies are not widely reported.

4.3 Chapter Aims

The aim of this chapter is to characterise the site-specific processes, including plume dispersion, involved in the disposal of dredged material and to determine the potential for loss of disposed material beyond the site boundaries. An additional aim is to make conclusions on the viability of the various field methodologies for future research. To achieve the above aims the following objectives will be addressed:

- assess weather and sea conditions during disposal operations with a focus on the magnitude of influence on sediment motions;
- consider the dredging and disposal method as a factor in dispersion of sediments released at the site;
- determine the temporal variability of suspended sediment following disposal;
- determine the spatial variability of suspended sediment following disposal; and
- characterise the material deposited on the seabed following disposal.

4.4 Background: Pine Harbour Marina Dredging

The applicant for establishment of the AMDG and recipient of the short-term consent was Coastal Resources Ltd. Owners of Coastal Resources Ltd. also own Pine Harbour Marina Ltd., the corporate body that manages Pine Harbour Marina located in Beachlands, southeast of Auckland city (Figure 1.1 and Figure 4.1).

Figure 4.1 Turbid plume entering Pine Harbour Marina, located along the Beachlands coastline, southwest of Auckland city (source: Pine Harbour Marina Ltd.).

Pine Harbour Marina is an example of an artificial semi-enclosed body of water that was unintentionally situated so that the marina entrance walls consistently catch and retain suspended littoral sediment (Figure 4.1). This has resulted in faster-than-expected sedimentation of the entrance channel and marina basin resulting in the need for annual maintenance dredging (Hull, 1996). However, such activities have been hampered by the lack of viable disposal sites in the Auckland area leading to a back-log of infilling sediment which, if left alone, will eventually reach the point when its channel and basin are no longer navigable (Flaim et al., 2010).

Therefore, the application for establishment of the AMDG was originally intended as a solution for the infilling problems of Pine Harbour Marina, as much as it was a solution for other ports and marinas in the Auckland area (and thus a potential source of revenue for the applicant). However, under the terms of the pilot study short-term consent permit, the allocated material was sourced from Pine Harbour Marina basin only.

4.4.1 Infilling Sediment Characteristics

Maintenance dredgings from the approach channel at Pine Harbour Marina were found to be 66 % silt, 18 % clay, and 16 % fine sand (Hull, 1996). That grain size

distribution was more consistent with that found by Golder Kingett Mitchell (2007) in the marina entrance, as opposed to the approach channel, with the exception of clay which was somewhat higher (~10 %). In the approach channel, Golder Kingett Mitchell (2007) found a much higher percentage of fine sand (~45 %) and a much lower percentage of clay (~5 %) than that found by Hull (1996) 10 years earlier. The historical data suggests that the distribution of littoral sediments getting trapped in the approach channel has coarsened with time.

Within the marina and close to the entrance, Bioresearches (2009) found a higher percentage of clay and a lower percentage of silt (~50 % and ~38 %) compared to that found by Golder Kingett Mitchell (2007) (~10 % and 65-80 %, respectively). In the marina basin, sites had very similar size distributions as that found near the entrance with approximately 80-90 % silt and clay (Bioresearches, 2009) (Table 4.1). At the sites within the marina basin that were sampled by Bioresearches (2009), the mean grain size ranged from 0.01 mm to 0.04 mm, with and overall mean of 0.02 m which falls in the class of medium silt (Table 4.1).

Hull (1996) assessed the bulk density and moisture content of material dredged from the Pine Harbour Marina approach channel. It was found that the material after having been disposed on the adjacent intertidal flats had an average bulk density between 1520 and 1800 kg/m^3 and a moisture content of approximately 45 %. As the material had been exposed to air and some de-watering after placement on the intertidal flats, it can be expected that the *in situ* bulk density might have been lower and the moisture content higher. As the apparent size distribution of the approach channel sediments are more coarsely skewed than in the marina basin, it can be expected that the *in situ* bulk density of the marina basin sediments could be lower and the moisture content higher than those within the approach channel due to the greater porosity typically associated with fine sediments though this would vary vertically within the area intended for dredging due to *in situ* compaction and de-watering (Whitehouse et al., 2000).

Table 4.1 Grain size data from samples collected within the marina basin at Pine Harbour Marina in 2009. Grain size means calculated based on data presented in Bioresearches (2009).

Grain size			Percent of total sample					
mm	**φ**	**Class**	**Site 2**	**Site 5**	**Site 6**	**Site 10**	**Site 11**	**Site 12**
>3.35	-2	gravel	5.29	0.00	0.00	0.00	3.42	0.87
3.35-2	-1	granules	0.22	0.19	1.25	0.77	2.15	1.74
2-1.18	0	very coarse sand	0.73	1.08	2.75	1.83	1.56	2.05
1.18-0.6	1	coarse sand	1.91	1.93	3.83	2.55	1.60	1.48
0.6-0.3	2	medium sand	2.04	1.78	2.08	1.93	1.30	0.87
0.3-0.15	3	fine sand	3.44	1.50	2.43	1.35	1.49	0.97
0.15-0.063	4	very fine sand	18.78	4.71	5.76	2.17	3.86	3.28
0.063-0.0442	4.5	coarse silt	0.23	0.12	0.65	0.66	0.00	0.08
0.0442-0.0312	5	coarse silt	4.57	2.91	1.80	0.53	1.09	0.31
0.0312-0.0221	5.5	medium silt	3.36	6.56	4.05	1.87	3.69	2.96
0.0221-0.0156	6	medium silt	3.15	4.39	3.93	5.00	3.95	2.37
0.0156-0.0078	7	fine silt	9.06	13.09	12.03	12.11	11.13	10.86
0.0078-0.0039	8	very fine silt	7.98	10.95	10.96	12.55	11.04	13.57
<0.0039	9	clay	39.23	50.79	48.47	56.68	53.73	58.65
<0.063	-	silt and clay	67.58	88.81	81.90	89.40	84.62	88.74
Site mean grain size (mm)			0.04	0.01	0.03	0.01	0.01	0.01
Mean overall grain size (mm)			0.02					

Hull (1996) found a high abundance of smectite clay in the dredgings removed from the approach channel at Pine Harbour and suggested that it reflected the contribution of the weathered shore platform and sea cliffs to the coastal sediment budget in the area, as well as that from the local Waitemata Formation. This is supported by the findings of Naish (1990) which showed that clays derived from the land catchment are rapidly converted to smectite upon contact with salt water. The findings of Naish (1990) pertained to the catchment draining into the Firth of Thames which, due to its proximity, is likely to have similar properties to the catchment surrounding the Beachlands/Pine Harbour area (Figure 1.1). Therefore, it is likely that the sediments within the Pine Harbour Marina basin have similar mineralogy.

4.4.2 Dredging Method

In March 2010, dredging began within the basin of Pine Harbour Marina. Material was removed using a back-hoe digger and hopper barge (Figure 4.2). When at capacity, the barge was transported and the material transferred to a larger split hull hopper, the *SB II Groper*, anchored outside the marina awaiting transport to the AMDG (Figure 4.3).

The dredged material was distinctly darker in colour than the suspended sediments comprising the background turbidity of the marina basin (Figure 4.2b). In person, the colour was almost black, which was most likely indicative of anoxic conditions where sediments are highly depositional and not frequently re-worked (Whitehouse et al., 2000).

From visual observations during the dredging operations, it was evident that the *in situ* structure of the dredged sediment was reasonably well retained (Figure 4.2b). This is not surprising considering the high clay content which implies high plasticity due to cohesion (Winterwerp & van Kesteren, 2004) and the dredging method used which has been shown to minimise re-working of the sediment (Bokuniewicz & Gordon, 1980; Poindexter-Rollings, 1990; USACE, 1983). The implications of this are that high clay-content material dredged in a method that minimises agitation of the material will be more resistant to dispersion during descent to the bed following release from the hopper (Bokuniewicz & Gordon, 1980; McAnally & Adamec, 1987).

Unfortunately, it was not possible to collect samples of the dredged material from inside the barge, so the exact properties are unknown. However, findings by Bioresearches (2009), Golder Kingett Mitchell (2007), and Hull (1996) are indicative and will be used where necessary throughout the remainder of this thesis.

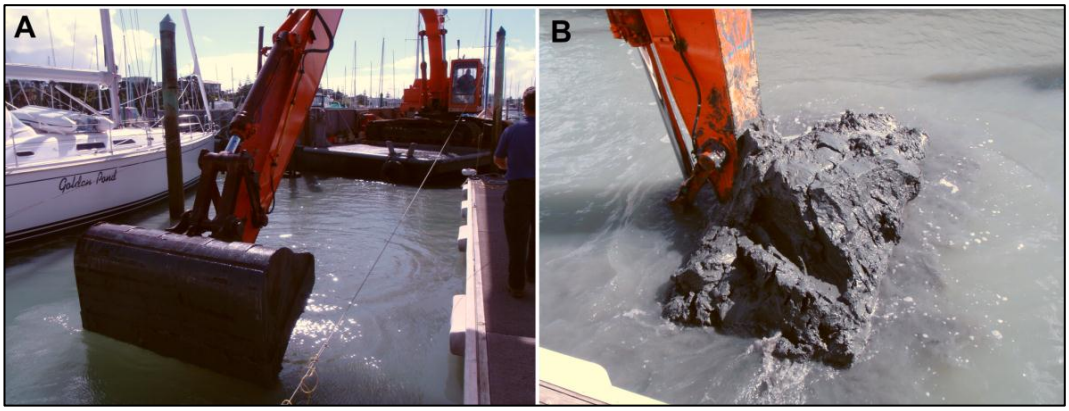

Figure 4.2 (a) Dredging of a berth at Pine Harbour Marina in March 2010 via back-hoe digger. Material was placed on a small hopper and transported to the larger main hopper (*SB II Groper*) outside the marina for transport to the AMDG. (b) dark colour of the dredged material is distinct from the background turbidity colour which indicates anoxic conditions at the bed.

Figure 4.3 *SB II Groper* split hull hopper anchored outside Pine Harbour Marina during dredging operations in March and April 2010; used to transport a maximum load of 765 m^3 of muddy dredged material to the AMDG for disposal.

4.4.3 Disposal Method

In March and April 2010, 9 separate loads of dredged material totalling 4873 m^3 were towed to the AMDG by the *MV Mina Campbell* and released at near the centre of the site (see Figure 3.1) via split hull hopper (*SB II Groper*) (Figure 4.4). The *SB II Groper* had a maximum capacity of 765 m^3, but this volume was not attained for any load transported to the site owing to weather conditions which often dictated a premature departure for the disposal grounds to avoid a costly situation where the hopper was full, but weather and sea conditions were unsafe for transport. The average volume disposed was 540 m^3, with maximum and minimum load sizes of 685 m^3 and 235 m^3, respectively (Table 4.2).

Table 4.2 Details of loads of dredged material transport to and disposed at the AMDG in March and April 2010 under the short-term pilot study consent permit.

Barge load no.	Date	Time (NZST)	Volume (m^3)	Cumulative volume (m^3)	Survey no.	Appx. release coordinates (NZTM)†
1	14-Mar-10	1940	530	530	-	-
2	20-Mar-10	905	540	1070	-	-
3	27-Mar-10	245	235	1305	-	-
4	31-Mar-10	2035	685	1990	-	-
5	2-Apr-10	1852	246	2236	-	-
6*	10-Apr-10	1107	720	2956	1	1851748.5 m E, 5989854.5 m N
7*	15-Apr-10	1002	685	3641	2	1851880.5 m E, 5989504.5 m N
8*	21-Apr-10	1004	570	4211	3	1851783.5 m E, 5989526.5 m N
9*	25-Apr-10	1033	662	4873	4	1851677.5 m E, 5989526.5 m N

*Disposed loads that were monitored for dispersion characteristics.

†Only coordinates for disposals corresponding to a field monitoring survey are shown.

In all cases, the *MV Mina Campbell* approached the AMDG on a path directed northeast from the southern tip of Great Barrier Island (in the Colville Channel) to

the centre of the AMDG. As an example, Figure 4.5a shows the way-point lines (red) and vessel track (blue/green) coming from Pine Harbour Marina to the southwest (not shown) through the Colville Channel and ending at the AMDG. The image is from a screen grab off the navigation computer of the *MV Mina Campbell* on 21 April 2010. Figure 4.5b shows a close-up view of the *MV Mina Campbell* path immediately following disposal of the load of material on 21 April 2010. The *MV Mina Campbell* typically travelled at a speed of 4-7 knots depending on the weather conditions and dredged material was released into the water column while underway in all cases. Opening of the hopper doors and insertion of the material into the water column was typically completed in less than 5 seconds.

Figure 4.4 *MV Mina Campbell* towing the split hull hopper *SB II Groper*, containing a load of maintenance dredged material from Pine Harbour Marina, to the AMDG on 20 March 2010.

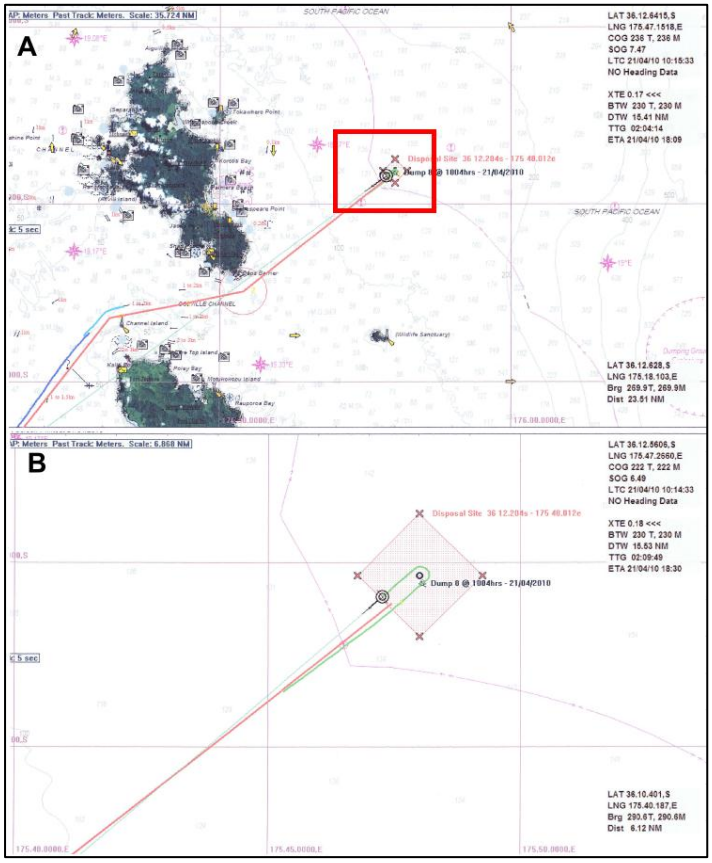

Figure 4.5 (a) C-plot screen grab of the vessel track from the navigation software aboard the *MV Mina Campbell* on 21 April 2010 immediately after release of dredged material. Vessel track indicated by the blue/green line. (b) close-up view of the centre of the disposal site (area inside the red rectangle in (a)) and the vessel track (green line) after turning back towards Auckland following disposal at the centre of the site.

4.5 Data Sources and Sampling Methodology

The data and findings discussed in the subsequent sections comprise 4 separate dispersion monitoring surveys undertaken in association with disposal operations at the AMDG that were consented as a pilot study to better understand the potential for loss of dredged material through dispersion processes. The surveys were undertaken immediately following the disposal of dredged material on 10, 15, 21, and 25 April 2010 and will be hereafter referred to as Surveys 1-4, respectively (Table 4.2). The methods used during each survey generally followed the same configuration, although small adjustments were applied where necessary to accommodate logistical issues encountered along the way.

Data collected at the AMDG before and after completion of all disposals will also be presented to complement and qualify some of the findings of the dispersion surveys. The majority of the ‘pre-‘ and ‘post-‘ disposal data will not be described because it relates more to the requirements of the consent and does not necessarily

enhance the findings of this chapter. However, detailed reports of the datasets are included in Flaim and de Lange (2011) (see Appendix III).

4.5.1 Meteorological Data and CTD Profiles

Refer to Sections 3.4.1 and 3.4.3 for descriptions of wind data and CTD profiling for the 2010 study period that correspond to the period in which all 9 loads of material were disposed at the AMDG.

4.5.2 Submerged Drifters

Submerged drifters, otherwise known as drogues, attached to surface buoys housing GPS transmitters and set to water depths of 10 and 30 m were deployed at the centre of the site AMDG prior to disposal on each of the four dispersion surveys (Figure 4.6). Drifters were left in the water for approximately 1 hour while GPS coordinates of each were received and recorded on the main survey vessel allowing for estimation of predominant current direction and velocity on the day of each survey. Coordinates were transmitted approximately every 5 min giving satisfactory resolution to the drifters' paths. Prior to arrival of the towed hopper, drifter observations were used to make decisions on where monitoring stations would be positioned. It should be noted however that often 2 or more hours passed between drifter deployment and the dispersion survey allowing time for changes in the current, especially with respect to the tide, that may not have been reflected in the drifters' paths.

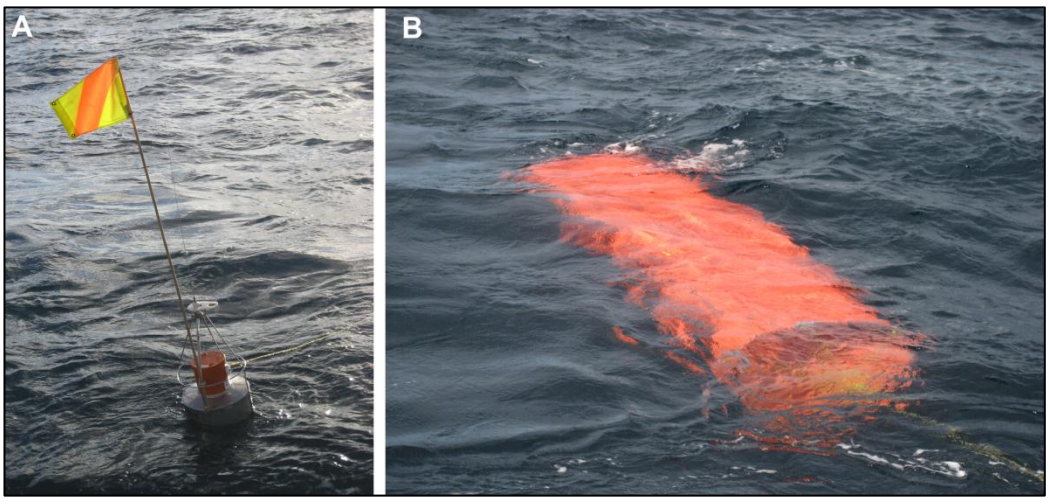

Figure 4.6 (a) Drifter buoy housing with a GPS transmitter. (b) Drifter sail immediately after deployment (as the hollow frame of the sail fills with water, it sinks to the designated depth).

On Survey 1, four drifters were deployed, two each at 10 and 30 m water depth. Due to time constraints involved in deployment and retrieval of the drifters and preparation of monitoring equipment in anticipation of the arrival of the towed hopper, for the remaining surveys, it was decided that only two drifters would be deployed, one each at 10 and 30 m water depth.

4.5.3 Water Samples

On each of the four surveys, water samples were collected at Stations A, B, and C at 5 and 10 m water depths (Figure 4.7). Sampling began approximately 5 min prior to release of the dredged sediment from the split hull hopper and was carried out at each depth every 5 min for the length of the survey. Sampling was undertaken for about an hour on each survey and was stopped after the surface plume was no longer visible (Table 4.3). Due to the transient nature of the surface plume, Stations A and B were not always located directly in the disposal plume. During Survey 1, Stations A and B were discovered to be located mainly at the southern end of the plume and should have been preferably situated closer together. A similar scenario arose on Survey 2 as well. To compensate for this miscalculation, during Survey 2, Stations A and B were relocated (new locations labelled Stations A2 and B2, respectively) (Figure 4.7). The move did allow for sampling directly in the plume, however technical difficulties encountered during the shift to the new sites resulted in only approximately 10 min of water sampling in the new locations.

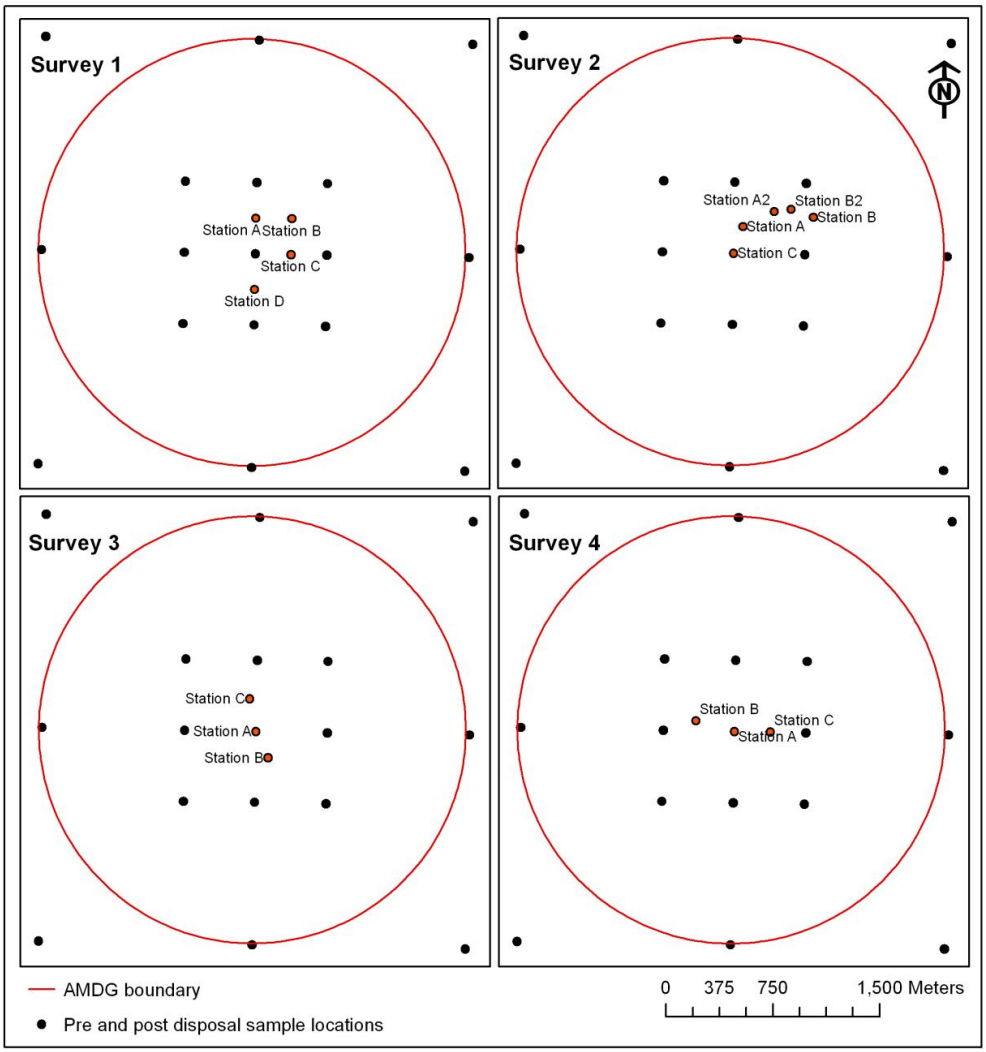

Figure 4.7 Locations of survey stations A, B, C, and D on Surveys 1-4.

Table 4.3 Water sampling period at each station during each survey. Samples were collected every 5 minutes for the length of the survey.

Survey no.	Disposal time (NZST)	Water sampling period		
		Station A	Station B	Station C
1	1107	1100-1155	1100-1155	1100-1155
2	1002	955-1125	955-1120	830-910
3	1004	1007-1117	957-1117	957-1117
4	1033	1035-1140	1025-1140	1025-1130

Water samples were collected nearly simultaneously at 5 and 10 m water depths using either 'Niskin' and 'Van Dorn' style samplers or 'Schindler-Patlas' traps. Approximately 1 L of water was retained from each collected sample and stored on ice initially, then frozen until sample processing was possible.

Following each survey, known volumes of the water samples were filtered through pre-rinsed, dried, and weighed filters to collect suspended particles (APHA, 1997). The labelled filters were then dried for 24 hours at 105°C and the

re-weighed. The following formula was then used to calculate suspended sediment concentration (mg/L):

$$SSC = [(x_2 - x_1)1000]/y \qquad \text{Equation 4-1}$$

where x_1 is the weight (g) of the rinsed and dried filter paper, x_2 is the weight (g) of the re-dried paper following filtration, and y is the volume (l) of sample filtered (APHA, 1997).

4.5.4 Optical Turbidity Measurements

Turbidity is a measurement of the transparency of the water which is directly proportional to the number of particles suspended in that water (Davies-Colley & Smith, 2001). So, although turbidity is not a direct measurement of suspended solids concentration (SSC), this value can be inferred and closely estimated through calibration procedures. Turbidity sensors are essentially optical sensors and function by measuring the amount of light scattered or the amount of light absorbed/attenuated by suspended particles through the use of a light source and a photo-detector (Davies-Colley & Smith, 2001). The photo-detector converts the light radiated by the water into a photocurrent usually in units of volts (V) or amperes (amps). The light radiated by the water is dependent on the number, size, shape, orientation, and colour of particles, and their reflection index. Individual turbidity sensors are usually designed to function in a set range of turbidity with maximum and minimum voltage outputs.

Optical backscatter measurements

To obtain stationary time series of turbidity levels in and near the disposal plume, optical backscatter type turbidity measurements were recorded during each of the 4 dispersion surveys. At each of the stations A, B, and C (and Station D on Survey 1) (Figure 4.7), sensors were deployed at 5 m and 10 m below the surface to coincide with water sampling depths (see Section 4.5.3). During some of the surveys, sensors were added at different depths to increase data coverage and to provide back up for some sensors that were less reliable. Appendix Table I.5 details the turbidity sensor deployments on each of the four surveys and each station. Where the data period is marked ‘none’, no data was recorded by the sensor due to technical problems.

Sensors were suspended off assisting vessels on lines at 5 m and 10 m below the surface with cables attached to loggers and batteries in water-tight containers at the surface (Figure 4.8). Each container was equipped with a power switch so that the sensors could be deployed well in advance without the necessity of recording extraneous data. Using radio communication from the main survey vessel, assistants were told when to turn on and off the sensors. This method also preserved battery power. Some of the sensors functioned with internal loggers and an internal power source. These sensors were programmed the morning of each survey to power on and off at the appropriate times.

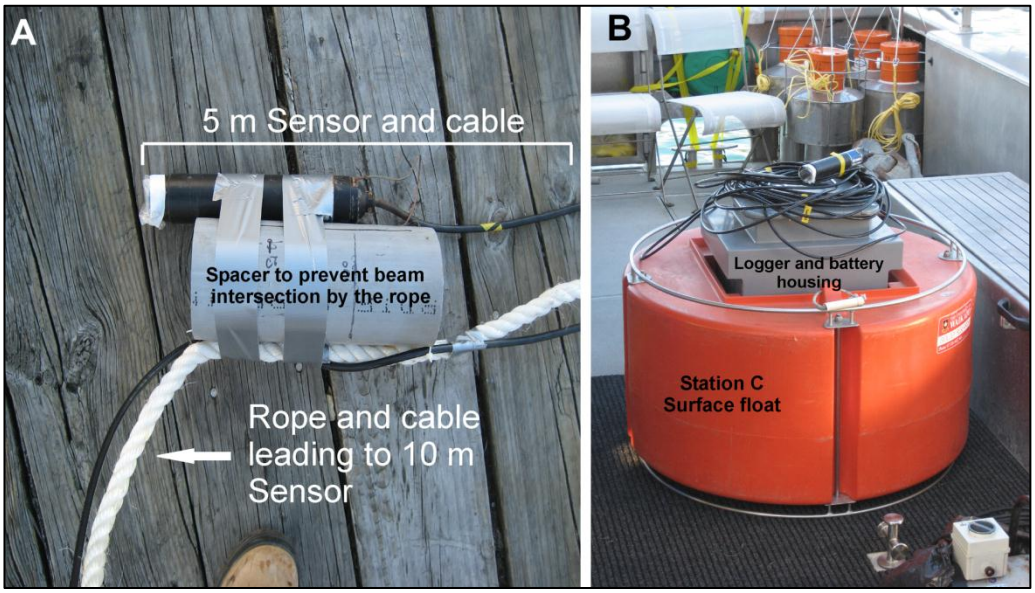

Figure 4.8 Sensor deployment configuration. (a) 5 m sensor attached to a rope with a second cable leading to the sensor attached at 10 m (spacer prevents light beam intersection by the rope). (b) surface float for Station C containing the water tight logger and battery housing from which the sensors were suspended (note: Stations A & B housings' were secured on deck of the assisting survey vessels).

During the four dispersion surveys, a variety of sensors were used, each with different specifications and functions (Campbell Scientific Inc., 2008; Greenspan Technology (a), n.d.; Greenspan Technology (b), n.d.; Turner Designs, 2002). Prior to the field surveys, tests were done on the sensors to determine their applicability for the presumed level of turbidity that would arise following release of dredged material at the site. Only in the case of Sensor 9 was the maximum range surpassed during the surveys. Sensor 9 was deployed during Surveys 3 and 4 as a replacement for a lost sensor and due to time constraints, full testing prior to deployment was not performed.

The sensors were programmed to take 1 reading per second, with the exception of sensors 5 and 6 that were internally programmed to a 9 s sampling interval (Appendix Table I.6). In most cases, data was recorded in millivolts (mV), with the exception of Sensor 9 which recorded in volts (V) and Sensor 8 which was pre-calibrated using Formazin standards allowing for direct conversion of the recorded photo current into Nephelometric Turbidity Units (NTU).

Following the dispersion surveys, the turbidity data was scaled to SSC (mg/l) using calibration coefficients determined by comparing sensor readings to known concentrations of marina basin sediment added progressively to continuously circulating water in a calibration tank. As turbidity sensors were deployed off the same stationary vessels were water sampling was undertaken, equally limited data recorded the levels of turbidity expected for the plume, therefore it was determined the majority of the sensor data was not useful.

Transmission measurements

BIO-FISH is a vessel towed multi-sensor probe linked to a PC system on deck where data are recorded (Figure 4.9) (ADM Elektronik, 2003). BIO-FISH has wings that can be controlled from the PC system; where wing-angle can be adjusted to allow undulation of the fish at desired intervals and water depths behind the boat. BIO-FISH is equipped with a turbidity sensor called a transmissometer. Unlike measurement by turbidity sensors described in the previous section, a transmissometer measures beam attenuation, which is also proportional to the quantity and type of suspended particles in the water column (Davies-Colley & Smith, 2001). BIO-FISH was towed from the main survey vessel on Surveys 3 and 4 for entire survey period. On Survey 3, BIO-FISH was undulated between approximately 5 m and 25 m below the surface for the length of the survey. On Survey 4, BIOFISH was undulated between approximately 10 m and 20 m below the surface for the length of the survey. Data was recorded as one continuous transect.

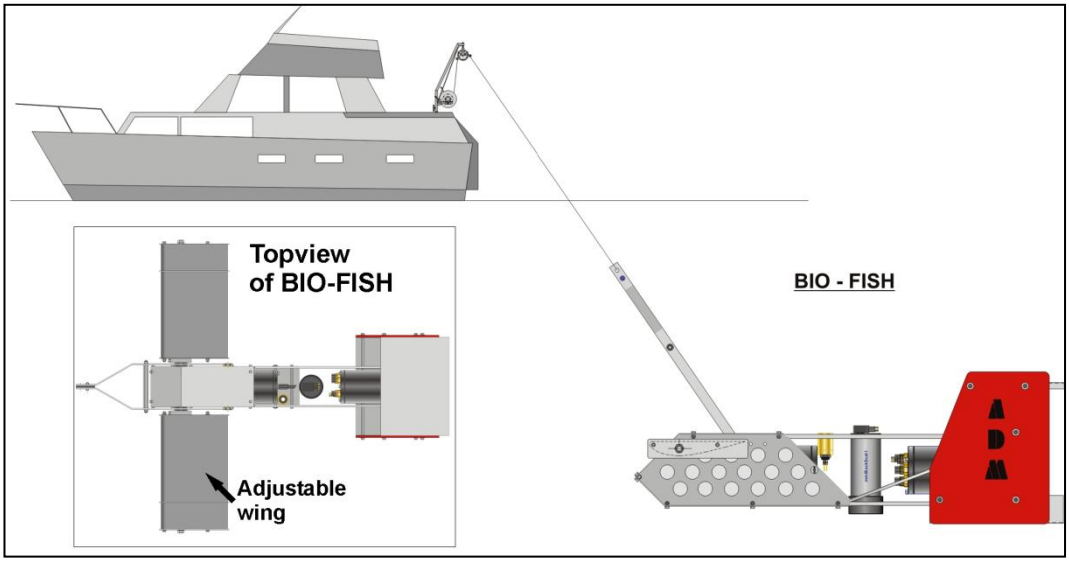

Figure 4.9 BIO-FISH deployment configuration (inset: top view showing adjustable wings that allow for vertical undulation of the fish).

4.5.5 ADCP Data Records

During each of the 4 dispersion surveys ADCP data were recorded by a boat-mounted system. Refer to Section 3.4.2 for details on the system used and conventions applied. The number and length of transects traversed during each survey varied depending on the visibility of the surface plume (Appendix Table I.7). Generally, the survey vessel was directed either across or along the axes of the visible surface plume until it was no longer visible typically 1 hour post-disposal. Locations of transects recorded during each survey are shown in Figure 4.10.

ADCPs are traditionally used to measure current velocity and direction based on the principle of the Doppler frequency shift of a moving object (Figure 4.11) (Puckette, 1998). The current velocity and direction ADCP data will be presented to make an assessment of the underlying hydrodynamics of each surveyed disposal. However, by using the amplitude of the reflected acoustic signal, otherwise known as backscatter, turbidity and thus suspended sediment concentration can also be inferred from these devices (Figure 4.11) (Gartner and Cheng, 2001).

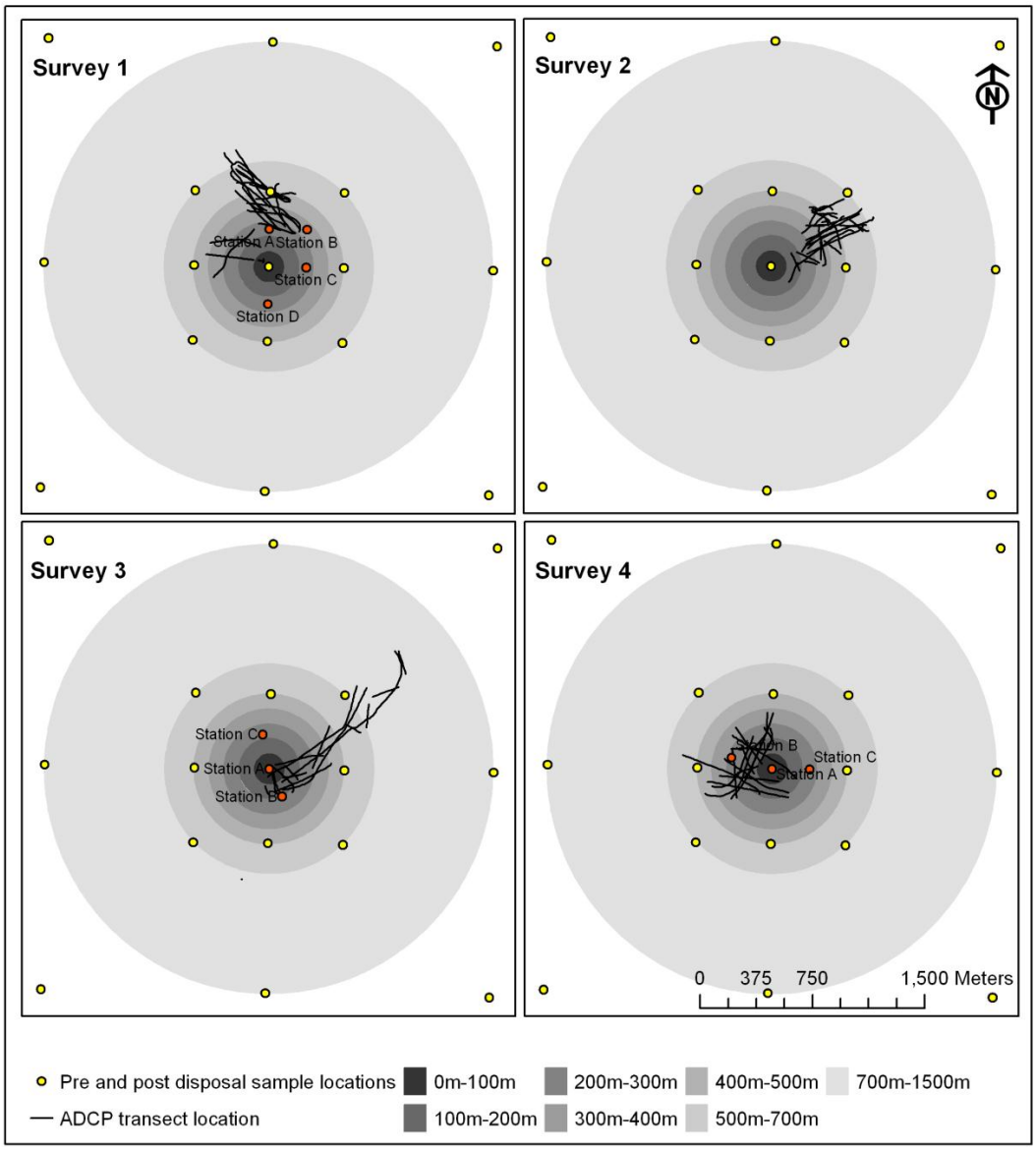

Figure 4.10 ADCP transect locations (black lines) for Survey 1-4.

Backscatter Strength is the ratio between backscatter and incident sound intensity after reflection off particles floating in the water column and is measured in decibels (dB). There are some limitations to this method (e.g. range of detected particle sizes; change in concentration is indistinguishable from change in particle size), but in general it can be very effective in detecting suspended particles. In the case of monitoring a plume, vessel mounted ADCPs can provide not only temporal turbidity data, similar to stationary turbidity sensors, but also data indicative of the spatial extent of the plume. Spatial data is dependent on the path of the vessel in that it must be congruent with the area of the plume.

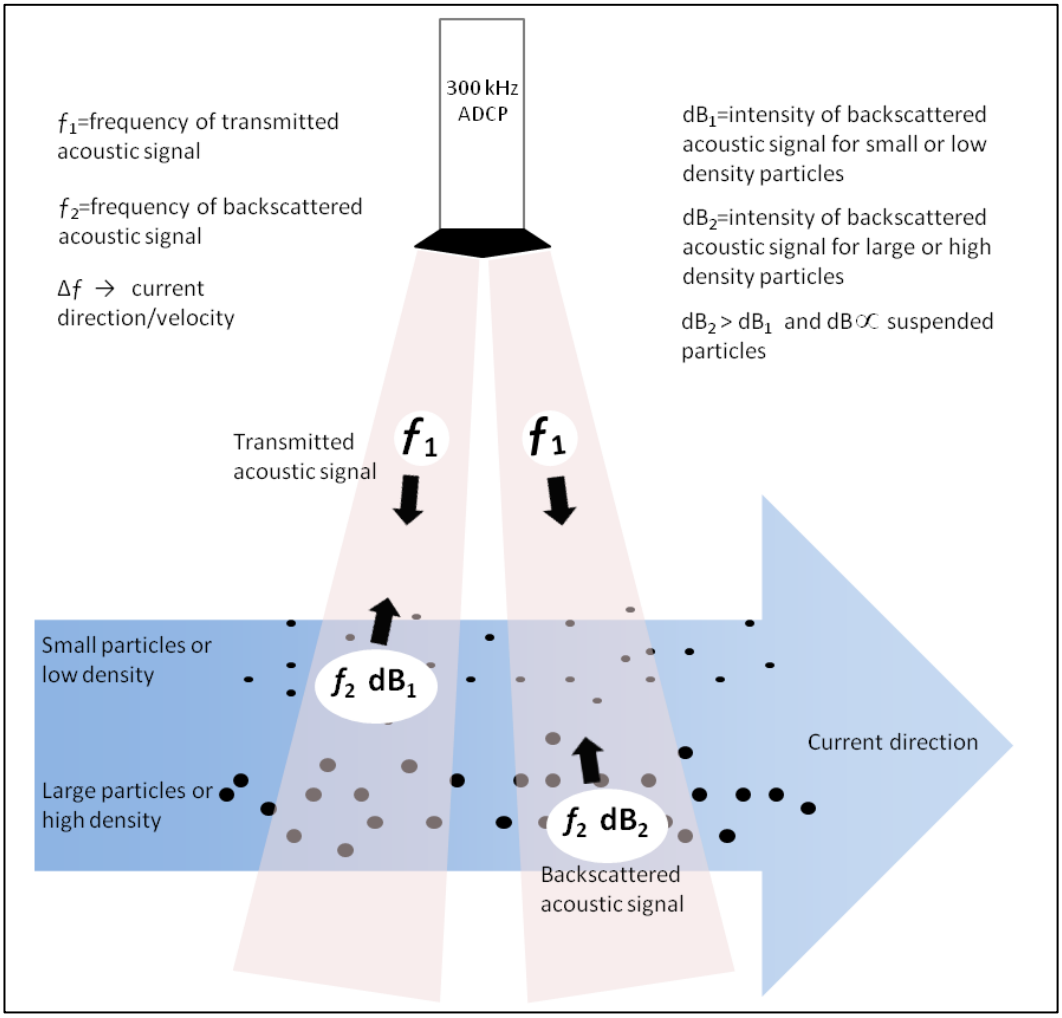

Figure 4.11 Diagram of ADCP "Doppler" frequency (*f*) shift principle and backscatter intensity (dB) relationship to suspended particles.

As reported by the manufacturer, the ADCP system used was capable of recording data in water depths up to approximately 165 m (Teledyne RD Instruments, 2008), which is slightly deeper than the maximum depth (~150 m) at the eastern boundary of the AMDG. However, achieving maximum resolution at the limits of the system is dependent on deployment factors such as power supply, cable length, and appropriate user settings.

By applying the Rayleigh (long wavelength) scattering model, the appropriateness of the device for inferring turbidity levels can also be determined (Gartner & Cheng, 2001). This theory is based on the particle size distribution and the frequency of the ADCP (300 kHz in this case). The model says that backscatter intensity will be most representative where the ratio of the particle circumference to the wave length of the acoustic signal is less than 1 or

$$\left[2\pi r_g / \lambda\right] < 1 \qquad \text{Equation 4-2}$$

and

$$\lambda = c / f \qquad \text{Equation 4-3}$$

where r_g is the radius (m) of the particle, λ is the wavelength (m) of the acoustic signal, c is the speed of sound (m/s) in water (~1500) and f is the frequency (Hz) of the acoustic signal. Where the above ratio is less than ~0.01, backscatter intensity is less representative of the suspended particles present. Within those ranges and with respect to the frequency of the ADCP used (300 kHz), the particle size distribution that is best represented by the backscatter intensity data is approximately 15 µm – 1.5 mm or medium sized silt to very coarse sand (Udden-Wentworth scale). In this case, representation of sediment size classes outside this range may not be as robust. However, flocculated clay-sized particles are effectually larger than individual clay particles and would likely be registered by the ADCP system (Gartner, 2004).

ADCP Backscatter Calibration

It is common practice to scale ADCP backscatter data into measures of SSC through calibration with SSC measured from water samples (viz. Gartner (2004); Hill et al. (2003); Hoitink and Hoekstra (2005); Holdaway et al. (1999)). In the present study, the main purpose of the water sampling described in Section 4.5.3 was for calibrating ADCP backscatter data to SSC. It was intended that the optical turbidity measurements (Section 0) would firstly serve as a back-up to the water sample derived SSC measurements because the raw photocurrent records could easily be lab-calibrated to values of SSC (Holdaway et al., 1999). Optical turbidity measurement can also serve as a validation of the scaled ADCP backscatter data records (viz. Hoitink and Hoekstra (2005)).

For successful calibration of ADCP backscatter data, measures of SSC, whether derived from field water samples or lab-calibrated optical turbidity sensors, need to be collected or recorded from nearby the ADCP transducer head or near an area of the water column ensonified by the transmitted acoustic signal without interfering with it. This is typically achieved through a moored ADCP configuration where the water samples are collected near the upward-facing transducer of the ADCP system (e.g. Traykovski et al. (2000); Bartholomä et al.

(2009)), though boat-mounted examples with corresponding water samples do exist (e.g. Schettini et al. (2010); Tubman et al. (1994)). In the present study, it was anticipated that calibration would be achieved by matching ADCP backscatter measurements from the ADCP bins nearest to 5 and 10 m below the surface to the time series of the corresponding water samples from the various stations as the vessel passed by at a semi-regular interval similar to the methods used by Alther (1984) and Fagerburg and Pratt (1995).

In practice though, it was not feasible to navigate the vessel closer than approximately 5-10 m of the stationary sampling stations. As a result and due to the unexpectedly transient nature of the disposal plume, very few measurements of SSC or optical turbidity from within the disposal plume could be confidently matched to a particular ADCP backscatter measurement. Further, more often than not, the sampling stations do not appear to have been located in the plume at all as evident by the overall very low turbidity levels recorded there. This was likely due to the fact that the majority of the disposal plume quickly descended to deeper parts of the water column where it was not feasible to collect water samples and record turbidity data. The small portion of the plume that remained at the surface may have easily passed by the sampling stations undetected. Such difficulties in collection of suitable data for calibration of ADCP backscatter were also experienced by Fagerburg and Pratt (1995) and Tubman et al (1994).

Due to the difficulties described above, the water sample data and optical turbidity sensor data were determined to be non-significant. Similarly, the turbidity data recorded by the BIOFISH, while more representative of the plume than the data collected using stationary measures because the instrument was towed directly through it, was also deemed to be non-significant because it was limited to only the near-surface areas. The water sample and turbidity datasets will, therefore, not be discussed within the context of this chapter, but are described and discussed in detail in Flaim and de Lange (2011) (see Appendix III).

Puckette (1998) reviewed the difficulties involved in the collection of water samples that represented the plume turbidity levels for direct correlation of backscatter measurements to SSC. Given the logistical problems, a method for converting backscatter directly into SSC through the use of acoustical theory has also been developed and used reasonably successfully, but is limited by the

information available on the suspended sediment and the system specifications (Ha et al., 2011; Holdaway et al., 1999; Tubman, 1995). The acoustical inversion method requires that the following conditions be met: particle size distribution of the suspended sediment is known, water properties (salinity, temperature, density, and speed of sound) are known, the acoustic system is calibrated, and constants relative to the transmitted and received signal strength have been determined (Tubman, 1995). Puckette (1998) reviewed the sonar equation with reference to Clay and Medwin (1977), Ogushwitz (1994), and Tubman (1995) as follows:

assuming Rayleigh scattering, the volume backscattering strength (S_v) is equal to

$$10\log_{10}\left(C_v k^4 r_g^3\right)+10\log_{10}\left(k_1\right)+20 \qquad \text{Equation 4-4}$$

where C_v=volume concentration scatterers, k=wave number of acoustic energy, r_g=particle radius, k_1=constant. S_v must be calculated for each grain size and because it is dependent on grain size to the third power, it is highly sensitive to small errors or changes in the grain size distribution. The sonar equation relates S_v to the backscatter measured at the transducer (RL) by

$$SL - AL + S_v - RV \qquad \text{Equation 4-5}$$

where SL=source level from transducer, AL=all acoustic losses, RV=ensonified volume. With a calibrated system, SL and RL are known and RV likewise depends on a calibrated system, but also the known geometry of the transducer. Acoustic losses (AL) can be calculated from acoustic theory and water column properties (i.e. temperature, salinity, density, and sound speed (Fisher & Simmons, 1977) and is also dependent on the concentration and particle size.

The only unknowns then are the suspended sediment concentration (C_v) and the particle size distribution, which are part of the S_v and AL terms. Assuming particle size distribution can be determined from sediment samples (either from filtered water samples or from the seabed where the suspended sediment originates), the sonar equation can be solved for concentration. If the system is uncalibrated, a reference concentration at a known depth can be used to provide the necessary constants to calculate the concentration within the remainder of the water column (e.g. Holdaway et al. (1999)). Unfortunately, the system used in this study was not calibrated, and as previously mentioned, attempts to collect reference

concentrations at known depths were unsuccessful, and so inversion of the backscatter dataset to SSC was not possible.

It is not expressly necessary to scale ADCP backscatter data to values of SSC to get information about the movements of suspended particles however, as the dB levels are still representative of relative turbidity and can also be used to show spatial and temporal variability of suspended sediment (e.g. Siegel et al. (2009) and Tsai et al. (1992)). As such, in the following sections, ADCP backscatter intensity data will be presented to show the important sediment dispersion pathways involved in the process of dredged material disposal at the AMDG. For this study, backscatter strength (dB) for all 4 dispersion surveys has been normalised to a universal scale of relative turbidity (RT) ranging from 0-1 so that comparisons could be drawn between patterns and variability of the different disposal events.

Acoustic shadowing of the lower parts of the water column commonly occurred during the first several transects of each survey due to very high initial turbidity levels in the upper parts of the water column prior to significant dilution of the inserted dredged material. This effect resulted in missing data in the ADCP bins directly below the highest turbidity regions. In transects with missing data within the measurable range, interpolation was undertaken to better visualise the full vertical distribution of the elevated turbidity.

4.5.6 Bottom Echo Sounder Record

During Survey 4, the screen display of the vessel echosounder aboard the *MV Ten Sixty* was filmed using a tripod mounted camcorder. Periodically throughout the footage, the current time was noted (filmed) so that the footage could be temporally correlated to the ADCP data from that survey. The screen display of the system included a vertical water depth scale which was visible in the footage, though some loss of resolution was evident due to sun glare and reflection of the camera on the screen display. The footage of the continuous echosounder record is used as a complement to the ADCP backscatter data records in that during periods of very high turbidity (i.e. 1-2 minutes after insertion of dredged material into the water column), the ADCP showed a complete data loss because the turbidity was beyond the measurable range of the system. It was not, however, out

of the measureable range of the vessel echosounder which confirmed that the data loss in the ADCP record was in fact due to extremely high turbidity.

4.5.7 MBES Datasets

In September 2008 and July 2010, which correspond to pre- and post-disposal periods, multibeam echosounder (MBES) surveys were undertaken using the Kongsberg (formally Simrad) EM3000 MBES (300 kHz) owned by the University of Waikato, Department of Earth and Ocean Sciences, Coastal Marine Group (Kongsberg, 2005). The set-up of the system on the *MV Ten-Sixty* involved surveying the locations of the sonar head, GPS antenna, and motion sensor with respect to a reference point near the centre of the vessel and the water level on the vessel while in motion. These measurements were used to account for any offsets in the data once acquired. An estimate of the sounding error budget for the surveys is included in Appendix Table I.8. The estimates correspond to soundings gathered at minimum, intermediate, and maximum depth levels and were based on system accuracies for the outer beams. Accuracy standards published by Land Information New Zealand (LINZ) are included and show that the system error estimates fall between MB-2 and MB-3 error standards.

Acquisition lines used to navigate the vessel during the survey were generated using Trimble HydroPro software based on the four coordinates encompassing the AMDG boundaries (175°45’57.593” E, 36°11’09.618”S; 175°49’26.857”E, 36°11’09.618”S; 175°49’26.857”E, 36°13’50.956”S; 175°45’57.593”E, 36°13’50.956”S) (Figure 4.12). The distances between acquisition lines were designated based on the swath width achieved in the 2008 MBES survey (~200 m), as well as on the time allocated for the survey. A small amount of overlap was allowed for in the data acquisition; however, as the system was operated at its depth limits, averaging was mainly over the noisy outer beams and, therefore, most likely did not improve accuracy greatly. MBES data was acquired with Triton Imaging Inc. Isis software. Bathymetry data was processed with Triton Imaging Inc. Bathypro software and gridded at a 1 m resolution. Tides were removed from the MBES bathymetric data based on modelled tides provided by

MetOcean Solutions Ltd.[8] which also accounted for the effects of forecasted atmospheric pressure. Backscatter data was processed using Hypack Geocoder software by which along-track banding effect was removed. Backscatter data was mosaicked at a resolution of 1 m.

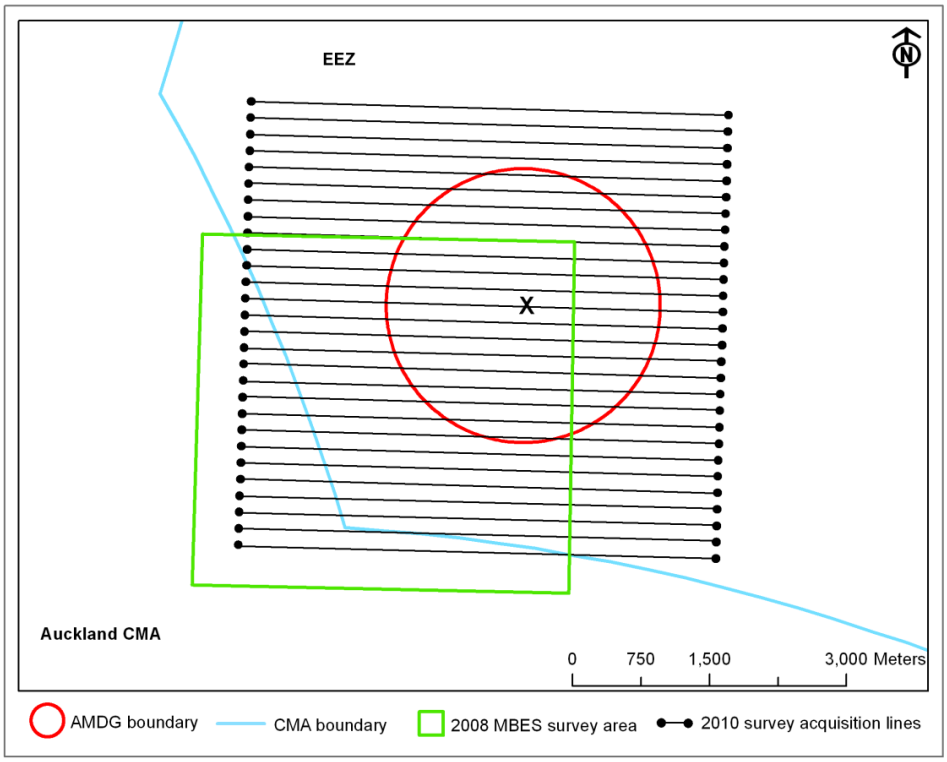

Figure 4.12 Survey areas of the 2008 and 2010 MBES records.

MBES systems are designed to measure sea floor topography with very high accuracy (Lurton, 2002). They are composed of a transmit array of transducers that emit an acoustic signal in direction of the seafloor, and of a receive array of transducers that record the signal reflected off targets in the water column or the seafloor. The principle for echo sounding in MBES is very similar to that of the single-beam echosounder (SBES) except for its formation of a high number of beams (up to 128 for the EM3000), in comparison to a unique beam for SBES, allowing for much denser coverage of the seafloor.

MBES bathymetry data show the variation in depths of the sea floor. The precision of the measured depth is dependent upon the transmitted frequency, sampling frequency, beam pointing angle, beam width, the technique used for

[8] MetOcean Solutions Ltd. employed the MSL implementation of the Princeton Ocean Model (POM) to hindcast tidal currents in the New Zealand region (Mellor, 2004). Boundaries were forced with tidal elevation and current velocity from the TPXO7.0 global inverse tidal solution (Egbert & Erofeeva, 2002).

bottom detection, and the actual water depth. The EM3000 in theory achieves a measurement accuracy of 5 cm RMS in shallow water (Kongsberg, 2005). However, due to increased sound absorption and heterogeneous physical conditions of the water column over large distances, this precision can be significantly less in deeper waters like those encountered during the pre- and post-disposal surveys. For a detailed description of the bathymetry of the AMDG based on data acquired using MBES methods please refer to Flaim and de Lange (2011) (see Appendix III).

Beyond determining the bathymetry of the sea floor, MBES systems are being increasingly used to determine sediment composition of the sea floor through the processing of its signal amplitude (backscatter) in a similar way as side-scan sonar (SSS) imagery (Beyer et al., 2007; Hughes Clarke et al., 1996; Preston et al., 2003). The use of backscatter in this case is also similar in principle to the use of ADCP backscatter to detect the quantity or density of particles in the water column described in Section 4.5.5.

MBES backscatter data, like SSS imagery, typically show the variations in seafloor "hardness" and "roughness". MBES backscatter data are processed into an imagery of the seafloor, which is like an "acoustic picture". Due to lack of calibration in commercial MBES systems and processing corrections being applied to the data for "cosmetic" purposes, the dB values in MBES imagery are, like that of SSS imagery, purely indicative. However, the variations in imagery tone and texture are useful to identify and position transitions from one sediment type to another, to be confirmed afterwards through ground-truthing surveys. In a general manner, a harder and/or rougher seafloor will present higher backscatter strength.

4.5.8 Sediment Samples

In 2008 and 2010, before and after the pilot study disposals at the AMDG, sediment samples were collected as a part of the preliminary studies in the former and as a requirement of the consent conditions in the latter. Samples were collected at locations across the AMDG and beyond (see Figure 4.7 for the positions of some of the sample locations) using a small gravity corer. Core barrels were 60 cm long by 70 mm wide (internal diameter). Due to the water

depth at the site, the corer never penetrated the seabed at a maximum velocity, which limited the length of the obtained core, however, other devices trialled for the purpose of sediment collection were even less successful.

For the requirements of the EIA and the disposal consent, samples were processed for benthic fauna and for various sediment characteristics such as particle size distribution, organic content, heavy metal concentrations, and total petroleum hydrocarbons. However, as the samples were not representative due to the barrel dimensions and shortened penetration depth, and because time limits restricted the number of replicates and sample spacing, statistical analysis was not possible. Findings on sediment characteristics will, therefore, not be described in detail, but will be drawn on in a qualitative manner to complement other findings of this thesis. A detailed description of results of analyses on collected sediment samples is provided in Flaim and de Lange (2011) (see Appendix III).

4.5.9 Seabed Video

Video of the seabed was recorded at locations indicated in Figure 4.13 at the AMDG on 26 July 2010, almost 3 months after the pilot study disposal operations had ceased. The purpose of filming the surface of the seabed was to identify the presence of deposited dredged material. The camera system was borrowed from Leigh Marine Lab of University of Auckland. Footage is recorded from approximately half a metre off the seafloor via a 4-legged frame (Figure 4.14). Though the frame was designed to be stationary, once set down on the seafloor, it was possible to pan the camera from approximately 0° to 90° vertically, and approximately 360° horizontally via a cable connected to an on deck control system (Figure 4.14b&c). Lighting could also be controlled via a dimmer housed in the same control box. Maximum and sustained brightness of the lighting units was compromised due to the length of cable required to reach the seabed. This resulted in a somewhat lower resolution to the video footage than was anticipated, but seabed characteristics were nonetheless identifiable.

Similar to the sediment characteristics, epi-benthic seabed characteristics at specific locations will be discussed to complement and qualify other findings of this thesis. Freeze-frame images of all locations filmed are included in Flaim and de Lange (2011) (see Appendix III).

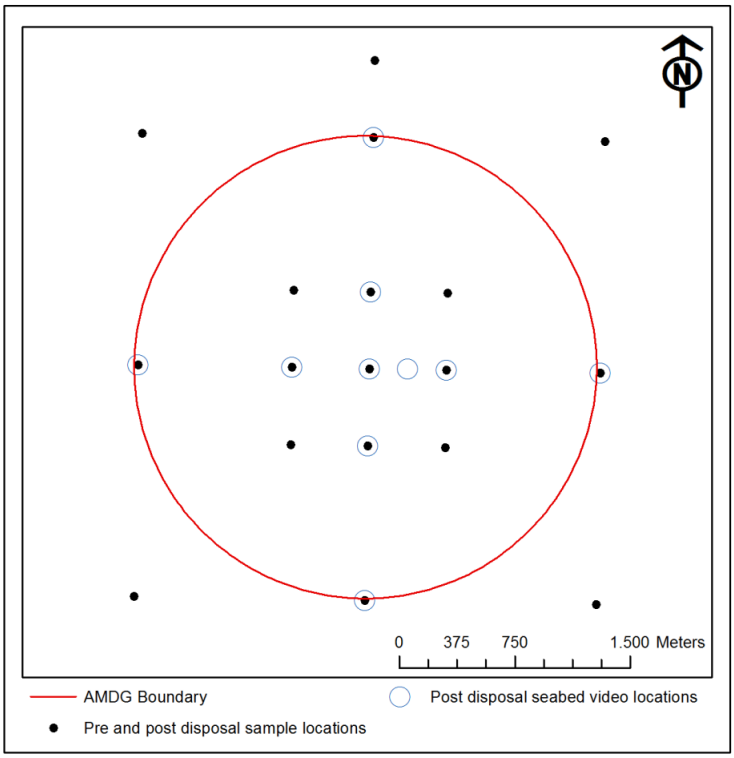

Figure 4.13 Sampling sites including locations of seabed video footage recorded after completion of all disposals.

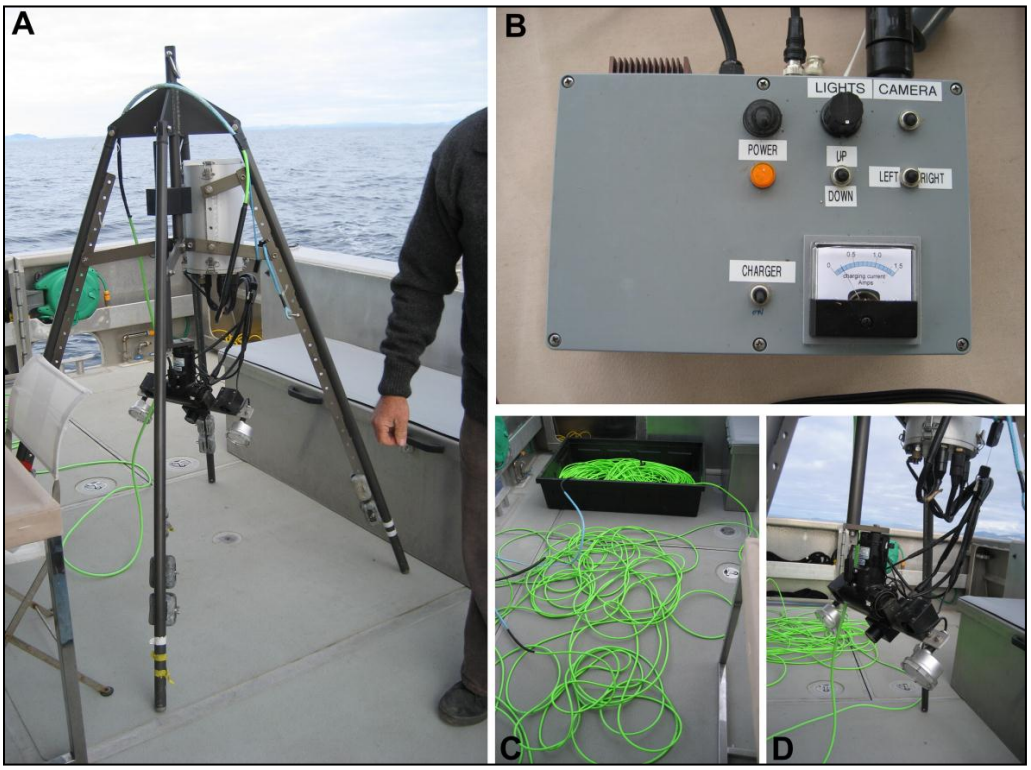

Figure 4.14 (a) frame-mounted underwater video recording system used to film the seafloor at the disposal site following disposal of 4873 m^3 of dredged material in March and April 2010, (b) onboard control system for panning and lighting, (c) cable for controlling camera and real-time viewing, and (d) close-up of camera flanked by lighting units.

4.6 Survey Setting: Environmental Conditions

Although it was envisaged that a variety of environmental conditions (e.g. weather and sea) would be incorporated in the dispersion surveys, the timing of the surveys were for the most part under control of the dredging contractor and the weather forecast. In general, it was not feasible for either the *MV Mina Campbell* or the survey vessels to operate in weather and sea conditions much less than optimal. To add to the complexity, the surveys could only take place during daylight hours, which meant that the comparably slow-moving tug and hopper had to depart Pine Harbour Marina approximately 12 hours prior to the designated disposal time. Therefore, when acceptable weather conditions aligned with an adequate barge load of dredged material and the opportunity for a night time departure, a survey would be scheduled the following morning. Fortunately, the environmental conditions of the 4 survey days were variable enough to be regarded as a 'variety' as stipulated by the consent requirements and though the conditions encountered certainly do not represent the full range of conditions that would occur at the AMDG, they can be regarded as characteristic of the conditions during which disposal would be feasible.

4.6.1 Wind and Sea Situation

Wind and sea conditions during each survey were obtained through first-hand observations (Table 4.4), the NIWA tide model (Figure 4.16), wind records from the CliFlo wind station at Mokohinau Islands (see Section 3.5 for details) (Figure 4.15), and CTD profiles recorded on the day of each survey (see Section 3.6). Density structure of the water column on each of the four 2010 survey days was discussed in depth in Section 3.6.3 of Chapter 3, but will be re-visited here for the purposes examining the effects of the environmental setting on disposal dynamics. It bears mentioning again that the density values derived from the CTD measurements did not originate from direct measurements of the water density, but from calculations of density using temperature, salinity, and pressure. Therefore, variations in the density structure of the water column observed during the surveys did not reflect contributions from suspended particles, which ordinarily would cause an increase in the local water density.

Table 4.4 Summary of conditions during Surveys 1-4.

Survey no.	Disposal Time	Tide	Wind	Sea State (observations)
1	1107	Early flood	SE 10 knots	Slight; 1m swell towards SE
2	1002	Mid ebb	SW 10-15 knots	1 m seas from the SW; wind chop strong
3	1004	Mid to late flood	SW 5 knots	Calm; 0.5 m swell from the SW
4	1033	Early flood	NE 10 knots	variable

Survey 1

During Survey 1, the tide stage was in early flood (Figure 4.16), wind was tending southeast at 10 knots, and the sea was slight with a 1 m swell towards the southeast. Conditions during Survey 1 were ideal for the survey methods (Table 4.4). Wind records from Mokohinau Islands agreed reasonably well with observer notes and showed that in the hours leading up to and during the survey, wind was from the southeast or east and the speed was ~5 m/s (~10 knots) (Figure 4.15). The density structure of the water column mirrored closely the thermal characteristics discussed in Section 3.6, which showed that the mixed layer extended to a depth of 70 m on the day of Survey 1 below which temperature decreased consistently. Figure 4.17a shows that a distinct pycnocline was present at the same depth. Smaller scale steps or kinks in the density profile representing a larger change in density are evident elsewhere in the water column as well. These steps or kinks will hereafter be referred to as *density transitions*. Beyond the principal pycnocline 70 m below the surface, additional significant density transitions were identified at 15, 25, 90, 110, 130 m below the surface. Density was 1025 kg/m^3 from the surface to 70 m and increased relatively consistently to a maximum of approximately 1027 kg/m^3 at the bed. The density at the principal pycnocline was 1026 kg/m^3.

Survey 2

Conditions during Survey 2 were less ideal for monitoring due to significant wind chop. Wind tended southwest at 10-15 knots with 1 m seas from the southwest (Table 4.4). Tide was ebbing (Figure 4.16). Antecedent winds matched observations well, with consistent >5 m/s winds from the southwest (Figure 4.15). The density profile measured during Survey 2 was slightly different than that measured during Survey 1 due to an increase in depth of the mixed layer to 80 m and the addition of a thin (5-10 m) slightly lower density layer centred approximately 20 m below the surface (Figure 4.17b). Additional small scale

density transitions were observed at 90, 110, and 120 m below the surface. Similar to that observed in Survey 1, density ranged from 1025 kg/m^3 at the surface to 1027 kg/m^3 at the bed. Density at the principal pycnocline was also 1026 kg/m^3.

Survey 3

During Survey 3, conditions were calm with winds tending southwest at 5 knots and 0.5 m seas from the southwest (Table 4.4). Tides were flooding (Figure 4.16). Wind records from Mokohinau Islands showed that winds were consistently stronger (~5 m/s or 10 knots) than what was observed at the site, but were similar in direction tending from either the south or the southwest in the day leading up to the survey (Figure 4.15). The mixed layer depth decreased significantly after Survey 2 with the principal pycnocline located only 30 m below the surface on the day of Survey 3 (Figure 4.17c). Additional notable density transitions were identified at 65, 90, 100, and 120 m below the surface. Density again ranged from 1025 kg/m^3 to 1027 kg/m^3, with a principal pycnocline density of 1026 kg/m^3.

Survey 4

Observations from Survey 4 noted that conditions were variable with a tendency from the northeast at 10 knots and the sea was relatively calm (Table 4.4). The tide was flooding (though only just past slack tide) (Figure 4.16). Mokohinau Islands wind records also showed variable conditions, but rather than tending northeast as was noted, wind direction appears to have transitioned from WSE 20 hours prior to the survey to southerly and then to south-easterly during the survey (Figure 4.15). Inconsistencies between observations and wind records could be a result of human error or possible differences in wind climate between Mokohinau Islands and the AMDG. By Survey 4, the mixed layer depth had re-established at 80 m after the previous rise observed during Survey 3 (Figure 4.17d). A pronounced low density (1024 kg/m^3) layer was present 20 m below the surface, below which density was consistent with that observed in the upper mixed layer for the study period (~1025 kg/m^3). Small scale density transitions were also observed at 90, 100, 110, and 130 m below the surface. With the exception of the low density spike 20 m below the surface, density ranged from 1025 kg/m^3 to 1027 kg/m^3 with the principal pycnocline at 1026 kg/m^3.

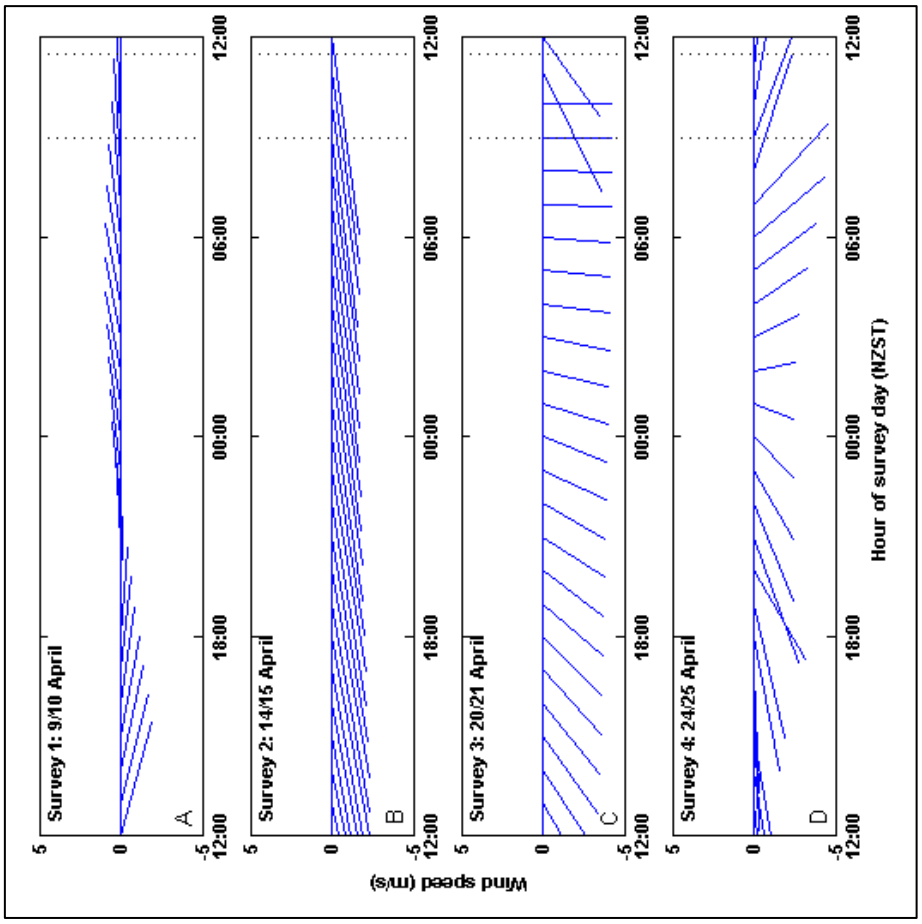

Figure 4.15 Hourly wind speed at Mokohinau Islands (CliFlo data record) starting at noon the day before through noon on the day of each dispersion survey. Scale of the feather plots are indicated by either the positive or negative y-axes. Dotted lines indicated approximate survey periods.

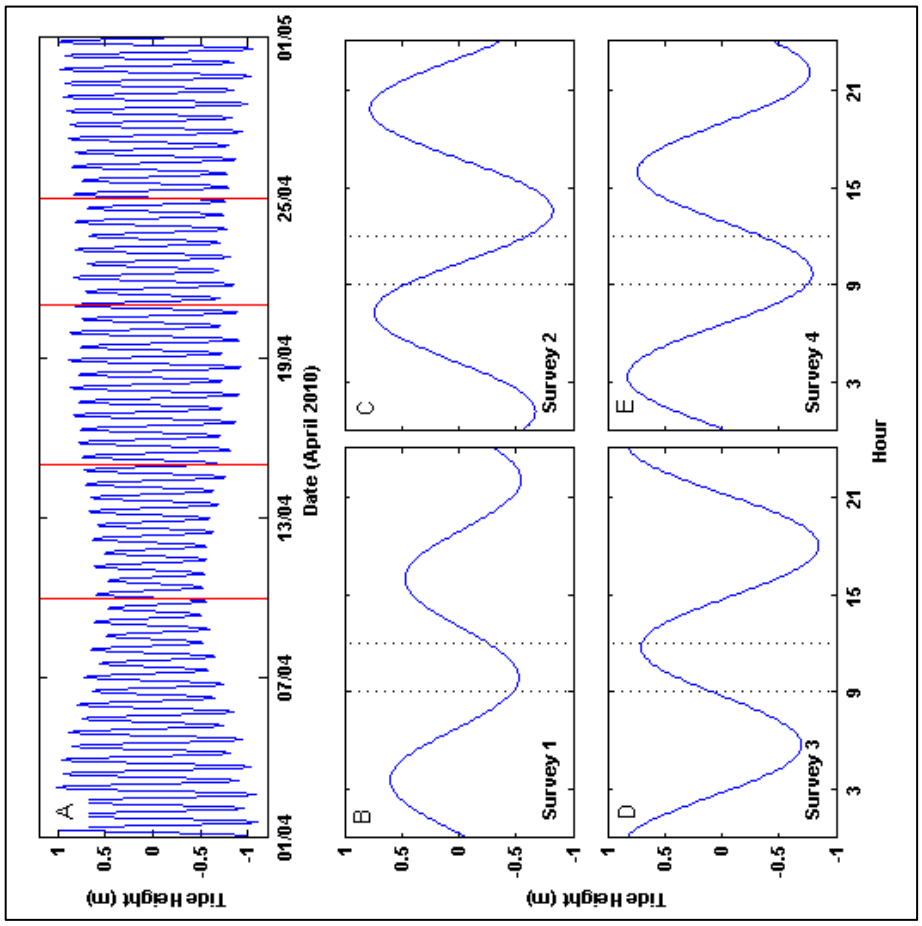

Figure 4.16 (a) Tide height for April 2010. Red lines indicate the 4 dispersion survey days. (b-e) Tide height on the day of Surveys 1-4. Approximate survey period indicated by dotted lines (source: National Institute of Water and Atmospheric Research (NIWA) tide model).

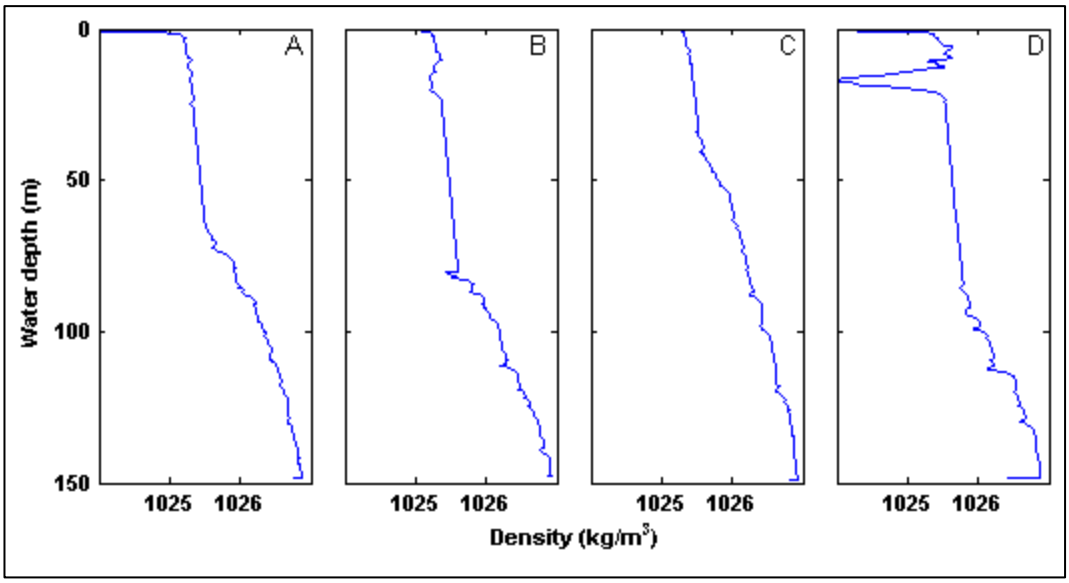

Figure 4.17 Density profiles recorded at the AMDG with a CTD profiler following the completion of each survey. Profiles a-d correspond to surveys 1-4 respectively. Profiles are identical to those present in Figure 3.10a-d in Chapter 3.

4.6.2 Ambient Current Observations

Current observations reported in the following text represent a 'snap-shot' of the hydrodynamics at the AMDG. For the purpose of evaluating the instantaneous movements of the plume, such observations can be considered comprehensive. However, mean patterns, which would be significant for evaluating the overall hydrodynamic setting, cannot be concluded from such a short-term dataset.

Records from the submerged drifter deployments indicated that the ambient current was directed northwest, northeast, south, and east prior to Surveys 1-4, respectively (Figure 4.18). The erratic path of drifters 3 and 4 for Survey 1 suggest that the GPS equipment may have been faulty, so a confident assessment of the ambient current patterns 30 m below the surface is not possible on that day, however, both drifters 1 and 2, indicated a north-westerly drift at 10 m below the surface. Drifters 3 and 4 were not used for the remainder of the surveys. For the deployments corresponding to Surveys 2-4, the paths of the 10 and 30 m drifters were essentially the same. Net drift distances were approximately 424 m, 679 m, 277 m, and 188 m corresponding to approximate ambient current speeds of 10 cm/s, 20 cm/s, 8 cm/s, and 4 cm/s in the ~1 hour drift period prior to each of the 4 surveys, respectively. Refer to Figure 4.18(a-d) for exact drogue deployment and retrieval times.

Figure 4.19 and Figure 4.20 show horizontal currents along transects recorded at the beginning and end of each survey; at least 30 minutes apart. The larger panels indicate the horizontal currents for the same transects at depths of 4, 32, and 60 m. Unfortunately, current data in the lower fourth of the water column was corrupt or missing for the majority of the surveys and is therefore not included. For all 4 surveys, there was no significant or consistent difference between transects recorded early in the survey versus those recorded 30-60 minutes later. Mean current speeds for both the early and late-survey transect in all 4 surveys are shown in Table 4.5. The ambient current for Surveys 1, 2, and 4 was in the range of 10-20 cm/s and that recorded during Survey 3 was 15-25 cm/s (Figure 4.19, Figure 4.20, and Table 4.5). There were no significant or consistent patterns in the vertical variation of current magnitude within or between surveys.

Table 4.5 Statistics of the horizontal current magnitude (cm/s) for an early and late-survey transect recorded during Surveys 1-4 at 4, 32, and 60 m below the surface.

Water depth (m)	Horizontal current magnitude (cm/s)							
	Survey 1		Survey 2		Survey 3		Survey 4	
	Mean	Std	Mean	Std	Mean	Std	Mean	Std
Early-survey transect								
4	14.82	4.38	14.06	5.05	20.89	6.28	8.95	4.16
32	12.49	5.20	13.07	4.56	23.89	6.18	9.02	4.55
60	15.89	7.08	11.00	9.45	17.45	9.11	9.94	5.20
Late-survey transect								
4	13.31	5.85	15.05	5.19	24.1	7.04	13.05	4.10
32	12.96	5.35	10.93	5.16	25.60	5.81	12.86	5.60
60	20.37	14.85	17.06	8.10	21.62	9.76	9.73	3.69

Near the surface, the ambient current was directed generally northwards on Surveys 1 and 2 (Figure 4.19), northeast on Survey 3 (Figure 4.20), and on Survey 4 there was no predominant direction (Figure 4.20). The 32 m records showed current direction to be similar to that at 4 m with a somewhat altered direction at 60 m for both Surveys 1 and 2 (Figure 4.19). During Survey 3, there was a distinct rotation towards the northwest at 60 m (Figure 4.20). Mid-depth (60 m) records from Survey 4 were similarly disordered as those nearer the surface (Figure 4.20).

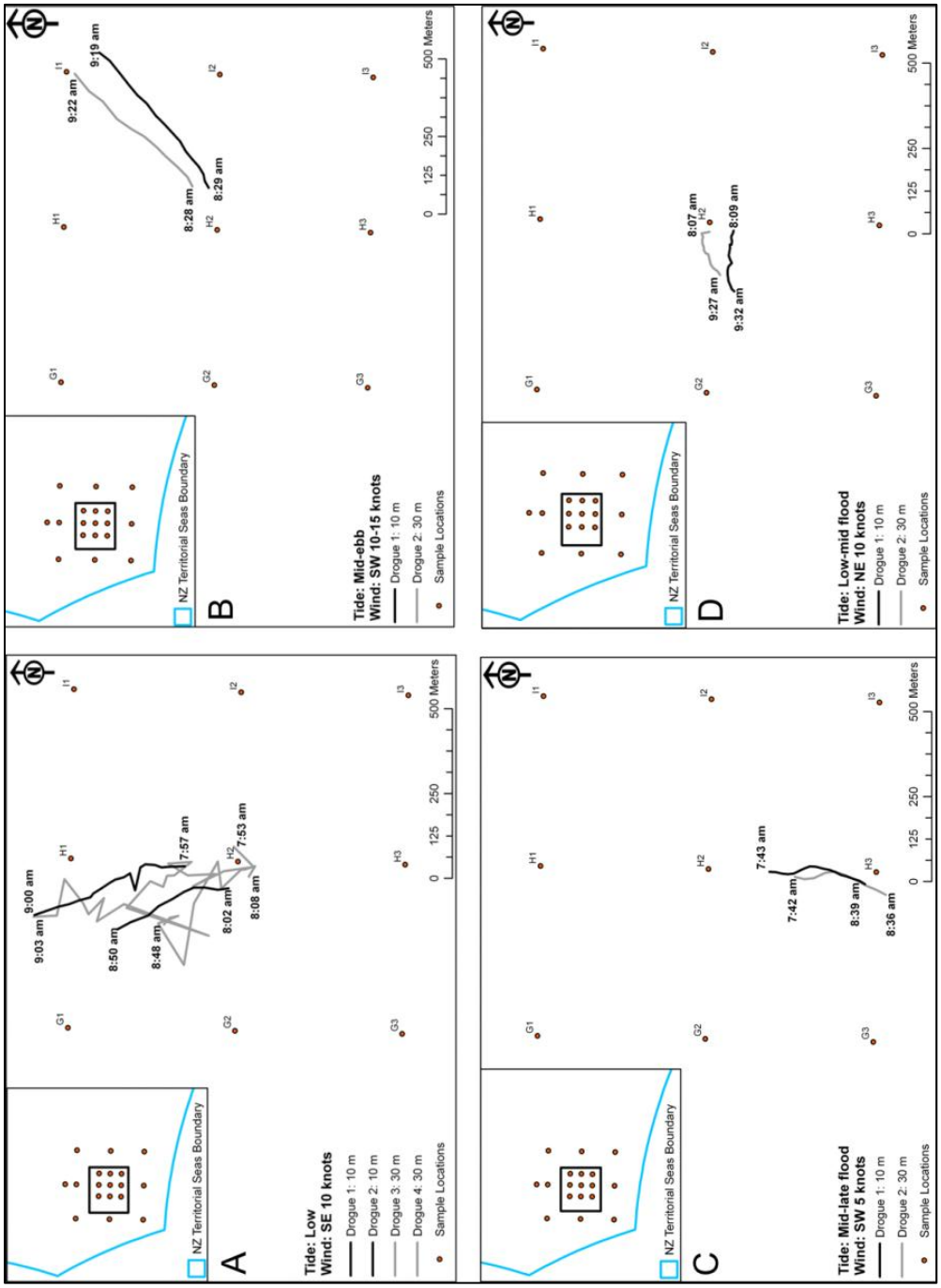

Figure 4.18 Path of drogues at 10 and 30 m below the surface immediately prior to Surveys 1-4 (a-b, respectively). First and last GPS transmit times as well as tide and wind conditions are noted.

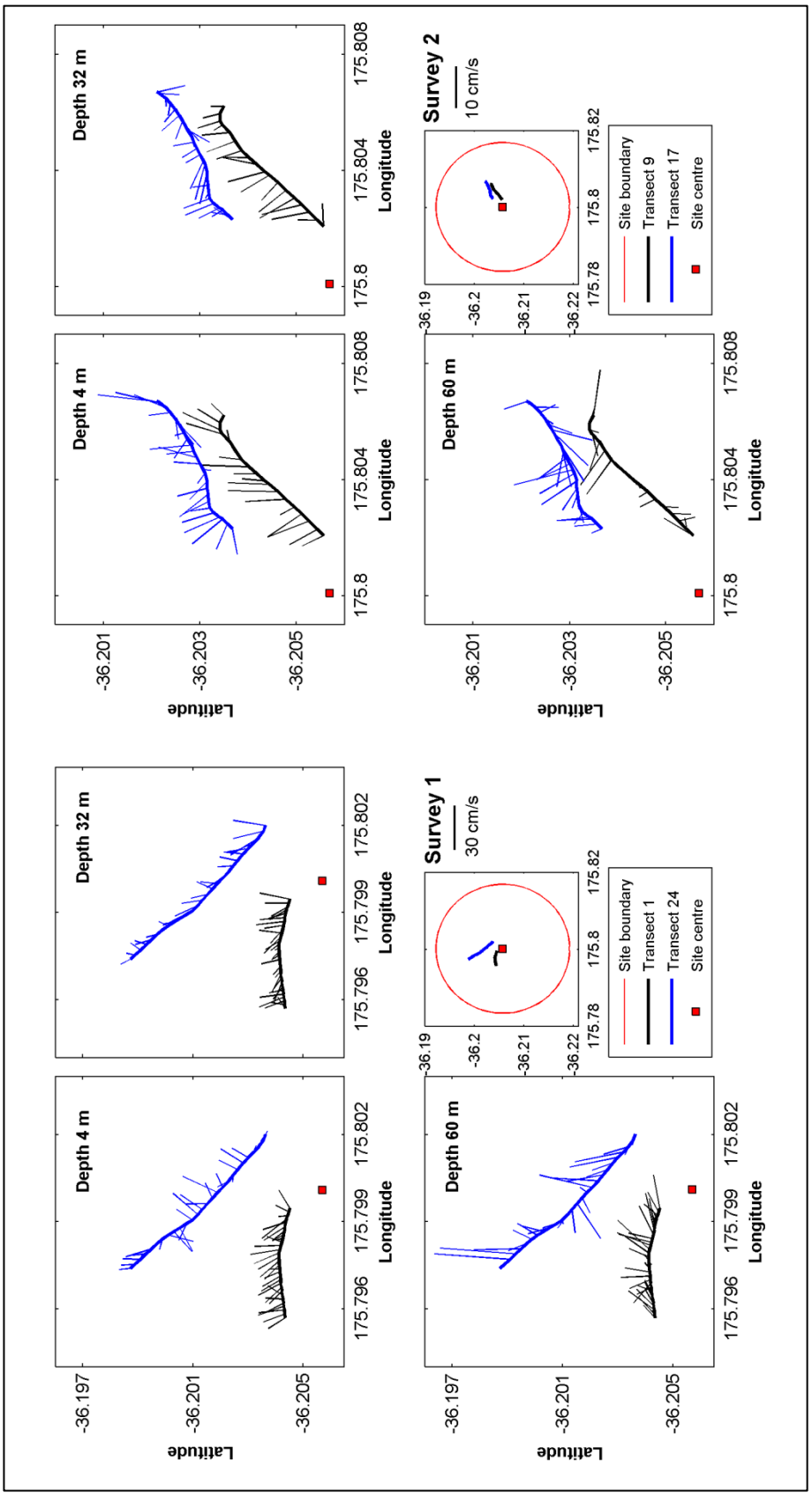

Figure 4.19 Horizontal current distribution measured during Surveys (a) 1 and (b) 2 for transects recorded near the beginning (black) and end (blue) of each survey at 3 different depth levels (4, 32, & 60 m).

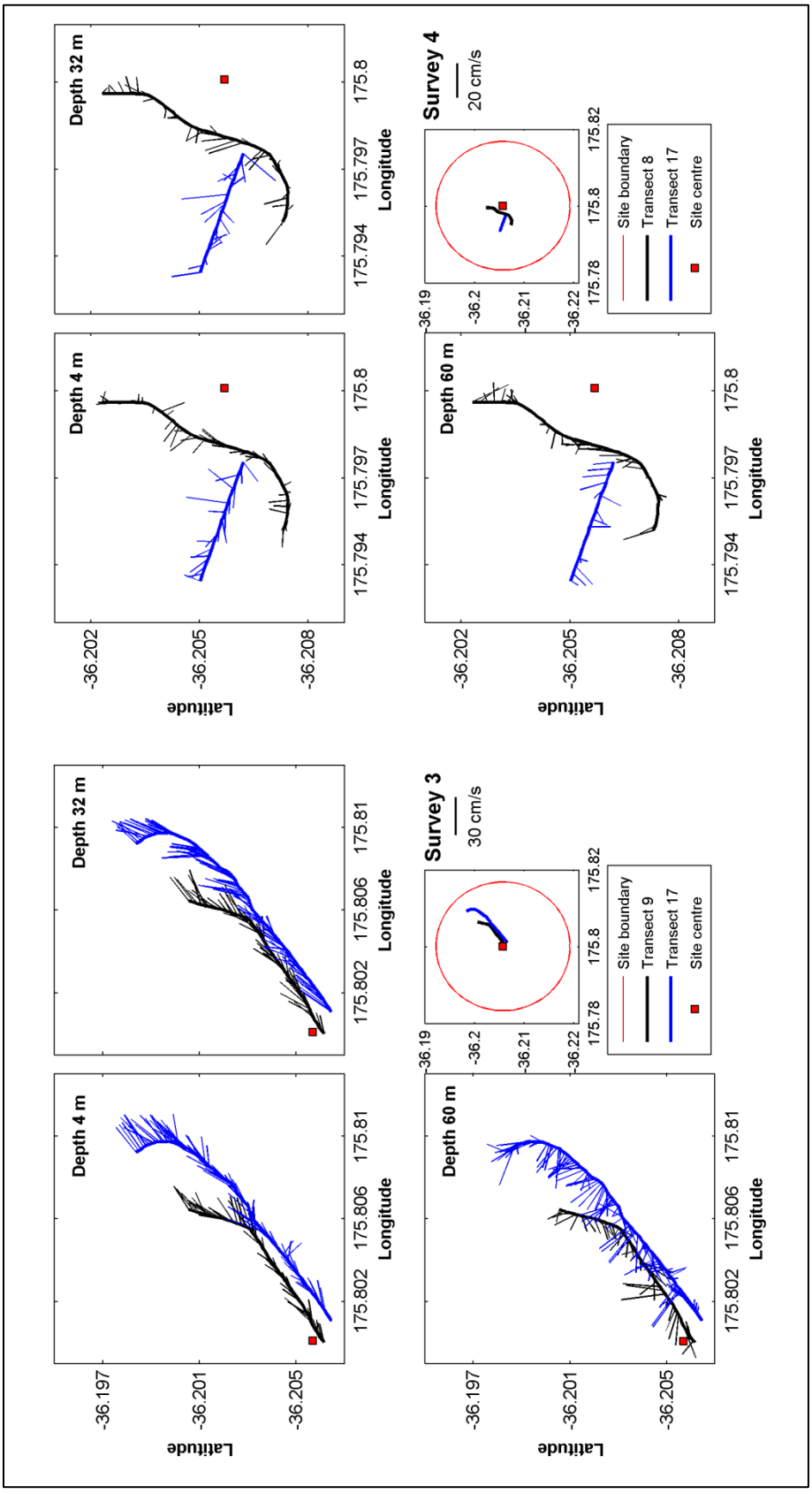

Figure 4.20 Horizontal current distribution measured during Surveys (a) 3 and (b) 4 for transects recorded near the beginning (black) and end (blue) of each survey at 3 different depth levels (4, 32, & 60 m).

Cross-shore (positive east) and alongshore (positive north) current components for the late-survey transects only (see Figure 4.19 and Figure 4.20) are shown in Figure 4.21 and Figure 4.22. Cross-shore and alongshore currents were directed weakly west and more strongly north, respectively, for the extent of the measured depth in Survey 1 (Figure 4.21a&b). This distribution indicates a NNW directed current, which lends some clarity to the interpretation of Figure 4.19a. In contrast, cross-shore and alongshore currents were directed more strongly west and weakly north, respectively, for the extent of the measured depth in Survey 2 (Figure 4.21c&d). This indicates a WNW ambient current, a finding that is not obvious in the plots of current magnitude and direction shown in Figure 4.19b.

The late-survey transect of Survey 3 shows a very strong flow reversal centred at 30 m in the cross-shore direction, with the surface layer directed strongly east and the lower layer directed strongly west (Figure 4.22a). A similar pattern occurred in the alongshore direction though to a lesser extent (Figure 4.22b). The flow reversal occurred at approximately 40 m below the surface, where the surface current was directed weakly north and the lower layer was directed weakly south. In the case of the alongshore currents, however, the lower layer opposing flow was not continuous to maximum measured depth; it was broken up by a secondary flow reversal resulting in a band of weak northerly directed currents located between 70 and 90 m below the surface.

Current component direction distributions for the late-survey transect corresponding to Survey 4 were more closely aligned with those from Survey 1 and 2, but with a few notable exceptions (Figure 4.22c&d). Cross-shore currents were similarly directed weakly west, but the alongshore current did not exhibit a predominant direction. Instead, high frequency, vertically uniform (between 0 and 70 m below the surface) oscillations between a northerly and southerly directed current were evident. The strength of the oscillations varied in magnitude along the transect with, at times, a current speed approaching, at times, 40 cm/s towards the north, but with an overall lower average velocity (~ 10 cm/s).

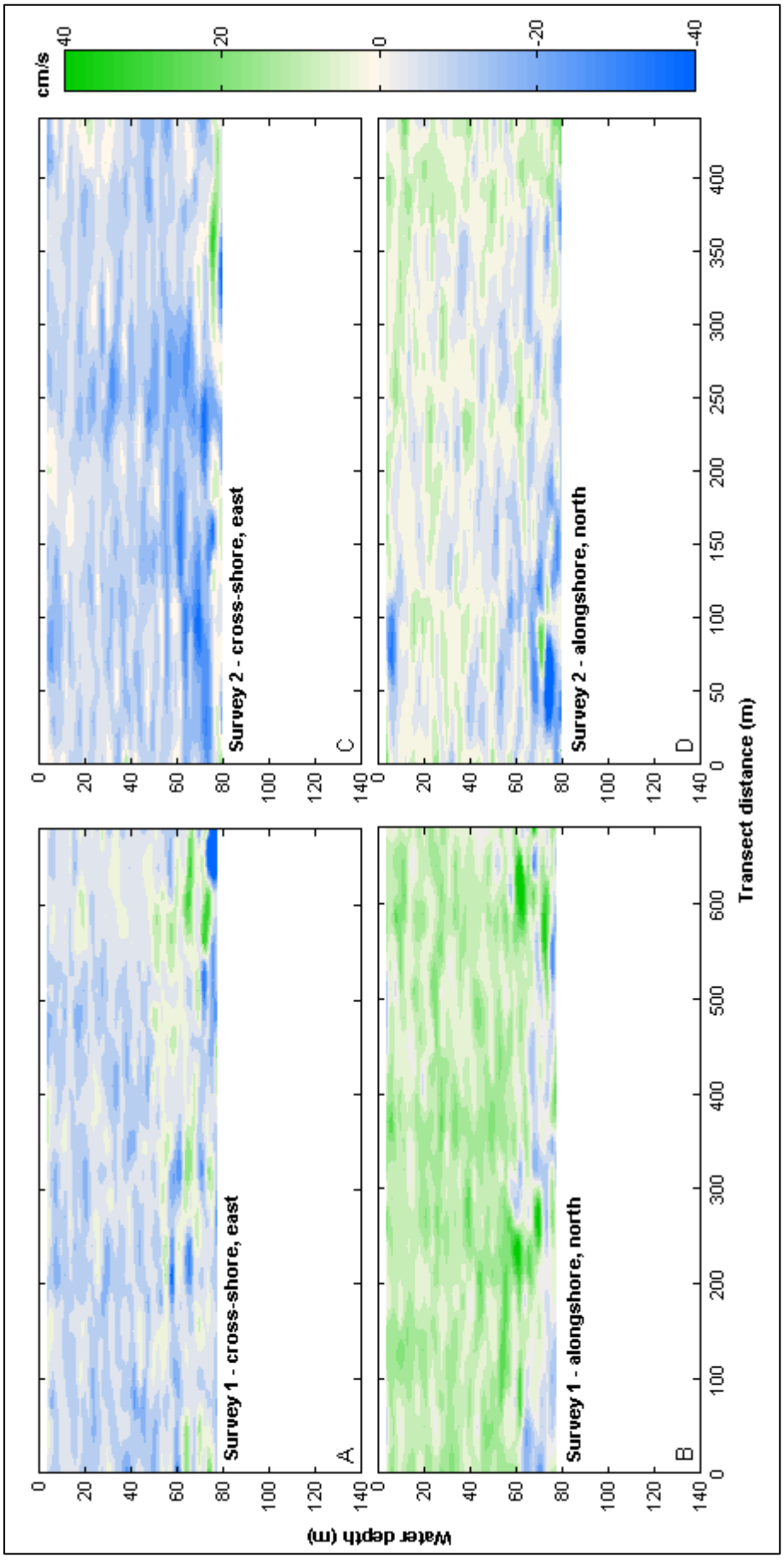

Figure 4.21 Horizontal current components (a&c) cross-shore (b&d) alongshore recorded during Transect 24 of Survey 1 and Transect 17 of Survey 2. White areas within the plot indicate locations of corrupt or missing data.

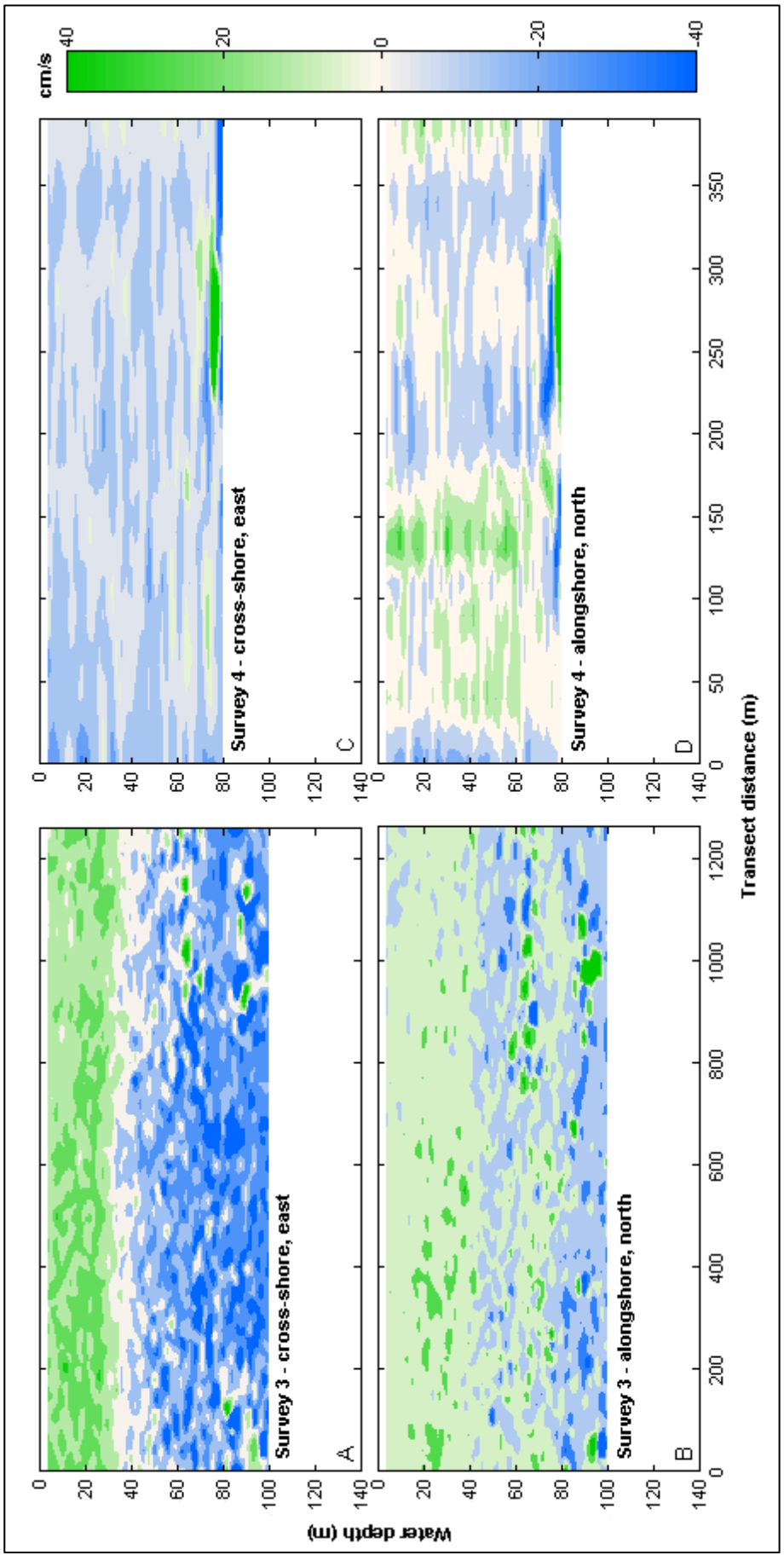

Figure 4.22 Horizontal current components (a&c) cross-shore (b&d) alongshore recorded during Transect 17 of Survey 3 and Transect 17 of Survey 4. White areas within the plot indicate locations of corrupt or missing data.

4.7 Background Turbidity Levels

A difficulty with the use of ADCP backscatter to identify suspended sediment distribution following disposal of dredged material is the presence of plankton and other suspended particles which also have the ability to reflect acoustic signals. Indeed, the study of plankton distribution through the use of acoustics is widespread (Lorke et al., 2004; Thomas & Kirsch, 2000; Wiebe & Green, 1994). Along the productive northeast coast of New Zealand, the distribution and abundance of phytoplankton populations tends to be seasonally variable, but their presence is nearly ubiquitous throughout the year (Chang et al., 2003; Hall et al., 2006; Murphy et al., 2001). Therefore, it is not unexpected that background levels of suspended particles at the AMDG recorded during the dispersion surveys of April 2010 did not amount to 'clear' water. Background relative turbidity at the AMDG on the day of Survey 1 is illustrated in Figure 4.23a. The transect was recorded prior to the arrival of the *MV Mina Campbell* and the towed hopper containing the dredged material which indicates that the regions of elevated turbidity were not a result of dispersed dredged material.

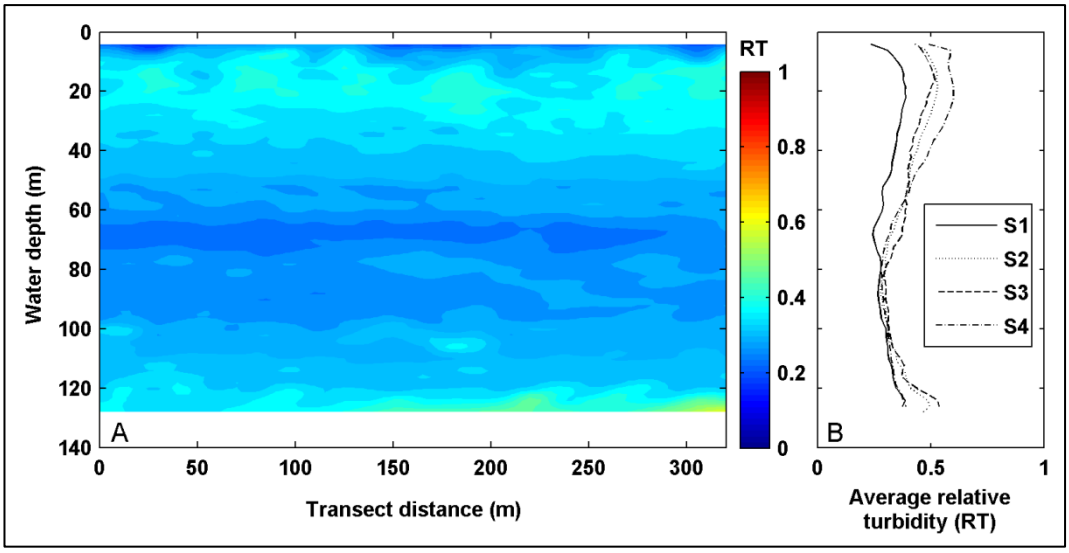

Figure 4.23 (a) Contour plot of relative turbidity (RT) levels recorded on Transect 2 of Survey 1 from normalised ADCP backscatter data prior to the disposal of dredged material at the AMDG. (b) Average background relative turbidity profiles corresponding to Surveys 1-4 (S1-S4).

The higher turbidity in the surface 40 m was likely due to the presence of photic zone phytoplankton, and though autumn phytoplankton abundances are known to be low in the region (Murphy et al., 2001), the recorded turbidity was approximately 2 % higher than the lowest recorded level situated 70 m below the

surface (Figure 4.23a). From approximately 120 m below the surface to the maximum measured depth, a secondary region of elevated background turbidity was evident. If this was a result of low level suspended sediment in the bottom boundary layer, then turbidity would be expected to increase with proximity to the bed (Grant & Madsen, 2003). A similar vertical distribution in background levels of relative turbidity were observed in Surveys 2-4 as well (Figure 4.23b).

To isolate the proportion of suspended particles originating solely from the dispersion of disposed dredged material, the average background turbidity profile recorded on each survey day (Figure 4.23b) was removed from the backscatter transects recorded during each of the corresponding surveys. A similar procedure as undertaken by Tubman and Corson (2000).

4.8 Convective Descent (Phase 1)

4.8.1 Entrainment

Dispersion processes during the convective descent phase (Figure 2.1) of the dredged material disposal process can be parameterised by the magnitude of ambient water entrainment along the lateral edges of the descending jet of dredged material. This process causes the cloud of turbid water to grow with time and usually with depth as well. Brandsma and Divoky (1976) described entrainment (E) as

$$E = Ae(\bar{v} - \bar{v}_a) \qquad \text{Equation 4-6}$$

where A=area of the hemispherical discharge, e=entrainment coefficient, $\bar{v}$=vector velocity of discharged material, $\bar{v}_a$=vector velocity of ambient water.

When $\bar{v} >> \bar{v}_a$,

$$dV/dt = eA(dz/dt) \qquad \text{Equation 4-7}$$

where V=volume of hemispherical discharge. Rearranging,

$$e = (1/A)(dV/dz), \qquad \text{Equation 4-8}$$

and for a hemispheric radius, r_h,

$$V = \left(2/3\right)\pi r_h^3, \quad \text{Equation 4-9}$$

and

$$A = 2\pi r_h^2 \quad \text{Equation 4-10}$$

so the formulation becomes

$$e = dr_h/dz \quad \text{Equation 4-11}$$

where the entrainment coefficient is simply the slope of the outer edge of the descending cloud of turbid water (Tsai et al., 1992).

Entrainment coefficients were estimated from early-survey transects (<5 min after disposal) recorded during each of the 4 surveys based on the normalised relative turbidity above the background level (Figure 4.24 and Table 4.6). For all 4 transects, the 0.35 turbidity contour level representing the edge of the highest turbidity portion of the descending plume was used to estimate dr_h and dz , and both ingress and egress (survey vessel travelling into and out of the plume, respectively) estimates were made. The entrainment coefficients ranged from 0.26 (egress) to 1 (ingress) during Surveys 3 and 2, respectively. The average entrainment coefficient estimates were 0.6 and 0.57 for the ingress and egress estimates, respectively.

Table 4.6 Details of entrainment coefficient and area of impact estimates for disposals undertaken during Surveys 1-4 based on the transects shown in Figure 4.24.

Survey no.	Water depth (m)	Transect no.	Entrainment coefficient (*e*)				$\bar{r}$ (m)	A_I (m^2)
			Ingress	*dz* (m)	Egress	*dz* (m)		
1	140	6	0.3	65	0.46	65	8.74	16806
2	140	1	1	64	0.98	46	8.74	69504
3	140	2	0.74	88	0.26	78	8.74	39648
4	140	1	0.36	56	0.58	60	8.74	25413
Mean			0.6		0.57			44855
Standard deviation			0.33		0.3			22502

$\bar{r}$=effective radius of orifice, *dz*=difference in depth along the vertical plume, A_I=area of impact

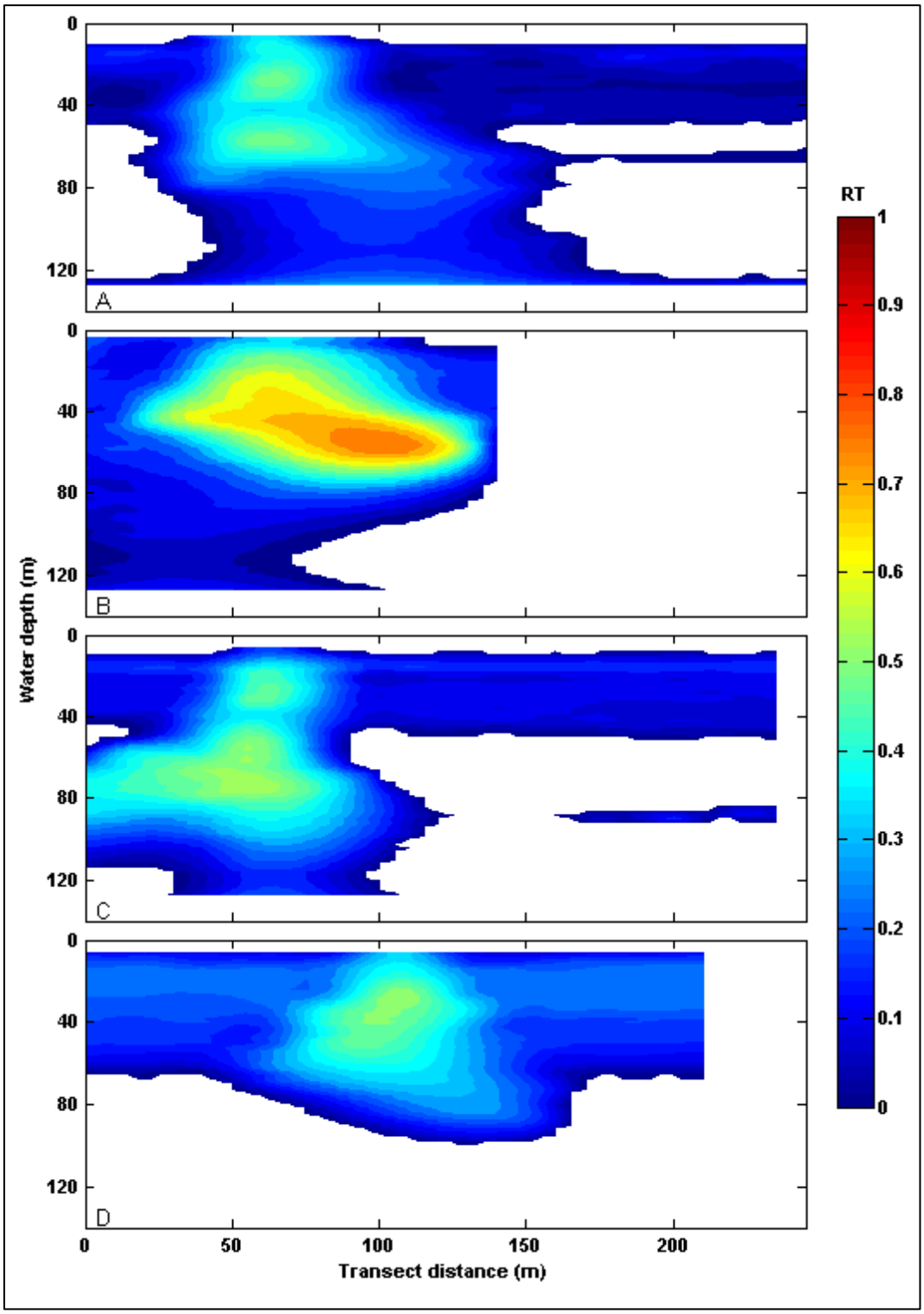

Figure 4.24 Relative turbidity (RT) above background level recorded during Surveys 1-4 (a-d). Transects were recorded (a) 3 min. (b) 2 min. (c) 5 min. and (d) 3 min. post-disposal, respectively. Transect numbers are 6, 1, 2, and 1 (see Appendix Table I.7).

4.8.2 Down-fall Velocity

During the convective descent phase the dredged material inserted into the water column descends rapidly as a large mass of material with a down-fall velocity much higher than that of any one individual sediment grain within that mass

(Gordon, 1974). Down-fall velocity of the mass of dredged material is dependent on the excess submerged weight per unit mass of submerged fluid or its negative buoyancy (F) where

$$F = \left({(\rho_s - \rho)} \middle/ {\rho} \right) g V_s \qquad \text{Equation 4-12}$$

and ρ_s=density of solid particles, ρ=density of water, g=gravitational acceleration, and V_s=volume of solid particles disposed as a mass (Drapeau et al., 1999). Krishnappan (1975) formulated the down-fall velocity (W_{fK}) as

$$\beta_k F^{1/2} / z \qquad \text{Equation 4-13}$$

where z=water depth, F=negative buoyancy, and β_k is defined as

$$\varphi_\beta \left(\gamma_s \rho D^3 \mu^{-2} \right) \qquad \text{Equation 4-14}$$

where γ_s=submerged weight [$(\rho_s$-$\rho)$g], D is the sediment grain size diameter, μ=viscosity of water, and the dimensionless parameter φ_β was determined experimentally.

Based on Equation 4-12, Equation 4-13 and Equation 4-14, down-fall velocity was estimated for the mass of material disposed on each of the 4 survey days (Table 4.7). Refer to Table 4.8 for details of the constants applied in the calculations. The estimates ranged from 0.91 m/s on Survey 1 to 0.81 m/s on Survey 3, and the mean was 0.87 m/s.

The down-fall velocity was also estimated from the relative turbidity above backscatter recorded in the 4 early-survey transects shown in Figure 4.24. Early (W_{fE}) and late (W_{fL}) phase down-fall velocities were estimated from each transect based on the maximum turbidity depth (z_E) and the leading edge depth of the higher turbidity region only (0.35 contour) (z_L), respectively and the time after disposal that the transect was recorded. The early phase estimates ranged from 1.27 m/s on Survey 1 to 0.67 m/s on Surveys 3 and 4, and the mean was 0.95 m/s. The late phase estimates ranged from 0.48 m/s on Survey 4 to 0.71 m/s on Survey 2, and the mean was 0.59 m/s (Table 4.7). The average down-fall velocities (W_{fM}) (early and late phase estimates) ranged from 0.97 m/s on Survey 1 to 0.58 m/s on Survey 4 and the mean for all four was 0.77 m/s.

Table 4.7 Details of down-fall velocity estimates for disposals undertaken during Surveys 1-4 based on the transects shown in Figure 4.24.

Survey no.	Water depth (m)	Transect no.	Estimate from early survey transect						Estimate from Krishnappan (1975)		*I* (m/s)
			t_{PD} (s)	z_L (m)	W_{fL} (m/s)	z_E (m)	W_{fE} (m/s)	W_{fM} (m/s)	*Vs* (m^3)	W_{fK} (m/s)	
1	140	6	101	68	0.67	128	1.27	0.97	720	0.91	0.60
2	140	1	107	76	0.71	128	1.20	0.95	685	0.88	0.57
3	140	2	191	98	0.51	128	0.67	0.59	570	0.81	0.48
4	140	1	146	70	0.48	98	0.67	0.58	662	0.87	0.55
Mean					0.59		0.95	0.77		0.87	0.55
Standard deviation					0.11		0.33	0.22		0.04	0.05

t_{PD}=time post-disposal, z_L=late phase estimate depth, z_E=early phase estimate depth, W_{fL}=down-fall velocity (late phase), W_{fE}=down-fall velocity (early phase), W_{fM}=mean down-fall velocity, *Vs*=volume of mass of disposed material, W_{fK}=down-fall calculated after Krishnappan (1975), and *I*=insertion speed.

Table 4.8 Constants applied in estimates using Equation 4-12, Equation 4-13 and Equation 4-14.

Constant	Value applied
ρ (kg/m3)	1026
ρ_s(kg/m3)	2650
g (m/s)	9.812
D (m)	0.000063
μ (Pa s)	0.00108
γ_s	15934
β_k*	1.2

*determined from empirical curves presented in Drapeau et al., (1999) and based on the term $[\gamma_s \rho D^3/\mu^2]$.

The down-fall velocity is thought to be correlated to the insertion speed (Bokuniewicz et al., 1978) which can be estimated as

$$\frac{\left(V_s / t_i\right)}{A_o} \qquad \text{Equation 4-15}$$

where V_s=volume of the mass of inserted material (m^3) (see Table 4.7), t_i=time for material to pass through the hopper doors (taken to be 5 sec (*pers. comm.*, R. McGregor)), and A_o=effective area of the orifice (taken to be 240 m^2). The insertion speeds were estimated to be 0.6, 0.57, 0.48, and 0.55 m/s for the material disposed during Surveys 1-4, respectively (Table 4.7).

To verify the estimates made through the methods described above, an additional estimate was made based on the timing of the ingress and egress plume depth recorded by the *MV Ten Sixty* echosounder during Survey 4 (Figure 4.25). The

timing of the echosounder screen image corresponds to the transect shown in Figure 4.24d. The ingress plume depth was 80 m, 134 seconds after insertion into the water column indicating a down-fall velocity of 0.6 m/s. On the egress run, 159 seconds after insertion, the plume depth was located approximately 90 m below the surface giving a down-fall velocity of 0.57 m/s.

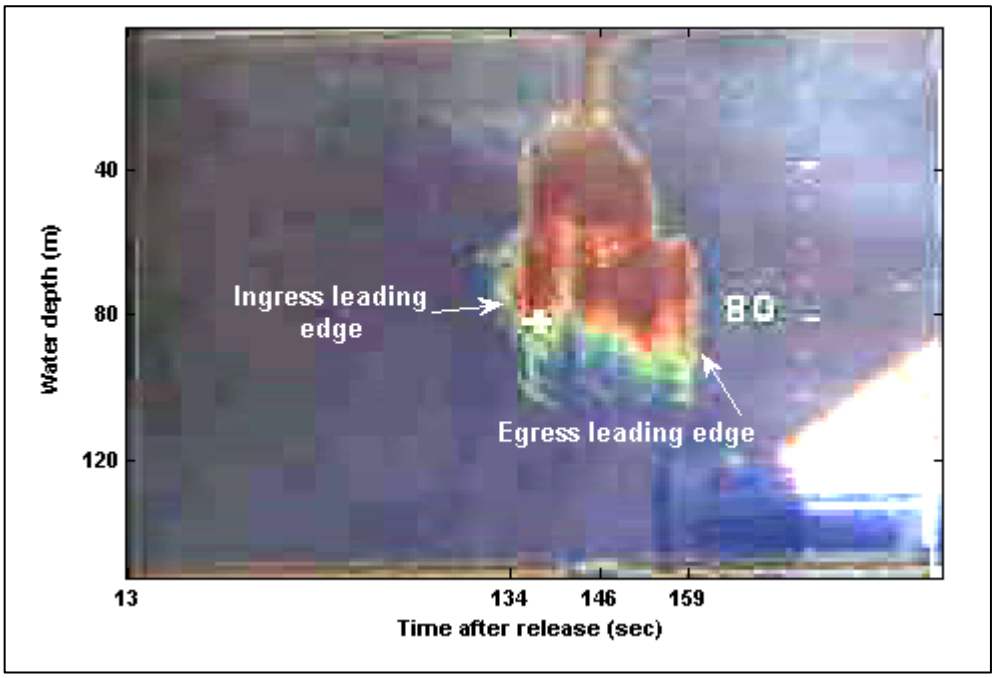

Figure 4.25 Screen image of the echosounder display aboard the *MV Ten Sixty* on Survey 4. Image corresponds to the transect shown in Figure 4.24d.

4.8.3 Area of Impact

If the descending dredged material retains enough energy during the descent process, it will impact with the seafloor which can initiate the second phase of the disposal process (dynamic collapse) (Winterwerp, 2002). The initial area of impact is defined here as the location of deposition of the material which deposits immediately on impact and is no longer subject to later phases of the disposal process. This proportion of the disposed load typically includes the clods, if any are present, of which the density is too high to be susceptible to suspension within the density current of the following phase, but if the down-fall velocity is slow enough there will be less available energy for initiation of the density current as part of Phase 2 (Bokuniewicz & Gordon, 1980).

The proportion of sediments settling directly at the point of impact (S), as defined by Drapeau et al. (1992), is

$$S = 1 - C(W_{fi} - W_s)/W_{fi} \qquad \text{Equation 4-16}$$

where W_{fi} is the down-fall velocity of the mass of disposed sediments at the moment of impact and W_s is the natural settling velocity of the sediment particles. C is a constant, which was suggested to be 0.5 (Drapeau et al., 1992). This formulation determines the excess energy available to form a density current, so if S=1, then all the material disposed will deposit on impact and there will be no subsequent density current. An estimate of the proportion of each monitored disposal that settled directly at the point of impact was made by applying the mean down-fall velocities (W_{fM}) (Table 4.7) as W_{fi} and the Stoke's settling velocity of the overall mean grain size of the sediments (Table 4.1) sampled by Bioresearches (2009) as. Based on the mean settling velocity for the clods and the jet, approximately 50 % of the disposed loads corresponding to Surveys 1 and 2 would settle on impact (Table 4.9). The settling velocity estimates derived for the loads disposed during Surveys 3 and 4 suggest that the proportion of the sediments to deposit on impact was close to 100 %, indicating that there would be little to no density current formed.

Table 4.9 Proportion of disposed load to settle on impact (%)[a,b]

Survey 1	Survey 2	Survey 3	Survey 4
50 %	50%	100%	100%

[a]estimated from Equation 4-16[c]
[b]values are approximate
[c] W_s=0.03 cm/s

The area of impact can be estimated from the entrainment coefficient (e) if data at the bed is not available. Bokuniewicz et al. (1978) stated that

$$A_I = \pi(\bar{r} + Z \tan\beta)^2 \qquad \text{Equation 4-17}$$

where A_I=area of impact, $\bar{r}$ =effective radius of the orifice, Z=the height of the orifice above the bottom, and β=the angle of spread of the plume of material and

$$\tan\beta = e \qquad \text{Equation 4-18}$$

The area of impact (A_I) was estimated from the derived entrainment coefficients which best represented the magnitude of spread throughout the water column (greatest value of dz), an effective orifice radius ($\bar{r}$) of 8.74 m (*SB II Groper* hopper doors area=240 m^2), and an orifice height above the seafloor of 140 m

(Table 4.6). The estimated area of impact ranged from 16,806 m^2 for the Survey 1 disposal to 69,504 m^2 for the Survey 2 disposal and the average was 44,855 m^2.

The estimated area of impact calculated for the disposal corresponding to each of the 4 surveys is shown in Figure 4.29 (Surveys 1 and 2) and Figure 4.30 (Surveys 3 and 4) as dashed line circles superimposed on maps of the near-bed interpolated relative turbidity. Interpolation was undertaken using only transects recorded in the first 15 min. following disposal on each survey so that higher turbidity areas better represented turbidity directly overlying the point of impact rather than suspended material that had been dispersed significantly away from the point of impact.

On the right-hand side of Figure 4.29 and Figure 4.30 the post-disposal MBES backscatter map is shown. The size and position of the relative turbidity map for each survey is shown as the region outlined in cyan on the post-disposal MBES backscatter map. The same MBES backscatter map is shown to the right of each relative turbidity map. Also indicated is the position of the centre of the highest turbidity area within the corresponding relative turbidity map (red marker) and the positions of sampling locations for sediment cores near the centre of the site which were 500 m apart for reference (yellow markers).

MBES backscatter data gives an indication of the density/roughness of the seafloor substrate represented in gray scale. Denser/rougher areas are indicated as patches of lighter gray colour. In this case, the lighter gray patches were presumed to be the area of impact for each separate disposed load of material near the centre of the site because the pre-disposal MBES backscatter map did not display any light gray patches (not shown). The disposed material would be expected to be denser/rougher than the naturally occurring seafloor sediment due to the presence of clods; large aggregates of dense, typically cohesive, material which retain their structure during the disposal process (Bokuniewicz & Gordon, 1980). Video footage recorded at the centre of the AMDG after the completion of all disposal operations affirmed the presence of clods (Figure 4.26).

Figure 4.26 Still images of video footage recorded at the seabed several months after the completion of disposal operations. Clods of dredged material were present at Site H2 which corresponds to the centre of the AMDG (approximate release location for all 9 loads of material disposed during March and April 2010).

Sediment cores collected before and after disposal operations further corroborate the claim that the light gray patches in the MBES backscatter map represent deposited dredged material. Figure 4.27a&b show photos of cores retrieved near the centre of the AMDG before and after disposal operations. The post-disposal core was collected in an area not impacted by the dredged material. Munsell colour code assignment shows that the sediments ranged from grayish yellow near the sediment-water interface to light gray deeper in the core (Table 4.10). The sediment colour did not change significantly in regions not impacted by the dredged material (Figure 4.27b). At the very centre of the AMDG, the sediment colour changed dramatically following completion of disposal operations (Figure 4.28). A dark blue-gray layer evident within the middle of the cores indicates the presence of the dredged material. After sequestration within the sheltered walls of the marina, infilling sediment would be expected to become somewhat anoxic especially that below the sediment water interface resulting in blue-black coloured sediment (Potter et al., 2005; Whitehouse et al., 2000). The post-disposal cores were collected several months after the completion of disposal operations so it is likely that the surficial layer of yellow gray material at the sediment-water interface represents dredged material that has undergone oxidation.

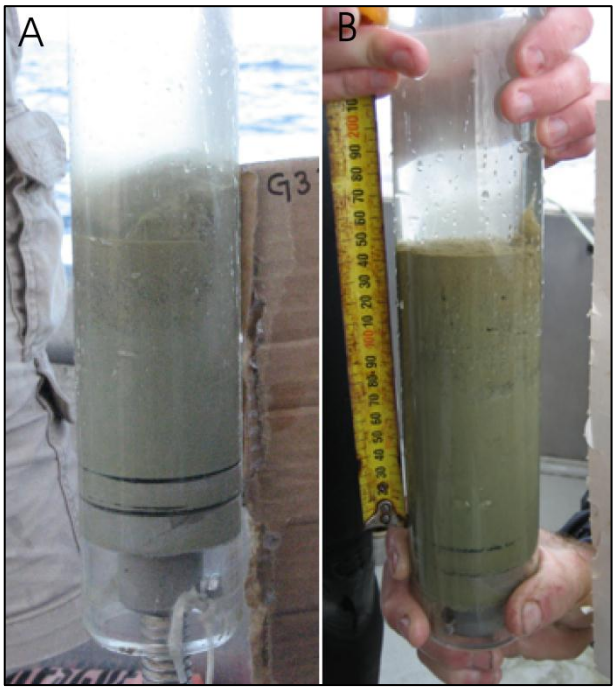

Figure 4.27 Sediment cores retrieved at the AMDG near the centre of the site a) before disposal and b) after completion of disposal operations. The post-disposal core was collected in an area not impacted by dredged material.

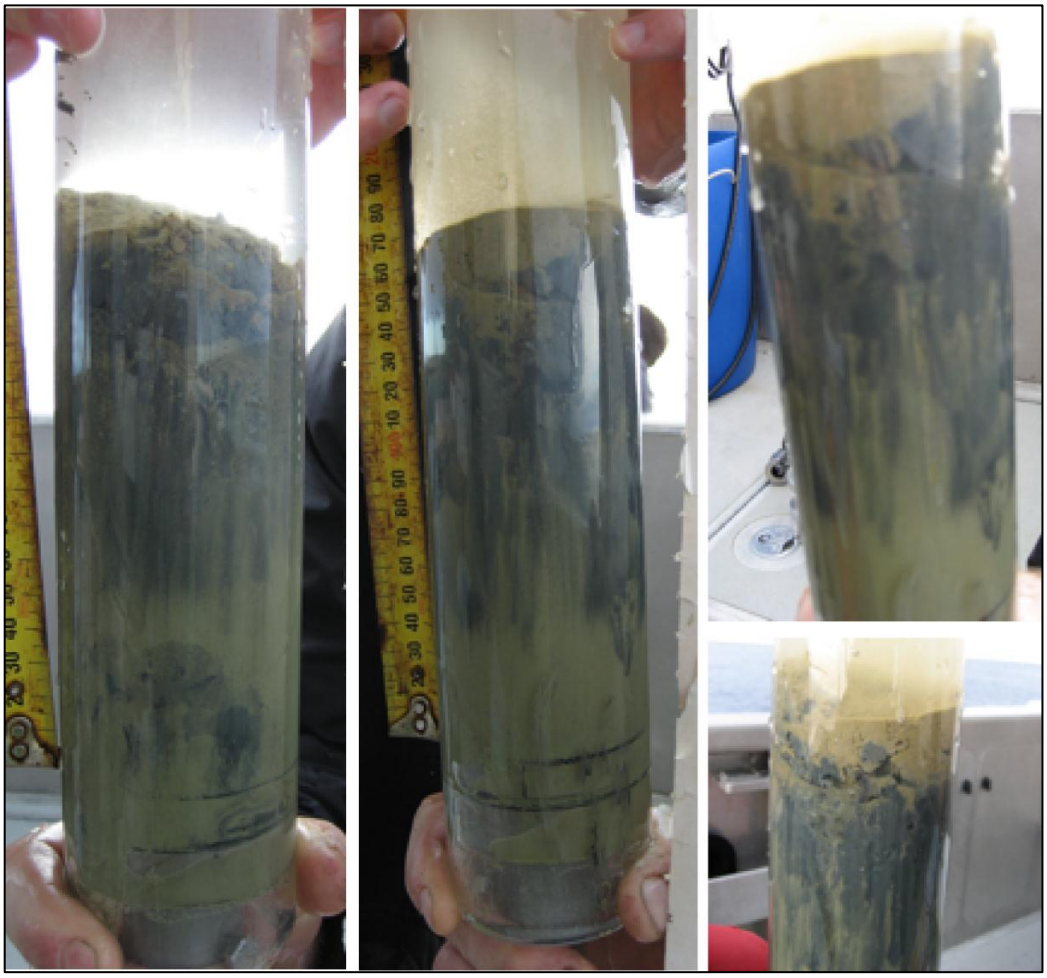

Figure 4.28 Two sediment cores collected at the centre of the AMDG following completion of disposal operations in June 2010. On right: close up views of each core.

Table 4.10 Munsell color description of sediment cores shown in Figure 4.27 and Figure 4.28.

Core	Layer	Type	Munsell color code	Description
Figure 4.27a	Top	Pre-disposal	2.5Y 7/2	Grayish yellow
Figure 4.27a	Bottom	Pre-disposal	2.5Y 7/1	Light gray
Figure 4.27b	Top	Post-disposal	2.5Y 6/4	Dull yellow
Figure 4.27b	Bottom	Post-disposal	10Y 7/2	Light gray
Figure 4.28	Top	Post-disposal	5Y 8/4	Light gray yellow
Figure 4.28	Middle	Post-disposal	N 5/0	Gray
Figure 4.28	Bottom	Post-disposal	10Y 7/2	Light gray

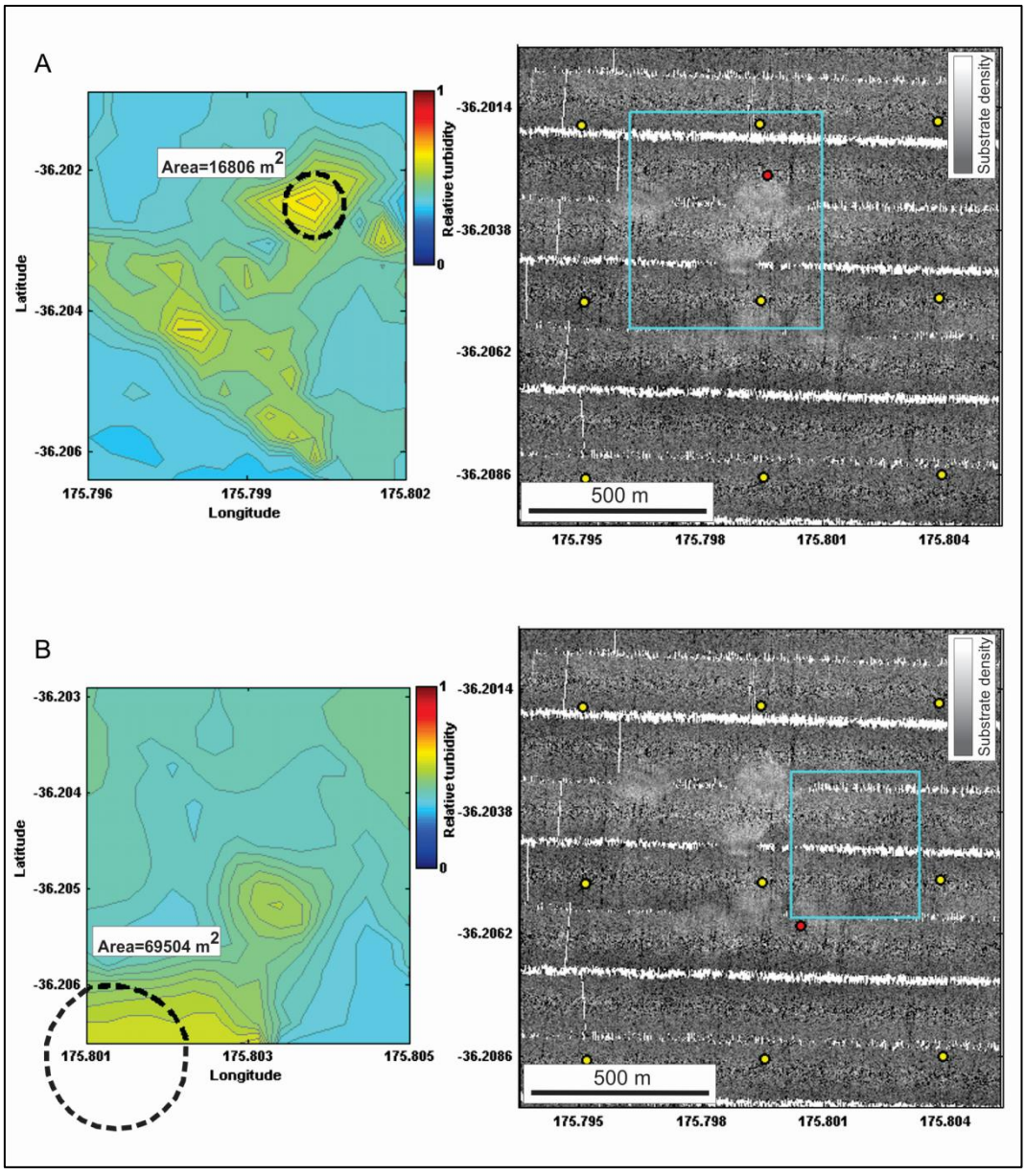

Figure 4.29 Left: Interpolated near-bed map of relative turbidity including background turbidity from (a) transects 5-9 of Survey 1 and (b) transects 1-8 of Survey 2. Black dashed line indicates the size of the area of impact derived using Equation 4-17 and Equation 4-18 centred over the area of highest turbidity. Right: MBES backscatter post-disposal map (all disposals completed). Cyan outline indicates the corresponding location of the relative turbidity map (at left) and the red marker indicates the centre of the high turbidity area in the map to the left. Yellow markers indicate sampling locations related to other parts of the study for reference.

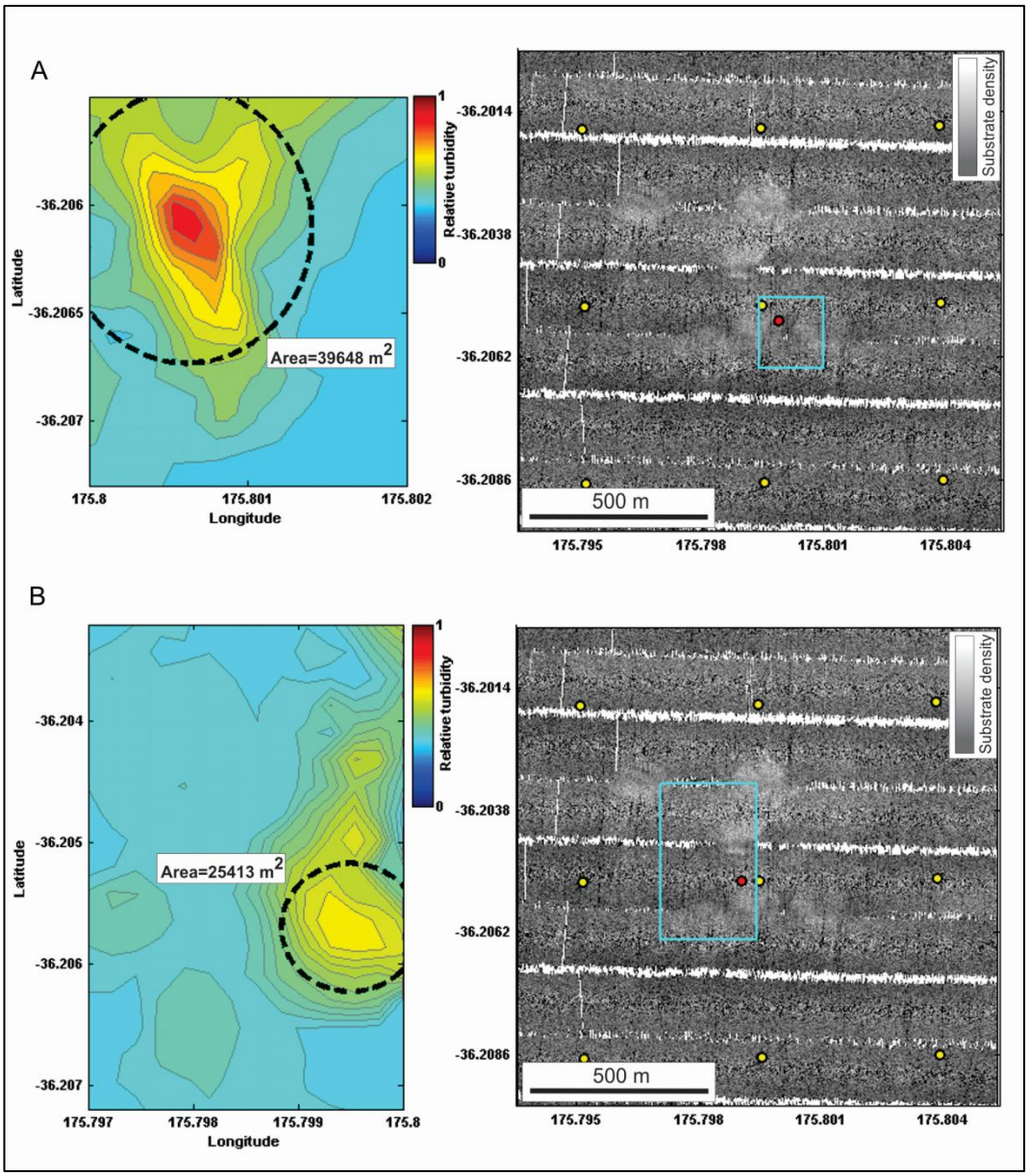

Figure 4.30 Left: Interpolated near-bed map of relative turbidity including background turbidity from (a) transects 2-5 of Survey 3 and (b) transects 1-5 of Survey 4. Black dashed line indicates the size of the area of impact derived using Equation 4-17 and Equation 4-18 centred over the area of highest turbidity. Right: MBES backscatter post-disposal map (all disposals completed). Cyan outline indicates the corresponding location of the relative turbidity map (at left) and the red marker indicates the centre of the high turbidity area in the map to the left. Yellow markers indicate sampling locations related to other parts of the study for reference.

To validate the impact area values derived using the entrainment coefficients, the area of the lighter gray patch nearest the centre of the high-turbidity area (red marker) was calculated for each survey. The edges of the lighter gray patches are not well-defined so the calculations are only an estimate. The patch nearest the high-turbidity centre for Survey 1 was located slightly to the south. The area of the patch was calculated to be 11,370 m^2. The Survey 2 patch, overlapping the southeast corner of the corresponding relative turbidity map, was calculated to be

23,203 m^2. In Survey 3, the nearest patch was centred slightly to the east of the high-turbidity centre and had an area of 18,796 m^2. The patch corresponding to Survey 4 had an area of 8,355 m^2 and was positioned somewhat further south and east of the high-turbidity centre. The area of impact values derived using the entrainment coefficients had corresponding radii that were, on average, 37 m larger than those of the area of impacts estimated from the MBES backscatter map

4.8.4 Discussion

Entrainment

Tsai et al. (1992) estimated the entrainment coefficients for 4 separate disposals at a Florida disposal site in 140 m of water. A mean of 0.68 was estimated which is similar to the ingress and egress estimates, 0.6 and 0.57, derived for this study. The range of estimates, however, was found by Tsai et al. (1992) to be much smaller compared to the present study. It was suggested that the presence of a pycnocline can act as a mechanism for altering the entrainment coefficient due to a change in slope of the turbidity contour at the level of the pycnocline (Tsai et al., 1992). Therefore, it is possible that the larger range of entrainment coefficients estimated for the 4 disposals included in this study is due to the variability of the water column density structure over the 4 survey days. This explanation is consistent with the density profiles recorded on each survey day as variability was observed in the position of the principal pycnocline (i.e. mixed layer depth) as well as in the strength and position of the additional small scale density transitions within the more stable overall density structure (Figure 4.17).

In principle, the pycnocline can act as a barrier which, depending on magnitude of stratification and the energy of the down-falling material, can cause spreading or entrainment at or just above the level of the pynocline and hinder the descent process. In some cases, the presence of a pycnocline can prohibit completely the descent to the seabed in which case all the down-falling material will hit the pycnocline and spread out radially in a premature mid-water-column dynamic collapse phase (Winterwerp, 2002). This occurs more commonly with dredging spill rather than disposal because dredging spill usually has a lower velocity ratio and excess density compared to loads of dredged material disposed as a mass (Winterwerp, 2002).

In the case of the disposals monitored at the AMDG, the presence of a pycnocline did not completely block the down-falling dredged material, but there is evidence that it did cause enhanced spreading in some cases. During Survey 1, strong spreading between 60 and 70 m below the surface was observed and was most likely associated with the maximum depth of the upper mixed layer, below which density increased towards the bed (Figure 4.17a and Figure 4.24a). Weaker enhanced spreading was also observed at approximately 40 m below the surface, but there was no obvious correlation to changes in the density profile at that depth.

During the disposal corresponding to Survey 2, increased spreading was observed 20 m below the surface which was likely associated with the narrow low density layer at the same depth evident in the density profile taken on that day[9] (Figure 4.17b and Figure 4.24b). A second zone of enhanced spreading was also observed 50 m below the surface which does not appear to be associated with a pycnocline. During Survey 2, the principal pycnocline depth appeared to occur approximately 80 m below the surface, which was just below the position of high turbidity plume recorded in the transect shown in Figure 4.24a, so it is not clear whether further enhanced spreading occurred in association with that density transition or others observed below it (Figure 4.17b). During Survey 3, zones of enhanced spreading associated with corresponding transitions in the density profile were observed at 30, 70, and 100 m below the surface (Figure 4.17c and Figure 4.24c). Similar zones of enhanced spreading were observed approximately 20, 50 and 80 m below the surface during Survey 4, which also may be associated with pycnoclines at similar depths (Figure 4.17d and Figure 4.24d).

[9] This feature was discussed in depth in Section 3.6 with regards to determining the origin of the low-density spike. It was assumed that as the profiles were recorded well after the release and dispersal of material into the water column, the low-density spike must have been caused by a remnant parcel of low density/low salinity marina water associated with the disposed material. However, the enhanced spreading observed in the early-survey transect (Figure 4.24b) of Survey 2 suggests that the low density spike was not a result of the disposed material, but inherently present as a part of the environmental setting of the site on that day. EAUC surface intrusion was already ruled out as a possible source of the low density layer as the salinity was lower than the mixed layer norm, therefore, the origin must be of a less saline source. The only other possible source of fresh water that far from the coastline is rain, so it is possible that a residual band of freshwater remained near the surface after the passing of a low pressure system in the days between Survey 1 and Survey 2. Enhanced spreading was also observed in the early-survey transect of Survey 4 at the depth of the low density spike in the profile recorded on the same day suggesting that a similar explanation may also apply to Survey 4.

As the zones of enhanced spreading act to increase the entrainment coefficient estimate, inaccuracies can arise if the estimates are made over depths that do not incorporate the pycnocline layers, in which case the derived coefficient would be an underestimate. Based on the timing of the transects used to estimate the entrainment coefficients and indications from the density profiles, it is possible that additional zones of enhanced spreading may have been present in the lower reaches of the water column which were not fully incorporated in the entrainment coefficient estimates especially on Surveys 3 and 4.

Down-fall Velocity

Estimation of the fall velocity of dredged material disposed at sea can be approached from a very simplistic perspective by considering the descending material to be a mass having only one descent speed (e.g. Drapeau et al. (1999) and Krishnappan (1975)) where the result represents an average fall velocity for the convective descent phase. Alternatively, if the field data allows, fall velocity can be determined based on the various components of the load of material each of which may have different descent characteristics and thus different fall velocities (e.g. Bokuniewicz et al. (1978)).

For the 4 dispersion surveys included in this study, an attempt was made to consider the down-fall velocity from both perspectives. Bokuniewicz et al. (1978) determined fall velocities of the "clods" of dredged material (mentioned previously) separately from the "jet" and defined each as independent, cohesive blocks of soil versus fine particles dispersed in fluid, respectively. For this study, the resolution of the ADCP backscatter is not high enough to distinguish individual clods, but there is an indication of them in the echosounder image presented in Figure 4.25 and underwater video recorded at the centre of the site (approximate release location for all 9 loads of material disposed at the AMDG) shows the presence of clods quite distinctly on the seafloor (Figure 4.26).

In this case, it was assumed that early-phase (W_{fE}) estimates were more representative of the independent clods of material as they would likely be positioned at the leading edge of the turbidity cloud or even preceding due their size and density (Bokuniewicz & Gordon, 1980). Likewise, late-phase (W_{fL}) estimates were assumed to be more representative of the average jet descent

velocity as the fluid component of the disposed load would lag behind the clods in descent to the seabed due to loss of momentum through entrainment processes (Bokuniewicz & Gordon, 1980). It should be noted that components of the load characterised somewhere between clod and jet are a likely to exist, but that level of detail was not considered here.

For the study done by Bokuniewicz et al. (1978), clod fall velocities ranging from 0.35 m/s to 1.53 m/s for clod sizes ranging in size from 2 cm to 13 cm were observed. In this case, all values of W_{fE} were within the range observed by Bokuniewicz et al. (1978) which suggests that W_{fE} is a sensible indictor of clod fall velocity; however, the values corresponding to Surveys 1 and 2 were significantly higher than those corresponding to Surveys 3 and 4 (~1.2 m/s vs. 0.7 m/s). There are several possible explanations for the lower W_{fE} speeds in Surveys 3 and 4 compared to Surveys 1 and 2. High current velocity can act to slow down vertical descent through horizontal displacement. Current measurements during Survey 3 were overall the highest recorded from the 4 surveys, but in the range of 20 to 25 cm/s, the currents would not sustain a clod in suspension that was larger than approximately 0.3 cm according to Hjulstrom's curve as cited in (McCave, 1984). This estimate assumes that a clod of cohesive material behaves similarly to an individual grain of non-cohesive sediment for which Hjulstrom's curve has been established as appropriate (McCave, 1984). The size of the clods shown in Figure 4.25 are unknown due to a lack of scale, however, the field of view has been estimated as 0.8 m by 0.6 m (*pers. comm.*, M. Birch), so they are likely on the order of 10 cm in size. Survey 4 was undertaken during slack tide, so current velocity was even lower than that of Survey 3. Therefore, it is not likely that high current speed is the reason for the low W_{fE} speeds estimated for Surveys 3 and 4.

Another possibility for the slower descent speeds may be due to the volume of the loads disposed as negative buoyancy is a function of the volume (Drapeau et al., 1999). Surveys 3 and 4 were indeed the smallest of the 4 disposed loads (Table 4.7), but the volume disposed during Survey 4 was only slightly less than that disposed during Survey 2 and so the large difference between the W_{fE} speeds determined for the 2 surveys does not seem sensible. A more plausible explanation, which may have been the case if the dredged material disposed

during Surveys 3 and 4 originated from areas of the marina which had lower clay content, is that there were simply fewer and/or smaller clods in the loads. Indeed Bioresearches (2009) characterised some areas of the marina as having a higher proportion of sand and gravel compared to areas predominantly composed of silt and clay. Sand and gravel are primarily considered to be non-cohesive and would therefore not promote the formation of clods. Additional possibilities are: increased agitation of the material in the hopper during transport to the site, less consolidation time in the hopper before release at the site, or increased turbulence during release due to the presence of surface waves and/or wind chop.

Estimates pertaining to the descent of the "jet" (W_{fL}) were also similar to those reported by Bokuniewicz et al. (1978) with the exception of one disposal where an unusually rapid descent speed (almost 3 m/s) was achieved. This was attributed to the high insertion speed, which was variable for the disposals monitored due to the use of different hoppers for each disposal. For the 4 disposals monitored in this study, the same hopper was used so the variable insertion speeds reported in Table 4.7 are purely a function of the volume of each load disposed (Equation 4-15). Based on that, the jet descent speed should be proportional to the volume of the disposed load (after Bokuniewicz et al. (1978)). To confirm whether this principle was true for the disposals monitored in this study, regression analysis was undertaken on W_{fL} and volume (Figure 4.31a). In this case, correlation was not significant, but a R^2-value of 0.45 suggests that there is probably some association between the two parameters. It is also feasible that experimental uncertainties influenced the poor correlation.

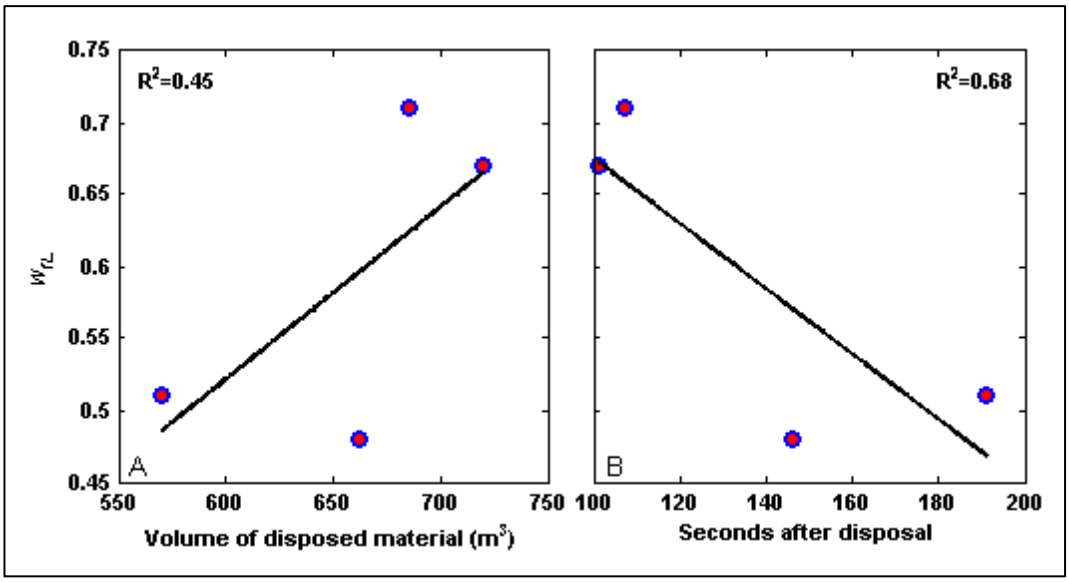

Figure 4.31 a) Regression analysis of W_{fL} and disposed load volume (m^3). b) Regression analysis of W_{fL} and time in seconds after disposal.

The transects used to estimate W_{fL} were recorded as close as possible to immediately after the disposal, but the timing ranged from 101 sec. to 191 sec. post-disposal for the 4 surveys, so it is possible the influence of time may have had an important effect on the derived W_{fL} estimates. Assuming the dredged material that was disposed was composed of a range of different grain sizes, the larger/heavier grains would be expected to reach the seafloor faster because they typically have a higher settling velocity. Due to this principle, it could be expected that the shorter the time between the disposal and the transect recording the estimate was made from, the higher the average jet descent velocity would be because the "jet" would, at that time, be composed of a larger proportion of the faster settling grain sizes.

Regression analysis of W_{fL} and time after disposal in seconds indicates a significant correlation with an R^2-value of 0.68 which is somewhat better than the relationship between W_{fL} and volume, but it is still not strongly correlated. Scanning electron microscope (SEM) imagery of filtrate from water samples collected near the surface was undertaken to attempt to validate the relationship between W_{fL} and time after disposal by determining whether the size distribution of the suspended particles became more finely skewed with time after disposal. Figure 4.32 shows examples of some of the SEM images of filtrate from the water samples collected during Survey 3 at Station A, which was at the location of release of the dredged material (Figure 4.7). The images represent the samples

collected between 10 min and 45 min after disposal at a depth of 5 m. The lighter coloured fibres are part of the filter paper that was used in the filtration of the water samples. The SSC for each sample ranged from 28 mg/L 10 min after disposal to 1.5 mg/L 45 min after disposal.

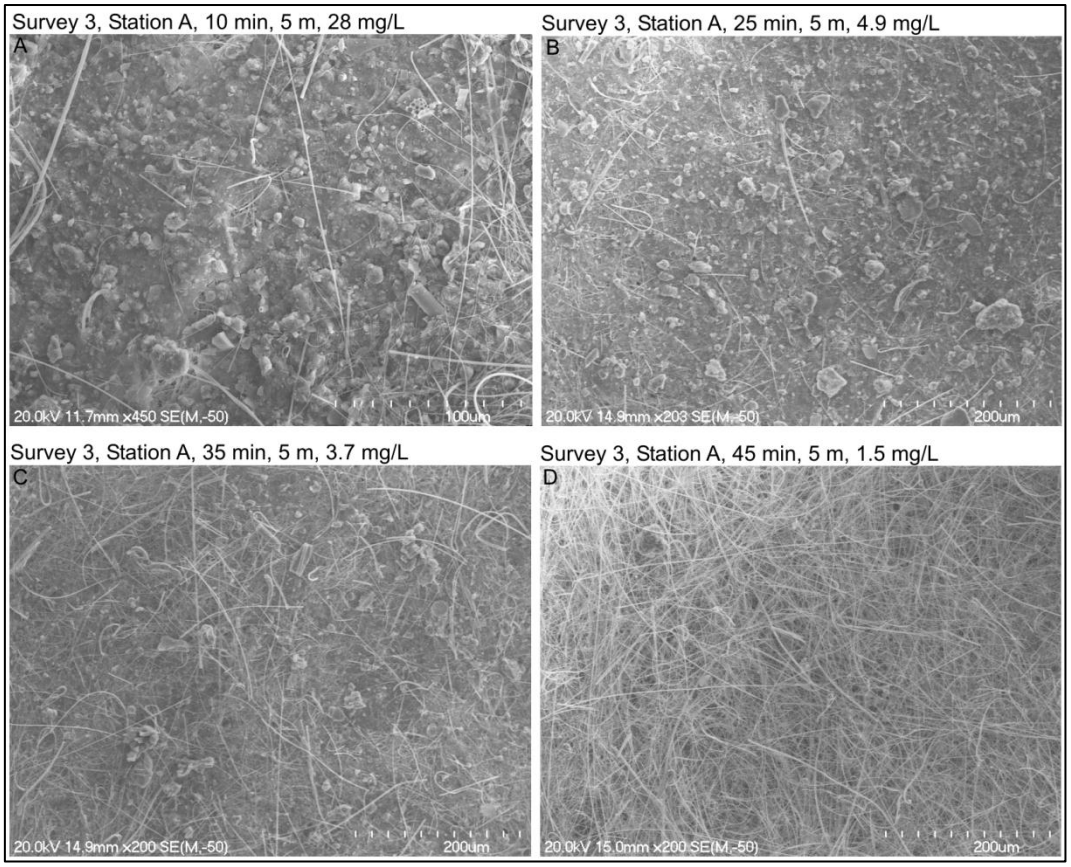

Figure 4.32 Scanning electron microscope images of the filtrate from water samples collected during Survey 3, 5 m below the surface a) 10 min b) 25 min c) 35 min and d) 45 min post-disposal. Light coloured fibres are part of the glass fibre filter used in the water sample filtration. Note the different scale of image A.

There is a clear decrease in the quantity of suspended particles which is visible as a thinning of the smooth layer of material obscuring the glass fibres. It would be expected that the smooth layer would be composed of the finer portion of the suspended particles as they would likely be laid down onto the filter paper during filtration in and even way, though disaggregation during the sample processing would be highly likely so the characteristics of the sediments on the filter papers may not accurately represent their *in situ* characteristics.

The larger particles are most likely representative of aggregated clay material that would be expected to settle out preferentially because they are heavier than the individual grains. It appears though that settling of the fines and the aggregates is almost simultaneous or possibly the fines are settling before the aggregates as

there are still some aggregates left in the later 2 samples. The mechanism for this is unknown, but it is possible that re-flocculation might have occurred due the presence of high organic content within the disposed material (Eisma, 1986) or that the portion of the filter papers shown in these images are not representative of the overall trend. In either case, the tendency for clays to aggregate makes it quite difficult to distinguish effects of the filtering and drying processes from patterns that were in place *in situ* when the samples were collected. So, no confident conclusions can be drawn on the validity of the correlation between W_{fL} and time from the SEM photos, other than to say that there is a definite decrease in the overall concentration as time progressed.

Despite this, the correlations indicate that time after disposal has a greater effect on the settling velocity of the jet than does the volume of the disposed load. However, as the analyses were only based on the data from 4 disposals, impact of errors from the estimation method may be high and indeed both parameters would be expected to be influential along with several other factors such as ambient current speed, water density, and sediment properties.

Estimates derived from Krishnappan's formulation of down-fall velocity (W_{fK}) are indicative of an average for both the clods and the jet portion of the disposed load because of the assumption that material falls as a single mass with one descent speed. Therefore, in principle W_{fK} should be similar to the average of W_{fE} and W_{fL} (W_{fM}). For Surveys 1 and 2, W_{fK} was slightly lower than W_{fM}, though within a reasonable margin of error, but for Surveys 3 and 4, W_{fK} was significantly larger than W_{fM} (Table 4.7). The evidence indicated that the material disposed during Surveys 3 and 4 may have had lower clay content and thus contained fewer and/or smaller clods which explained the low W_{fE} estimates compared to Surveys 1 and 2. Assuming that explanation is valid, Krishnappan's formulation for downfall velocity most likely does not adequately account for the unique properties of clods within a load of disposed dredged material. Equation 4-14 shows that W_{fK} only takes into consideration properties of the individual grains within the load. As such, this formulation would be more appropriate for dredged material with mainly non-cohesive sediment, such as sand and silt. For dredged material with a high clay content, an additional cohesion parameter may improve results.

Area of Impact

The area of impact was defined as the location of deposition for the component of the disposed load that settled on impact with the seabed. The estimates for the proportion of the loads that settled on impact seemed reasonable for Surveys 1 and 2, but it is unlikely that 100% of the loads disposed during Surveys 3 and 4 settled on impact. The estimates should, therefore, be regarded as an indication only. Most likely, the values are somewhat overestimated because the settling velocity applied does not represent the significant clay fraction of the material dredged from the marina.

In general, the derived area of impact estimates correspond well with the size of the near-bed higher turbidity areas recorded during the first several transects of each survey, however, it is clear that on Survey 2 (Figure 4.29b), the high turbidity area resulting from the point of impact, was beyond the range of the transects recorded in the first 15 min of the survey. The position of the dashed line circle in that case was estimated based on the location of the nearest patch of denser substrate as determined from the MBES backscatter map. In all other cases, the position of the red marker on the MBES backscatter map reflects the position of the high-turbidity centre within the relative turbidity map to the left. For all 4 surveys, the red marker is positioned very close to at least one lighter gray patch of a size similar to the corresponding high turbidity zone. The area of impact values showed a linear correlation between the two estimate methods (R^2=0.77) (Figure 4.33), however, values derived based on the entrainment coefficient were somewhat larger than those based on measurements from the MBES backscatter map.

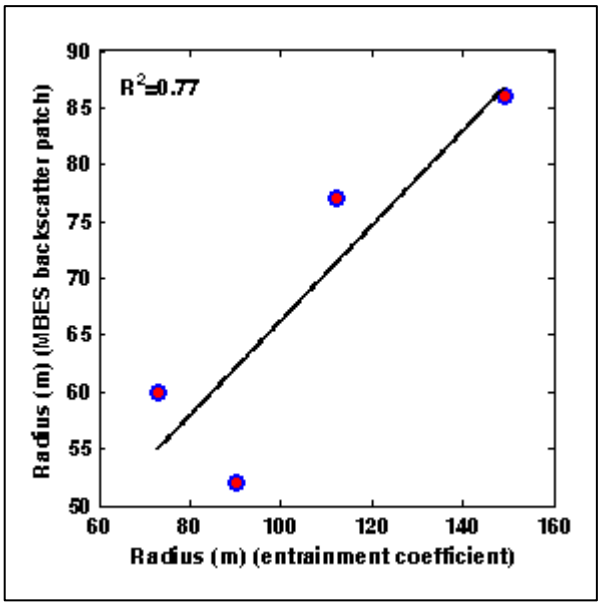

Figure 4.33 Regression of radius values (based on area of impact values) derived from entrainment coefficients versus those derived from the post-disposal MBES backscatter map.

Offsets in the position of the centre of the highest turbidity zones within the relative turbidity maps compared to the location of the light gray patches within the MBES backscatter map are most likely due to the fact that the extent of the ADCP backscatter data is 128 m below the surface which is approximately 10 m above the bed. Horizontal displacement within that distance would result in the actual point of impact being shifted slightly in the direction of the ambient current. Interpolation procedures applied to the ADCP backscatter datasets and experimental errors may have also contributed to the inconsistencies.

Based on the variation in the area of impact estimated for each disposed load, there may be a negative correlation to the volume discharged. This seems reasonable as the larger the load disposed, the higher the negative buoyancy and descent velocity, which would have the effect of preventing entrainment and lateral spreading during descent. However, the negative correlation is only consistent if the load corresponding to Survey 2 is treated as an outlier (Figure 4.33). This load may have exhibited different characteristics because the sea state conditions were considerably more turbulent than on the other 3 survey days based on observations from on board the monitoring vessel, though it should be noted that according to the horizontal current magnitude records (Table 4.5), starting from 4 m below the surface, the currents on that day were neither the strongest, nor the most variable of the four survey days. In that case, a plausible explanation is that turbulence at the surface caused disaggregation of clods and

mixing of the fluid component within the hopper during transport to the site. This process would have made what was in fact the largest load, more susceptible to entrainment resulting in an increased entrainment and an area of impact. Though this idea is somewhat counterintuitive to the higher downfall velocities associated with the load disposed during Survey 2 (see Section 4.8.2).

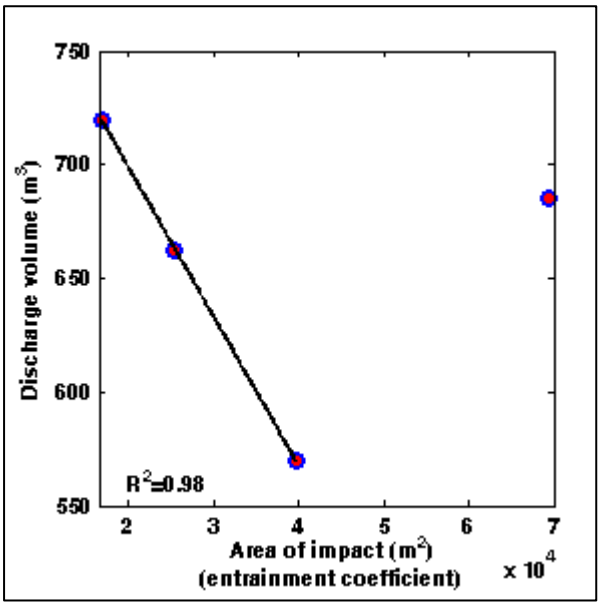

Figure 4.34 Regression of area of impact values derived from entrainment coefficients versus discharge volume for each disposal surveyed.

4.8.5 Summary of Dispersion During Phase 1

During the Convective Descent phase of the disposal process, horizontal dispersion mainly takes place through entrainment processes, which manifest through spreading of the jet of semi-liquid disposed material away from the release location. The magnitude of spreading typically increases with depth, but can be enhanced preferentially at points corresponding to significant water density transitions. The transitions, however, are not depth-dependent. In this study enhanced spreading due to density layers was evident, but overall the greatest spreading was observed at the leading edge of the disposal plume (Figure 4.24) so it is reasonable to assume that the radius (R_I) of the area of impact calculated using the entrainment coefficient (A_I) is an appropriate estimate of the maximum horizontal dispersion distance incurred during Phase 1 of each monitored disposal assuming that advection by the ambient current is minimal during the first few minutes after disposal. Use of the A_I values in this case is more appropriate than use of the estimates derived from the MBES backscatter map because A_I is

derived from suspended particles which are susceptible to dispersion. Those values derived from the MBES backscatter map, on the other hand, are only a measure of material that was dense enough alter the seafloor properties and appear as a distinct patch in backscatter grayscale and, as such, that material may not have been susceptible to passive dispersion through entrainment during descent.

Maximum horizontal dispersion during the Convective Descent phase, can therefore, be estimated as 73 m, 149 m, 112 m, and 90 m, with distances decreasing with proximity to the surface for each of the loads monitored. Dispersion distances were based on the area of impact (A_I) estimates (16,806 m^2, 69,504 m^2, 39,648 m^2, and 25,413 m^2) for the disposals corresponding surveys 1 - 4, respectively. Variation in the area of impact between the 4 loads disposed may be negatively correlated to the volume of the load, such that larger loads may be less susceptible to entrainment due to higher negative buoyancy, though the evidence for this is limited and requires a larger dataset to form a more robust conclusion.

4.9 Dynamic Collapse

At the point of transition between the *Convective Descent* phase and the *Dynamic Collapse* phase (Figure 2.1), the disposed material has either deposited on the bed at the point of impact or it is in suspension. If it is deposited on the seafloor, it can be considered unavailable for dispersion at least in terms of the short-term fate of the disposed material (Drapeau et al., 1992). The proportion of sediment in suspension, therefore available for dispersion by a density current, was described earlier with Equation 4-16. This suspension forms the initial conditions for the propagation of the density current radially away from the initial area of impact.

4.9.1 Density Current Formation

At the moment of impact the mass of sediments impacting the seafloor has a vertical flux that was described by Drapeau (1992) as

$$\pi R_I^2 W_{fi} \qquad \text{Equation 4-19}$$

where R_I=radius of the area of impact (A_I) cloud and W_{fi}=the downfall velocity at the moment of impact. The initial flux of the density current formed at the moment of impact can be described as

$$2\pi R_{Di} H_{Di} V_{Di} \qquad \text{Equation 4-20}$$

where R_{Di}=the initial radius of the density current, H_{Di}=the initial thickness of the density current, and V_{Di}=the initial velocity of the density current. Since R_I and R_{Di} are equal at the moment of impact, Equation 4-19 and Equation 4-20 can be equated to give

$$R_I W_{fi} = 2H_{Di} V_{Di} \qquad \text{Equation 4-21}$$

in which case the two unknowns, initial thickness and initial velocity of the density current, must be determined.

4.9.2 Thickness of the Density Current

Through conservation of flux the initial thickness of the density current (H_{Di}) can be described as

$$\left[(R_{Di} W_{fi})^2 / \left(4Fr^2 g D_{Di}\right)\right]^{1/3} \qquad \text{Equation 4-22}$$

where Fr=densiometric Froude number determined to be constant at a value of 0.75 for density currents generated by sediments in suspension flowing over a horizontal bottom (Middleton, 1966), and D_{Di}=difference density of the density current defined as

$$\rho_e / \rho \qquad \text{Equation 4-23}$$

where ρ=the density of water and ρ_e=excess density of the density current which can be determined as

$$\rho_{plume} - \rho \qquad \text{Equation 4-24}$$

where ρ_{plume}=density of the suspended component of the disposal plume after impact with the seafloor. The value for ρ_e is equivalent to the concentration of suspended sediment. In essence, the lower the concentration, the higher the initial

thickness of the plume as it is more susceptible to turbulent processes. This is particularly relevant in deeper water because entrainment during convective descent is more extensive which results in a lower initial concentration of the density current (Bokuniewicz & Gordon, 1980).

To estimate the initial thickness of the density current during each of 4 monitored disposals in this study the above equations were applied. The input values and results are shown in Table 4.11. The area of impact radius (R_I) estimated from the MBES backscatter map for each monitored disposal was applied as R_{Di}. In this case, use of the MBES backscatter map estimates is more appropriate than the entrainment value estimates because the density current will form based on excess energy after the bulk of the material impacts with the seafloor, thus, intuitively, initiation of the density current should coincide with the high density patches identified on the MBES backscatter maps.

The early-phase down-fall velocity estimates (W_{fE}) were applied as W_{fi} in Equation 4-22. As near-bed sediment concentrations were not sampled due to the significant water depth, a range of values for ρ_e were considered. The water depth of the AMDG indicates that the excess density of the disposal plume in the moment after impact would be significantly diluted due to entrainment during descent and deposition of the portion of the load on impact with the seabed so the applied values of ρ_s correspond to 2 concentrations in the fluid mud range (McAnally et al., 2007) and 2 at lower concentrations. As a reference, the maximum concentration sampled near the surface was 0.07 g/l, which was visibly very dilute.

The estimated density current thicknesses range from 14 to 29 m above the bed at a ρ_e of 20 kg/m^3 and from 38 m to 79 m above the bed at a ρ_e of 1 kg/m^3. During Survey 1, one ADCP transect of relative turbidity above background levels recorded approximately 6 minutes after disposal, showed indications of a density current that had propagated away from the area of impact (Figure 4.35). It appears that only the upper edge of the density current is visible due to the limits of the system settings, but the indication is that the density current had an initial thickness of approximately 40 m ATB which decreased over a distance of 200 m to approximately 15 m ATB. Unfortunately, none of the transects recorded during Surveys 2-4 adequately captured evidence of a density current.

Table 4.11 Details of thickness of density current estimates for the 4 monitored disposals.

ρ_e (kg/m^3)(g/l)	Plume density (kg/m^3)	H_{Di} (m)			
		Survey 1	Survey 2	Survey 3	Survey 4
20	1047	24	29	18	14
10[a]	1037	30	37	23	18
5	1032	37	46	29	22
1[b]	1028	64	79	50	38
Constants					
R_{Di} [c](m)		60	86	77	52
W_{fi} [d](m/s)		1.27	1.20	0.67	0.67
Fr=0.75, g=9.812, ρ=1027 (kg/m^3)					

[a]generally accepted concentration minimum for fluid mud (McAnally et al., 2007)

[b]approximate maximum concentration measured from near-surface water samples

[c]radius of the density current is equal to the radius of area of impact, which was derived from the MBES backscatter map (Table 4.6 and Section 4.8.3)

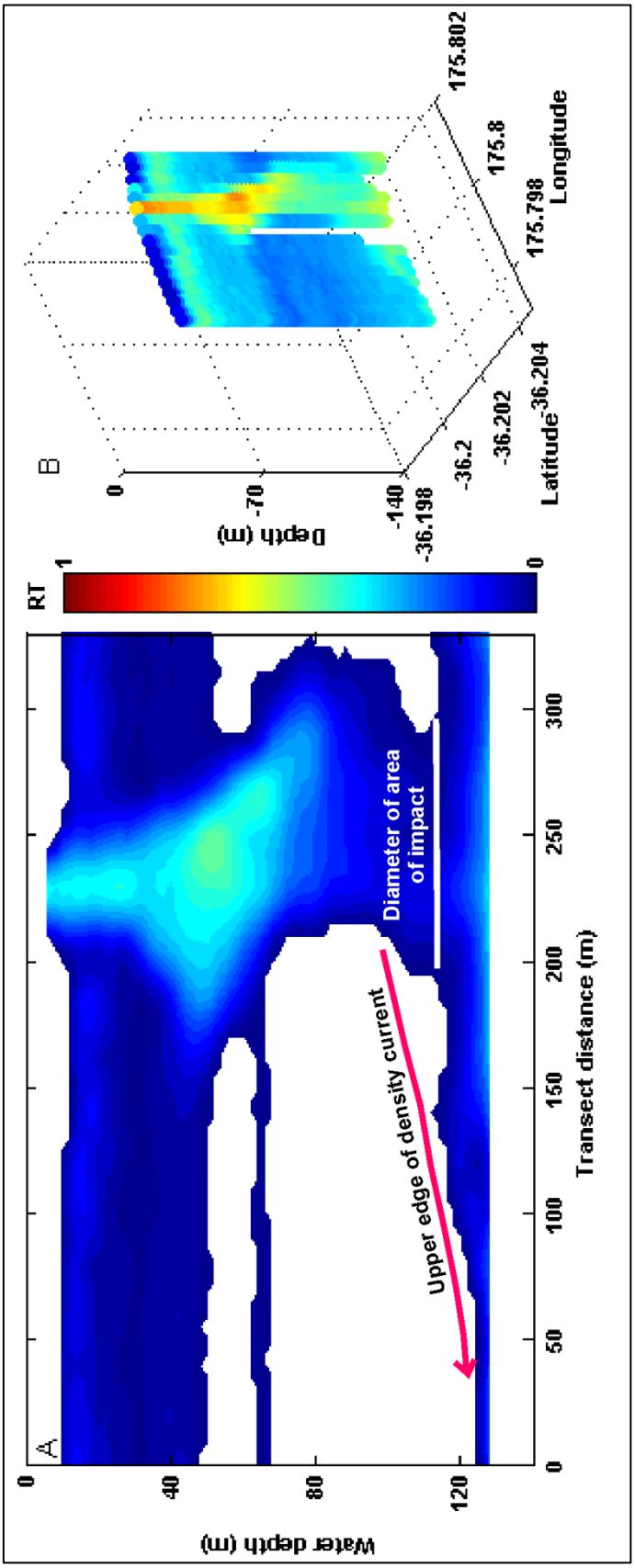

Figure 4.35 a) Transect of relative turbidity above background recorded 6 min after disposal during Survey 1. Red arrow indicates the upper edge of the density current. b) Location of the transect (un-interpolated and including background turbidity)

4.9.3 Velocity of the Density Current

The velocity of the density current will decrease with propagation time due to friction over the seabed and entrainment of ambient water (Bokuniewicz et al., 1978), but the initial velocity at the moment of formation can be estimated as

$$V_{Di} = Fr\left(D_{Di} g H_{Di}\right)^{1/2} \qquad \text{Equation 4-25}$$

where Fr=densiometric Froude number previously defined as 0.75, D_{Di}= initial difference density of the density current (previously defined), and H_{Di}=initial thickness of the density current (Drapeau et al., 1992).

From Figure 4.35, the initial thickness of the density current appeared to be approximately 40 m ATB for the load disposed during Survey 1. The data presented in Figure 4.35 shows that at an initial thickness of approximately 40 m, the concentration of the density current would be expected to be between 1 kg/m^3 (g/l) and 5 kg/m^3 (g/l). Using that range of possible concentrations for a potential initial thickness of 40 m and Equation 4-25, the initial velocity for the Survey 1 case was calculated (Table 4.12).

Table 4.12 Details of analysis of initial velocity of the density current for the load disposed during Survey 1.

Initial concentration of the density current (ρ_e) (kg/m3) (g/l)	Initial velocity* (V_{Di}) (m/s)
1	0.46
2	0.66
3	0.8
4	0.93
5	1

*H_{Di}=40 m

For an initial concentration ranging from 1 kg/m^3 to 5 kg/m^3, the initial velocity of a potential density current would be expected to vary from 0.46 m/s to 1 m/s, respectively, based on the theoretical understanding..

4.9.4 Density Current Propagation

A feedback loop exists between the velocity, thickness, and concentration of the density current, where each aspect is affected by, and also affects, the other parameters equally. To gain a better understanding of the propagation potential of

a density current at the AMDG, iterative analysis was undertaken, based on the method of Drapeau et al. (1999), to derive the temporal and spatial adjustments within the current. This method was applied to Survey 1 conditions only due to the lack of field collected bottom surge information for Surveys 2-4, and the method assumes that the density current takes the form of a torus of constant width and volume.

The iteration was initialised using an initial density current velocity (V_{Di}), given by Equation 4-25. Refer to Table 4.13 for all initial values and constants applied in the iteration.

The potential density current thickness was determined as

$$H_D = M_D / A_D \qquad \text{Equation 4-26}$$

where M_D=the volume of the density current and A_D=surface area of the density current (Drapeau et al., 1999). The initial value for A_D was determined based on the initial radius of the density current (R_{Di}) (see Table 4.6) assuming an inner radius of zero and the initial value for M_D was taken as the product of the initial value of A_D and the initial thickness of the density current (H_{Di}) (see Figure 4.35).

Table 4.13 Values applied in iterative analysis of the potential density current propagation associated with the disposal corresponding to Survey 1.

Variable	Initial value	
Density current velocity (V_D)	0.66 m/s	
Radius of the density current (R_{Di})	60 m	
Density current thickness (H_D)	40 m	
	Constants	
Gravitational acceleration (g)	9.81 m/s	
Densiometric Froude number (Fr)	0.75	
Ambient water density (ρ)	1027 kg/m^3	
Excess density of the density current (concentration) (ρ_e)	2 kg/m^3 (g/l)	
	Mud	Sand
Mean settling velocity (W_s)*	0.00035 m/s	0.024 m/s
Sediment entrainment threshold velocity (U_{crit})†	0.2 m/s	0.35 m/s

*based on Stokes settling velocity
†based on Sheilds entrainment parameter

The change in excess density (concentration) of the density current as it propagates over the bed was accounted for by comparing an idealised settling

velocity (W_s) for either sand or mud, to an idealised sediment entrainment threshold (U_{crit}) for either sediment type (see Table 4.13). If the velocity of the density current exceeded the sediment entrainment threshold, the concentration was not adjusted. In that, the assumption was made that the amount of erosion of the bed by the density current balances out the amount of deposition to the bed. If the velocity of the density current was less than the entrainment threshold, the amount lost due to settling was then calculated giving a new concentration for the density current.

Finally, by again applying Equation 4-25 using the adjusted values for the potential thickness and concentration, a new density current velocity was calculated. The iteration was terminated after the calculated settling distance exceeded the potential thickness of the density current, when the concentration of the density current was no longer meaningful (minimum concentration=0.001 g/l), or after 3600 iterations (equivalent to 3600 seconds; the approximate length of the surveys).

In the case of a density current composed of fine sand-sized sediment (0.2 mm), the iteration method gave a maximum propagation distance of approximately 250 m from the centre, a distance attained after approximately 1800 seconds (Figure 4.36). In this case, the potential thickness of the density current was still approximately 7 m, but the iteration was terminated because the concentration was less than the minimum allowed and was, therefore, no longer meaningful as a density current.

When the density current is composed of only mud-sized sediment (0.02 mm), the analysis indicated that a current would still have momentum more than 600 m from the centre and after more than 3500 seconds (Figure 4.36a&d). A density current, after such a point, could potentially have a concentration of approximately 1.25 g/l (Figure 4.36c&f), but with a thickness of only 1 metre or less.

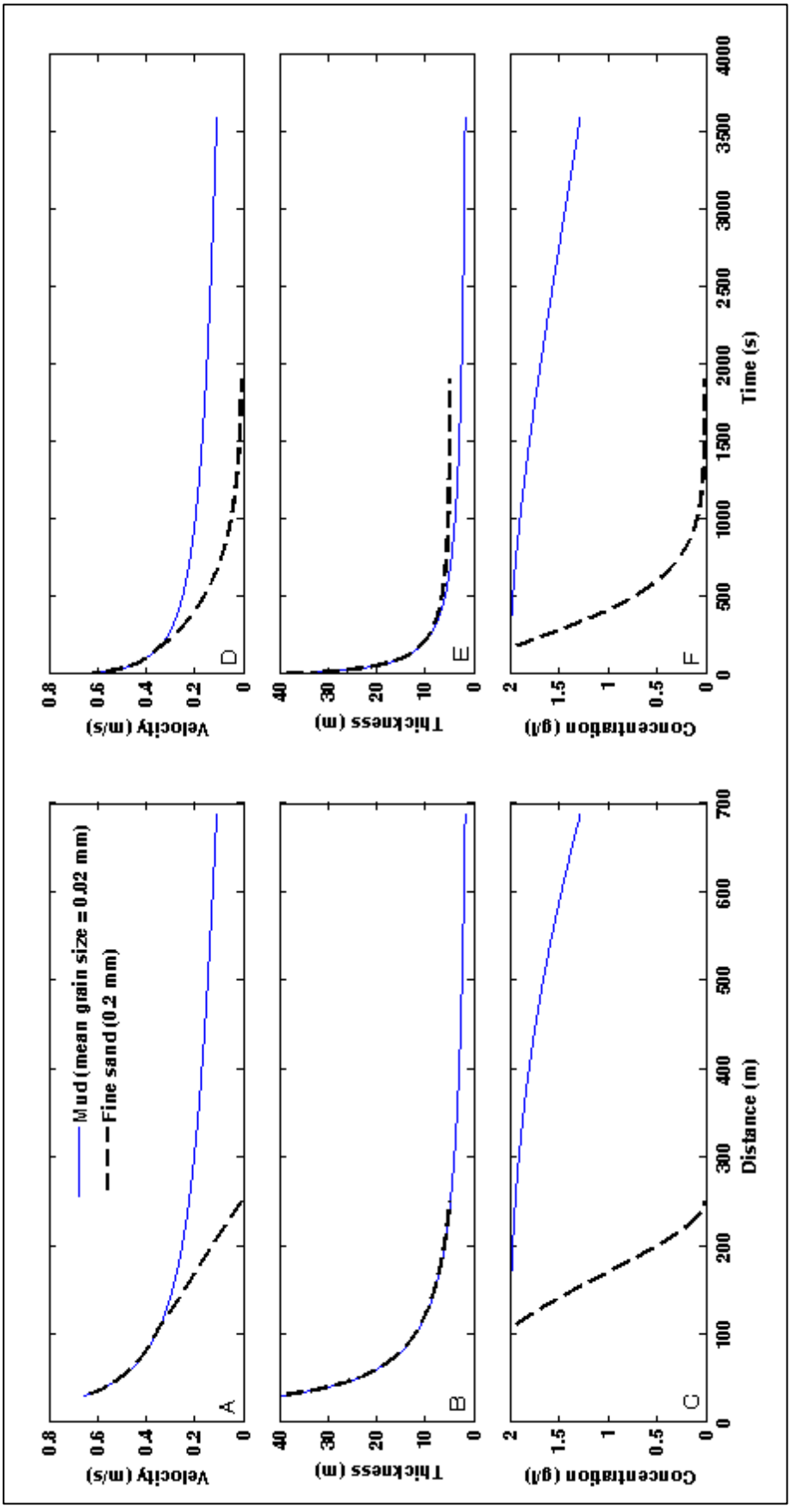

Figure 4.36 Potential velocity, thickness, and concentration of the bottom surge relative to (a-c) distance (radius) and (d-f) time for the mean grain size of the material disposed at the AMDG (solid blue line) and for fine sand (dashed black line) with an initial density current thickness of 40 m.

4.9.5 Discussion

One ADCP transect recorded during Survey 1 showed what can be interpreted as the upper edge of the density current which was located approximately 40 m ATB (Figure 4.35). However, what is not possible to see in the transect is the leading edge of the density current, often referred to as a 'tore' (e.g. Drapeau et al. (1999)). Based on approximate descent speeds, the transect was most likely recorded several minutes after initiation of the density current and, therefore, the tore had probably already propagated to a point beyond the end of the transect; however this is not certain due to the missing data in the lowest 20 m of the water column.

The 'tail' of the density current, the region stretching from the tore backwards to the area of initiation, typically has higher flow velocities than the leading edge due to the internal turbulence of the density current (Bokuniewicz et al., 1978). This area is, therefore, subject to increased entrainment of ambient water, which causes the thickness of the tail region to increase. This disparity in the thickness of the density current from tore to tail has been illustrated quite clearly *in situ* by Bokuniewicz et al. (1978) and Tsai et al. (1995), as well as by Middelton (1966) and Sparks et al. (1993) in the laboratory setting.

As the ADCP transect from Survey 1 showing the upper edge of the density current probably more closely illustrates the thickness of the tail region, it is possible that the density current thickness estimate of 40 m ATB may be somewhat exaggerated for application in the relevant calculations as the thickness of the tore. Indeed, Bokuniewicz et al. (1978) reported that typically tore thicknesses were approximately 15 % of the water depth, which in the case of the AMDG, indicates a thickness closer to 20 m, rather than 40 m.

On the other hand, when considering the thickness estimates made by applying Equation 4-22 (see Table 4.11) to the Survey 1 disposal, an estimate of 40 m does not seem improbable. It should be mentioned, however, that the thickness estimates are highly sensitive to the excess density (ρ_e) (concentration) value. For example, an increase in ρ_e by 1 order of magnitude more than doubled the thickness of the density current (Table 4.11). So, even though the derivation implied that a ρ_e range of 1 – 5 kg/m^3(g/l) was reasonable, in fact previous studies

suggest that a slightly larger value (e.g. 10 kg/m^3 (g/l)) is no less sensible (e.g. Bokuniewicz et al. (1978), Wolanski et al. (1992), Drapeau et al. (1999)), though in those examples, the water depth of the disposal sites were typically less than that of the AMDG. Nonetheless, a density current (tore) thickness closer to 20 m, may be accurate for potential density currents at the AMDG.

Potential propagation distance of a density current associated with the disposal monitored during Survey 1 was somewhat higher than expected, especially in the case of a density current composed of mud, but also in the case of fine sand. The maximum distance ranged from approximately 250 m to ~500 m, whereas Bokuniewicz (1978) reported propagation distances in the range of 150 m to 300 m. The disparity could be due to differences in the conditions, i.e. water depth, dredged material properties, or disposal methods, but it could also be the result of errors in the values applied to initiate the iteration in this case.

With so many variables, it is difficult to pinpoint a single parameter as the source of the problem, but as already mentioned, one possibility could be an error in the initial thickness value. By adjusting the initial thickness (H_{Di}) to 20 m, rather than 40 m (Figure 4.36), more realistic propagation distances were derived for the mud (~300 m) and fine sand cases (140 m) (Figure 4.37).

One further validation of the derived density current characteristics based on the conditions monitored during Survey 1 was undertaken based on the dimensional analysis presented by Tsai et al. (1995). In that, it was found that the ratio of the propagation distance (length; L_s) to the water depth (H) is proportional to the 0.15 power of the ratio of the discharged volume (V_0) to the third power of the water depth (H). A similar relationship was also found with respect to the density current thickness, except the power dependence was 0.1 rather than 0.15 (see Table 4.14 for details and additional constants).

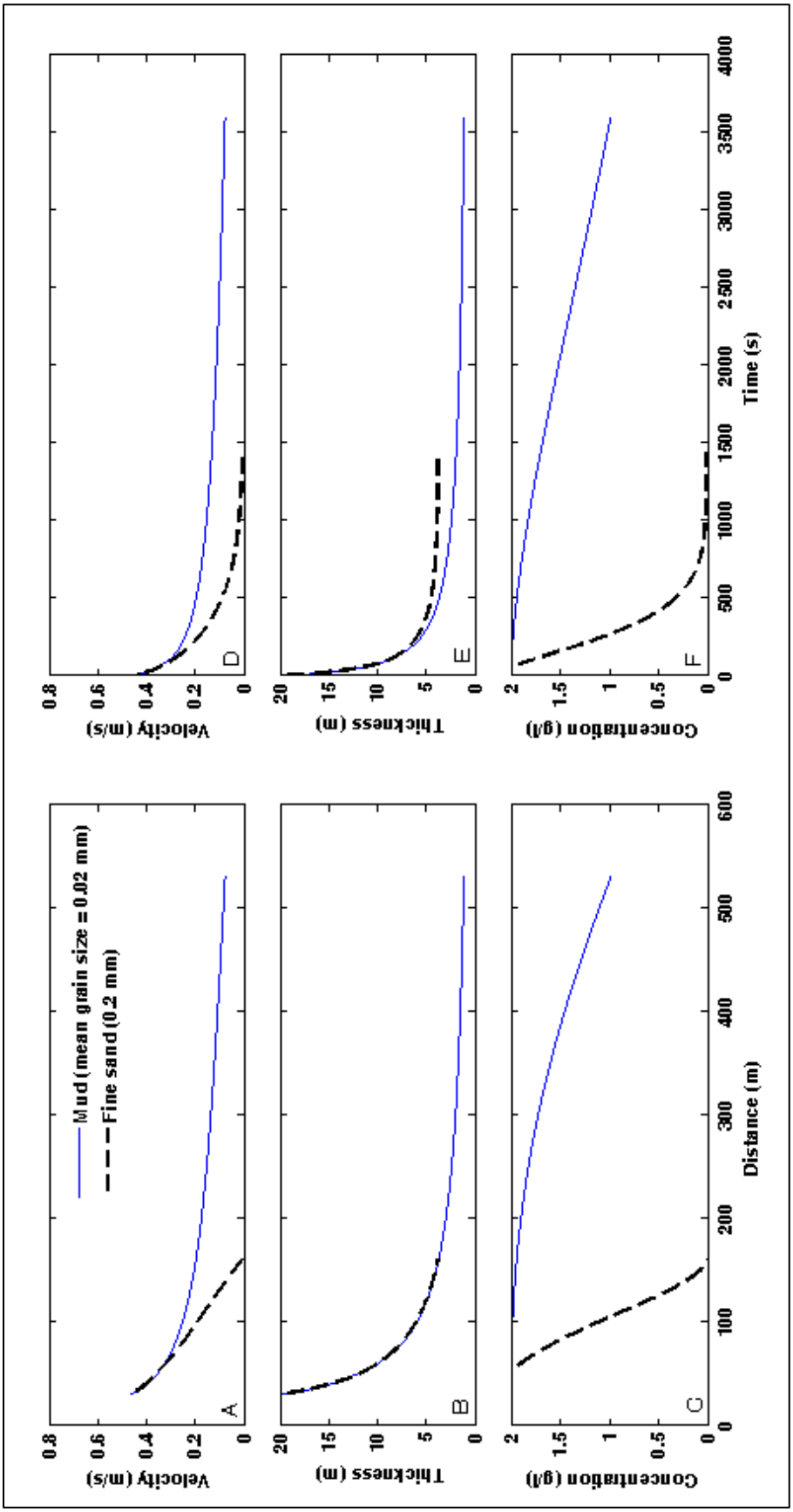

Figure 4.37 Potential velocity, thickness, and concentration of the bottom surge relative to (a-c) distance (radius) and (d-f) time for the mean grain size of the material disposed at the AMDG (solid blue line) and for fine sand (dashed black line) with an initial density current thickness of 20 m.

The ratios of the sand and mud propagation distances to the water depth (L_s/H), derived from the iterative analysis, range from 1.6 (sand) to 3.6 (mud), assuming an initial thickness of 40 m (Table 4.14). The corresponding value based on the relationship described above $\left(c\left(\frac{V_0}{H^3}\right)^d\right)$ is 2.14, which falls approximately in between the latter two values. Mean grain sizes of the discharged material from which the above relationship was derived was not mentioned by Tsai et al. (1995), but as most 'maintenance' type dredged material is of the fine to silty range, then it is reasonable assume that the relationship may be applicable to the present study. In which case, since the material disposed at the AMDG was neither purely fine sand, nor merely mud, but rather a mixture, then the density current propagation distances derived from the iterative analysis using the initial thickness of 40 m agrees surprisingly well with the relationship found by Tsai et al. (1995). The respective values derived for a density current with an initial thickness of 20 m also fit the dimensional relationship reasonably well, but more so in the case of a density current composed of mainly mud (Table 4.14).

Table 4.14 Evaluation of potential density current characteristics (Survey 1) using the dimensional relationships described by Tsai et al. (1995).

Depth H (m)	V_0 (m^3)	Initial thickness H_{Di} (m)	Surge length L_s (m)*		Dimensional analysis (thickness)		Dimensional analysis (length)		
			Sand	Mud	H_{Di}/H	$a\left(\frac{V_0}{H^3}\right)^b$	L_s/H		$c\left(\frac{V_0}{H^3}\right)^d$
							Sand	Mud	
140	720	40	225	500	0.29	0.11	1.61	3.57	2.13
140	720	20	140	300	0.14	0.11	1	2.14	2.13

a=0.256, b=1/10, c=7.353, d=0.15 (after Tsai et al. (1995))

*based on values derived using the iterative method described in Section 4.9.4 (see Figure 4.36 and Figure 4.37).

When considering density current thickness, however, the dimensional relationship described by Tsai et al. (1995) is more representative in the case that the initial thickness is 20 m, rather than 40 m, where the ratios of initial thickness to water depth (H_{Di}/H) are 0.14 and 0.29, respectively, and the corresponding ratio based on the relationship $\left(a\left(\frac{V_0}{H^3}\right)^b\right)$ is 0.11 (Table 4.14).

Thus, it is not clear whether the values applied in the iterative analysis are entirely appropriate, but it can be said that in general the results are most likely indicative. The only possibility for a more accurate account of the density current

propagation at the AMDG would be through further field studies, which ideally would focus more heavily on the near-bed conditions. In that, further studies should include deployment of current measuring devices at the presumed area of impact and at intervals radiating away from there. Mounted on those devices should be water sampling and/or turbidity measuring instruments to gather information on the excess density associated with a potential density current. Further, stationary ADCP backscatter records from an ideal location approximately 50 m to 100 m from the estimated area of impact would be of value so long as it is possible to collect data from the complete water column.

4.9.6 Summary of Dispersion During Phase 2

The *Dynamic Collapse* phase of the disposal process has been reasonably well documented in previous field studies (Bokuniewicz et al., 1978; Gordon, 1974; Tsai et al., 1995; Wolanski et al., 1992). Most of the previous studies on the Dynamic Collapse phase have been limited to field sites with water depths less than 50 m, however, with the exception of that from Tsai et al. (1995). One likely reason for this is that it is a complex task to collect field data detailed enough to observe the important features of this phase which, occur within a relatively short temporal scale, but over a large spatial scale. Shallow water sites are, therefore, more feasible to monitor as it is less difficult to deploy instruments at the bed and monitor from a vessel at the sea surface. The implications are that differences in the Dynamic Collapse phase due to water depth are not well documented and, therefore, further study is required at deep water disposal sites, especially as the offshore zone is becoming an increasingly more favourable option for disposal activities (Flaim et al., 2010).

Advances in acoustic technology have opened up new avenues for monitoring the density current associated with the *Dynamic Collapse* phase of the disposal process, which allow for data collection over a larger temporal and spatial scale. The use of echosounders is fairly common in the tracking of disposed dredged material, but relatively few have applied the technology specifically to the tracking of the density current (e.g. Bokuniewicz et al. (1978) and Wolanski et al. (1992)) and even fewer have attempted to use the backscatter data from ADCP records to do the same (e.g. Tsai et al. (1995)).

In the present study, the use the ADCP backscatter data to track potential density currents at the AMDG after disposal was, for the most part, unsuccessful due to the loss of the near-bed acoustic reflections. These problems were, in part, caused by technical issues related to the water depth and the system limitations, which illustrates again the difficulty in monitoring such processes at deep water sites. To attempt to compensate for this lack of direct information, a variety of theoretical calculations and analyses were undertaken, which were supported as much as possible by realistic values taken from the literature and any applicable data that could be harvested from the 'upstream' portions of the surveys.

Dispersion during the *Dynamic Collapse* phase takes place in the form of the density current propagating outward from the area of impact of the disposed material. Based on the average propagation distances for 'sand' and 'mud' density currents, derived iteratively for the potential density current associated with the disposal monitored during Survey 1, dispersion may occur over distances ranging from approximately 200 m to 350 m from the area of impact. The range is based on an initial density current height of either 20 m or 40 m, both of which are sensible according to the ADCP backscatter records from Survey 1, as well as previous studies and the theoretical understanding of the process. However, it should be noted again that most of the previous knowledge on density currents from the disposal of dredged material was developed based on shallow water examples. Further, variations in the local conditions, such as disposal technique, ambient current, dredged material characteristics, and volume discharge are likely to have an important effect on the potential propagation of a density current.

4.10 Passive (Long-Term) Dispersion (Phase 3)

Phase 3 of the disposal process can be defined as the point when dispersion of the disposed material is driven more by the ambient currents and turbulence than by the momentum formed by the dynamics of the disposal operation (Figure 2.1) (McAnally & Adamec, 1987). In the disposal process, the majority of this type of dispersion occurs after completion of Phases 1 and 2 and is therefore also referred to as long-term dispersion (McAnally & Adamec, 1987; Truitt, 1988), but passive dispersion can occur the moment any portion of the material disposed takes on a buoyancy similar to that of the ambient water. For example, entrainment of ambient water around the perimeter of the descending jet during the Convective Descent Phase will result in an increase in buoyancy eventually causing the affected particles to disperse away from the jet in the direction of the ambient current. However, the magnitude of passive dispersion during the first few minutes after disposal is small compared to that driven dynamically by the disposed material itself.

Overall, suspended particles associated with the disposal operations have the potential to be dispersed great distances over a long period of time depending on the ambient currents and the nature of the dredged material. The following sections will consider direction, distance, and time with respect to dispersion of the material disposed at the AMDG during the 4 monitoring surveys.

4.10.1 Disposal Plume Direction

Passive dispersion of disposed dredged material would be expected to occur in the direction of the ambient current, but the boundary between dynamic and passive processes is not always distinct. Turbulent forces may dominate during the transition from dynamic to passive dispersion as the buoyancy of the suspended particles reaches a neutral level. During such processes the suspended particles may be subject to dispersion in a direction that is not necessarily consistent with the ambient current. To characterise the main dispersal directions of the disposed material, interpolated relative turbidity levels (including background levels) along north/south and east/west transects intersecting at the disposal release location, at 15 minute intervals after the disposal time and at a range of depths were plotted in Figure 4.38 through Figure 4.45. The maximum distance of the peak turbidity

level from the disposal release location (dist=0) was approximated as the maximum dispersion distance for each survey. The dispersion patterns often varied between the upper and lower half of the water column, so they were considered separately. Table 4.15 includes the maximum alongshore (Δy) and cross-shore (Δx) dispersion distances approximated from Figure 4.38 through Figure 4.45. Positive and negative symbols indicate north or east dispersion and south or west dispersion, respectively. The magnitude (P) and overall direction (θ) are also shown.

Table 4.15 Approximate alongshore (+/north) and cross-shore (+/east) disposal plume drift distance (m) within the upper (0-70 m) and lower (70-140 m) parts of the water column based on peak relative turbidity along N/S and E/W transects through the disposal location for Surveys 1-4.

Survey no.	0-70 m (Upper water column)						70-140 m (Lower water column)					
	Alongshore		Cross-shore		θ	P	Alongshore		Cross-shore		θ	P
	+/N	Δy (m)	+/E	Δx (m)			+/N	Δy (m)	+/E	Δx (m)		
1	+	420	-	300	NW	516	C	0	+	150	E	150
2	+	250	-	150	NW	292	+	100	-	150	WNW	180
3	+	400	+	700	NE	806	+	500	+	500	NE	707
							-	100			ENE	510
4	+	200	-	150	NW	250	-	250	-	100	SSW	269

C=center (no drift), θ=overall direction, P=dispersion magnitude.

During Survey 1, the maximum dispersion distance was approximated as 500 m northwest and 150 m east in the upper and lower half of the water column, respectively. Dispersion during Survey 2 was approximately 300 m northwest in the upper half of the water column and 180 m west-northwest in the lower half of the water column. Survey 3 data indicates an upper water column dispersion distance of 700 m northeast and that of the lower water column varied between 700 m northeast and 500 east-northeast. The disposal plume drifted approximately 250 m northwest and 100 m southwest, in the upper and lower half of the water column, respectively, during Survey 4. Figure 4.46 summarises the findings described above.

The approximated dispersion distances are representative of only of the area surveyed and thus it is possible that the derived values may underestimate maximum dispersion, though the direction is likely to at least be indicative.

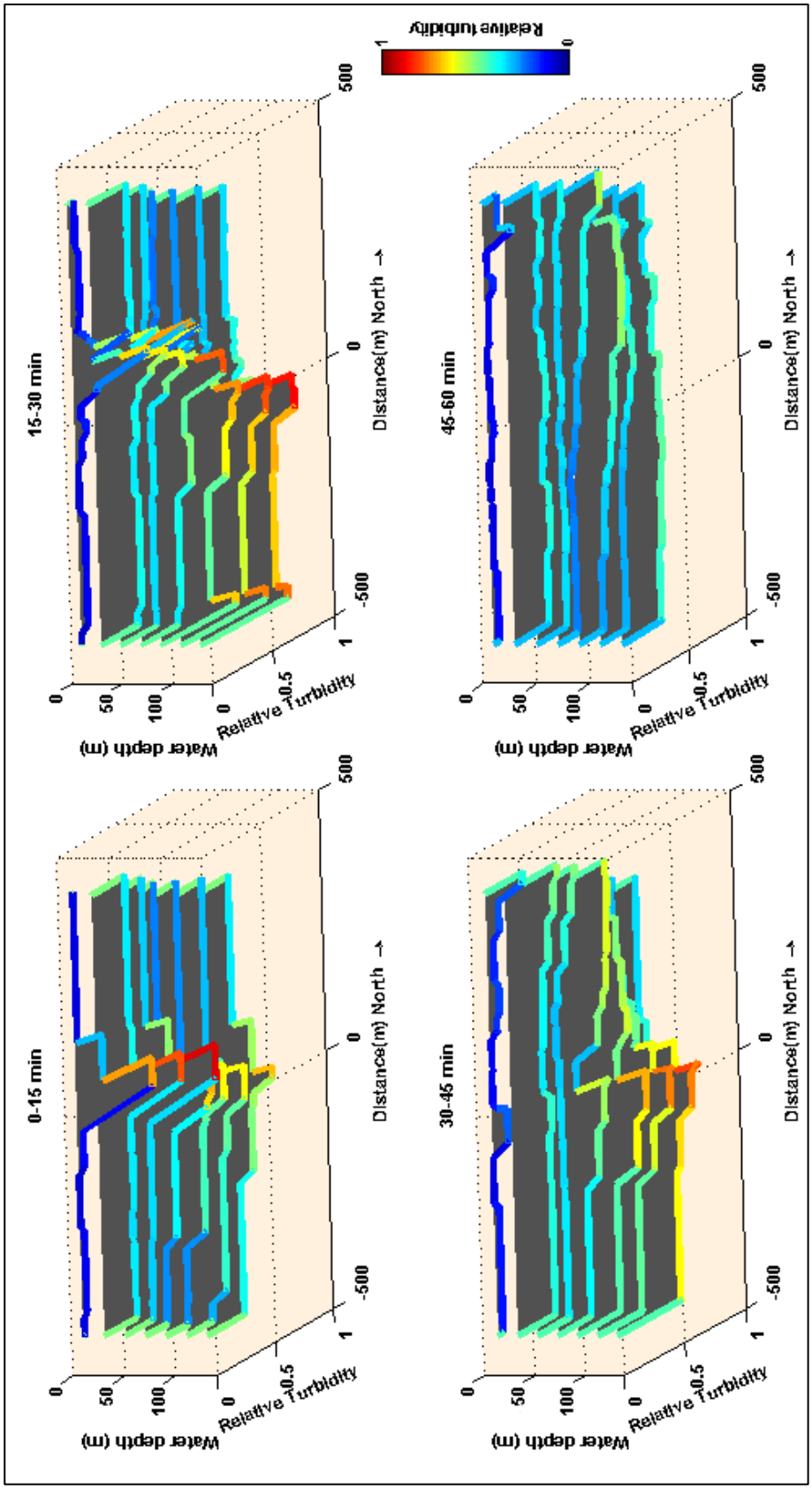

Figure 4.38 Temporal (dt=15 min.) evolution of the Survey 1 disposal plume along a north/south transect through the disposal release location (Dist.N.=0) at a range of water depths. Relative turbidity is including background level.

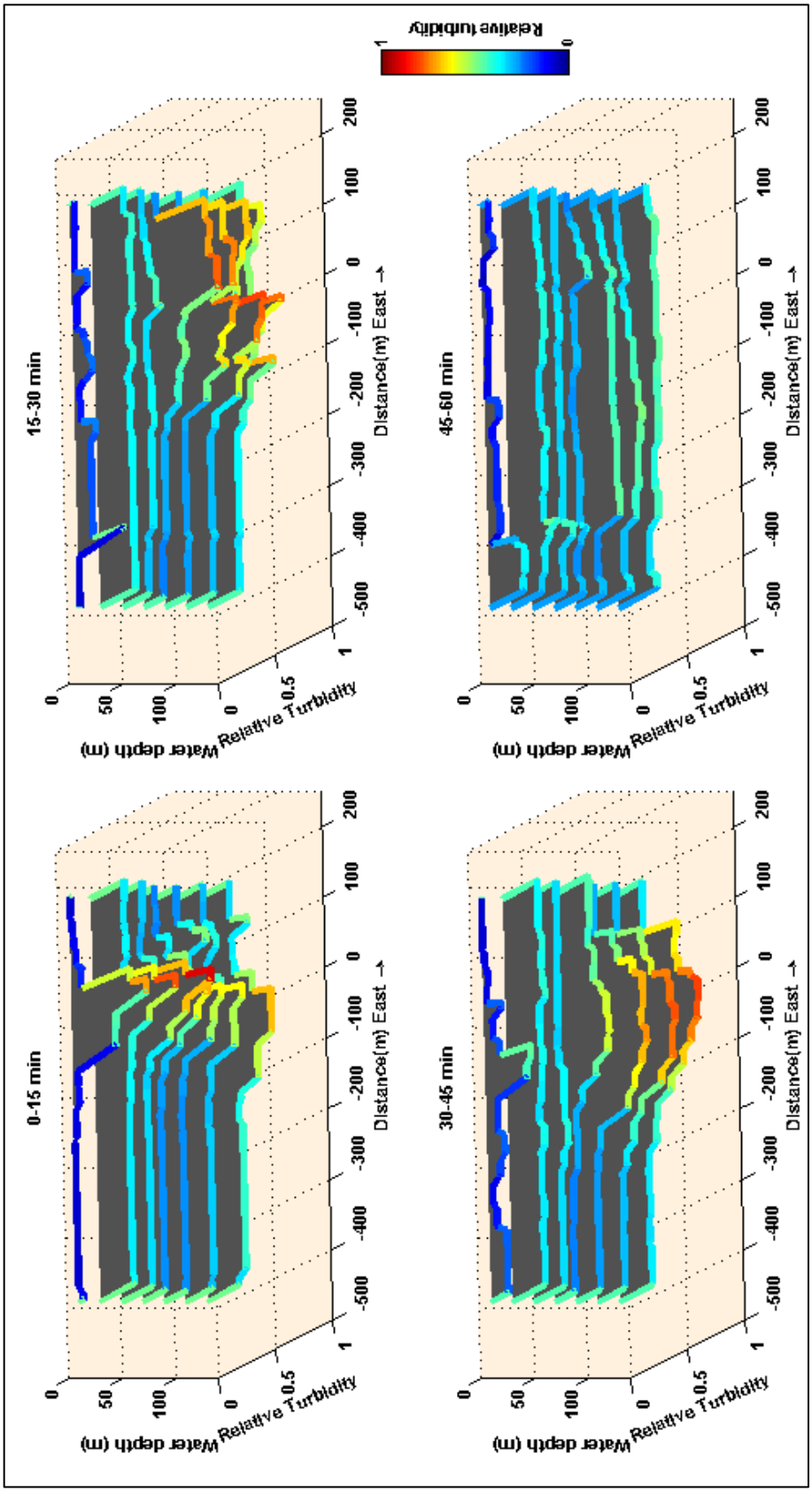

Figure 4.39 Temporal (dt=15 min.) evolution of the Survey 1 disposal plume along a east/west transect through the disposal release location (Dist.E.=0) at a range of water depths. Relative turbidity is including background level.

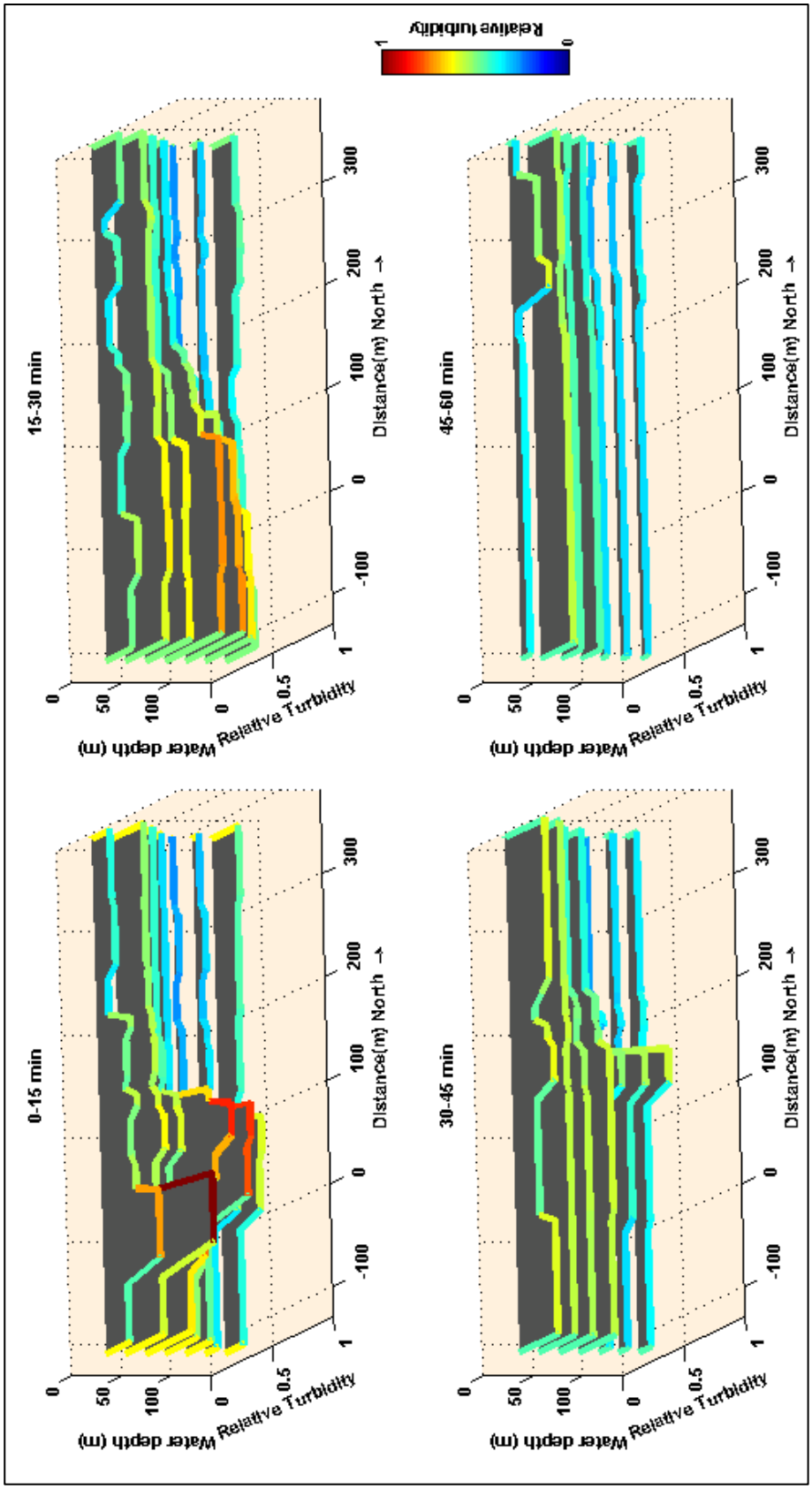

Figure 4.40 Temporal (dt=15 min.) evolution of the Survey 2 disposal plume along a north/south transect through the disposal release location (Dist.N.=0) at a range of water depths. Relative turbidity is including background level.

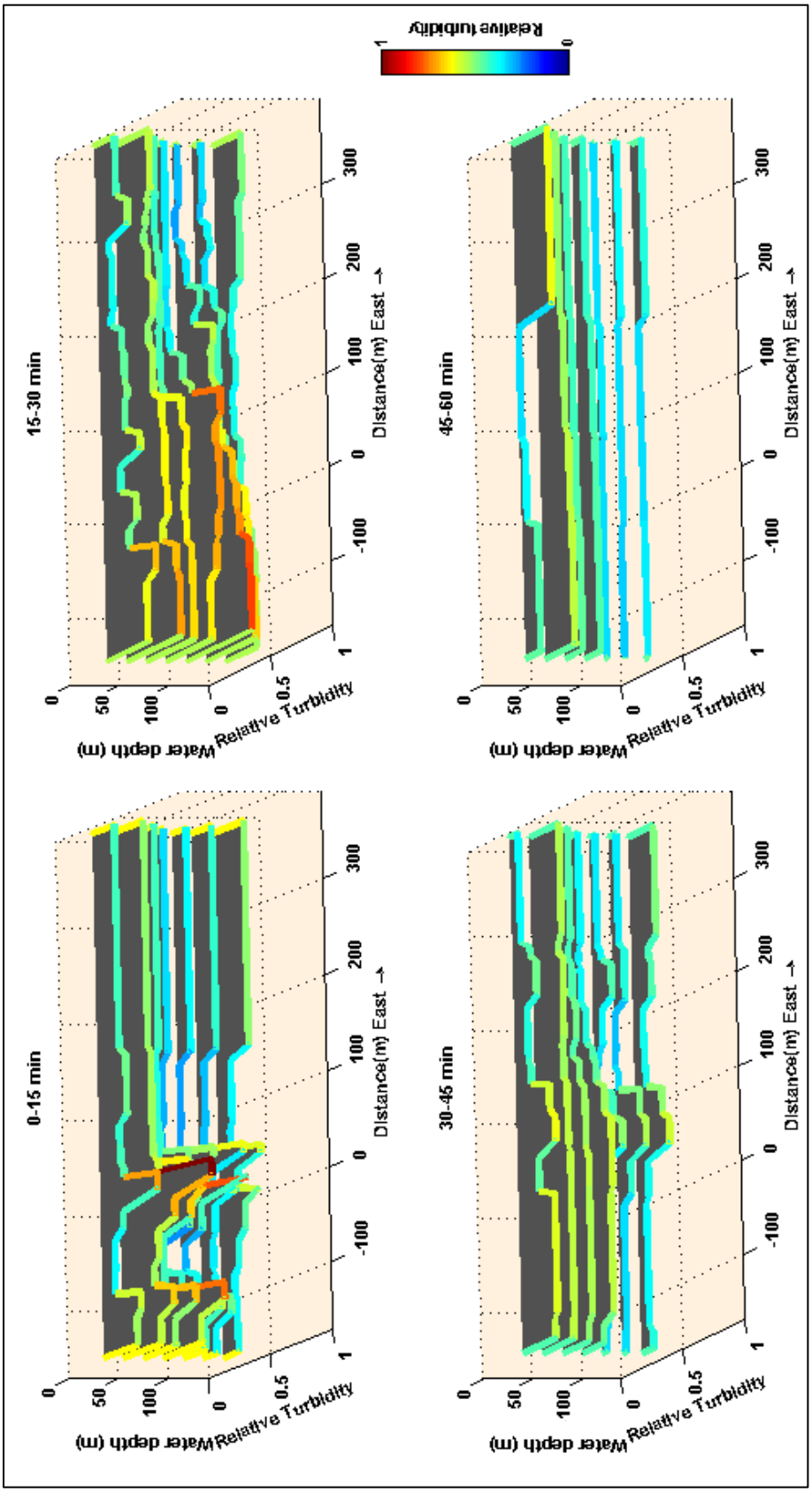

Figure 4.41 Temporal (dt=15 min.) evolution of the Survey 2 disposal plume along a east/west transect through the disposal release location (Dist.E.=0) at a range of water depths. Relative turbidity is including background level.

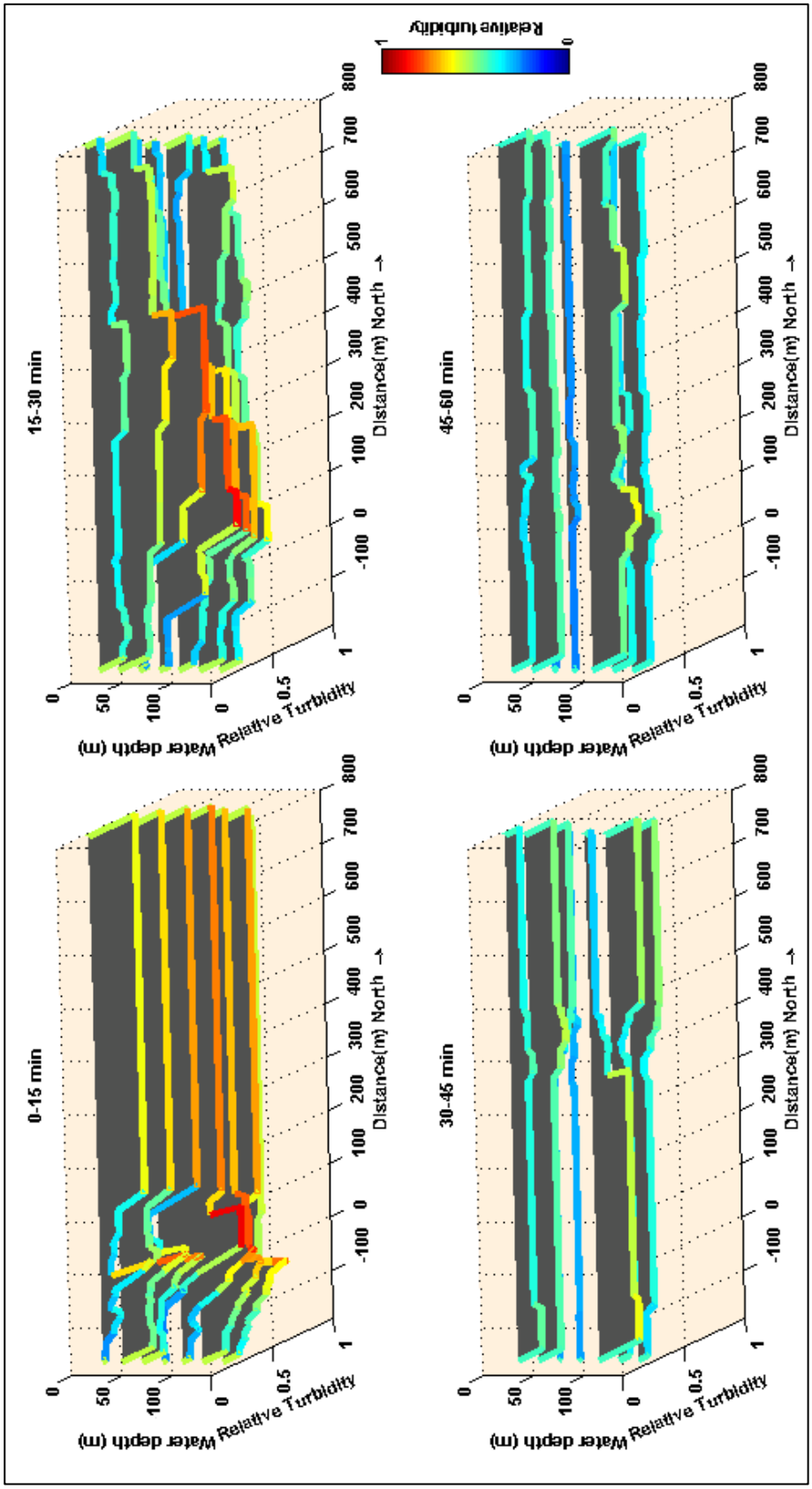

Figure 4.42 Temporal (dt=15 min.) evolution of the Survey 3 disposal plume along a north/south transect through the disposal release location (Dist.N.=0) at a range of water depths. Relative turbidity is including background level.

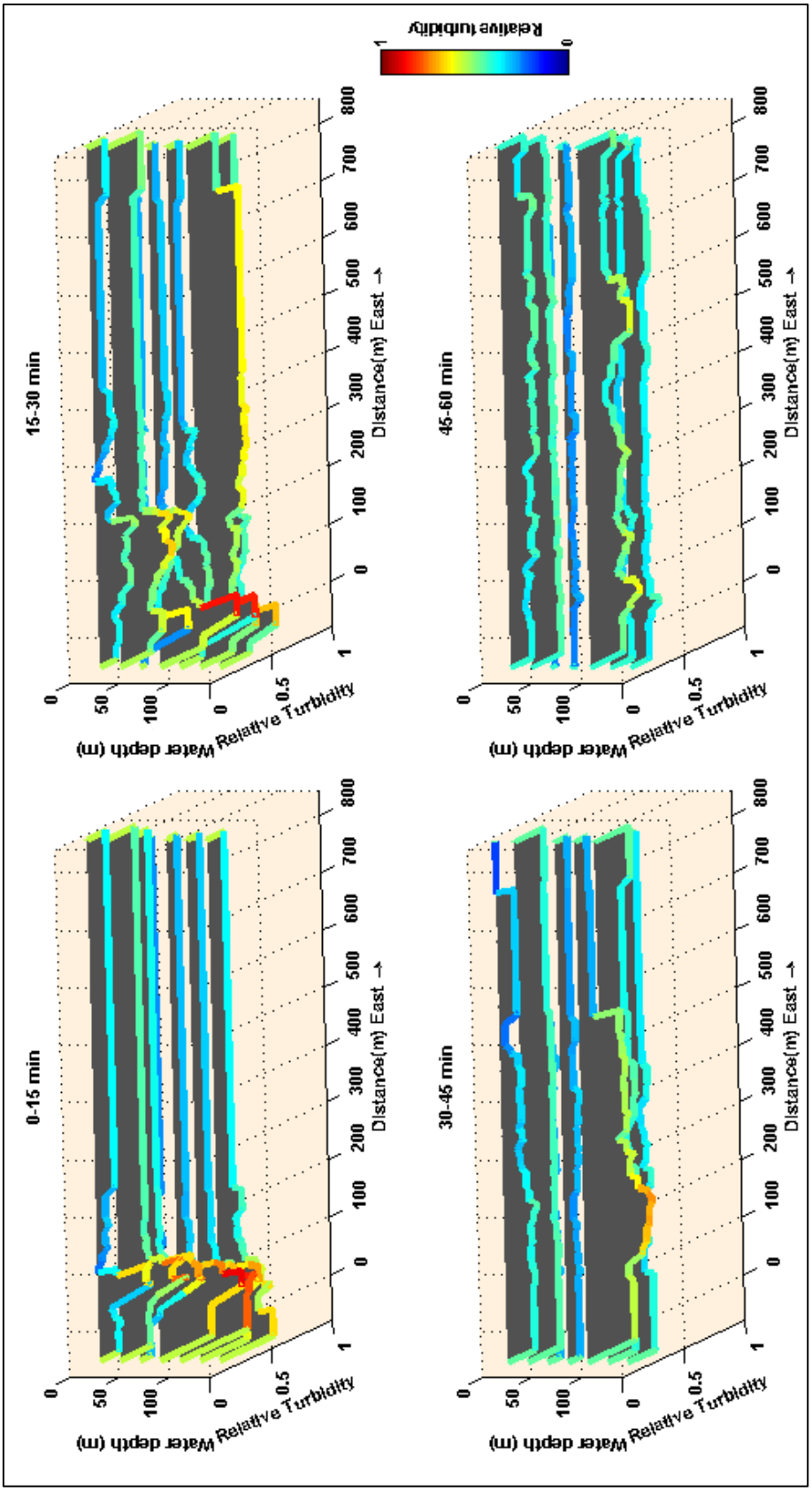

Figure 4.43 Temporal (dt=15 min.) evolution of the Survey 3 disposal plume along a east/west transect through the disposal release location (Dist.E.=0) at a range of water depths. Relative turbidity is including background level.

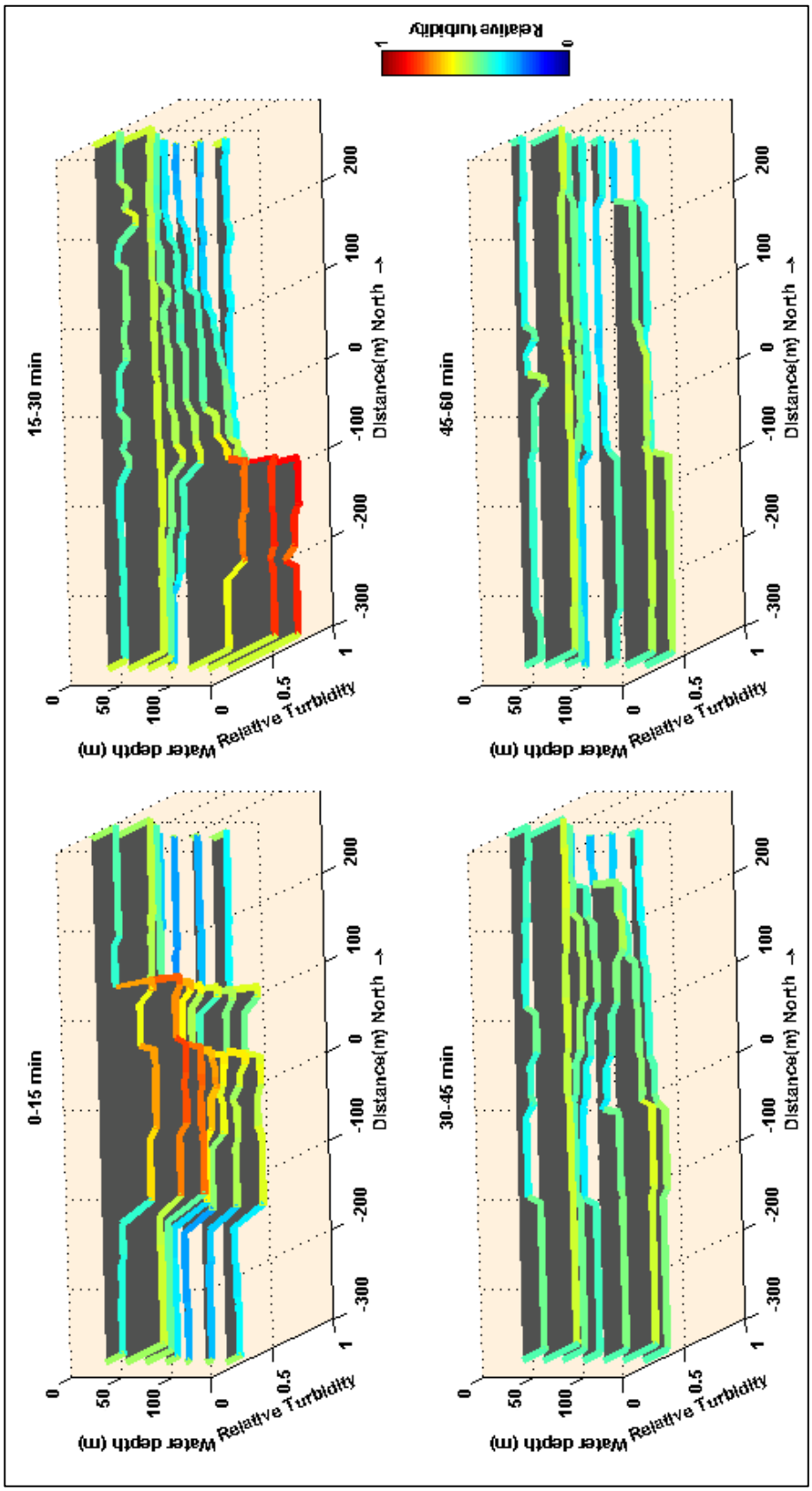

Figure 4.44 Temporal (dt=15 min.) evolution of the Survey 4 disposal plume along a north/south transect through the disposal release location (Dist.N.=0) at a range of water depths. Relative turbidity is including background level.

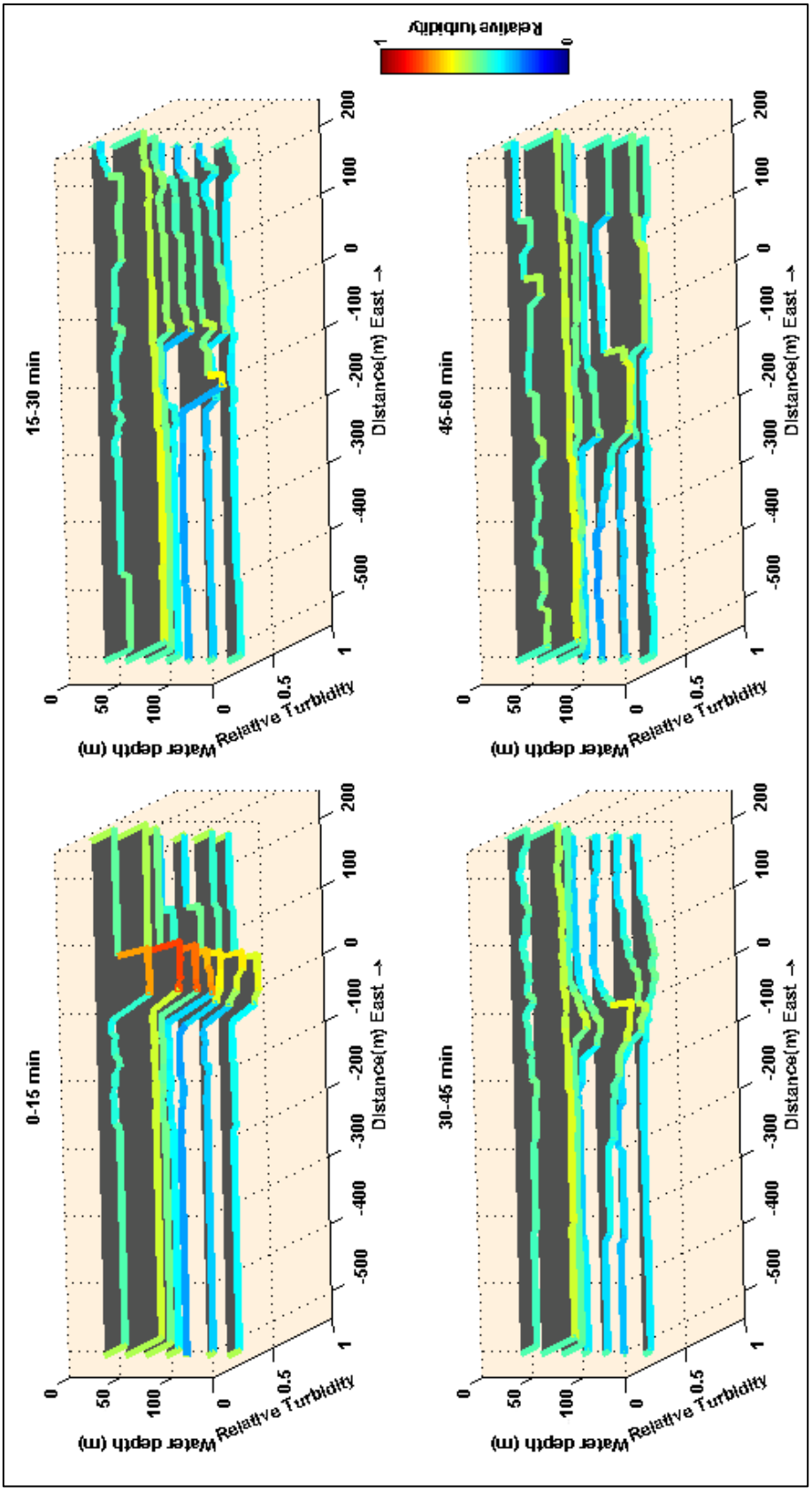

Figure 4.45 Temporal (dt=15 min.) evolution of the Survey 4 disposal plume along a east/west transect through the disposal release location (Dist.E.=0) at a range of water depths. Relative turbidity is including background level.

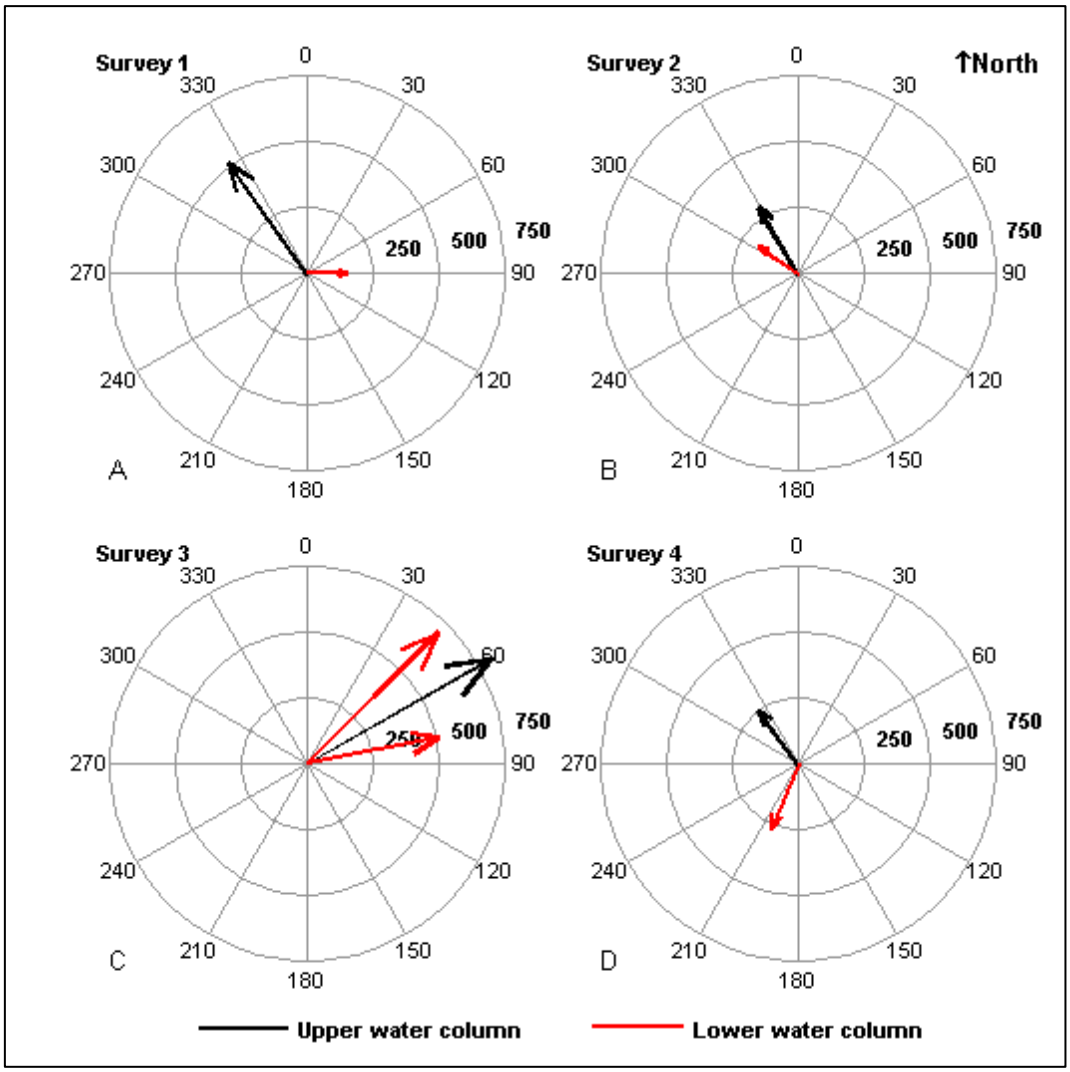

Figure 4.46 Rose plots of disposal plume drift in the upper half of the water column (black arrow) and lower half of the water column (red arrow) for Surveys 1-4. Tabulated data shown in Table 4.15

4.10.2 Dispersion Magnitude

To gain a better understanding on the magnitude of dispersion of the dredged material at the AMDG, relative turbidity data above the background levels, from all 4 surveys was grouped based on time after disposal and then further grouped by distance from the centre of the site. Table 4.16 and Figure 4.47 highlight the time and distance grouped data.

As the background level turbidity has been removed, the assumption has been made that the data included in Table 4.16 and Figure 4.47 represent the approximate range of turbidity associated with the disposal plume. The maximum turbidity levels ranged between 0.63 (0-15 min & 0-100 m) and 0.08 (15-30 min & 700-1500 m). The mean turbidity ranged from 0.26 (0-15 min & 0-100 m) to

0.02 (15-30 min & 700-1500 m). The variance (*VAR*) was highest 15-30 min after disposal and between 100 m and 200 m from the centre at 0.029. The lowest variance occurred 15-30 min after disposal between 700 m and 1500 m from the centre at <0.001. The respective range of standard deviations was 0.17 to 0.02.

Table 4.16 Details of disposal plume evolution based on relative turbidity data above background from all 4 surveys.

Time after disposal (min)	Statistic	Distance from Centre (m)						
		≤100	**≤200**	**≤300**	**≤400**	**≤500**	**≤700**	**≤1500**
0-15	Max	0.630	0.520	0.580	0.580	0.510	0.120	-
	Mean	0.260	0.130	0.090	0.120	0.050	0.030	-
	VAR	0.020	0.013	0.012	0.015	0.006	0.001	-
	Stdev.	0.142	0.113	0.109	0.124	0.074	0.032	-
15-30	Max	0.550	0.620	0.560	0.620	0.480	0.240	0.080
	Mean	0.190	0.200	0.160	0.150	0.090	0.030	0.020
	VAR	0.018	0.029	0.021	0.024	0.010	0.001	0.000
	Stdev.	0.135	0.169	0.146	0.155	0.100	0.036	0.020
30-45	Max	0.300	0.390	0.330	0.400	0.340	0.370	0.260
	Mean	0.120	0.140	0.090	0.090	0.080	0.060	0.060
	VAR	0.006	0.010	0.005	0.006	0.006	0.004	0.002
	Stdev.	0.076	0.098	0.071	0.076	0.079	0.067	0.049
45-60	Max	0.340	0.400	0.440	0.440	0.330	0.380	0.330
	Mean	0.110	0.120	0.080	0.060	0.060	0.060	0.040
	VAR	0.009	0.009	0.008	0.005	0.003	0.003	0.002
	Stdev.	0.095	0.093	0.092	0.068	0.053	0.057	0.043

- no transects recorded

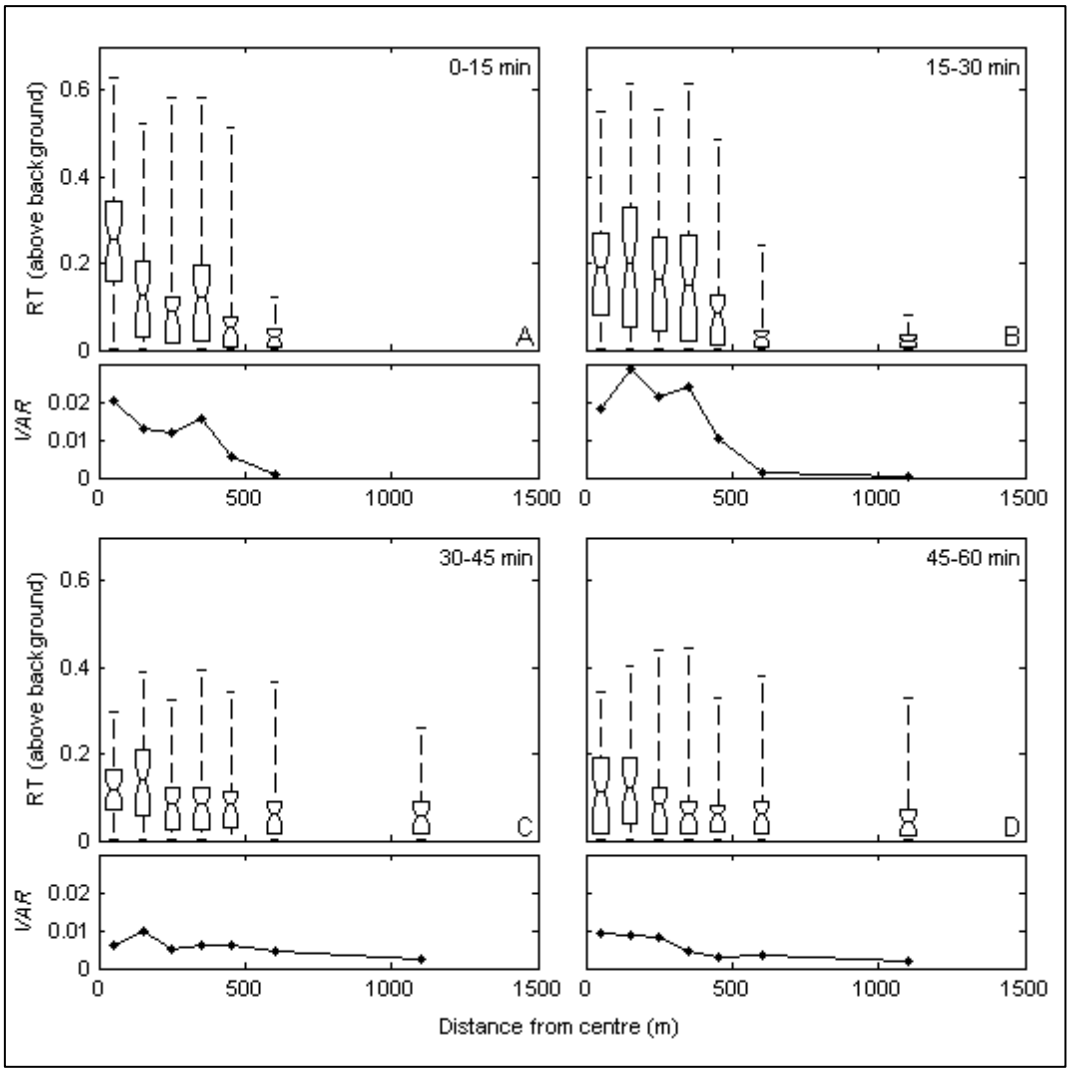

Figure 4.47 Relative turbidity above background level for Surveys 1-4 at a range of distances from the centre of the AMDG at 15 minute time intervals after the release of dredged material. Lower plots show the variance of the data within each distance interval.

4.10.3 Dispersion Characteristics

Patterns in the rate of dispersion of the disposed material, with respect to both time and space, can be identified by the following ratios

$$D_{Ft} = {RT_{t1}}/{RT_{t4}} \qquad \text{Equation 4-27}$$

$$D_{Fs} = {RT_{s1}}/{RT_{s5}} \qquad \text{Equation 4-28}$$

where D_{Ft} and D_{Fs} are dispersion factors relative to time and space, respectively; RT_{t1} and RT_{s1} are the mean relative turbidity at time=1 (0-15 min) and space=1 (0-100 m); and RT_{t4} and RT_{s5} are the mean relative turbidity at time=4 (45-60 min) and space=5 (400-500 m). The same method was applied to the

standard deviation of each value to determine a spread factor (S_F) which represents the change in the range of data relative to space and time.

Figure 4.48 is a plot of the time and space dispersion factors (D_{Ft} and D_{Fs}). Near the disposal location and within a short period after disposal, the values for D_F were 5.2 and 2.4, respectively. In both instances, S_F was high at 1.9 and 1.5, respectively. Between 100 and 300 m from the disposal location and from 15 to 45 min after the disposal, the D_F values decreased to 2.1 and 1.5 in the time domain and to 1.08 and 1.13 in the space domain. The values for S_F were small both in time and space, ranging from 0.96 to 1.3. In the last time bin, 45 to 60 min after disposal as well as between 300 and 400 m from the disposal location, the D_F values increased to approximately 2 for both time and space. The corresponding S_F values also increased to approximately 2 in both time and space. In the last space bin (400 m to 500 m from centre), D_F decreased to 0.83 and S_F decreased to 1.4. Based on the trends identified in the space domain, an additional time bin (60-75 min after disposal) was plotted in Figure 4.48 using projected values of D_F and S_F to complete the conceptual picture of dispersion characteristics.

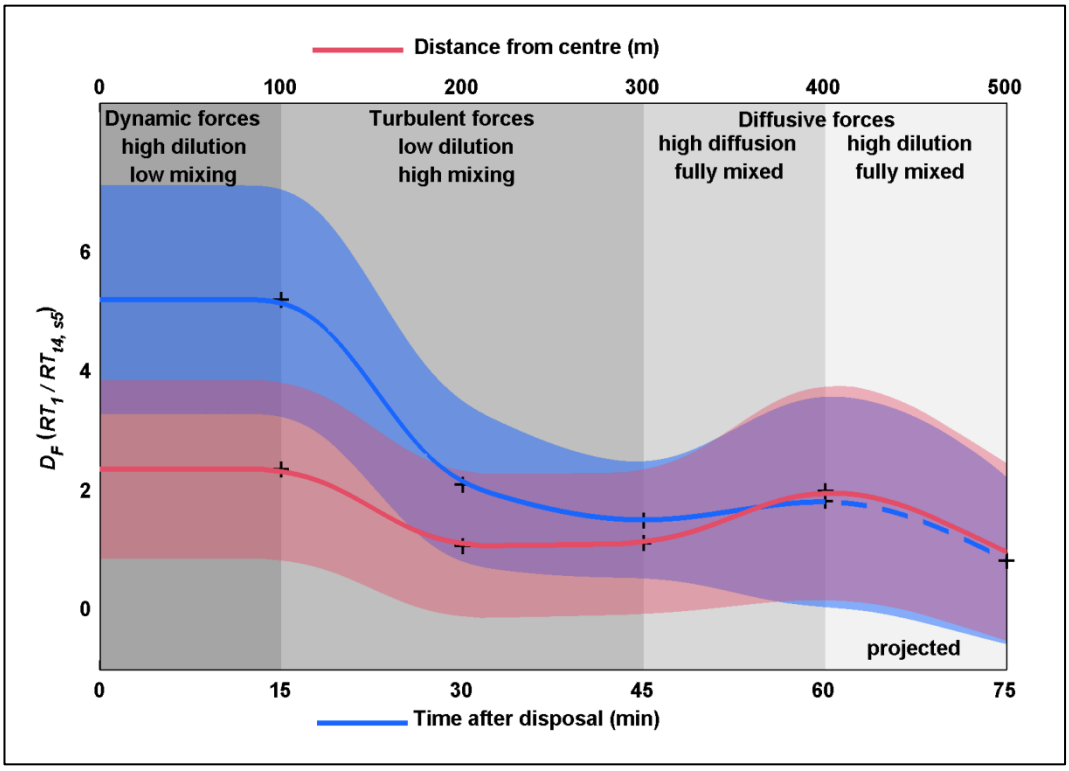

Figure 4.48 Dispersion factor (DF) curves relative to time (blue) and space (red) showing a decrease until diffusive forces exceed turbulent forces, which results in a slight increase before it drops off to zero. Corresponding spread factors (SF) are also shown for each parameter (shaded area in corresponding colour, 1 Stdev from each DF value). Projected DF and SF values for the period of 60-75 min are represented by the dashed blue line and the corresponding light blue shaded area.

4.10.4 Discussion

Environmental Conditions

Movement of the drifters deployed during Survey 1 was toward the northwest, which was consistent with the ADCP data recorded during the survey, although neither technique captured the ambient current direction in the bottom half of the water column (Figure 4.18a and Figure 4.21a&b). Directional analysis of the plume corresponding to Survey 1 indicates that in the upper water column, dispersion direction was also directed toward the northwest (Figure 4.46a). In the lower water column, dispersion was minimal, but appeared to be directed eastward. On the day of Survey 1, wind was from the southeast, which is generally consistent with the north-westerly directed dispersion in the upper half of the water column. Although Ekman dynamics dictates that at the lower limit of the wind-affected layer, dispersion would be directed toward the west, this can only occur if the wind direction had persisted long enough for a fully developed Ekman spiral to be established.

Survey 2 drifters indicated that the disposal plume would be likely to drift northeast from the disposal location and possibly at a significant speed (~20 cm/s) (Figure 4.18b). However, ADCP records showed a northwest directed current in the period after the disposal and directional analysis showed a predominant northwest drift of the plume in both the upper and lower water column (Figure 4.21b and Figure 4.46b). Inconsistency between the drifter direction prior to the disposal and the current measured with the ADCP during the survey suggests that wind was not an important forcing mechanism as the direction would not have varied so greatly over the span of 2 hours. This is somewhat surprising as the wind was the strongest during Survey 2 out of the 4 surveys, but it is possible that even though the wind was strong, it was not persistent and therefore did not result in strongly developed wind-driven currents.

Higher frequency tidal variations seem to be a more plausible explanation for the rotation in the ambient current after the initial drifter deployment especially as the survey was mainly conducted during a peak tidal stage (Figure 4.16c). Neither the upper or lower water column demonstrated the expected strong dispersion that the

drifters indicated. The maximum measured dispersion distance was approximately 300 m. The similarity in the dispersion direction of the upper and lower water column may possibly be attributable to the depth of the mixed layer which was at its deepest on the day of Survey 2 compared to the other 3 surveys (Figure 4.17b). If so, the nearly fully-mixed conditions may have resulted in one predominant dispersion direction throughout the water column.

The paths of drifters deployed prior to Survey 3 were, again, inconsistent with the ambient current observed during the survey itself. The drifters indicated a weak southward directed ambient current in the upper water column, but ADCP records showed a strong northeast directed upper water column current (Figure 4.18c and Figure 4.22a&b). The upper water column plume did appear to disperse a significant distance towards the northeast (Figure 4.46c), but lower water column dispersion was not in the expected direction of southwest (Figure 4.22a&b). Rather, apparent dispersion both north and south, combined with cross-shore east dispersion, resulted in what appeared to be variable northeast dispersion in the lower water column (Figure 4.46c).

In this case however, the directional analysis may have been distorted by a narrow region of focused dispersion which was observed in most of the late-survey ADCP backscatter transects recorded during Survey 3; some of them recorded at significant distances from the disposal location (e.g. Figure 4.49). On the day of Survey 3, the depth of the mixed layer had risen to approximately 30 m below the surface, which resulted in a distinct pycnocline at the same depth (Figure 4.17c). However, the focused dispersion was located significantly deeper than that (80-100 m below the surface). There were additional density transitions observed at similar depths to that of the narrow dispersive layer, but they were less distinct than the pycnocline at 30 m and were most likely not strong enough to initiate the focused dispersion.

ADCP current records from Survey 3, however, did show characteristics that may explain the source of the narrow dispersive layer. In the cross-shore direction, currents were directed essentially eastward in the surface-most 30-40 m (Figure 4.22a). Across the same depths, the alongshore currents were directed northwards (Figure 4.22b). This area corresponds to the depth of the mixed layer observed in

the density profile recorded on the same day (Figure 4.17c) and also by the higher relative turbidity zone near the surface in Figure 4.49, which is likely due to the presence of phytoplankton. The northeast current easily explains the northeast directed dispersion in the upper water column (Figure 4.46c).

Starting at 40 m below the surface to at least 128 m, the cross-shore current was directed west (Figure 4.22a). In the alongshore direction however, such a simple two-layer system was not observed (Figure 4.22b). Instead, in addition to the north-directed surface mixed layer, there was a band of southerly currents from 50 m to 60 m, a secondary band of northerly-directed currents from 60 m to 80 m, and finally a secondary band of southerly-directed currents from 80 m to at least 100 m. It appears that the dispersive layer was associated with the secondary southerly-directed band of currents. Figure 4.50 shows a conceptual diagram of this system and the corresponding relative turbidity based on the transect shown in Figure 4.49.

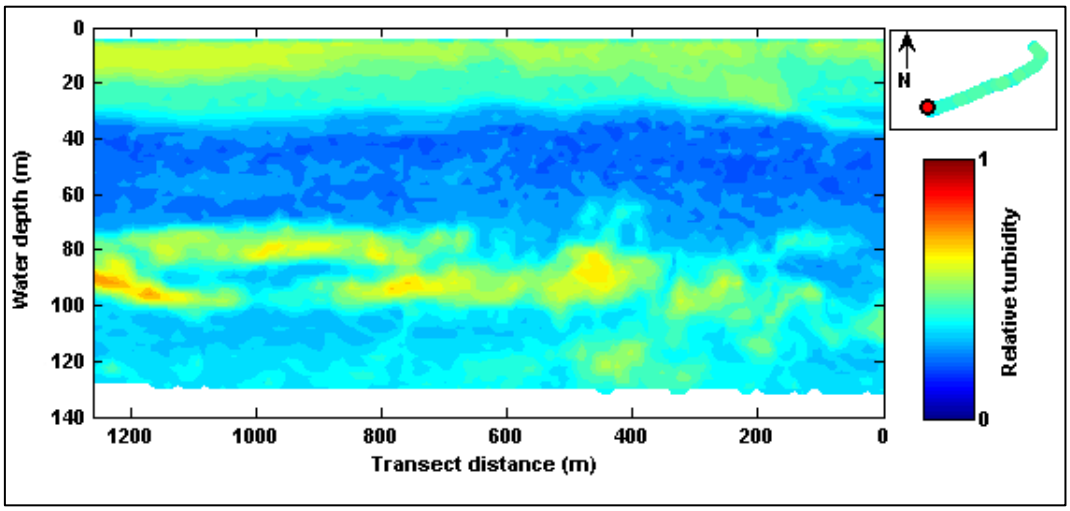

Figure 4.49 Relative turbidity (including background levels) recorded approximately 1 hour after disposal during Survey 3. Inset: location of transect relative to the disposal location (red marker).

Although the position of the secondary southerly directed current layer between 80 m and 100 m below the surface suggests that it may be the mechanism behind the dispersive layer at the same depth, there is some question whether this is a valid theory. The transect shown in Figure 4.49 was recorded starting from northeast of the disposal location and moving towards it in a south-westerly direction (see inset of Figure 4.49). The relative turbidity in the layer appeared to increase as the vessel approached the disposal location, which indicates that

dispersion within the layer was directed from the disposal location towards the northeast. This pattern is consistent with the directional analysis (Figure 4.46c), but not consistent with the ADCP current data which showed that from 80 m to 100 m, the currents were directed west in the cross-shore direction and south in the alongshore direction. A clear mechanism for this feature is not obvious from the available data, but it seems plausible that interfacial instabilities caused by the shearing of the stratified velocity layers may have driven the enhanced dispersion (Strang & Fernando, 2001). It is likely, though, that the dispersion within other regions of the lower water column was at a much smaller scale and probably more consistent with the current structure shown in Figure 4.50.

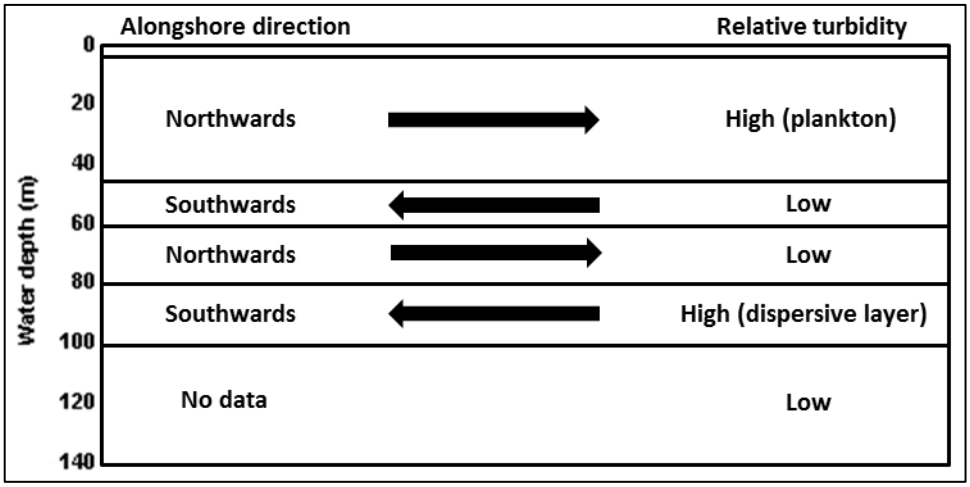

Figure 4.50 Conceptual diagram of alongshore current direction during Survey 3 and approximate relative turbidity levels 60 min after disposal.

Fortunately, the environmental indicators observed during Survey 4 were more consistent with the observed dispersion. Drifters deployed prior to the survey indicated a weak westerly directed current (Figure 4.18d). During the Survey, the ADCP records of the upper water column indicated weak westerly directed cross-shore currents and weak variable alongshore currents (Figure 4.22c&d). These patterns were consistent with the directional analysis which showed dispersion to distance of approximately 250 m directed towards the northwest in the upper water column and towards the southwest in the lower water column.

Spatial and Temporal Evolution

Observations from comparisons of relative turbidity (RT) above background levels showed an evolution of the disposal plume with respect to time and space

(Figure 4.47). Maximum and mean RT levels underwent a general decrease by a factor of 2 to 4 at each distance from the first 30 min to the second 30 min which indicates dilution of the plume with time. Finer scale trends can be more easily identified by examination of the maximum RT levels. The change in slope of a best-fit line through the max RT level of each distance bin and at each 15 min interval shows a general movement of the plume away from the centre of the site as a transition from a negative slope to a positive slope with respect to time (Figure 4.51). The same trend is not evident in changes in the mean RT levels, however mean levels do illustrate the underlying trend of an overall dilution of the plume with time (note the change in the y-axis range) (Figure 4.52).

Variance of spread of the data was generally highest between 15 min and 30 min after disposal; within that time period, variance was highest between approximately 200 m and 400 m from the centre of the site (Figure 4.47). Before and after this period, the ranges (variance) of RT levels at each distance from the centre are significantly lower. This hints at another pattern not specifically related to the changes in the relative turbidity, but to the forces that drive the changes in turbidity during the disposal process and will be discussed further in the follow section.

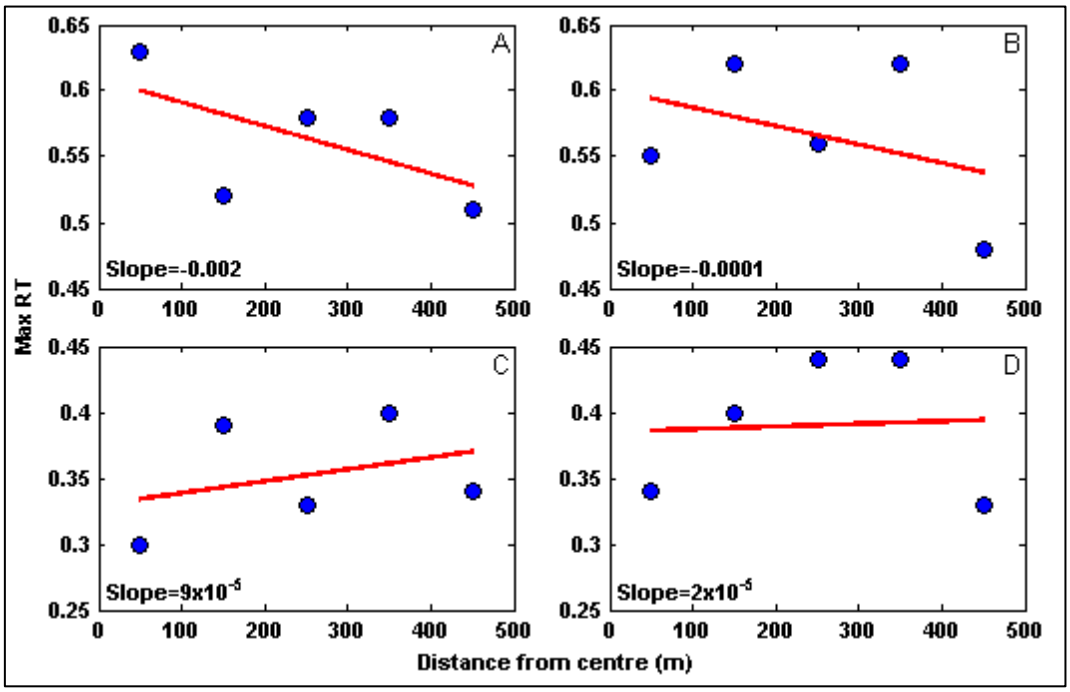

Figure 4.51 Slope of best-fit linear regression of maximum relative turbidity above background relative to distance from centre a) 0-15 min, b) 15-30 min, c) 30-45 min, and d) 45-60 min after disposal.

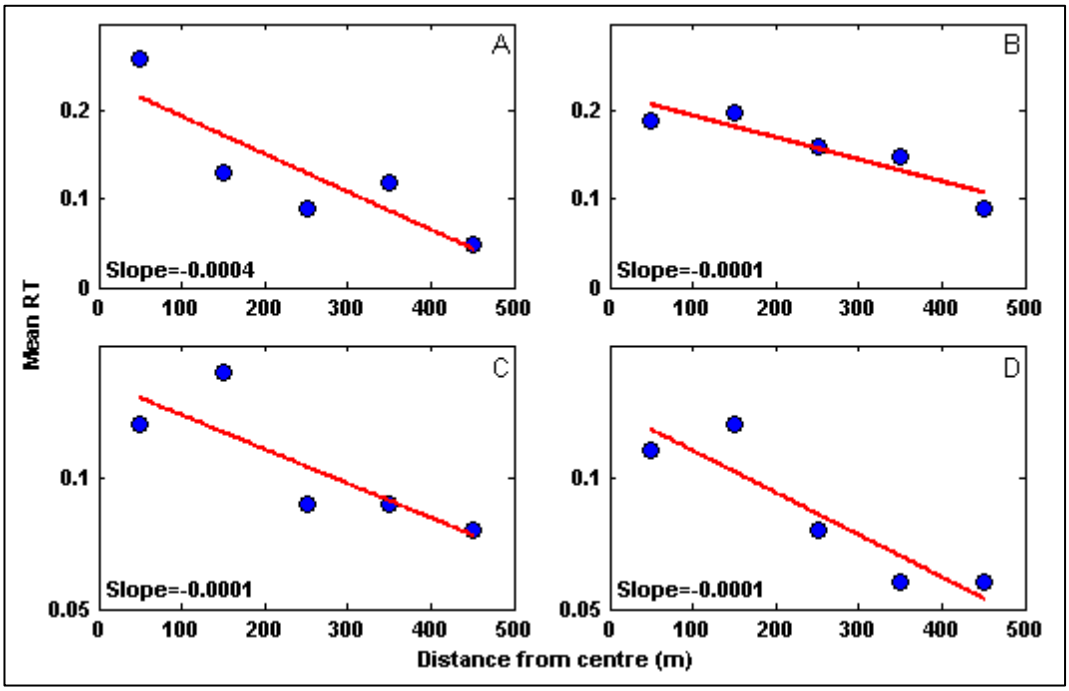

Figure 4.52 Slope of best-fit linear regression of mean relative turbidity above background relative to distance from centre a) 0-15 min, b) 15-30 min, c) 30-45 min, and d) 45-60 min after disposal.

Dispersive Forces

Figure 4.48 illustrated the change in dispersion factors (D_F) and spread factors (S_F) with respect to time and space. Three distinct zones along the time and space domains are evident (Figure 4.53). Zone 1 occurs close to the disposal location, both in time and space and is characterised by high D_F values and large S_F values (i.e. a large change in RT levels and data range through time near the centre and in space soon after the disposal). Zone 2 generally occurs between 15 min and 45 min after disposal and approximately 200 m to 400 m from the centre of the site. In this zone, the mean RT levels were relatively constant through time and space which is shown as low D_F and S_F. Zone 3, beyond approximately 400 m from the disposal location and starting around 1 hour after release, is characterised by a higher D_F and S_F which indicates similar processes to that of zone 1, but at a smaller scale.

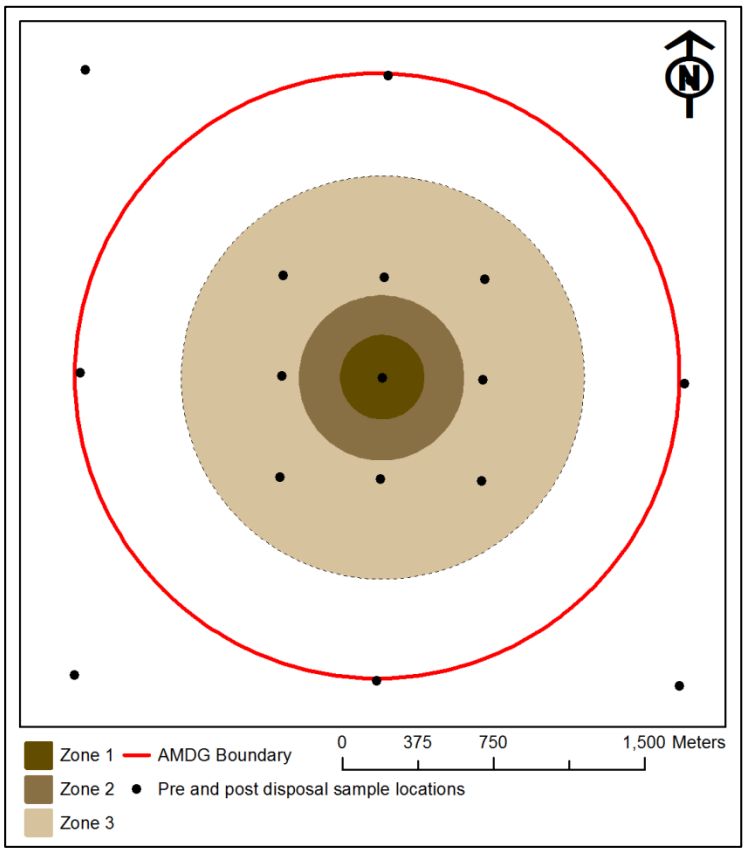

Figure 4.53 Plan view of the spatial extent of the 3 main dispersion zones at the AMDG (see Figure 4.48 for a description of zonal characteristics).

The distinct change in the dispersion characteristics between Zone 1 and Zone 2, both in time and space, suggests that there are different underlying dispersive forcing mechanisms. The forcing mechanism controlling the area near the disposal location in the period immediately following the disposal is the dynamic force of the disposed material itself (Figure 4.54). The dynamic force has already been discussed in depth in previous sections as Phase 1 (*Convective Descent*) of the disposal process, but in review, is responsible for high dilution as the majority of the material descends rapidly to the sea floor (i.e. high D_F) and a large change in the range of turbidity (i.e. high S_F). Phase 2 of the disposal process (*Dynamic Collapse*) is most likely also contained within this zone as the significant water depth, in this case, precludes a density current from propagating very far from the centre and over a long period after impact with the sea floor.

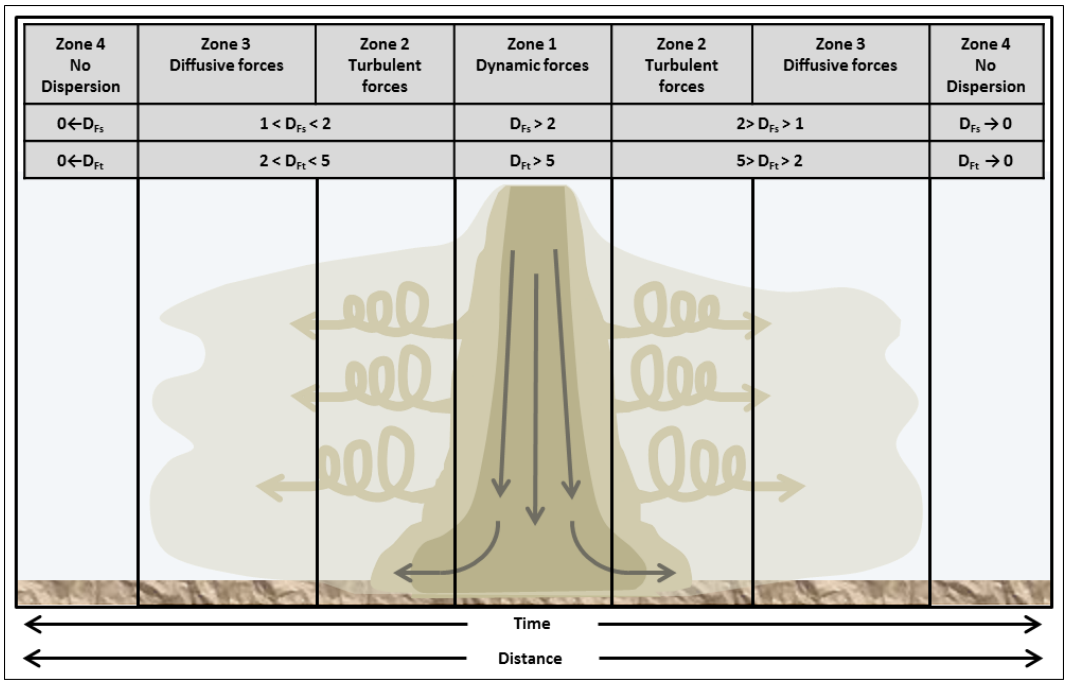

Figure 4.54 Profile view of the spatial extent of the 3 main dispersion zones (and a theoretical 'Zone 4') at the AMDG (see Figure 4.48 for a description of zonal characteristics). The approximate non-dimensional dispersion factor values (D_F), with respect to space and time, are also shown in the associated zone.

Zone 2 would most likely fall into the category of Phase 3 (*Passive Dispersion*), but it is not wholly characteristic of the passive dispersion described in the literature and that is probably because it serves as more of a transition between the dynamic and passive stages. At intermediate distances and periods from the disposal, there was low dilution (low D_F) and little change in the range of RT levels (low S_F). Completion of the dynamic phases of the disposal process suggests that most of the suspended material still present in the water column several hundred metres from the disposal location, and more than 15 min after disposal, is of the finer type and is likely to be subject to the force of the ambient current. However, if suspended material dispersed away with the ambient current, high D_F and S_F values would be expected as the RT levels would decrease over time and space, but this is not the case for Zone 2. Instead, it appears that the important force prevented a decrease in RT levels, as well as a change in the range of RT levels. Turbulence brought about by the interaction of the perimeter of the dynamic jet with the ambient water may be the possible source of this force. Such an interaction could set the ambient water in motion, which may take some time to return to a natural state. Turbulence could potentially disperse the suspended particles in circular pathways such that the material does not actually get

transported in one particular direction (Figure 4.54). This process would manifest as a low change in RT levels (low D_F) and a low change in the range of RT levels (low S_F).

Turbulence, as such, is not commonly discussed in the literature as an important dispersive force during the disposal process because typically discussions proceed directly onto dynamic collapse following convective descent. The areas of the water column not affected by the density current, usually at least the upper half of the water column, are mostly disregarded because they are thought not to have a large quantity of suspended material (typically cited as 1-5 % of the disposed load (e.g. Bokuniewicz and Gordon (1980), Gordon (1974), and Truitt (1988)). However, references to the water surrounding the jet of the Convective Descent phase being 'set in motion' have been made (Bokuniewicz et al., 1978).

After the energy available for the turbulent motions is spent, the ambient water would be expected to return to its usual direction and speed, thereby entering Zone 3 of the dispersive forces. As described above, suspended particles under the influence of a force from a uniform direction would result in a residual transport direction and RT levels would again change over time and in space (i.e. high D_F and S_F). Although, due to the early deposition of the majority of the material disposed, D_F and S_F did not increase to the levels observed in Zone 1 of the disposal process. The important force in Zone 3 can be more accurately described as diffusive because the suspended material would be well-mixed after the turbulent mixing of Zone 2 and would be dispersed more homogenously throughout the water column. Diffusive forces would result in a consistent decrease in RT levels and, therefore, also a decrease in the range. After RT returns to background levels, there would be no further change in the levels and range, thus, resulting in a decrease in D_F and S_F in the final domains of Zone 3 (Figure 4.48). Accordingly, as D_F values approach zero, it can be inferred that dispersion is insignificant because there are fewer and fewer suspended particles left in the water column to undergo dispersion. Based on this notion, a theoretical 'Zone 4', representing the area where dispersion would not be expected can be hypothesized (Figure 4.54).

4.10.5 Summary of Dispersion After Phase 3

The magnitude of dispersion at the end of Phase 3 (*Passive Dispersion*) was estimated using directional analysis of alongshore and cross-shore transects with the disposal location as their intercept. Using those measures, maximum dispersion was approximately 500 m, 300 m, 800 m, and 250 m for the disposals corresponding to Surveys 1-4, respectively. Dispersion was always greater in the upper water column compared to the lower water column. The values determined were based only on the alongshore and cross-shore transects analysed, so it is possible that the dispersion distance may have been somewhat larger in some cases. In Survey 3, for example, the narrow dispersion layer shown in Figure 4.49 was recorded some 1000 m from the disposal location, whereas the directional analysis determined maximum dispersion to be approximately 800 m. This was due to the fact that the dispersive layer was directed toward the northeast mainly and the dispersion distance along the flanks, that which would have been picked up in the alongshore and cross-shore transects in the analyses, was most likely lower than that at its leading edge.

Additionally, due to the large component of clay in the disposed material it is probable that material was dispersed far greater distances than that observed in the time and space of the surveys, however, the concentrations of such far-reaching material would have been so low that it would not be distinguishable from the ambient turbidity level of the surrounding waters. Based on that, it can be said that Phase 3 is not technically complete until all particles have deposited on the seabed. For the intents and purposes of monitoring dispersion after disposal of material at the AMDG, however, a more realistic endpoint is the distance and time at which turbidity returns to background levels, after which it is difficult to effectively distinguish between anthropogenic and naturally occurring suspended particulate matter in the acoustic record.

In the present study, Maritime New Zealand (MNZ) is ultimately concerned about the dispersing characteristics of dredged material disposed at the AMDG in order to mitigate adverse ecological impacts in the surrounding areas. To avoid adverse ecological impacts, the use of one standard deviation as a conservative upper limit for an acceptable increase in turbidity has been suggested, to better account for

natural variability in suspended sediment levels (Orpin et al., 2004). However, such a limit is more applicable for shallow water environments, where the seabed is more easily stirred by surface waves. The water depth at the AMDG precludes high variability in naturally occurring suspended sediment because the predominant waves do not typically penetrate to the seabed (see Section 2.3.2 for more details) and, thus, the actual background level is more appropriate as the upper limit for persistent dispersed material (i.e. material that is dispersed beyond the boundary of the site).

4.11 Summary and Conclusions

Four field campaigns were undertaken within the period of disposal of dredged material at the AMDG in April 2010. The focus of each field campaign was to monitor as many aspects of the disposal process as was feasible. On each day, a variety of monitoring instruments were used to record conditions prior to and during disposal with the aim of recording both the ambient conditions, as well as the changes incurred by the addition of dredged material to the water column and the seabed. From the field data records, it was possible to interpret the dispersive characteristics of the AMDG through the movements of the dredged material. Dispersion and the potential for dispersion were assessed from the perspective of each of the three disposal process phases: Phase 1 – *Convective Descent*, Phase 2 – *Dynamic Collapse*, and Phase 3 – *Passive Dispersion* as a means of organising and comparing the findings to those from previous works.

4.11.1 Dispersion During the 3 Phases of Disposal at the AMDG

Dispersion can be defined as any movement of sediment particles away from the source location (i.e. the orifice of the hopper in the case of disposed dredged material). Thus, during the 3 phases of the disposal process, discharged material is mainly dispersed in either the vertical or horizontal direction, but also in a multitude of directions in between. In terms of the environmental and legal restrictions, horizontal dispersion is the main concern as potential adverse impacts from the presence of the disposed material should not be detected beyond the boundary of the site.

Phase 1 – Convective Descent

During phase 1 of the disposal process, maximum horizontal dispersion, in the form of entrainment and subsequent lateral spreading of the descending jet of dredged material, was observed during all four surveys nearest the bed and decreasing with proximity to the surface. In surveys 1 – 4, the maximum dispersion was 73 m, 149 m, 112 m, and 90 m, respectively in any direction away from the source location (Table 4.17). A possible negative correlation to the discharge volume was identified such that larger loads may be less susceptible to entrainment and lateral spreading due to higher negative buoyancy.

This may have implications for the operational procedures employed during future dredging and disposal missions at the AMDG, as only 1 out of 9 hopper loads disposed at the site were filled to near capacity (Table 4.2). It was often the case that it was more economical to transport a partial load to the site prior to the onset of unfavourable weather conditions, which might delay transport for several days. In this case, the balance between economic costs and environmental costs would need to be considered because even though the horizontal spreading during phase 1 is relatively minor, dispersion in the subsequent phases is at least partially linked to the quantity of material entrained during phase 1.

Table 4.17 Summary of maximum dispersion distances during each phase of the disposal process for each of the four monitoring surveys.

Disposal Phase	Horizontal Dispersion Distance (m)- Survey No.			
	1	**2**	**3**	**4**
Convective Descent	73	149	112	90
Dynamic Collapse	200 – 350	-	-	-
Passive Dispersion	500	300	800	250

- indicates where no data was available

Phase 2 – Dynamic Collapse

Dispersion during phase 2 occurs in the case that a density current is generated from the excess energy available after the impact of the disposed material with the seabed. In this sense, a density current can act as a dispersing mechanism by propagating radially away from the point of impact. In this process, depending on the energy available and the characteristics of the dredged material, there is great potential for horizontal dispersion in the near-bed region. However, due to the

small temporal and large spatial scales that phase 2 occurs under, documentation is difficult and can be further complicated when the water depth is significant. In the present study, insufficient instrumentation in the near-bed region prevented adequate quantification of potential density currents that may have been generated during the 4 surveys. Theoretical estimates, based on values from the literature and gleaned from the field data where possible, were instead derived in an attempt to determine the potential for density current propagation at the AMDG. The analyses, only undertaken for the case of Survey 1, indicated that a density current has the potential to propagate (horizontally disperse) 200 m to 350 m from the area of impact (Table 4.17). At the AMDG, variation in the propagation range is dependent on the ambient sea state conditions, the volume discharged, and the characteristics of the dredged material.

Phase 3 – Passive Dispersion

After a time in the disposal process, dispersion forces transition from dynamical, in phases 1 and 2, to passive, in phase 3, at which time sediment particles still in suspension begin to be transported in the direction of the ambient current. This transition generally occurs within 15 minutes after disposal, but passive dispersion can initiate at any time after disposal: from seconds (in the case of entrainment at the perimeter of the jet) to several minutes (in the case of entrainment at the interface of the decelerating bottom density surge).

In the present study, horizontal dispersion was the most significant during this phase, with distances of approximately 500 m, 300 m, 800 m, and 250 m, respectively, for the disposed material corresponding to surveys 1 – 4 (Table 4.17). With the exception of Survey 3, passive horizontal dispersion decreased with proximity to the bed, which makes sense considering that a typical velocity profile reduces to zero at the bed (Schlichting, 1968). Focused dispersion at depths between approximately 80 m and 100 m significantly increased the magnitude of horizontal dispersion observed during Survey 3. An obvious mechanism for such a feature was not identified, but may be the result interfacial instabilities driven by the shearing of the stratified velocity layers (Strang & Fernando, 2001).

Evidence of a short-lived phase was identified by quantifying the rates of decrease of the relative turbidity and the rate of change in the standard deviation of the relative turbidity. The patterns identified indicated that a transitional phase occurs, in the mid to upper water column after the passage of the jet of material (Convective Descent), at which point the surrounding water column is set into turbulent motion, such that the forces are neither directly dynamic, nor directly passive. In this zone, the suspended sediment may be dispersed, but if the motion is turbulent, as the evidence suggests, the residual transport may be essentially zero. These findings are interesting, as evidence of the process is not commonly discussed in literature on disposal mechanics theory, but the implications for dispersion are minimal.

4.11.2 Recommendations for Future Monitoring at the AMDG

The majority of the processes that occur during the disposal of dredged material in open water are rapid by nature, with the exception of passive dispersion, which instead, can be long-lasting, but inherently transient, making all stages of disposal difficult to document and quantify through field monitoring methods. Adding to the complexity of documenting disposal processes at sea are:

i. the need to coordinate monitoring surveys with the dredging/disposal operators, optimal weather and sea conditions, and daylight hours;

ii. the extensive instrumentation requirements with respect to: costs, deployment, operation in potentially unfavourable conditions, and the challenges involved in managing the deployment and operation of multiple devices concurrently; and

iii. the availability and costs of field assistants, multiple monitoring vessels, and the licensed skippers.

Many lessons were learned in the planning and execution of the disposal plume monitoring surveys in the present study from which recommendations can be made to improve the effectiveness of future potential surveys. Recommendations will be presented from the perspective of the 3 main phases described in the previous sections as the optimal monitoring techniques for each phase varies.

Pre-Disposal Data Collection

The pre-disposal surveys should be undertaken as close as possible before the start of disposal operations so that changes detected after the disposal operations can be validly attributed to the effects of the disposal operations rather than other variables such as storms or seasonal changes.

1. Multibeam echosounder (MBES) survey:
    - Bathymetry information
    - Textural characteristics of the seabed (backscatter)
    - MBES frequency should ideally be able to detect small scale bathymetry changes.
2. Dredged material samples:
    - Depth-dependent sediment samples from within the hopper
    - Sample collection should be undertaken close to the time of release into the water column
    - Samples should be analysed for stratification within the vessel, grain size, bulk density, water content.
3. Site sediment samples:
    - Collection sites should be on a regular grid
    - 3 replicate samples should be collected at each site
    - Sample sites should be focused over the centre of the site
    - A boxcorer would be the ideal sampling device, but it would depend on the capabilities of the vessel
    - Sub-cores can be taken for benthic fauna identification and sediment analysis
    - Sediment analysis should consider depth variations within the core, organics, grain size, texture, heavy metals or other contaminants, colour, water content, and possibly viscosity or shear strength.
4. Seabed video:
    - The camera should be suspended approximately 1 m above the bed
    - Transects on a regular grid should be recorded across the centre of the site
    - Transect grid should pass over the sediment sample collection sites.
5. CTD casts:

- 2 – 3 casts should be recorded near the centre of the site on the day of each survey
- Casts should be recorded before the dredged material is released into the water column so profiles represent the ambient conditions.

Phase 1 – Convective Descent

1. Bottom-mounted (upward-facing) ADCP data:
    - The ADCP should be deployed in the estimated area of impact
    - Current data will show descent velocity of the disposed material and backscatter intensity will show turbidity
    - ADCP should be programmed to start sampling at least 30 minutes before the schedule disposal time, but a long term deployment spanning all disposals would be optimal
    - If a long-term deployment will be used, the material needs to be released from the hopper as close to directly over the ADCP as possible (this may prove difficult if the material is released while the tug is underway).
2. Turbidity sensor data:
    - Ideally, a string of self-contained (internal battery and logger) turbidity sensors with large optical ranges should be moored at the bed adjacent to the bottom-mounted ADCP
    - Laboratory calibration of the sensors can be undertaken after each disposal with a representative sample of the material in the hopper
    - Sensor string should be held taut using surface buoyancy sufficient to prevent significant drifting of the mooring line in the upper water column
    - Sensors should be suspended at regular intervals along the mooring line so that calibration of the ADCP backscatter data throughout the water column is possible
    - Sensors should be programmed to start sampling approximately 30 min before the schedule disposal time.
3. Boat-mounted (downward-facing) ADCP:
    - Two vessels should be equipped with a downward-facing ADCPs
    - Transects should be recorded along a regular grid over the centre of the site
    - The two vessels should drive mirroring transects simultaneously on either side of the release location
    - The vessels should proceed initially away from the centre and then making their way back towards the centre, repeating the cycle until the plume is no longer visible

- The real-time backscatter display screen on board should be used to identify the presence of elevated turbidity in the water column.

4. Water samples:
    - Samples should be collected from a set depth at regular and representative time intervals
    - The collection depth should coincide with at least one (more than one is ideal, but this depends on manpower) of the upper water column ADCP bins
    - Samples should be collected on the same side of the boat as the mounted ADCP
    - Water samples should be processed for suspended sediment concentration (SSC) as soon as possible after collection (if processing is not possible immediately, samples should be refrigerated).
5. Boat-mounted turbidity sensor:
    - A self-contained turbidity sensor should be mounted on the vessel
    - The sensor should be mounted at a depth as close as possible to that of the water samples
    - The sensor should be mounted nearby the ADCP to ensure that the backscatter and turbidity data reflect the same 'parcel' of water.

Phase 2 – Dynamic Collapse

1. Bottom-mounted ADCP and moored turbidity sensor string (described above):
    - Data can also be used for recording the initial stages of the dynamic collapse in the area of impact
2. Additional bottom-mounted ADCPs and turbidity sensors:
    - Ideally, 2 additional bottom-mounted (upward-facing) ADCPs should be deployed
    - A turbidity sensor should be secured to each additional ADCP frame at a height at least above the blanking distance of the ADCP
    - The ADCPs should be deployed approximately 50 m and 100 m from the centre (area of impact) on the same side
    - The sensors should be calibrated as described above.
3. Boat-mounted (downward-facing) ADCP (described above):
    - Backscatter data from the downward-facing ADCPs of the 2 traversing vessels can also be used for recording the presence of a density current at the bed

- Density current thickness can be observed from the backscatter record
- If there is sufficient information on SSC, determined from the calibrated turbidity sensors, concentration of the density current can be determined from the ADCP backscatter record after calibration.

Phase 3 – Passive Dispersion

In general, the measurements described above should be carried out until no elevated turbidity is visible in the water column by referring to the backscatter contour plot of the data-acquisition screen on board the survey vessel. The only changes that may be required in order to fully document the passive dispersion phase is that the traversing vessels equipped with the downward-facing ADCPs and turbidity sensors may need to extend the distance away from the centre that the transects are recorded. The pre-designated grid should include the additional recording areas, but they should only be driven if the on board display of ADCP backscatter indicates that the plume has drifted beyond the areas previously visited.

Post – Disposal Data Collection

A post-disposal survey should be undertaken as close to the completion of all disposals as possible to determine the short-term fate of the disposed material. If long-term fate is also of interest, several months should pass and at least one significant weather system before a second post-disposal survey is undertaken.

1. Multibeam echosounder (MBES) survey:
    - MBES survey should follow the same procedure as described in the pre-disposal methods
2. Site sediment samples:
    - Sample collection should follow the same procedure as described in the pre-disposal methods
3. Seabed video:
    - Seabed video should follow the same procedure as described in the pre-disposal methods

4.11.3 Relevance to the Thesis Aims and Objectives

The majority of the findings in this chapter contribute the understanding on the site specific processes involved in the disposal of dredged material (Objective 2) and provide information about the potential for loss of disposed sediment at the AMDG (Objective 3). However, as the disposal monitoring surveys were undertaken over a relatively narrow range of sea state conditions, further investigations that contribute to the completion of Objectives 2 and 3 were undertaken utilising numerical modelling techniques and are described in Chapter 5. Findings related to the definition hydrodynamic forcing mechanisms at the AMDG, based on data recorded during the plume monitoring studies, further contributed to the completion of Objective 1 in this Chapter. However, additional information on forcing mechanisms was obtained through the numerical modelling studies described in Chapter 5.

CHAPTER 5

NUMERICAL MODELLING EXERCISES FOR IMPROVED UNDERSTANDING OF DISPERSION AT THE AUCKLAND MARINE DISPOSAL GROUND

5.1 Introduction

Evaluating the suitability of a site for the purposes of disposal of dredged material involves determining the dispersive characteristics, or the potential for the disposed material to be transported beyond the boundaries of the site (Langtry et al., 2009; McAnally & Adamec, 1987; Sheehan & Harrington, 2012). In most cases, contaminated sediments are not permitted to be disposed in open-water in most cases as defined by the international conventions (Bolam & Rees, 2003; Flaim et al., 2010; Tay et al., 2008), but in some cases low levels of contamination are allowed if adverse impacts are minimal (Flaim et al., 2010). In such cases, legal provisions may stipulate that the material must not be detected beyond the boundaries of the site for the purposes of minimising adverse impacts to the surrounding environment (Flaim et al., 2010; Langtry et al., 2009; Sheehan & Harrington, 2012).

Thus, a comprehensive understanding of the spatial and temporal characteristics of the hydrodynamics related to the potential for dispersion is critical for the permitting of sites proposed for disposal operations.

5.2 Motivation and Relevance to the Thesis Objectives

Field surveys and deployments targeted at determining the potential for dispersion at the AMDG have provided valuable information related to the potential for dispersion there, but the contribution of these data to a comprehensive understanding are limited in that they only represent the time periods and conditions under which they were collected. A numerical model representing the characteristics of the site can offer additional information about the pathways for sediment transport during conditions that were not documented during the field campaigns. Another benefit to the development of a numerical model of the disposal of dredged material at the AMDG is the potential to isolate the influencing forces and quantify the significance of each. Such information can be

valuable in developing an on-going plan for operation of the site to minimise dispersion, should the site be approved for long-term use.

The findings of this chapter satisfy the objectives set out in Chapter 1 of this thesis by contributing to an improved understanding of the various forcing mechanisms of dispersion and by allowing, through the development of a representative model, for further assessment of dispersion characteristics under conditions not encountered during the field surveys.

5.3 Chapter Aims

This chapter aims to:

- develop a 3-dimensional numerical flow model that is representative of the hydrodynamic conditions at the AMDG;
- develop and couple a mud transport model that simulates the dispersion characteristics of disposed dredged material with the flow model;
- based on results, assess the capability of the model for simulation the disposal process; and
- investigate the influence and effects of forcing mechanisms on dispersion at the AMDG that were not previously observed in the field campaigns through the modelling of a range of idealised scenarios representing potential conditions at the AMDG.

5.4 Forcing Considerations in the Shelf Environment

Bounded by land on only one side, the shelf region is inherently unconstrained. This makes the task of developing calibrated shelf models complex on several levels. Shelf flow regimes may be influenced not just by shelf-specific mechanisms, but also those originating from the presence of the coastal boundary and the deep ocean (Csanady, 1997).

5.4.1 Physical Processes

A typical accounting (e.g. de Lange et al. (2003), Heath (1985), Longdill (2007), and Sharples and Greig (1998)) of the various mechanisms influencing shelf flows in the New Zealand region usually include discussions on the following:

- winds;
- tides;
- density gradients;
- boundary currents; and
- coastal trapped waves.

Any number of these mechanisms may influence the regional and/or local current regime. Therefore, modelling efforts which attempt to replicate the shelf flows at the AMDG should consider the significance, and possibly account for, each influencing factor. It should be added that for the purposes of sediment transport modelling, which is also considered in this chapter, the local wave climate can also have a significant influence on transport. However, as it was previously mentioned in Section 2.3.2, the water depth at the AMDG precludes any major contribution from waves, so they will not be considered further.

5.4.2 Data Availability

A critical factor in the development of a representative model is the availability of data for *i*) boundary conditions, *ii*) initial conditions, and *iii*) calibration and validation steps. Possibilities for acquiring the necessary data include field deployments and, in some cases, extraction of output from openly available regional models, such as Bluelink (oceanic circulation; Oke et al. (2008)) and TPXO6.2, referenced earlier in the thesis as used by MetOcean Ltd. to develop a New Zealand tide model (Egbert et al. (2002)).

A significant number of modelling studies have been undertaken for purposes of improving the understanding of coastal processes in New Zealand waters (Hume et al., 1992). Generally speaking, efforts have focused mainly on near-shore areas,

through the use of 2-dimensional hydrodynamic and sediment transport models. Even as recently as 2007, only 2 examples of 3-dimensional coastal models exist (Black et al., 2000; Longdill, 2007), both undertaken in the northeast coast region, but neither domain covering the location of the AMDG. There are currently no known model studies that focus on the shelf area in the vicinity of the AMDG.

This is likely due to the difficulty in constraining such an environment, which is not only characterised by deep water, but also by the presence of a variety of different forcing mechanisms. As a result of the latter, then, field data requirements for initialising, forcing, and calibrating a model must be extensive and representative of the variability on all levels, which is made all the more complex by the former. Generally speaking, the collection of the appropriate type and amount of field data for the development of such a model would require a large scale operation composed of several large vessels, availability of a large range of instrumentation and multiples of each type, and the ability to measure conditions on at least a seasonal scale.

As previously mentioned, use of freely available global model data can reduce the need for field measurements. Typically, such data is used for boundary forcing purposes and thus, the resolution is a crucial factor in considering its suitability as finer scale processes may not be well-represented on at a coarse grid scale. In such circumstances, use of this type of data is impractical. In a related matter, another consideration for use of global model datasets to force a smaller scale model is the whether the purpose of the global model corresponds with the purpose of the model that is being developed. If the forces that need to be represented in the small scale model are not represented in the larger scale model, then use of such data would, again, be impractical.

5.5 Numerical Model Description

The models described in the following sections were developed using the MIKE 21 FM and MIKE 3 FM modelling systems, which are commercially available from DHI Water & Environment. The programs are designed to simulate two- and three-dimensional flows, respectively, over a flexible element mesh grid, where elements can be unstructured triangles or quadrilaterals in the horizontal plane and in the case of the 3D version, structured prisms or bricks in the vertical domain.

The systems are based on the numerical solution of two or three-dimensional incompressible Reynolds averaged Navier-Stokes equations invoking the assumptions of Boussinesq and hydrostatic pressure. Therefore, the models account for the continuity, momentum, temperature, salinity, and density equations and use a turbulent closure scheme. In the 3D version, the free-surface is based on the sigma-coordinate transformation approach. The systems use a cell-centred finite volume spatial discretization method and the domain is discretized through subdivision of the continuum into non-overlapping elements. Details of the governing equations and the numerical solutions are described in DHI (2011a).

Time integration is explicit in the 2D version and semi-implicit in the 3D version, where horizontal terms are treated explicitly and vertical terms are treated implicitly.

Each version is comprised of a hydrodynamic module that provides the underlying flow behaviour, and the following possible transport modules:

- Transport Module;
- ECO Lab/Oil Spill Module;
- Particle Tracking Module;
- Mud Transport Module; and
- Sand Transport Module

In the present study, the Mud Transport Module was applied within the MIKE 3 version of the modelling system. The Mud Transport Module is coupled with the Hydrodynamic Module to solve the advection-dispersion equation for sediment transport. The module can account for multiple mud fractions, multiple bed layers, wave-current interaction, flocculation, hindered settling, inclusion of a sand fraction, transitions of sediments between layers, and simple morphological calculations. Details of the governing equations and numerical solutions of the Mud Transport Module are included in DHI (2011b).

Within the Mud Transport Module addition of sediment via dredging activities can be included in the model using the Dredging Dialogue. Within that Dialogue, sediment can be removed from the bed (dredging) or added to the water column

(dredger spill or disposal). In the present study, dispersion characteristics after disposal of dredged material at the AMDG were simulated by designation of source elements in the surface layer of the 3D model domain.

5.6 Two-Dimensional Regional Tide Model

A two-dimensional regional tide model was initially developed as the basis for a shelf circulation model. From this, it was intended that the boundary conditions of a local flow model could be extracted to simulate the dynamics of dispersion of dredged material at the AMDG. However, it was found during the initial stages of developing a regional circulation model that the situation in the AMDG was complex and ultimately too unconstrained, as was previously alluded, to justify continuing attempts to build such a model. The following sections describe the initial steps undertaken in developing the regional model, and the justification for abandoning the effort in favour of a more simplified modelling approach, which is described in Section 5.7.

5.6.1 Model Domain and Boundary Conditions

Tidal dynamics were simulated over a computational domain that covered the majority of New Zealand's northeast coastline, from Sandy Bay at Whanaki in the Northland, to Maketu southeast of Tauranga Harbour on the Bay of Plenty coastline (Figure 5.1). Due to the physiography of the New Zealand landmass in the region, the eastern boundary of the model domain extends a significant distance offshore, some 150 km, on the northern end, but only small distance on southern end with the grid corner located approximately offshore from Opotiki. Most offshore islands and reef systems were included in the model domain. In some cases, very small islands and estuaries were excluded from the grid as their influence on the regional dynamics would be insignificant.

The model domain was built using a flexible mesh of triangular elements. The majority of the grid contains mesh elements that were fitted based on a maximum mesh element area of 12 km^2, which corresponds to a triangle with sides approximately 5 km in length (Figure 5.1). Within areas of interest, such as at the AMDG and at calibration locations, a decreased mesh element size was applied in order to increase the accuracy of model output for a particular location. A 10 km

by 10 km area surrounding the AMDG was designated with a maximum mesh element size of 1 km^2 corresponding to triangles with sides approximately 1400 m in length.

The model bathymetry was interpolated over the flexible mesh based on hydrographic data digitised from hydrographic charts published for the North Island east coast region[10] (LINZ, 1999, 2002, 2004, 2007, 2009). All water depths were adjusted to an average MSL based on the chart datum of each hydrographic chart included in the model domain. The interpolated model bathymetry is based on over 34,000 data points with a decreasing density with distance from the coastline. For the purposes of decreasing computation time, water depths greater than 500 m were truncated to a constant value of 500 m, which had a negligible impact on the modelled currents. A small amount of smoothing in the southeast corner of the model grid was required to increase the stability of the model.

Model boundary conditions for all three open boundaries (north, east, and south) were applied as specified tidal heights varying in space and time. Tide heights along each boundary and for the length of the model run were extracted from a global tide model dataset available within the MIKE 21 Tide Predictor Toolbox. The global tide data is based on TOPEX/POSEIDON altimetry data and represents the major diurnal (K_1, O_1, P_1, and Q_1) and semi-diurnal tidal constituents (M_2, S_2, N_2, and K_2) at a resolution of 0.25° × 0.25° (Andersen, 1995).

[10] Sourced from Land Information New Zealand data. Crown Copyright Reserved.

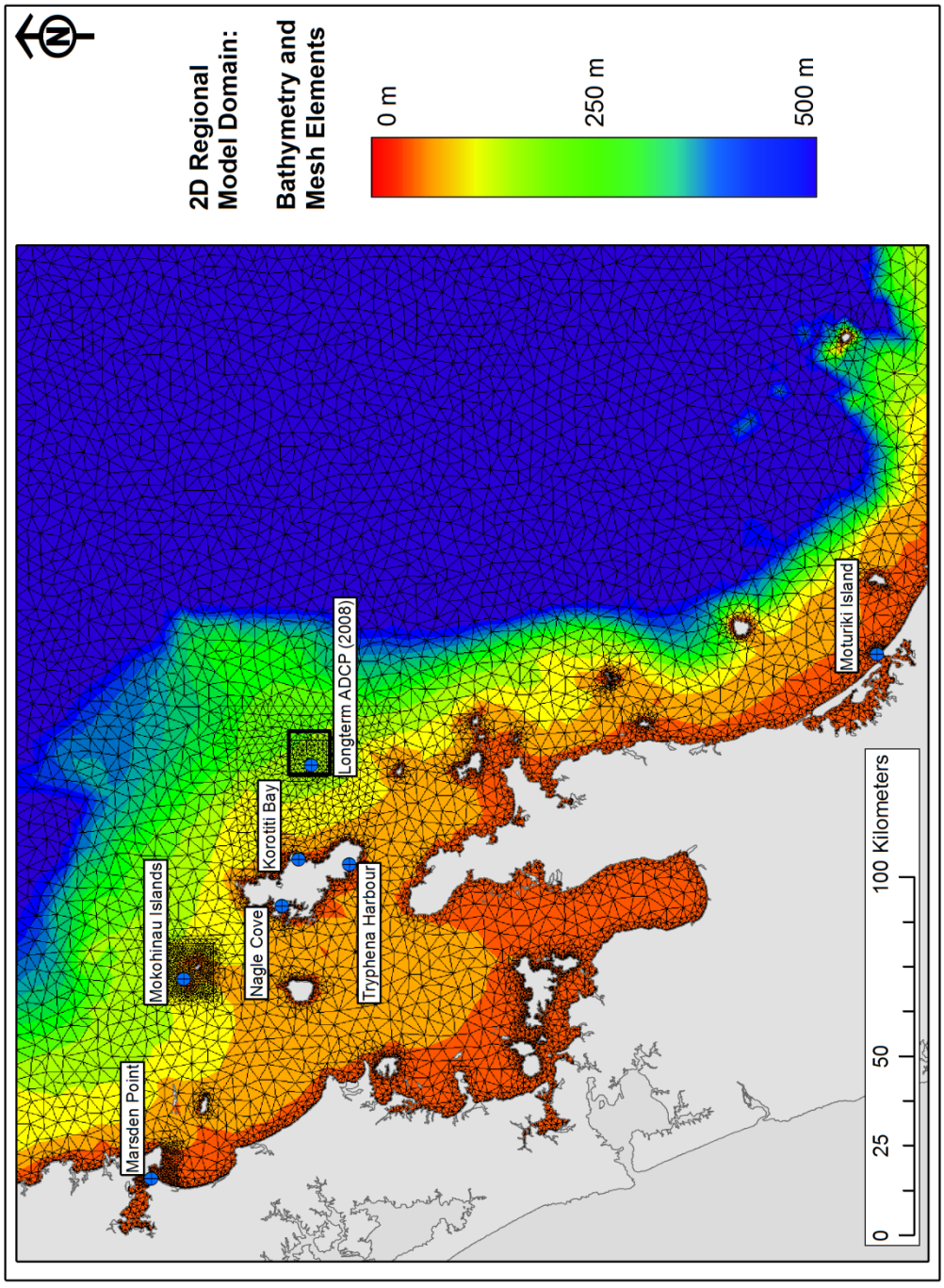

Figure 5.1 Model domain and flexible triangular mesh bathymetry grid used for the 2D tidal model. Finer resolution mesh elements were applied in areas of interest.

5.6.2 Model Comparisons and Calibration

The 2D tidal model simulation was run for a period of approximately 2 months corresponding to the long-term ADCP record of 2008 (see Chapter 3). However, the ADCP was not equipped with a pressure sensor, so a water level record at the location of the AMDG was not available.

Tide Height

To verify the accuracy of the modelled tide heights, output from several locations within the model domain was extracted and compared to observed tidal records sourced from various organisations within the New Zealand maritime and oceanographic community. Table 5.1 details the tidal records used to calibrate and validate the 2D tidal model of the northeast coast region. Refer to Figure 5.1 for positions of calibration locations within the model domain.

Table 5.1 Details of observed tide height records used for calibration and validation of the 2D tide model.

Calibration Locations	Record Type	Coordinates (NZTM)		Processing details	Source
		Northing	Easting		
Marsden Point	Water level	6033364.146	1734604.824	De-tided (T_tide harmonic analysis)	North Port water level gauge
Mokhinau Islands	Tide height	6024280.882	1790486.611	Predicted tides from historical water level gauge record	NIWA tide model
Nagel Cove	Tide height	5996825.736	1810800.604	Predicted tides from historical water level gauge record	Land Information New Zealand (LINZ)
Tryphena Harbour	Tide height	5978032.387	1822500.04	Predicted tides from historical water level gauge record	Land Information New Zealand (LINZ)
Korotiti Bay	Water level	5992200.128	1823815.665	De-tided (T_tide harmonic analysis)	GeoNet National Tsunami Gauge Network
Moturiki Island	Tide height	5830400.96	1881180.521	Predicted tides fom water level gauge record	NIWA tide model

The records for Marsden Point and Korotiti Bay were extracted from water level gauge datasets that are, at present, still in use. Water level data is not only influenced by tidal oscillations, but also by such factors as atmospheric conditions and wind set-up. In order to obtain a tidal height record from such data, it is necessary to undertake a processing step which separates the tidal frequencies from the non-tidal frequencies (residual). The de-tiding step was undertaken using

the harmonic analysis package T_TIDE in the MATLAB environment (Pawlowicz et al., 2002). For the 122 day Marsden Point record, 18 significant (95 % level) constituents were resolved, explaining 93.3 % of the variance. The Korotiti Bay record was somewhat shorter in length than the Marsden Point record (50 days) and as such, only 12 significant constituents were resolved; however, these constituents explained 97 % of the variance at that location. All other records obtained were based on tidal predictions from locations where tidal constituent information is well known and applied for the purposes of modeling or for navigation (Table 5.1). These records were used to calibrate and validate the model.

In the two-dimensional model, there are two main parameters that can be adjusted to calibrate the model; the bed resistance parameter and the eddy viscosity parameter. For large grids with a significant change in water depth, use of the Manning number to define the bed resistance is recommended (DHI, 2010). The model was relatively insensitive to large changes in the Manning number, so the default (recommended) value of 32 $m^{1/3}s^{-1}$ was applied. For the eddy viscosity parameter, the Smagorinsky formulation was applied and calibration efforts showed that the model was also insensitive to changes in the applied value, so the default values for the coefficient and the range of possible viscosities were used. Please refer to Table 5.2 for applied parameters and details of the model set-up.

A period including two neap tides and two spring tides was assessed for model validation following calibration efforts. Modelled (red) and observed (black) tidal heights are shown in Figure 5.2 for each of the six tide height calibration locations within the model domain (see Table 5.1 for details). Figure 5.3 shows the regression-scatter plots corresponding to the model versus observation data for each location during the period of interest. Patterns in the regression-scatter plots indicate the type of errors in the modelled values (Winter, 2007).

Marsden Point values (Figure 5.2a and Figure 5.3a) indicate that the model underestimated the amplitude of the tidal signal and the closed hysteresis loop indicates the presence of a lag error. Mokohinau Island values (Figure 5.2b and Figure 5.3b) show error patterns similar to the Marsden Point location, but the errors were on a smaller scale (R^2-values of 0.93 versus 0.91 for Marsden Point). At Nagel Cove (Figure 5.2c and Figure 5.3c), the model-observation agreement

was quite good, with no significant errors indicate by the high R^2 value (0.99) and the low mean absolute error (MAE) (0.06). Errors at the Tryphena Harbour (Figure 5.2d and Figure 5.3d) also indicated an underestimation of the tidal amplitude and a lag error that was slightly larger than that at the Mokohinau Island location. Errors at Korotiti Bay (Figure 5.2e and Figure 5.3e) were significant (R^2=0.52; MAE=0.37), indicating that the model did not represent the tidal signal well at that location. The model significantly underestimated the tidal amplitude and a large lag error was also present. Values at the Moturiki Island location (Figure 5.2f and Figure 5.3f) showed a slightly different trend than that at the other calibration locations; there was no indication of a lag error, and only a small amplitude error. However, in this case the model over-estimated the tidal amplitude.

Table 5.2 Numerical parameters for the two-dimensional barotropic tide model of the northeast coast of New Zealand's North Island.

Parameter	Value
Time step	10 sec
Number of time steps	596160
Model start time	20/09/2008 00:00:00 GMT
Bed resistance	Manning number = 32 $m^{1/3}s^{-1}$
Eddy viscosity	Smagorinsky formulation: 0.28 constant in domain (Min =1.8e^{-6} (m^2/s); Max = 1e^7 (m^2/s))
Coriolis Forcing	Varying in domain
Grid type	Flexible mesh (triangular elements)
Max element area	Main area: 12 km^2; eastern Great Barrier Island: 4 km^2; AMDG: 1 km^2; Tide height calibration locations: 0.4 km^2;
Grid orientation	True north 0°
Grid origin	1715473.9398 m E, 5812489.7915 m N, NZTM
Grid latitude (centre)	-36°
Drying depth (m)	0.005
Flooding depth (m)	0.05
Wetting depth (m)	0.1
North boundary	Specified level global tide model data (Andersen, 1995)
East boundary	Specified level global tide model data (Andersen, 1995)
South boundary	Specified level global tide model data (Andersen, 1995)

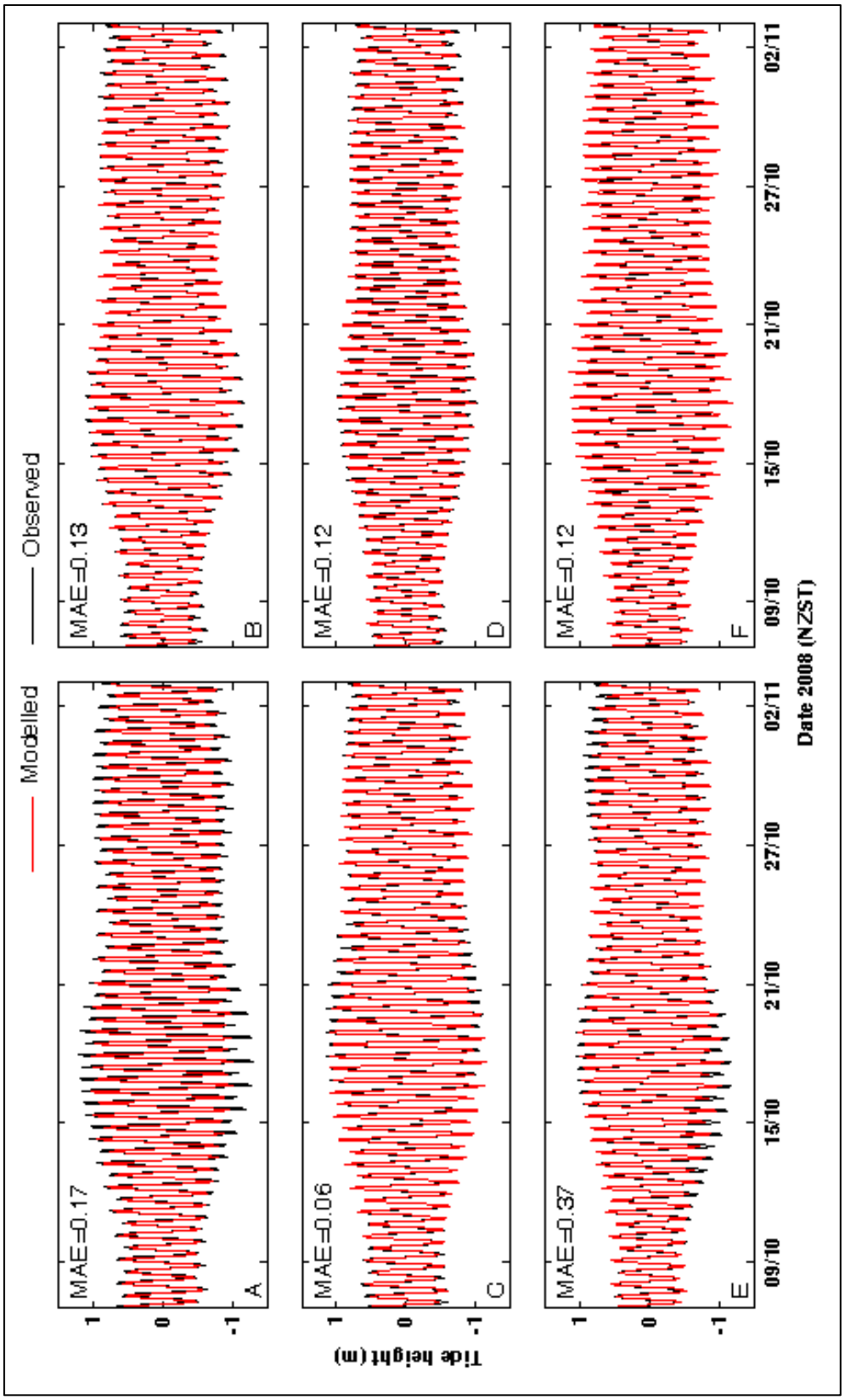

Figure 5.2 Observed-gauge tidal predictions (black) and modelled (red) tide heights with the corresponding mean absolute error (MAE) for (a) Marsden Point, (b) Mokohinau Islands, (c) Nagle Cove, (d) Tryphena Harbour, (e) Korotiti Bay, and (f) Moturiki Island. See Figure 5.1 for the

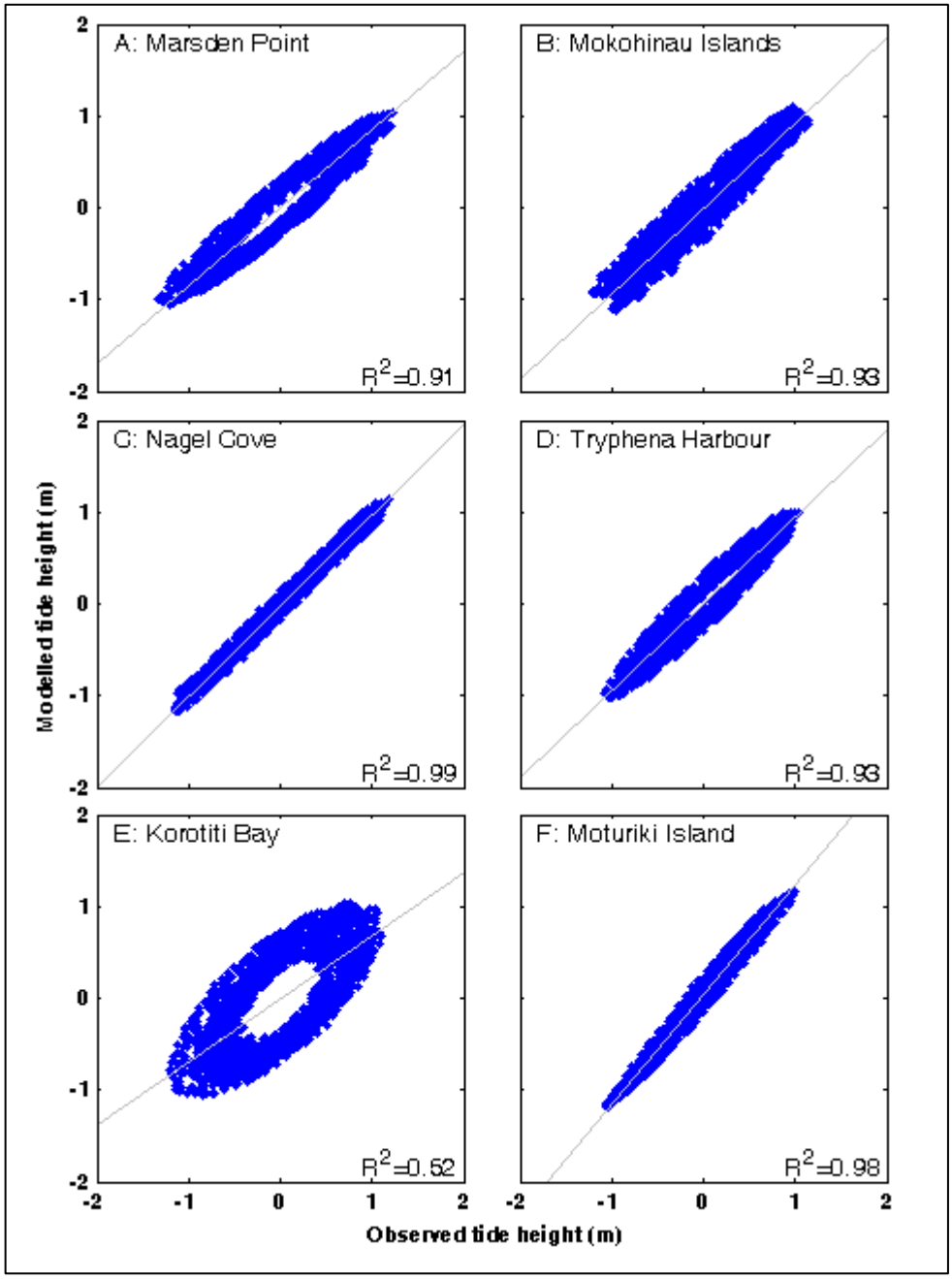

Figure 5.3 Scatter plots and R^2-values from linear regression of modelled and observed tide height records presented in Figure 5.2 ((a) Marsden Point, (b) Mokohinau Islands, (c) Nagle Cove, (d) Tryphena Harbour, (e) Korotiti Bay, and (f) Moturiki Island). Observed tide heights are based on tidal predictions from tide gauge records at locations within the regional model domain (see Figure 5.1 for locations).

Depth-Averaged Tidal Currents

The tidal component comprised approximately 25 % of the total current velocity at the AMDG during the long-term ADP deployment in 2008 (Chapter 3), therefore for a representative flow regime, it is crucial that the model is capable of reliably simulating the tidal currents at the AMDG. To verify the accuracy of the 2D regional tide model with regards to tidal current simulation, current

components output from the same period of interest assessed for the tide height validation, was extracted at the location corresponding to the deployment site of the ADP used for the long-term record of 2008 (Figure 5.1). The output was extracted from the same simulation used to assess the tidal height (above) (see Table 5.2 for applied settings).

Figure 5.4 shows the modelled (red) and observed (black) cross-shore (u) and alongshore (v) tidal currents at the AMDG during the period of interest and the corresponding MAE-values for each. Observed tidal currents were separated from the depth-averaged raw signal using harmonic analysis (T_TIDE) in the MATLAB environment (Pawlowicz et al., 2002)) (see Chapter 3 for more details).

It is clear that at the AMDG location in the model domain, the current velocities are not well represented (MAE=3.13 and 2.27 for *u*- and *v*- currents, respectively). It appears that the cross-shore currents are underestimated and the alongshore currents over-estimated. Regression-scatter plots patterns and low R^2-values reveal what can most likely be attributed to a range of different types of errors (constant factor, amplitude, lag, and frequency (Winter, 2007)) in the representation of both the cross-shore and alongshore tidal current components (Figure 5.5). It should be noted, however, that the current velocity ranges are not unreasonable, despite the aforementioned under- and over- estimates of the cross-shore and alongshore components, respectively.

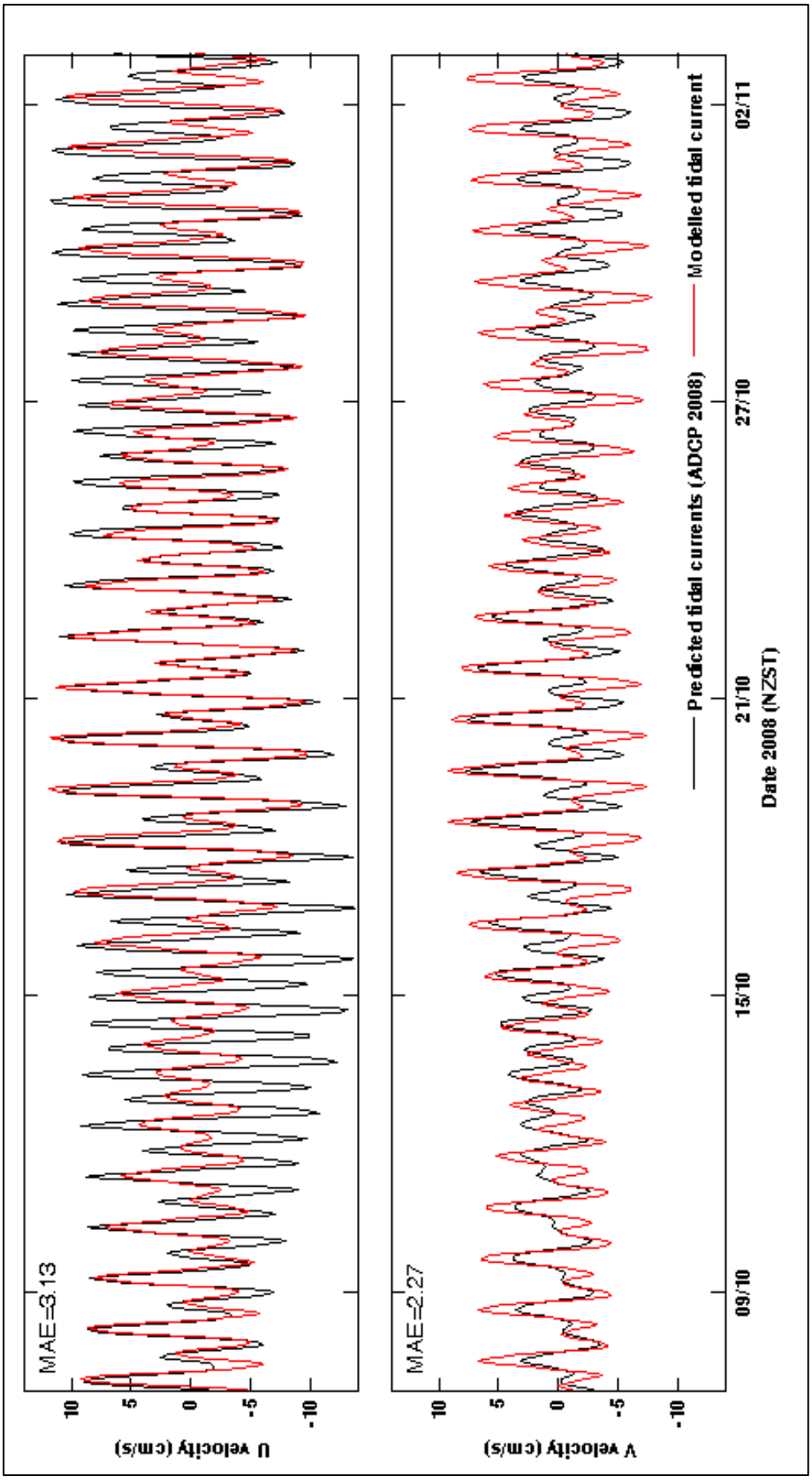

Figure 5.4 Observed cross-shore (u) and alongshore (v) tidal currents predicted from the long-term 2008 ADCP record (black) and modelled u- and v- tidal currents (red) from the location corresponding to the ADCP mooring within the model domain. The records shown correspond to the same period shown in Figure 5.2. Mean absolute error (MAE) is given for each component.

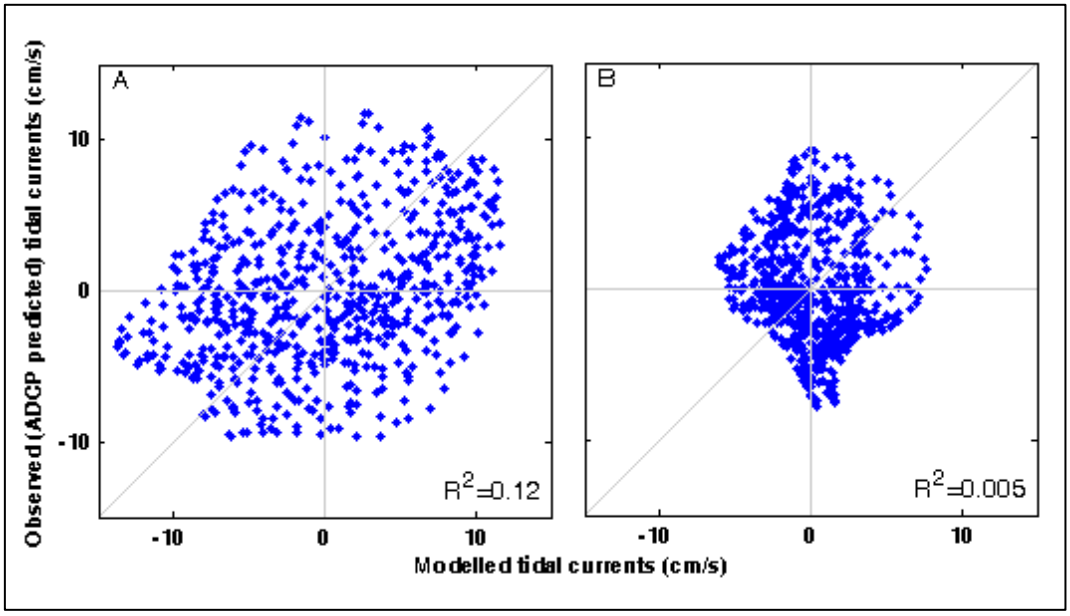

Figure 5.5 Scatter plots and R^2-values from linear regression of modelled and observed tidal current component records ((a) *u* and (b) *v*) presented in Figure 5.4. Observed currents are based on tidal predictions from the long-term ADCP record of 2008. Model output was extracted from a location within the model domain that corresponded to the long-term ADCP mooring (see Figure 5.1 for location).

5.6.3 Tidal Currents in the Northeast Coast Region

The output from the 2D regional tide model, though not without error for all locations, is at least indicative of the major features of the tidal component of flow for the northeast continental shelf region. These features are evident in Figure 5.6 and Figure 5.7, which depict the depth-averaged tidal current flow field from the model domain at a mid-ebb and mid-flood stage of the tide during a spring tide, respectively. Tidal currents are, overall, relatively weak in this area with the highest velocities (~50 cm/s) occurring during the ebbing stage in the Colville Channel, which funnels water from within the Hauraki Gulf onto the adjacent shelf. It appears that due to the proximity of the AMDG to the Colville Channel, tidal current velocity may be somewhat enhanced compared to shelf regions to the north or south, but velocities are almost an order of magnitude lower (~5 - 10 cm/s) in the AMDG area compared to in the Colville Channel.

According to the model output, current direction may also influenced by the ebb-dominance in the region. It appears that the flow field at the AMDG may be additionally influenced from currents flowing out of the northern end of the Hauraki Gulf and around the tip of Great Barrier Island, as seen by the ebb vectors at the AMDG, which are directed northwest to southeast (Figure 5.6). Unlike a

symmetrical tidal regime, the corresponding flood stage vectors at the AMDG are directed northeast to southwest (Figure 5.7). These patterns suggest the existence of a possible tidal current pathway that flows clockwise, flooding through the Colville Channel and ebbing through the northern end of the Hauraki Gulf and around the northern tip of Great Barrier Island.

5.6.4 Discussion

The tidal elevation representation within the 2D regional tide model was acceptable in the nearshore regions, but with increasing distance from New Zealand's main coastline, disparities between modelled and observed tidal heights increased. This may be the result of two main factors: 1) the model bathymetry was based on digitised hydrographic charts that had a decreasing density of water depth points with distance from the coastline and 2) the model boundaries were forced by a global tide model that did not account for several tidal constituents, which have been shown to be of increasing importance in the shelf areas.

In a coastal environment with a highly variable bathymetry, such as rocky reefs, high-resolution bathymetric datasets are required for accurate numerical simulations of the area. Rocky reef habitats have been found in areas east of Great Barrier Island, but mainly at shelf depths shallower than approximately 100 m; deeper than that, bottom relief was found to be low (Sivaguru & Grace, 2002). The data density for the hydrographic charts used to create the model bathymetry in this research decreased starting at approximately the 100 m depth contour. Furthermore, if the bathymetry of the AMDG area surveyed with MBES during these studies is any indication of the overall bathymetric relief of the northeast coast shelf, a highly variable bottom topography is not a concern (Flaim & de Lange, 2011). Therefore, low resolution bathymetric data for the offshore areas of the model domain is most likely sufficient for reliable numerical simulations.

This indicates that the main source of error in the model output is the boundary forcing. The global tide model used as boundary forcing, only accounted for the main tidal constituents. An assumption of low significance of longer period constituents such as the M_m (monthly lunar) is generally acceptable for models of coastal areas. However, it has been speculated that the long period tidal waves have an increasing influence in shelf areas due to minimal damping by the bottom

topography (Hendershott & Munk, 1970). In Chapter 3 of this thesis, this theory was proposed as the explanation for the strength of the M_m tidal constituent derived from harmonic analysis of the long-term ADP data recorded at the AMDG in 2008. Thus, it is probable that neglecting such usually unimportant constituents in a model that includes deeper shelf areas would result in errors that tend to increase in magnitude with distance from the coastline. This pattern is exemplified in the case of the 2D regional model described here. Errors in the tide height were minimal at calibration locations close to the main coastline of New Zealand (e.g. Mokohinau Islands and Moturiki Islands (Figure 5.3b&f, respectively)). At sites closer to the shelf margin, for example Tryphena Harbour and Korotiti Bay (Figure 5.3d&e, respectively) the model error increased. This principle is further supported by the quite low agreement between the modelled and observed currents at the AMDG calibration location (Figure 5.5).

The model appears to have represented some of the main tidal component features relatively well, as evidenced by the current magnitude difference between the Colville Channel and the AMDG, which is confirmed by the results of Greig (1990), Manighetti and Carter (1999), and by the findings of this research (Chapter 3). However, contrary to descriptions by Manighetti and Carter (1999), the model output indicated a clockwise component to the tidal wave propagation around Great Barrier Island. Harmonic analysis of the long-term ADP record from the AMDG also indicated a clockwise propagation of the main tidal wave (M_2), which was explained as a possible local tidal flow generated by the proximity of Great Barrier Island (Chapter 3). It should be mentioned, however, that the under- and over- estimates of the cross-shore and alongshore current velocities, respectively, at the AMDG would primarily manifest in the model output as errors in current direction and such results should be regarded with caution.

The results of this tidal modelling study, while acceptable for a general indication of regional tidal dynamics, are less than optimal when the end result is simulation of local scale dynamics. This is especially true considering that the potential for representative results would diminish significantly with the addition of non-tidal factors. Consequently, a more simplified modelling approach is presented in the following section, the results of which will comprise the core findings of this chapter.

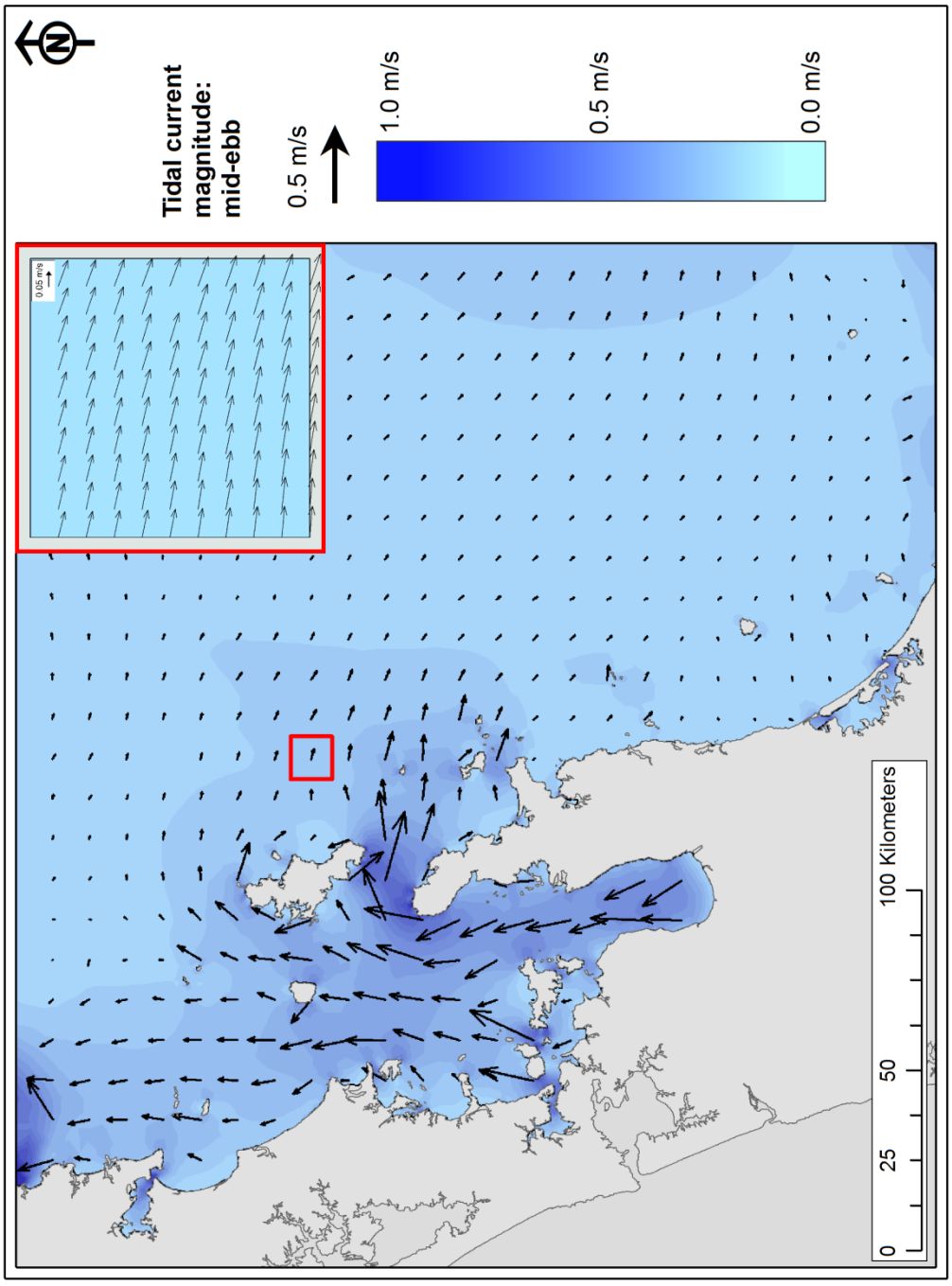

Figure 5.6 Tidally generated currents in the northeast coast region during spring tides at mid-ebb stage. Inset is a close-up view of the current vectors in the region of the AMDG (note the separate vector scale for the close-up).

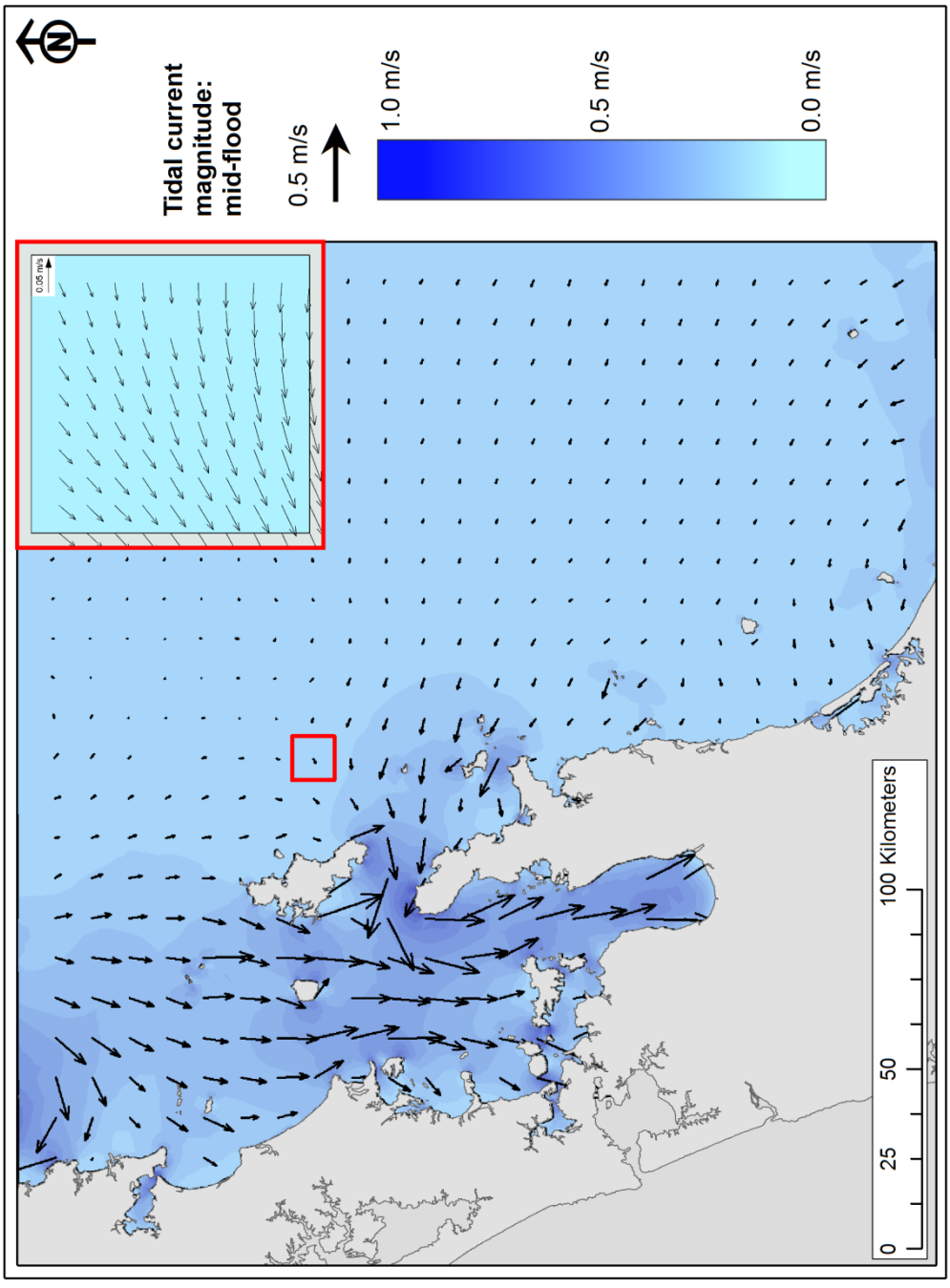

Figure 5.7 Tidally generated currents in the northeast coast region during spring tides at mid-flood stage. Inset is a close-up view of the current vectors in the region of the AMDG (note the separate vector scale for the close-up).

5.7 A Three Dimensional Near-Field Flow Model

As described in the previous section, development of a 2D regional circulation model for the purposes of forcing a near field model of the disposal of dredged material proved too complex, even at the baseline stage of tidal forcing. Initial results of the tidal dynamics model showed that ultimately a regional model would not provide satisfactory results. Therefore, an alternative approach was taken, which can be described as semi-empirical as it focuses on and utilises the conditions directly measured at the AMDG during the field campaigns. As such, it was not possible to 'field calibrate' in the standard sense, but rather the model was tuned to the conditions so that it is representative of conditions that have been observed.

5.7.1 Model Domain and Boundary Conditions

Model Grid

Near-field flows were simulated over a 3D computational domain that covered the AMDG and the surrounding area (Figure 5.8). The grid dimensions correspond to an area of 10 km by 10 km, with the AMDG positioned at the centre. The model domain was chosen to be large enough to minimise boundary stability concerns at the centre, but small enough to ensure a practical computation time. Due to the distance of the AMDG from the nearest coastline, approximately 25 km from the east coast of Great Barrier Island (see inset Figure 5.8), and the small area of interest, the model domain consists of 4 completely open boundaries oriented relative to true north.

The model domain was built on a flexible mesh of triangular elements. The majority of the grid contains mesh elements that were fitted based on a maximum mesh element sized of 1 km^2, which corresponds to an approximately equilateral triangle with sides around 1400 m in length (Figure 5.8). At the centre of the model domain an area of interest was designated corresponding to the AMDG, where a decreased mesh element size (maximum area = 1250 m^2; side length ≈ 50 m) was applied in order to increase the accuracy of model output for that location.

At the step of mesh generation, the DHI software ensures a smooth transition between areas with differing applied mesh settings. Use of a decreased mesh element size in the area of the AMDG is also crucial for the subsequent mud transport modelling, as the 'sediment' is introduced at a constant concentration within the source element. That element should, therefore, be at a scale analogous to the scale of dispersion at the AMDG otherwise dilution across the source element would obscure the relevant dispersion patterns. This aspect will be discussed further in Section 5.8.

The vertical domain of the 3D model grid was applied as four layers of variable thickness, where thinner higher resolution layers were used near the bed and at the surface for the purposes of coupling the mud transport module (Table 5.3) (see Section 5.8). Layer 3 is much thicker as minimal mud transport occurs within this zone.

Table 5.3 Structure of the vertical domain used in the 3D near-field model of the AMDG.

Layer No. (1=near-bed)	Layer Thickness (m)	Depth at the base of the layer (m)*
4	20	20
3	80	100
2	20	120
1	20	140

*depths correspond to the centre of the model domain

The model bathymetry was generated under the same conditions as that of the regional model described above (Section 5.6.1), but only bathymetry data points coinciding with the model domain were included in the interpolation step.

Model boundary conditions for all 4 open boundaries (north, east, south, and west) were applied as specified current velocities (cross-shore (u) and alongshore (v)) varying in time and constant along a boundary. The boundary condition tidal current velocities were determined from the depth-averaged value, assuming a logarithmic profile in the vertical domain. The applied boundary conditions were derived based on conditions representative of the AMDG flow regimes, including tidal and non-tidal forces; however limitations in the available data and restrictions within the model software constrained the complete replication of all conditions observed. The procedure and explanation of boundary data derivation is described further below.

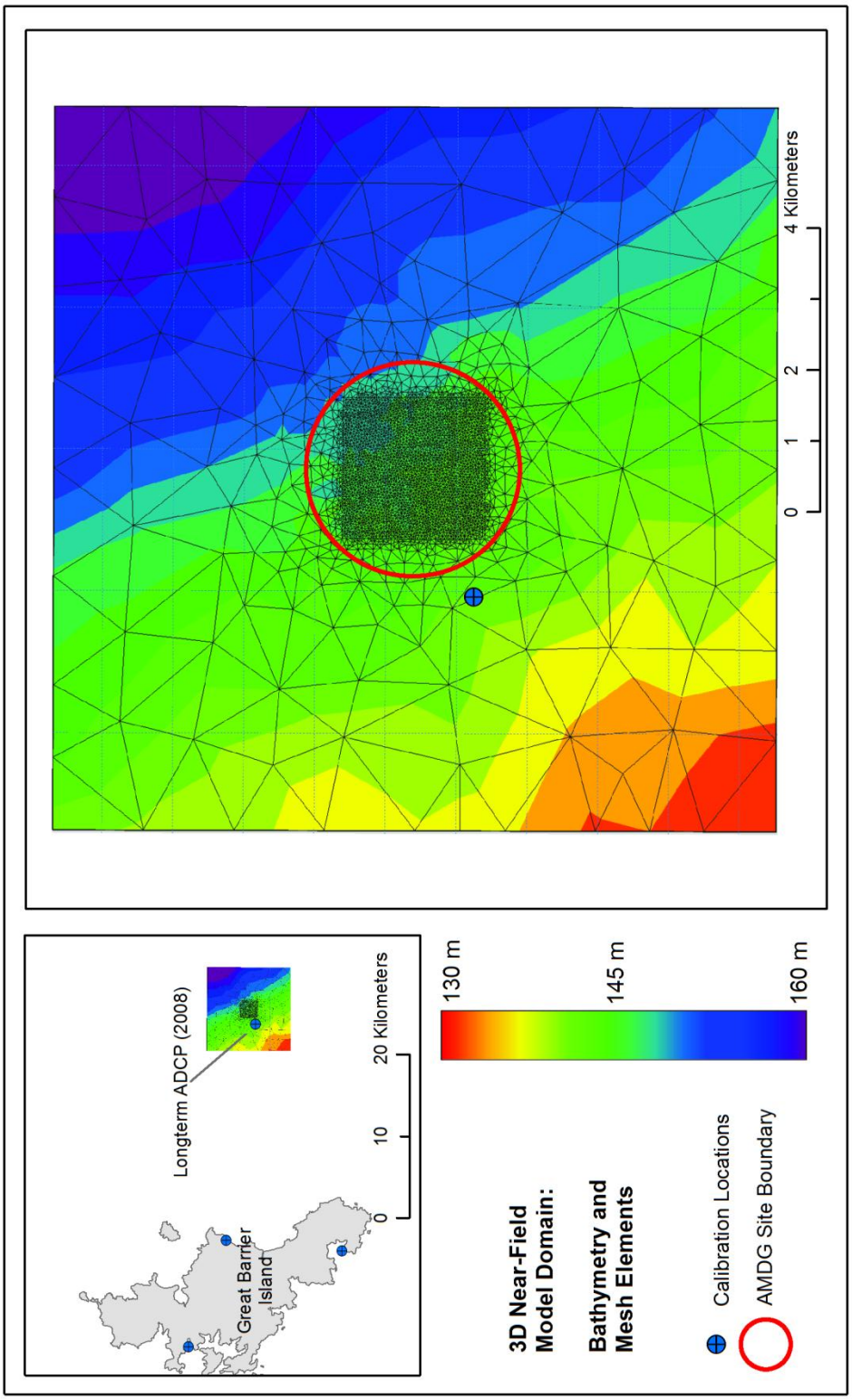

Figure 5.8 Model domain and flexible triangular mesh bathymetry grid used for the 3D near-field model. At the centre a finer resolution mesh element area was applied.

Tidal Boundary Condition

Output extracted from the 2D regional tide model at the locations corresponding to the boundaries of the 3D near-field model show that there is very little observed difference in the tidal currents across the near-field model domain (Figure 5.9a) (MAE =0.004, 0.006, and 0.004, respectively, for E, S, and W relative to N). A linear regression of the modelled tidal elevation from the location of the north boundary (mid-point) of the near-field model to that of each of the other three boundary locations (mid-point) gives R^2-values of 0.99, 0.99, and 1 for the east, south, and west boundaries, respectively (Figure 5.9b). Owing to the small area of the near-field model domain and the high correlations, it is thus considered sufficient to assume a constant flow in space.

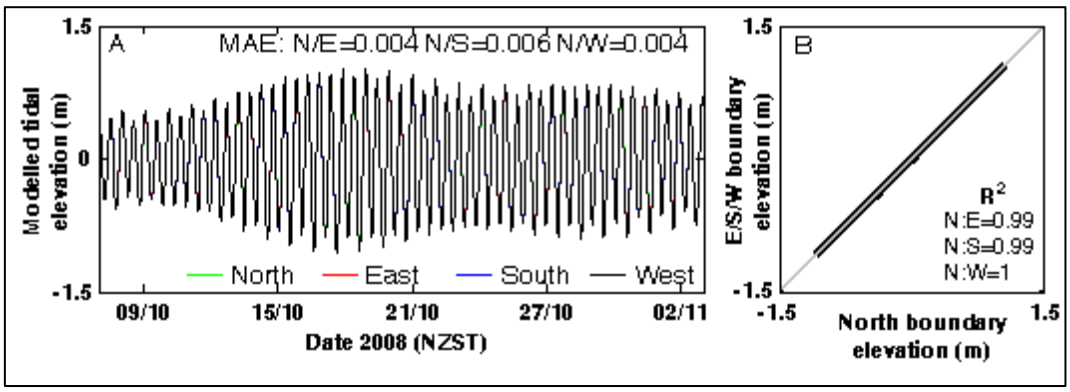

Figure 5.9 (a)Tidal elevation extracted from the output of 2D regional model simulation described in Section 5.6 at locations corresponding to the mid-point of each boundary (north, east, south, and west) of the near-field model domain (see black outlined box in Figure 5.1) with corresponding MAE values for the E, S, and W records relative to the N record. (b) Linear regression and R^2-values of the N boundary elevation versus the E, S, and W boundary elevations.

However, as it was already proven by comparing the output from the regional model to the long-term ADCP record (Figure 5.4), tidal velocities at the location corresponding to the AMDG were not well represented. Therefore, it was determined that the means for optimal representation of the tidal component of flow during the period of interest was through the use of the tidal current signal derived through harmonic analysis of the long-term ADCP record (see Section 3.7), predicted for the disposal operations period (April 2010) (Figure 5.10). These tidal current predictions provided the basis for the spatially constant, temporally varying, boundary condition used to force each boundary of the 3D near-field flow model and to which a non-tidal component was subsequently added. The non-tidal condition is described in detail below.

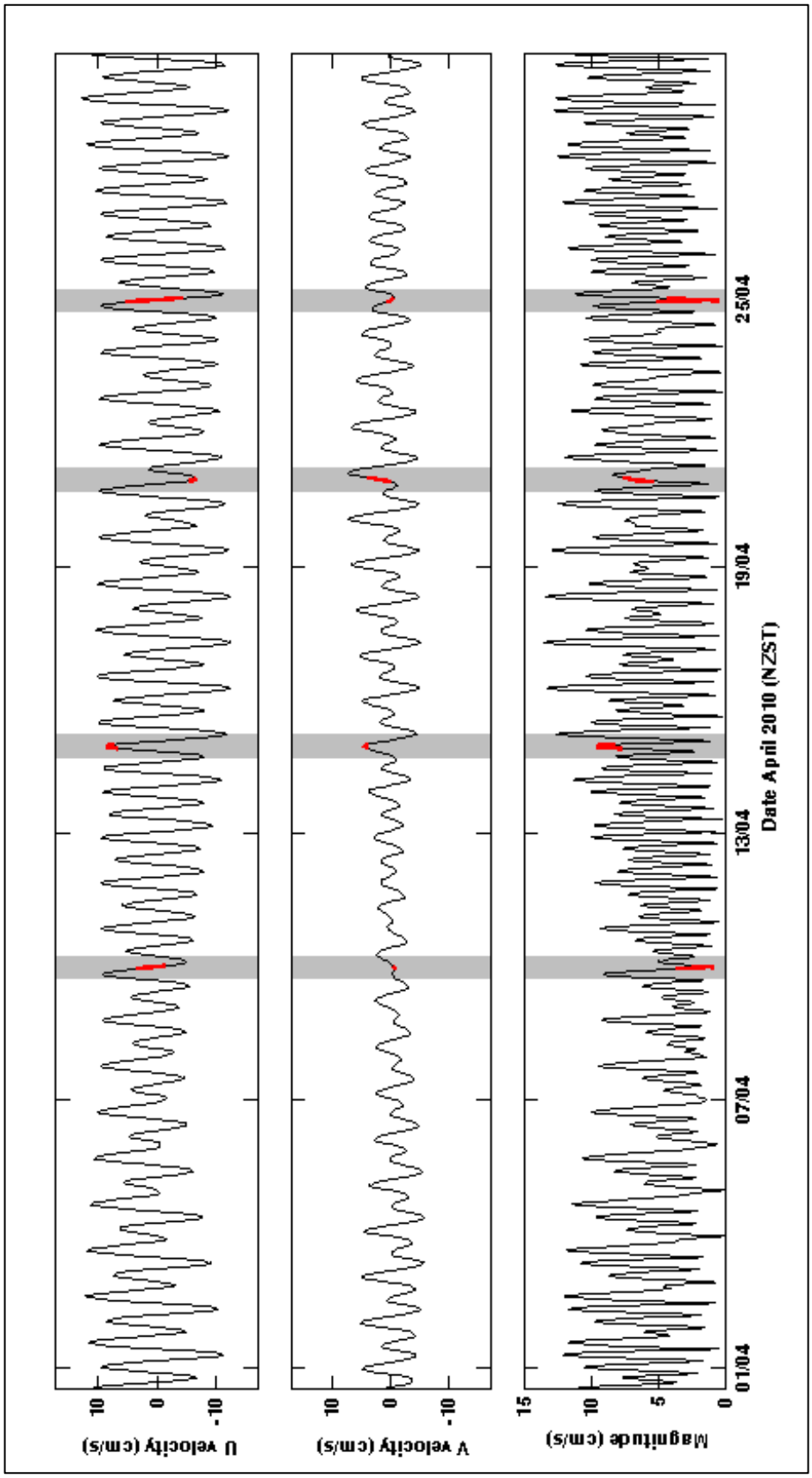

Figure 5.10 Predicted tidal currents for the April 2010 survey period. Survey times are highlighted in red and back-shaded in gray.

Non-Tidal Boundary Condition

Data pertaining to flow conditions during each of the four plume monitoring surveys were only recorded over short periods (~1.5 hours), and not as a continuous stationary record, but as downward-facing ADCP transects varying in location and length. Therefore, it is not possible to derive the non-tidal, or residual component of flow through harmonic analysis as was done in the case of the long-term ADCP record from 2008 (see Section 3.8).

As an alternative approach, the semi-instantaneous residual component was estimated for the period of each plume monitoring survey. The predicted tidal velocity components were first averaged for the period of each survey. Areas highlighted in red in Figure 5.10 show the data periods over which the averaged tidal velocity for each survey day was derived. The averaged values, were then removed from the ambient current velocity (tidal and non-tidal components combined) recorded during each of the four surveys using the downward-facing ADCP. Use of the averaged tidal current value is sufficient because tidal currents do not change greatly over the period of an hour, the approximate length of each survey. The resultant velocities, therefore, represent an estimate of the semi-instantaneous non-tidal flow component for each survey period.

Analysis presented in Chapter 4 (see Section 4.6.2) showed that over the short period of each monitoring survey (~1.5 hours each), the ambient current did not change significantly. Therefore, conclusions regarding the flow conditions on each day were primarily drawn from the examination of one representative transect recorded during each survey. Data from those transects are shown in Figure 4.21 and Figure 4.22. Accordingly, the non-tidal component estimate procedure described above was undertaken using the data from those same transects. Figure 5.11 and Figure 5.12 show the data from transects adjusted to represent the non-tidal component only.

To obtain a single non-tidal component factor for each survey period, for the eventual addition to the near-field boundary condition, the ‘non-tidal’ data along each transect was averaged to give one velocity profile for each survey period (Figure 5.13), followed by vertical averaging. All tidal and non-tidal data derived for each survey period is presented in Table 5.4.

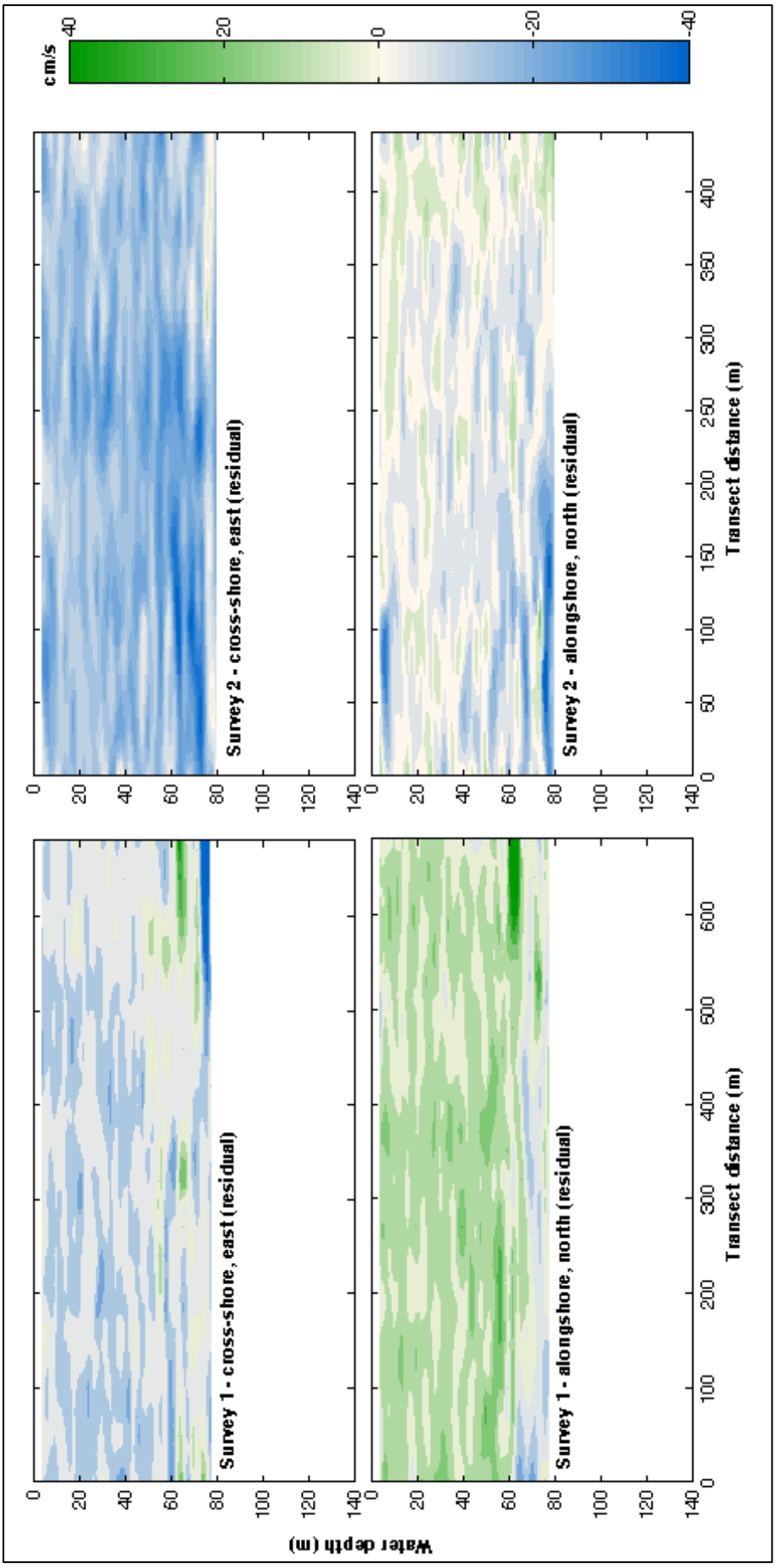

Figure 5.11 Estimated residual (non-tidal) currents for ADCP transects shown in Figure 4.21 for Surveys 1 and 2.

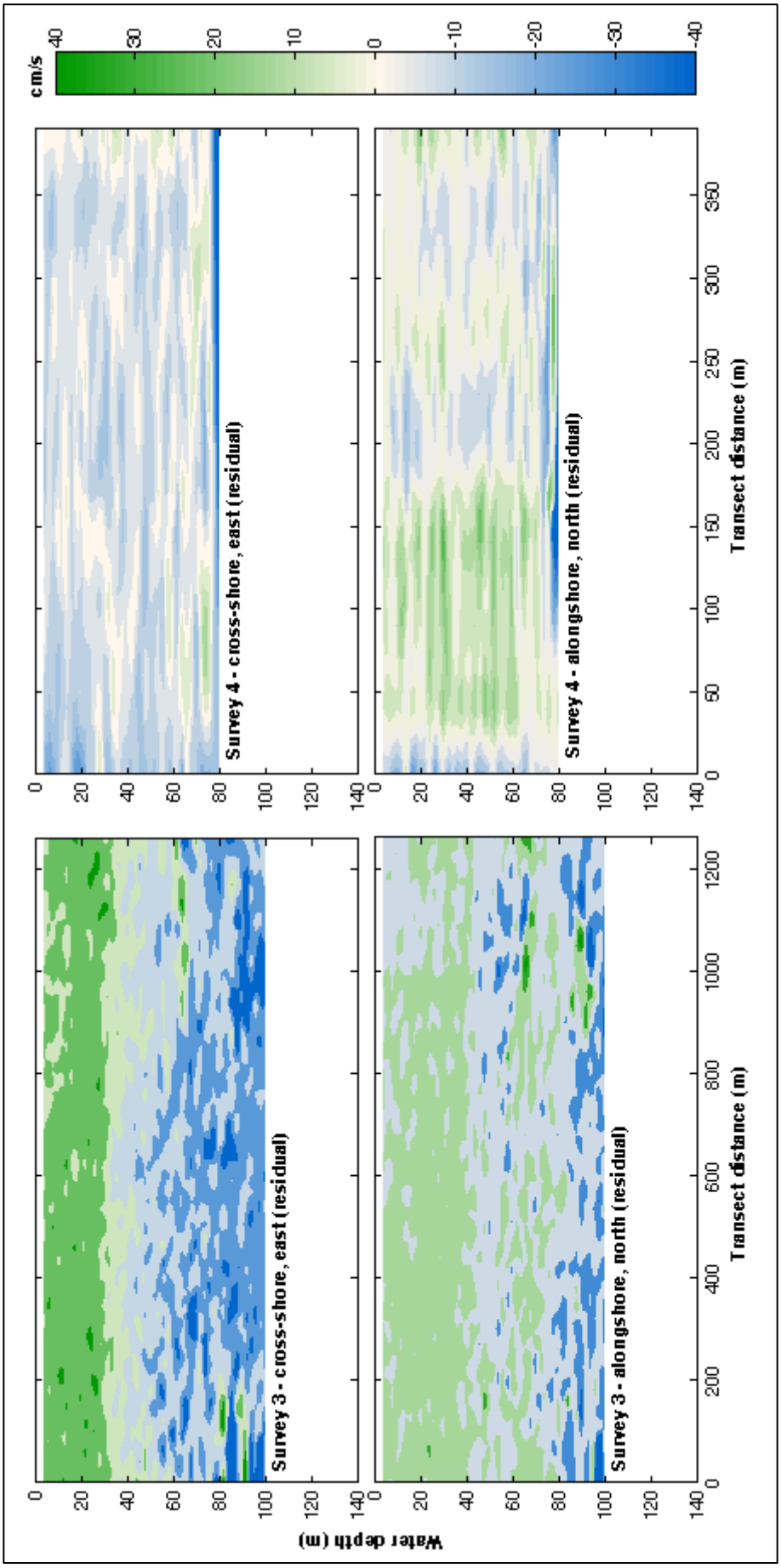

Figure 5.12 Estimated residual (non-tidal) currents for ADCP transects shown in Figure 4.22 for Surveys 3 and 4.

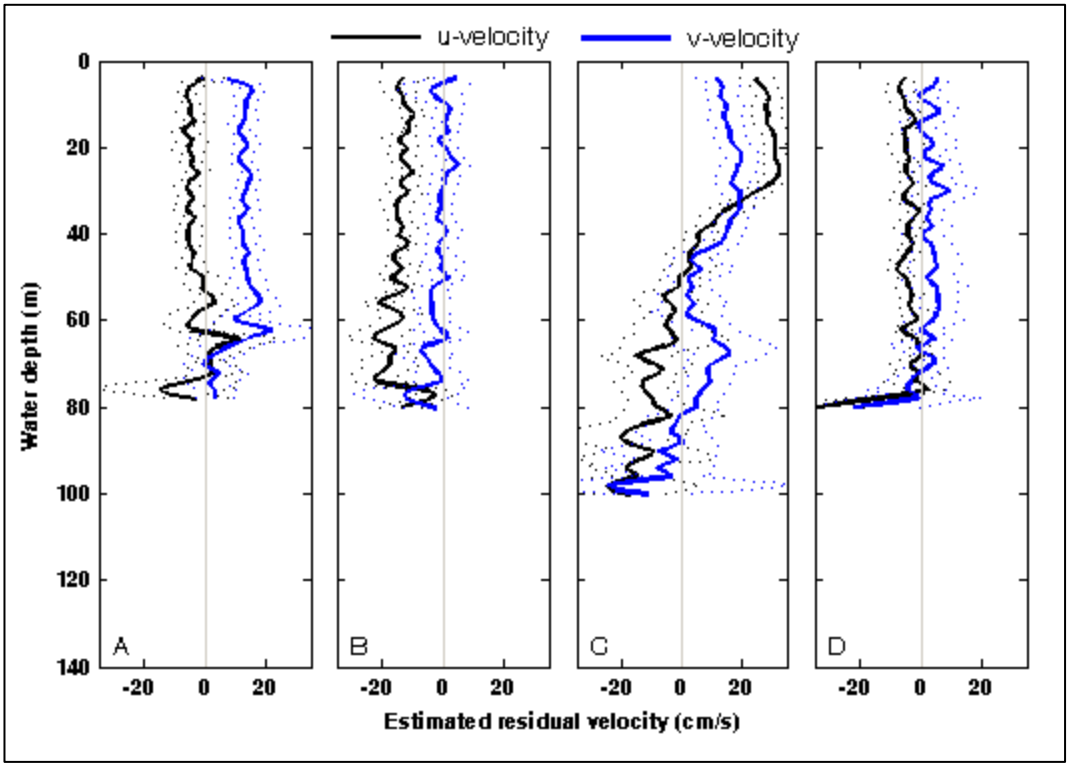

Figure 5.13 Estimated average residual cross-shore (*u*, black) and alongshore (*v*, blue) velocity profiles for Surveys 1-4 (a-d). Averages are based on transects shown in Figure 4.21 and Figure 4.22.

Table 5.4 Details of the ambient current during Surveys 1-4. *P* and *θ* are the current magnitude and direction, respectively.

Survey No.	Depth-averaged tidal component				Depth-averaged residual component*			
	u-velocity (cm/s)	*v*-velocity (cm/s)	*P* (cm/s)	*θ* (deg)	*u*-velocity (cm/s)	*v*-velocity (cm/s)	*P* (cm/s)	*θ* (deg)
1	1.16±1.5	-0.81±0.1	1.41	123	-2.95±4	11.99±1.5	12.34	346
2	7.78±0.6	4.19±0.1	8.84	62	-14.13±3.7	-1.26±2.9	14.19	264
3	-6.73±0.4	1.82±1	6.9	285	4.76±2.3	8.18±2.4	9.46	30.19
4	0.69±3	-1±0.3	1.21	145	-4.36±1.9	2.53±4.8	5.04	59.87

*estimated from ADCP transects shown in Figure 4.21 and Figure 4.22 and the predicted tidal component based on the long-term 2008 ADP record.

Representative Boundary Flows

To approximate a time series for the non-tidal component of flow for April 2010, the four values derived as representative of the residual current during the four survey periods (Table 5.4) were interpolated (piecewise cubic Hermite method) (see red line in Figure 5.14). This time series is only an approximation, but the 4 data points used in the interpolation (black markers, Figure 5.14) represent conditions over a regular interval (~5 days) covering the majority of the month, with only the beginning and end not represented. Residual forcing tends to have a frequency of 5-7 days in the northeast coast region, usually linked to the passing

of local weather systems (Harris, 1985), and in the case of boundary currents, the frequency can be even longer (Sharples, 1997). Hence, the derived time series probably represents the non-tidal component over the disposal period adequately. For the periods outside the survey days, the time series was padded with zeros. The interpolation step included one 'zero' data point several days before the first survey day and several days after the last survey day. This approach was used to allow for a ramp-up of the added residual flow component, which is important for preventing a model crash. Thus, only the period of interest was supplied with the complete magnitude of the non-tidal forcing. The interpolated time series for each current component was then added to the respective predicted tidal current component records (blue line, Figure 5.14). The resultant time series were applied to each boundary of the near-field model to simulate flow conditions during each survey day.

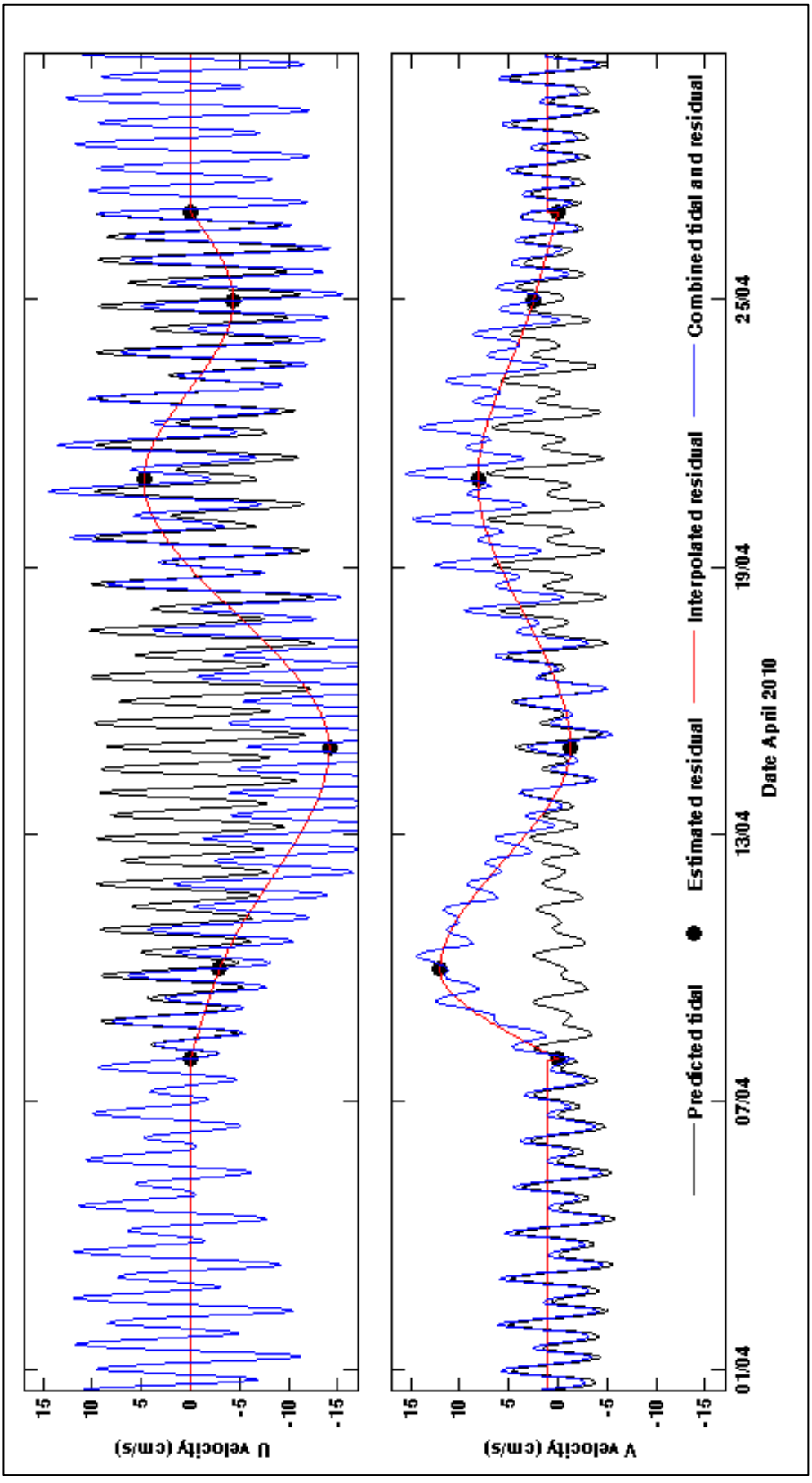

Figure 5.14 Cross-shore (*u*) and alongshore (*v*) components of the predicted tidal current (black), estimated residual current (red with black markers), and the combined tidal and residual current (blue) which is supplied as the boundary forcing for the hydrodynamic models.

5.7.2 Model Comparison and Calibration

The 3D near-field flow model was run over four separate periods corresponding to each of the four plume monitoring surveys undertaken in April 2010 at the AMDG. Each model was forced with the corresponding portion of the boundary condition time series described in the previous section. The four model periods are highlighted in red in Figure 5.15. Each model run included a ramp-up period corresponding to two model days prior to each survey period to allow for flows to stabilise before the period of interest. Details of the model periods are included in Table 5.5.

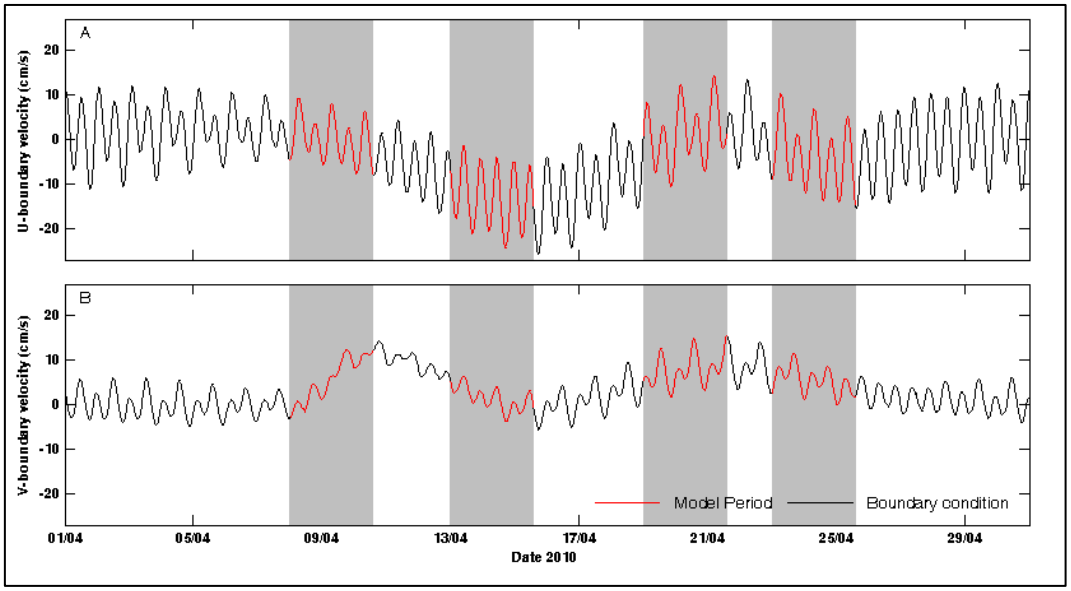

Figure 5.15 Cross-shore (*u*) (a) and alongshore (*v*) (b) current velocity time series of the near-field model boundary condition (black) with model run periods, corresponding to each of the four plume monitoring surveys undertaken in April 2010 including a 2-day ramp-up period prior to each, highlighted in red with gray back-shading.

Table 5.5 Model run periods for the 3D near-field flow model.

Model/Survey No.	Model Time (NZST)*		Period of Interest (NZST)	
	Start	End	Start	End
1	08/4/2010 00:00	10/4/2010 14:00	10/4/2010 00:00	10/4/2010 14:00
2	13/4/2010 00:00	15/4/2010 14:00	15/4/2010 00:00	15/4/2010 14:00
3	19/4/2010 00:00	21/4/2010 14:00	21/4/2010 00:00	21/4/2010 14:00
4	23/4/2010 00:00	25/4/2010 14:00	25/4/2010 00:00	25/4/2010 14:00

*run times include a 2day ramp-up period at the beginning of each simulation

Data observations from the site during April 2010 indicated a baroclinic flow regime, most obviously on the day of Survey 3 (see Section 4.6.2). However implementation of baroclinic conditions in the model was not possible due to

limitations in available boundary forcing data. This lead to the approach described in the previous section, which is applicable to a barotropic situation. Thus the model was set-up in barotropic mode and forced with the boundary condition described in the previous section.

Velocity Profile Structure

As the model was forced with a boundary condition that was synthesized to represent the depth-averaged flow conditions during each period of interest, it is not likely that the model output will vary significantly from the forcing in the depth-averaged sense. However, the model assumes a logarithmic velocity profile near the bed, which is applied according to parameters of the vertical domain. In this case, calibration is necessary to ensure that vertical variation in the velocity output is representative of the conditions at the AMDG.

Loss of data in the lower portion of the water column during the April 2010 plume monitoring surveys due to technical problems precluded velocity profile calibration based on the recorded downward ADCP data. However, since the model requires barotropic profile information and the measurement period of 2008 showed essentially barotropic conditions, the long-term ADCP record described in Chapter 3 of this thesis was used for tuning the modelled velocity profile.

Residual current analysis showed a 2 – 4 cm/s decrease in the mean residual velocity profile from near-surface to near-bed (Figure 3.20) for both the cross- and alongshore current components. Mid-depth (~40-80 m) velocities were, however, several cm/s faster than those at near the surface. Although it is not possible to recreate the mid-depth maximum current through simple calibration adjustments, it was possible to control the velocity range between the near-surface and near-depth regions.

Calibration parameters in the 3D model are similar to those in the 2D model described above: eddy viscosity (horizontal and vertical) and bed resistance. Using the Survey 1 model period, a range of calibration parameters was tested to identify the settings needed to achieve the optimal representation of the velocity profile. The model was insensitive to adjustments in both the horizontal and

vertical eddy viscosity parameter and, therefore, the default settings for constant eddy viscosity parameters were chosen because use of a constant formulation decreased the computation time. Adjustment of the bed resistance using the quadratic drag coefficient formulation produced the most sensible results in terms of the vertical profile for period 1. Model periods 2-4 were then simulated to validate the applied settings.

Details of the model settings are shown in Table 5.6. Figure 5.16 through Figure 5.19 illustrate the 3-dimensional flow conditions during the period of interest for each model run following velocity profile calibration. Time series of the model output from each layer (plots (a) cross-shore and (b) alongshore in each figure) show an acceptable relationship to the original depth-averaged boundary condition (i.e. a 2 – 4 cm/s range between the surface layer (4) and the bed layer (1)). Contour plots (plots (b) cross-shore and (d) alongshore) of the vertical velocity profiles further illustrate that the current structure for each simulation is sensible.

Table 5.6 Numerical parameters for the 3D near-field flow model of the AMDG and surrounding area.

Parameter	Value
Time step	10 sec
Number of time steps	22320
Model start time	See Table 5.5
Bed resistance	Quadratic drag coefficient = 0.05
Horizontal eddy viscosity	Constant eddy formulation, constant in domain = 0.2 m^2/s
Vertical eddy viscosity	Constant eddy formulation, constant in domain = 0.2 m^2/s
Coriolis Forcing	Constant in domain
Grid type	Flexible mesh (triangular elements)
Max element area	Main area: 1 km^2; AMDG: 1250 m^2
Grid orientation	True north 0°
Grid origin	1846524.93 m E, 5984371.89 m N, NZTM
Grid latitude (centre)	-36°
North boundary	Specified velocities (synthesized conditions, see Section 5.7.1)
East boundary	Specified velocities (synthesized conditions, see Section 5.7.1)
South boundary	Specified velocities (synthesized conditions, see Section 5.7.1)
West boundary	Specified velocities (synthesized conditions, see Section 5.7.1)

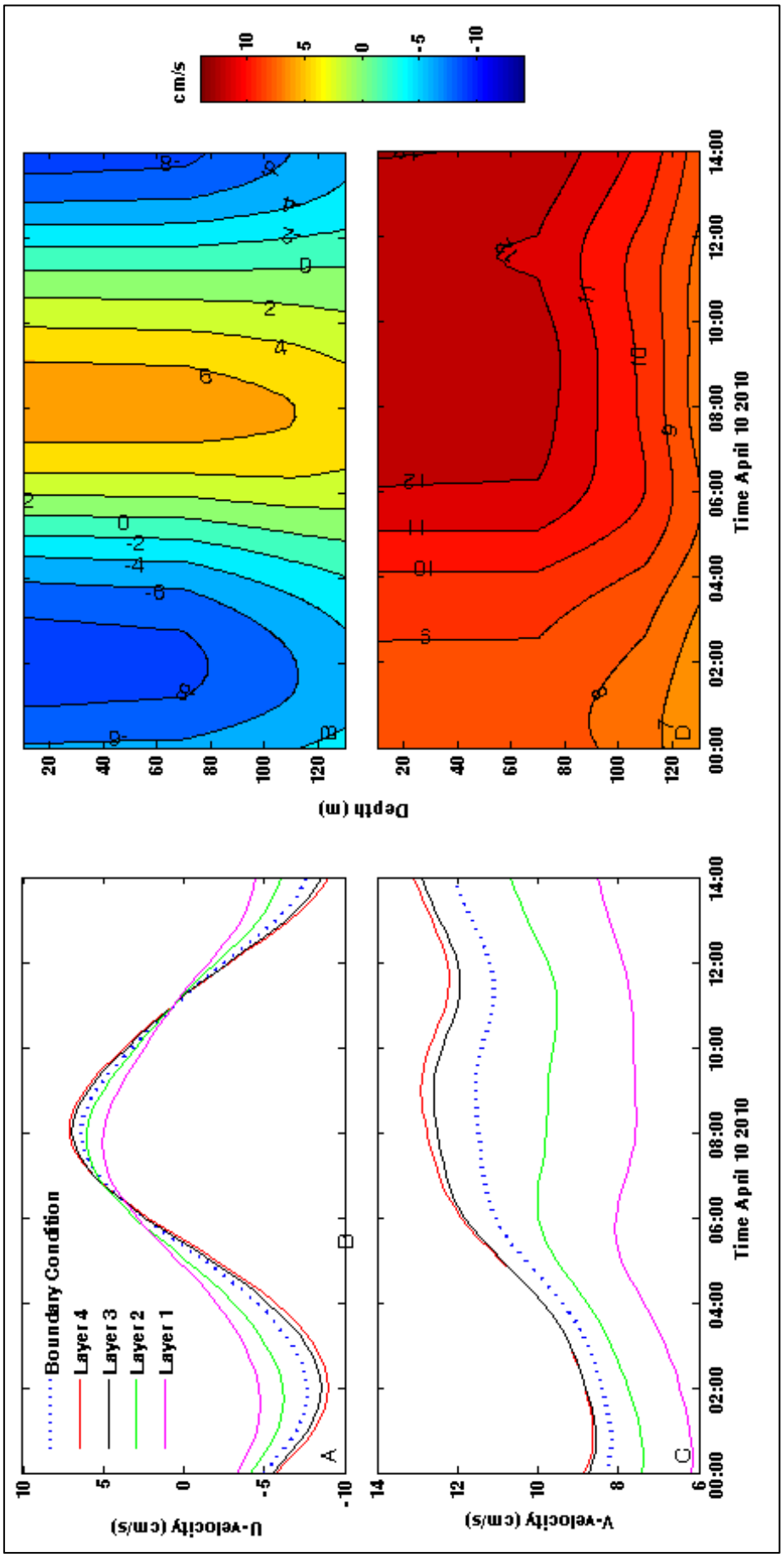

Figure 5.16 (a & c) Time series of cross-shore (*u*) and alongshore (*v*) current velocities from model output of each layer at the centre of the domain (solid lines) and the boundary condition (dashed line) for the model period corresponding to Survey 1 undertaken on 10 April 2010. (b & d) Contour plots of the cross-shore and alongshore model output current velocities based on the four vertical layers of the near-field model for the same period shown in a and c.

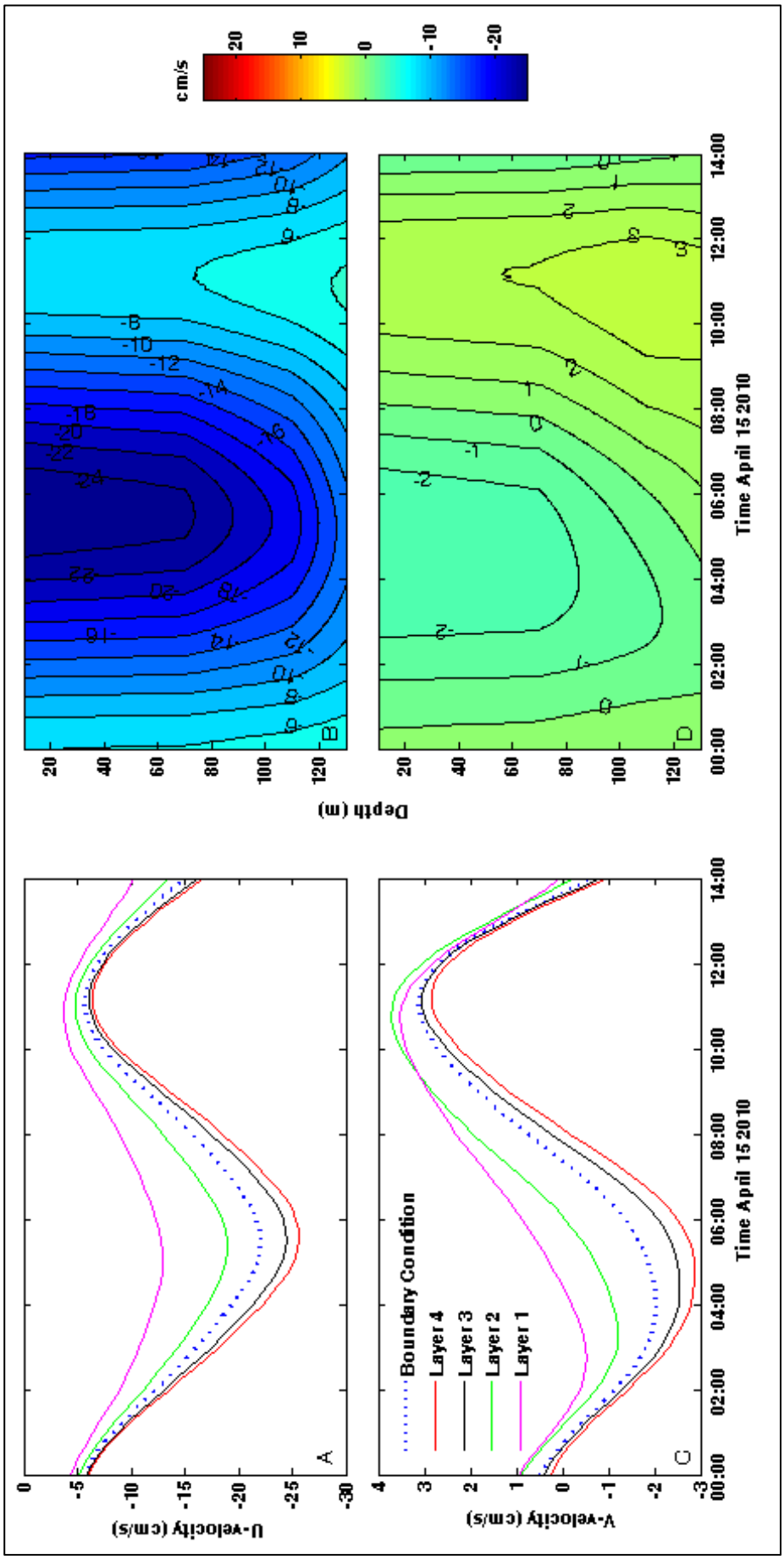

Figure 5.17 (a & c) Time series of cross-shore (*u*) and alongshore (*v*) current velocities from model output of each layer at the centre of the domain (solid lines) and the boundary condition (dashed line) for the model period corresponding to Survey 2 undertaken on 15 April 2010. (b & d) Contour plots of the cross-shore and alongshore model output current velocities based on the four vertical layers of the near-field model for the same period shown in a and c.

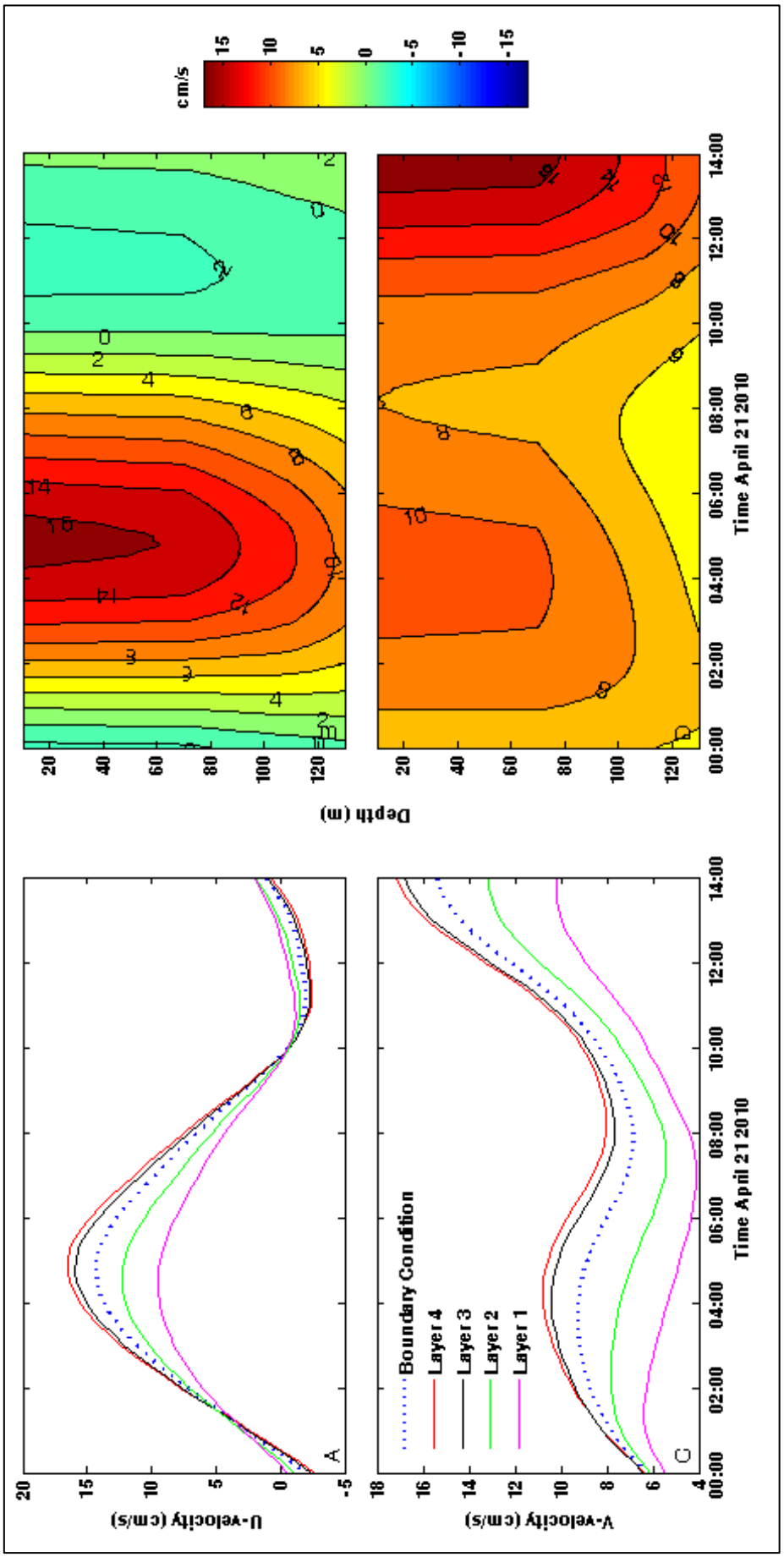

Figure 5.18 (a & c) Time series of cross-shore (*u*) and alongshore (*v*) current velocities from model output of each layer at the centre of the domain (solid lines) and the boundary condition (dashed line) for the model period corresponding to Survey 3 undertaken on 21 April 2010. (b & d) Contour plots of the cross-shore and alongshore model output current velocities based on the four vertical layers of the near-field model for the same period shown in a and c.

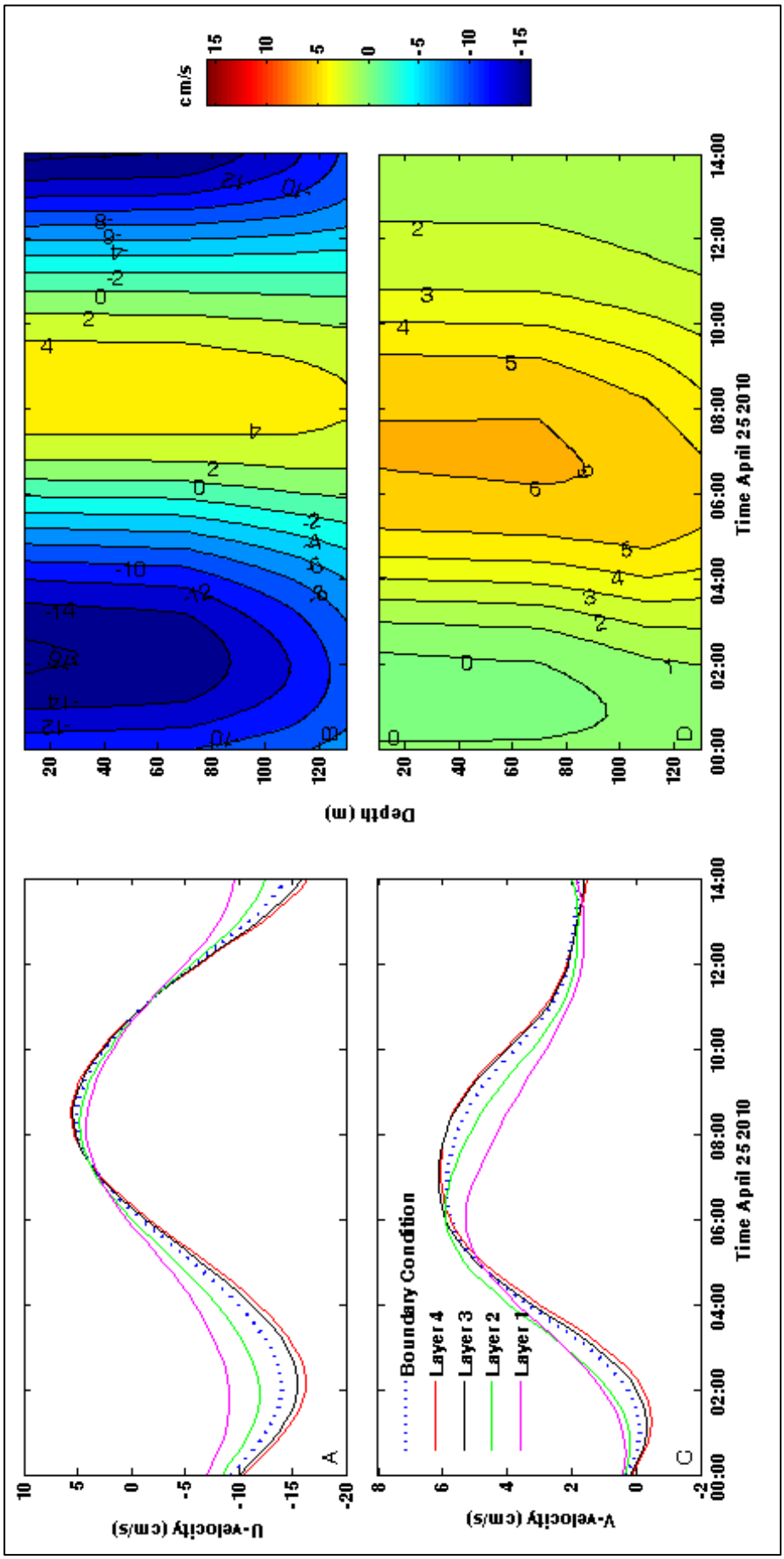

Figure 5.19 (a & c) Time series of cross-shore (*u*) and alongshore (*v*) current velocities from model output of each layer at the centre of the domain (solid lines) and the boundary condition (dashed line) for the model period corresponding to Survey 4 undertaken on 25 April 2010. (b & d) Contour plots of the cross-shore and alongshore model output current velocities based on the four vertical layers of the near-field model for the same period shown in a and c.

Depth-Averaged Current Validation

Time series plots of output from each model layer in the 4 simulations indicated that the current velocity at the centre of the model domain represents the boundary condition adequately in magnitude and frequency, but for a more complete assessment, the model, output was depth-averaged and again compared to boundary condition to verify that instabilities did not affect the model output. Figure 5.20 and Figure 5.21 show the results of comparisons from each of the four model runs for both the cross-shore and alongshore current components along with the corresponding MAE values for each velocity component. The time series plots indicate that in all four cases, only slight variations in the amplitude occurred between the model results and the respective boundary condition. R^2-values are close to 1 in all cases, however, errors due to a systematic bias are evident especially in the case of the period 1 *v*-velocity current component. The calibration parameters used gave the optimum results, so improvement to the error would be difficult. The magnitude of error associated with a MAE value of 0.63, such as that of the period 1 *v*-velocity case, is nonetheless small, which suggests that the model is relatively stable and the intended spatially constant flow conditions are simulated adequately.

Flow Conditions

The plume monitoring surveys were undertaken in all cases between the hours of 10:00 am and 12:30 pm on each survey day. Details of the average flow velocities at the centre of the model domain during that period for each model run are shown in (Figure 5.20). Flow direction and magnitude for each model layer and simulation period are shown in Figure 5.22. The modelled current was directed towards the NNW, W, NE, and NW during simulations 1-4, respectively. Of the average velocities for each simulation period, a maximum current speed of 15 cm/s occurred during period 2 and a minimum of 6 cm/s occurred during period 4, while the current magnitude was approximately 12 cm/s during both periods 1 and 3. As was previously shown, in all cases the current magnitude decreased by 2 – 4 cm/s from the surface layer to the bed layer, with exception of period 2, when the range was closer to 6 cm/s. A slight vertical phase shift was apparent in all simulations except during period 3.

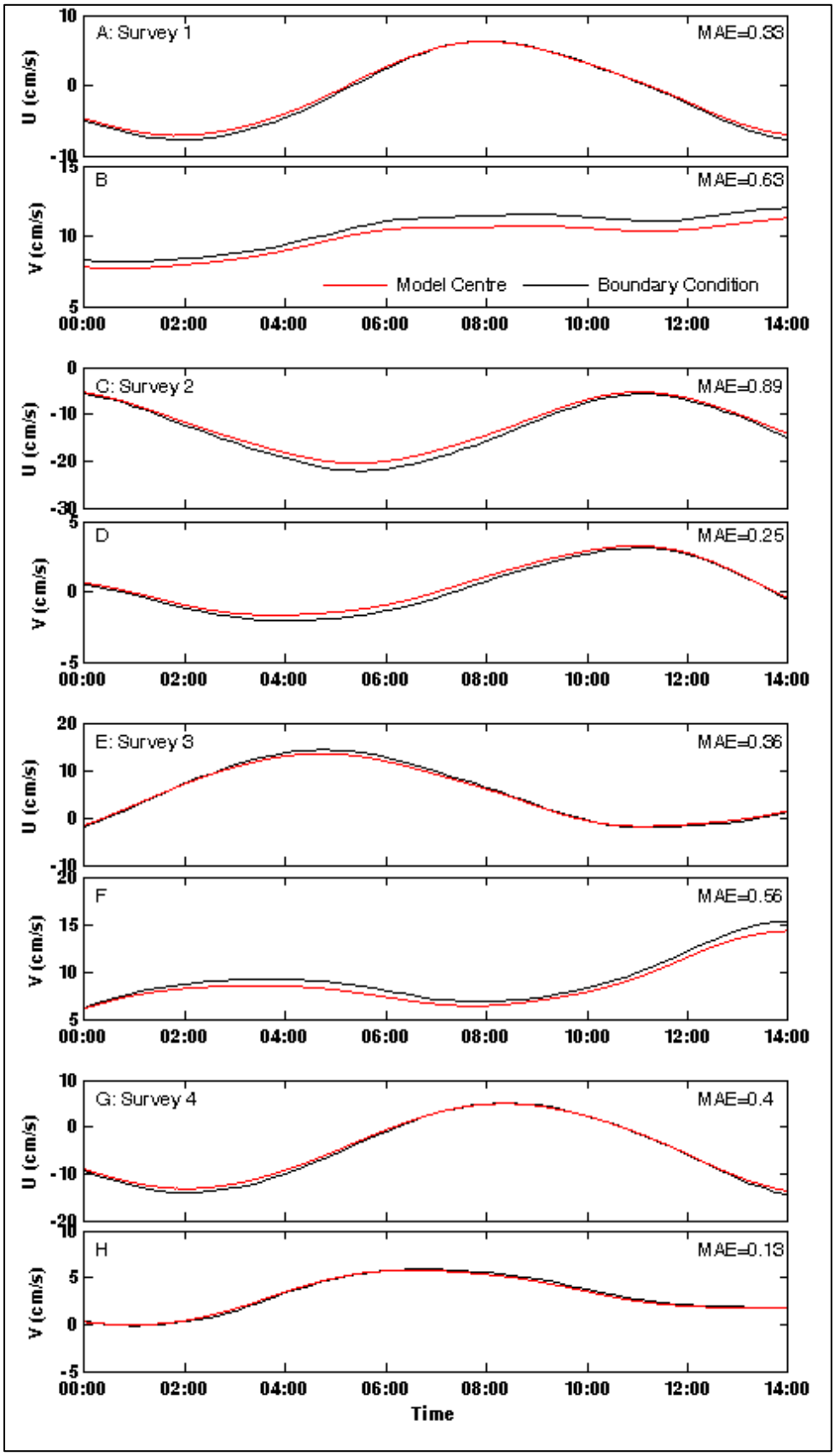

Figure 5.20 Cross-shore (*u*) (a, c, e, & g) and alongshore (*v*) (b, d, f, & h) current velocity of the boundary condition (black) and depth-averaged model output at the centre of the domain (red) for each of the model period corresponding to the four plume monitoring surveys undertaken in April 2010. Ramp-up period prior to each modelled survey period is not included. MAE values are included for each velocity component.

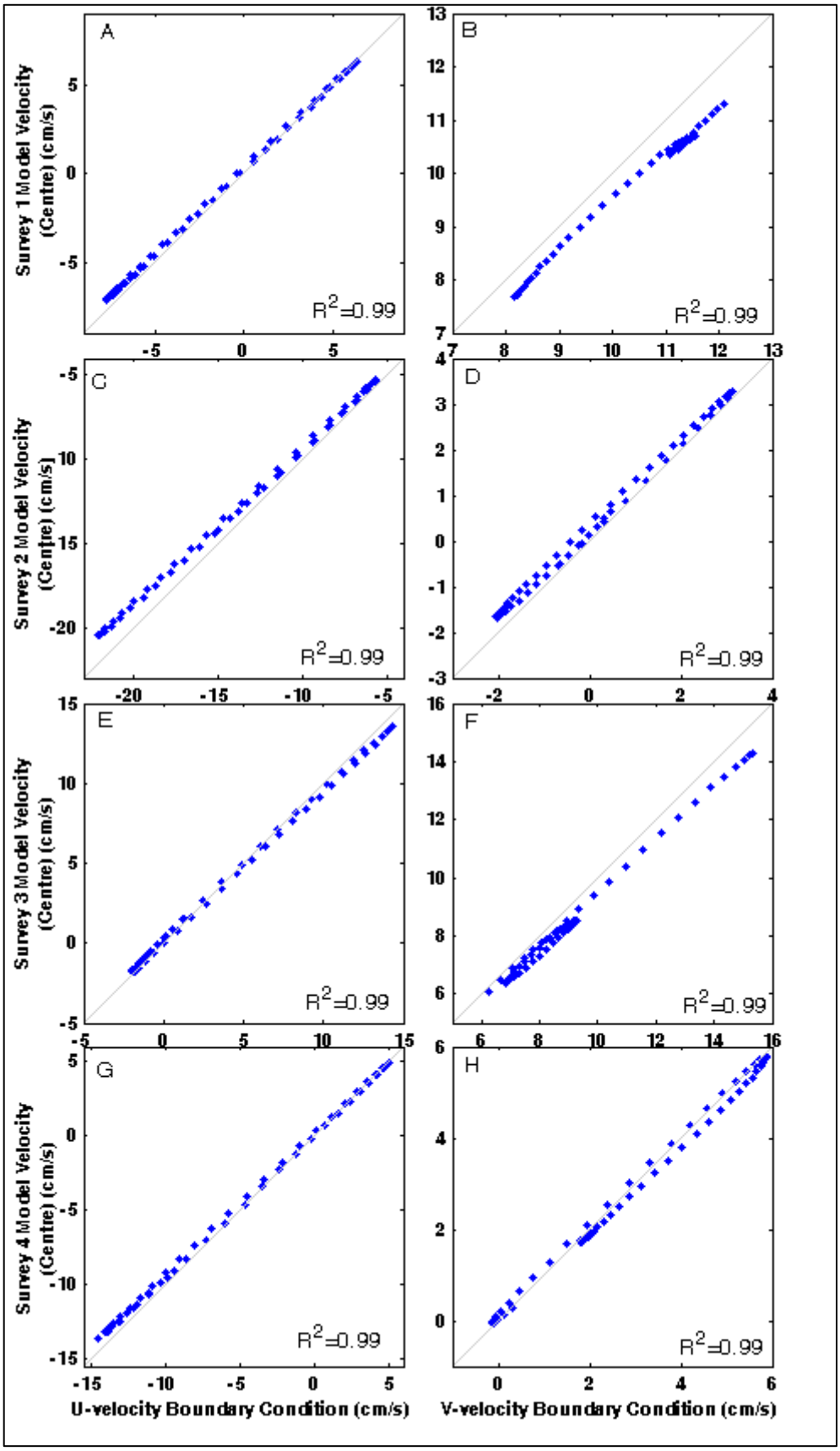

Figure 5.21 Scatter-regression plots and corresponding R2-values of the boundary condition and respective model output from the centre of the domain for the cross-shore (*u*) (a, c, e, & g) and alongshore (*v*) (b, d, f, & h) current velocities of each model period corresponding to the 4 plume monitoring surveys undertaken in April 2010.

Table 5.7 Details of model output flow velocities for each simulation period

Model Layer No.	Model Period							
	1		2		3		4	
	u **(+, east)**	***v*** **(+, north)**	***u*** **(+, east)**	***v*** **(+, north)**	***u*** **(+, east)**	***v*** **(+, north)**	***u*** **(+, east)**	***v*** **(+, north)**
1	-1.09	11.13	-15.54	-0.42	6.81	9.63	-5.08	3.21
2	-0.93	10.98	-14.83	-0.15	6.58	9.36	-4.81	3.29
3	-0.13	9.10	-11.67	1.01	5.35	7.28	-3.47	3.29
4	0.11	7.37	-8.45	1.37	4.31	5.79	-2.59	2.96

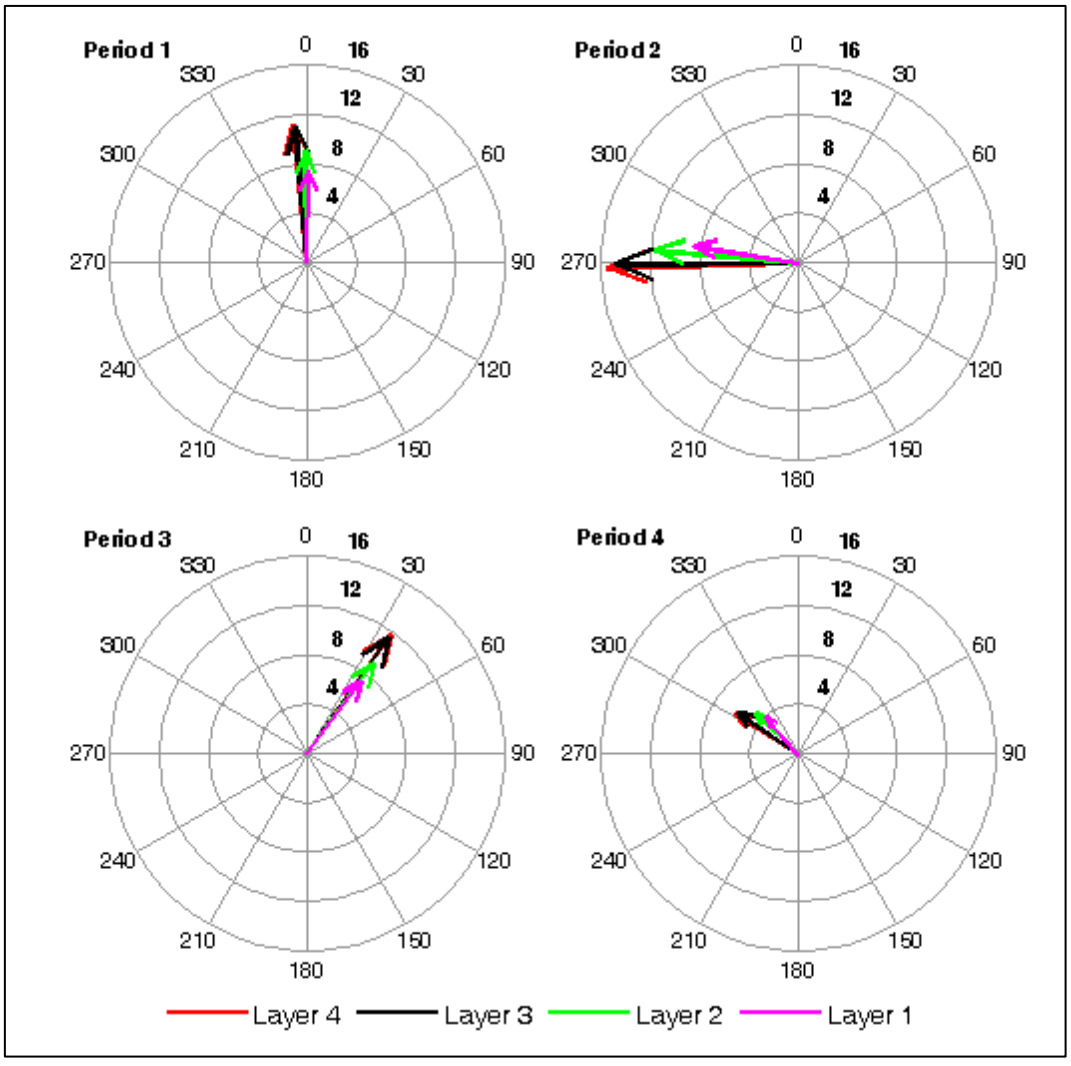

Figure 5.22 Rose plots of the model output flow conditions for the period corresponding to 10:00 am to 12:30 pm on each survey day for model layers 1 (near-bed, magenta) to 4 (surface, red).

5.7.3 Discussion

Simulated flows during each model run exhibited the general characteristics, both in magnitude and direction, of the current regime observed during each of the corresponding plume monitoring surveys (see Section 4.6.2). The results also

correspond surprisingly well to the plume dispersion characteristics derived in Section 4.10.1 (summarised in Figure 4.46). Differences between the general dispersion characteristics and the model output flow conditions can be attributed to the barotropic model set-up, whereas the observed situation was baroclinic.

Data collected during the plume monitoring surveys indicated the baroclinic situation. ADCP current data was limited in the lower part of the water column due to power problems with the ADCP system, but baroclinic characteristics were also observed in CTD data and ADCP backscatter data, which covered a larger portion of the water column. In fact, CTD casts showed that the missing portion of ADCP current data appears to have corresponded with the location of the main pycnocline (80 m) on Surveys 1, 2, and 4. This is probably not a coincidence as the strong density gradient so far from the transducer head may have hindered the already attenuated acoustic signal. During Survey 3, however, the pycnocline was located closer to the transducer head (30 m) and most likely had less effect on the transmit/receive paths of the signal. The result was that more of the water column was recorded and the 2-layer structure was more apparent during Survey 3.

The non-tidal component of the boundary condition was essentially derived from the depth-averaged current velocity values from the shortened ADCP records. Therefore, the modelled flow conditions only represent the portion of the water column recorded by the ADCP. Even though a baroclinic situation was indicated in all four cases, only during Surveys 1 and 4 was the dispersion direction significantly different between the top half and the bottom half of the water column. In those cases, the model flows reflect patterns in the upper half of the water column only as seen by comparing Figure 4.46 to Figure 5.22. The implications of this is that after coupling with the mud transport model, dispersion simulations would not be representative of the situation in the lower half of the water column, and would over-estimate the transport in the direction of the flow within the upper half.

This may only be problematic in the case of Survey 4 where the dispersion magnitude was essentially equal in the upper and lower halves of the water column. The output flow conditions described here would, therefore, under-estimate dispersion magnitude and give an incorrect prediction of the dispersion

direction in the lower half of the water column. During Survey 1, however, dispersion was minimal in the lower half of the water column. The vertical structure of the output flow conditions are consistent with this pattern and would only be inaccurate in direction, which is less important in the case of a small observed dispersion magnitude.

Dispersion during Surveys 2 and 3 appeared to follow a barotropic situation in direction, with vertical differences only manifesting as a reduced magnitude with depth. In those cases, despite the lack of baroclinic conditions in the model, the output flow conditions can be expected to simulate the correct dispersion characteristics after coupling with the mud transport model reasonably well.

Overall, the 3D model will not be able to simulate the situation during each survey period exactly, but the flow output can be expected to influence dispersion in a representative way, such that errors will mainly exist in the lower half of the water column and predominantly involve directional inaccuracies. Dispersion in the lower half of the water column was observed to be minimal compared to the upper half, so the implications of the failings of the model are not expected to be important.

Model Flow Mechanisms

The distinction between the forcing mechanisms incorporated into the model is only addressed as tidal or non-tidal due to limitations in the type of data available. However, under the classification of non-tidal or residual forcing, several types of mechanisms have been suggested as important drivers, such as winds, boundary currents, and coastal trapped waves.

This study did not obtain of the type of field datasets necessary to distinguish the presence of coastal-trapped waves and as such their contribution at the AMDG cannot be addressed in the model. Analysis of the long-term ADP record indicated that the residual forcing was dominated by a southeasterly flowing current during the 2008 measurement period. This was attributed to the East Auckland Current, the boundary current which is known to flow along, and sometimes over, the shelf margin of the northeast coast of New Zealand's North Island. During the April 2010 monitoring period, information on distinct forcing mechanisms was limited,

but analysis indicated that the residual component was more variable, directed northwest and southwest during Surveys 1 and 2, respectively, and northeast during Surveys 3 and 4. Lack of a southeasterly directed component and the significant changes in direction over a short temporal scale is consistent with the passing of local weather systems. This suggests that wind forcing may have been the dominant non-tidal forcing mechanism. Therefore, the residual component incorporated into the model presented above, is most likely predominantly the result of wind-driven and tidal currents, however, other unresolved mechanisms may have also had a role.

5.8 A Three Dimensional Mud Transport Model

Disposal of dredged material at the AMDG was simulated for the model periods, which corresponded to each survey, by coupling the relevant sediment transport calculations to the designated flow conditions. To do this, the Mud Transport Module was enabled within the MIKE 3 FM Hydrodynamic Module. Unless otherwise stated, the flow conditions used to drive the mud transport simulations were those reported in the previous section and as such, will not be described below.

5.8.1 Testing the Model Functionality for Disposal Simulations

As previously described in Chapters 2 and 4, it is well known that dredged material disposed at sea behaves both dynamically and passively, depending on the time after disposal and the distance from the disposal location. It was crucial, therefore, to test the ability of the mud transport module to accurately simulate both behaviours.

The Dredging Dialog within the Mud Transport Module, as evidenced by the name itself, was originally designed to simulate the ‘spill’ that typically occurs during dredging activities. Such spill can either occur at the dredging location, owing to the loss of sediment due to the mechanical actions of the dredger, or at the surface due to overflow losses at the holding vessel. The type of material typically associated with this type of ‘spill’ is a fluid-like slurry that is susceptible to entrainment, where the material behaves mostly passively or under the

influence of the individual grains or floc properties. Aggregates are not usually part of the 'spill' because they are typically trapped within the dredging bucket.

In typical disposal activities, it has been shown that only a small percentage of the material disposed acts passively, or under the influence of the individual grain or floc properties. The majority of the material descends dynamically, due to its negative buoyancy, at a rate much greater than the typical settling velocity of the individual grains and flocs contained within the descending load. This dynamic settling velocity can be thought of as the 'bulk' settling velocity. For this process, it was unknown whether the options available within the Dredging Dialogue were applicable for true disposal operations, where a large quantity of material is inserted into the water column at the surface, almost instantaneously, as in the situation with a split-hull hopper. No published research using the Mud Transport Module via the Dredging Dialog to simulate dredge disposal was available, so a series of tests were undertaken to determine its applicability.

To simulate spill, the main parameter for defining the behaviour of the material is the settling velocity. It is also possible to indicate whether the material behaves as sand or mud. For the tests, 5 disposal scenarios were run:

1. One *mud* fraction with a settling velocity representative of individual grains or flocs;
2. Two *mud* fractions – 1 with a settling velocity representative of the dynamic aggregate portion of the disposed load, and 1 with a slightly lower settling velocity representative of the dynamic jet of material having a lower negative buoyancy than the aggregate portion;
3. Three *mud* fractions – 1 and 2 the same as in scenario 2, and the 3rd with a settling velocity representative of the individual grains or flocs, as in scenario 1;
4. Four *mud* fractions – 1-3 the same as in scenario 3, and the 4th with a slightly lower settling velocity, intended to represent individual grains or flocs with a lower mean grain size;
5. Five fractions – 1-4 the same as in scenario 4, and the 5th designated as *sand* with a settling velocity representative of individual grains.

Details of the applied settings used in the test scenarios are included in Table 5.8. The results of the disposal scenarios are shown in Figure 5.23.

Table 5.8 Details of Dredging Dialog test scenarios.

Scenario No.	Behaviour	Material	Settling velocity (m/s) (Fraction No.)				
			1	2	3	4	5
1	Individual	Mud	0.0005	-	-	-	-
2	Bulk	Mud	1	0.6	-	-	-
3	Bulk + Individual	Mud	1	0.6	0.0005	-	-
4	Bulk + Individual	Mud	1	0.6	0.0005	0.0003	-
5	Bulk + Individual	Mud + Sand	1	0.6	0.0005	0.0003	0.03

The test scenarios were not designed to produce field-calibrated model results, rather, the purpose was to examine the function of the model with respect to a range of different fraction types and combinations, with a special focus on fractions that did not behave as expected and, therefore, that the model was, presumably, not specifically designed to simulate. In Scenario 1, all the material discharged into the model domain was given a settling velocity corresponding to a medium silt particle (5 Φ / 30 µm). Even though the material was added at a very high rate, suggesting that in reality, the material would have a high negative buoyancy and, thus, would settle to the seabed very quickly, modelled sediment concentrations 3 minutes after discharge were highest near the surface (Figure 5.23). This result shows that the model relies predominantly on the settling velocity parameter, rather than the discharge rate, for determining the vertical position of the discharged material.

Scenario 2 was used to determine whether the model could accurately simulate the movement of the dynamic components of the disposed load. To achieve the rapid descent associated with the dynamic components, high settling velocities were assigned. The profiles shown in Figure 5.23 indicate that within 3 minutes after the discharge, both of the dynamic fractions (F1 and F2) had reached the seabed, suggesting that the enhanced settling velocities do not destabilise the model. Scenarios 3 and 4 were designed to determine whether the behaviour of the dynamic fractions were consistent after the addition of the non-dynamic fractions (F3 (5 Φ / 30 µm) in Scenario 3; F3 and F4 (6 Φ / 20 µm) in Scenario 4) (Figure

5.23). These scenarios showed that while the dynamic fractions settled rapidly to the bed, the non-dynamic fractions remained at the surface, which is consistent with their low settling velocities. The fifth scenario included the addition of a sand fraction, which was important to test because the material disposed at the AMDG included a small sand component. Three minutes after the discharge, the model results showed that the highest concentration of the sand component (F5 (0.25 Φ / 200 µm)) was located near the surface, but at lower concentrations than the mud fractions (F3 and F4), suggesting that more of the sand fraction had settled to the bed (Figure 5.23). This behaviour is what would be expected based on the difference in settling velocities between sand and mud.

The results of the test scenarios indicate that the Mud Transport Module can support not only simulations of 'spill' due to dredging, but also the bulk settling properties that would be expected of material disposed through a split hull hopper.

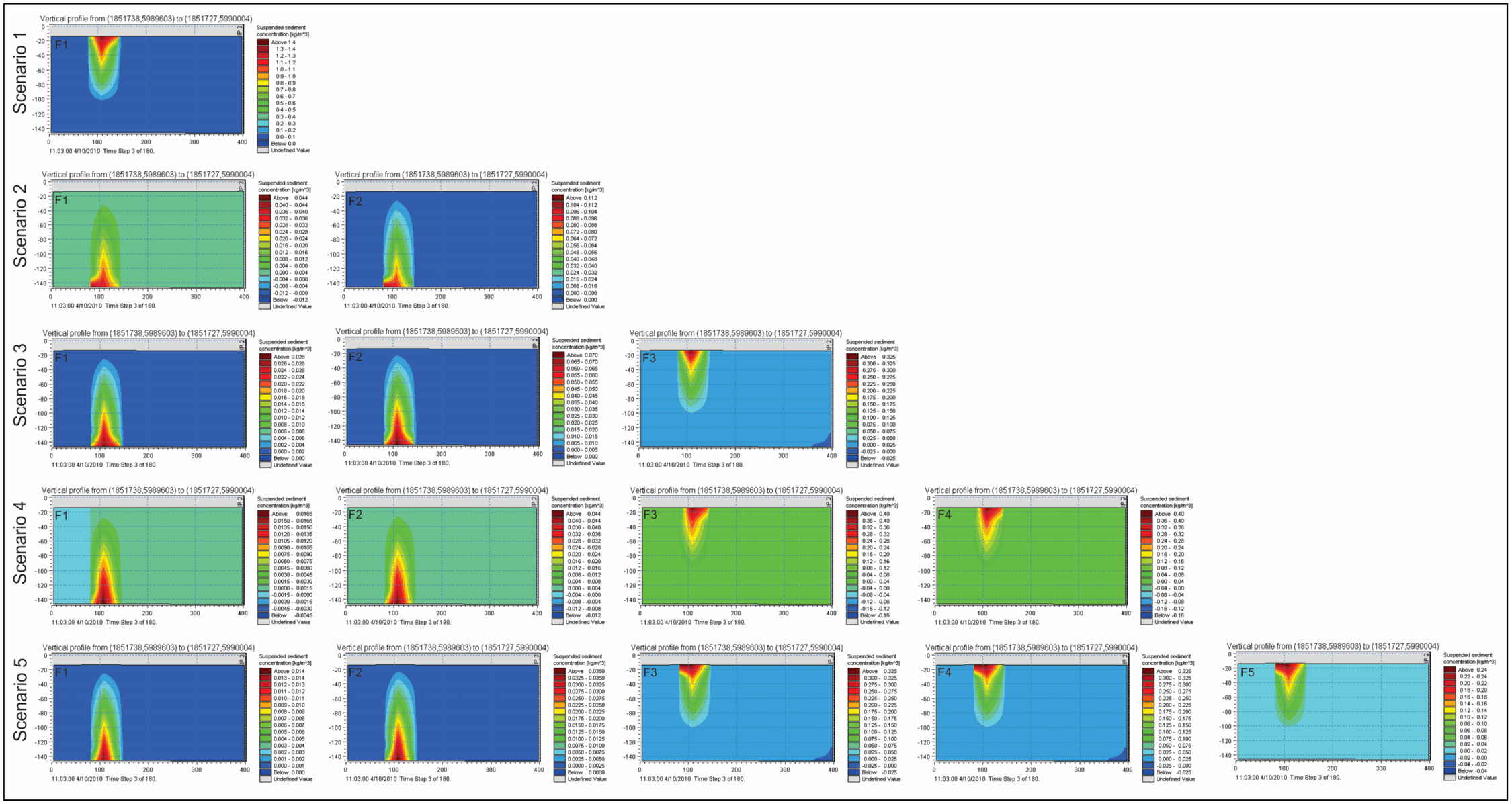

Figure 5.23 Transects of modelled sediment concentration profiles for each fraction in each test scenario. The time step shown corresponds to 3 minutes after disposal. Note the different colour scales. F1 – F5 refer to fractions 1 - 5 in each of the scenarios.

5.8.2 Model Set – Up

Implementation of muddy sediment transport within the 3D model is determined by its physical characteristics, such as the number of size fractions and their distribution, settling velocities, critical erosion/deposition thresholds, and volume and method added. The values applied for such parameters should, ideally, be representative of the situation being modelled, while calibration parameters, such as horizontal and vertical dispersion factors can be used to adjust for optimal results. The model runs were set-up based on the results of the test scenarios described in the previous section, as well as on the conditions of each disposal event monitored during the four surveys described in Chapter 4.

Sediment Fractions

Five fractions, including 2 bulk and 3 individual (2 mud and 1 sand), were defined for the mud transport calculations based on the commonly accepted behaviour of dredged material disposed in open-water (that was also essentially observed during disposal operations at the AMDG), as well as what was known about the characteristics of the material disposed at the AMDG during the plume monitoring surveys of April 2010. Details of the applied sediment fractions used for the modelling are included in Table 5.9.

Table 5.9 Summary of the characteristics of the sediment fractions implemented in the mud transport module of the 3D model.

Fraction No.	Description	Settling velocity (m/s)	Critical threshold for deposition (Nm^{-2})
1	Negatively buoyant bulk fraction; represents dense aggregates (clods)	1	0.2
2	Negatively buoyant bulk fraction; represents 'jet' and is susceptible to entrainment	0.6	0.07
3	Medium silt (20 μm)	0.0003†	0.05
4	Clay (3.9 μm)	0.00001†	0.02
5	Fine sand (200 μm)	0.03†	0.07

† Based on Stokes settling velocity

The bulk fractions (1 and 2) are characterised as such because they represent the material that descends rapidly to the seafloor during the *Convective Descent* phase due to their negative buoyancy. Fraction 1 represents the portion of the negatively buoyant material that is dense due to the presence of larger sediment aggregates.

Fraction 2 represents the 'jet' portion of the descending material. The 'jet' can be characterised as a negatively buoyant slurry that is susceptible to entrainment at the perimeter, but not within the body of the jet. The sediment grains within those fractions do not behave as individual particles; rather, they behave with bulk characteristics. The settling velocity was chosen to be 1 m/s and 0.6 m/s for fractions 1 and 2, respectively, based on field observations described in Chapter 4. Fractions 3 – 5 represent material that acts with the properties of the individual grains or flocs and were designated as medium silt (20 µm), clay (3.9 µm), and fine sand (200 µm), with Stokes settling velocities of 0.0003 m/s, 0.00001 m/s, and 0.03 m/s, respectively.

The critical threshold for deposition is the minimum shear stress required to maintain a particle in suspension. As fractions 1 and 2 do not behave passively or as individual grains/flocs, higher threshold values (0.2 and 0.07 Nm^{-2}) were chosen to ensure that under most flow conditions, the material would settle to the seabed. Fractions 3 and 4 were assigned progressively lower thresholds (0.05 and 0.02 Nm^{-2}) to represent the reduced shear stress associated with a progressive decrease in grain size and Fraction 5 was assigned a threshold of 0.07 Nm^{-2}, which matches the jet component (Fraction 2).

For model initialisation, all fraction concentrations within the water column were set to zero and no sediment was added at the boundary because the aim was to track the plume arising from disposal operations only and no other important sediment sources exist within the area corresponding to the model domain. It should be noted, however, that naturally occurring background turbidity does exist at the AMDG as described in Chapter 4, the level of which is influenced not only by ambient suspended sediment, but also from other floating particulates, such as plankton. However, including the background level in the model would only obscure the modelled concentrations resulting from the simulated disposal.

Bed Parameters

Erosion of the seabed was implemented using the default parameters corresponding to the 'soft mud' situation in the model. Critical shear stress for erosion was defined as 0.05 Nm^{-2} based on an assessment of the seabed sediments

at the AMDG and assuming that, once deposited, the non-dynamic fractions will behave similarly to the naturally occurring sediments. The density of the seabed (based on a dry weight) was defined as 180 kg/m^3 as recommend by DHI (2011b) for soft mud. Bed roughness was applied as 0.001 m for a flat bed. The initial thickness of the bed was set to 10 cm based on core observations of the depth of the upper soft layer (see Section 4.8.3). The initial fraction distribution within the bed was set to 0, 0, 40, 40, and 20 for fractions 1-5, respectively, based on sediment texture analyses undertaken on seabed sediments prior to disposal operations at the site (Flaim & de Lange, 2011) (see Appendix III). Fractions 1 and 2 were set to zero for the initial bed definition because they are specific to characteristics of the bulk portion of the dredged material, which would presumably be less susceptible to erosion following initial deposition.

Dredging Dialog

Dredged material was added to the model domain through the implementation of the Dredging Dialog within the Mud Transport Module. Within the Dialog, it is necessary to specify the type of spill, the distribution of the fractions within the applied spill, the position of the spill within the model domain, the dredge/discharge rate, and the percent spill. It should be noted that use of the term 'spill' applies to the dredging function within the Dialog, where if a dredging rate is applied, the 'spill' represents the percentage and location in the water column that material is spilled from the dredging operations and the spill location, in the vertical dimension, is a characteristic of the type of dredging used.

In the case of disposal of dredged material, 100 % of the material was 'spilled' in the top layer of the model domain to simulate disposal at the surface via split-hull hopper. The discharge rate represents the volume disposed as a negative value in kg/s. Estimation of the discharge rate should take into consideration the discharge method (i.e. insertion speed), the time step, the volume disposed, and its bulk and dry densities. At the AMDG, the tug and towed hopper approached the disposal ground from the southwest and material was released from the hopper over approximately 5 seconds as the tug proceeded northeast across the site (Figure 5.24). Immediately following disposal, a small, elongated plume of suspended material was observed at the surface as a trail behind the hopper. Based on the

observed patterns, the discharge was initiated at 11:00 am in each model simulation on the model day corresponding to the day each disposal was monitored at the AMDG. Material was discharged along a diagonal track (SW-NE) across the model domain at approximate disposal locations observed during each of the 4 surveys (Figure 5.24), over a period of 5 seconds with the sediment source (moving hopper) proceeding across the model domain at a speed equivalent to approximately 3 m/s (~6.5 knots (*pers. comm*, R. McGregor)). Discharge rates for each simulation, corresponding to the volume disposed, are included in Table 5.10 along with other parameters applied in the Dredging Dialog.

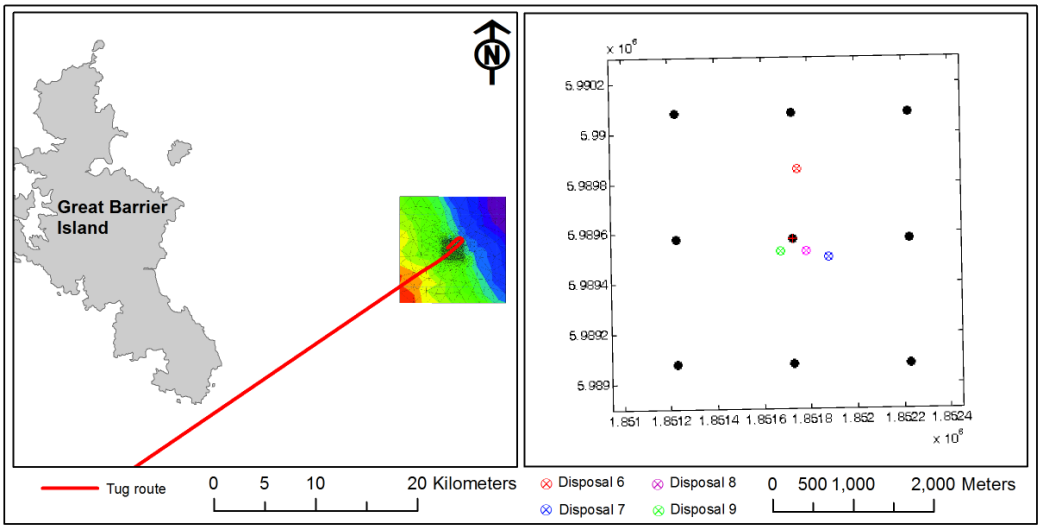

Figure 5.24 Left: Tug and hopper approach route for disposal of dredged material at the AMDG during the April 2010 operations superimposed on the 3D model domain. Right: approximated disposal locations for loads 6 – 9, corresponding to Surveys 1 – 4, with respect to the centre of the site and sampling locations related to other parts of the study (black markers).

Table 5.10 Details of parameters applied in the Dredging Dialog within the Mud Transport Module for model simulations corresponding to the disposals monitoring during Surveys 1 - 4.

Parameter			**Value/Option applied**				
Type of spill			100% in the top layer				
Fraction distribution			Fraction No.	1	2	3	4	5
			%	35	35	10	15	5
Survey No.	**Discharge starting location (NZTM)**	**Discharge time**	**Discharge time series (kg/s)**				
			T1	**T2**	**T3**	**T4**	**T5**
1	1851748.5 m E, 5989854.5 m N	11:00	10,000	40,000	85,000	181,920	5,000
2	1851880.5 m E, 5989504.5 m N	11:00	10,000	40,000	85,000	166,270	5,000
3	1851783.5 m E, 5989526.5 m N	11:00	10,000	40,000	85,000	114,850	5,000
4	1851677.5 m E, 5989526.5 m N	11:00	10,000	40,000	85,000	155,980	5,000

The distribution of the fractions within the disposed load was based on the conceptual model for the behaviour of dredged material during the disposal, where typically, the quantity of the disposed load available for passive dispersion makes up a very small percentage of the total load. Within the 'passive' component, which is controlled by the influence of the individual grain or floc properties (fractions 3 and 4), proportions were approximated by the known grain size distributions of sediments that accumulate within Pine Harbour Marina (Bioresearches, 2009). The quantity that descends dynamically is usually composed of a solid or dense portion representing the aggregates, as well as the 'jet' component that descends as a fluid-like slurry. The aggregate component usually only makes up a small proportion of the total volume compared to the slurry (Bokuniewicz & Gordon, 1980). However, as the model requires the discharge in units of dry weight per second, it was assumed that in the absence of the interstitial water, the two dynamic components of the dredged load would actually have similar weight values.

Discharge rate was calculated based on an assumed bulk density (wet) of 1300 kg/m^3 and the volumes disposed on each of the four survey days (Table 4.2). For conversion to dry weight (ρ_d), the following formula was used as recommended by DHI (2011b):

$$\frac{\rho_s(\rho_b - \rho)}{(\rho_s - \rho)} \qquad \text{Equation 5-1}$$

where ρ_d=bulk density (wet) (1300 kg/m^3), ρ_s=grain density (2650 kg/m^3), and ρ=water density (1026 kg/m^3). The total dry weight calculated for each load was then distributed over the 5 second discharge period such that the highest quantity exiting the hopper door coincided with discharge time step 3 (T3) in order to simulate the reduced rate during the initial 2 seconds before the hopper doors were fully open (Table 5.10). The quantity exiting the hopper at T3 never exceeded the maximum amount possible, which was calculated to be about 220,000 kg/s based on the area of the hopper doors and an estimated insertion speed of 2 m/s.

5.8.3 Near – Field Dispersion Calibration

Two values are primarily used for calibration of suspended sediment concentrations (SSC) and bed morphological changes within the Mud Transport Module: horizontal and vertical dispersion parameters. Dispersion can be tuned in three ways: scaled eddy viscosity formulation, dispersion coefficient formulation, or no dispersion.

For calibration of the model a simulation corresponding to the Survey 1 situation was run. The optimal dispersion parameters for each of the 5 included fractions are shown in Table 5.11.

Table 5.11 Details of applied calibration parameters in the Mud Transport Module.

Fraction No.	Formulation	Horizontal dispersion	Vertical dispersion
1	No dispersion	-	-
2	Dispersion coefficient formulation	0.1	0.01
3	Scaled eddy viscosity formulation	1	1
4	Scaled eddy viscosity formulation	1	1
5	Scaled eddy viscosity formulation	1	1

To evaluate the accuracy of the model in simulating the disposal process and the subsequent dispersion of the muddy material, the following characteristic features from the model results were compared to field observations: impact area, impact location, deposit thickness, and near-surface and near-bed dispersion.

Impact Area

In Chapter 4, the position of the light gray patches in the post-disposal backscatter map were compared to the ADCP backscatter data recorded during each of the 4 surveys to identify which patch represented the deposit resulting from each disposal event (Figure 4.29a). The Survey 1 patch was identified as lying approximately 300 m north of the centre of the site. Figure 5.25 shows the same MBES backscatter map presented in Chapter 4 superimposed with the modelled bed thickness change (cm) contours. The impact footprint of the model results is notably more detailed in shape than that recorded in the field; however, this is likely due to the low resolution of the acquired MBES data. Initial visible comparisons of the modelled and observed footprints indicate that the model tends to slightly underestimate the size of the impact area, but the results are still

sensible. Figure 5.26 shows the geometric approximation of the footprints for a more accurate estimate of the area covered, which also gives an indication of the accuracy of the modelled impact location.

The approximate area of the patch corresponding to the Survey 1 disposal is 11,370 m^2 and model predicted footprint was indeed ~27 % less at 8,345 m^2 (Table 5.12). This difference, however, corresponds to an effective difference in radius of only 8 m. The results suggests that, at least based on the dense deposited portion comprising the light gray patch in the MBES backscatter map, the model simulates the lateral spreading of the disposed material during descent to the seafloor with reasonable accuracy.

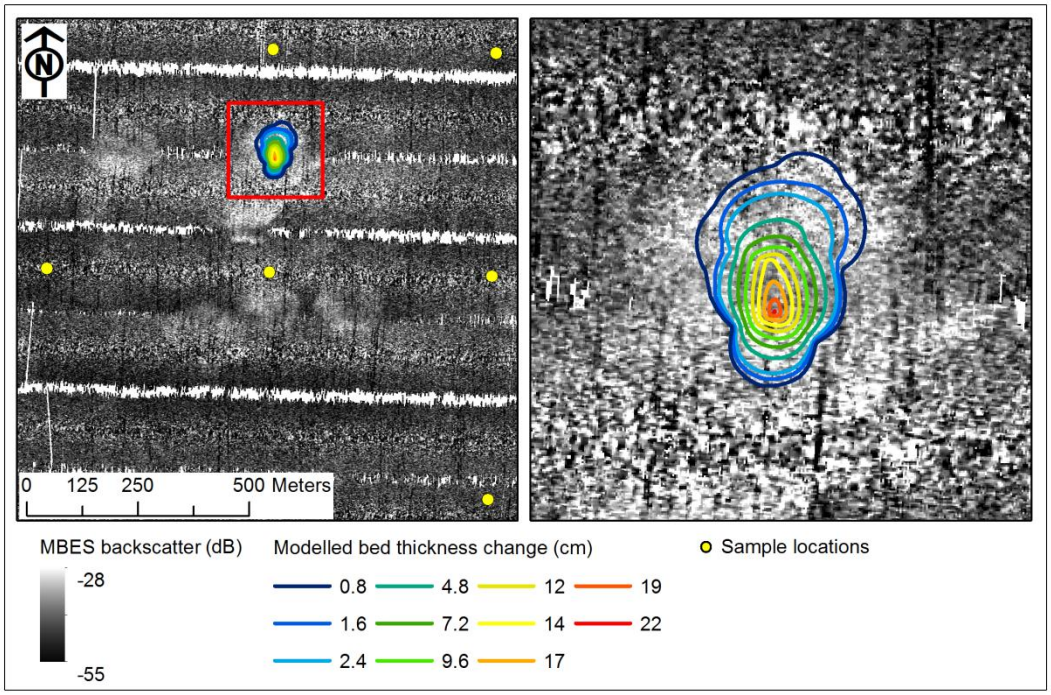

Figure 5.25 Modelled change in bed thickness contours corresponding to the load disposed during Survey 1 superimposed on the MBES backscatter data recorded at the AMDG after completion of the disposal operations. On the right is a close-up view of the area indicated by the red square on the left-hand map.

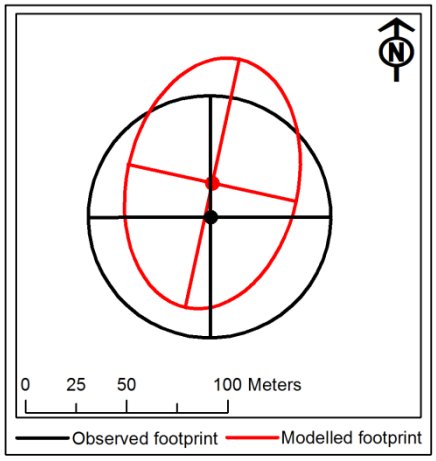

Figure 5.26 Approximate footprints of observed (black, from MBES map) and modelled (red) data used to compare impact area and location.

Based on the centre point of the approximated geometric representation of the observed and modelled footprints, the difference in impact location was also assessed (Figure 5.26). The results indicated only a 17 m shift in the modelled footprint compared to the observed footprint; however, if the thickest point of the modelled deposit is considered as the centre, rather than the geometric centre, the disparity in impact location is then even.

Table 5.12 Details of model results and the corresponding field observations from each of the 4 monitored disposals.

Survey No.	Impact area (m^2) / radius (m)		Impact location diff. (m)[‡]	Bed thickness change (cm)		Surface dispersion[†]			Bottom dispersion[†]		
	Obs.	Mod.		Obs.[§]	Mod.*	Obs. (m)	Mod.		Obs. (m)	Mod.	
							Δx (m)	*Δt* (min)		*Δx* (m)	*Δt* (min)
1	11370 / 60	8345 / 52	17	10	22	516	446	59	150	63	5
2	23203 / 86	9028 / 54	60	10	17	292	349	72	180	57	4
3	18796 / 77	6531 / 46	73	10	14	806	518	63	510	199	28
4	8355 / 52	9321 / 54	58	10	26	250	253	83	269	72	38

*maximum thickness
[†]dispersion at SSC ≤ 15 mg/l corresponding to the contrast limit of the plume against the ambient water
[‡]relative to the centre of the area of impact
[§]Estimate based on core observations only

Deposit Thickness

The predicted thickness of the deposit is indicated by the colour-graded contours of the modelled deposit (Figure 5.25). At its maximum thickness, the modelled deposit was 22 cm, which covered only a very small area (Table 5.13). Based on the area covered by each contour level, the area-weighted average thickness of the modelled deposit is approximately 4 cm (Table 5.13).

Table 5.13 Values used for calculation of the area-weighted average modelled deposit thickness.

Contour level (cm)	Area covered (m^2)
0.8	1972
1.6	1074
2.4	1747
4.8	995
7.2	613
9.6	463
12	380
14	263
17	161
19	42
22	0.18
Area-weighted average (cm)	4.27

The thickness of each deposit corresponding to the 4 monitored disposals is not known specifically because the resolution of MBES bathymetry data was not high enough to resolve deposits approximately less than 50 cm in thickness. However, cores retrieved near the centre of the site following the completion of all disposals indicated a deposit thickness in the order of magnitude of 10 cm (Figure 4.28). Due to the low degree of location accuracy in the core retrieval, it is not known which deposit in particular the material shown in Figure 4.28 represents; however, presumably, the thickness of the deposits were similar for each load disposed based on the consistency in disposal method and material disposed. Without knowing the specific thickness of the deposit corresponding to the Survey 1 disposal, it can only be suggested that the model results are sensible and within the expected range based on the limited field observations.

Dispersion Magnitude

For the case of the AMDG, the distance that disposed material is dispersed from the disposal location is a critical factor in deciding whether long-term use of the site should be allowed. Therefore, it is crucial that the magnitude of dispersion be represented as accurately as possible in the model. In general, the term ‘magnitude’ will, hereafter, refer to the distance and direction of dispersion, as well as the associated time after disposal.

For calibration of modelled dispersion magnitude, results were compared to field observations based on ADCP backscatter data, which was first presented in Chapter 4. Figure 5.27a&b show slices of interpolated backscatter data superimposed with the corresponding model layer SSC contours. Though the interpolated data slices shown in these figures were not specifically presented in Chapter 4, they were used, in part, to develop the passive dispersion plots presented in Section 4.10.1, and thus provide a useful visual representation of the findings on Chapter 4 for comparison to the model results here.

During the field surveys, ADCP data was recorded until the plume was nearly indistinguishable from the ambient water at the surface. Water samples collected in the last 15 min of each survey had an average SSC between 5 mg/l and 12 mg/l (Flaim & de Lange, 2011) (refer to Appendix III). In general, the plume was not located near any of the water sampling stations at the end of the surveys, so the average SSC values measured in those locations can be considered to represent the range of background SSC. A value of 15 mg/l, therefore, is a reasonable estimate for the concentration of the plume at the surface at the point when observers from the survey vessel noted that it was nearly indistinguishable from the ambient water. Hereafter, this limit will be referred to as the 'contrast limit'.

For comparison to model results, the transects comprising the final 15 min (approximately 45 – 60 min after disposal) of each survey are considered here to represent the period when the SSC had reached the contrast limit. This assumption is necessary because calibration of ADCP backscatter data to units of mg/l was not possible (refer to Section 4.5.5 for details) and therefore, the model results, in units of mg/l, must be related directly to the measured data in units of dB.

Figure 5.27a, shows the comparison of the near-bed modelled plume at the contrast limit and the corresponding measured plume. From the spread of the contours, it is clear that the measured near-bed plume covered a larger surface area than the modelled plume; however, the position of the centroid of the two plumes are very close, with the model centroid located only slightly west of the measured centroid[11]. The near-bed dispersion distance was determined to be

[11] The feature at the northern end of the measured data area in Figure 5.27a, indicating a small high turbidity zone directly adjacent to a small low turbidity zone, is mostly likely spurious,

150 m based on the measured data, and that of the model was 100 m (Table 5.12). The modelled near-bed plume corresponding to the contrast limit occurred only 5 min 'post-disposal', whereas that observed in the measured data occurred some 45 to 60 min after disposal.

This inconsistency is linked to the disparity in the spread of the contours in that the model does not allow for adjustment of the flow patterns due to the dynamic movements (*Dynamic Collapse Phase*) of the disposed material. In reality, turbulence near the bed created by the impact of the material with the bed causes increased dispersion (i.e. contour spread), thus resulting in an increased settling time (i.e. the time after disposal for SSC to decrease to the contrast limit).

Furthermore, the applied flow conditions, as described in Section 5.7, do not accurately represent the near-bed situation due to lack of measured forcing data in that region. In reality, however, the effects of the dynamic collapse would be expected to outweigh the dispersion due to the ambient current near the bed, and because such a deficiency in the model cannot be improved by calibration methods, the results can be expected to always underestimate the degree of dispersion at the bed.

resulting from the interpolation procedure, which likely extrapolated the higher surface turbidity in that area (see Figure 5.27b) towards the bed. Therefore, the feature is disregarded for model comparisons.

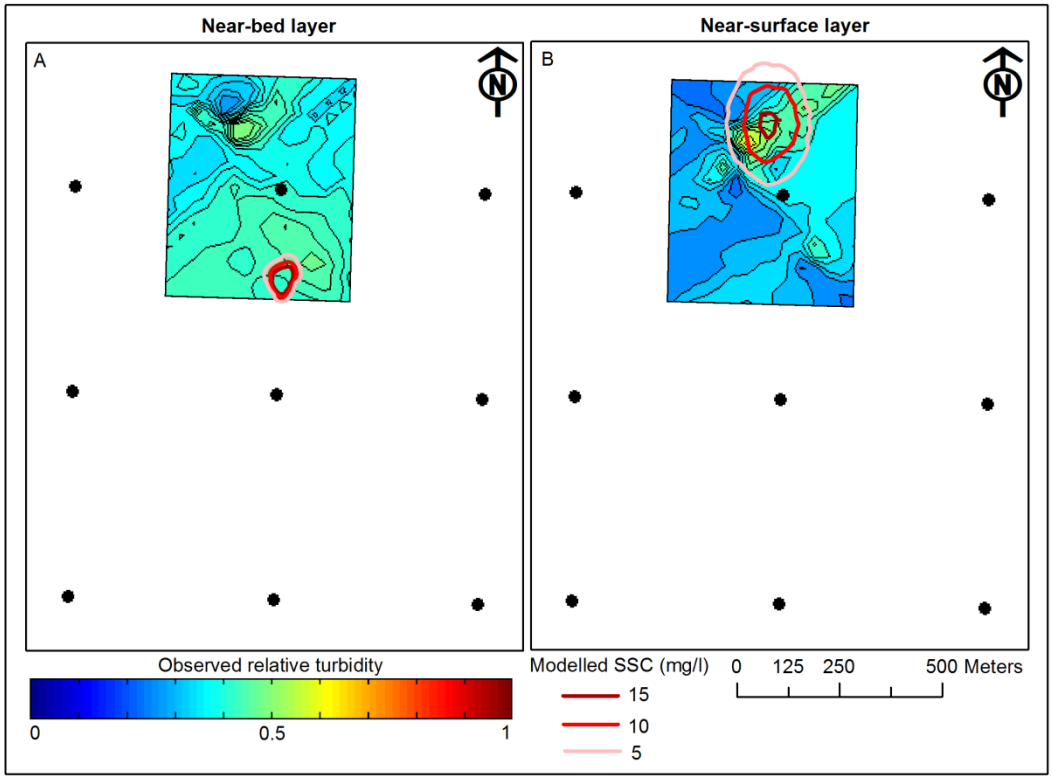

Figure 5.27 Interpolated relative turbidity from ADCP backscatter recorded 45-60 min after disposal during Survey 1, superimposed with modelled SSC (mg/l) contours (red scale) at the point corresponding approximately to the limit of visibility (~15 mg/l) for the (a) near-bed and (b) near-surface layers.

Near the surface, where dispersion is mainly influenced by the ambient current, the modelled magnitude of dispersion matches that of the measured quite well. Figure 5.27b shows that the near-surface modelled centroid, representing the position at the contrast limit, is located very close (slightly east) to the measured centroid in the last 15 min of the survey. The corresponding dispersion distances were 446 m and 516 m, respectively (Table 5.12). The dispersion period for these distances also matched reasonably well, with the model centroid reaching the distance of 446 m 59 min after disposal, compared to the 45-60 min window for that of the measured data. Figure 5.28 further illustrates the modelled dispersion distance, in profile view, 1 hour 'post-disposal'. The spread of the contours appears to be over-estimated by the model, a disparity which, in theory, can be calibrated for; however, the results shown represent the optimal settings when considering all the aspects that must be reproduced in the model.

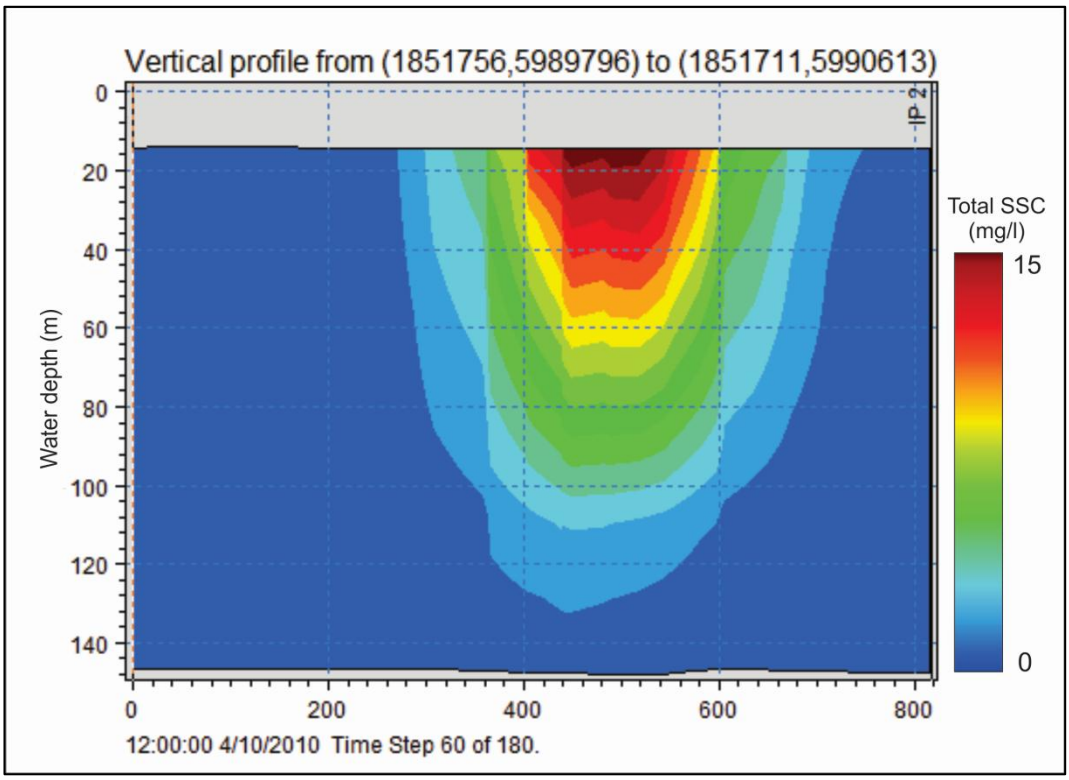

Figure 5.28 Profile view of modelled SSC concentration for simulation corresponding to Survey 1 showing the distance from the source (x-axis = 0 m) (disposal location) to the minimum visibility point (~15 mg/l) (x-axis = 500 m) in the surface layer.

Model Performance

Based on the optimised settings, the model was capable of reproducing some, though not all, of the important aspects of the disposal process corresponding to that monitored in Survey 1 at the AMDG. It was shown that the model simulates the following processes reasonably well:

- lateral spreading during descent of the dredged material;
- deposition of the dynamic portion of the disposed load; and
- temporal and spatial aspects of dispersion of the passive portion of the disposed load near the surface.

The model was deficient in reproducing the flow effects induced by the *dynamic collapse* phase, therefore, did not accurately simulate the following processes:

- temporal and spatial aspects of dispersion of the passive portion of the disposed load near the bed.

5.8.4 Model Validation

To validate the above conclusions on the performance of the model, 3 more simulations were run corresponding to the disposals monitored during the 3 subsequent plume monitoring surveys using the optimised settings. Table 5.12 includes the results from calibration (Survey 1) and validation (Surveys 2-4) simulations and the corresponding measured values. For Surveys 2 and 3, the difference between the modelled impact footprints and those identified on the MBES backscatter map corresponds to a difference in the effective radius of approximately 30 m, with the model under-predicting the area compared to the measured data (Table 5.12). The results from the Survey 4 simulation were much closer to the measured data and the difference in the effective radii was not significant (Figure 5.29).

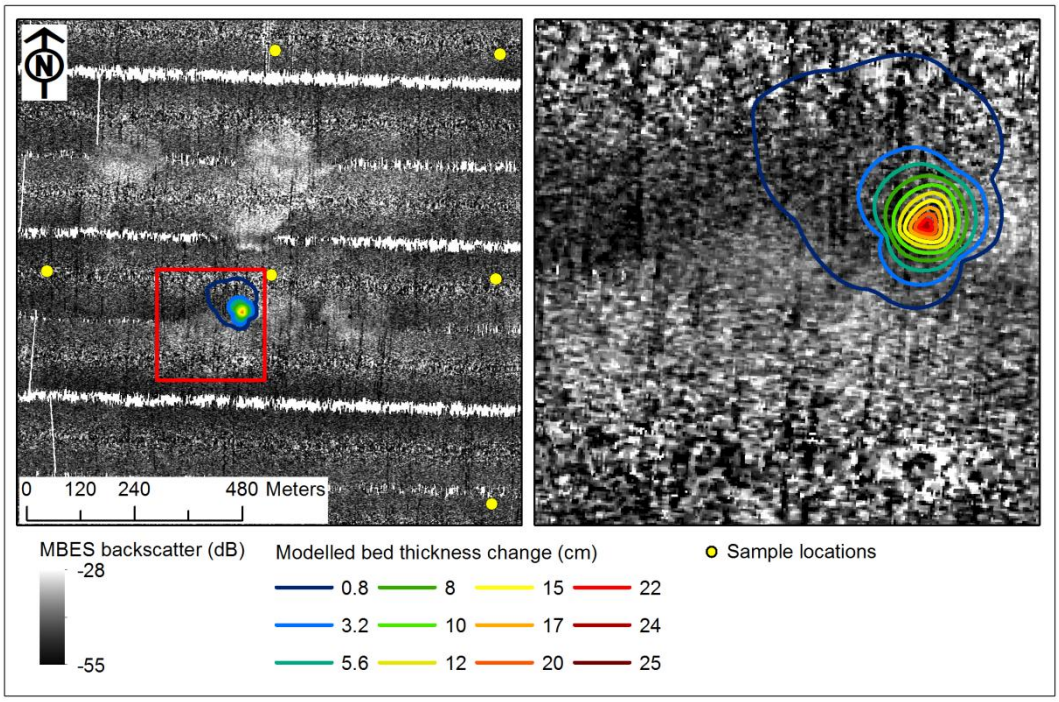

Figure 5.29 Modelled change in bed thickness contours corresponding to the load disposed during Survey 4 superimposed on the MBES backscatter data recorded at the AMDG after completion of the disposal operations. On the right is a close-up view of the area indicated by the red square on the left-hand map.

The location of the predicted point of impacts for the three validation simulations, based on the centroid of modelled deposits, was somewhat further away from the measured point of impact compared the simulation of the Survey 1 disposal, with an average difference of approximately 65 m for simulations of Surveys 2-4.

The modelled maximum thickness of the deposits for each of the three validation runs were 17 cm, 14 cm, and 26 cm, respectively, with corresponding area-weighted averages of 4 cm, 2.5 cm, and 2.5 cm. These values are within the expected range based on observations from collected cores (refer to Figure 4.28)).

Dispersion characteristics predicted by the model for the disposal corresponding to Survey 2 were partly in line with the ADCP backscatter data (see Section 4.10.1 for details on measured dispersion patterns). In the surface layer of the model, maximum dispersion to the point corresponding to the contrast limit was 350 m, 72 min 'post-disposal', compared to about 300 m approximately 1 hour after disposal as measured in the ADCP backscatter record (Table 5.12). At the bed, however, the model significantly under-predicted the extent of dispersion (57 m predicted, compared to 180 m measured), as well as the time it took to reach the extent of dispersion (only 4 min compared to the measured range which was 45-60 min).

Measured dispersion was greatest, both near the bed and near the surface, during Survey 3. Compared to the other simulations, the Survey 3 simulation also showed the greatest dispersion extent at the surface and near the bed with distances of 518 m and 199 m, respectively, but the model significantly under-predicted the extent of dispersion by about 300 m in both zones (Figure 5.30). It is also clear from Figure 5.30 that the model did not accurately reproduce the direction of dispersion, particularly near the surface.

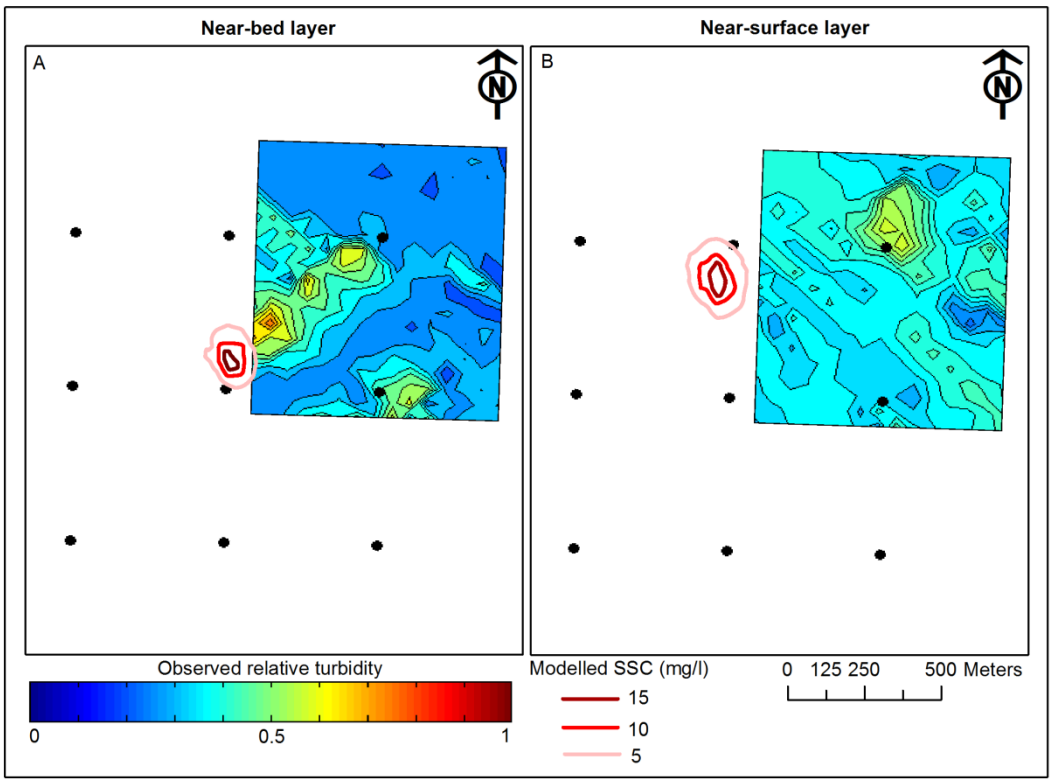

Figure 5.30 Interpolated relative turbidity from ADCP backscatter recorded 45-60 min after disposal during Survey 3, superimposed with modelled SSC (mg/l) contours (red scale) at the point corresponding approximately to the limit of visibility (~15 mg/l) for the near-bed (a) and near-surface (b) layers.

The Survey 4 simulation, showed very good agreement with the measured data in the surface layer, with a maximum dispersion of 253 m compared to 250 m shown in the ADCP backscatter record, however, the distance was achieved only after 83 min, compared to the range of 45-60 min in the measured data. Similar the result of the three other simulations, the extent of dispersion near the bed in the Survey 4 simulation was significantly under-predicted by the model.

5.8.5 Discussion

Errors associated with the model results, were affected by the local resolution of the grid. However, because a flexible mesh grid was used, there was no consistent grid size, and hence, consistent error. With respect to surface dispersion and impact location, the model performed reasonably well, with errors in the same order of magnitude or less than the length of the side of one grid element (~50 m) in the area of interest of the model domain, so the significance of the error is low. The exception was the modelled dispersion for the Survey 3 simulation, which was underestimated by about 300 m, both near the bed and near the surface. The

direction of dispersion was also inaccurate, which, in the case of surface dispersion, was unexpected because the direction of modelled flows at the surface were reasonably well represented by the hydrodynamic model (compare Figure 4.46 (measured) to Figure 5.22 (modelled)). Near the bed, it is clear from Figure 5.30 that the model results do not reflect the focused dispersion along a density layer that was observed in the measured data (see Figure 4.49), but this is not surprising because the modelled flow conditions were implemented as barotropic, so density stratification was not included. However, dispersion was better represented for the Survey 1, 2, and 4 simulations.

The main discrepancy between the modelled and measured dispersion characteristics were in the near-bed zone with the model significantly under-predicting the spatial and temporal extent of dispersion in all four simulations. Although there are several areas where lack of information on initial conditions (e.g. dredged material properties) and forcing data (e.g. flow conditions at near the bed) may contribute to inaccuracies in the model results, it appears that the main source of error is related to the inability of the model to feed-back dynamic sediment movement (i.e. development of a density surge after impact of the disposed material with the bed) into the flow model. As such, after the material impacts with the seabed in the model, it deposits immediately and only fractions that were susceptible to advection via the ambient current are further transported, and then, in that case, only in directions and at distances corresponding to flow conditions originating from the provided boundary conditions. Thus, only a very small amount of material is available for dispersion, which then settles very quickly because the ambient modelled flow at the bed is weak (Figure 5.22). If development of a density surge could be implemented in the model, much more of the disposed material would be dispersed over a greater distance and over a longer time period due to the enhanced near-bed current associated with the transfer of energy after the material impacts with the bed. Such a scenario would show better agreement with the measured data.

Another issue with using the Mud Transport Module for simulations of dredged material disposal is that, because the model requires that the quantity of discharged sediment be provided in dry weight units, the negative buoyancy due

to the interstitial water cannot be accurately simulated. This is not so much of a problem for dredging spill because the material acts as if it were all individual grains, which is what the model was designed for. In attempting to model the dynamic components (i.e. fractions 1 and 2), however, it would be better if the model accepted bulk properties, so that the differences between the aggregate portions and the jet portions could be achieved. In this case, one possible approach was to artificially increase the proportion of sediment in the jet component to mimic the increased volume of the jet, but this would result in a thicker deposited layer, and thus, less accurate results. In this study, increased dispersion and decreased settling velocity was used to distinguish between the two dynamic portions.

Despite these deficiencies, according to the measured data, surface dispersion was, in almost all cases, more extensive than near-bed dispersion and because the model reproduced surface dispersion sufficiently, it can, in that sense, still be considered useful. However, for more accurate simulation of the initial disposal phases, especially *dynamic collapse*, implementation of another model, such as STFATE (Johnson & Fong, 1995), is recommended. This model incorporates the dynamics of the developed density surge and accepts information on the bulk properties of the dredged material, such as water and aggregate (clump) content. Based on the complementary capabilities of STFATE and the Mud Transport Module (MIKE 3FM, by DHI) used here, it would be possible to utilise the former to simulate the initial two phases (*Convective Descent* and *Dynamic Collapse*) and then use the results to implement the initial conditions of the third phase (*Passive Dispersion*) within the latter. For multiple disposals, new dynamic results via STFATE could be fed into the set-up of the MIKE model, which would allow for simulation of potential resuspension events of old deposits and dispersion and settling of the passive component from newly disposed material. This was not done for this study as it would exceed the original scope of the project.

5.9 Wind Scenarios for Dispersion at the AMDG

Based on the validation results described above, it was determined that surface plume dispersion processes were sufficiently well reproduced by the model. For improved insight into the potential dispersion at the AMDG, simulations of

scenarios of wind conditions not encountered during the field surveys were undertaken. As wind driven currents are primarily focused near the surface, which the model simulated reasonably well, the results presented herein can be regarded as indicative of wind effects of dispersal for a wide range of conditions at the AMDG.

5.9.1 Scenario Set-Up

During the four plume monitoring surveys undertaken at the AMDG, the maximum wind speed observed was approximately 15 knots (Survey 2, April 15). At this speed, the sea conditions were unfavourable for monitoring due to wind chop, and marginal for use of the tug-towed hopper disposal method that was employed. According to the operators, the maximum possible wind speed where disposal operations would be feasible using a tug-towed hopper is 20 knots (10 m/s) (*pers. comm.*, Simon Male). As this condition was not encountered during any of the four monitoring surveys, modelling of scenarios involving dredged material disposal at the AMDG for 20 knot (10 m/s) wind conditions were undertaken.

In the calibration and validation simulations presented in Section 5.8, modelled flows were forced with the tides, as well as a non-tidal component, which included the force of wind-driven currents and any other non-tidal forcing, such as the East Auckland Current (EAUC). However, due to lack of a long-term current record during the monitoring period, it was not possible to distinguish between the various non-tidal forcing mechanisms that may have been present during the monitoring surveys.

For wind scenarios, therefore, the simulations were forced only with tides (see Section 5.7.1 for a description of the tidal forcing used) and a constant wind speed of 10 m/s. Under this forcing scheme, tests showed that the plume persisted longer than what was predicted in the calibration and validation runs described in Section 5.8, so the model simulation durations were increased by 1 hour; ending four hours after the simulated disposal rather than 3 hours. The simulated scenarios were either a ‘high current’ type or a ‘low current’ type, corresponding to mid-ebb and near slack tide, respectively. Tidal conditions from Survey 2 (April 15, 2010)

were applied as the 'high current' situation, where, at the time of disposal within the simulation (11:00), the tide was at a mid-ebb stage during spring tides. The 'low current' case was represented by the tidal conditions during Survey 1 (April 10), where, at the time of disposal (11:00), it was nearly slack water during neap tides.

Eight separate scenarios were run, with 4 high current cases and 4 low current cases. The constant wind speed of 10 m/s was applied from each of the four quadrants (north, east, south, and west) for the entirety of the model simulation time, which started approximately 2.5 days prior to the disposal for each simulation (Table 5.5). This length of time was required to ensure that the wind-driven current was sufficiently well developed. All other model settings matched those described in Sections 5.8.3 and 5.8.4.

5.9.2 Results

High Current Case

During the high current condition, which was the situation during Survey 2 (April 15, 2010), the tidal current magnitude for the period of interest (11:00 – 15:00) started at 9.5 cm/s during mid-ebb, and decreased to 1.1 cm/s around low tide before increasing again to 5.4 cm/s in early flood stages (Table 5.14) (see also Figure 5.10). The average current velocity during the simulation period for each of the high current scenarios (1-4), including the added corresponding wind component, was 5.9 cm/s, 5.4 cm/s, 6.8 cm/s, and 6.1 cm/s, respectively (Table 5.14). During the simulation period the tidal current was initially directed east-northeast, and following the turning of the tide towards the end of the simulation (14:00), the current was directed west-southwest.

In Scenario 1 (northerly wind), the maximum dispersion distance was predicted to be 852 m towards the northwest (74°) (Table 5.14 and Figure 5.31). The corresponding maximum SSC at that location was 40 mg/l. Maximum dispersion distances were estimated as 678 m, 902 m, and 1001 m for Scenarios 2-4 (east, south, and west), respectively (Table 5.14 and Figure 5.31). Similar to Scenario 1, the plume drifted northeast in the remaining three scenarios, ranging from about 60° in Scenarios 2 and 4, to 48° in Scenario 3. The maximum concentration of the

modelled plume at the extent of dispersion was the highest during Scenario 2 (easterly wind) at 48 mg/l and lowest during Scenario 3 and 4 (southerly and westerly winds) at 32 mg/l (Table 5.14 and Figure 5.31).

In the high current scenarios, the maximum dispersion distance did not correspond to the end of the simulation (15:00). Following the turning of the tide at 14:00, the dispersion direction of the plumes was, in all cases, reversed in the direction of the newly flooding tide (west-southwest) until the completion of the simulation at 15:00 (Table 5.14, plume images not shown).

Table 5.14 Details of modelled wind scenario simulations. Tidal stage figures depict (top) the current vectors, which indicate current magnitude (cm/s) and direction and (bottom) the tide height (m) for the high and low current cases used in the scenarios for the model periods corresponding to the time of disposal to the end of the simulation.

Scenario No.	Applied wind†	Avg. current velocity (cm/s)	Tidal stage	Dispersion distance‡ (m)	Dir. (°)	SSC* (mg/l)
High current case			Mid-ebb through early-flood			
1	N	5.9±3.4	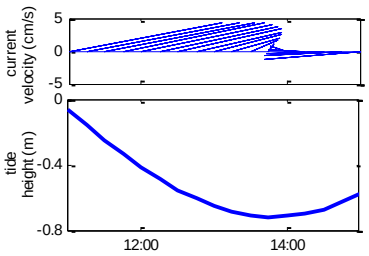	852	74	40
2	E	5.4±2.5		678	60	48
3	S	6.8±2.9		902	48	32
4	W	6.1±3.0		1001	63	32
Low Current Case			Low-tide through mid-flood			
5	N	3.8±1.0	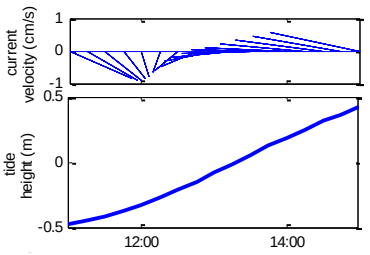	454	211	40
6	E	4.3±2.2		564	252	40
7	S	3.9±1.9		532	312	40
8	W	2.8±1.4		175	322	80

†Wind applied at a constant speed of 20 knots for the period of interest preceded by a 2 day ramp-up period.
‡Value corresponds to the farthest distance along the 15 mg/l SSC contour (see Figure 5.31 and Figure 5.32).
*Value corresponds to the maximum concentration at that location.

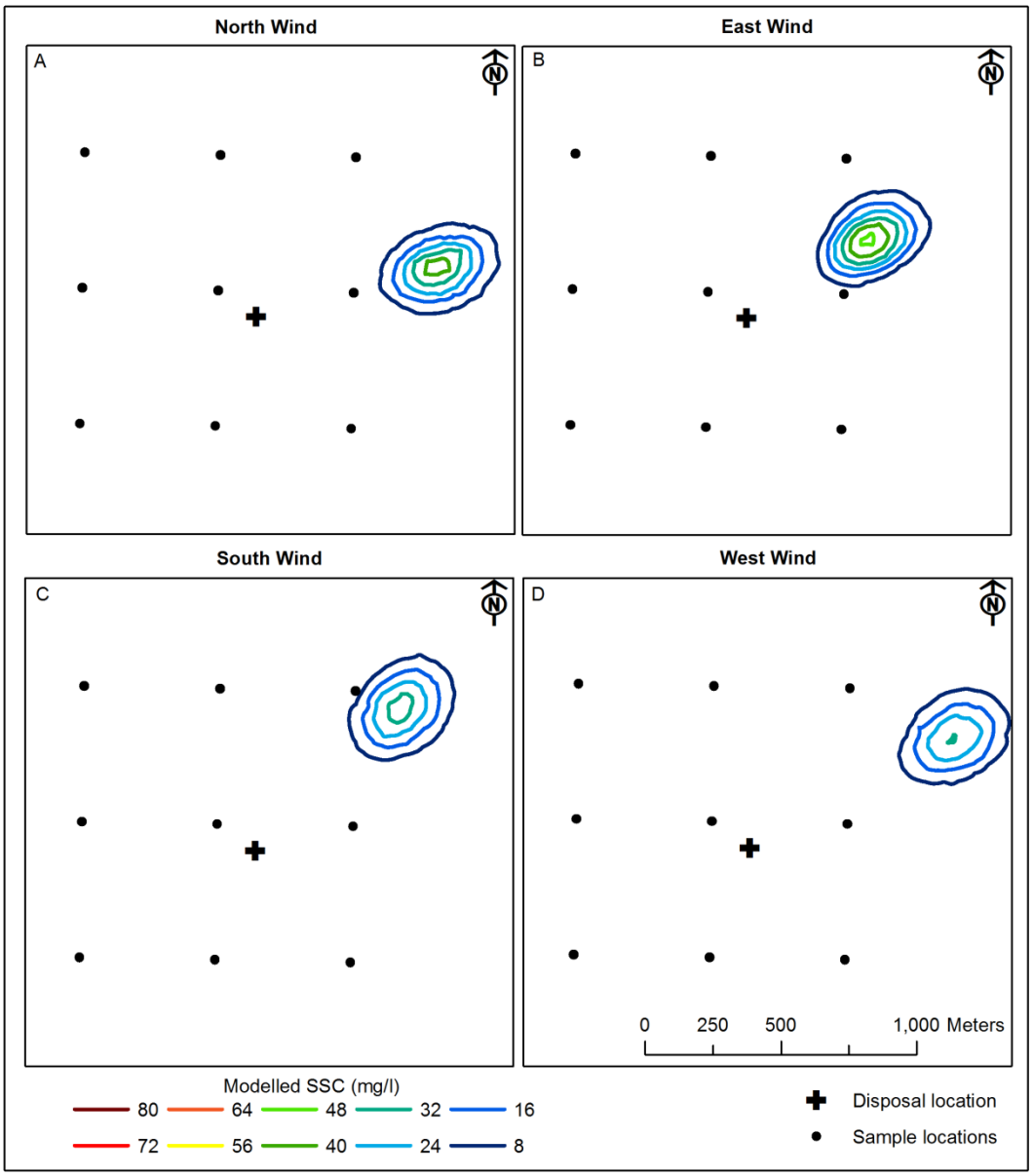

Figure 5.31 Modelled SSC concentration (mg/l) at the surface (model layer 4) during a high tidal current and with (a) northerly, (b) easterly, (c) southerly, and (d) westerly applied wind conditions. The black cross indicates the disposal location.

Low Current Case

The tidal current conditions during Survey 1 (April 10, 2010) were employed as the low current case for the scenario simulations. During the period of interest (11:00 – 15:00), the tidal current magnitude started at 3.6 cm/s and decreased to 0.8 cm/s at slack water ebb just after low tide, before increasing again in the second half of the period to a mid-flood velocity of 4.9 cm/s (Table 5.14(see also Figure 5.10). Initially, the current was directed southeast and then rotated towards the west-southwest (Table 5.14). The average current velocity during the simulation period for each of the low current scenarios (5-8), including the added

corresponding wind component, was 3.8 cm/s, 4.3 cm/s, 3.9 cm/s, and 2.8 cm/s, respectively (Table 5.14).

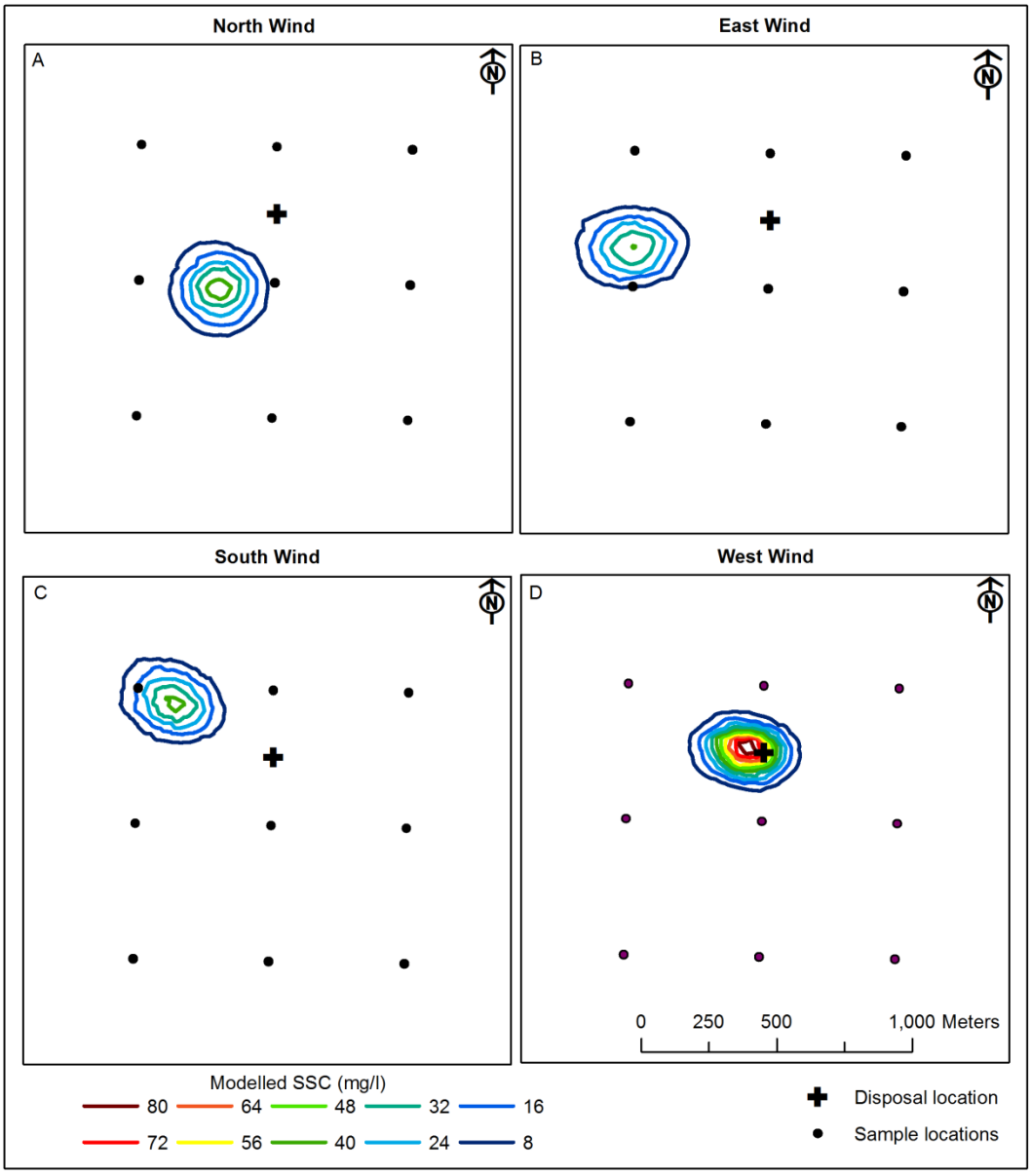

Figure 5.32 Modelled SSC concentration (mg/l) at the surface (model layer 4) during a low tidal current and with (a) northerly, (b) easterly, (c) southerly, and (d) westerly applied wind conditions. The black cross indicates the disposal location.

In the first half of the simulation, the modelled plume drifted only a small distance in all four low current scenarios (<100 m). After the tidal current turned westward in the second half of the simulation period, which is consistent with a newly flooding tide, the modelled plumes began to drift. In the case of a northerly, southerly, or easterly wind, the modelled plume drifted a similar distance (454 m, 532 m, and 564 m, respectively) towards the west in response to the westerly tidal current (Table 5.14 and Figure 5.32). The influence of the wind was most

apparent in the drift direction, where the plume drifted southwest (211°) under a northerly wind, northwest (312°) with a southerly wind, and on an easterly wind, the plume drifted west (252°) (Table 5.14 and Figure 5.32).

The decrease in SSC was greatest during the Scenario 6 simulation (easterly wind), with a maximum predicted concentration of 40 mg/l at the extent of dispersion (Table 5.14 and Figure 5.32). This level was consistent with those predicted in Scenarios 5 (northerly wind) and 7 (southerly wind), but the area covered by the maximum concentration was much smaller than that in the latter two cases (Table 5.14 and Figure 5.32).

For the case of the westerly wind (Scenario 8), the plume dispersion patterns were distinctly different than the other three low current cases. The plume drifted the smallest distance east (227°) of the four low current scenarios (175 m), and SSC levels were significantly higher than in the other 3 scenarios with a maximum concentration of 80 mg/l (Table 5.14 and Figure 5.32).

5.9.3 Discussion

In both the low and high current simulation scenarios, the results showed that plume dispersion at the surface was not greatly influenced by wind-driven currents, but rather it followed the tidal current patterns. Maximum dispersion distances were greatest during the high current scenarios, and were approximately twice the length predicted in the low current scenarios. This pattern corresponds to the average current velocity for each case (Table 5.14).

The influence of the wind was most apparent in plume dispersion direction. In most cases, the dispersion direction was predominantly in the direction of the tidal current, but favouring the quadrant opposite the applied wind (e.g. on and easterly tidal current and a northerly wind, the plume drifted southwest). The influence of the wind was stronger in the low current scenarios as evident from the 111° range of predicted directions compared to only a 26° range of directions in the high current cases. This is consistent with the reduced influence of the tidal current during slack water.

Other notable contributions from the wind were observed when the applied wind direction directly opposed the tidal current (i.e. Scenarios 2 and 8). In these cases, wind was not strong enough to overcome the prevailing current direction driven by the tides, even in the low current case, but dispersion was hindered by the effect of the wind-driven current opposing the tidal current, which also had the result of preventing dilution of the plume. This effect was most obvious in Scenario 8 (low current), where the plume was essentially held stationary (within about 100 m of the disposal location). In this case, by the end of the simulation (four hours after disposal), the maximum SSC had only reduced to 80 mg/l, which is approximately twice the level predicted in the other scenarios.

Somewhat unexpectedly, in the scenarios where the wind was aligned with the tidal current (Scenarios 4 and 6), the maximum dispersion distances were only slightly enhanced from the scenarios where the wind was at a 90° angle to the tidal current (~100 m and 30 m in Scenarios 4 and 6, respectively). This is further evidence that a persistent 20 knot wind and resultant wind-driven currents are not important mechanisms for dispersion at the AMDG.

The model simulations presented in Section 5.8 were forced with tides and a residual component, which had the influence of winds and other non-tidal forcing mechanisms, such as the East Auckland Current (EAUC). For the idealised simulations presented above, the influence of other non-tidal forcing was not considered. From the results, therefore, it can be concluded that during disposal operations at the AMDG, the influence of the wind can, for the most part, be expected to be insignificant in comparison to tidal currents and probably, other non-tidal forcing mechanisms.

The exception to this conclusion may be for conditions similar to those of Scenario 4, where during a 'high' tidal current, such as during mid-flood or mid-ebb of a spring tide, the prevailing wind is aligned with tidal current direction. In this situation, the greatest dispersion was observed (~1000 m). In the modelled scenario, the final maximum concentration was predicted to be 32 mg/l, which is about twice that which estimated as the contrast limit (see Section 5.8.3), suggesting that the plume has the potential to be dispersed a significant distance further and possibly beyond the boundary of the site. However, the area covered

by SSC levels higher than the contrast limit was small (Figure 5.31d) and because of the tidal influence, the plume can only be dispersed in one direction at a maximum velocity for approximately 3 hours. The model results suggest that in the absence of other non-tidal forcing mechanisms, this is not long enough to disperse a plume 1500 m, or from the centre of the site to its boundary. The results of Scenario 4 showed that after dispersion some 1000 m northwest from the disposal location, the dispersion direction reversed in response to the turning of the tide, so that the plume began traversing back towards the centre of the site. Based on this pattern, continued dilution at similar rates would be expected and by the next turning of tide, the plume would no longer be detectable.

Due to the environmental limitations of the tug-towed hopper disposal method, it is not possible to undertake disposals at the AMDG in wind conditions exceeding that which was simulated in the idealised scenarios (*pers. comm*., Simon Male). Accordingly, the model results are indicative of the 'extreme' situation for wind-driven forcing at the AMDG. In which case, it can be concluded that disposal plumes from the centre of the AMDG will be unlikely to disperse beyond the boundary of the site. However, if the disposal location is shifted a great distance (>200 m) from the centre of the site, and a strong wind coincides with the tidal flow, then it is possible that a plume may be dispersed beyond the boundary of the site.

Furthermore, the effects of non-tidal forcing beyond wind were not accounted for here. It would be beneficial to simulate the effect of the EAUC in combination with winds and tides. This is an area of research that deserves further examination, but requires more data than that obtained during the field programme for this study.

5.10 Summary and Conclusions

The numerical modelling programme presented in this chapter was designed to provide additional information towards the completion of Objectives 1-4 of this thesis, especially in the case of knowledge gaps due to lack of necessary field data. In this respect, the main aim of this Chapter was to develop a representative model and use it to examine the dispersion characteristics of the AMDG during

environmental conditions not encountered in the field. In doing so, the influence of various forcing mechanisms were examined (Objective 1), the importance of the range of processes that occur during disposal of dredged material was investigated (Objective 2), the potential for loss of disposed material beyond the boundaries of the site was estimated (Objective 3), the findings of which contribute to the required knowledge for developing a plan to minimise dispersion in potential future disposal operations (Objective 4).

5.10.1 Success of the Modelling Programme

The development of a model representative of hydrodynamic conditions at the AMDG initially focussed on reproducing the regional characteristics with the intention of nesting smaller grids at a scale feasible for reproducing near-field dispersion patterns. The choice of an initial regional model was related to the distance of the site offshore, and concerns that the model would not be stable with four open boundaries. In practice though, the lack of suitable boundary conditions limited the accuracy of the regional model and it was determined that the stability of a completely open model grid was not an issue.

The modelling programme then focussed on developing only a near-field model and extending it to the third dimension, which was necessary as the aim was simulate the disposal process and its vertical variability. With lack of representative boundary conditions still a significant issue, development of the near-field model required a somewhat creative view on how to force the boundaries. In the end, a technique that incorporated both predicted and measured data from both the 2008 and 2010 study period was developed to produce representative boundary conditions. While it was not possible to ensure high vertical accuracy in the flow conditions, the modelled results showed encouraging agreement with observations in the surface zone, which was determined to be the more important region for dispersion.

Following development of the 3D near-field flow model, the Mud Transport Module and the Dredging Dialog within it, was used to simulate disposal of dredged material. Field data from Survey 1 was used to calibrate the model, and data from Surveys 2-4 was used to validate the model. Again, the model showed

reasonable agreement with the dispersive characteristics near the surface observed in the field surveys and even with the initial fate of the disposed sediment on the seabed. However, the results showed that the MIKE model was not capable of simulating the density surge formed during the *Dynamic Collapse* phase, and due to lack of accuracy in the flow model near the bed, passive dispersion in that region was also not well represented. The limitations in the model results were, therefore, a result of both the model itself, as well as lack of field data for boundary and initial conditions.

However, the modelling efforts did have several positive outcomes:

- the capability of the MIKE 3D Mud Transport model for modelling the disposal process was tested, which was required because prior to this work, there was little to no available literature on the use of the model for the purposes it was applied in this thesis;

- a semi-empirical technique for dealing with limited forcing data in the offshore zone was developed, which resulted in reasonable model predictions, thus, making possible the next stage in the modelling process; and

- the influence of wind-driven currents on surface dispersion of disposed dredged material was defined with respect to the influence of the tides and it was determined that wind forcing only plays a relatively minor role in surface dispersion.

5.10.2 Optimal Use of the AMDG

The findings of this chapter provide some of the information that was not obtained from the field campaigns, but is necessary for making recommendations on optimal use of the AMDG to minimise dispersion during potential future disposal operations. Development of an operational plan that ensures safe and sustainable use the AMDG is an important step for long-term use.

Scenarios of potential wind conditions were designed to estimate the affect wind and the resultant currents on the dispersion of dredged material at the AMDG. The

scenarios only simulated conditions that could be encountered during the disposal operations, which are less extreme than what may actually occur in the region due to the limitations of the tug-towed hopper disposal method employed.

The findings showed that wind-driven currents had minimal effect on dispersion compared to both low and high tidal current conditions. However, in the case of a wind-driven current that coincides with a strong tidal current, especially if the load of material is released on the side of the site corresponding to the direction of the current (e.g. east of the centre when the current is directed to the east), there is a possibility that dispersion of the plume at detectable levels may occur beyond the boundary of the site. All other cases examined, present no indication that dispersion at detectable levels greater than 1500 m (the radius of the AMDG) would occur.

Based on the findings of the simulations undertaken in this Chapter and the known environmental limitations of the employed disposal method, the following tactics are recommended for potential future use of the AMDG to minimise disposal:

i. release of material from the hopper should be undertaken in the shortest amount of time that is feasible in order to limit the area of dispersion and maximise the initial negative buoyancy which acts to sequester material at the seabed where it is less likely to be dispersed;

ii. the location of disposal should be at or within ~200 m of the centre of the site so that the distance from the boundary is kept relatively constant at 1500 m because during certain environmental conditions, a decreased distance may result in dispersion beyond the boundary;

iii. if wind conditions in the days prior to a planned disposal are variable in direction and/or less than a speed of 20 knots, disposal operations can be undertaken regardless of the tidal current conditions (mid- or slack-tide);

iv. if wind conditions are consistent (in direction and speed) for two days or more, prior to a planned disposal and are at least 20 knots, disposal should

not be undertaken during high current conditions when the tidal current coincides with the wind direction; and

v. without further investigation, disposal of material with a predominantly fine, but mostly non-cohesive component should not be undertaken because this type of material was not considered in the simulations undertaken here and would be expected to be more susceptible to dispersion than the material type studied in this thesis.

The recommendations may require some revision; however, because full influence of non-tidal forcing was not considered in the scenarios. In fact, at no time was the combined effect of the tides, wind, and EAUC on dispersion definitely investigated. During the long-term deployment study period (Chapter 3), the data indicated that the predominant non-tidal forcing was the EAUC and the wind forcing was insignificant. On the other hand, during the 2010 monitoring period (Chapter 4), the variable nature of the data recorded over the month indicated that wind was most likely the predominant non-tidal forcing, as the residual component did not exhibit the characteristic consistent southeasterly directed flow as would be expected from the EAUC. Finally, modelling efforts presented in this chapter either did not distinguish between the non-tidal forcing mechanisms, or only focussed on wind effects.

As such, the above recommendations should be applied with caution and preferably only after further investigations into the combined effects of wind, tides, and the EAUC on dispersion of disposed dredged material are undertaken.

5.10.3 Relevance to the Thesis Aims and Objectives

Findings of this Chapter primarily contribute to an improved understanding of the potential for loss of disposed sediment at the AMDG (Objective 3), and from that, the ability to make recommendations on how to minimise dispersion in potential future use of the site (Objective 4). Through the process of model development, additional knowledge was gained regarding the influence of the various forcing mechanisms, both with respect to the hydrodynamic setting, as well as the forces driving the disposal process, which further contribute to Objectives 1 and 2, respectively.

An unexpected outcome of this Chapter was the finding that the MIKE model is limited in its capability for simulation of all aspects of the disposal process. Evaluation of the model for these purposes was not an initial objective of this thesis because its capabilities were assumed. So, in fact, determination of the limits of the model, in this regard, is an important result that may prove useful in future research.

CHAPTER 6
SUMMARY AND CONCLUSIONS: DISPERSION POTENTIAL AT THE AUCKLAND MARINE DISPOSAL GROUND

6.1 Introduction: Completion of Thesis Aims and Objectives

This thesis has identified and quantified the main pathways for dispersion of suspended sediment at the AMDG, with a focus on the potential for dispersion of disposed dredged material and the determination of the dispersive classification of the site.

Dispersion potential was examined through consideration of the inherent characteristics of the study site and the conditions under which it was utilised for disposal of dredged material. Objectives designed to meet the overall aim of the thesis were satisfied as follows:

Objective 1 Resolve the forcing mechanisms and influences driving the hydrodynamics on the continental shelf in the region of the new disposal ground.

The primary findings relating to the hydrodynamic forcing mechanisms were developed in Chapter 3, in which long and short-term data records from 2008 in the region of the AMDG were examined. ADCP data from a two month long deployment allowed for separation of tidal, wind, and boundary influences. The average tidal contributions were 45 % and 15 % of the recorded signal for the cross-shore and alongshore components, respectively. The average tidal current velocity was 6 cm/s under the influence, primarily, of the principle lunar, semi-diurnal M_2 constituent. The data suggested that the dominant non-tidal forcing mechanism during the 2008 deployment period was the East Auckland Current (EAUC), which is known to flow southeast on and along the shelf edge in the northeast coast region.

Additional findings based on short-term records from monitoring surveys during the 2010 study period were presented in Chapter 4. These data showcased a hydrodynamic setting that was very different from that described in Chapter 3.

During this period, it was found that the water column was stratified with a variable thermocline position through the month. Lack of a consistent non-tidal signature suggested the wind-driven currents were most likely the predominant forcing mechanism, as opposed to the EAUC, which was predominant during the 2008 measurement period; however, definitive conclusions were not possible due to the lack of long term data for the 2010 study period.

Model simulations undertaken in Chapter 5 underscored the findings developed in Chapters 3 and 4 and also further highlighted the influence of the wind on the ambient current. It was shown that under conditions where it would be possible to undertake disposal operations, the wind-driven currents are weak compared to tidal currents and do not represent a significant forcing mechanism.

The data observations made in Chapters 3 and 4, and model results described in Chapter 5 showed that the hydrodynamic setting of the AMDG is not characterised by extreme forces in general, but is variable in nature and, therefore, dispersion potential can be expected to be dependent on a range of forcing mechanisms.

Objective 2 Determine the site-specific processes involved in the disposal of dredged material.

Through an intensive field campaign to monitor the disposal of dredged material at the AMDG on four separate occasions, the processes that occur after disposal were characterised and described in Chapter 4. Monitoring surveys designed to track the disposed material and the resultant plumes were undertaken in April 2010 during disposal operations at the site. A variety of different data reflecting the level of suspended sediment at various locations in the water column were recorded. However, the ADCP backscatter dataset provided the highest resolution both spatially and temporally. Features of the three main disposal phases, well-described in the literature, were identified using this dataset and variations on those features due to site specific characteristics were described. A conceptual model of the disposal process at the AMDG was developed based on data recorded during the plume monitoring survey.

The numerical modelling programme described in Chapter 5, drew on the findings of Chapter 4, as well as other aspects such as, the characteristics of the dredged material released during the monitoring surveys, and the dredging and disposal methods for development of the model. Results emphasised the influence of each of the disposal phases, as well as the role external aspects on the disposal process.

Objective 3 Assess the potential for loss of disposed sediment from the disposal site.

The assessment of the loss of disposed sediment beyond the boundary of the site was addressed either directly or indirectly in each of the main Chapters of this thesis (Chapters 3-5). In Chapter 3, dispersion distance of a passive particle was estimated based on current records from the 2008 study period and using progressive vector techniques. Chapter 4 illustrated, in particular, the actual passive dispersion of suspended sediment using ADCP backscatter data. Analysis of drift patterns during each survey allowed for quantification of dispersion distances. Model simulations of a variety of tidal and wind conditions presented in Chapter 5 illustrated the potential dispersion distances under conditions that were not encountered in the field, but could be expected at the AMDG during future disposal operations.

In all instances, measured and predicted dispersion distances were found to be less than the radius of the AMDG (1500 m) for a representative time frame after disposal. The findings revealed some specific conditions that were observed or simulated that may result in dispersion beyond the boundary of the site, but in general, those cases are few and are not likely to occur during disposal at the site. Through completion of this objective, it became clear that the AMDG behaves as a retentive site; one where disposed material is retained within its boundary.

Objective 4 Recommend operational restrictions on disposal methodology to minimise dispersal during disposal.

The information needed to make recommendations for minimisation of dispersion for future use of the site was primarily developed through employment of scenario simulations presented in Chapter 5. Although understanding in this regard was gained through the approaches taken in Chapters 3 and 4 as well, conclusions

were global in perspective because the environmental conditions on which they were based could not be described as 'extreme'. The scenario simulations, presented in Chapter 5, produced predictions of 'extreme' conditions and highlighted the potential maximum surface dispersion that could be expected at the operational limits of the tug-towed hopper. Based on the combination of forces (tidal and wind) examined in each scenario, optimal conditions were identified. Conclusions drawn in Chapters 3 and 4, along with those based on the scenario simulations, were applied to develop recommendations for optimising disposal operations for minimisation of dispersion after disposal of dredged material.

6.2 Potential for Dispersion at the AMDG

The physical characteristics of the suspended sediment (i.e. the disposed dredged material) dictate what dispersion forces are important. This principle is somewhat confounding because the forces themselves influence the state of the suspended sediment, but transitions from one dominant force to another are essentially driven by the state the sediment is in because there are bidirectional feed backs.

In a general sense, dispersion in the initial stages after release of dredged material in the water column is driven by the negative buoyancy of the material itself, with only insignificant influence by the ambient environment. In this *Convective Descent* phase, the characteristics of the material being disposed and the disposal methods are the driving forces. Due to the high negative buoyancy, horizontal dispersion is minimal, but mainly occurs in the form of entrainment at the perimeter of the jet leading to lateral spreading.

After the disposed material impacts with the bed, depending on the available momentum, a density surge may develop that can disperse dredged material, as well as entrained site sediment, significant distances along the seabed away from the point of impact. In this *Dynamic Collapse* phase, dispersion of suspended sediment continues to be dynamic (sediment derived), resulting from the potential energy of the load before release from the hopper and the excess density of the material maintained in the suspension.

When the initial momentum of the dynamically moving sediment is spent (e.g., through friction with the seabed and dilution via entrainment of surrounding or

overlying water), the important drivers of dispersion transition to passive forces (environmentally derived). During this *Passive Dispersion* phase, the properties of the individual grains are still influential (e.g. settling velocity), but there is no longer a bulk influence originating from the disposed load unit and, therefore, the ambient currents and other predominant hydrodynamic forces take over as the dispersion mechanism. Sediment still in suspension during this phase will be dispersed in the direction of the predominant environmental forcing mechanisms, as long as that force is able to overcome the settling velocity of individual grains.

Passive dispersion does not wait for the completion of phases 1 and 2, rather, as soon as the suspended material is in its passive form, it may be subjected to the ambient forcing mechanisms. As an example, material entrained around the perimeter of the descending jet quickly loses its dynamic characteristics after separation from the column of descending material. It was observed at the AMDG that there was a transition zone where there was no residual dispersion, but the entrained material was maintained in suspension, suggesting a turbulent zone of surrounding water set in motion by the jet. After a time, however, the turbulent forces weakened and passive forces took over dispersing the individual grains in the direction of the ambient current.

The dispersion patterns reported in this thesis generally fall in line with theories previously published, with the exception of the suggestion of the role of turbulent forces within a transition zone between dynamic and passive forces. The phenomenon has not been covered in previous literature, with the exception of a possible reference to it by Bokuniewicz et al. (1978). However, previous studies have predominantly occurred in much shallower water depths. Hence, it is possible that due to the significant water depth of the study site in this case, there was increased the entrainment that magnified the process. In shallower sites the pattern may not have been as easy to observe.

The primary finding of this research in relation to the AMDG, however, was that in all circumstances examined, dispersion of suspended sediment due to disposal operations was not observed beyond the boundary of the site. In fact, the maximum recorded dispersion from the disposal location was detected (at a very low level), some 500 m inside the boundary of the 1500 m radius site. Based on

the findings, the AMDG can, therefore, be classified as a non-dispersive (retentive) site. This classification has some caveats, however, which will be discussed in the following section with regards to the implications for ongoing use of the site.

6.3 Considerations for Ongoing Operation of the AMDG

Classification of the AMDG as a retentive disposal site is dependent on the following aspects:

- the disposal method used;
- environmental limitations on disposal methods; and
- the type of material being disposed;

Dredging and disposal operations carried out in association with the monitoring surveys at the AMDG were undertaken using the same methods for each disposal event (i.e. back-hoe dredging, and disposal via towed split-hull hopper). Furthermore, all model simulations were designed to represent these operational aspects. A change in the dredging and/or disposal method for future use of the site may result in a change in the classification of the site. For example, if suction dredging were employed, rather than back hoe, little of the *in situ* structure of the dredged material would be retained, which would lead to an increased proportion that would descend as the 'jet' and be more susceptible to entrainment and resuspension, though self-consolidation in the hopper might result in little difference between the two dredging methods. If the disposal operation was altered so that the hopper doors opened more slowly, the discharging material would be spread over a larger area and the descending material would fall at a lower speed, which would likewise increase its susceptibility to entrainment and dispersion.

Use of the tug-towed hopper for transport of the material to the site, introduces another set of limitations, which relate to the site classification. Essentially, this method requires that the towing cable remain constantly taut. Momentary loss of tension due to, for example, a large wave, can put the tug in danger, or possibly

cause a snap-back that might break the cable. Therefore, in this case, it is not possible to undertake disposal operations under poor environmental conditions (i.e. large swell or high winds). The environmental limitations to disposal with this method mean that ambient conditions can be expected to be calm with decreased dispersion potential. If, however, the disposal method were to change such that operation could be undertaken in rough seas, then the retentive classification may cease to be applicable.

The material disposed at the AMDG was a sandy mud with a high clay content. Depending on the structural integrity of the clay aggregates, which can be influenced by the transport to the site and other forces such as, wind waves upon entry to the water column, this type of material can be considered more resistant to entrainment and, thus, dispersion due to its cohesive properties. In the case that there is a need to dispose material with different characteristics than those examined in this study, it would be necessary to ensure that the material is not more susceptible to dispersion, which might be the case, for example, if the material was predominantly silt, with a small grain size, but low cohesion. If the dredged material had a similar clay content or possibly a larger component of coarse material, it is likely that it will be equally or less susceptible to dispersion, which means that the retentive classification would still be valid.

If all variables remain essentially the same, it is reasonable to expect that the AMDG can be used as a retentive open-sea disposal grounds for many years to come. The water depth at the site is sufficient that mound development would not encroach on navigational regions of the water column. In fact, to prolong the period before the site reaches capacity, the aim should not be to form a single mound where all disposed material comes to rest, rather, material should be released near the centre (away from the boundaries), but not in the exact same location, so that the probability will be higher that each deposit will have more time to consolidate before another load is deposited on top of it, which decreases the potential for resuspension of old deposits. In practice, due again to the water depth and the use of a moving split hull hopper for disposal, it would actually be very difficult to form a single mound, so the tendency will be to employ the dispersion minimizing method anyway.

One final aspect to consider is the potential for resuspension in extreme storm conditions. This aspect was not examined in this thesis due to the rarity of occurrence, based on known wave conditions in the northeast coast region, of waves that would be capable of resuspending deposited material at the bed. For dispersion of the resuspended material beyond the boundary of the site, the increased orbital velocities would also need to be sustained, a highly unlikely scenario. More likely would be the potential for enhanced dispersion through such processes as density stratification (as demonstrated in this thesis), internal waves, and/or coastal trapped waves. For quantification of the potential for dispersion by the latter two processes, they would first need to be documented at the site and then analysed for their transport potential.

To minimise dispersion at the AMDG, it was found that the following factors should be considered:

- material type;
- disposal method;
- tidal current speed and direction;
- wind speed and direction; and
- the characteristics of currents derived from other non-tidal forcing, such as the EAUC.

The research in this thesis showed that under calm conditions the AMDG behaves as a retentive site. Conditions that are considered calm can be described as non-persistent and/or low wind speeds less than 20 knots from any quadrant, tidal currents at any stage of the tide, and weak to normal input from additional non-tidal forcing, such as the EAUC. Model simulations indicated that caution should be exercised when wind conditions reach or exceed 20 knots, especially if the disposal is planned during a period of strong tidal currents. It was recommended that the same disposal method be employed and only material types with equal or lower susceptibility to dispersion be disposed in future disposal operations at the AMDG to ensure that the retentive characteristics of the

site be upheld. Conditions outside these constraints may result in the dispersion of material beyond the boundary of the site, which would be in breach of permit conditions and international law even though the environmental implications may be only small.

The studies used to develop the conclusions and recommendations described above, while diverse, may not be completely robust. Aspects that were not possible to investigate in detail in this thesis, but may add valuable knowledge for the ongoing use of the AMDG and its potential for dispersion include the influence of the EAUC, internal waves, coastal trapped waves, and seasonal variability.

6.4 Innovations and Advancements of this Research

This thesis represents advancement in scientific knowledge in 4 main areas of research:

- the physical setting of the northeast shelf east of Great Barrier Island;
- the study of the mechanics of disposal of dredged material in a deep-water setting;
- the use of ADCP backscatter to track plumes arising from disposal of dredged material; and
- use of the MIKE 3FM coupled Mud Transport Model for simulating the disposal process.

Though the northeast shelf is one area of New Zealand that has been studied with some degree of thoroughness, the majority of the research has been limited to the Hauraki Gulf, and the Northland and Coromandel/Bay of Plenty coasts, leaving a noticeable gap in knowledge on the shelf region east of Great Barrier Island. Prior to the work presented in this thesis, information for the area east of Great Barrier Island has been obtained by studies looking mainly at one type of data only (i.e. temperature records only), or is based on assumptions developed from work done in areas to the north and south. The findings presented primarily in Chapter 3, and to some extent in Chapter 4, help to close that gap by describing the physical

dynamics of the shelf area in the vicinity of the AMDG using the most diverse and long-term datasets available to date. The research has shown that the area, while in some respects follows the expected behaviour, in other respects possesses its own unique features not previously observed in other areas along the northeast coast. The main findings of this work that generally diverge from commonly understood characteristics of the northeast coast shelf include:

- the indication of locally influenced tidal wave propagation;
- the influence of the longer period tidal constituent M_m;
- the presence of a strong southeasterly flow signature throughout the water column; and
- the potential influence of the local shelf morphology on the initiation of upwelling events.

One reason that the area east of Great Barrier is under-represented in the scientific literature is that it is far from the nearest mainland and is characterised by relatively deep water making it more difficult to study compared to nearshore areas. This is a theme that has also dictated the study of the mechanics of dredged material disposal. While the topic is far from neglected in the scientific literature, it is surprising how few studies have been undertaken at depths greater than 50 m. As such, examination of the mechanics of disposal of dredged material in this study, at a water depth of 140 m, provides confirmation of the key processes, but also identifies how deep water disposal differs from the commonly accepted theories developed from studies undertaken in shallower waters. This is an important advancement, because in absence of other disposal options, it is becoming more desirable to dispose of dredged material in offshore areas; where it is less likely that the material will be resuspended and transported back to the dredged area or to local beaches.

The methods employed in this thesis for monitoring and tracking the sediment plumes arising from disposal of dredged material also represent an advancement on published studies, partly due to the identification of methods that were not well-suited for resolving the plume characteristics, such as stationary OBS

measurements and water samples, and more importantly, the successful use of ADCP backscatter as a proxy for turbidity. In such an unconstrained and unknown environment, it was very difficult to predict which techniques would provide the most comprehensive data. So, in that respect, the defining of the optimal methods in this study allows for the avoidance of impractical methods in potential future surveys at the AMDG or elsewhere. Moreover, the use of ADCP backscatter as a proxy for turbidity, while well-known for its usefulness in other realms, has not been greatly employed for the monitoring of dredged material disposal. The application in this case required some adjustment due to the highly transient nature of the plume, which was somewhat underestimated, but the experiences gained in this study can be used to greatly enhance the resolution of disposal plumes in future studies.

Finally, the use of the MIKE 3FM Mud Transport Model for simulation of the disposal process was examined. This model includes a 'Dredging Dialog' which allows for the removal (dredging) or discharge (disposal) of sediment at specified locations within the model domain. However, the discharge function is designed to simulate dredging spill (e.g. relatively small amounts of fluid-like slurry material released from hopper). This material has very different properties to those of dredged material disposed as a reasonably coherent mass through split hopper doors. As a consequence, there are several deficiencies in the model, which make simulation of the disposal process inaccurate, such as the requirement that the discharged material be define as a dry weight, lack of consideration for the bulk properties of the dredged material, and the lack of capability for the development of a density surge.

Despite these deficiencies, the model produced reasonable results with respect to surface dispersion of the plume, with the main errors, most likely, a result of insufficient boundary data. The conclusions on the applicability of the model has brought about the suggestion that it could be used in a coupled setting with the USACE model STFATE, which can provide better results on the dynamic phases of the disposal process, but itself lacks the capability for long-term passive dispersion simulation. This combination could prove to be a valuable tool for

future work on the development of a field calibrated model for the disposal process.

6.5 Suggestions for Future Research

Within each approach described in this thesis, there were avenues for achieving each set of objectives that, due to lack of resources and/or time, were not taken, but that offer possibilities for improvements to the findings presented herein. The following set outs methods that can and should be used if further information is required with regard to the physical characteristics of the AMDG and its dispersion potential. The suggestions given below can also be applied for similar purposes at other locations for understanding the physical dynamics of an open sea location, plume dispersion due to disposal of dredged material or that from other sources, and for setting up and implementing a numerical model for simulating dispersion of disposed dredged material.

6.5.1 Hydrodynamic Observations (Chapter 3)

Certain details that were not possible to resolve with the dataset discussed in Chapter 3 remain unknown due mainly to lack of information on seasonal variation and lack of spatial coverage of the area. Therefore, the following additions are recommended for future research:

- long-term ADCP deployments resolving the entire water column throughout or encompassing all seasons and deployed at strategic locations to allow for collection of data that can be used for forcing a near-field model, resolving other features, such as coastal trapped waves and internal waves, and for identifying seasonal variability;

- long-term deployments should include the deployment of a pressure sensor for resolution of local tidal fluctuations;

- temperature and salinity measurements throughout the year(s) for determining the vertical structure of the water column and how it varies seasonally, as well as for boundary forcing of a baroclinic hydrodynamic model; and

- wind measurements from a nearby location (e.g. Cuvier Island in the case of the AMDG), which would allow for more accurate resolution of the influence of wind on the residual current at the AMDG.

6.5.2 Disposal Plume Resolution (Chapter 4)

Despite the significant effort in recording the plumes arising from the disposal of dredged material at the AMDG, as described in Chapter 4, their unexpectedly transient nature resulted in data gaps that may have been avoided if alternative tactics had been employed. The following are recommendations for improved measurement and tracking of disposal-related plumes, as well as other sediment plumes:

- deployment of an upward-facing ADCP spanning the length of all monitoring periods to complement boat-mounted ADCP records and if resources permit, two simultaneous upward-facing deployments would allow for improved resolution of potential density surges related to impact of sediment with the seabed[12];

- use of strategic transect locations for boat-mounted ADCP measurements (i.e. on a grid) using a system and settings that can resolve both the current velocity and backscatter throughout the whole water column;

- use of a calibrated ADCP system (i.e. where terms such as, source level from transducer (*SL*), acoustic losses (*AL*), and ensonified volume (*RV*) are known) to allow for inversion of ADCP backscatter data (turbidity) to the more commonly accepted units of mg/l via the sonar equation; and

[12] Ideally, the deployment locations of two upward-facing ADCPs on the seabed would be such that one could record the descent of the material and its impact with the bed, and the other could record the passing of a density surge. However, in practice, accurate placement would be very difficult at such water depths, both in the placement of the instruments, as well as with regards to the requirement that the material be released precisely over the position of the ADCP; not to mention the possibility that the transducers may be damaged by aggregates falling at a high velocity. These suggestions would require further consideration as to their feasibility in the setting of the ADCP.

- collection of water samples and/or OBS measurements near the first or second bin of each ADCP system used for acquiring the necessary info to calibrate backscatter measurements to mg/l.

6.5.3 Modelling of the Disposal Process (Chapter 5)

Development of a representative model that accurately reproduces flow conditions and the dispersive characteristics of a site, is inherently complex. In this case, it was further complicated due to the water depth at the AMDG (requiring multiple model layers and, thus, increased computation time (>8 hours for just 4 layers and 2.5 model days) and detailed vertical boundary information), its offshore location (better suited to a far-field model), and the transient nature and other unique aspects of disposal plumes (better suited to a near-field model). The above aspects contributed to limitations in the model developed in Chapter 5. Improvements to the accuracy of the model results could be achieved with the following steps:

- coupling of the results of STFATE, for improved simulation of disposal phases 1 and 2, with the MIKE 3FM Mud Transport model, for simulation of disposal phase 3 and multiple disposal (long-term) scenarios;

- use of improved boundary condition data (see recommendations for instrument deployments in Section (6.5.1);

- collect detailed information on the characteristics of the dredged material within the hopper immediately prior to disposal;

- undertake idealised model scenarios that focus on the effects of waves, and possible variations in the disposal method and dredged material type.

6.6 Closing Remarks

This thesis presents research that, on the surface, is very applied in nature. The overall aim of the research was essentially to answer the questions raised by Maritime New Zealand (MNZ) and to assist them in decision-making for future use of the AMDG. In that respect, the research contributes to the environmentally

sustainable ambitions of the New Zealand Government, a worthy achievement in itself.

Aside from the applied contributions of this thesis, however, several fundamental outcomes have evolved that advance knowledge on both a national and international scale. The findings of Chapter 3 contribute to the understanding of New Zealand's continental shelf, as well as continental shelves in a more general sense. Chapter 4 results contribute to the body of knowledge on the process of disposal of dredged material, but also serve as a general guide for measuring any sediment plumes. The experience in the numerical simulation of the processes in question described in Chapter 5, highlight an area for improvement in the capability of the model applied, but also serve as an account of pitfalls that, in some cases, can be avoided if the special circumstances of the situation being modelled are better accounted for.

The application of science in this case, therefore, has improved the fundamental understanding, which in turn may one day improve the application of the science.

> *'There is no such thing as a special category of science called applied science; there is science and its applications, which are related to one another as the fruit is related to the tree that has borne it.'*
>
> -Louis Pasteur

LITERATURE CITED

Aarninkhof, S., & Luijendik, A. (2010). Safe disposal of dredged material in a sensitive environment based on innovative plume predictions. *Terra et Aqua, 119*, 21-28.

ADM Elektronik. (2003). *BIO-FISH Towed-system (Serial number 8-102): User's manual*: Analoge und digitale Meßsysteme (ADM) Elektronik. 77p.

Allen, J. S., & Kundu, P. K. (1978). On the momentum, vorticity and mass balance on the Oregon Shelf. *Journal of Physical Oceanography, 8*, 13-27.

Alther, G. R. (1984). Monitoring of descending dredged material plumes. *Ohio Journal of Science, 84*(1), 19-28.

Andersen, O. B. (1995). Global ocean tides from ERS 1 and TOPEX/POSEIDON altimetry. *J. Geophys. Res., 100*(C12), 25249-25259.

Anderson, K., Wang, T., Cappellino, S., John, S., Lyons, M., & Morton, J. (2002). *Developing a Los Angeles region dredged material management plan: a coordinated effort.* Paper presented at the Dredging '02, Orlando, FL.

APHA. (1997). *2540 D Total suspended solids dried at 103-105°C.*: American Public Health Association (APHA), American Water Works Association, Water Environment Federation.

Auckland Council. (2010). Harbour Master; Recreational boating. Retrieved July 15, 2011, from http://www.arc.govt.nz/environment/coastal-and-marine/harbourmaster/recreational-boating.cfm

Australian Government Bureau of Meteorology. (2011). Southern Oscillation Index. Retrieved 28 October, 2011, from http://www.bom.gov.au/climate/current/soi2.shtml

Australian Government Bureau of Meterology. (2011). Southern Oscillation Index. Retrieved 28 October, 2011, from http://www.bom.gov.au/climate/current/soi2.shtml

Bartholomä, A., Kubicki, A., Badewien, T., & Flemming, B. (2009). Suspended sediment transport in the German Wadden Sea - seasonal variations and extreme events. *Ocean Dynamics, 59*(2), 213-225.

Battisti, D. S., & Hickey, B. M. (1984). Application of remote wind-forced coastal trapped wave theory to the Oregon and Washington coasts. *Journal of Physical Oceanography, 14*(5), 887-935.

Bell, R. G., & Goring, D. G. (1996). Techniques for analyzing sea level records around New Zealand. *Marine Geodesy, 19*(1), 77-98.

Beyer, A., Chakraborty, B., & Schenke, H. (2007). Seafloor classification of the mound and channel provinces of the Porcupine Seabight: an application of the multibeam angular backscatter data. *International Journal of Earth Sciences, 96*(1), 11-20.

Bioresearches. (2009). *Pine Harbour Marina Limited - Pre dredging marina basin biological and sediment characteristics report, September 2009*. Auckland.

Black, K. P., Bell, R. G., Oldman, J. W., Carter, G. S., & Hume, T. S. (2000). Features of 3-dimensional barotropic and baroclinic circulation in the Hauraki Gulf, New Zealand. *New Zealand Journal of Marine and Freshwater Research, 34*, 1-28.

Black, K. S., Athey, S., Wilson, P., & Evans, D. (2004, 20-22 September, 2004). *Particle tracking: a new tool for coastal zone sediment management.* Paper presented at the Littoral 2004, Aberdeen, Scotland.

Black, K. S., Athey, S., Wilson, P., & Evans, D. (2007). The use of particle tracking in sediment transport studies: a review. *Geological Society, London, Special Publications, 274*(1), 73-91.

Bokuniewicz, H. J., Gilbert, J., Gordon, R. B., Higgins, J. L., Kaminsky, P., Pilbeam, C. C., et al. (1978). *Field study of the mechanics of the placement of dredged material at open-water disposal sites.* (No. D-78-7). Vicksburg, MS: US Army Engineer Waterways Experiment Station.

Bokuniewicz, H. J., & Gordon, R. B. (1980). Deposition of dredged sediment at open water sites. *Estuarine and Coastal Marine Science, 10*(3), 289-303.

Bolam, S. G., Barry, J., Bolam, T., Mason, C., Rumney, H. S., Thain, J. E., et al. (2011). Impacts of maintenance dredged material disposal on macrobenthic structure and secondary productivity. *Marine Pollution Bulletin, In Press, Corrected Proof*.

Bolam, S. G., & Rees, H. L. (2003). Minimizing Impacts of Maintenance Dredged Material Disposal in the Coastal Environment: A Habitat Approach. *Environmental Management, 32*(2), 171-188.

Bolam, S. G., Rees, H. L., Somerfield, P., Smith, R., Clarke, K. R., Warwick, R. M., et al. (2006). Ecological consequences of dredged material disposal in the marine environment: A holistic assessment of activities around the England and Wales coastline. *Marine Pollution Bulletin, 52*(4), 415-426.

Bowden, D., Fenwick, M., Spong, K., Chin, C., & Miller, A. (2010). *Bay of Islands OS20/20 survey report. Chapter 9: seafloor assemblage and habitat assessment using DTIS.* http://www.os2020.org.nz/browse-data-boi.

Bradshaw, B. E., Healy, T. R., Dell, P. M., & Bolstad, W. M. (1991). Inner Shelf Dynamics on a Storm-Dominated Coast, East Coromandel, New Zealand. *Journal of Coastal Research, 7*(1), 11-30.

Bradshaw, B. E., Healy, T. R., Nelson, C. S., Dell, P. M., & de Lange, W. P. (1994). Holocene sediment lithofacies and dispersal systems on a storm-dominated, back-arc shelf margin: The east Coromandel coast, New Zealand. *Marine Geology, 119*(1-2), 75-98.

Brandsma, M. G., & Divoky, D. J. (1976). *Development of models for prediction and short-term fate of dredged material discharged in the estuarine environment* (No. D-76-5). Vicksburg, MI: US Army Engineering Waterways Experiment Station.

Brodie, J. W. (1960). Coastal surface currents around New Zealand. *New Zealand Journal of Geology and Geophysics, 3*, 235-252.

Campbell Scientific Inc. (2008). *OBS3+ Suspended solids and turbidity monitor: operators manual.* 40p.

Chang, F. H., Zeldis, J., Gall, M., & Hall, J. (2003). Seasonal and spatial variation of phytoplankton assemblages, biomass and cell size from spring to summer across the north-eastern New Zealand continental shelf. *Journal of Plankton Research, 25*(7), 737-758.

Chapman, D. C. (1987). Application of Wind-Forced, Long, Coastal-Trapped Wave Theory Along the California Coast. *J. Geophys. Res., 92*(C2), 1798-1816.

Chin, J. L., & Ota, A. Y. (2001). Disposal of dredged material and other waste on the continental shelf and slope. In H. A. Karl, J. L. Chin, E. Ueber, P. H. Stauffer & J. W. Hendley (Eds.), *Beyond the Goldengate-Oceanography, geology, biology and environmental issues in the Gulf of Farallones* (pp. 193-206). Menlo Park, C.A.: U.S. Geological Survey.

Chiswell, S. M. (2000). Tidal Energetics over the Chatham Rise, New Zealand. *Journal of Physical Oceanography, 30*(9), 2452-2460.

Chiswell, S. M., & Moore, M. I. (1999). Internal Tides near the Kermadec Ridge. *Journal of Physical Oceanography, 29*(5), 1019-1035.

Clay, C. S., & Medwin, H. (1977). *Acoustical oceanography*. New York: John Wiley and Sons.

Clyde, M. J., & Christian, C. (1993). *Mobilisation of dredge spoil by wave action.* Paper presented at the 11th Australian Conference on Coastal and Ocean Engineering: Coastal Engineering a Partnership with Nature, Townsville, Australia.

Cresswell, G. (1994). Nutrient enrichment of the Sydney continental shelf. *Australian Journal of Marine and Freshwater Research, 45*, 677-691.

Crossley, J. (2010, June 24, 2010). Wairoa river canal plans rejected. *The National Business Review*, from http://www.nbr.co.nz/article/wairoa-river-canal-development-plans-rejected-125130

Csanady, G. T. (1997). On the theories that underlie our understanding of continental shelf circulation. *Journal of Oceanography, 53*, 207-229.

Davies-Colley, R. J., & Smith, D. G. (2001). Turbidity, suspended sediment, and water clarity: a review. *Journal of the American Water Resources Association, 37*(5), 1085-1101.

Davies, A. M. (1983). Comparison of computed and observed residual currents during Jonsdap '76. In B. Johns (Ed.), *Elsevier Oceanography Series, 35: Physical oceanography of coastal and shelf seas* (pp. 357-386). Amsterdam, The Netherlands: Elsevier.

de Lange, W. P., Bell, R. G., Gorman, R., & Ried, S. (2003). Physical oceanography of New Zealand waters. In J. Goff, S. L. Nichol & H. L. Rouse (Eds.), *The New Zealand coast Te tai o Aotearoa* (pp. 59-77). Palmerston North, New Zealand: Dunmore Press.

Delogu, O. E. (1990). "NIMBY" is a national environmental problem. *South Dakota Law Review, 35*, 198-219.

Denham, R. N., Bannister, R. W., Guthrie, K. M., & Crook, F. G. (1984). Surveys of the east Auckland and East Cape Currents, New Zealand. *Australian Journal of Marine and Freshwater Research, 35*(5), 491-504.

Dever, E. P. (1997). Wind-Forced Cross-Shelf Circulation on the Northern California Shelf. *Journal of Physical Oceanography, 27*(8), 1566-1580.

DHI. (2010). *MIKE 21 Flow Model FM, Hydrodynamic Module, User Guide*: DHI Water & Environment. 108 p.

DHI. (2011a). *MIKE 21 & MIKE 3 Flow Model FM*: DHI Water & Environment. 50 p.

DHI. (2011b). *MIKE 21 & MIKE 3 Flow Model FM Mud Transport Module Scientific Documentation*: DHI Water & Environment. 40 p.

Dinehart, R. L., & Burau, J. R. (2005). Repeated surveys by acoustic Doppler current profiler for flow and sediment dynamics in a tidal river. *Journal of Hydrology, 314*(1–4), 1-21.

Disposal Options Advisory Group. (1994). *Assessment of the options available for the disposal of dredged material from the Port of Auckland* (No. 1-5). Auckland.

Doneker, R. L., Nash, J. D., & Jirka, G. H. (2004). Pollutant transport and mixing zone simulation of sediment density currents. *Journal of Hydraulic Engineering, 130*(4), 349-359.

Drapeau, G., Gauthier, D., & Lavallee, D. (1999). In Situ Deposition versus Transport by Density Currents of Dredged Sediments Dumped in Coastal Waters. *Journal of Coastal Research, 15*(1), 87-96.

Drapeau, G., Lavallee, D., Dumais, J. F., & Walsh, G. (1992). *Dispersion model of dredge spoil dumped in coastal waters.* Paper presented at the Coastal Engineering, Venice, Italy.

Dvorak, M. J., Archer, C. L., & Jacobson, M. Z. (2010). California offshore wind energy potential. *Renewable Energy, 35*(6), 1244-1254.

Ebisuzaki, W. (1997). A Method to Estimate the Statistical Significance of a Correlation When the Data Are Serially Correlated. *Journal of Climate, 10*(9), 2147-2153.

Egbert, G. D., & Erofeeva, S. Y. (2002). Efficient Inverse Modeling of Barotropic Ocean Tides. *Journal of Atmospheric and Oceanic Technology, 19*(2), 183-204.

Eggleton, J., & Thomas, K. V. (2004). A review of factors affecting the release and bioavailability of contaminants during sediment disturbance events. *Environment International, 30*(7), 973-980.

Eisma, D. (1986). Flocculation and de-flocculation of suspended matter in estuaries. *Netherlands Journal of Sea Research, 20*(2â€“3), 183-199.

Endler, R. (2009). Sediment physical properties of the DYNAS study area. *Journal of Marine Systems, 75*(3-4), 317-329.

EPA. (2012). The United States Environmental Protection Agency. Retrieved December 11, 2012, from http://www.epa.gov/aboutepa/

EPA/USACE. (2008). *Miami ocean dredged material disposal site: site management and monitoring plan*: U.S. Environmental Protection Agency and the U.S. Army Corps of Engineers.

Fagerburg, T. L., & Pratt, T. (1995). Field application using acoustic Doppler systems for current and sediment flux measurements. *Hydrological Science and Technology, 11*, 17-25.

Fisher, F. H., & Simmons, V. P. (1977). Sound absorption in sea water. *Journal of the Acoustical Society of America, 62*(3), 558-564.

Flaim, B. K., & de Lange, W. P. (2011). *Post-disposal monitoring of the Auckland Marine Disposal Ground*. Hamilton, New Zealand: Coastal Marine Group, University of Waikato. 186 p.

Flaim, B. K., & Healy, T. R. (2008). *Proposal for dredged sediment disposal on the continental shelf in the EEZ: environment impact assessment*. Hamilton, New Zealand: Coastal Marine Group, University of Waikato. 96 p.

Flaim, B. K., Healy, T. R., & Weir, P. (2010). Establishment of a dredged material disposal site in the Exclusive Economic Zone: New Zealand. *Coastal Management, 38*(5), 474-500.

Flaim, B. K., Stark, N., Moon, V., de Lange, W. P., Healy, T. R., & Kopf, A. (2011). *Monitoring a dredged material disposal site on the continental shelf using the dynamic penetrometer Nimrod.* Paper presented at the Coastal Sediments 2011, Miami, USA.

Foster, G. A., Healy, T. R., & Lange, W. P. D. (1996). Presaging Beach Renourishment from a Nearshore Dredge Dump Mound, Mt. Maunganui Beach, New Zealand. *Journal of Coastal Research, 12*(2), 395-405.

Fredette, T. J., & French, G. T. (2004). Understanding the physical and environmental consequences of dredged material disposal: history in New England and current perspectives. *Marine Pollution Bulletin, 49*(1–2), 93-102.

Freeland, H. J., Boland, F. M., Church, J. A., Clarke, A. J., Forbes, A. M. G., Huyer, A., et al. (1986). The Australian coastal experiment: a search for coastal-trapped waves. *Journal of Physical Oceanography, 16*, 1230-1249.

Freudenburg, W. R., & Gramling, R. (1994). *Oil in troubled waters*. Albany: State University of New York Press.

Gao, S., & Jia, J.-j. (2002). Modeling suspended sediment distribution in continental shelf upwelling/downwelling settings. *Geo-Marine Letters, 22*(4), 218-226.

Garner, D. M. (1961). *Hydrology of New Zealand Coastal Waters* (New Zealand Department of Scientific and Industrial Research Bulletin 138, Memoir No. 8). Wellington, New Zealand: New Zealand Oceanographic Institute.

Gartner, J. W. (2004). Estimating suspended solids concentrations from backscatter intensity measured by acoustic Doppler current profiler in San Francisco Bay, California. *Marine Geology, 211*(3-4), 169-187.

Gartner, J. W., & Cheng, R. T. (2001). *The promises and pitfalls of estimating total suspended solids based on backscatter intensity from acoustic Doppler current profiler.* Paper presented at the Seventh Federal Interagency Sedimentation Conference, Reno, Nevada.

Germano and Associates Inc. (2010). *Review/synthesis of historical environmental monitoring data collected at the San Francisco Deep Ocean Disposal Site (SF-DODS) in support of EPA regulatory decision to revise the site's management and monitoring plan*. Bellvue, WA: USEPA Region 9.

Giddings, N. C. (2011). Go offshore young man! The categorical exclusion solution to offshore wind farm development on the outer continental shelf. *Journal of Energy and Environmental Law*(Winter), 75-86.

Golder Kingett Mitchell. (2007). *Pine Harbour sediment assessment September 2007* (No. PINHAAKL002). Auckland: Golder Kingett Mitchell.

Gordon, N. D. (1985). The Southern Oscillation: A New Zealand perspective. *Journal of the Royal Society of New Zealand, 15*(2), 137-155.

Gordon, R. B. (1974). Dispersion of dredge spoil dumped in near-shore waters. *Estuarine and Coastal Marine Science, 2*, 349-358.

Gorman, R. M., Bryan, K. R., & Laing, A. K. (2003). Wave hindcast for the New Zealand region: deep-water wave climate. *New Zealand Journal of Marine and Freshwater Research, 37*, 589-612.

Grace, R. V. (1988). *Ecological investigation of the Auckland Harbour Board's alternative dredge spoil dump site off Brown's Island, Waitemata Harbour.*: Report prepared for the Auckland Harbour Board.

Grant, W. D., & Madsen, O. S. (2003). The Continental-Shelf Bottom Boundary Layer. *Annual Review of Fluid Mechanics, 18*(1), 265-305.

Greenspan Technology (a). (n.d.). *Turbidity sensor TS100: user manual (edition 3.0)*. 26p.

Greenspan Technology (b). (n.d.). *Turbidity sensor TS1200: user manual (edition 1.2)*. 29p.

Greig, M. J. (1990). Circulation in the Hauraki Gulf, New Zealand. *New Zealand Journal of Marine and Freshwater Research, 24*, 141-150.

Ha, H. K., Maa, J. P. Y., Park, K., & Kim, Y. H. (2011). Estimation of high-resolution sediment concentration profiles in bottom boundary layer using pulse-coherent acoustic Doppler current profilers. *Marine Geology, 279*(1-4), 199-209.

Halka, J., Panageotou, W., & Sanford, L. (1991). Consolidation and erosion of deposited cohesive sediments in Northern Chesapeake Bay, USA. *Geo-Marine Letters, 11*(3), 174-178.

Hall, J. A., Safi, K., James, M. R., Zeldis, J., & Weatherhead, M. (2006). Microbial assemblage during the spring-summer transition on the northeast continental shelf on New Zealand. *New Zealand Journal of Marine and Freshwater Research, 40*, 195-210.

Hands, E. B., & Allison, M. C. (1991). *Mound migration in deeper water and methods of categorizing active and stable mounds.* Paper presented at the Coastal Sediments, Seattle, Washington.

Harris, T. F. W. (1985). *North Cape to East Cape aspects of the physical oceanography*. Leigh, New Zealand: University of Auckland.

Healy, T. R. (2002). Muddy coasts of mid-latitude oceanic islands on an active plate margin-New Zealand. In T. R. Healy, Y. Wang & J.-A. Healy (Eds.), *Muddy coasts of the world: processes, deposits, and function* (Vol. 4, pp. 347-374). Amsterdam, the Netherlands: Elsevier Science B.V.

Heath, R. A. (1984). Tidal observations on the west coast, South Island, New Zealand. *New Zealand Journal of Marine and Freshwater Research, 18*, 251-261.

Heath, R. A. (1985). A review of the physical oceanography of the seas around New Zealand - 1982. *New Zealand Journal of Marine and Freshwater Research, 19*, 79-124.

Hendershott, M., & Munk, W. (1970). Tides. *Annual Review of Fluid Mechanics, 2*(1), 205-224.

Herbich, J. B. (1981). Chapter 7 Environmental Effects of Unconfined and Confined Disposal of Dredged Materials in Open Water. In A. G. Richard (Ed.), *Elsevier Oceanography Series* (Vol. Volume 27, Part B, pp. 241-260): Elsevier.

Hill, D. C., Jones, S. E., & Prandle, D. (2003). Derivation of sediment resuspension rates from acoustic backscatter time-series in tidal waters. *Continental Shelf Research, 23*(1), 19-40.

Hitchcock, D. R., & Bell, S. (2004). Physical Impacts of Marine Aggregate Dredging on Seabed Resources in Coastal Deposits. *Journal of Coastal Research*, 101-114.

Hoitink, A. J. F., & Hoekstra, P. (2005). Observations of suspended sediment from ADCP and OBS measurements in a mud-dominated environment. *Coastal Engineering, 52*(2), 103-118.

Holdaway, G. P., Thorne, P. D., Flatt, D., Jones, S. E., & Prandle, D. (1999). Comparison between ADCP and transmissometer measurements of suspended sediment concentration. *Continental Shelf Research, 19*, 421-441.

Holliday, B. W. (1978). *Processes affecting the fate of dredged material* (No. DS-78-2). Vicksburg, M.S.: U.S. Army Engineer Waterways Experiment Station Environmental Laboratory.

Holligan, P. M., Pingree, R. D., & Mardell, G. T. (1985). Oceanic solitons, nutrient pulses and phytoplankton growth. *Nature, 314*(6009), 348-350.

Howlett, E., Galagan, C., Clausner, J., & Johnson, B. H. (2000). *DREDGEMAP: a GIS-based dredging model system.* Paper presented at the Oceans 2000 MT S/IEEE Conference and Exhibition, Providence, RI.

Hsu, S. A., Meindl, E. A., & Gilhousen, D. B. (1994). Determining the Power-Law Wind-Profile Exponent under Near-Neutral Stability Conditions at Sea. *Journal of Applied Meteorology, 33*(6), 757-765.

Hughes Clarke, J. E., Mayer, L. A., & Wells, D. E. (1996). Shallow-water imaging multibeam sonars: A new tool for investigating seafloor processes in the coastal zone and on the continental shelf. *Marine Geophysical Researches, 18*(6), 607-629.

Hull, J. M. (1996). *Wave induced sediment transport on intertidal flats in a fetch limited environment, Pine Habour Marina, Auckland.* University of Waikato, Hamilton.

Hume, T. M., Bell, R. G., de Lange, W. P., Healy, T. R., Hicks, D. M., & Kirk, R. M. (1992). Coastal oceanography and sedimentology in New Zealand, 1967-91. *New Zealand Journal of Marine and Freshwater Research, 26*(1), 1-36.

Hume, T. S. (1983). *Upper Waitemata Harbour sediments and the inferred impact of future catchment and estuary use change*. Hamilton: Auckland Regional Authority.

Huyer, A. (1990). Shelf Circulation. In B. Le Mehaute & D. M. Hanes (Eds.), *The sea: ideas and observations on the progress in the study of the seas, Ocean Engineering Science 9 (Part A)* (pp. 423-466). New York: John Wiley and Sons.

International Maritime Organisation. (2003). *Convention on the prevention of marine pollution by dumping of wastes and other matter 1972 and 1996 protocol* (2003 ed.). London, England: International Maritime Organisation.

Jiang, N., Hay, J. E., & Fisher, G. W. (2004). Classification of New Zealand synoptic weather types and relation to the Southern Oscillation Index. *Weather and Climate, 23*, 3-23.

Johnson, B. H., & Fong, M. T. (1995). *Development and verification of numerical models for predicting the initial fate of dredged material disposed in open water; report 2, theoretical developments and verification results* (No. DRP-93-1). Vicksburg, MS: US Army Engineers Waterways Experiment Station.

Johnson, D. (1987). *New Zealand's maritime heritage*. Auckland: William Collins.

Joyce, J. (1979). On the behaviour of dumped dredger spoil. *Marine Pollution Bulletin, 10*(6), 158-160.

Kagan, R. A. (1994). Dredging Oakland Harbor: implications for ocean governance. *Ocean and Coastal Management, 23*, 49-63.

Kaltschmitt, M., Streicher, W., & Wiese, A. (2007). *Renewable Energy*. Berlin: Springer.

Kneller, B., & Buckee, C. (2000). The structure and fluid mechanics of turbidity currents: a review of some recent studies and their geological implications. *Sedimentology, 47*, 62-94.

Koh, R. C. Y. (1971). Ocean Sludge Disposal by Barges. *Water Resour. Res., 7*(6), 1647-1651.

Koh, R. C. Y., & Chang, Y. C. (1973). *Mathematical model for barged ocean disposal of waste*. Washington, D.C.: US Environmental Protection Agency. 178 p.

Kongsberg. (2005). *Product description EM3000 Multibeam echo sounder*. Horten, Norway: Kongsberg Maritime. 36p.

Krishnappan, B. G. (1975). *Dispersion of granular material dumped in deep water* (No. 55): Environment Canada, Inland Waters Directorate.

Lambert, I. B. (2001). Mining and sustainable development: considerations for minerals supply. *Natural Resources Forum, 25*(4), 275-284.

Langtry, S., Rayson, M., Makarynskyy, O., & Zapata, M. (2009). *Optimal selection of sediment disposal sites in open coast locations.* Paper presented at the Coasts and Ports 2009, Wellington, New Zealand.

Lentz, S., & Winant, C. D. (1986). Subinertial currents on the southern California shelf. *Journal of Physical Oceanography, 16*(11), 1737-1750.

Li, M. Z., Parrott, D. R., & Yang, Z. (2009). Sediment Stability and Dispersion at the Black Point Offshore Disposal Site, Saint John Harbour, New Brunswick, Canada. *Journal of Coastal Research, 25*(4), 1025-1040.

LINZ. (1999). Firth of Thames NZ533, *North Island - New Zealand*: Land Information New Zealand (LINZ), Hydrographic Office of the Royal New Zealand Navy, scale: 1:100,000.

LINZ. (2002). Bream Head to Slipper Island including Hauraki Gulf NZ53, *North Island - East Coast*: Land Information New Zealand (LINZ), Hydrographic Office of the Royal New Zealand Navy. scale: 1:200,000.

LINZ. (2004). Cape Brett to Cuvier Island NZ52, *North Island - East Coast*

Land Information New Zealand (LINZ), Hydrographic Office of the Royal New Zealand Navy. scale: 1:200,000.

LINZ. (2007). Cuvier Island to East Cape NZ54, *North Island - East Cape*: Land Information New Zealand (LINZ), Hydrographic Office of the Royal New Zealand Navy, scale: 1:300,000.

LINZ. (2009). Mayor Island to Okurei Point NZ541, *North Island - East Coast*: Land Information New Zealand (LINZ), Hydrographic Office of the Royal New Zealand Navy, scale: 1:100,000.

Longdill, P. C. (2007). *Environmentally sustainable aquaculture: an eco-physical perspective.* University of Waikato, Hamilton.

Longdill, P. C., Healy, T. R., & Black, K. P. (2008). Transient wind-driven coastal upwelling on a shelf with varying width and orientation. *New Zealand Journal of Marine and Freshwater Research, 42*, 181-196.

Loomb, C., & Healy, T. R. (2000). Muddy sedimentation in a sheltered estuarine marina, Auckland, New Zealand. *Journal of Coastal Research, ICS 2000 Proceedings*, 357-369.

Lorke, A., McGinnis, D. F., Spaak, P., & Wüest, A. (2004). Acoustic observations of zooplankton in lakes using a Doppler current profiler. *Freshwater Biology, 49*(10), 1280-1292.

Louisse, C. J., Akkerman, R. J., & Suylen, J. M. (1986). A fluorescent tracer for cohesive sediment. *In: International conference on measuring techniques of hydraulics phenomena in offshore, coastal and inland waters* (pp. 367-391). London, England, 9-11 April, 1986.

Lurton, X. (2002). *An introduction to underwater acoustics, principles, and applications*. Chichester: Praxis Publishing, Ltd.

Lynch, J. F., Irish, J. D., Gross, T. F., Wiberg, P. L., Newhall, A. E., Traykovski, P. A., et al. (1997). Acoustic measurements of the spatial and temporal structure of the near-bottom boundary layer in the 1990-1991 STRESS experiment. *Continental Shelf Research, 17*(10), 1271-1295.

Manighetti, B., & Carter, L. (1999). Across-shelf sediment dispersal, Hauraki Gulf, New Zealand. *Marine Geology, 160*(3-4), 271-300.

Maurer, D., Keck, R. T., Tinsman, J. C., Leathem, W. A., Wethe, C., Lord, C., et al. (1986). Vertical Migration and Mortality of Marine Benthos in Dredged Material: A Synthesis. [10.1002/iroh.19860710106]. *Internationale Revue der gesamten Hydrobiologie und Hydrographie, 71*(1), 49-63.

McAnally, J. W. H., & Adamec, J. S. A. (1987). Designing open water disposal for dredged muddy sediments. *Continental Shelf Research, 7*(11-12), 1445-1455.

McAnally, W. H., Friedrichs, C., Hamilton, D., Hayter, E., Shrestha, P., Rodriguez, H., et al. (2007). Management of fluid mud in estuaries, bays, and lakes. I: present state

of understanding on character and behavior. *Journal of Hydraulic Engineering, 133*(1), 9-22.

McCave, I. N. (1984). Erosion, transport and deposition of fine-grained marine sediments. In D. A. V. Stow & D. J. W. Piper (Eds.), *Fine-grained sediments: deep-water processes and facies* (pp. 35-69). Oxford, England: Blackwell Scientific Publications.

Mellor, G. L. (2004). Users guide for "A three-dimensional, primitive equation, numerical ocean model". Princeton University, Princeton, NJ., from http://www.aos.princeton.edu/WWPUBLIC/htdocs.pom/

Middleton, G. V. (1966). Experiments on density and turbidity currents: I. motion of the head. *Canadian Journal of Earth Sciences, 3*(4), 523-546.

Ministry for Culture and Heritage (Ed.). (2009). *New Zealanders and the sea*. Auckland, New Zealand: David Bateman, Ltd.

Mitchener, H., & Torfs, H. (1996). Erosion of mud/sand mixtures. *Coastal Engineering, 29*(1–2), 1-25.

Moritz, H. R., & Randall, R. E. (1995). Simulating Dredged-Material Placement at Open-Water Disposal Sites. *Journal of Waterway, Port, Coastal, and Ocean Engineering, 121*(1), 36-48.

Murphy, R. J., Pinkerton, M. H., Richardson, K. M., & Bradford-Grieve, J. M. (2001). Phytoplankton distributions around New Zealand derived from SeaWiFS remotely-sensed ocean colour data. *New Zealand Journal of Marine and Freshwater Research, 35*, 343-362.

Naish, T. R. (1990). *Late holocene mud sedimentation and diagenesis in the Firth of Thames: bentonites in the making.* University of Waikato, Hamilton, New Zealand.

Naito, R., & Nakamura, Y. (2009). Strategies for the Beneficial Use of Dredged Material in Japan. In E. Moksness, E. Dahl & J. Stottrup (Eds.), *Integrated Coastal Zone Management* (pp. 237-250). Oxford: Wiley-Blackwell.

National Institute of Water and Atmospheric Research (NIWA). CliFlo: NIWA's national climate database on the web. Retrieved 5 August 2011, from Retrieved 5 August 2010: http://cliflo.niwa.co.nz: http://cliflo.niwa.co.nz

National Oceanographic and Atmospheric Administration (NOAA). NCEP_Reanalysis 2 data. from NOAA/OAR/ESRL PSD: http://www.esrl.noaa.gov/psd/ http://www.esrl.noaa.gov/psd/

Neal, R. W., Henry, G., & Greene, S. H. (1978). *Evaluation of the submerged discharge of dredged material slurry during pipeline dredge operation* (No. D-78-44). Wilmigtion, MA: US Army Waterways Experiment Station.

New Zealand Government. (2000). Hauraki Gulf Marine Park Act 2000. Retrieved from http://www.legislation.govt.nz/act/public/2000/0001/latest/DLM52558.html

New Zealand Press Association. (2010, July 13, 2011). NZ's $500m superyacht deals. from http://www.stuff.co.nz/business/industries/4259139/NZs-500m-superyacht-deals

Nichols, M., Thompson, G., & Faas, R. (1978). *Field study of fluid mud dredged material: its physical nature and dispersal* (No. D-78-40). Vicksburg, USA: U.S. Army Engineer Waterways Experiment Station.

Ogushwitz, P. R. (1994). Measurement of acoustical scattering from plumes of sediment suspended in open waters. *Journal of Marine Environmental Engineering, 1*(2), 119-130.

Oke, P. R., Brassington, G. B., Griffin, D. A., & Schiller, A. (2008). The Bluelink ocean data assimilation system (BODAS). *Ocean Modelling, 21*(1-2), 46-70.

Oldman, J. W., Senior, A., Haskew, R., & Ramsay, D. (2004). *Hauraki regional harbour model: set-up, calibration and verification* (No. HAM2004-038). Hamilton, New Zealand: National Institute of Water & Atmosphere Research, Ltd.

Orpin, A. R., Ridd, P. V., Thomas, S., Anthony, K. R. N., Marshall, P., & Oliver, J. (2004). Natural turbidity variability and weather forecasts in risk management of

anthropogenic sediment discharge near sensitive environments. *Marine Pollution Bulletin*, *49*(7–8), 602-612.

Palumbo, L. (2007). Sediment management of nations in Europe. In G. Bortone & L. Palumbo (Eds.), *Sustainable Management of Sediment Resources Sediment and Dredged Material Treatment* (Vol. 2, pp. 11-58). Amsterdam, The Netherlands: Elsevier.

Parliamentary Commissioner for the Environment. (1995). *Dredgings disposal in the Hauraki Gulf: final report of the technical review panel*. Wellington, New Zealand: Parliamentary Commissioner for the Environment.

Pawlowicz, R., Beardsley, B., & Lentz, S. (2002). Classical tidal harmonic analysis including error estimates in MATLAB using T-TIDE. *Computers & Geosciences*, *28*(8), 929-937.

Peart, R. (2006). *Managing New Zealand's Coastal Development: The Role of National Policy*. Paper presented at the Coast to Coast 2006, Melbourne, VIC, Australia.

Peart, R. (2007). *Beyond the tide*. Auckland, New Zealand: Environmental Defence Society Inc.

Pickrill, R. A., & Mitchell, J. S. (1979). Ocean wave characteristics around New Zealand. *New Zealand Journal of Marine and Freshwater Research*, *13*(4), 501-520.

Poindexter-Rollings, M. E. (1990). *Methodology for analysis of subaqueous sediment mounds* (No. D-90-2). Vicksburg, MS: US Army Engineer Waterways Experiment Station.

Ports of Auckland Ltd. (2009). Ports of Auckland consent heralds final preparations for larger container ships. *Media release* Retrieved July, 22, 2009, from http://www.poal.co.nz/news_media/2009_mediareleases/090527_ConsentLargerShips.htm

Potter, P. E., Maynard, J. B., & Depetris, P. J. (2005). *Mud and mudstones: introduction and overview*. Berlin, Germany: Springer.

Preston, J. M., Parrott, D. R., & Collins, W. T. (2003). *Sediment classification based on repetitive multibeam bathymetry surveys of an offshore disposal site*. Paper presented at the Oceans, San Diego, C.A.

Proctor, R., & Greig, M. J. (1989). A numerical model investigation of the residual circulation in Hauraki Gulf, New Zealand. *New Zealand Journal of Marine and Freshwater Research*, *23*, 421-442.

Puckette, T. P. (1998). *Evaluation of dredged material plumes - physical monitoring techniques* (No. TN DOER-E5). Vicksburg, MS: US Army Engineer Research and Development Center.

Reine, K. J., Clarke, D. G., & Dickerson, C. (2002). *Acoustic characterization of suspended sediment plumes resulting from barge overflow* (No. (ERDC TN-DOER-E15)). Vicksburg, MS: U.S. Army Engineer Research and Development Center.

Ridgway, K. R., & Godfrey, J. S. (1997). Seasonal cycle of the East Australian Current. *J. Geophys. Res.*, *102*(C10), 22921-22936.

Roemmich, D., & Sutton, P. (1998). The mean and variability of ocean circulation past northern New Zealand: Determining the representativeness of hydrographic climatologies. *J. Geophys. Res.*, *103*(C6), 13041-13054.

Rogers, D. (2012). *The skeletal carbonate contribution to mixed terrigenous-carbonate sediments on the temperate northeastern Northland continental shelf, New Zealand.* University of Waikato, Hamilton, New Zealand.

Schettini, C., de Almeida, D., Siegle, E., & de Alencar, A. Ã. n. (2010). A snapshot of suspended sediment and fluid mud occurrence in a mixed-energy embayment, Tijucas Bay, Brazil. *Geo-Marine Letters*, *30*(1), 47-62.

Schlichting, H. (1968). *Boundary-layer theory* (6th ed.). New York, NY: McGraw-Hill.

Schumann, E. H., & Brink, K. (1990). Coastal-trapped waves off the coast of South Africa: generation, propagation and current structures. *Journal of Physical Oceanography*, *20*, 1206-1218.

Scott, K. J., & Redmond, M. S. (1989). The effects of a contaminated dredged material on laboratory populations of the Tubicolous Amphipod Ampelisca abdita. In U. M. Cowgill & L. R. Williams (Eds.), *Aquatic Toxicology and Hazard Assessment* (Vol. 12). Philadelphia, PA: American Society for Testing and Materials.

Sharples, J. (1997). Cross-shelf intrusion of subtropical water into the coastal zone of northeast New Zealand. *Continental Shelf Research, 17*(7), 835-857.

Sharples, J. (1998). Physical processes on the New Zealand shelf and the rest of the world's islands. In A. R. Robinson & K. Brink (Eds.), *The Sea, Volume 11* (Vol. 11, pp. 965-996): Wiley & Sons, Inc.

Sharples, J., & Greig, M. J. (1998). Tidal currents, mean flows, and upwelling on the north-east shelf of New Zealand. *New Zealand Journal of Marine and Freshwater Research, 32*, 215-231.

Sharples, J., Moore, M., & Abraham, E. R. (2001). Internal tide dissipation, mixing, and vertical nitrate flux at the shelf edge of NE New Zealand. *Journal of Geophysical Research, 106*(C7), 14069-14081.

Sheehan, C., & Harrington, J. (2012). Management of dredge material in the Republic of Ireland – A review. *Waste Management, 32*(5), 1031-1044.

Shi, Z., Ren, L. F., Zhang, S. Y., & Chen, J. Y. (1997). Acoustic imaging of cohesive sediment resuspension and re-entrainment in the Changjiang Estuary, East China Sea. *Geo-Marine Letters, 17*(2), 162-168.

Shirtcliffe, T. G. L., Moore, M. I., Cole, A. G., Viner, A. B., Baldwin, R., & Chapman, B. (1990). Dynamics of the Cape Farewell upwelling plume, New Zealand. *New Zealand Journal of Marine and Freshwater Research, 24*(4), 555-568.

Siegel, H., Gerth, M., Heene, T., Ohde, T., Rüß, D., & Kraft, H. (2009). Hydrography, currents and distribution of suspended matter during a dumping experiment in the western Baltic Sea at a site near Warnemünde. *Journal of Marine Systems, 75*(3-4), 397-408.

Sivaguru, K., & Grace, R. V. (2002). *Habitat and species diversity of deep reefs and sediments at Great Barrier Island*. Auckland, New Zealand: Department of Conservation.

Sparkes, D. (2012). Count the dredges as harbour projects go full steam ahead. *The Observer*. Retrieved from http://www.gladstoneobserver.com.au/news/count-dredges-harbour-projects-go-full-steam-ahead/1595377/

Sparks, R. S. J., Bonnecaze, R. T., Huppert, H. E., Lister, J. R., Hallworth, M. A., Mader, H., et al. (1993). Sediment-laden gravity currents with reversing buoyancy. *Earth and Planetary Science Letters, 114*(2-3), 243-257.

Stanton, B. (1977). Preliminary observations of the internal tide over the shelf west of New Zealand. *New Zealand Journal of Marine and Freshwater Research, 11*(4), 703-712.

Stanton, B., Goring, D. G., & Bell, R. G. (2001). Observed and modelled tidal currents in the New Zealand region. *New Zealand Journal of Marine and Freshwater Research, 35*, 397 - 415.

Stanton, B., Sutton, P., & Chiswell, S. M. (1997). The East Auckland Current, 1994-95. *New Zealand Journal of Marine and Freshwater Research, 31*, 537-549.

Stephens, S. A., Bell, R. G., & Black, K. P. (2001). Complex Circulation in a Coastal Embayment: Shelf-Current, Wind and Density-Driven Circulation in Poverty Bay, New Zealand. *Journal of Coastal Research, SI 43 (ICS 2000)*, 45-59.

Strang, E. J., & Fernando, H. J. S. (2001). Entrainment and mixing in stratified shear flows. *Journal of Fluid Mechanics, 428*, 349-386.

Sutton, P., & Roemmich, D. (2001). Ocean temperature climate off north-east New Zealand. *New Zealand Journal of Marine and Freshwater Research, 35*, 553-565.

Swanson, J. C., Isaji, T., Ward, M., Teeter, A., & Clarke, D. G. (2000). *Demonstration of the SSFATE numerical modeling system* (No. ERDC TN-DOER-E12). Vicksburg, MS: U.S. Army Engineer Research and Development Center.

Tay, K.-L., Osborne, J., & Wang, L. K. (2008). Ocean disposal technology and assessment. In L. K. Wang, N. K. Shammas & Y. T. Hung (Eds.), *Handbook of*

Environmental Engineering, Volume 7: Biosolids Engineering and Management (Vol. 7, pp. 443-477). Totowa, NJ: The Humana Press.

Teledyne RD Instruments. (2008). *Workhorse Sentinel self-contained 1200, 600, 300 kHz ADCP* Poway, CA: Teledyne RD Instruments. 2p.

Thomas, G. L., & Kirsch, J. (2000). Nekton and plankton acoustics: an overview. *Fisheries Research, 47*(2-3), 107-113.

Tilburg, C. E., Hurlburt, H. E., Brien, J. J., & Shriver, J. F. (2001). The Dynamics of the East Australian Current System: The Tasman Front, the East Auckland Current, and the East Cape Current. *Journal of Physical Oceanography, 31*(10), 2917-2943.

Tomczak, G. (1964). Invesitgations with drift cards to determine the influence of the wind on surface currents. *Studies on Oceanography, Tokyo University (1964)*, 129-139.

Traykovski, P., Geyer, W. R., Irish, J. D., & Lynch, J. F. (2000). The role of wave-induced density-driven fluid mud flows for cross-shelf transport on the Eel River continental shelf. *Continental Shelf Research, 20*(16), 2113-2140.

Trocine, R. P., & Trefry, J. H. (1983). Particulate metal tracers of petroleum drilling mud dispersion in the marine environment. *Environmental Science & Technology, 17*(9), 507-512.

Troell, M., Joyce, A., Chopin, T., Neori, A., Buschmann, A. H., & Fang, J.-G. (2009). Ecological engineering in aquaculture — Potential for integrated multi-trophic aquaculture (IMTA) in marine offshore systems. *Aquaculture, 297*(1–4), 1-9.

Truitt, C. L. (1988). Dredged material behaviour during open-water disposal. *Journal of Coastal Research, 4*(3), 489-497.

Tsai, J. J., Huang, H., & Proni, J. R. (1995). Acoustic Observations of Bottom Surge From Dredged Material Discharge in the Open Ocean. *Chemistry and Ecology, 10*(1-2), 71-85.

Tsai, J. J., Proni, J. R., Dammann, P. W., & Kraus, N. (1992). Dredged material disposal at the edge of the Florida Current. *Chemistry and Ecology, 6*, 169-187.

Tubman, M. (1995). *Plume Measurement System (PLUMES) technical manual and data analysis procedures* (No. DRP-95-1). Vicksburg, MI: US Army Corps of Engineers Waterways Experiment Station.

Tubman, M., Brumley, B., & Puckette, P. (1994). *Deep-water dredged material disposal monitoring offshore of San Francisco using the PLUme MEasurement System (PLUMES).* Paper presented at the Second International Conference on Dredging and Dredged Material Placement, Lake Buena Vista, Florida.

Tubman, M. W., & Corson, W. D. (2000). *Acoustic monitoring of dredging-related suspended sediment plumes* (No. ERDC TN-DOER-E7). Vicksburg, M.S.: U.S. Army Engineer Research and Development Center.

Turner Designs. (2002). *SCUFA self-contained underwater fluorescence apparatus: user's manual (2.1)*. 44p.

USACE. (1983). *Engineering and design: dredging and dredged material disposal* (Engineer manual No. EM 1110-2-5025). Washington D.C.

Vennell, R., & Moore, M. (1993). Acoustic doppler current profiler measurements of the semi-diurnal internal tide on the west coast of New Zealand. *New Zealand Journal of Marine and Freshwater Research, 27*(1), 31-38.

Walters, R. A., Goring, D. G., & Bell, R. G. (2001). Ocean tides around New Zealand. *New Zealand Journal of Marine and Freshwater Research, 35*, 567-579.

Wang, W., & Jiang, W. (2008). Study on the seasonal variation of the suspended sediment distribution and transportation in the East China Seas based on SeaWiFS data. *Journal of Ocean University of China, 7*(4), 385-392.

Warren, S. K. (1992). *Geomechanics and dispersion of dredge spoil.* University of Waikato, Hamilton.

Weston Solutions Inc. (2010). *Guam deep ocean disposal site - site management and monitoring plan*. Carlsbad, CA: Department of the Navy.

Whitehouse, R., Soulsby, R. L., Roberts, W., & Mitchener, H. (2000). *Dynamics of estuarine muds*. London: Thomas Telford Ltd.

Wiebe, P. H., & Green, C. H. (1994). The use of high frequency acoustics in the study of zooplankton spatial and temporal patterns. *Proceedings of the NIPR Symposium Polar Biology, 7*, 133-157.

Wienberg, C., & Bartholomä, A. (2005). Acoustic seabed classification in a coastal environment (outer Weser Estuary, German Bight)--a new approach to monitor dredging and dredge spoil disposal. *Continental Shelf Research, 25*(9), 1143-1156.

Wienberg, C., Dannenberg, J., & Hebbeln, D. (2004). The fate of dumped sediments monitored by a high-resolution multibeam echosounder system, Weser Estuary, German Bight. *Geo-Marine Letters, 24*(1), 22-31.

Wilber, D. H., & Clarke, D. G. (2001). Biological Effects of Suspended Sediments: A Review of Suspended Sediment Impacts on Fish and Shellfish with Relation to Dredging Activities in Estuaries. *North American Journal of Fisheries Management, 21*(4), 855-875.

Winter, C. (2007). On the evaluation of sediment transport models in tidal environments. *Sedimentary Geology, 202*(3), 562-571.

Winterwerp, J. C. (2002). Near-Field Behavior of Dredging Spill in Shallow Water. *Journal of Waterway, Port, Coastal & Ocean Engineering, 128*(2), 96.

Winterwerp, J. C., & van Kesteren, W. G. M. (2004). *Introduction to the physics of cohesive sediment in the marine environment*. Amsterdam, The Netherlands: Elsevier.

Wolanski, E., Gibbs, R., Ridd, P., & Mehta, A. (1992). Settling of ocean-dumped dredged material, Townsville, Australia. *Estuarine, Coastal and Shelf Science, 35*(5), 473-489.

Wu, J., Huanting, S., & Zhang, S. (2003, November 9-11). *Acoustic observations of fine sediment dispersal and the deposition during dredged sediment release in the Yangtze Estuary*. Paper presented at the International Conference on Estuaries and Coasts, Hangzhou, China.

Wu, J., Liu, J. T., Shen, H., & Zhang, S. (2006). Dispersion of disposed dredged slurry in the meso-tidal Changjiang (Yangtze River) Estuary. *Estuarine, Coastal and Shelf Science, 70*(4), 663-672.

Yell, D., & Riddell, J. (1995). *Dredging*. London, England: Thomas Telford Publications.

Zeldis, J. R. (2004). New and remineralised nutrient supply and ecosystem metabolism on the northeastern New Zealand continental shelf. *Continental Shelf Research, 24*(4-5), 563-581.

Zeldis, J. R., Walters, R. A., Greig, M. J. N., & Image, K. (2004). Circulation over the northeastern New Zealand continental slope, shelf and adjacent Hauraki Gulf, during spring and summer. *Continental Shelf Research, 24*(4-5), 543-561.

Zhang, H.-M., Bates, J. J., & Reynolds, R. W. (2006). Assessment of composite global sampling: Sea surface wind speed. *Geophys. Res. Lett., 33*(17), L17714.

APPENDIX I
INSTRUMENT AND DATA SPECIFICATIONS

Appendix Table I.1 Instrument specifications for the long-term ADP deployment.

ADP	
Instrument type	SONTEK®
Frequency	250 kHz
Serial number	C550
No. of beams	3
Blanking distance	1.5 m
Cell size	8 m
No. of cells	20
Averaging interval	600 s (10 min)
Profiling interval	3600 s (1 hour)
Coordinate system	East, North, Up (ENU)
Compass reference	Magnetic North
Current speed accuracy	±1% of measured velocity, ±0.5 cm/s
Compass accuracy	±2°
Current meter	
Instrument type	InterOcean®
Serial number	06292545
Sample interval	2 Hz (0.5 sec)
Burst length	600 s (10 min)
Burst interval	3600 s (1 hour)
Coordinate system	East, North
Compass reference	Magnetic North
Current speed accuracy	±2% of measured velocity, ±1 cm/s
Compass accuracy	±2° within tilt angles of 5°
Temperature Sensor	
Instrument type	Thermistor (SONTEK® standard)
Sampling interval	1 Hz (1 sec)
Burst length	600 s (10 min)
Burst interval	3600 s (1 hour)
Accuracy	±0.1°C

Appendix Table I.2 Instrument specifications for the short-term ADCP surveys.

ACDP	
Instrument type	RD Instruments®
Frequency	300 kHz
Serial number	0459
No. of beams	4
Blanking distance	1m
Cell size	2 m
No. of cells	93
No. of pings per ensemble	8
Coordinate system	East, North, Up (ENU)
Coordinate Reference	Bottom Track
Compass reference	Magnetic North
Current speed accuracy	±0.5% of measured velocity, ±0.5cm/s
Compass accuracy	±2°
Temperature Sensor	
Instrument type	Temperature sensor (RD Instruments® standard)
Sampling Interval	Once per ensemble
Accuracy	±0.4°C

Appendix Table I.3 Details of accessed climate stations from CliFlo-NIWA's national online climate database.

Agent No.	Location	NZTM easting	NZTM northing	Data type	Sample interval	Height above MSL	Record start date	Record end date	Period accessed
9654	MI	1790861	6024521	Surface wind speed/direction	Hourly	60 m	7/12/93	present	1/12/05 – 30/11/10
31827	SI	1861709	5895307	As above	Hourly	103 m	4/10/05	present	1/12/05 – 30/11/10

Appendix Table I.4 Details of data accessed from the NOAA BSWD.

Site Name	NZTM easting	NZTM northing	Data type	Sample interval	Height above MSL	Record start date	Record end date	Period accessed
E5	1847095	5984814	Surface wind speed	6 Hourly	10 m	9/07/87	present	1/09/08 – 1/05/10
MI	1802803	6013710	As above	As above	As above	As above	As above	As above
SI	1889215	5900188	As above	As above	As above	As above	As above	As above

Appendix Table I.5 Details of the turbidity sensor deployments during each of the 4 plume monitoring surveys.

Survey no.	Disposal time (NZST)	Station	Station type	Sensor no.	Depth (m)	Data period (NZST)	Sampling interval (s)
1	1104	A	Suspended from assisting fishing vessel	1	5	None	-
				2	10	None	-
		B	Suspended from assisting fishing vessel	3	5	1059 -1154	1
				4	10	1059 -1154	1
		C	Suspended from manned rubber dingy	5	5	1100-1154	9
				6	10	1100-1154	9
		D	Suspended from unmanned rubber dingy	7	5	None	-
				8	10	950-1236	1
2	1000	A	Suspended from assisting fishing vessel	1	5	None	-
				8	7	950-955 1004-1056 1115-1126	1
				2	10	None	-
		B	Suspended from assisting fishing vessel	3	5	1107-1115	1
				4	10	1107-1115	1
		C	Suspended from main survey vessel before disposal	5	5	832-909	9
				6	10	832-909	9
3	1002	A	Suspended from assisting fishing vessel	2	1	None	-
				1	5	None	-
				9	7	1000-1034 1040-1114	1
				8	10	1007-1115	1
		B	Suspended from assisting fishing vessel	7	5	None	-
				10	7	None	-
				4	10	952-1120	1
		C	Suspended from manned rubber dingy	5	5	1000-1120	9
				6	10	1000-1120	9
4	1030	A	Suspended from assisting fishing vessel	2	1	None	-
				1	5	None	-
				9	5	1038-1104 1110-1144	1
				8	10	1036 -1145	1
		B	Suspended from assisting fishing vessel	7	5	None	-
				10	7	None	-
				4	10	1028-1144	1
		C	Suspended from manned rubber dingy	5	5	None	-
				6	10	None	-

Appendix Table I.6 System details of deployed turbidity sensors (sensors which did not record usable data are not included).

Sensor no.	Brand/Model	Data Logger	Measurement type	Range		Recorded units
				Raw	NTU	
3	Greenspan TS100	Campbell Scientific	Optical backscatter	4-20 mA	0-2000	millivolts
4	Greenspan TS100	Campbell Scientific	Optical backscatter	4-20 mA	0-2000	millivolts
5	Greenspan TS100	Campbell Scientific	Optical backscatter	4-20 mA	0-2000	millivolts
6	Greenspan TS1200	Campbell Scientific	Optical backscatter	4-20 mA	0-2000	millivolts
8	Scufa	Internal	Optical backscatter	0-5V	0.05-200	NTU
9	OBS-3	DOBIE	Optical backscatter	0-5V	0-50	volts

Appendix Table I.7 Summary of ADCP transects for Surveys 1-4.

Disposal time (NZST)	1104		1000		1002		1030	
Survey no.	1		2		3		4	
Transect no.	Start	Finish	Start	Finish	Start	Finish	Start	Finish
1	*832	835	1000	1002	*911	911	1031	1033
2	*835	839	1002	1002	1005	1007	1033	1035
3	*840	840	1003	1005	1008	1010	1035	1038
4	*841	845	1005	1007	1011	1013	1039	1040
5	1101	1105	1007	1008	1015	1017	1040	1042
6	1105	1107	1009	1010	1017	1020	1043	1048
7	1107	1110	1010	1011	1021	1027	1049	1053
8	1110	1113	1012	1013	1027	1028	1054	1100
9	1113	1113	1014	1017	1028	1036	1101	1107
10	1115	1117	1018	1019	1038	1049	1108	1110
11	1118	1119	1020	1023	1051	1052	1112	1113
12	1120	1122	1023	1026	1053	1055	1115	1117
13	1123	1124	1027	1032	1057	1058	1118	1123
14	1125	1126	1032	1035	1058	1100	1124	1127
15	1128	1131	1036	1040	1100	1102	1129	1132
16	1131	1134	1041	1044	1103	1105	1134	1136
17	1134	1137	1045	1048	1105	1121	1136	1139
18	1138	1140	1049	1049	-	-	-	-
19	1141	1143	1051	1052	-	-	-	-
20	1143	1145	1053	1054	-	-	-	-
21	1145	1146	1108	1110	-	-	-	-
22	1147	1149	1110	1111	-	-	-	-
23	1150	1152	1112	1114	-	-	-	-
24	1152	1156	1114	1116	-	-	-	-
25	-	-	1118	1119	-	-	-	-
26	-	-	1120	1121	-	-	-	-

Transects recorded prior to the arrival of the hopper are marked by *

Appendix Table I.8 Sounding error budget for MBES surveys at the AMDG[13]

Error type[14]	Source of error	Water depth (m)		
		100	**130**	**160**
A	Draught Setting	0.05	0.05	0.05
B	Variation of Draught	0.05	0.05	0.05
C	Sound Velocity	0.29	0.36	0.43
D	Spatial Variation in SV	0.1	0.1	0.1
E	Temporal Variation in SV	0.05	0.05	0.05
F	Application of Measured SV	0.05	0.05	0.05
G	Depth Measurement (Instrument)	1.50	1.95	2.40
H	Depth Measurement (Resolution)	0.01	0.01	0.01
I	Heave	0.5	0.5	0.5
J	Settlement and Squat	0.2	0.2	0.2
K	Roll, Pitch and Seabed Slope	NA	NA	NA
L	Tidal Readings	0.5	0.5	0.5
M	Co-Tidal Correction	NA	NA	NA
N	Tide Corrections	0.05	0.05	0.05
O	Trace Reading	NA	NA	NA
	Total Standard Error $\sqrt{a^2 + b^2 + \ldots}$	1.70	2.12	2.55
LINZ accuracy standards[15]				
	MB Special	0.79	1.01	1.23
	MB-1	1.19	1.51	1.84
	MB-2	1.58	2.01	2.45
	MB-3	1.98	2.52	3.06

[13] Sounding error budget compiled by Dr. Alexandre Schimel, University of Waikato, Department of Earth and Ocean Science.

[14]

A No bar check was carried out. Worst-case value estimated from total station measurements standard error, and static waterline visual estimation.

B Estimation from temporal variation in tanks.

C Based on SV-plus accuracy (0.0024 x depth + 0.05).

D,E Worst-case estimation considering size of survey area and frequency of SV casts.

F SV applied in EM3000 at time of acquisition.

G,H Worst-case estimation of 1.5% of the water depth.

I Estimated from data artefacts.

J Maximum error in dynamic draught estimation procedure.

K Not applicable. Single-beam only.

L Significant potential error as tide models were used instead of measurements. Maximum error estimated from comparison between lines and cross-lines.

M Not applicable. Tide models were used.

N Tide data sampled at 6 minutes and interpolated by the processing software.

O Not applicable. Soundings were derived digitally.

[15] LINZ standards derived as multiples of Single-beam special order depth accuracy (SO). MB-special = 1xSO, MB-1=1.5xSO, MB-2=2xSO, MB-3=2.5xSO, where $SO = \sqrt{(0.25^2 + (0.0075 \text{ x depth })^2]}$.

APPENDIX II
RESEARCH PAPERS ASSOCIATED WITH THE PROJECT

Coastal Management, 38:474–500, 2010
 ISSN: 0892-0753 print / 1521-0421 online DOI: 10.1080/08920753.2010.498109

Establishment of a Dredged Material Disposal Site in the Exclusive Economic Zone: New Zealand

BRYNA K. FLAIM, TERRY R. HEALY, AND PHILLIP WEIR

Coastal Marine Group, Department of Earth and Ocean Science, University of Waikato, Hamilton, New Zealand

Disposal options for muddy dredged material, especially if lightly contaminated, is an issue facing many countries, particularly if environmental protection and adherence to the Protocols of the London Dumping Convention is a regulatory requirement. For the case of the oceanic islands of New Zealand, disposal of muddy dredged material has become an issue for the prime city of Auckland. Accordingly, it has been necessary to investigate a suitable marine disposal site outside of the territorial seas in the EEZ. Ideal properties for such a disposal site include a near flat surface on the continental shelf, with sediments of similar textural characteristics to the material being disposed, a site of non-critical benthic ecology, water depths sufficient to enable the disposal site to be monitored (as required under the London Dumping Convention), a site experiencing low shelf currents, not affected by significant wave agitation and a site not of cultural significance. The approach for site establishment and gaining consent for disposal activities is reviewed. Preliminary investigations supporting a proposed site on the continental shelf in the EEZ are presented.

Keywords: disposal site establishment, environmental impact assessment, ocean disposal, regulatory requirements

Introduction

Harbours of the steep to mountainous oceanic islands comprising New Zealand suffer from accumulation of significant quantities of sediment that require removal for the maintenance of port operations. For the case of the ports and marinas of east Auckland (Figure 1), New Zealand's largest city, approximately 100 000 m^3 of muddy dredged material removed annually needs disposal (Maritime New Zealand, 2009). On rare occasions, some dredged material has been used for reclamation or nourishment, but for the most part, the material is either unsuitable or unneeded for such purposes. The dredged material has in the past been disposed in the territorial seas (TS) adjacent to Auckland City (hereafter referred to as the Coastal Marine Area (CMA)) (Grace, 1988; Roberts *et al*., 1991; Parliamentary Commissioner for the Environment, 1995). Aucklanders' affinity to the coast for recreation as well as the expanding international tourism industry (Peart, 2007), have made nearshore disposal sites less desirable. Future capital dredging works in Auckland will likely continue to increase in response to larger commercial ships and their deeper drafts (Keown, 2009).

This research was funded in part by Kaipara Limited and the University of Waikato, Hamilton, New Zealand doctoral research scholarship. This manuscript was written in part at The Institute of Cybernetics of Tallinn University of Technology, Tallinn, Estonia, under funding from FP6 Marie Curie RTN project SEAMOCS (MRTN-CT-2005-019374) and Estonian block grant SF0140077s08.

Address to Bryna K. Flaim, Coastal Marine Group, Department of Earth and Ocean Science, University of Waikato, Private Bag 3105, Hamilton 3240, New Zealand. E-mail: bkf3@waikato.ac.nz

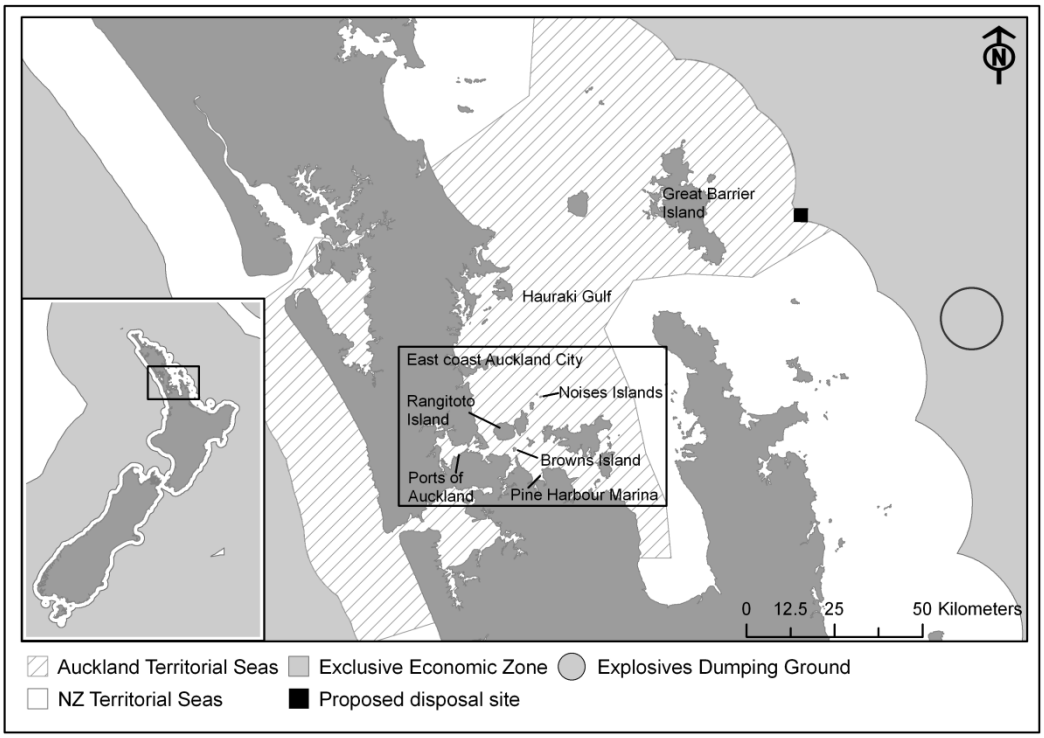

Figure 1. New Zealand territorial seas (TS)[1] and surrounding EEZ[1] of the east coast of Auckland's coastal marine area (CMA) (relevant locations mentioned in the text are noted).

At-sea disposal of contaminated material on Auckland's east coast has been and continues to be controversial, due to the lack of acceptable disposal sites in the CMA (Figure 1) (Healy *et al*., 1988). Ultimately, scarcity of disposal sites threatens the ability for ports and marinas to dredge approach channels and marina basins (Kagan, 1994; Gibb, 1997; Maninno *et al*., 2002). The implications of such restrictions could both undermine the profitability of ports and marinas, as well as create a safety hazard to both recreational boaties and commercial shipping interests (Marine Board, 1985).

Prior to the enactment of the Resource Management Act 1991 (RMA), historical disposal sites located within New Zealand's TS were established under the Town and Country Planning Act (TCPA). Under this legislative framework, dredged material disposal sites were typically located close to the origin of the dredged material. This near shore disposal approach was consistent with the underlying philosophy of the TCPA which was to balance economic profitability with environmental sustainability. For the east coast of Auckland, establishment of alternative and/or additional sites in response to greater demand has been increasingly restricted in the CMA. The enactment of the RMA and its associated reforms in 1991 ushered in a more environmentally conscious approach to management of New Zealand's natural and physical resources.

The RMA approach was a direct product of both the international sustainability movement (Rio Earth Summit and the Brundtland Report) and market based reforms to the New Zealand economy, which resulted in significant deregulation and consolidation of decision-making functions and the formation of a system of effects-based planning. This effects-based system requires that new developments meet underlying biophysical bottom lines bringing about the oft-repeated mantra of "ensuring that effects are no more than minor".

This paradigm shift has created a practical management problem whereby no new or existing sites have been consented under the RMA to dispose of slightly contaminated muddy dredged material, a product of ongoing maritime maintenance and development on the east coast of Auckland.

In response to increased pressure in nearshore waters from both, permitting authorities as well as local residents (DOAG, 1994; Parliamentary Commissioner for the Environment, 1995), port and marina operators, like other ocean industrialists, such as aquaculturalists and renewable energy developers, are increasingly considering offshore waters in the Exclusive Economic Zone (EEZ) as potential development sites. Such a shift would facilitate the avoidance of restrictive permitting systems and existing nearshore stakeholders (Healy *et al.*, 1988) harboring Not In My Backyard ($NIMBY^2$) concerns. In Auckland and other coastal cities, such as Baltimore, in the United States, established political and environmental interests, such as advocacy groups and concerned citizens, have imposed significant restrictions on the development of nearshore coastal environments (Poltrack, 2001). For Auckland port and marine operators, the benefits and drawbacks offered by a move to deeper more removed offshore locations are summarized in Table 1.

Table 1
Benefits and drawbacks to establishing a dredged material disposal site in the offshore areas adjacent to Auckland City, New Zealand.

Offshore disposal of dredged material	
Advantages	Disadvantages
Reduced competition with established user rights of fishing, recreation and shipping industries.	Higher cost of transporting material
Reduced NIMBY complaints from coastal residents.	Deeper water means research required for establishment is a greater financial investment
No negative historical precedents, making the consenting process less burdensome.	More involved to adequately monitor environmental impacts
Ecosystem complexity decreases with distance from the coast in the Auckland area, so shelf waters are generally not habitat for significant species (i.e. commercial or endangered species)	Some uncertainty in the effectiveness of the management framework as an offshore site is unprecedented.

This paper describes a case study for establishment of a dredged material disposal site in New Zealand's EEZ. The establishment process is reviewed and discussed, with the intention that the conclusions drawn may be useful as a template for other ports and marinas with looming difficulties for future disposal of dredged material in territorial seas.

Background

History of Dredged Material Disposal in the East Auckland Territorial Seas

Several dredged material disposal sites located within the Hauraki Gulf, namely at Browns, Rangitoto, and Noises Islands (Figure 1), were used by the Ports of Auckland and marina developers with varying degrees of success from the early 1980s through 1991 (Table 2). Generally, ongoing use of each of the sites was hampered by public concern over the perceived environmental impacts. Environmental monitoring undertaken either during or after disposal of dredged material revealed general degradation or alteration of benthic habitat, which was perceived as a negative impact. Of the three historical sites, the Noises Islands site resulted in the greatest controversy and can be most closely linked to present management concerns and the continued absence of suitable ocean disposal sites. (Parliamentary Commissioner for the Environment, 1995).

Table 2
Details of 3 disposal sites used within the CMA which led to the management problems of dredged material disposal.

Location (Figure 1)	Browns Island	Rangitoto Island	Noises Islands
Time period used	1987	1980s	1992
Controlling authority	Auckland Harbour Board (consent awarded by Ministry of Transport)	Auckland Harbour Board	Auckland Regional Water Board
Perceived environmental impact	Degradation of snapper feeding and spawning grounds (Grace, 1988) (*Pagrus auratus*, a commercially and recreationally important species in NZ)	Degradation of habitat leading to an undesirable permanent change in species composition (Roberts *et al*., 1991)	Significant loss offsite of disposed sediment (quantity unspecified); other impacts inconclusive (Parliamentary Commissioner for the Environment, 1995)

Noises Islands Disposal Site: a Cause for Controversy

Controversy over disposal operations in the Hauraki Gulf peaked with the awarding of consent to the Ports of Auckland by the Auckland Harbour Board in 1991 for dredging and disposal of 270,000 m^3 of harbor sediments that had accumulated over the previous 5 – 6 years. The consent included conditions that mandated an extensive monitoring program to assess the effects of the disposal operations, but even before the dredging began the project was a topic of extensive media coverage and significant public opposition (Parliamentary Commissioner for the Environment, 1995).

In an effort to address both public concern and provide an impartial review of the consented activities, the Parliamentary Commissioner for the Environment

established an independent technical review panel (hereafter referred to as 'the panel') made up of a multi-disciplinary group of qualified scientists. The panel produced a series of reports that evaluated the findings of monitoring surveys and made recommendations on methods to both reduce environmental effects and alleviate public concerns (Parliamentary Commissioner for the Environment, 1995).

Generally, the panel determined that the monitoring program suffered from deficiencies in the pre-disposal base-line sampling, meaning that post-disposal comparisons were inconclusive. Uncertainty associated with the magnitude of unknown impacts prompted Ports of Auckland to withdraw a pending disposal application for additional disposal of dredged sediment at the site. As a result, the Noises Islands disposal ground was only used once for the disposal of the 270 000 m^3 of dredged sediment.

Shortly after controversy over the Noises site, a second review group was formed as a result of public concern. The Disposal Options Advisory Group (DOAG), established in 1993, was tasked with the responsibility of examining and reporting on the disposal options for dredged materials. The DOAG provided specific focus to the Ports of Auckland's disposal operations at the Noises Islands disposal site. The DOAG cast its review wider than the technical review panel with reports detailing potential Ports of Auckland dredged material disposal options with respect to cost and environmental effects (Disposal Options Advisory Group, 1994). The DOAG considered harbor edge and land-based disposal options in addition to the more traditional means of marine disposal. In the absence of any planned reclamation projects, the DOAG ultimately recommended that future disposal of maintenance and capital works dredged sediment be disposed of at sites with a water depth in excess of 100 m (Disposal Options Advisory Group, 1994).

Current Disposal Activity

With a backlog of infilling sediment in the Auckland waterfront areas, New Zealand's Maritime Safety Authority, now Maritime New Zealand (MNZ), intervened and began to award consents for disposal of dredged material at the Explosives Dumping Ground (EDG) The EDG is located some 80 km distance from the city of Auckland, on the continental slope in water depths between 500 and 1300 m, and importantly, is outside the CMA and the jurisdiction of the RMA (Figure 1). It was established primarily for the Royal New Zealand Navy to dispose of unexploded munitions abandoned on the sea floor since WWII. The EDG is considered a safe disposal location for the munitions because of its water depth and distance from the coastline.

The EDG has never been surveyed or monitored exclusively for dredge material disposal. The extreme water depth and danger in sampling in the vicinity of the munitions make such activities virtually impossible. Therefore, the impacts from years of disposal operations at the EDG and effects on the surrounding areas are unknown. When the site was first used for dredged material disposal (mid-90s), long-term consents were granted with little regulation as to the quantity of material being placed there. Under recent management regimes, however, dredged material disposal is capped at 50,000 m^3 per annum, a portion of which is allocated to each applicant to alleviate some of the need, but applications routinely exceed the total allocations (*pers. comm.*, Tara Ross-Watt, 2009).

The EDG is generally considered a temporary solution in its present state (*pers. comm.*, Tara Ross-Watt, 2009). In order to acquiesce with the London Dumping Convention, to which New Zealand is a party, management controls need to be implemented to monitor the site or alternatively, disposal of dredged material should be relocated away from the site, an option not currently considered for lack of alternatives.

Other options for disposal of muddy and/or slightly contaminated dredged material, such as containment islands and mound capping have been used with some degree of success in the United States (Gibb, 1997), but these sorts of methods are not always appropriate for all types of dredged material (i.e. muddy and slightly contaminated). Consequently, none other than the occasional reclamation and nourishment project have as yet been deemed appropriate for such material originating from the east Auckland area.

The Need for a New Site

The severe limitations for disposal options within the 12 nm limit east of Auckland City was further compounded by the establishment of the Hauraki Gulf Marine Park in 2000, evidence of the community push to preserve and protect coastal areas. Accordingly, consideration of deeper more distant waters for disposal of dredged material seems to be a logical next step. Beyond the CMA, New Zealand's continental shelf waters range from approximately 50 – 200 m water depth, with the EEZ boundary beginning at approximately the 100 m depth contour. Beyond this boundary, water depths increase appreciably to 2000 m. Not only would establishing a site in the shelf zone, and therefore the EEZ, bring actions in line with the recommendations made by the Disposal Options Advisory Group (1994), but more importantly, at such water depths, monitoring is still a feasible activity. As such, disposal operations would not be in breach of the London Dumping Convention as they are currently at the EDG.

However, it should be emphasized that as the shelf zone is a relatively new area for commercial activities, a precautionary approach to the management of these environments should be applied through the establishment of a monitoring program to identify and then avoid environmental effects. This concept has been reviewed by Hall (2002), who feared that shelf resources would become over-used, as in nearshore areas, as a result of anthropogenic pressures particularly in developing nations where strict controls are not as easily enforced. With an established consenting process, New Zealand does not fall into this category, but other developing nations looking to move offshore for various commercial intents, should be aware of the potential consequences that could result if offshore sites are developed in the absence of appropriate environmental management mechanisms.

The Proposal

In 2006, Pine Harbour Marina, requested the University of Waikato, Hamilton, New Zealand, to investigate the possibility of a new dredged material disposal site. It was envisioned that the site would serve two purposes, pending consent conditions; a disposal site for maintenance dredgings from the marina and a new commercial venture for the company, as other ports and marinas from the area would likely pay to dispose quantities of dredged material beyond their disposal allowance at the EDG.

The primary criteria for identifying a potential site, in this case, was to avoid the regulatory requirements of the CMA where history and public sentiment suggests that another consent application for a disposal site establishment would result in a long, drawn-out and ultimately unsuccessful outcome.

Typically, a dredged material disposal site is established as a dispersal site (active) or a non-dispersive site (in-active) (Palermo, 2000). Non-dispersive sites are more easily monitored because sediments are not readily re-suspended and dispersed beyond the boundaries of the site. It was determined that a non-dispersive site would be required to accommodate dredged sediments from Auckland ports and marinas due to the presence of the generally low levels of contamination caused from both terrestrial run-off and vessel discharges. A non-dispersive (in-active) site is required in these circumstances to ensure contaminated materials remain at the disposal site and do not migrate away from the site to potentially cause what would be unknown adverse effects.

Accordingly, 'ideal site' features, some of them generic to any disposal site and some specific to non-dispersive type sites, were then considered. The following were identified as key features in site selection:

i. no historical or cultural significance
ii. not an important recreational or commercial area
iii. non-sensitive ecology
iv. flat seafloor topography
v. seafloor sediments texturally similar to those intended for disposal
vi. slow tidal and ambient currents throughout the water column
vii. minimal wave effects for sediment entrainment at the sea floor
viii. long-term economic and operational feasibility

Under traditional site selection methodology, a number of sites would have been identified and studied to determine the most appropriate (Palermo, 2000). In this instance, this method was considered to be cost-prohibitive and rather, an initial review of studies on the deeper water environments of the northeast coast of New Zealand was undertaken. A proposed site was then selected on the basis of the initial review, its suitably deep water (>100 m, as per the DOAG (1994) recommendations), and being located outside the CMA.

A Potentially Suitable Site

The proposed site, selected by meeting the aforementioned criteria, is located 25 km east of Great Barrier Island in the EEZ, which makes up the eastern boundary of the Hauraki Gulf, the gateway to most of east Auckland's ports and marinas (Figure 1). Preliminary analysis of hydrographic charts and sediment maps of the area indicated that the proposed site has water depths ranging from 130 m to 150 m over a generally low gradient shelf terrace (Frisken, 1992). Seafloor sediments were shown to be composed of muddy/sand to sandy/mud, texturally similar to sediments known to be accumulating in some of the ports and marinas in the Auckland area (Carter and Eade, 1980; Loomb, 2001; Golder Kingett Mitchell, 2007; BioResearches, 2009).

Literature describes the wave climate on the northeast coast as typically mild compared to that of the west coast of New Zealand (Pickrill and Mitchell, 1979; Harris, 1985). A predominant southeasterly flowing boundary current (the

East Auckland Current (EAUC)) has been commonly reported (Heath, 1980; Stanton *et al*., 1997; Stanton and Sutton, 2003) which may or may not have an effect on disposal operations on the shelf.

Based on these observations and assumptions, the site was cautiously flagged for further study, which initially included a more in depth desktop study, a preliminary field survey, and consultations with likely stakeholders. This early stage research was employed to determine whether the more detailed and costly research/analysis required to fulfil the established regulatory environment would be a worthwhile effort.

New Zealand Framework for Site Establishment and Dredged Material Disposal

In order to contextualize the drivers for the establishment of a site suitable for disposal of lightly contaminated muddy dredged material in New Zealand's EEZ, rather than within New Zealand's TS, the following sections outline the management approach to New Zealand's Coastal Marine Area (CMA) as well as that of the EEZ.

Territorial Seas: New Zealand's management of its Coastal Marine Area (CMA)

By definition, New Zealand's TS and the CMA are one in the same[3]. The dominant environmental management mechanism applied in these waters, as well as to terrestrial areas, is the RMA. Its application is wide reaching and includes the management of allocation of space, authorizing coastal reclamations and dredging works, state-of-the-environment monitoring and managing the effects of aquaculture developments. While the RMA has acted to consolidate environmental management into a centralized legislative arrangement, on-the-ground decisions and actions are devolved to local territorial and regional authorities (sections 30 and 31) (Figure 2 and Table 3).

The RMA applies a neo-market effects based approach to environmental management, where biophysical bottom lines are established, under which developments are assessed. The approach provides flexibility to developers in that the medium of management is the effects of development and not a prescribed activity itself. While broadly enabling, the approach has been criticized as being overly onerous for developers in that its enabling provisions require every project to demonstrate what the effects of their development will be rather than assess broadly the proposed activity.

New Zealand Exclusive Economic Zone: Disposal of Dredged Material

In contrast to the management mechanisms described for the RMA, establishment processes for a disposal site beyond the CMA, but still within New Zealand's EEZ would be subject to central government permitting procedures lead by Maritime New Zealand (MNZ). In this environment, management approaches are generally more closely aligned to guidelines established through international conventions. The National Policy on the Sea Disposal of Waste-Marine Pollution Prevention (Maritime New Zealand, 2002) broadly describes New Zealand's position on disposal of waste at sea.

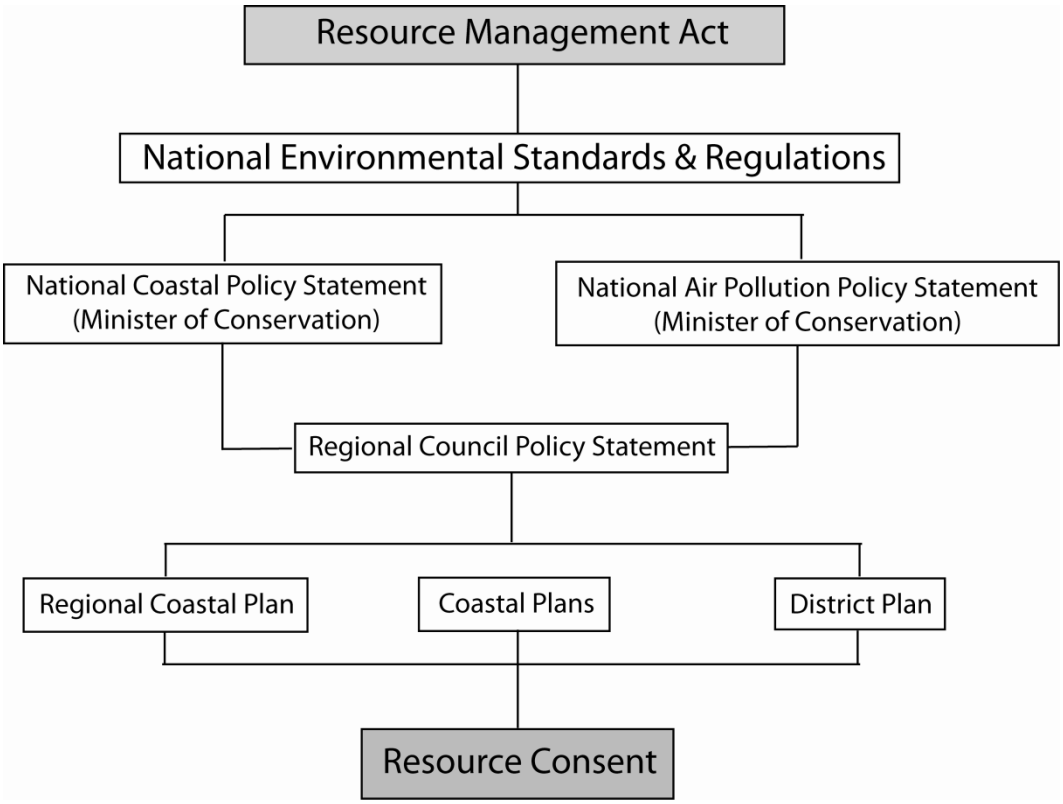

Figure 2. Hierarchical system for issuing resource consents in the Resource Management Act (1991) which has jurisdiction to the 12 nm limit in coastal areas of New Zealand.

For the case of disposal site establishment and dredged material disposal, the London Dumping Convention and its 1996 Protocol are the international conventions that shape New Zealand's management of such activities. Generally, the precautionary approach is required, where avoidance of disposal at sea is the aim and effects are the focus. The Maritime Transport Act (MTA) (1994) establishes the framework for the application and enforcement of the standards and processes set out in the 1996 Protocol within the EEZ. Marine Protection Rules-Part 180-*Dumping of Wastes and Other Matter* implements the requirements of the MTA.

The New Zealand Guidelines for the Sea Disposal of Waste (hereafter referred to as the Guidelines) (Maritime Safety Authority, 1999), prepared jointly by the Maritime Safety Authority of New Zealand (now MNZ) and the Ministry for the Environment, were developed to assist in the assessment and issuing of disposal permits. The Guidelines provide detailed technical information that

Table 3
Summary of the underlying RMA coastal management functions in New Zealand.

New Zealand Coastal Policy Statement (NZCPS)	The RMA requires that the Minister of Conservation prepare the NZCPS which is New Zealand's only mandatory policy statement (Figure 2). The NZCPS provides overarching advice on the management of the coastal space. It is, however, comprehensively vague in that it provides a number of broad directives despite leaving the 'on-the-ground' management and policy setting functions to the discretion of local authorities. The NZCPS sets priorities for the preservation and protection of the natural character of New Zealand's coastal space from inappropriate use and development by encouraging development in locations where the natural character of the coastal space has been compromised (Ashby, 2004).`	
Regional Councils	Regional Policy Statements	Policy statements set broad goals and provide policy guidance to the management of the each region's resources.
	Regional Coastal Plan	Coastal plans describe the management of Coastal Resources within the CMA of each region.
	Regional Plans	Outlines the biophysical bottom lines to be achieved in the terrestrial environment.
	Consents	Permissions procedure to allow developments to proceed or otherwise.

supports the assessment of proposals for at-sea disposal. The aims of the Guidelines are to:

- assist applicants for resource consents and permits to dump wastes at sea from ships, aircraft or offshore installations, or to dump ships and offshore installations
- assist the issuing authorities tasked with making decisions on such applications
- promote a consistent, practical consenting/permitting regime for dumping in accordance with the 1996 Protocol in all areas of the sea that New Zealand has jurisdiction and responsibilities for dumping.

(Maritime Safety Authority, 1999, p. 6)

The process for application and assessment of permits for disposal in areas beyond the TS (i.e. the EEZ) are summarized in Figure 3. The Guidelines are an intricate part of the establishment process because they designate the specific information, on both the proposed site as well as the material intended for disposal that MNZ requires when assessing applications. Accordingly, for the present case, this document has provided direction for necessary site investigations.

Disparity Between Regulatory Authorities

Generally, the regulatory frameworks for the TS and the EEZ treat dredged material disposal activities similarly. There is an over-arching theme of a pre-cautionary effects-based approach where the focus is on ensuring environmental sustainability. Within New Zealand, the management problem of finding a suitable site for dredged material disposal is mainly confined to the east Auckland coastal areas. So, one might question (*i*) the reason for the management problem itself and (*ii*) what makes the EEZ preferable and potentially more feasible for disposal operations compared to the CMA in this area, as opposed to others.

There seem to be two factors driving the events surrounding the present case. For the east coast of Auckland, there is a negative historical precedence of disposal operations in the CMA which appears to be based on a closely involved and environmentally sensitive community with decisions made by the regional council, to some extent, on their behalf. Moreover, the regional council, in this case ARC, operates under the RMA, both complex and restrictive, as well as sustainability-focused. Under that, ARC regulates not just the TS adjacent to Auckland, but terrestrial areas as well. While the ARC's purpose as directed by the RMA Sections 5 and 30 require economic factors to be considered in making a balanced decision, it seems that in the case of dredging disposal the required balancing act favors non-development of ARC coastal areas. On the other hand, MNZ in its name has a distinctive maritime focus. While seeking to uphold the pre-cautionary approach to disposal activities, the establishment of the EDG for disposal of dredged material demonstrates a willingness to provide specific support to commercial maritime entities affected by the aforementioned difficulties in establishing a dredged material disposal site. Whatever, the motivation, it is clear that despite the similarity between the underlying principles of the two regulatory frameworks, disposal of dredged material is regarded as less problematic in the EEZ adjacent to east Auckland compared to the CMA.

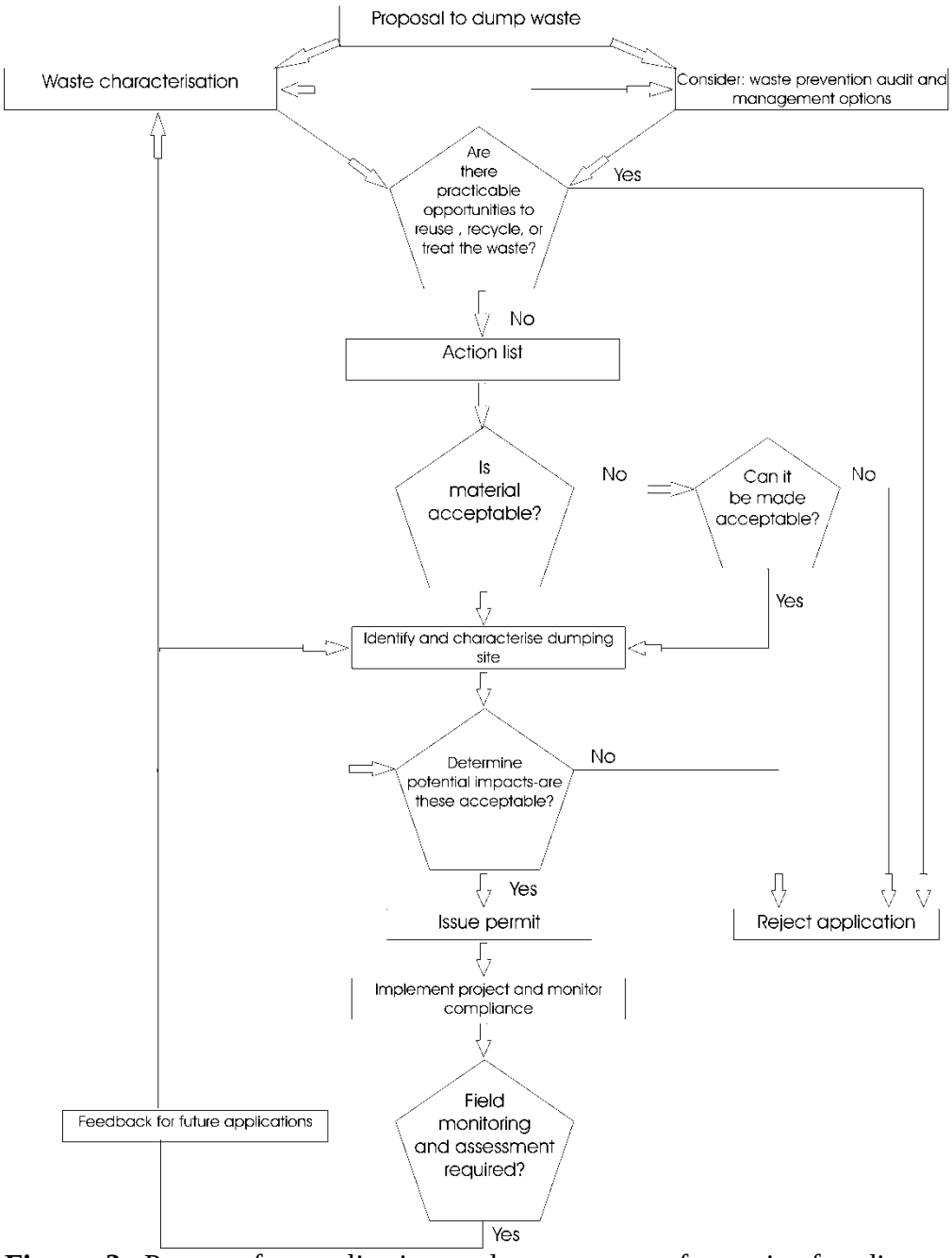

Figure 3. Process for application and assessment of permits for disposal of dredged material in the EEZ as designated in the Guidelines (adopted from Maritime Safety Authority (1999)).

Initial Site Investigations

Initial site investigations for the case of Pine Harbour Marina dredged basin sediments were undertaken in the form of a detailed desktop study, stakeholder consultations, and a preliminary field survey. These were carried out in accordance with the Guidelines, described above.

As emphasized in the Guidelines, a primary aim is to avoid at-sea disposal of dredged material through reduction and re-use methods. In the present situation, such 'at the source' management techniques were not deemed possible and hence are outside the scope of this communication. The following provides a

review of the initial investigations pertaining to the disposal of Pine Harbour Marina dredged basin sediments at the proposed site (Figure 1).

Waste Characterization

The Guidelines describe a 4-level waste characterization process with each level requiring an increased level of characterization. Level 1 involves reviewing the existing information on the waste. Level 2 requires a physical and chemical characterization of the waste. Levels 3 and 4 require various toxicity and bioaccumulation testing. It is specified that if the lower levels of investigation are sufficient to provide the required information on the waste, then higher levels of investigation are not necessary.

Pine Harbour Marina regularly undertakes sampling and testing of both channel and basin sediments, so reports are available as recent as 2009 (Bioresearches, 2009). Sediment texture, as well as chemical characteristics of the material intended for disposal, is considered important in determining compatibility with a proposed disposal site. It is thought that in the case of disposal of dredged material, the principle of 'like on like' applies to minimize biological impacts (e.g. smothering of benthic fauna) (Hirsch *et al*., 1978). For example, vertical migration of benthic fauna would be expected of some species if the deposited material was similar to native sediments (Mauer *et al*., 1980; 1981; 1982; Harvey *et al*., 1998).

Bioresearches (2009) sampled 6 locations within the basin of Pine Harbour Marina. Five out of the 6 samples were between 80% and 90% silt and clay fractions (3.9 – 63 µm) with the remaining sample 66% silt and clay. Sorting was generally poor in all 6 samples, indicating the presence of a range of size classes. Comparison of these sediments to the naturally occurring sediments of the proposed site is described below (see Table 4).

Historically, contaminants of concern at Pine Harbour Marina are heavy metals, of which the main concern has been Copper. Golder Kingett Mitchell (2007) found that all the heavy metal concentrations in the entrance and approach channels to be below the ISQG-low standard (interim sediment quality guideline-low) recommended by ANZECC (2000). In more recent testing of the marina basin, Bioresearches (2009) found all heavy metals except Copper to be below Effects Range-Low (ER-L) (ANZECC, 1998) levels, the chosen criterion of the Guidelines (Maritime Safety Authority, 1999). Copper levels were slightly elevated above ER-L, but still well below the Effects Range-Medium (ER-M) level. According to the Guidelines, if all samples showed levels below ER-L standards and no heavy metal levels are detected above ER-M levels, the material can be considered suitable for unconfined ocean disposal without further testing. For the case of the slightly elevated Copper concentrations, a level 3 elutriate test was undertaken. Bioresearches (2009) found that Copper concentrations did not exceed the ANZECC marine water quality criterion (the standard suggested in the Guidelines). In fact, the concentration decreased because it was adsorbed onto the sediments, meaning that it would not be bio-available to fauna inhabiting the sediments.

Level 1 and 3 investigations indicated that Pine Harbour Marina basin sediments fall into category 2, '*Wastes that contain substances below the relevant lower levels and that are of little environmental concern*', as designated in the Guidelines (Maritime Safety Authority 1999, p.25). Category 2 sediments are acceptable for unconfined disposal at sea.

Assessment of the Proposed Disposal Site

A literature review on studies located at the northeast coast of New Zealand revealed a variety of relevant information on the regional characteristics of the site location. However, no specific studies have been undertaken at the specific coordinates of the proposed site. Desktop calculations and a preliminary field survey (November 2007) filled some knowledge gaps pertaining to the following: oceanographic setting, shelf morphology and sediments, and biological characteristics.

Oceanographic setting

An understanding of the oceanographic setting of a proposed disposal site is critical in determining its suitability for such operations. Regional current patterns drive local forcing at any site which can greatly influence the geo-mechanical behaviour of the dredged material once it has been released into the water column (Truitt, 1988). During the descent process, current speeds and directions determine what portion of the material will be entrained in the water column, how far it will be advected, how persistent a turbid plume will be, where the material will deposit, and how far a bottom density flow will travel from the point of impact. Additionally, bottom currents and waves can have the effect of agitation of this deposited material, re-entrainment, and dispersion long after disposal has occurred (Mathews, 1997). The extent of these actions can also influence the consolidation process of the deposited material (Halka, 1991). For these reasons, the proposed site was evaluated with respect to its known oceanographic influences.

In New Zealand, the dominant tidal wave is the semi-diurnal M_2 constituent with a period of 12.42 hours (Heath, 1977). It propagates anti-clockwise around the New Zealand landmass as a trapped Kelvin wave and is maintained by incoming tidal wave additions from its easterly and westerly situated amphidromic points (Heath, 1977; Walters *et al*., 2001). In the region of the proposed site, M_2 tidal current velocities are 5-10 cms^{-1}, but under certain conditions the M_2 tide may be induced to separate into its M_4 and M_6 tidal harmonics resulting in elevated tidal velocities (Sharples and Grieg, 1998).

Along the northeast coast, the prevailing waves are from the northeast and are generated from short-period weather cycles associated with larger scale weak seasonal cycles (Harris, 1985). Sheltering due to the northeast aspect of the landmass results a less energetic wave climate in this region compared to others around New Zealand. Measured, as well as modelled, waves have been reported to range from 0.5 m to 3 m in height and 5 sec to 9 sec in period (Pickrill and Mitchell, 1979; Heath, 1985; Gorman *et al.*, 2003). El Niño Southern Oscillation (ENSO) can have the effect of decreasing mean wave height in the El Niño phase and increasing mean wave height during La Niña. However, under typical conditions, it is unlikely that wave motions will be strong enough to stir sediments at 140 m, the depth of the proposed site. To confirm this, a calculation of current velocity due to wave motions was undertaken.

Wave orbital velocity in deep water was calculated using:

$$\overline{U}_{\infty} = \left(\frac{\pi H_{\infty}}{L_{\infty}} \right)^2 C_{\infty} e^{2kz} \qquad (1)$$

where H_∞ is the wave height (m), L_∞ is the wavelength (m), C_∞ is the phase velocity (ms^{-1}), k is the wave number (m^{-1}), and z is the water depth (m) (Komar, 1976). Calculations were based on wave data from the NOAA Wavewatch III hindcast model (Tolman, 2009) for the northeast coast region of New Zealand for the period of Jan 1, 1998 – June 1, 2003 (Table 4). From the 4 year dataset, the mean significant wave height and period were ~1.5 m and ~7 sec, respectively. The maximum significant wave height and period were ~6 m and ~16 sec, respectively. Results indicate that wave orbitals typical of the region of the proposed site would attenuate such that current velocities due to surface waves would be negligible at 60 m below the surface (Table 4). At 140 m, initiation of motion by wave induced currents of deposited material at the proposed site would not be likely under typical conditions.

Table 4
Wave data from NOAA Wavewatch III model hindcast (Jan 1, 1998 – June 1, 2003), with depth calculated wave orbital velocity.

	Wave height (m)	Wave period (m)	Depth below surface (m)	Orbital velocity (cms^{-1})
Maximum*	***5.8**	9.8	10	10
			20	4
			40	0.8
			60	0.2
	2.05	***15.79**	10	0.5
			20	0.4
			40	0.2
			60	0.1
Mean	1.59 (σ=0.83)	7.21 (σ=2.41)	10	0.9
			20	0.2
			40	0.009
			60	$4x10^{-4}$

Generally, the tide is a minor influence on shelf dynamics compared to other geostrophic flows (Sharples and Greig, 1998). Given the depths at the proposed site, it is also unlikely that wave action will have a significant impact on the seabed. The most influential force on shelf dynamics is instead, likely to be The East Auckland Current (EAUC). Formed from subtropical waters of the East Australian Current (EAC), it typically flows offshore and southeasterly with respect to the northeast coastline of New Zealand. Near surface velocities for this current have been estimated to be between 20 and 30 cms^{-1} (Heath, 1980), but variability is significant along the northeast coast (Stanton *et al.*, 1997). Under some conditions, the current has been observed to intrude onshore, thought to be a result of either prolonged summertime easterly winds or stratification of the water column (Denham *et al.*, 1984; Sharples, 1997; Zeldis *et al*., 2004).

The major effect of currents on the long-term stability of dredged material is the applied bed shear stress. Bed shear stress was estimated based on a logarithmic current profile with a boundary layer current velocity of 20 cms^{-1} 100 cm above the seabed after the von Karman-Prandtl equation (Dyer, 1986)

$$u(z) = \frac{u_*}{\kappa} \ln\left(\frac{z}{z_0}\right) \quad (2)$$

where u_* is the shear velocity, κ is von Karman's constant, z is the depth profile of the bottom boundary layer, z_0 is the bed roughness for an hydraulically smooth bed given as

$$z_0 = \frac{\nu}{9u_*} \quad (3)$$

and ν is the kinematic viscosity of seawater (20°C) (1.004×10^{-6} m^2s^{-1}). Using the derived current profile and the related u_*, Reynold's number (Re) and Shield's parameter (θ) were calculated by:

$$\mathrm{Re} = \frac{u_* d}{\nu} \quad (4)$$

and

$$\theta = \frac{\tau_0}{(\rho_s - \rho)gd} \quad (5)$$

where ρ_s is the density of sediment (2650 kgm^{-3} for quartz type sediment), ρ is the density of seawater (1025 kgm^{-3}), g is the acceleration due to gravity, d is the diameter of the median grain size sediment (36 μm for medium silt) and τ_0 is the bed shear stress given as

$$\tau_0 = \rho u_*^2 \quad (6)$$

Based on Shield's curve published by Miller *et al.* (1977), a boundary layer current of 20 cms^{-1} (producing a bed shear stress of 0.05 Nm^{-2}) is below the critical velocity for entrainment. A similar procedure was also undertaken to calculate the critical shear stress under typical conditions at the proposed disposal site. Calculations specify that a boundary layer current of 32 cms^{-1} would induce a critical shear stress of 0.12 Nm^{-2}. This would initiate sediment motion for silt-sized particles according to the Shield's curve. This estimation is in line with that reported by Peterson (1999) and Friedrichs *et al*. (2000), 0.1 Nm^{-2} for mud and fine grained beds.

Based on these initial calculations, typical oceanographic conditions at the proposed site seem conducive to disposal operations (i.e. conditions where sediment disposed at the site is not likely be disturbed by currents or waves and be transported away from the site). Although these assessments are mainly indicative and additional *in situ* measurements such as current velocity and sediment mobility are needed for confirmation, the above findings increase the confidence that further research will more conclusively establish the suitability of the site.

Shelf morphology and sediments

Similar to the oceanographic setting, knowledge of the morphology and sedimentology of a proposed site are important factors for determining its suitability. By assessing both regional and local characteristics of the proposed

site area, it can be determined whether the site will be appropriate for long-term usage and what, if any, environmental concerns there may be.

Along the northeast coast of New Zealand, where the proposed site is located, the continental shelf ranges in width from just 11 km to ~100 km (Harris, 1985). At the latitude where the site has been proposed, the shelf-break occurs at the 200 m contour proceeding onto the continental slope (Harris, 1985). The sediments at the mid-shelf depths in the area of the proposed site are typically muddy/sand to sandy/mud (Carter, 1980).

Initial site inspection in November 2007, using a single depth sounder and drop camera video images indicated a flat plain seafloor only varying 1-3 m in depth over the proposed site area. Also notable is a lack of bedforms, the presence of which typically indicates active sediment transport. Twenty samples, taken at regular intervals across the site, were retrieved using a 'SHIPEK' grab sampler which has the capability of collecting approximately 0.4 m^2 of surficial sediment (Figure 4). Textural analyses of the samples confirmed the previously reported sediment types.

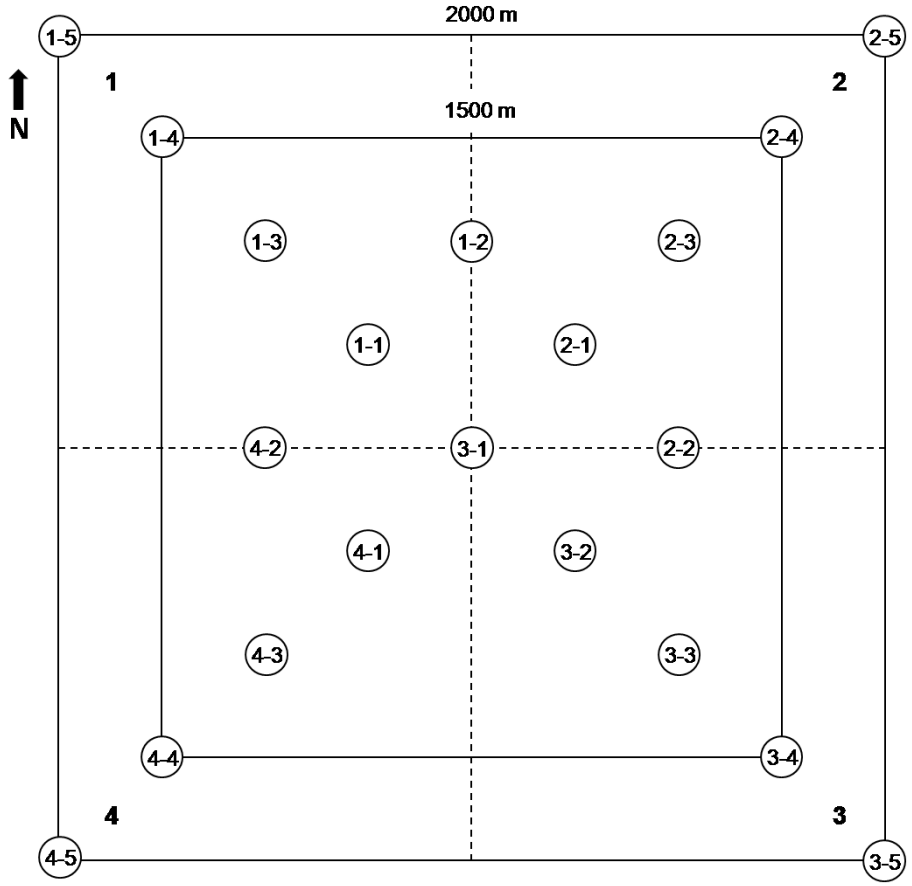

Figure 4. Diagram of locations sampled during the preliminary field survey for sediment texture and benthic faunal assessment (dashed lines indicate the four quadrants referred to in Figure 5). Site 3-1 is located at 175° 48' 0" E, 36° 12' 20" S.

Sediment texture of the retrieved samples was undertaken using laser-sizer analysis (Malvern Mastersizer-S 300RF). For the majority of samples, the dominant sediment size class ranged from approximately 0.8 µm to 35 µm or clay through to coarse silt sized particles. However, another textural component was sizes ranging from 50 µm to 350 µm. These were classified as very fine sand

through medium sand. The major textural class for all sample locations is that of clay sized particles. Particles classified as very fine sand make up the second largest size class for all sampling locations. Medium sized sand particles make up the smallest size class of the locations sampled. Comparisons between sample locations showed very little variation across the site area.

Table 5 shows the median grain size (µm) of the sample collected at site 3-1 of the proposed disposal site (Figure 4), as well as the sorting. Also included are the median grain sizes and sorting of the 6 sites sampled by Bioresearches (2009) in the basin of Pine Harbour Marina. Comparison of these values illustrates the similarity between the sediments naturally occurring at the proposed site and the sediments that may potentially be disposed there. The sediments at the proposed site are slightly coarser in texture than those of Pine Harbour Marina basin, but poor sorting indicates a significant overlap in size classes between the two locations.

Table 5

Median grain size (µm) and sorting of sediment from the center of the proposed site (3-1), as well as of sediments from 6 samples collected by Bioresearches (2009) in Pine Harbour Marina basin.

Site	Median grain size (µm)	Type	Sorting	Type
Proposed disposal site (3-1)	35.90	coarse silt	2.78	poorly - very poorly sorted
PHM 2	5.15	fine silt	3.2	very poorly sorted
PHM 5	3.91	fine silt	2.21	poorly - very poorly sorted
PHM 6	4.49	fine silt	2.83	poorly - very poorly sorted
PHM 10	2.40	clay	2.15	poorly - very poorly sorted
PHM 11	3.40	clay	2.72	poorly - very poorly sorted
PHM 12	3.17	clay	2.28	poorly - very poorly sorted

The generally flat shelf area where the proposed site is located suggests that dredged material disposed there will not be subject to ‘slips’ leading to a loss of material beyond site boundaries. The similarity between sediments proposed for disposal and those occurring naturally at the site indicate that environmental effects on benthic fauna from introduction of significantly different sediment type will be minimal.

Biological characteristics

An understanding of the baseline state of the ecosystem is essential to identify significant species as well as in determining post-disposal impacts on the site and surrounding areas. Comparisons can be undertaken by determining changes in

species richness, diversity and evenness (Roberts *et al*., 1998; Smith and Rule, 2001; Simonini *et al*., 2005) and also by quantifying changes in contaminant levels of an indicator species (Hirsch *et al*., 1978; Roberts and Forrest, 1999).

Biological assessments that include actual identification of species present on the northeast New Zealand shelf are rare. However findings of one such study undertaken by Sivaguru and Grace (2002) were relevant to the proposed site. Conclusions made from their study were that species richness in the deep-water areas was lower than that of the shallower sample locations, indicating that richness may be a function of depth. It was also noted that the polychaetes identified are typical of low energy environments, which is particularly relevant for disposal operations.

Although Sivaguru and Grace (2002) provide an indication of the ecosystem at the proposed site, their findings are not sufficient to make any definite conclusions. Therefore, the preliminary field survey of 2007 also included a benthic fauna assessment. A sample was retrieved, again with the 'SHIPEK' grab sampler, at each location (Figure 4). Samples were representative of the bioactive zone, the top several centimetres of the seafloor substrate. For the purposes of the initial investigations, specimens were sorted into major classes. Within each class, the number individuals per species, per grab were counted (Table 6). At each sample location, species richness (R), the Shannon Diversity Index (H'), and evenness (E) were determined (Krebs, 1989) (Table 6).

Average ecosystem indices (R=species richness, H'=Shannon Diversity Index, E=evenness) for quadrants 1, 2, 3, and 4 (Figure 4) are plotted in Figure 5. Each quadrant included 5 sample locations (Table 6). Average species richness (R) ranged from 8.4 to 11.8 across the 4 quadrants with similar variability amongst samples per quadrant. The average Shannon Diversity Index (H') ranged from 1.94 in quadrant 1 to 2.36 in quadrant 2. Variability amongst samples per quadrant was similar across the site. Average evenness was close to 1 (0.93 – 0.98) in all 4 quadrants with negligible variability amongst samples per quadrant. An evenness (E) value of 1 represents the maximum diversity evenness. Ecosystem indicators within the benthos at baseline conditions show similar trends across the site, with exception of the Shannon Diversity Index (H') which was more varied. Future surveys based on a finer sampling grid would increase confidence in the index trends.

At the proposed site, the pelagic ecosystem is equally important as the benthic ecosystem, but often draws more attention as it includes more 'popular' marine fauna such as fin fish and cetaceans. A review of the literature indicates that important pelagic species typically move with the EAUC in the northeast coast region (Francis, 1996). Seasonally, there may be transient visits in the vicinity of the site by large species such as tunas and marlins. Small, rare reef fishes also known to populate the region under specific temperature conditions, but would likely remain closer to the coastline where rock reef habitat predominates (Francis *et al*., 1999).

Table 6

Number of individuals per class, per grab for the 6 benthic faunal classes* identified at the 20 sample locations, total number of individuals collected (N), and the respective indices species richness (R), Shannon Diversity Index (H') and evenness (E).

Quadrant/Sample	P	W	B	G	M	O	N	R	H'	E
1										
1-1	3	2	0	0	9	1	15	10	2.08	0.90
1-2	4	0	0	0	1	0	5	5	1.61	1.00
1-3	16	4	0	1	3	0	24	15	2.59	0.96
1-4	7	0	1	0	1	1	10	8	2.03	0.97
1-5	0	2	0	0	2	0	4	4	1.39	1.00
2										
2-1	6	0	0	0	3	0	9	9	2.16	0.98
2-2	10	1	2	0	5	0	18	15	2.66	0.98
2-3	6	1	1	0	2	0	10	8	2.03	0.97
2-4	9	0	1	0	3	0	13	9	2.14	0.97
2-5	16	1	2	1	2	2	24	18	2.81	0.97
3										
3-1	5	0	0	2	2	0	9	9	2.20	1.00
3-2	7	1	1	0	2	0	11	6	1.42	0.79
3-3	9	2	0	0	2	0	13	9	2.14	0.97
3-4	10	0	0	0	3	0	13	10	2.21	0.96
3-5	9	1	2	1	9	1	23	17	2.75	0.97
4										
4-1	9	1	1	2	8	2	23	15	2.52	0.93
4-2	6	0	0	0	12	1	19	12	2.07	0.83
4-3	1	1	0	1	4	0	7	6	1.73	0.97
4-4	8	3	0	2	2	1	16	12	2.43	0.98
4-5	7	0	0	0	0	0	7	5	1.55	0.96

*P=Polycheates, W=Other worms, B=Bivalves, G=Gastropods, M=Malacostracans, O=Ophiuroids

Similarly, studies by Gaskin (1968), Visser (2000), Neumann *et al*. (2002) and McDonald (2006) on a variety of cetaceans in the northeast coast region suggest that apart from transient passage, such species do not spend a significant amount of time in the vicinity of the proposed site. These species spend most of their time feeding and are unlikely to frequent areas like the farther reaches of the northeast coast shelf, where the seafloor is flat and muddy and does not attract a large fin fish community (*pers. comm*., Alan Baker, 2008). However, it should be noted that as certain species do seasonally pass through the area, encounters could be mitigated during disposal operations by employing a 'watch' post to pause operations until the individual(s) have passed through the area.

Overall, based on the review and findings from the preliminary field survey, it does not appear that the seabed in the vicinity of the proposed site provides habitat for any key species in a food chain, nor is the water column frequented by any significant species.

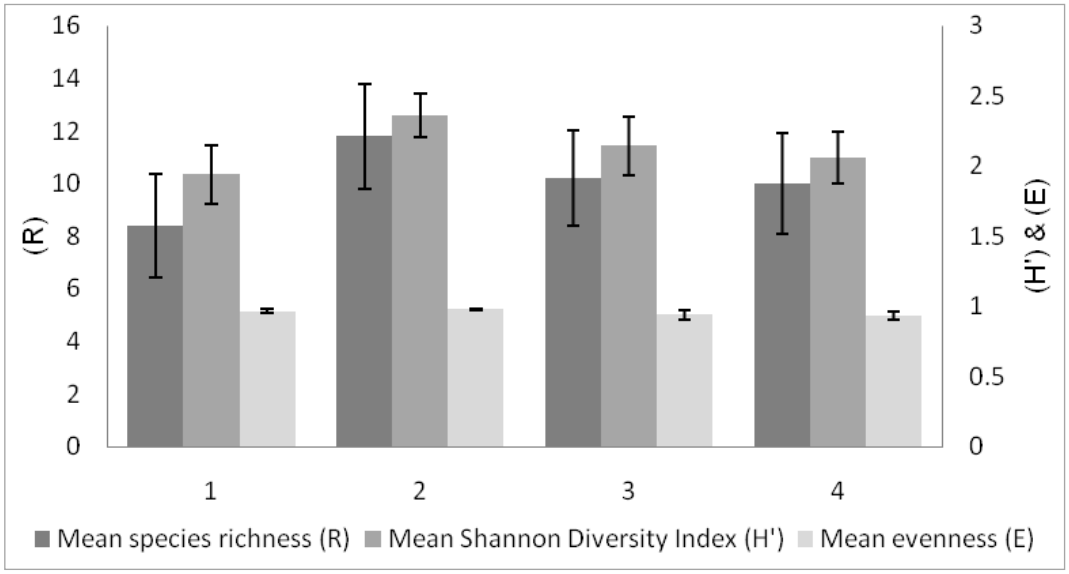

Figure 5. Mean ecosystem indices (species richness (R), Shannon Diversity Index (H'), evenness (E)) for quadrants 1, 2, 3, and 4 of the proposed site. Average values are based on 5 samples per quadrant (see Figure 4). Bars indicate the standard error.

With regard to the reported benthic ecosystem indices, the findings will become more useful should the proposed site be approved for disposal operations. A required monitoring program will involve a comparison of those indices to post-disposal conditions in order to assess any shifts in assemblage and any decreases in diversity or evenness, all of which could be perceived as adverse impacts.

Stakeholder concerns

Consultations with various government organisations and relevant interest groups were undertaken to assess the issues associated with the proposed disposal site and associated operations. The aim was to determine if the proposed site would be subject to internal spatial conflict and to more broadly allow for a review of the proposed activities. Seventeen stakeholders including local fishermen's associations, regional governments, local *iwi* groups (indigenous peoples groups), NZ military, and government conservation departments were engaged regarding the proposed activities (see Flaim and Healy (2008) and Maritime New Zealand (2009) for details). A public notification was also made in this period in accordance with Rule 180.5(1)(a) of the Maritime Protection Rules for permit applications (see the proceeding section for details on submission of the application). Responses were mixed, however all parties following concessions by the applicant and MNZ provided endorsement for the proposed disposal site subject to conditions (highlights from feedback listed in Table 7).

Of particular significance were discussions with ARC regarding the flux of disposed material into the CMA (Figure 1). As the CMA is under the legislative jurisdiction of the RMA, it was argued that operations at the proposed site would have offsite effects within the CMA and as such, an additional RMA consent would be required. As a technicality, this is a legitimate point. However, as the RMA and the MTA essentially uphold similar principles of sustaining the

Table 7
Details of feedback provided by interested stakeholders during the consultation process for disposal site assessment and permit application assessment.

Stakeholder	Concern	Feedback	Action taken
Auckland Regional Council (ARC)	Proximity of the site to the CMA	Contaminants could easily be transported into the CMA	Provision in future consents for monitoring of disposal plumes and suspension of operations should the plume drift into the CMA.
Iwi groups	*Mauri* (life-force) of New Zealand waters	A long-term consent would not allow for proper monitoring of impacts, jeopardizing the *Mauri* (life-force) of the waters.	Conditions on any consent issued that would require a strict and thorough monitoring plan to identify impacts.
MAF Biosecurity	Acceptability of dredged material for disposal at the site with regard for the spread of invasive species	No invasive species of concern identified in Pine Harbour Marina sediments	None
Ministry of Fisheries	Commercial fishing activities at the proposed site	No commercial fishing activities occur in the specified area of the proposed site	None
NZ Defence Force	Naval exercise grounds in the vicinity of the site	Possible conflicts between disposal barges and naval vessels operating in similar areas	Conditions in future consents requiring notification of disposal operations to mitigate interference with naval exercises

environment and preventing adverse impacts, any material transported over the boundary would be very unlikely to have any impact at all. While assessment and justification is required to demonstrate that material disposal effects will be no more than minor, it seems onerous to require the applicant to repeat the MNZ consent process for effects within the CMA to the ARC. Furthermore, the quantities of land-derived (and therefore potentially contaminated) sediment flushed into the Hauraki Gulf and other parts of the CMA by rivers, has the potential to result in high background levels of suspended sediment in some areas and a small transient increase from a disposal event would likely be insignificant if it reached the CMA boundary. This point is made especially pertinent when considering that the typical quantity of material lost as a 'plume' during disposal is only 1 – 5 % of the total quantity disposed (Truitt, 1988).

Other Site Assessment Considerations

The size and capacity of a proposed site are also important factors in its long term suitability for disposal operations, which is related to the loading rates and the type of site (i.e. dispersive or non-dispersive). Dredged material fate models, such as STFATE by the US Army Corps of Engineers, were designed to predict mound formation which can be used to determine how long a site can be used before vessels can no longer safely navigate over the deposited material (Moritz *et al*., 2000). For the present case, the significant water depth suggests that capacity will not be an important issue unless future permitting of the site allows for heavy usage. In that case, capacity issues will probably be related to loss of sediment outside the site boundaries, not vessel draught interference with disposal mounds though further analysis would be beneficial.

A Pilot Study

Concurrent with stakeholder consultations was the submission of the formal application to MNZ for consent to dispose dredged material at the proposed site. All findings from the initial investigations, feedback from stakeholder consultations, and discussions on potential impacts were included in the application submission in the form of an environmental impact assessment (EIA) (Flaim and Healy, 2008). After pending feedback was received, the information was reviewed by MNZ during assessment of the application. The original application was for a 35-year consent, with the understanding that regular monitoring would be part of the conditions. MNZ determined that there was not enough background information in order to award a 35-year consent. They, like ARC, were concerned about what would happen to the material after release into the water column and queried whether the material would be transported into the CMA.

As a compromise and in order to allow the missing data to be collected, MNZ awarded the applicant a short-term consent for a pilot study comprising a one-off disposal of 7,000 m^3 of dredged material. Conditions of the consent include rigorous plume monitoring surveys during disposals and a detailed post-disposal survey to identify the location of the disposed material and any potential impacts (Maritime New Zealand, 2009). It is anticipated by MNZ that if the pilot study shows no adverse impacts and raises no further concerns from the ARC, then a long-term consent would be suitable. In this case, the proposed site could

potentially be usable for other interested parties as per the original intentions of the applicant, though alteration of the consent would likely be required.

Conclusions

As illustrated in this paper, the continued use of the CMA east of Auckland City for disposal of dredged material is not assured. This communication describes the process by which a New Zealand maritime entity has attempted to establish a suitable dredged material disposal site beyond those boundaries. The described approach illustrates procedural lessons that can be learned with respect to the establishment of an offshore disposal site. For nations whom are yet to develop systems for the assessment of new disposal sites, the New Zealand approach presented here, taken by MNZ in the EEZ and by regional councils in the TS may offer a starting point for initiating such directives.

For the present case, findings of the initial investigations indicate that the proposed site is suitable for disposal operations and adverse environmental impacts are unlikely. However, data collected and analysed from the upcoming pilot study shall provide verification of these assumptions. Data from the plume dispersal monitoring, and post-disposal surveys will be examined by MNZ to determine the extent of environmental effects and to assess whether the consent period of 35 years, proposed by the applicant, is appropriate.

For New Zealand, as for other countries, offshore disposal sites could be a viable alternative to nearshore sites. Offshore sites are likely to be removed from 'NIMBY' concerns with increased distances reducing the interaction between the sites and coastal populations. In the case of east Auckland, bureaucratic slowing due to past controversies, would in theory also be largely circumvented, with ARC involvement limited to disposed material which may float into waters under their jurisdiction (CMA). While developments in the EEZ are still subject to environmental assessment regulation, historically limited developments in this spatial environment may result in management mechanisms that are less fragmented, more centralized, more efficient, and more closely aligned with international directives.

However, moving the proposed site even further offshore to acquiesce with, in this case, the regional council would increase operational costs as well as the difficulty for monitoring, in the end making it a less attractive option. Logistically, the proposed site appears to be in the ideal location when considering all perspectives, but some aspects of the environmental sustainability of the site have yet to be determined. Clearly though, gaining the desired long term dredged material disposal consent in EEZ would solve a decades-long coastal management problem for east Auckland as well as illustrate the benefit that moving such activities offshore would provide.

Notes

1. Sourced from Land Information New Zealand data. Crown Copyright Reserved. DATA IS NOT COMPLIANT WITH AND CANNOT BE USED IN LIEU OF DATA REQUIRED UNDER SECTION 31.1 OF THE TERRITORIAL SEA [CONTIGUOUS ZONE] AND EXCLUSIVE ECONOMIC ZONE ACT 1977. NOT TO BE USED FOR NAVIGATION.

2. Not In my Backyard describes the situation where residents oppose development based on geographic proximity, rather than being fundamentally opposed to the effects which may arise upon the environment (Delogu, 1990). Increased industrialization of the ocean environment will be opposed by local residents with effects on visual amenities commonly cited effects. The very same residents however may believe that the project proposed is suitable, as long as it is somewhere else.
3. Refer to the United Nations Convention on the Law of the Seas (UNCLOS) Part II, Section 2, Articles 3, 4, 5, 7, and 9 for a definition of what is meant by the territorial seas. Details on the definition of the Coastal Marine Area can be found in the Resource Management Act's Section 2.

References

ANZECC. 2000. Australia and New Zealand guidelines for fresh and marine water quality 2000. Australia and New Zealand Environment and Conservation Council, Agriculture and Resource Management Council of Australia and New Zealand.

ANZECC, 1998. Australia and New Zealand Environment and Conservation Council: interim disposal guidelines.

Ashby, M. 2004. *Winds up: planning for the future now*. Wellington: Connell Wagner.

Bioresearches. 2009. Pine Harbour Marina Limited pre dredging marina basin biological and sediment characteristics report. 9p.

Carter, L., and J.V. Eade. 1980. Hauraki sediments, New Zealand Oceanographic Institute Chart, Coastal Series 1:200 000.

Delogu, O.E. 1990. "NIMBY" is a national environmental problem. *South Dakota Law Review* 35: 198-219.

Denham, R.N., R.W. Bannister, K.M. Guthrie, and F.G. Crook. 1984. Surveys of the East Auckland and East Cape Currents, New Zealand. *Australian Journal of Marine and Freshwater Research* 35: 491-504.

Disposal Options Advisory Group (DOAG). 1994. Assessment of the options available for the disposal of dredged material from the Port of Auckland. New Zealand. Part 1 - 5.

Dyer, K.R. 1986. *Coastal and Estuarine Sediment Dynamics*. Chichester: John Wiley & Sons.

Flaim and Healy, 2008. Proposal for Dredged sediment disposal on the continental shelf in the EEZ: Environmental Impact Assessment. Coastal Marine Group, University of Waikato, Hamilton, New Zealand. 88 pp.

Francis, M. P. 1996. Geographic distribution of marine fishes in the New Zealand region. *New Zealand Journal of Marine and Freshwater Research* 30: 35-55.

Francis, M. P., C. J. Worthington, P. Saul, and K. D. Clements. 1999. New and rare tropical and subtropical fishes from northern New Zealand. *New Zealand Journal of Marine and Freshwater Research* 33: 571-586.

Friedrichs, C.T., L.D. Wright, D.A. Hepworth, and S.C. Kim. 2000. Bottom-boundary-layer processes associated with fine sediment accumulation in coastal seas and bays. *Continental Shelf Research* 20: 807-841.

Frisken, W.D. 1992. New Zealand North Island east coast: Breamhead to Slipper Island including Hauraki Gulf 1: 200 000. Auckland, Hydrographic Office of the Royal New Zealand Navy.

Gaskin, D. E. 1968. Distribution of Delphinidae (Cetacea) in relation to sea surface temperatures off eastern and southern New Zealand. *New Zealand Journal of Marine and Freshwater Research* 2: 527-534.

Gibb, B. 1997. Dredging, environmental issues and port experience in the United States. *Maritime Policy and Management* 24:313-318.

Golder Kingett Mitchell. 2007. Pine Harbour Sediment Assement. Report prepared for Pine Harbour Marina Ltd. Report No. PINHAAKL002, 9pp.

Gorman, R.M., K.R. Bryan, and A.K. Laing. 2003. Wave hindcast for the New Zealand region: deep-water wave climate. *New Zealand Journal of Marine and Freshwater Research* 37: 589-612.

Grace, R.V. 1988. Ecological investigation of the Auckland Harbour Board's alternative dredge spoil dump site off Brown's Island, Waitemata Harbour. Report prepared for the Auckland Harbour Board.

Halka, J., W. Panageotou, and L. Sanford. 1991. Consolidation and erosion of deposited cohesive sediments in Northern Chesapeake Bay, USA. *Geo-Marine Letters* 11:174-178.

Hall, S.J. 2002. The continental shelf benthic ecosystem: current status, agents for change and future prospects. *Environmental Conservation* 29(3):350-374.

Harris, T.F.W. 1985. North Cape to East Cape aspects of the physical oceanography. University of Auckland Department of Physics and Marine Laboratory, Leigh, 178pp.

Harvey, M., D. Gautheir, and J. Munro. 1998. Temporal changes in the composition and abundance of the macro-benthic invertebrate communities at dredged material disposal sites in the Anse à Beaufils, Baie des Chaleurs, eastern Canada. *Marine Pollution Bulletin* 36:41-55.

Healy, T.R., S.G. Ryan, and C. Harms. 1988. Recent environmental issues concerning dredge spoil dumping. Proceedings of the Ecopolitics III Conference, Hamilton, 98 -102, University of Waikato, Hamilton, New Zealand.

Heath, R.A. 1977. Phase distributions of tidal constituents around New Zealand. *New Zealand Journal of Marine and Freshwater Research* 11(2): 383-392.

Heath, R.A. 1980. Eastwards oceanic flow past northern New Zealand. *New Zealand Journal of Marine and Freshwater Research* 14 (2): 169-182.

Heath, R.A. 1985. A review of the physical oceanography of the seas around New Zealand- 1982. *New Zealand Journal of Marine and Freshwater Research* 19: 79-124.

Hirsch, N.D., L.H. Disalvo, and R. Peddicord. 1978. Effects of dredging and disposal on aquatic organisms. Technical Report No. DS-78-5, Dredged Material Research Program, US Army Corps of Engineers, 41pp.

Kagan, R.A. 1994. Dredging Oakland Harbour: implications for ocean governance. *Ocean & Coastal Management* 23: 49-63.

Keown, J. 2009. Auckland disputes need for dredging. *The Dominion Post*, 22 October 2009, http://www.stuff.co.nz/business/industries/2987770/Auckland-disputes-need-for-dredging. Fairfax New Zealand Limited: accessed 2 April, 2010.

Komar, P.D. 1976. *Beach processes and sedimentation*. Englewood Cliffs: Prentice-Hall Inc.

Krebs, C.J. 1989. *Ecological Methodology*. New York: Harper & Row.

Loomb, C.A.M. 2001. Muddy sedimentation in a sheltered estuarine marina, Westpark Marina, Auckland, New Zealand. Unpublished Msc Thesis.

University of Waikato, Department of Earth Science, Hamilton, New Zealand. p 33-60.

Mannino, I., S. Soriani, and G Zanetto. 2002. Management of port dredged material: and eco-political issue. Proceedings of Littoral 2002 The Changing Coast, EUROCOAST/EUCC, 75-79, Porto, Portugal.

Marine Board. 1985. *Dredging Coastal Ports: An Assessment of the Issues.* Washington D.C.: National Academy Press.

Maritime New Zealand. 2009. Dumping permit application report - Coastal Resources Limited (Pine Harbour Marina): disposal of dredged spoil at new EEZ site east of Great Barrier Island. 12pp.

Maritime New Zealand. 2002. National policy on the sea disposal of waste. 8 pp.

Maritime Safety Authority. 1999. New Zealand Guidelines for the Sea Disposal of Waste. Maritime Safety Authority, Wellington, New Zealand.

Mauer, D., R.T. Keck, J.C. Tinsman, and W.A. Leatham. 1980. Vertical migration and mortality of benthos in dredged material: part I-mollusca. Marine *Environmental Research* 4:229-319.

Mauer, D., R.T. Keck, J.C. Tinsman, and W.A. Leatham. 1981. Vertical migration and mortality of benthos in dredged material: part II-crustacea. Marine *Environmental Research* 5:301-317.

Mauer, D., R.T. Keck, J.C. Tinsman, and W.A. Leatham. 1982.Vertical migration and mortality of benthos in dredged material: part III-polychaeta. Marine *Environmental Research* 6:49-68.

McDonald, M. A. 2006. An acoustic survey of baleen of whales off Great Barrier Island, New Zealand. *New Zealand Journal of Marine and Freshwater Research* 40: 519-529.

Miller, M.C., I.N. McCave, and P.D. Komar. 1977. Threshold of sediment motion under unidirectional currents. *Sedimentology* 24(4): 507-527.

Moritz, H.R., B.H. Johnson, and N.W. Scheffner. 2000. Numerical models for predicting the fate of dredged material placed in open water. In Handbook of coastal engineering, ed. J.B. Herbich, 16.1-16.27. New York: McGraw-Hill.

Neumann, D.R., A. Leitenberger, and M.B. Orams. 2002. Photo-identification of short-beaked common dolphins (*Delphinus delphis*) in the north-east New Zealand: a photo-catalogue of recognisable individuals. *New Zealand Journal of Marine and Freshwater Research* 36: 593-604.

Palermo, M.R. 2000. Disposal and placement of dredged material. In Handbook of dredging engineering (2nd edition), ed. J.B. Herbich, 11.1-11.52. New York: McGraw-Hill.

Parliamentary Commissioner for the Environment. 1995. Dredgings disposal in the Hauraki Gulf. Final report of the technical review panel, Parliamentary Commissioner for the Environment, New Zealand.

Peart, R. 2007. *Beyond the tide – integrating the management of New Zealand's coasts*. Auckland: Environmental Defence Society Incorporated.

Peterson, E.L. 1999. Benthic shear stress and sediment condition. *Aquacultural Engineering* 21: 85-11.

Pickrill, R.A., and J.S. Mitchell. 1979. Ocean wave characteristics around New Zealand. *New Zealand Journal of Marine and Freshwater Research* 13(4): 501-520.

Poltrack, S. 2001. The maritime industry and our environment: the delicate balance of economic and environmental concerns, globally, nationally, and

within the Port of Baltimore. *University of Baltimore Journal of Environmental Law* 8.1: 51-78.

Roberts. R.D., M.R. Gregory, and B.A. Foster. 1991. The Rangitoto spoil ground: impact of dumping dredge spoil from the Port of Auckland on a shallow seafloor. In Proceedings of the 10th Australasian Conference on Coastal and Ocean Engineering, ed. R.G. Bell, T.M. Hume, and T.R. Healy, 35-40. Auckland, New Zealand.

Roberts, R.D., M.R. Gregory, and B.A. Foster. 1998. Developing an efficient macrofauna monitoring index from an impact study – a dredge spoil example. *Marine Pollution Bulletin* 36(3): 231-235.

Roberts, R.D. and B.M. Forrest. 1999. Minimal impact from long-term dredge spoil disposal at a dispersive site in Tasman Bay, New Zealand. *New Zealand Journal of Marine and Freshwater Research* 33: 623-633.

Sharples, J. 1997. Cross-shelf intrusion of subtropical water into the coastal zone northeast of New Zealand. *Continental Shelf Research* 17(7):835-857.

Sharples, J., and M.J.N. Grieg. 1998. Tidal currents, mean flows, and upwelling on the north-east shelf of New Zealand. *New Zealand Journal of Marine and Freshwater Research* 32: 215-231.

Simonini, R., I. Ansaloni, F. Cavallini, F. Graziosi, M. Iotti, G. Massamba N'Siala, M. Mauri, G. Montanari, M. Preti, D. Prevedelli. 2005. Effects of long-term dumping of harbour-dredged material on macrozoobenthos at four disposal sites along the Emilia-Romagna coast (Northern Adriatic Sea, Italy). *Marine Pollution Bulletin* 50: 1595-1605.

Sivaguru, K., and R. Grace. 2002. Habitat species diversity of deep reefs and sediments at Great Barrier Island. Report for the Department of Conservation, Auckland Conservancy, 25 pp.

Smith, S.D.A., and M.J. Rule. 2001. The effects of dredge-spoil dumping on a shallow water soft-sediment community in the Solitary Islands Marine Park, NSW, Australia. *Marine Pollution Bulletin* 42:1040-1048.

Stanton B.R. and P. Sutton. 2003. Velocity measurements in the East Auckland Current north-east of North Cape, New Zealand. *New Zealand Journal of Marine and Freshwater Research* 37: 195-204.

Stanton, B.R., P.J.H. Sutton, and S.M. Chiswell. 1997. The East Auckland Current, 1994-95. *New Zealand Journal of Marine and Freshwater Research* 31: 537-549.

Tolman, H.L. 2009. User manual and system documentation of WAVEWATCH III™ version 3.14. NOAA / NWS / NCEP / MMAB Technical Note 276, 194 pp + Appendices.

Truitt, C.L. 1988. Dredged material behaviour during open-water disposal. *Journal of Coastal Research* 4:489-497.

Visser, I.N. 2000. Orca (*Orcinus orca*) in New Zealand waters. Ph.D. Thesis. University of Auckland, Auckland, New Zealand, 200 pp.

Walters, R.A., D.G. GORING, and R.G. Bell. 2001. Ocean tides around New Zealand. *New Zealand Journal of Marine and Freshwater Research* 35: 567-579.

Zeldis, J.R., R.A. Walters, M.J.N. Grieg, and K. Image. 2004. Circulation over the northeastern New Zealand continental slope, shelf and adjacent Hauraki Gulf, during spring and summer. *Continental Shelf Research* 24(4-5): 543-561.

Tidal components of flow at a proposed dredged material disposal site on the continental shelf, northeast New Zealand

Bryna K. Flaim[1], Terry R. Healy[1] and Willem de Lange[1]
[1]University of Waikato, Hamilton, New Zealand

Abstract
As a regulatory requirement of the London Dumping Convention, the suitability of a site for proposed disposal operations must be determined prior to establishment. The tidal flow components at a proposed disposal site on the continental shelf of the northeast of New Zealand have been examined. Harmonic analysis of acoustic Doppler profiler (ADP) data showed that the cross-shore component of tidal variance was significant, often in the range of 50%, through the water column during the sampling period. The horizontal tidal component was influenced mainly by semi-diurnal tidal constituents, namely the M_2 tidal wave, with a small diurnal inequality. M_2 tidal amplitudes were approximately 8 cm/s throughout the water column, but other constituents showed more variation from sea surface to seafloor. The 3-dimensional barotropic tide model shows reasonable agreement with the measured data, but requires calibration for accurate tidal simulation. For establishment of the proposed disposal site, the findings of this study suggest that tidal currents will not be a significant driver for either the advection or re-suspension of disposed material.

1 Introduction

The natural, infilling tendencies of many harbours and marinas of New Zealand result in the accumulation of significant quantities of sediment that must ultimately be removed to maintain normal shipping and boating operations. For the case of Auckland, New Zealand's major city, an annual average of approximately 50 000 – 100 000 m^3 of lightly contaminated muddy dredged material is deemed unsuitable for alternative disposal options, such as reclamation and nourishment activities, and requires disposal in the seas adjacent to Auckland city (Disposal Options Advisory Group 1994). Previously, disposal sites have been established and used in the relatively shallow seas of the Hauraki Gulf near Auckland city (Fig. 1), only to be shut down due to the discovery of adverse environmental impacts (Grace 1988, Kingett Mitchell & Associates 1990, Roberts *et al.* 1991, Flaim, 2008).

Due to these effects and the establishment of the Hauraki Gulf Marine Park in 2000 (Department of Conservation 2000) (Fig. 1), traditional at-sea disposal activities within the Auckland territorial seas have, effectively, stopped. Companies, such as the Ports of Auckland have sponsored much research on the identification of new and more environmentally suitable sites within the Gulf, but none have been deemed acceptable for long term use (Grace 1988; Disposal Options Advisory Group 1994; Parliamentary Commissioner for the Environment 1995).

Consequently, a disposal site has been proposed beyond the boundaries of the territorial seas in waters deeper than 100 m, as recommended by Disposal Options Advisory Group (1994). Compared to shallower sites, it is thought that a proposed deep water site will result in significantly fewer environmental impacts from disposal operations.

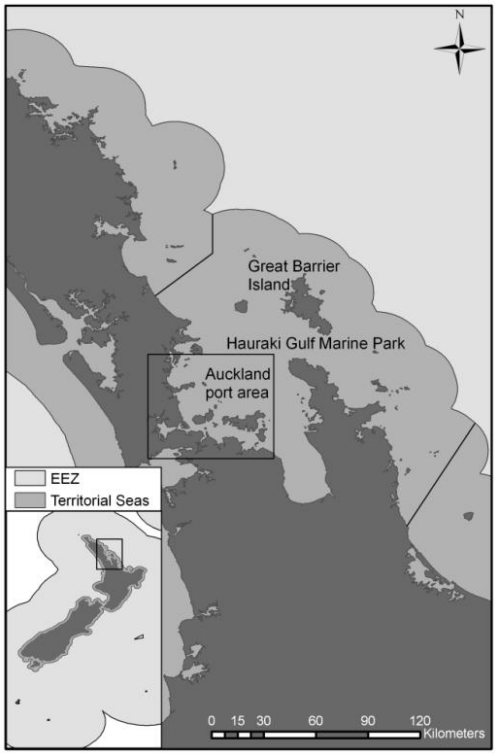

Figure 1. The Auckland port area, boundaries of the Hauraki Gulf Marine Park (black line), Territorial Seas, and the EEZ.

Its location on the continental shelf is not home to, or in the vicinity of the ecologically sensitive communities present in the shallow territorial seas. As the proposed site is located in the Exclusive Economic Zone (EEZ) (Fig. 1), it is under the jurisdiction of Maritime New Zealand, the national authority, and is therefore subject to the international policies, namely, the

London Dumping Convention (International Maritime Organisation 2003), to which New Zealand is a signatory. This study details the influence of the tides at the proposed disposal site through analysis of ADP measurements, the findings of which will be used for the purpose of calibrating a comprehensive numerical model that can be used to estimate sediment transport pathways. Ultimately, the flow direction and concentration of suspended sediment potentially resulting from disposal operations will be a major factor for site suitability.

1.1 Study site setting

The tides on northeast coast of the North Island of New Zealand are, like all other New Zealand regions, predominantly semi-diurnal, with the M_2 tide as the principal constituent. This wave travels anti-clockwise as a trapped Kelvin wave around the bathymetric platform (Heath 1985), which on the northeast coast, ranges in width from 11 km – 100 km (Harris 1985). It has a period of 12.42 h with typical current amplitudes of 5 – 10 cm/s (Sharples and Greig 1998). Other semi-diurnal constituents, such as the N_2 and the S_2, are weak on the east coast (Heath 1985). Diurnal constituents in this region are generally complex, owing to the complex bathymetry between the east coast and the amphidrome located east of New Zealand (Stanton *et al*. 2001). The largest of these diurnal components are the K_1 and O_1 and while generally less important than the semi-diurnal components, Heath (1985) reported larger-than-expected flows for the K_1. Internal tides, associated with the stratified conditions of the summer months, have been observed on the northeast coast by Sharples and Greig (1998).

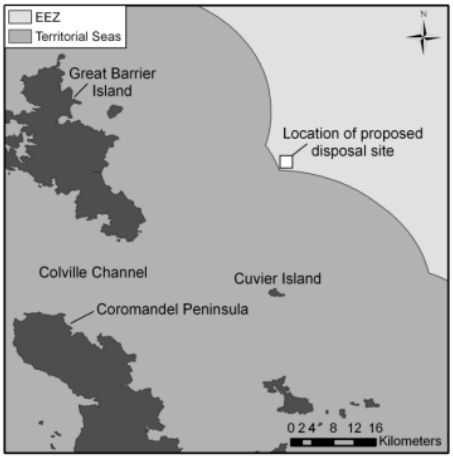

Figure 2. Location of the proposed disposal site in relation to: Great Barrier Island, Cuvier Island, Coromandel Peninsula, Colville Channel, Territorial Seas, and the EEZ.

The proposed disposal site is located on the continental shelf at water depths ranging from 135 – 145 m. Shelf-break in this area occurs at approximately 200 m. The site lies 25 km east of Great Barrier Island and 22 km north of Cuvier Island, just inside the boundaries of the EEZ (Fig. 2). It extends over 4 km^2, with the centre coordinates at 175° 47' 00''E and 36° 13' 00''S.

The site is characterised by flat featureless topography, with sediments comprising mainly silt and fine sand deposited as a thin (<20 cm) layer, over a hard foundation (Flaim 2008). To the southwest of the proposed site lies the Colville Channel, an entrance to the Hauraki Gulf. It is bounded by the southern end of Great Barrier Island to the north, and the northern tip of the Coromandel Peninsula to the south (Fig. 2). Within this channel, due to morphological constriction, tidal currents have been estimated to reach 25 cm/s (Greig and Proctor 1988).

2 Methodology

2.1 Field measurements

On 26 September 2008, an upward facing Sontek 500kHz ADP was deployed on the seafloor at the centre of the study site for ~2 months. Horizontal and vertical current velocities (U,V & W) were logged at hourly intervals in 7 m bins over the total depth of 140 m. ADP data from the lowest 7 m, and cells 15 - 20 (near surface) were not usable and were not included in the analysis. At the same time, a CTD survey was undertaken across the study site. Twenty CTD casts were taken at 500 – 1000 m intervals, giving reasonable coverage of the site.

2.2 Field data preparation

Tidal analysis was undertaken using the Matlab T_TIDE harmonic analysis package (Pawlowicz *et al.* 2002). For the 63 days of ADP data, 35 tidal constituents were estimated for the U, V and W velocities, and used to determine the tidal contribution to variance, constituent significance, tidal ellipse parameters (amplitude, inclination and phase). These analyses were performed for cells 1 – 14, corresponding to mid-cell water elevations of approximately 10 - 117 m above the seafloor.

2.3 Model set-up

Assessment of CTD profiles showed that during the sampling period, the water column was fully mixed with respect to temperature, salinity, and density. With that in mind, a 3-dimensional barotropic model was run to simulate the tidal dynamics for a

regional domain including the study site. As the results of the CTD have no bearing on the model set up, they will not be discussed further. The 3DD model (Black, 1995) was designed to simulate 2-dimensional currents and 3-dimensional wind driven and buoyancy forced flows. The model has successfully been applied in New Zealand and international waters since the 1980s (Black 1987, 1989, Black and Gay 1987, Black *et al*. 1993, 2000, Middleton and Black 1994, Young *et al*. 1994, Hume *et al*. 2000). It uses an explicit, finite difference (Eulerian) scheme to solve momentum and continuity equations for velocity and sea level (Black, 1995). The vertical layers are linked by the vertical eddy viscosity coefficient. The model accounts for spatial variation through bed roughness length and horizontal eddy viscosity. The model can also account for various non-linear terms and Coriolis forcing.

Tidal dynamics were simulated over a computational domain that extends from Great Barrier Island in the north to the northern part of the Coromandel Peninsula in the south (Fig. 3).

The model domain is a 500 m x 500 m grid oriented north-south (j=111 km) and east-west (i=118 km). All off-shore islands have been included and some land smoothing has been applied. The grid origin is located at 351216.45 E, 5931565.39 N (UTM 60). The shelf bathymetry was interpolated into the model grid based on the hydrographic chart (NZ53) produced by the Royal New Zealand Navy (Frisken 1992). Four vertical layers were applied to the model. Layers 1, 2, and 3 were 20 m, 105 m, and 20 m from sea surface to 145 m water depth, respectively, and layer 4 was 1629 m. This allowed for greatest vertical resolution in water depths corresponding to the study site.

2.4 Model run

Water level fluctuations were extracted from the National Institute of Water and Atmospheric Research (NIWA) tidal model (forced using data from the U.S.-French oceanographic satellite TOPEX/Poseidon) along all open boundaries of the grid. Sea-levels were interpolated across the north, east, and south boundaries. The model run spanned a spring and neap period from 10 October – 8 November 2008; a period that coincides with the ADP sampling period described above. Model parameters are included in Table 1.

Table 1. Model parameters

Parameter	Value
Time step	1.8 sec
Roughness length	0.005 m
Horizontal eddy viscosity coefficient	1 m^2s^{-1}
Model start time	10/10/2008 GMT+12hr
Grid resolution	500 m x 500 m
Grid dimensions	236 x 221
Orientation	0°true
Grid latitude (centre)	-36°20’
Coastal slip	100%
Effective drying depth	0.3 m
Drying height	0.05 m
Open boundaries	NIWA tide model: Sea-level values

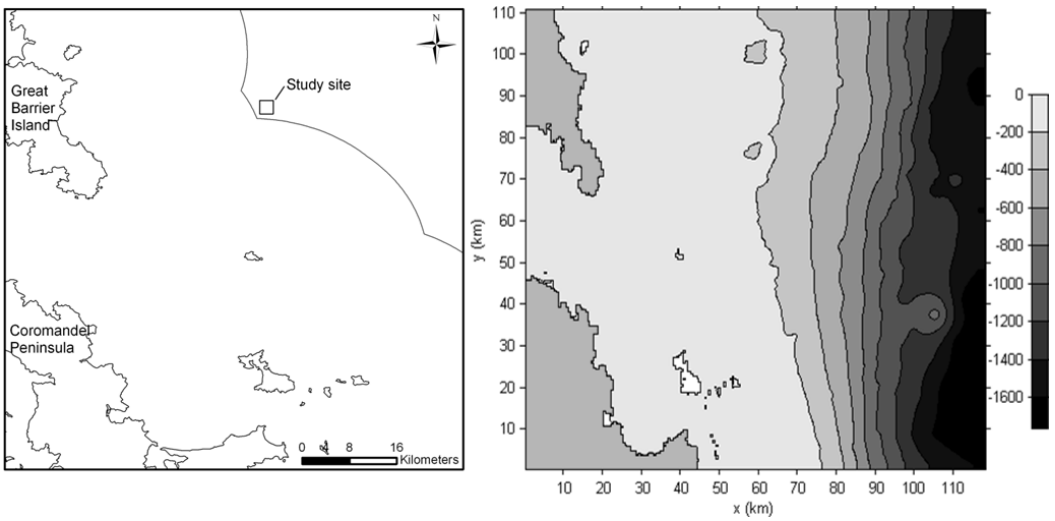

Figure 3. Geographic model domain (including location of the study site) and the 500 m x 500 m bathymetric grid used in the numerical simulation. The grid is oriented north-south (y) and east-west (x). Grid origin is located at 351216.45 E, 5931565.39 N (UTM 60).

3 Results

3.1 Tidal variance

The contribution of tidal energy was derived through harmonic analysis of the ADP time series of the U (cross-shore), V (alongshore), and W (vertical) currents from the centre of the study site (Fig. 4). The greatest tidal contribution (>50%) was in the cross-shore currents (30 - 90 m above the seafloor (ASF)). 10 - 30 m ASF, tidal contribution is just below 50% of the total variance. Close to the surface (100 – 120 m ASF) tidal contribution ranged from 45 – 30%, respectively. Tidal contribution in the alongshore and vertical directions was substantially less than that in the cross-shore direction. However, for the vertical direction, there is a notable increase in tidal energy nearbed (10 – 20 m AFS). It decreases towards the sea surface and becomes negligible 80 m AFS.

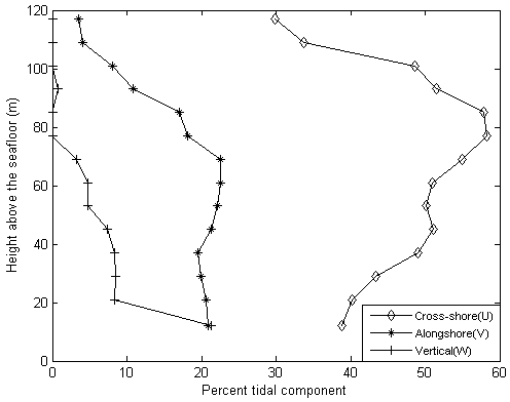

Figure 4. Percent tidal contribution to flow at the centre of the study site during the measured period.

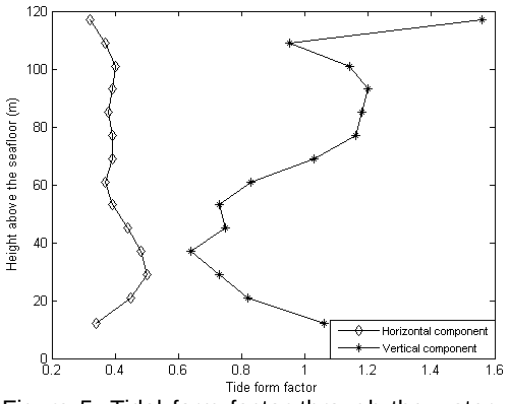

Figure 5. Tidal form factor through the water column, based on the M_2, S_2, K_1, and O_1 constituents.

To quantify contributions by semi-diurnal constituents versus diurnal constituents, a tidal form factor was derived based on the semi-major axes of the M_2, S_2, K_1, and O_1 constituents (Fig. 5). In the horizontal direction, semi-diurnal constituents are dominant with little variation throughout the water column. In the vertical direction, diurnal and semi-diurnal constituents have a more equal presence, with the diurnal constituents strongest near-bed and near-surface.

The tidal ellipses for M_2, S_2, N_2, K_1, and O_1 are plotted in Figure 6. Seven of the 14 ADP sampling cells are shown, describing the constituent ellipse at 21, 37, 53, 69, 85, 101, and 117 m above the seafloor. The M_2 semi-major axis dominates at approximately 8 cm/s. This amplitude is consistent throughout the water column, whereas the M_2 semi-minor axis varies, decreasing in strength closer to the seafloor. The tidal ellipse also rotates anticlockwise with increasing depth.

The S_2 tide amplitude is small throughout the water column compared to the M_2 tide. Generally, the semi-minor axis decreases towards the seafloor, but the ellipse inclination and phase does not change significantly. The N_2 tide semi-major amplitude is larger than the S_2 tide close to the sea surface (~4 cm/s). However, the two are similar in magnitude closer to the sea floor. The N_2 ellipse rotates anti-clockwise with depth. The K_1 tide has relatively strong amplitudes along the semi-major and minor axes (~4 and ~2 cm/s, respectively). The signal, as well as inclination and phase, remains consistent throughout the water column. Slightly weaker than the K_1 tide, the O_1 tide (~1 cm/s for semi-major and minor) is strongest in the middle of the water column.

3.2 Numerical modelling

The ultimate aim of this research is to develop a comprehensive numerical model that can be used to simulate sediment transport in the region of the study site so that effects of dredged material disposal can be predicted. The present 3-dimensional barotropic tide model is a scenario simulation, whereby results are uncalibrated, but indicative. Figure 7 includes comparison plots of observed versus modelled cross-shore currents from the centre of the study during a spring (12 Oct – 24 Oct 2008) and neap (24 Oct – 2 Nov) period. The data represents the average velocity between 21 and 117 m above the seafloor. These depths were chosen for analysis because they correspond to depths where measured (ADP) velocities were the most complete. Modelled data corresponding to these depths were taken from the mid-depth layer (layer 2) of the model output.

As tidal contribution during the measured period was not significant in the along-shore and vertical directions, modelled tidal currents were best represented in the cross-shore direction. In general, the neap period was simulated better than the spring period, with a mean absolute error (MAE) of 3.54. For the spring period, MAE was 4.58. Most of the model prediction error occurred toward the end of the spring period.

Overall, velocity magnitude was reasonably simulated for an uncalibrated model, although the timing is not quite correct. Additional current and pressure data are available from a bottom mounted InterOcean S4 current meter. Once these data are analysed, they will be used to calibrate the model.

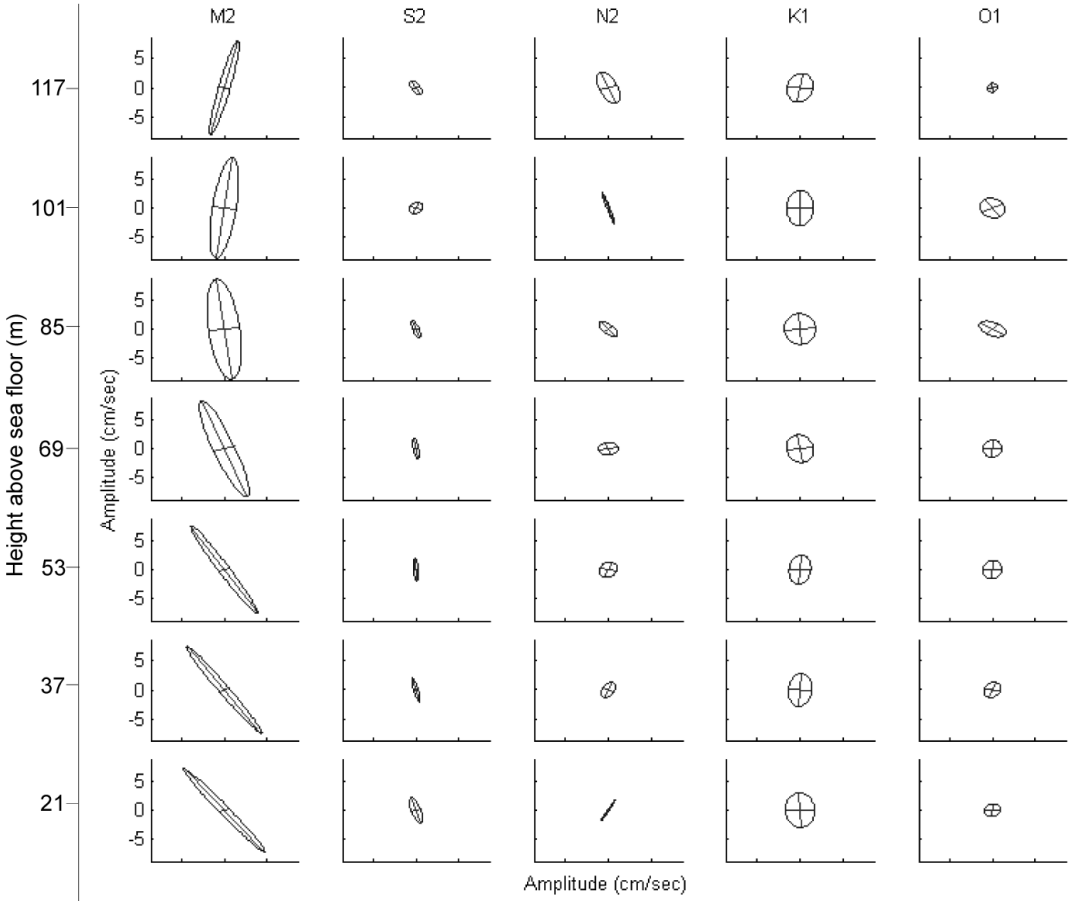

Figure 6. Tidal ellipses of the M_2, S_2, N_2, K_1, and O_1 constituents at 21, 37, 53, 69, 85, 101, and 117 m ASF, derived by harmonic analysis of ADP data from the centre of the study site (Sept. – Dec., 2008).

4 Conclusions

Patterns of the M_2 tidal wave observed during the measured period were consistent with the findings of Heath (1985) for the east coast of New Zealand. It is a trapped progressive wave so little energy is lost as it propagates around the southern end of New Zealand, making it the dominate constituent on the east coast. The S_2 tide has a dominant standing wave component on the west coast of New Zealand, which is not transmitted around the southern end of New Zealand to the east coast (Heath, 1985). This explains the observed small signal of this constituent during the sampling period.

Walters *et al.* (2001) found that the N_2 tide was similar to the M_2 tide except in amplitude, which was smaller. For the present study, the N_2 tide did have a smaller signal than the M_2, however, ellipticity was less consistent, with inclination and phase quite variable through the water column. The larger K_1 amplitudes were consistent with Heath (1985) and Stanton *et al.* (2001). Although, those previously reported findings were from regions to the south of the study site over the Chatham Rise. If the present findings represent those previous observed patterns, it can be suggested that these stronger-than-expected diurnal flows may be consistent with the generation of continental shelf waves, which may influence sedimentation and mixing.

Not previously discussed for the east coast region of New Zealand are the 3-dimensional features of the tides. Stanton *et al.* (2001) suggested that despite the barotropic nature of the tide, vertical variation is still feasible in the form of internal tides (occurring only during baroclinic conditions), as well as frictional effects.

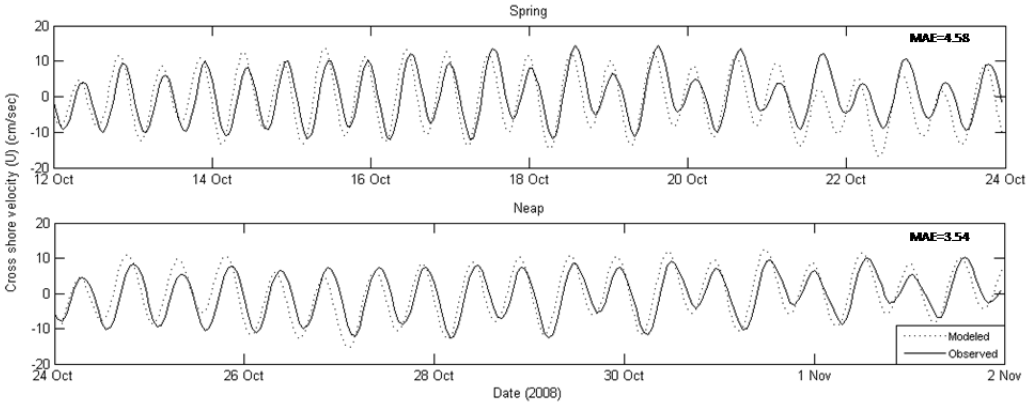

Figure 7. Observed and modelled cross-shore currents during a spring (12 Oct – 24 Oct 2008) and neap (24 Oct – 2 Nov 2008) period from the centre of the study site. Mean absolute error (MAE) was 4.58 and 3.54 for the spring and neap periods, respectively. The data represent the average cross-shore velocity for mid-water column depths (21 - 117 m above the seafloor).

It is clear that a vertically variable tide is a feature of the study site, most likely explained by friction and interaction with bottom topography. For the most part, the main constituents showed relatively consistent semi-major amplitudes, but there was an obvious decrease in semi-minor amplitudes toward the seafloor for several of the described constituents. Inclination and phase were also highly variable with depth for most of the observed constituents.

These findings suggest that a 3-dimensional tide model is required to resolve tidal behaviour. For the present study, a 3-dimensional tide model was only attempted for the region of interest surrounding the proposed disposal site. The presented results have not been calibrated, but velocity magnitudes for the cross-shore direction, the component with the greatest tidal contribution, were reasonably well simulated at mid-water column depths.

For the purposes of establishing the proposed disposal site, the findings of this study are fundamental to developing a comprehensive model of the circulation of the region of interest, which can then be used to predict sediment transport pathways and steps are currently being taken in that process. However, the findings also show that tidal currents will not be the major force driving either the advection or re-suspension of disposed material at the proposed site.

5 Acknowledgements

The measurement data and analysis work included in this paper was funded by Kaipara Ltd and the University of Waikato Doctoral Scholarship. The authors would like to thank the National Institute of Water and Atmospheric Science for the use of tide model sea level data. Data collection was directed by Dirk Immenga of the University of Waikato Coastal Marine Group. We also wish to thank Peter McComb of MetOcean Solutions Ltd. for the use of the ADP system.

6 References

Black, K.P. (1987) A numerical sediment transport model for application to natural estuaries, harbours and rivers. In: Noye, J. (Ed). *Numerical modelling applications to marine systems*. Elsevier, North Holland, pp. 77 - 105.

Black, K.P. (1989) Numerical simulation of steady and unsteady meso-scale eddies. Proceedings of the 9th Australasian Conference on Coastal and Ocean Engineering (Adelaide), pp. 204 - 208.

Black, K.P. (1995) The hydrodynamic model 3DD and support software, Occasional Report 19, Department of Earth Science, University of Waikato, 53 p.

Black, K.P. and Gay S.L. (1987) Eddy formation in unsteady flows. *Journal of Geophysical Research*, Vol. 92, 9514 - 9522.

Black, K.P., Hatton, D., and Rosenberg, M. (1993) Locally and externally-driven dynamics of a large semi-enclosed bay in southern Australia. *Journal of Coastal Research*, Vol. 9 No. 2, 509 - 538.

Black, K.P., Bell, R.G., Oldman, J.W., Carter G.S., and Hume, T.M. (2000) Features of 3-dimensional barotropic and baroclinic circulation in the Hauraki Gulf, New Zealand. *New Zealand Journal of Marine and Freshwater Research*, Vol. 34, 1 - 28.

Department of Conservation (2000) Hauraki Gulf Marine Park Act 2000. Department of Conservation, 34 p.

Disposal Options Advisory Group (DOAG) (1994) Assessment of the options available for the disposal of dredged material from the Port of Auckland. Report prepared for the

Commissioner of the Environment, New Zealand, Part 1 - 5.

Flaim, B.K. (2008) The continental shelf as a site for dredged material disposal, northeast New Zealand. MSc thesis, University of Waikato, New Zealand (unpublished), 169 p.

Frisken, W.D. (1992) New Zealand North Island east coast: Breamhead to Slipper Island including Hauraki Gulf 1: 200 000. Auckland, Hydrographic Office of the Royal New Zealand Navy.

Grace, R.V. (1988) Ecological investigation of the Auckland Harbour Board's alternative dredge spoil dump site off Brown's Island, Waitemata Harbour. Report prepared for the Auckland Harbour Board.

Greig, M.J. and Proctor, R. (1988) A numerical model of the Hauraki Gulf, New Zealand. *New Zealand Journal of Marine and Freshwater Research*, Vol. 22, 379 - 390.

Harris, T.F.W. (1985) North Cape to East Cape aspects of the physical oceanography. University of Auckland Department of Physics and Marine Laboratory, Leigh, 178 p.

Heath, R.A. (1985) A review of the physical oceanography of the seas around New Zealand- 1982. *New Zealand Journal of Marine and Freshwater Research*, Vol. 19, 79 - 124.

Hume, T.M., Oldman, J.W., and Black, K.P. (2000) Sediment facies and pathways of sand transport about a large deep water headland, Cape Rodney, New Zealand. *New Zealand Journal of Marine and Freshwater Research*, Vol. 34, 695 - 717.

International Maritime Organisation (2003) Convention on the Prevention of Marine Pollution by Dumping of Wastes and Other Matter 1972 and 1996 Protocol 2003 Edition. International Maritime Organisation, London, 39 p.

Kingett Mitchell & Associates (1990) Ports of Auckland Environmental Studies, Environmental assessment of the disposal of dredged material at the Hauraki Gulf disposal site. Report 9, Prepared for the Ports of Auckland Ltd., Part 2, 127 p.

Longdill, P.C. (2008) Environmentally sustainable aquaculture: an eco-physical perspective. PhD thesis, University of Waikato, New Zealand, 280 p.

Middleton, J.F. and Black, K.P. (1994) The low frequency circulation in and around Bath Strait: a numerical study. *Continental Shelf Research*, Vol. 14 No.13/14, 1495 - 1521.

Parliamentary Commissioner for the Environment (1995) Dredgings disposal in the Hauraki Gulf. Final report of the technical review panel, Parliamentary Commissioner for the Environment, New Zealand, 71 p.

Pawlowicz, R., Beardsley, B. and Lentz, S. (2002) Classical tidal harmonic analysis including error estimates in MATLAB using T_TIDE. *Computers and Geosciences*, Vol. 28, 929 - 937.

Roberts, R.D., Gregory, M.R. and Foster, B.A. (1991) The Rangitoto spoil ground: impact of dumping dredge spoil from the Port of Auckland on a shallow seafloor. Proceedings of the 10th Australasian Conference on Coastal and Ocean Engineering, R.G. Bell, T.M. Hume and T.R. Healy (Eds.) (Auckland), pp.35 - 40.

Sharples, J. and Greig, M.J.N. (1998) Tidal currents, mean flows, and upwelling on the north-east shelf of New Zealand. *New Zealand Journal of Marine and Freshwater Research*, Vol. 32, 215 - 231.

Stanton, B.R., Goring, D.G., and Bell, R.G. (2001) Observed and modelled tidal currents in the New Zealand region. *New Zealand Journal of Marine and Freshwater Research*, Vol. 35, 397- 415.

Walters, R.A., Goring, D.G., and Bell, R.G (2001) Ocean tides around New Zealand. *New Zealand Journal of Marine and Freshwater Research*, Vol. 35, 567 – 579.

Young, I.R., Black, K.P., and Heron, M.L. (1994) Circulation in the ribbon reef region of the Great Barrier Reef. *Continental Shelf Research*, Vol.14 No. 2/3, 117- 142.

MONITORING A DREDGED MATERIAL DISPOSAL SITE ON THE CONTINENTAL SHELF USING THE DYNAMIC PENETROMETER *NIMROD*

BRYNA FLAIM[1], NINA STARK[2], VICKI MOON[1], WILLEM DE LANGE[1], TERRY HEALY[1]* AND ACHIM KOPF[2]

*1. Department of Earth and Ocean Sciences, University of Waikato, Private Bag 3105, Hamilton 3240, New Zealand. bkf3@waikato.ac.nz; v.moon@waikato.ac.nz; delange@waikato.ac.nz. *Deceased July 20 2010*

2. MARUM, University of Bremen, Leobener Strasse, 28359 Bremen, Germany. nstark@uni-bremen.de; akopf@uni-bremen.de.

Abstract: During three surveys at a new dredged material disposal site on the northeast continental shelf of New Zealand's North Island, the dynamic penetrometer *Nimrod* was deployed to determine sediment strength characteristics of the site before and after disposal of dredged material. From the *Nimrod* data records, shear strength profiles were derived at 40 deployment positions. Interpreted shear strengths ranged from 0.6-1.3 kPa with associated impact velocities and decelerations of ~1.8 m/s and ≤3 g, respectively. Interpreted values correspond reasonably with laboratory measurements. Four types of shear strength profiles were identified after each of the post-disposal surveys, suggesting spatial distribution from dredged material disposal processes. Despite the small quantities of material disposed, a sequence of events was identified, attesting that turbidity current erosion and/or mixing may have contributed to an increase in strength of the shallow sub-seafloor material by appx. a factor of 2 in the eastern and southeastern portion of the disposal site.

Introduction

The fate of dredged material can be monitored using acoustic devices such as multibeam backscatter (MBES) and side-scan sonar (SSS), as well as through ground-truth methods such as diver observation and sample collection (Birchenough et al 2006; Li et al 2009). Using these methods, disposed material is typically identified based on topographic change, or changes in sediment properties such as type, texture, and density. Dynamic penetrometers, capable of profiling small vertical changes in seafloor sediment properties (Stark and Wever 2008), have the potential to be used as a complementary disposal monitoring technique by detecting changes in the strength of the sediment following disposal of dredged material. However, like most methods, some form of ground-truth should be undertaken to confirm results (Birchenough et al 2006; Li et al 2009).

In the Hauraki Gulf, comprising the nearshore waters of the Auckland region of New Zealand's North Island (Fig. 1), controversy over historical disposal sites has resulted in an absence of suitable long-term options for disposal of maintenance and capital works dredgings from ports, harbors, and marinas of the region (Flaim et al. 2010). In response, research began in February 2007 on the assessment of a proposed disposal site on the continental shelf of New Zealand's northeast coast (Fig. 1). The site, well beyond the shallow waters of the Hauraki Gulf, is located some 50 nm east of the coastal city of Auckland at water depths ranging from approximately 145-150 m. The continental shelf in this area is gently sloping with little to no morphologic features and the seafloor is composed of coarse silt to clay sized sediments (after Udden 1914, and Wentworth 1922). In the region of the site, currents tend to be relatively small owing to sheltering from predominant winds (Harris 1985) but are dominated by the East Auckland Current (EAUC) which flows toward the southeast along the northeast coast. Bottom currents measured during recent monitoring surveys were in the range of 5-20 cm/s.

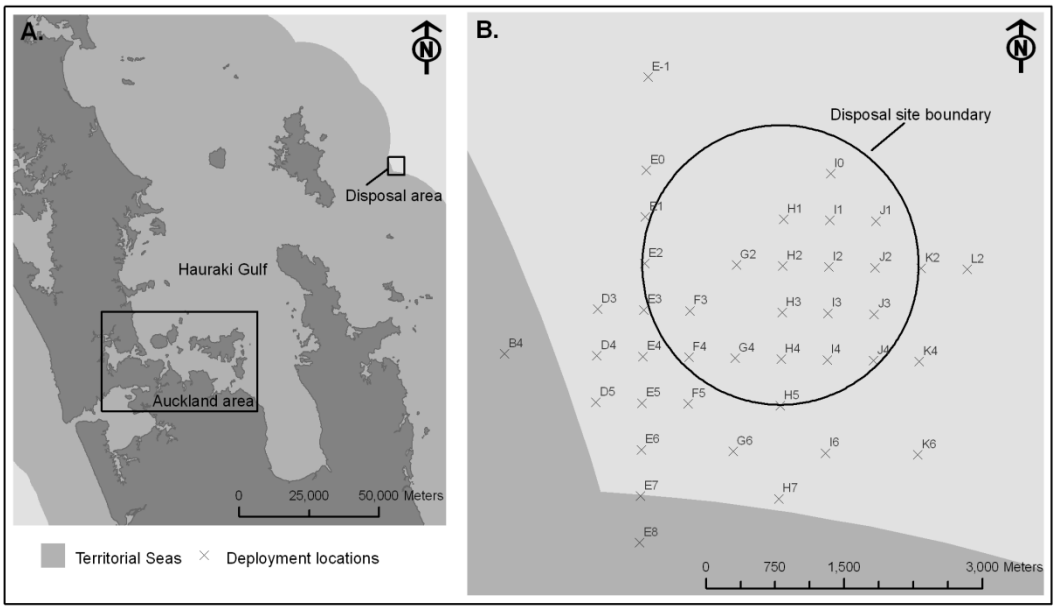

Fig. 1. A). Map of a section of the North Island of New Zealand including the Auckland area and the disposal area. B). *Nimrod* deployment locations including the boundaries of the disposal site.

In December 2009, consent was granted for a pilot study disposal of 5,000 m^3 of muddy sediments (silty-clay after Udden (1914) and Wentworth (1922)) dredged from the basin of an Auckland area marina for the purposes of determining whether the site was dispersive or non-dispersive (Maritime New Zealand 2009). A baseline survey (followed by two post-disposal surveys) of site sediments was undertaken using the small dynamic penetrometer, *Nimrod*, with the aim of determining the fate of the disposed material (Fig.2). This device was designed to be highly sensitive to small vertical changes in sediment resistance through the possibility of variable tip geometries (flat cylinder, hemisphere, or cone), the ability for true free-fall along with high-speed data acquisition, and the inclusion of four accelerometers varying in range and resolution (Stark et al. 2009a). Unlike the other monitoring methods, which were used to assess the total quantity disposed (10 loads of ~500 m^3 each), the objective of the *Nimrod* surveys were to identify small-scale changes in sediment strength following two individual disposals. Following disposal operations, core samples were collected across the proposed site. Shear strength was determined using a laboratory shear vane and compared to estimated undrained shear strength derived from profiles recorded by *Nimrod* at the same locations.

Fig. 2. *Nimrod* being readied for a free-fall deployment (assembled with hemispherical tip).

Methodological Approach

Deployed by hand, *Nimrod* penetrates the seafloor after free-fall through the water column. Sensors measure deceleration and pressure over time allowing for the calculation of velocity and penetration depth (Stark et al. 2009a). Although vertical variation in sediment properties such as strength and density can be inferred through the deceleration-depth profiles, the impact velocity and in consequence the deceleration, is also influenced by water column effects (e.g. currents) and other deployment factors (e.g. tether drag) (Stoll et al. 2007; Stark and Wever 2008). Given these uncertainties, it has been considered more useful to assess bearing capacity and undrained shear strength (Aubeny and Shi, 2006; Stoll et al 2007; Stark et al. 2009b). Deceleration after the probe contacts the seafloor is proportional to the resistive force of the sediment which is dependent on its undrained shear strength (Stoll and Akal 1999). Following that principle, an approach first introduced by Dayal and Allen (1975) and advanced by Aubeny and Shi (2006) can be used to determine the undrained shear strength from the deceleration profile. By applying the power law, sediment resistance force F_{sr} can be obtained:

$$W_b\, dec = F_{sr} \tag{1}$$

where W_b is the buoyant weight of *Nimrod* (with hemispherical tip, ~9 kg) and *dec* is the measured deceleration. Due to the very small penetration depths, inertial forces and probe soil buoyancy are neglected. Following Aubeny and Shi (2006) and by employing the empirical relationship introduced by Dayal and Allen (1975), the bearing factor N_c can be estimated as

$$N_c = N_{c0}[1 + K\log_{10}(v/v_{ref})] \tag{2}$$

where v is the instantaneous velocity of the penetrometer, v_{ref} is a reference velocity chosen to be 0.02 m/s after Lunne et al (1997), K is a strain rate multiplier (chosen to be 0.03-0.09) determined by applying the scaling formula (Aubeny 2010, *pers. comm.*).

$$K_2 = K_1/[1 + K_1(v_{ref2}/v_{ref1})] \tag{3}$$

where K_1 is a previously established strain rate multiplier, chosen to be 1 after Dayal et al (1975) for very low strength sediment and impact velocities > 0.3 m/s, v_{ref1} is the associated reference velocity or reference strain rate, and v_{ref2} is 0.02 m/s. Based on Eq. 2, N_{c0} is the dimensionless bearing capacity factor for clay type sediment determined after Aubeny and Shi (2006) as

$$N_{c0} = 8.55(h/d)^{0.756},\ h/d \leq 1.2 \tag{4a}$$

$$N_{c0} = 9.60(h/d)^{0.21},\ h/d > 1.2 \tag{4b}$$

with h=depth and d=diameter of the penetrometer. An approximated instantaneous undrained shear strength c_0 can then be derived as

$$c_0 = F_{sr}/N_c A \tag{5}$$

where A is the area of the plain subjected to load.

Field and Laboratory Evaluation

In June 2009 and March 2010, *Nimrod* was deployed at selected locations within and around the disposal site boundaries (Fig. 1B). Deployment positions visited during the March 2010 post-disposal surveys were located further east than those of the June 2009 baseline survey as a result of a mandated eastward shift in the disposal site boundaries, though some positions were visited on all 3 surveys. *Nimrod* was deployed twice at each position making up a total of 40, 44, and 44 deployments on 23 June 2009, 16 March 2010, and 20 March 2010, respectively. On 14 March 2010, the first load of dredged material (530 m^3) was released at Site H2 (Fig.1). The first of the two post-disposal surveys using *Nimrod* was undertaken on 16 March 2010. On 20 March 2010, the second load of dredged material (540 m^3) was transported to the disposal site and again released at Site H2. The second *Nimrod* survey took place within hours after release of the second load of dredged material. On 10 April 2010, three core samples were collected at each of the

Nimrod deployment positions G4, H5, I3, and I6 using a lightweight gravity corer (barrel inner diameter=70 mm). Total core lengths ranged between 7 and 14 cm bsf (below sea floor) and correspond to the embedment depths of *Nimrod* deployments (6-19 cm bsf). Laboratory vane shear tests were undertaken in the upper and lower half of the core. Generally, the upper and lower tests were taken at 3 cm and 8 cm below the mud-line, respectively. Results are presented together with those from *Nimrod* deployments in Figure 3.

Results

Shear Strength Profiles

Figure 3a-d shows interpreted sediment strength profiles from *Nimrod* deployments superimposed with shear strength profiles from the laboratory vane shear tests. It can be seen from all profiles that the pronounced peak in shear strength in the upper 5 cm of the profile are related to the high impact velocity of the dynamic penetrometer (Fig. 3). Below 5 cm bsf, shear strength decreases to a value of approximately 1 kPa. In contrast to this ± constant strength, vane shear data show a gradual increase in strength with depth. In the examples shown, the interpreted shear strengths tend be lower than the laboratory shear strength values (Fig. 3). However, two aspects hamper the interpretation. First, the mismatch between in situ and laboratory data could be related to the fact that positioning during the various surveys is inaccurate. Consequently, the core could have been taken slightly adjacent to the earlier Nimrod site and small-scale regional variations may account for the differences observed. Second, coring took place about a month after the second post-disposal *Nimrod* survey, the samples of which were not tested with the lab vane for another several weeks after that. Hence, the core may have been slightly altered during transport and storage in that loss of pore water may account for the increase in strength during laboratory measurements. Given these possibilities, the interpreted profiles from positions G4, H5, and K4 appear to be within a reasonable agreement of the respective lab strength tests (Fig. 3a-b&d).

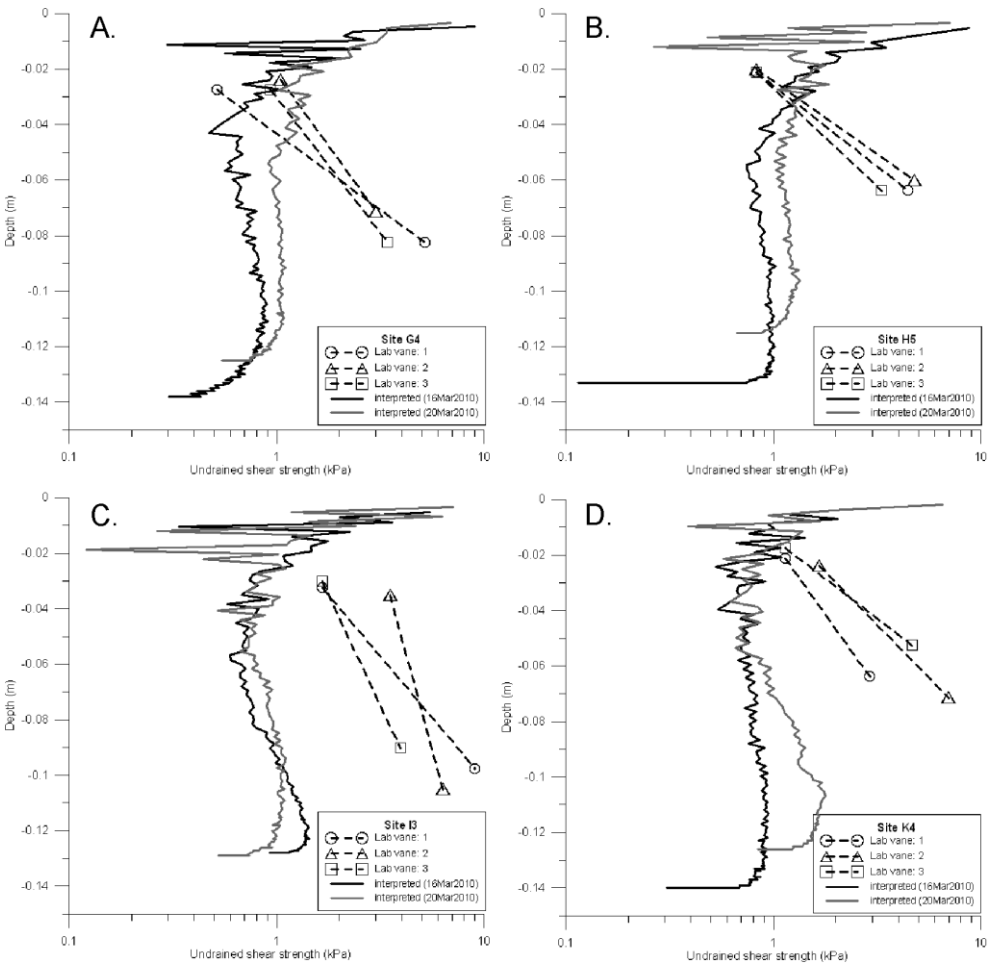

Fig. 3. Examples of interpreted strength profiles from 16 and 20 March 2010 at position A). G4, B). H5, C). I3 and D). K4 superimposed with lab shear vane profiles.

Sediment strength characteristics

Four main strength signatures were identified from the *Nimrod* results:

i. Type A: The deceleration increases approximately linearly with depth. Shear strength is mostly uniform along the depth profile (occasionally a slight increase with depth, but similar to deceleration, the increase is approximately linear) (Fig. 4).

ii. Type B: The deceleration profile takes a "concave-down" shape with an "S"-shaped strength profile (when considering the entire profile). Below ~5 cm and above the deepest 1-2 cm of the profile, the shear strength increases more dramatically with depth (Fig. 5).

iii. Type C: The deceleration increases sharply at a certain depth reflected by a "kink" in the profile. A sharp increase in the strength can likewise be identified at that depth in the profile (Fig. 6).

iv. Type D: The deceleration profile takes a "concave-up" shape with an uncharacteristic strength pattern. Although less pronounced in Figure 7a, typically, the strength appears to be highest in the upper part of the profile (even well below upper 5 cm where the highest values are encountered right after the impact).

Type A and B signatures were the most common throughout the surveys. All deployments from the baseline survey in June 2009 were of these two types. In Type A profiles, maximum deceleration ranged from 1.71-2.75±0.27 g with associated impact velocities of 1.59-1.96±0.1 m/s. Average interpreted shear strengths for this type were between 0.68 ±0.07 and 1.18±0.1 kPa. Impact velocities of Type B profiles ranged from 1.53-1.95±0.12 m/s with maximum decelerations from 1.89-3.22±0.31 g. Average sediment strengths ranged along the profile between 0.64±0.17 – 1.16±0.19 kPa. Type C signatures are characterized by an upper layer of lower strength material with an underlying higher strength material. The thickness of the upper layer ranged from 6-11 cm with an average shear strength of 0.97±0.2 kPa, and was tentatively interpreted as disposed silty-clay from the marina. The higher strength underlying sediment, most likely the natural shelf deposits, had an average shear strength of 1.21±0.18 kPa. The impact velocities and maximum decelerations associated with Type C profiles were 1.73-1.94±0.07 m/s and 2.53-3.6±0.34 g, respectively. Type D profiles, the least common of the surveys, only identified on 4 deployments (possibly less depending on interpretation). Impact velocities ranged from 1.45-1.74±0.12 m/s with associated maximum decelerations of 1.82-2.24±0.19 g. Shear strength in these profiles did not show commonalities as in the other signatures, but deceleration increased rapidly in the upper part of the profile followed by a slower increase with depth.

In map view, the pattern of shear strength profile types across the study site is shown in Figure 8. The most notable observation is that between the two post-disposal surveys, the strength profile type at the majority of deployment positions changed. Also, within a 1km-radius of the disposal release location (H2) and during the first post-disposal survey, there are several positions showing a Type C (i.e., layered) strength profile. During the second post-disposal survey, Type C profiles were identified further away from the disposal release location (>1 km). Less typical Type D profiles were predominantly found during the second survey and near the disposal release location (H2). Spatial variations of Type A and B profiles during the post-disposal surveys are less obvious (Fig. 8).

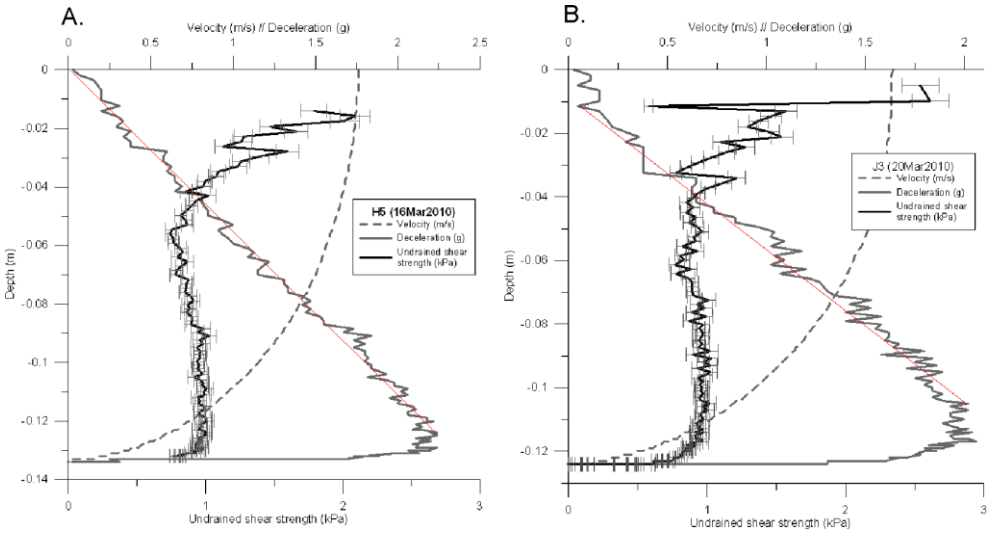

Fig. 4. "Type A" profiles from *Nimrod* deployments on the A) Mar16 & B) Mar 20 2010.

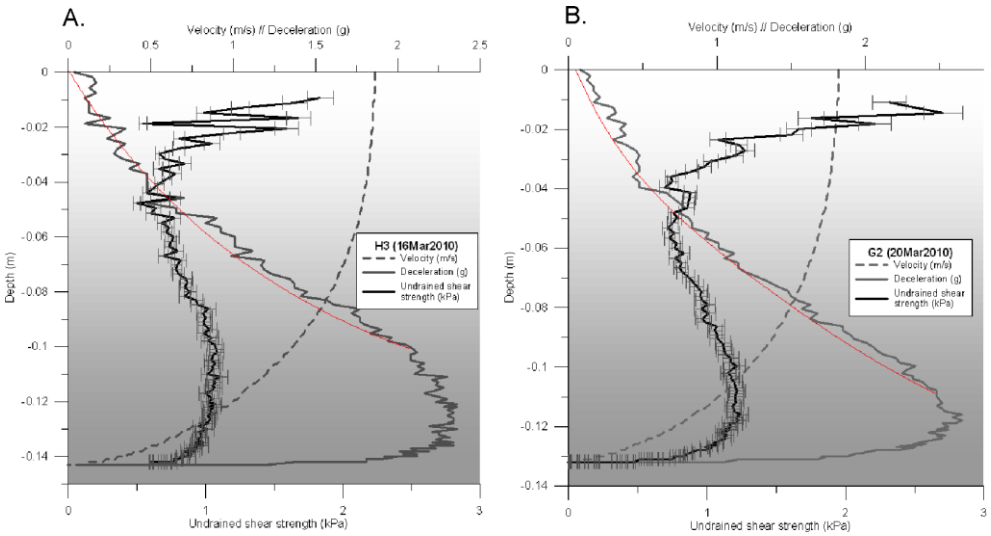

Fig. 5. "Type B" profiles from *Nimrod* deployments on the A) Mar16 & B) Mar 20 2010.

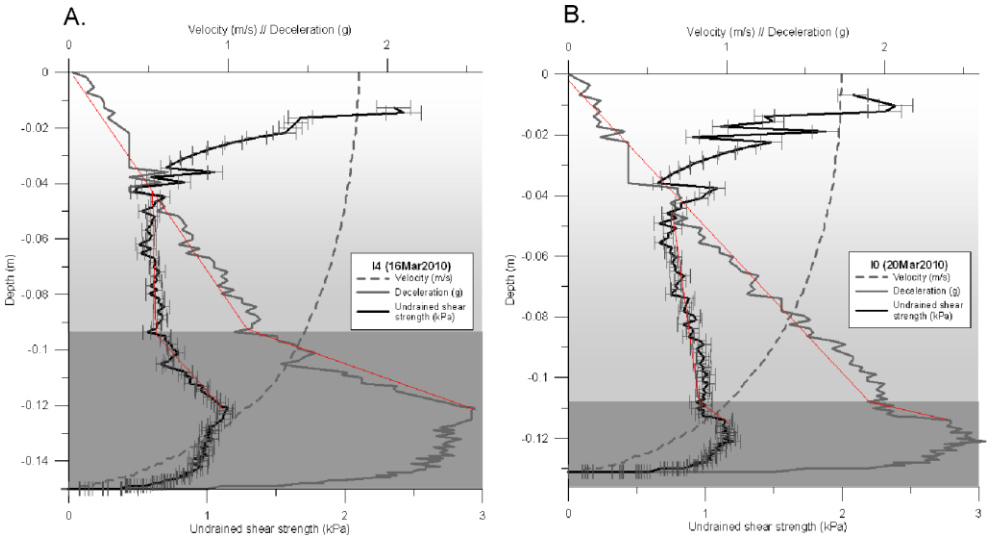

Fig. 6. "Type C" profiles from *Nimrod* deployments on the A) Mar16 & B) Mar 20 2010.

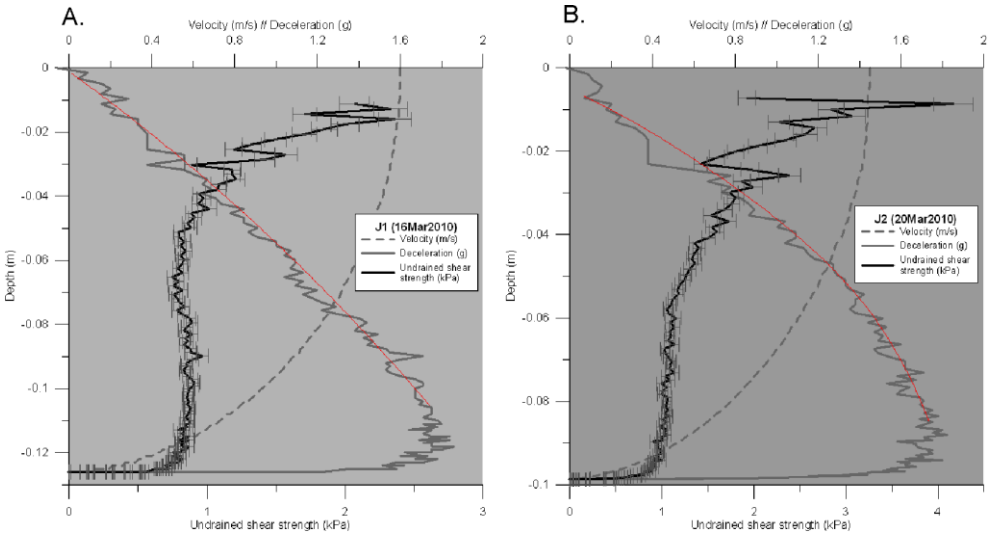

Fig. 7. "Type D" profiles from *Nimrod* deployments on the A) Mar16 & B) Mar 20 2010.

The average interpreted shear strength at each deployment location on each of the post-disposal *Nimrod* surveys is shown in Figure 9. On both occasions, the average calculated shear strength was elevated at positions directly east and of the disposal location (H2) (Fig. 9). After the second post-disposal survey, there also seems to be a general increase in average shear strength at positions south and southeast of the disposal location (H2) compared to those of the first post-disposal survey (Fig. 9).

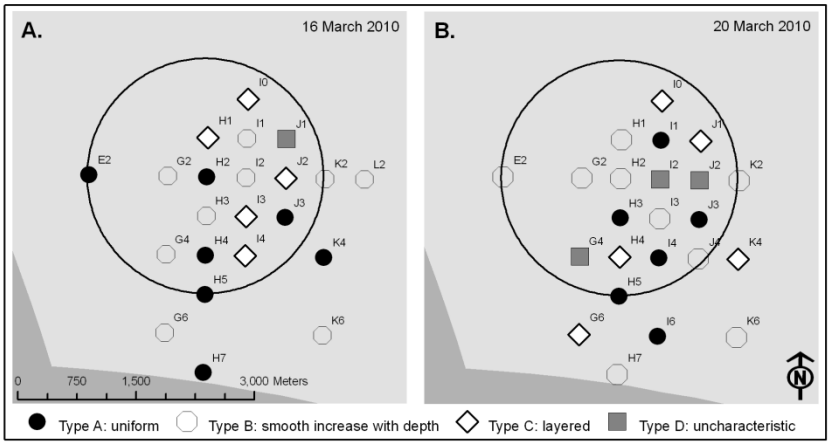

Fig. 8. Sediment strength characteristics indicated from interpretations of *Nimrod* deployments on A). 16 March 2010 and B). 20 March 2010.

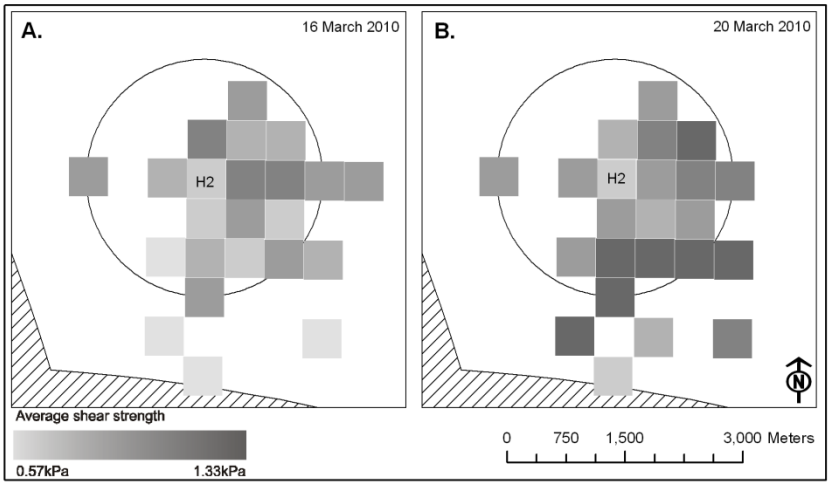

Fig. 9. Average shear strength indicated from interpretations of *Nimrod* deployments on A). 16 March 2010 and B). 20 March 2010.

Discussion

The discussion will focus on two aspects: (i) the geological significance of the *Nimrod* data for future disposal of dredged sediment and (ii) the validity of the interpreted shear strength profiles from dynamic *in situ* testing.

Geological Implications

The range of shear strengths determined from the *Nimrod* deployments is small and does not vary greatly between surveys. Yet, four distinct profile signatures, observed throughout the surveys, were identified. This suggests variability, however small, in an otherwise homogenous environment. The changeability of profile type between deployment locations and between surveys alludes to some influential process acting on the site. Since typical disposal mechanics include three main temporal stages: descent through the water column as a turbulent jet, impact with the seafloor, and spread of the resulting turbidity current (Gordon 1974), the time between disposal and the penetrometer survey is important. The first post-disposal *Nimrod* survey was undertaken two days after disposal, whereas the second survey took place within 4 hours after disposal. Significant water depths which increase entrainment during descent and the increased erosion potential of a turbidity current on a soft seafloor are additional factors to consider (Bokuniewicz and Gordon 1980). It is possible that Type C profiles observed near the disposal location on the first survey were influenced by turbidity current processes and later deposition of entrained fines (see typical 2-layer structure; Fig. 6). In similar locations after the second survey, Type D profiles had only hours to develop and could have resulted from mixing and erosion by a turbidity current, but with insufficient time for settling of the fines. The observed elevated shear strengths to the east and southeast of the disposal location may potentially be the result of erosion by the turbidity current and/or settling of deposited material on either occasion. However, effects from natural processes (e.g. the EAUC) cannot be ruled out. In Type B profiles, typical for the central portion of the H2 site during either survey (Fig. 8), the gradual change in the lower portion of the strength profile seems to be related to amalgamation of the uppermost seafloor deposits and the disposed silty-clay. This process is facilitated by the similarity in strength and sediment consistency when comparing the disposal and natural shelf materials.

Methodological Assessment

Although the interpretation method includes several assumptions and use of empirical relationships that likely do not perfectly describe the present case (Dayal and Allen, 1975; Aubeny and Shi 2006). The procedure has resulted in interpreted shear strength values that are within a reasonable range of the laboratory shear vane values. The results are comparable to the interpretations by Aubeny and Shi (2006) on soft marine muds, and also agree well with earlier penetrometer surveys in which ground-truthing with cores was possible (e.g. Stegmann et al. (2007)). The most significant deficiencies related to the interpretation method are in the upper 5cm and the final 1-2 cm of the profile. Aubeny and Shi (2006) attribute the defects to the neglect of inertial forces and elastic rebound in the soil as velocity decreases to zero in Eq. (1). However, the middle range of the profile values can be regarded as more reliable (Aubeny and Shi 2006). In that area of the depth profiles, there is some overlap between the lower of the vane shear data (see Fig. 3a-b&d). Further below towards the lower end of the gravity cores, the discrepancy between in situ strength estimate and laboratory vane measurement increases (Fig. 3). The lab shear vane measurements may have been compromised by sample disturbance during collection, a common problem with sediment coring, especially that of fine material (Blomqvist 1991) as well as from consolidation of the sample itself during storage and extrusion which could be enhanced due to drainage of the core upon recovery in the field. In addition, the somewhat higher strength of the sediment may result from “apparent over-consolidation”, which is typical for superficial sediments and has been explained by physico-chemical and biogeochemical processes in the sediments (e.g. Sultan et al. (2000)).

Conclusions

In summary, the observations on sediment strength from the *Nimrod* surveys are yet to be fully explained considering that patterns are probably somewhat masked by the combination of the low strength of both native and disposed material, the significant water depth, possible tether drag effects, and the small of quantities of material disposed. However, despite the lack of concrete explanations for the patterns observed, several successes have come from this work. As had been previously demonstrated, the empirical formulation included in the methods of Dayal and Allen (1975) and Aubeny and Shi (2006) also resulted in reasonable interpretations of shear strength for this study. Despite the large water depths and the low strength of the material, fine scale strength variations were detected temporally as well as spatially and in both two and three dimensions. This suggests that *Nimrod* and other dynamic penetrometers can be used effectively for disposal site monitoring, although preferably at sites with larger quantities of disposed material. As far as the authors know, aside from this study, dynamic penetrometers have not been considered previously for these purposes. Following the completion of the *Nimrod* surveys, 8 more loads of dredged material were released at the site bringing the total amount to approximately 5,000 m^3. Undertaking a follow-up *Nimrod* survey would shed more light on the spatial and temporal evolution of dredged material disposal on the shelf northeast of the Hauraki Gulf, New Zealand.

Acknowledgements

This research was funded by the University of Waikato Doctoral Scholarship, Kaipara Limited, the German Research Association (via MARUM and GLOMAR, University of Bremen), and the German Academic Exchange Service (DAAD). We would also like to thank Alan Drinkrow, Mike Roycroft, and Gary Larsen for their field assistance. We are particularly indebted to Matthias Lange (MARUM), Christian Zoellner (MARUM), and Matthias Colsmann (AVISARO, Hannover). Professor Terry Healy passed away on July 20 2010. We were fortunate to have his energetic support during the early stages of this work and for that we are sincerely grateful.

References

Aubeny, C.P. and Shi, H. (2006). "Interpretation of Impact Penetration Measurements in Soft Clays," *Journal of Geotechnical and Geoenvironmental Engineering*, 132(6), 770-777.

Birchenough, S., Boyd, S., Coggan, R., Limpenny, D., Meadows, W., and Rees, H. (2006). "Lights, camera, and acoustics: assessing the macrobenthic communities at a dredged material disposal site off the northeast coast of the UK," *Journal of Marine Systems*, 62, 204-216.

Blomqvist, S. (1991). "Quantitative sampling of soft-bottom sediments: problems and solutions", *Marine Ecology Progress Series*, 72, 295-304.

Bokuniewicz, H. and Gordon, R., 1980. Deposition of dredged sediment at open water sites. *Estuarine and Coastal Marine Science*, 10(3), 289-303.

Dayal, U., Allen, J.H., and Jones, J.M. (1975). "Use of an Impact Penetrometer for the Evaluation of the In-Situ Strength of Marine Sediments," *Marine Georesources and Geotechnology*, 1(2), 73-89.

Flaim, B.K., Healy, T.R., and Weir, P. (2010). "Establishment of a dredged material disposal site in the Exclusive Economic Zone: New Zealand," *Coastal Management*, 38(5), 474-500.

Gordon, R. (1974). "Dispersion of dredge spoil dumped in near-shore waters," *Estuarine and Coastal Marine Science*, 2, 349-358.

Harris, T.F.W. (1985). "*North Cape to East Cape aspects of the physical oceanography*," University of Auckland Department of Physics and Marine Laboratory, 178 p.

Li, M.Z., Parrott, D.R., and Yang, Z. (2009). "Sediment stability and dispersion at the Black Point Offshore Disposal Site, Saint John Harbour, New Brunswick, Canada," *Journal of Coastal Research*, 24(4), 1025-1040.

Lunne, T., Robertson, P.K., and Powell, J.J.M. (1997). *"Cone penetration testing in geotechnical practice,"* Spon Press, London.

Maritime New Zealand, (2009). "Dumping permit application report—Coastal Resources Limited (Pine Harbour Marina): disposal of dredged spoil at new EEZ site east of Great Barrier Island," Maritime New Zealand, Wellington, New Zealand.

Stark , N. and Wever, T. (2008). "Unravelling the subtle details of e*x*pendable *b*ottom *p*enetrometer (XBP) deceleration profiles," *Geo-Marine Letters*, 29(1), 39-45.

Stark, N., Hanff, H., and Kopf, A. (2009). "Nimrod: a tool for rapid geotechnical characterization of surface sediments," *Sea Technology*, 50(4), 10-14.

Stark, N., Hanff, H., Stegmann, S., Wilkens, R., and Kopf, A. (2009). "Geotechnical investigations of sandy seafloors using dynamic penetrometers," *Proceedings of the MTS/IEEE OCEANS'09*, Biloxi.

Stegmann, S., Strasser, M., Anselmetti, F.S., and Kopf, A. (2007). "Geotechnical *in situ* characterisation of subaquatic slopes: The role of pore pressure transients versus frictional strength in landslide initiation," *Geophysical Research Letts.*, 34(7), doi:10.1029/2006GL029122.

Stoll, R.D. and Akal, T. (1999). "XBP-tool for rapid assessment of seabed properties," *Sea Technology*, 40(2), 47-51.

Stoll, R.D., Sun, Y., and Bitte, I. (2007). "Seafloor properties from penetrometer tests," *IEEE Journal of Oceanic Engineering*, 32(1), 57-63.

Sultan, N., Cochonat, P., Dennielou, B., Bourillet, J.F., Savoye, B. and Colliat, J.L. (2000). "Sur consolidation apparente et pression osmotique dans un sédiment marin," *Comptes Rendus de l'Académie des Sciences - Series IIA - Earth and Planetary Science*, 331, 379-386.

Udden, J.A. (1914). "Mechanical composition of clastic sediments," *Bulletin of the Geological Society of America*, 25, 655–744.

Wentworth, C.K. (1922). "A scale of grade and class terms of clastic sediments," *Journal of Geology*, 30, 377-392.

APPENDIX III
CONSULTING REPORTS

The following consulting reports cited in this thesis and arising as a part of the contractual obligations of the project are included on the CD-ROM secured to the back cover of this thesis:

- Flaim, B.K. and Healy, T.R. (2008). Proposal for dredged sediment disposal on the continental shelf in the EEZ: environment impact assessment. Coastal Marine Group, University of Waikato. 96 p.

- Flaim, B.K. and de Lange, W.P. (2011). Post-disposal monitoring of the Auckland Marine Disposal Ground. Coastal Marine Group, University of Waikato. 186 p.